

Structural and Viscoelastic Studies of Flexible Polyurethane Foams

by

Dimitrios V. Dounis

Dissertation Submitted to the Faculty of the
Virginia Polytechnic Institute and State University
In Partial Fulfillment of the Requirements for the Degree

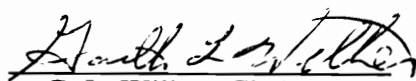
of

Doctor of Philosophy

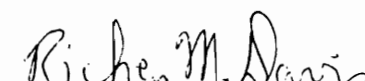
in

Chemical Engineering

Approved:


G. L. Wilkes, Chairman


T. C. Ward


R. M. Davis


J. S. Riffle


D. A. Dillard

Blacksburg, VA

September, 1995

STRUCTURAL AND VISCOELASTIC STUDIES OF FLEXIBLE POLYURETHANE FOAMS

by

Dimitrios V. Dounis

Chairman: Garth L. Wilkes
Chemical Engineering

(ABSTRACT)

In this study, the viscoelastic and morphological characterization of molded foams was the main focus. A series of molded foams based on toluene diisocyanate (TDI) and glycerol initiated polyethylene-oxide-capped propylene-oxide was studied in terms of the structure property features. The results were in many instances compared to those obtained on conventional slabstock foams based on TDI and glycerol initiated propylene-oxide. These comparisons were made to delineate and clarify distinct differences between these two different and very important systems. It was found that high temperatures and humidities "plasticized" the viscoelastic behavior of molded foams to a greater extent than that of slabstock foams; the molded foams displayed higher load decay values in the viscoelastic measurements than slabstock foams.

In an attempt to understand these dramatic differences, the two types of "cross-links" (covalent cross-links and urea based phase separated hard segment domains) were evaluated. It was discovered that the structure of the hard segment domains dictated the foam's behavior, especially at elevated temperatures and humidity. Furthermore, it was found that the hard segment domains in slabstock foams had a much higher level of short range ordering. This was confirmed by wide-angle x-ray scattering (WAXS) and fourier transform infrared (FTIR) which revealed that the conventional slabstock foams had much more organized hard segment domains. It is thus concluded that the dramatic differences between the mechanical properties of molded and slabstock foams are due to the lower and weaker ordering of the hard segments in molded systems making these physical "cross-

links" more labile at higher temperatures and humidities. These morphological differences were shown to be due primarily to differences in the formulation components between the two studied systems. First, the ethylene-oxide capping used in the polyol of molded foams to increase the reactivity is known to also increase the compatibility between the hard and soft segments thus promoting some phase-mixing. Second, the addition of diethanolamine (DEOA) added in the molded foam formulation to decrease demold times by enhancing cross-linking clearly resulted in the prevention of the full development of the hard-segment domains.

It was also found that the copolymer polyol particles (CPP), added to molded foams to increase load bearing capabilities, had a negative effect on the viscoelastic properties. The viscoelastic properties of the CPP containing foams were more time-dependent than those of the foams lacking these particles. As expected, the incorporation of these particles increased the initial load and decreased the initial strain over the foams lacking the particles suggesting that the initial stiffness of these materials was increased. However, over a period of time, the amount of this initial load that decayed was greater for the CPP containing foams and furthermore, at elevated conditions, the load decreased to levels below those of the CPP lacking foams.

A series of slabstock foams was also studied to evaluate the effect of toluene diisocyanate (TDI) index on the physical properties, and morphology of the foams. Extraction experiments using dimethyl formamide (DMF) showed that increasing the index increased the level of covalent cross-linking with perhaps a maximum being reached at an index of 100. Viscoelastic measurements also supported the claim of increased cross-linking with TDI index. The initial load in load relaxation experiments systematically increased with increasing TDI while the percent decay in a three hour period decreased. Temperature and/or humidity "plasticized" the load relaxation behavior in all the foams studied indicating that the hard segment domain physical "cross-links" play a significant role in the properties of these materials. The morphology of the foams was also found to

be influenced by the TDI index. Small angle x-ray scattering (SAXS), differential scanning calorimetry (DSC), and dynamic mechanical analysis (DMA) all provided evidence that an increase in the TDI index promoted phase mixing. FTIR and WAXS showed that the short range ordering within the hard segment domains displayed a maximum at an index of 100 and decreased as the index was increased.

Finally, the influence of transient moisture conditions on the viscoelastic behavior was also investigated. In creep extractions, as the moisture conditions were cycled from low to high humidity while maintaining constant temperature, the compressive strain increased in subsequent steps where the strain levels under cyclic moisture conditions surpassed those observed at the highest constant relative humidity. This overall phenomenon of enhanced creep under cyclic moisture levels was attributed to water interacting with the hydrogen bonded structure within the foam. These hydrophilic interactions, principally promoted within the hard segment regions due to high hydrogen bonding, are disrupted causing slippage and increases in strain. As the foam is rapidly dried, regions of free volume are induced by the loss of water thus causing further increases in strain prior to the re-establishment of well ordered hydrogen bonding.

Acknowledgments

First, I would like to extend my utmost gratitude to my Lord, Jesus Christ, without his mercy and grace nothing I have accomplished would be possible. He has given me the talent and discipline to achieve my goals and has given me the ability through my deeds and actions to further glorify his name. Second, I would like to thank my mother and father who have supported and encouraged me tremendously through my educational years. Their accomplishments are a testament to the rewards of hard work. Furthermore, their sacrifices for my sake to make my years as painless as possible are beyond what any parents should sacrifice. The rewards and accomplishments that I have attained are very much credited to them. Through my high school, to my undergraduate, and now my graduate years, they have given up personal comforts, both monetary and psychological so that they can help me accomplish my goals. I would also like to thank my sister who has given me as much encouragement, love and admiration as anyone. I am truly blessed and honored to be loved and respected to such a degree as my sister does.

In my graduate school years, I met my wife who has added meaning and inspiration to my life. She has shown support and love that only she could and has truly felt my happiness and well as my frustrations and has made the road I've traveled smoother and more meaningful. She has also given me the greatest gift of all; the most wonderful, beautiful, inspirational son of all. He is the meaning of life, the center of my universe and has given me more happiness than any other person or thing. He can magically turn the most frustrating and disappointing day into the most pleasant. Just over two years old, he has given me more joys than any other accomplishment or gift I have experienced.

To this point in my life, I can truly say I have two heroes. The first is my father. If I can be half the man he is, I would be a great man. I have yet to meet a person more honest, sincere, hard working, and dedicated to his family than my father. Philosophically, this is the man I want to model my life after. My second hero is my

advisor. I have yet to meet a person more dedicated to his work and students than Professor Garth L. Wilkes. His patience, expertise and support was instrumental in my accomplishments. He is a perfect educator, in and out of the classroom and the laboratory, as well as academically and socially. He never restrained me from carrying out specific experiments even when he knew that the outcome would be less than positive. He allowed me to learn from my own mistakes and offered advice when necessary. My career goal is to dedicate the amount of energy to my work as he has to his work and with as much enthusiasm. I am truly blessed to have had him as an advisor. My future successes can definitely be in part attributed to the positive impact that he has had on me.

I would also like to thank my other committee members (professors Rick Davis, Dave Dillard, Judy Riffle, and Tom Ward) for they were also very instrumental, from my proposal defense to their teachings within the classroom. Some of the most challenging classes I took, were taught by my committee members. I'll never forget the way Dr. Ward taught *Physical Chemistry of Polymers* . He taught that class with as much passion and brilliance as any professor I have had with any class. Each committee member has left a unique positive enlightening impression that will definitely aid me in the future.

I am also grateful to my fellow group members. Their presence and broad research interests have also broadened my familiarity with polymeric materials. I have learned a great deal from each member of Dr. Wilkes' research group both technically oriented as well as socially. A special thanks goes to Sandy Simpkins who was a great help over the years and especially near the end of my graduate career.

I am also very grateful to people who had positive influences on my earlier years that led me to take the path I did. For example it was my tenth and eleventh grade science teachers who began my interest in chemical engineering. I am also grateful to Professor Larry Drzal and his colleagues at Michigan State who gave me the opportunity to "taste" graduate school which I immensely enjoyed.

Finally, I would like to express my gratitude to the Dow Chemical Co. and especially the people that have been directly involved in providing the funding that has allowed me to pursue this research as well as those that have an interest in the work and have collaborated with me on this project.

I feel that in many ways, I have already received part of my reward for my hard work. My reward is my enlightenment and therefore since everyone I have mentioned above was instrumental in that, I am truly grateful to them all. *Among many, one of my goals is to share my experiences and expertise with others and positively influence them as those mentioned above have influenced me.*

Table of Contents

Chapter 1	1
1.1 Introduction	1
1.2 Applications	4
Chapter 2	8
2.0 Literature Review	8
2.1 Chemistry	8
2.1.1 Formulation Components	10
2.1.1.a Polyols	10
2.1.1.b Isocyanates	21
2.1.1.c Water	27
2.1.1.d Surfactants	27
2.1.1.e Catalysts	30
2.1.1.f Blowing Agents	34
2.1.2 Foam Process	35
2.1.3 Molded Foam Processing Technique	38
2.1.4 Reaction Sequences	39
2.2 Morphology and Structure	41
2.2.1 Scanning Electron Microscopy	43
2.2.2 Transmission Electron Microscopy	43
2.2.3 Dynamic Mechanical Spectroscopy	46
2.2.4 Differential Scanning Calorimetry	46
2.2.5 Wide-Angle X-ray Scattering	48
2.2.6 Small-Angle X-ray Scattering	51
2.2.7 Fourier Transform Infrared	54
2.3 Mechanical Properties of Polyurethane Foams	62

2.3.1	Basic Foam Properties	62
2.3.2	Stress Strain Behavior	65
2.3.2.a	Open-Cells	67
2.3.2.b	Closed-Cells	73
2.3.3	Viscoelastic Properties	76
2.3.3.a	Stress Relaxation	77
2.3.3.b	Creep	83
2.3.3.c	Compression Set	93
2.3.4	Mechano-Sorptive Behavior	96
2.4	Summary	99
Chapter 3		101
3.0	Experimental Materials and Procedures	101
3.1	Materials	101
3.2	Experimental Techniques	110
3.2.1	Scanning Electron Microscopy	112
3.2.2	Transmission Electron Microscopy	112
3.2.3	Differential Scanning Calorimetry	113
3.2.4	Dynamic Mechanical Analysis	113
3.2.5	Small-Angle X-ray Scattering	113
3.2.6	Wide-Angle X-ray Scattering	114
3.2.7	Fourier Transform Infrared	114
3.2.8	Extraction Studies	114
3.2.9	Load Relaxation	115
3.2.10	Compression Creep Experiments	117
3.2.11	Compression Set and Recovery Experiments	119
3.2.12	Compression and Tensile "Stress"-Strain Determinations	119

3.2.13	Mechano-Sorptive Experiments	120
Chapter 4	121
4.1	Cellular Structure	121
4.1.1	Effect of Copolymer Polyols on Cellular Structure	125
4.2	Fine Structure	131
4.3	Microphase Separation	134
4.3.1	Thermal Properties	134
4.3.2	Small Angle X-ray Scattering	142
4.3.2.1	Effect of Water/TDI Content on SAXS	145
4.3.2.2	Influence of CPP Dispersions on SAXS	148
4.3.3	Wide Angle X-ray Diffraction	149
4.3.4	Fourier Transform Infrared	153
4.4	Solvent Extraction Studies	160
4.4.1	Effect of Copolymer Polyols	160
4.4.2	Effect of Water/TDI Content	162
4.5	Compression "Stress"-Strain	163
4.5.1	Effect of Copolymer Polyols	171
4.5.2	Effect of Formulation Water Content	174
4.6	Viscoelastic Behavior	175
4.6.1	Load Relaxation Behavior	175
4.6.1.1	Effect of Temperature and Relative Humidity	176
4.6.1.2	Effect of Copolymer Polyols	206
4.6.1.3	Effect of Formulation - Water/TDI Content	218
4.6.2	Compression Creep	218
4.6.2.1	Effect of Temperature and Relative Humidity	222
4.6.2.2	Effect of Copolymer Polyols	238
4.6.2.3	Effect of Water/TDI Content	248

4.6.3	Compression Set	249
4.6.3.1	Effect of Temperature and Relative Humidity on Compression Set	249
4.6.3.2	Effect of Copolymer Polyols	251
4.6.3.3	Effect of Water/TDI Content	252
4.6.3.4	Compression Set Recoverability	252
4.7	Characterization of Foams Made with Diethanolamine	253
4.7.1	Influence of Diethanolamine on Structure and Properties	254
4.7.1.1	Influence Cellular Structure	255
4.7.1.2	Influence on Fine Structure	255
4.7.1.3	Influence of DEOA on Solvent Extraction Behavior .	258
4.7.1.4	Influence of DEOA on Microphase Separation	258
4.7.1.4.a	Thermal Analysis	258
4.7.1.4.b	Small Angle X-ray Scattering	261
4.7.1.4.c	Wide Angle X-ray Scattering	266
4.7.1.4.d	Fourier Transform Infrared	268
4.7.1.5	Load Relaxation Behavior	270
4.7.2	Influence of Diethanolamine on Structure and Properties of Foams Made with a 3000 MW All PO Polyol	273
4.7.2.1	Influence on Cellular Structure	273
4.7.2.2	Influence on Fine Structure	276
4.7.2.3	Influence of DEOA on Solvent Extraction Behavior .	280
4.7.2.4	Influence of DEOA on Microphase Separation	280
4.7.2.4.a	Thermal Analysis	282
4.7.2.4.b	Wide Angle X-ray Scattering	282
4.7.2.5	Load Relaxation Behavior	285
4.7.3	Influence of EO Capped Polyols	289
4.8	Summary	290

Chapter 5	295
5.0 Influence of TDI Index on Structure-Property Behavior of Flexible Slabstock Polyurethane Foams	295
5.1 Influence of Index on Cellular Structure	296
5.2 Influence of Index on Solvent Extraction Results(Covalent Cross-linking)		300
5.3 Influence of TDI Index on the Microphase Separation	304
5.4 Effect of Index on the Mechanical Properties	318
5.5 Influence of TDI Index on the Viscoelastic Behavior	320
5.6 Summary	335
Chapter 6	337
6.0 Mechano-Sorptive Behavior	337
6.1 Effect of Transient Moisture Conditions on the Creep Response	337
6.2 Effect of Transient Moisture Conditions on the Load Relaxation Behavior		346
6.3 Summary	352
Chapter 7	353
7.0 Conclusions and Recommendations	353
7.1 Conclusions	353
7.2 Recommendations	359
References	362

List of Figures

Figure 1.1.	Schematic representation of different types of cellular polymers: (a) low-density open-cell foam, (b) high-density closed-cell foam, (c) structural foam with cellular core and integral skin, (d) multicomponent structural foam, (e) fiber-reinforced closed-cell foam and (f) syntactic foam. [ref 1]..2
Figure 1.2.	Applications of Polyurethane foams. [ref 5].....5
Figure 2.1.	Reactions in urethane formation. (a) primary gellation reaction and (b) secondary reaction leading to allophanate.....9
Figure 2.2.	Reactions in urea formation. (A) primary blowing reaction, (B) chain extension reaction, and (C) secondary reaction leading to biuret.....11
Figure 2.3.	Formation of trifunctional polyol.....14
Figure 2.4.	Formation of primary hydroxyl derived from ethylene oxide.....16
Figure 2.5.	Formation of block copolymer polyol.....17
Figure 2.6.	Reactivity of polyols. (A) effect of primary hydroxyl content (B) effect of monol and primary hydroxyl content. [ref 6].....20
Figure 2.7.	Formation of isocyanates.....22
Figure 2.8.	Secondary reactions in isocyanate formation.....23
Figure 2.9.	Toluene diisocyanate isomers.....24
Figure 2.10.	Production of 80:20 isomer mixture of toluene diisocyanate. [ref 6]25
Figure 2.11.	Production of diphenylmethane diisocyanate. [ref 6]26
Figure 2.12.	Formation of silicone based surfactant.....29
Figure 2.13.	Formation of isocyanate-amine complex. [ref 5].....31
Figure 2.14.	Formation of active hydrogen amine complex. [ref 5].....32
Figure 2.15.	Mechanism for activated complex formation. [ref 5].....33
Figure 2.16.	Representation of multiphase separated structure in conventional slabstock polyurethane foams. [ref 6].....42
Figure 2.17.	Typical SEM micrographs of a conventional slabstock polyurethane foam (a) parallel to the rise direction and (b) perpendicular to the rise direction. [ref 33].....44
Figure 2.18.	TEM micrographs of four slabstock polyurethane foams varying in water content (A) Foam 1 (B) Foam 2 (C) Foam 3 (D) Foam 4. [ref 33].....45

Figure 2.19.	Normalized DMS spectra for slabstock polyurethane foams (a) storage modulus (b) $\tan \delta$. [ref 31].....	47
Figure 2.20.	DSC thermogram of slabstock polyurethane foams varying in water content. [ref 6].....	49
Figure 2.21.	WAXS patterns for four slabstock polyurethane foams varying in water content. [ref 33].....	50
Figure 2.22.	SAXS profiles for four slabstock polyurethane foams varying in water content. [ref 33].....	52
Figure 2.23.	IR spectra in the N-H and C=O regions at 29°C and 98°C for a polyurethane elastomer. [ref 40].....	55
Figure 2.24.	Temperature dependence of the bonded N-H region of a semicrystalline polyurethane upon (A) heating and (B) cooling. [ref 41].....	58
Figure 2.25.	Simultaneous FTIR-DSC results for 2,4-TDI polyurethane. [ref 42].....	60
Figure 2.26.	Compression hardness and indentation force deflection tests. [ref 3].....	64
Figure 2.27.	Stress-strain behavior for elastomeric foams in (A) compression and (B) tension. [ref 57].....	66
Figure 2.28.	(A) Cubic model for an open-cell foam undergoing (B) cell edge bending and then (C) elastic buckling in cell walls. [ref 1].....	68
Figure 2.29.	Comparison of theory to experimental data for Young's modulus. Solid line represents theory. [ref 57].....	70
Figure 2.30.	Comparison of theory to experimental data for the elastic collapse stress. Solid line represents theory. [ref 57].....	72
Figure 2.31.	Compressive stress-strain. [ref 64].....	75
Figure 2.32.	Effect of temperature on stress relaxation of 2 pph water content foam. [ref 79].....	80
Figure 2.33.	Effect of temperature on stress relaxation of 5 pph water content foam. [ref 79].....	82
Figure 2.34.	Flexural Creep for a 25% reinforced foam. [ref 91].....	86
Figure 2.35.	Master curves of flexural creep for (a) 25% and (b) 40% reinforced foams. [ref 91].....	87
Figure 2.36.	Creep rate as a function of initial penetration. [ref 80].....	89
Figure 2.37.	Long column buckling. [ref 80].....	90

Figure 2.38.	Compressive creep behavior for two foams varying in hard segment content. [ref 79].....	92
Figure 2.39.	Compression set tests at (A) 90% deflection, (B) 75% deflection and (C) 50% deflection. [ref 96].....	95
Figure 2.40.	Creep and delayed failure of beech wood under cyclic moisture conditions. [ref 102].....	98
Figure 3.1.	Illustration of load relaxation apparatus.....	116
Figure 3.2.	Illustration of creep apparatus.....	118
Figure 4.1.	Scanning electron micrographs of foam Fmc4 shown both (a) parallel to the rise direction and (b) perpendicular to the rise direction.....	124
Figure 4.2.	Scanning electron micrographs of foams (a) Fmo4, (b) Fmo2, (c) Fmc4, and (d) Fmc2. (mag = 30x).....	126
Figure 4.3.	Scanning electron micrographs of foams (a) Fmo4, (b) Fmo2, (c) Fmc4, and (d) Fmc2. (mag = 80x).....	128
Figure 4.4.	Scanning electron micrographs of foam Fme4 shown both (a) parallel to the rise direction and (b) perpendicular to the rise direction.....	130
Figure 4.5.	Transmission electron micrograph of foam Fmc4 (mag. = 27kx).....	132
Figure 4.6.	Transmission electron micrograph of foam Fme4 (mag. = 27kx).....	133
Figure 4.7.	Transmission electron micrograph of foam Fmc4 after 90% compression at 150°C (mag. = 27kx).....	135
Figure 4.8.	DSC thermograms of Fmc4 showing both the (a) first and (b) second heating cycles.....	137
Figure 4.9.	TGA thermogram of Fmc4 showing the weight loss associated with the observed endotherm.....	138
Figure 4.10.	Oscillating DSC of Fmc4 illustrating both the (a) reversible and (b) irreversible transitions.....	139
Figure 4.11.	DSC thermograms of Fmo4 showing both the (a) first and (b) second heating cycles.....	140
Figure 4.12.	Influence of the formulation ingredients on the Tan Delta of the six molded foams. Foams are listed in terms of decreasing order of the magnitude of the tan delta peak: (a) Fmo2, (b) Fme2, (c) Fmc2, (d) Fmo2, (e) Fmc4, and (f) Fme4.....	143
Figure 4.13.	Influence of the CPP particles on the Tan Delta peak of the molded foams illustrated using (a) Fmc4 and (b) Fmo4.....	144

Figure 4.14.	SAXS profiles of 4 molded foams illustrating the influence of the CPP particles and water/TDI content on the microphase separation: (a) Fmc4, (b) Fmo4, (c) Fmc2 and (d) Fmo2.....	146
Figure 4.15.	SAXS profiles of 4 molded foams illustrating the influence of the experimental CPP particles and water/TDI content on the microphase separation: (a) Fmc4, (b) Fme4, (c) Fmc2 and (d) Fme2.....	147
Figure 4.16.	WAXS patterns illustrating the short range ordering of the HS domains of the molded foams: (a) Fmo4, (b) Fmo2, (c) Fmc4, (d) Fmc2, (e) Fme4, and (f) Fme2.....	150
Figure 4.17.	WAXS patterns illustrating the short range ordering of the HS domains of a conventional slabstock foam (a) before extraction and (b) after extraction.....	152
Figure 4.18.	FTIR spectra in the carbonyl region of the molded foams (a) Fmc4 and (b) Fmc2 as well as slabstock foam (c) Fs5.....	155
Figure 4.19.	FTIR spectra in the carbonyl region of molded foams (a) Fmo4 and (b) Fmo2.....	156
Figure 4.20.	Influence of temperature on carbonyl absorbance in FTIR spectra of Fmc4.....	157
Figure 4.21.	FTIR spectra in the carbonyl region of the slabstock foam (a) before extraction and (b) after extraction.....	159
Figure 4.22.	Load-strain behavior for Fmo4 illustrating hysteresis upon (a) loading-unloading and (b) first loading-second loading following a 5 min. recovery period.....	164
Figure 4.23.	Load-strain behavior for Fmo2 illustrating hysteresis upon (a) loading-unloading and (b) first loading-second loading following a 5 min. recovery period.....	166
Figure 4.24.	Load-strain behavior for Fmc4 illustrating hysteresis upon (a) loading-unloading and (b) first loading-second loading following a 5 min. recovery period.....	167
Figure 4.25.	Load-strain behavior for Fmc2 illustrating hysteresis upon (a) loading-unloading and (b) first loading-second loading following a 5 min. recovery period.....	168
Figure 4.26.	Load-strain behavior for Fme4 illustrating hysteresis upon (a) loading-unloading and (b) first loading-second loading following a 5 min. recovery period.....	169
Figure 4.27.	Load-strain behavior for Fmc4 illustrating hysteresis difference between (a) first loading-unloading and (b) second loading-unloading following a 5 min. recovery period.....	170

Figure 4.28.	Load relaxation behavior of Fmc2 at 30°C-35%RH under a constant deformation of 65%.....	177
Figure 4.29.	Load Relaxation Behavior of Fmo4 as a function of temperature/relative humidity, (a) 30°C-35%RH, (b) 100°C-35%RH, (c) 30°C-98%RH, and (d) 100°C-98%RH.....	178
Figure 4.30.	Load Relaxation Behavior of Fmo2 as a function of temperature/relative humidity, (a) 30°C-35%RH, (b)100°C-35%RH, (c) 30°C-98%RH, and (d) 100°C-98%RH.....	182
Figure 4.31.	Variable temperature load relaxation behavior for Fmc4 at 35%RH.....	186
Figure 4.32.	Variable temperature load relaxation behavior for Fmc4 at 98%RH.....	188
Figure 4.33.	Load Relaxation Behavior of Fmc4 as a function of temperature/relative humidity, (a) 30°C-35%RH, (b) 30°C-98%RH, (c) 50°C-35%RH, (d) 50°C-98%RH, (e) 80°C-35%RH, (f) 80°C-98%RH, (g) 100°C-35%RH, and (h) 100°C-98%RH.....	190
Figure 4.34.	Variable temperature load relaxation behavior for Fmc2 at 35%RH.....	192
Figure 4.35.	Variable temperature load relaxation behavior for Fmc2 at 98%RH.....	195
Figure 4.36.	Load Relaxation Behavior of Fmc2 as a function of temperature/relative humidity, (a) 30°C-35%RH, (b) 30°C-98%RH, (c) 50°C-35%RH, (d) 50°C-98%RH, (e) 80°C-35%RH, (f) 80°C-98%RH, (g) 100°C-35%RH, and (h) 100°C-98%RH.....	196
Figure 4.37.	Load Relaxation Behavior of Fme4 as a function of temperature/relative humidity, (a) 30°C-35%RH, (b) 30°C-98%RH, (c) 50°C-35%RH, (d) 50°C-98%RH, (e) 80°C-35%RH, (f) 80°C-98%RH, (g) 100°C-35%RH, and (h) 100°C-98%RH.....	198
Figure 4.38.	Load Relaxation Behavior of Fme2 as a function of temperature/relative humidity, (a) 30°C-35%RH, (b) 30°C-98%RH, (c) 50°C-35%RH, (d) 50°C-98%RH, (e) 80°C-35%RH, (f) 80°C-98%RH, (g) 100°C-35%RH, and (h) 100°C-98%RH.....	202
Figure 4.39.	Figure 4.39. Master curves of the load relaxation behavior of foam Fme4 using horizontal shifts of curves at (A) different temperatures (ref. T=30°C, RH=35%) and (B) different humidity levels (ref. RH=35%,T=30°C)..	205
Figure 4.40.	Load relaxation behavior at 30°C-35%RH for the 4 pph water content foam as a function of the CPP used, (a) Fme4, (b) Fmc4 and (c) Fmo4.....	207
Figure 4.41.	Load relaxation behavior at 30°C-35%RH for the 2 pph water content foam as a function of the CPP used, (a) Fme2, (b) Fmc2 and (c) Fmo2.....	208
Figure 4.42.	Load relaxation behavior at 100°C-35%RH for the 4 pph water content foam as a function of the CPP used, (a) Fme4, (b) Fmc4 and (c) Fmo4.....	210

Figure 4.43.	Load relaxation behavior at 100°C-35%RH for the 2 pph water content foam as a function of the CPP used, (a) Fme2, (b) Fmc2 and (c) Fmo2.....	211
Figure 4.44.	Load relaxation behavior at 30°C-98%RH for the 4 pph water content foam as a function of the CPP used, (a) Fme4, (b) Fmc4 and (c) Fmo4.....	213
Figure 4.45.	Load relaxation behavior at 30°C-98%RH for the 2 pph water content foam as a function of the CPP used, (a) Fme2, (b) Fmc2 and (c) Fmo2.....	214
Figure 4.46.	Load relaxation behavior at 100°C-98%RH for the 4 pph water content foam as a function of the CPP used, (a) Fme4, (b) Fmc4 and (c) Fmo4.....	215
Figure 4.47.	Load relaxation behavior at 100°C-98%RH for the 2 pph water content as a function of the CPP used, (a) Fme2, (b) Fmc2 and (c) Fmo2.....	217
Figure 4.48.	Load relaxation behavior at 30°C-35%RH of molded foams without the use of CPPs as a function of water/TDI content (or density), (a) Fmo2 and (b) Fmo4.....	219
Figure 4.49.	Load relaxation behavior at 30°C-35%RH for the CPP containing molded foams as a function of water/TDI content (or density), (a) Fmc2 and (b) Fmc4.....	220
Figure 4.50.	Normalized load relaxation behavior at 30°C-35%RH for the CPP containing molded foams as a function of water/TDI content, (a) Fmc2 and (b) Fmc4.....	221
Figure 4.51.	Creep response of Fmc4 as a function of temperature/relative humidity, (a) 30°C-35%RH, (b)30°C-98%RH, (c) 50°C-35%RH, (d) 50°C-98%RH, (e) 80°C-35%RH, (f)80°C-98%RH, (g) 100°C-35%RH (h) 100°C-98%RH.....	223
Figure 4.52.	Creep response of Fmc2 as a function of temperature/relative humidity, (a) 30°C-35%RH, (b)30°C-98%RH, (c) 50°C-35%RH, (d) 50°C-98%RH, (e) 80°C-35%RH, (f)80°C-98%RH, (g) 100°C-35%RH (h) 100°C-98%RH.....	227
Figure 4.53.	Creep response of Fme4 as a function of temperature/relative humidity, (a) 30°C-35%RH, (b)30°C-98%RH, (c) 50°C-35%RH, (d) 50°C-98%RH, (e) 80°C-35%RH, (f)80°C-98%RH, (g) 100°C-35%RH (h) 100°C-98%RH.....	229
Figure 4.54.	Creep response of Fme2 as a function of temperature/relative humidity, (a) 30°C-35%RH, (b)30°C-98%RH, (c) 50°C-35%RH, (d) 50°C-98%RH, (e) 80°C-35%RH, (f)80°C-98%RH, (g) 100°C-35%RH (h) 100°C-98%RH.....	231
Figure 4.55.	Creep response of Fmo4 as a function of temperature/relative humidity, (a) 30°C-35%RH, (b)30°C-98%RH, (c) 100°C-35%RH and (d) 100°C-98%RH.....	234

Figure 4.56.	Creep response of Fmo2 as a function of temperature/relative humidity, (a) 30°C-35%RH, (b) 30°C-98%RH, (c) 100°C-35%RH and (d) 100°C-98%RH.....	236
Figure 4.57.	Effect of temperature on the initial strain at 35%RH, (a) Fme2, (b) Fmc2, (c) Fme4, (d) Fmc4, (e) Fmo2, and (f) Fmo4.....	239
Figure 4.58.	Effect of temperature on the creep decay at 35%RH, (a) Fme2, (b) Fmc2, (c) Fme4, (d) Fmc4, (e) Fmo2, and (f) Fmo4.....	240
Figure 4.59.	Creep response at 30°C-35%RH as a function of the CPP used and water/TDI content, (a) Fme2, (b) Fmc2, (c) Fme4, (d) Fmc4, (e) Fmo2, and (f) Fmo4.....	241
Figure 4.60.	Creep response at 100°C-35%RH as a function of the CPP used and water/TDI content, (a) Fme2, (b) Fmc2, (c) Fme4, (d) Fmc4, (e) Fmo2, and (f) Fmo4.....	243
Figure 4.61.	Creep response at 30°C-98%RH as a function of the CPP used and water/TDI content, (a) Fme2, (b) Fmc2, (c) Fme4, (d) Fmc4, (e) Fmo2, and (f) Fmo4.....	245
Figure 4.62.	Creep response at 100°C-98%RH as a function of the CPP used and water/TDI content, (a) Fme2, (b) Fmc2, (c) Fme4, (d) Fmc4, (e) Fmo2, and (f) Fmo4.....	247
Figure 4.63.	Scanning electron micrographs of foam FeD-0 shown both (a) parallel to the rise direction and (b) perpendicular to the rise direction.....	256
Figure 4.64.	Scanning electron micrographs of foam FeD-2 shown both (a) parallel to the rise direction and (b) perpendicular to the rise direction.....	257
Figure 4.65.	Transmission electron micrographs of foam (a) FeD-0 and (b) FeD-2 at a magnification of 69.6kx.....	259
Figure 4.66.	DSC thermograms of the first heating cycles of (a) FeD-0 and (b) FeD-2.....	262
Figure 4.67.	DSC thermograms of the second heating cycles of (a) FeD-0 and (b) FeD-2.....	263
Figure 4.68.	Influence of the DEOA content on the Tan Delta peak of the molded foams: (a) FeD-0 and (b) FeD-2.....	264
Figure 4.69.	SAXS profiles of (a) FeD-0, (b) FeD-2 illustrating the influence of the DEOA content on the microphase separation.....	265
Figure 4.70.	WAXS patterns illustrating the influence of DEOA content on the short range ordering of the HS domains: (a) FeD-0, (b) FeD-1 and (c) FeD-2.....	267
Figure 4.71.	Influence of DEOA content on bidentate absorbance in the FTIR spectra of foams (a) FeD-0 and (b) FeD-2.....	269

Figure 4.72.	Influence of temperature and relative humidity on the load relaxation behavior of (A) FeD-0 and (B) FeD-2. In each figure the letters designate the following conditions: (a) 30°C-35%RH, (b) 30°C-98%RH, (c) 100°C-35%RH, and (d) 100°C-98%RH.....	271
Figure 4.73.	Influence of the DEOA content on the load relaxation behavior at (A) 30°C-35%RH, and (B) 100°C-98%RH. In each figure the letters designate: (a) FeD-0 and (b) FeD-2.....	272
Figure 4.74.	Scanning electron micrographs of foam FD-0 shown both (a) parallel to the rise direction and (b) perpendicular to the rise direction.....	274
Figure 4.75.	Scanning electron micrographs of foam FD-0.5 shown both (a) parallel to the rise direction and (b) perpendicular to the rise direction.....	275
Figure 4.76.	Scanning electron micrographs of foam FD-1 shown both (a) parallel to the rise direction and (b) perpendicular to the rise direction.....	277
Figure 4.77.	Transmission electron micrographs of foam (a) FD-0 at a magnification of 54kx.....	278
Figure 4.78.	Transmission electron micrographs of foam FD-0.5 at a magnification of 54kx.....	279
Figure 4.79.	Influence of DEOA content on the Tan Delta peak of foams (a) FD-0, (b) FD-0.5 and (c) FD-1.....	283
Figure 4.80.	Influence of DEOA content on the storage modulus of foams (a) FD-0, (b) FD-0.5 and (c) FD-1.....	284
Figure 4.81.	WAXS patterns illustrating the influence of DEOA content on the short range ordering of the HS domains: (a) FD-0, (b) FD-0.5 and (c) FD-1.....	286
Figure 4.82.	Influence of temperature and relative humidity on the load relaxation behavior of (A) FD-0 and (B) FD-0.5. In each figure the letters designate the following conditions: (a) 30°C-35%RH, (b) 30°C-98%RH, (c) 100°C-35%RH, and (d) 100°C-98%RH.....	287
Figure 4.83.	Influence of the DEOA content on the load relaxation behavior at (A) 30°C-35%RH, and (B) 100°C-98%RH. In each figure the letters designate: (a) FD-0 and (b) FD-0.5.....	288
Figure 5.1.	Scanning electron micrographs of foam F85 shown both (A) parallel to the rise direction and (B) perpendicular to the rise direction.....	297
Figure 5.2.	Scanning electron micrographs of foam F100 shown at magnifications of (A) 30x and (B) 140x.....	298
Figure 5.3.	Scanning electron micrographs of foam F110 at a magnification of 30x.....	299
Figure 5.4.	Scanning electron micrographs of foams following extraction process: (A) F85, (B) F100, and (C) F110.....	302

Figure 5.5.	DSC thermograms of the (A) first heating scans and (B) second heating scans. In each figure letters designate the following foams: (a) F85 and (b) F95, (c) F100, and (d) F110.....	306
Figure 5.6.	Influence of the TDI index on the Tan Delta peak: (a) F85 and (b) F95, (c) F100, and (d) F110.....	308
Figure 5.7.	SAXS profiles of slabstock polyurethane foams (a) F85, (b) F100, and (c) F110 illustrating the influence of TDI index on the microphase separation.....	309
Figure 5.8.	WAXS patterns illustrating the influence of TDI index on the short range ordering of the HS domains: (A) F85, (B) F100 and (C) F110.....	312
Figure 5.9.	WAXS diffractometer scan illustrating the influence of TDI index on the short range ordering of the HS domains: (a) F85 and (b) F110.....	313
Figure 5.10.	Influence of TDI index on the bidentate absorbance in the FTIR spectra of foams (a) F85 and (b) F100, and (c) F110.....	315
Figure 5.11.	Influence of TDI index on the NH absorbance in the FTIR spectra of foams (a) F85 and (b) F100, and (c) F110.....	316
Figure 5.12.	Influence of TDI index on the free isocyanate absorbance in the FTIR spectra of foams (a) F85 and (b) F100, and (c) F110.....	317
Figure 5.13.	Tensile stress-strain behavior for the foam (a) F85, (b) F100, (c) F105, (d) F110.....	319
Figure 5.14.	Load relaxation behavior of F85 as a function of temperature/relative humidity, (a) 30°C-35%RH, (b) 30°C-98%RH, (c) 50-35%RH, (d) 50-98%RH, (e) 80°C-35%RH, (f) 80°C-98%RH, (g) 100°C-35%RH, and (h) 100°C-98%RH.....	321
Figure 5.15.	Load relaxation behavior of F110 as a function of temperature/relative humidity, (a) 30°C-35%RH, (b) 30°C-98%RH, (c) 50-35%RH, (d) 50-98%RH, (e) 80°C-35%RH, (f) 80°C-98%RH, (g) 100°C-35%RH, and (h) 100°C-98%RH.....	324
Figure 5.16.	Load relaxation behavior at 30°C-35%RH of the foams varying in index (a) F85, (b) F90, (c) F95, (d) F100, (e) F105, and (f) F110.....	326
Figure 5.17.	Load relaxation behavior at 100°C-35%RH of the foams varying in index (a) F85, (b) F90, (c) F95, (d) F100, (e) F105, and (f) F110.....	327
Figure 5.18.	Load relaxation behavior at 30°C-98%RH of the foams varying in index (a) F85, (b) F90, (c) F95, (d) F100, (e) F105, and (f) F110.....	328
Figure 5.19.	Load relaxation behavior at 100°C-98%RH of the foams varying in index (a) F85, (b) F90, (c) F95, (d) F100, (e) F105, and (f) F110.....	329
Figure 5.20.	Creep response of (A) F85 and (B) F110 as a function of temperature/relative humidity, (a) 30°C-35%RH, (b) 30°C-98%RH, (c) 50-	

	35%RH, (d) 50-98%RH, (e) 80°C-35%RH, (f) 80°C-98%RH, (g) 100°C-35%RH, and (h) 100°C-98%RH.....	331
Figure 5.21	Compression set recovery as a function of index.....	334
Figure 6.1.	Mechano-sorptive behavior for slabstock foam Fs4 under a constant load and temperature (40°C). Curves correspond to (a) constant 20%RH (b) constant 98%RH, and (c) cyclic moisture conditions.....	339
Figure 6.2.	Mechano-sorptive behavior for slabstock foam Fs5 under a constant load and temperature (40°C). Curves correspond to (a) constant 20%RH (b) constant 98%RH, and (c) cyclic moisture conditions.....	340
Figure 6.3.	Mechano-sorptive behavior for slabstock foam Fme2 under a constant load and temperature (40°C). Curves correspond to (a) constant 20%RH (b) constant 98%RH, and (c) cyclic moisture conditions.....	342
Figure 6.4.	Simplified morphological model illustrating the mechanism behind the observed mechano-sorptive behavior.....	343
Figure 6.5.	Mechano-sorptive behavior for slabstock foam Fs5 under a lower constant load and a high temperature (90°C). Curves correspond to (a) constant 20%RH (b) constant 98%RH, and (c) cyclic moisture conditions.....	345
Figure 6.6.	Mechano-sorptive behavior for slabstock foam Fme2 under a constant load and a high temperature (90°C). Curves correspond to (a) constant 20%RH (b) constant 98%RH, and (c) cyclic moisture conditions.....	347
Figure 6.7.	Mechano-sorptive behavior for a polyurethane elastomer under constant load and temperature (40°C), but cyclic moisture conditions.....	348
Figure 6.8.	Influence of cyclic moisture conditions on the load relaxation behavior of Fs5 at a constant 65% strain and constant 40°C.....	350
Figure 6.9.	Influence of cyclic moisture conditions on the load relaxation behavior of Fs5 at a constant 65% strain and constant 90°C.....	351

Chapter 1

1.1 Introduction

A cellular solid derived from the Latin word "cell", meaning a small enclosed space, is the assembly of cells with solid edges or faces packed together. Cellular solids are made up of an interconnected network of solid struts forming the edges and faces of the cells. The simplest cellular solid is a two-dimensional array of polygons called honeycombs. Three dimensional packing of the cells are called foams. The foam is said to be open-celled if only the cell edges are solid, where the foam is closed-celled if the cell faces as well are solid.

Cellular polymers are multiphase materials consisting of a polymer and a fluid phase, e.g. air. The majority of cellular polymers used in industry are polyurethanes, polystyrene, poly(vinyl chloride), and polyolifins. Polymer foams have been classified by their cellular morphology, mechanical behavior, composition, or cellular structure such as cell openness. In closed-cell foams, the gas phase is discrete and the polymer phase is continuous. In open-cell materials, both the solid and fluid phases are continuous. A schematic representation of the different types of cellular solids is shown in Fig. 1.1. The mechanical properties of cellular solids largely depend on the gas transport through the medium which, in the case of open-cells, flows freely through the medium, but in closed-cells, the gas transport takes place by diffusion through cell walls.

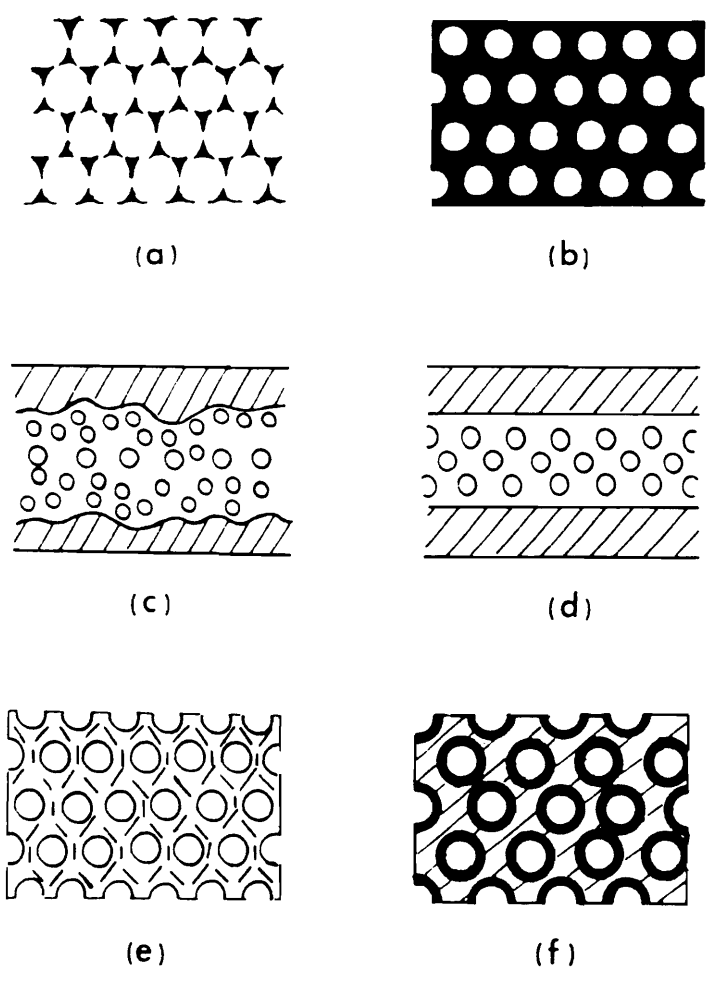


Figure 1.1: Schematic representation of different types of cellular polymers: (a) low-density open-cell foam, (b) high-density closed-cell foam, (c) structural foam with cellular core and integral skin, (d) multicomponent structural foam, (e) fiber-reinforced closed-cell foam and (f) syntactic foam. [ref 1]

Cellular solids are also classified according to their stiffness, i.e. rigid versus flexible. A rigid foam is one in which the polymer exists in the semi-crystalline or glassy amorphous state. A flexible foam is one in which the polymer matrix exists above the glass transition in the rubbery state. Rigid polyurethane foams are often subdivided according to their application such as load-bearing structural materials or non-load-bearing applications. Flexible polyurethane foams are classified as either slabstock foams or molded foams. In short, slabstock foams involve the pouring of the components on to large conveyers producing large semi-continuous blocks from which specific shape and size samples are cut for end use. In molded foams, the components are poured into a mold having the desired shape and size thereby eliminating the need for cutting. Further details on molded foams will be given in a later section. Within each category, these foams can be further classified as cold-cured foams also referred to as high resiliency (HR) versus hot-cured foams. This classification also relates to the mechanical hysteresis which in the case of HR foams is between that of open-cell flexible polyurethane foams and that of rubber latex foam.

A very important feature of cellular solids is their density or relative density, ρ^* / ρ_s (foam density/solid density). Polymeric foams used for cushioning, packaging or insulation have relative densities between 0.05 and 0.2. As the relative density increases, the cell walls generally thicken and the pore space decreases.

Polyurethanes are polymeric products of reactions between an isocyanate and a hydroxyl group or polyol. They are polymers which contain the urethane linkage. The first polyurethanes were discovered in 1937 by Otto Bayer and co-workers.¹ The first commercial polyurethane foams were developed in 1954 using a German technology which used an aromatic isocyanate and a polyester polyol. Two years later, the first polyether polyols were introduced which provided for a foam which was more durable and less affected by hydrolysis. In 1958, the more economic "one shot" foam technology was developed where the polyether polyols, catalysts, and silicone-based surfactants (which are

all needed to produce a quality foam) were combined all at once to produce foams with improved physical properties.

1.2 Applications

There are four major areas of application of cellular solids: thermal insulation packaging, structural use, buoyancy, and furnishings. Since plastic foams have a low thermal conductivity, they are used as insulation from coffee cups to insulation in booster rockets. Another advantage is their low thermal mass which allows them to be heated or cooled with a minimum amount of energy. Foams are also used in packaging since they can absorb energy of impact and undergo large compressive strains without subjecting the contents to damaging stresses. The ease of molding along with their low density also make foams ideal for packaging. Cellular solids such as wood, bone, and coral are all structural foams used to support large loads. Wood is the most widely used natural cellular structural material. However, increasingly, man-made foams are used in structural applications such as sandwich panels, made of plywood skins bonded to balsa wood cores and more recently glass or carbon-fiber composite skin with a rigid polymer foam core. These sandwich panels used in space vehicles, skis, yachts and portable buildings, provide excellent specific bending strength for lightweight materials. Cellular materials, primarily polystyrene, and polyethylene, are used as supports for floating structures and portions of boats such as the hull or deck. By controlling their density, a given buoyancy factor can be achieved. Another advantage is that these foams are much more damage tolerant than other flotation devices such as bags or chambers and when damaged they can still retain their buoyancy.

Figure 1.2 is a block diagram illustrating the wide versatility and wide application of flexible polyurethane foams. As can be seen, the majority of flexible foams are used as cushioning in the furniture industry, but extend from vibration and sound dampening to

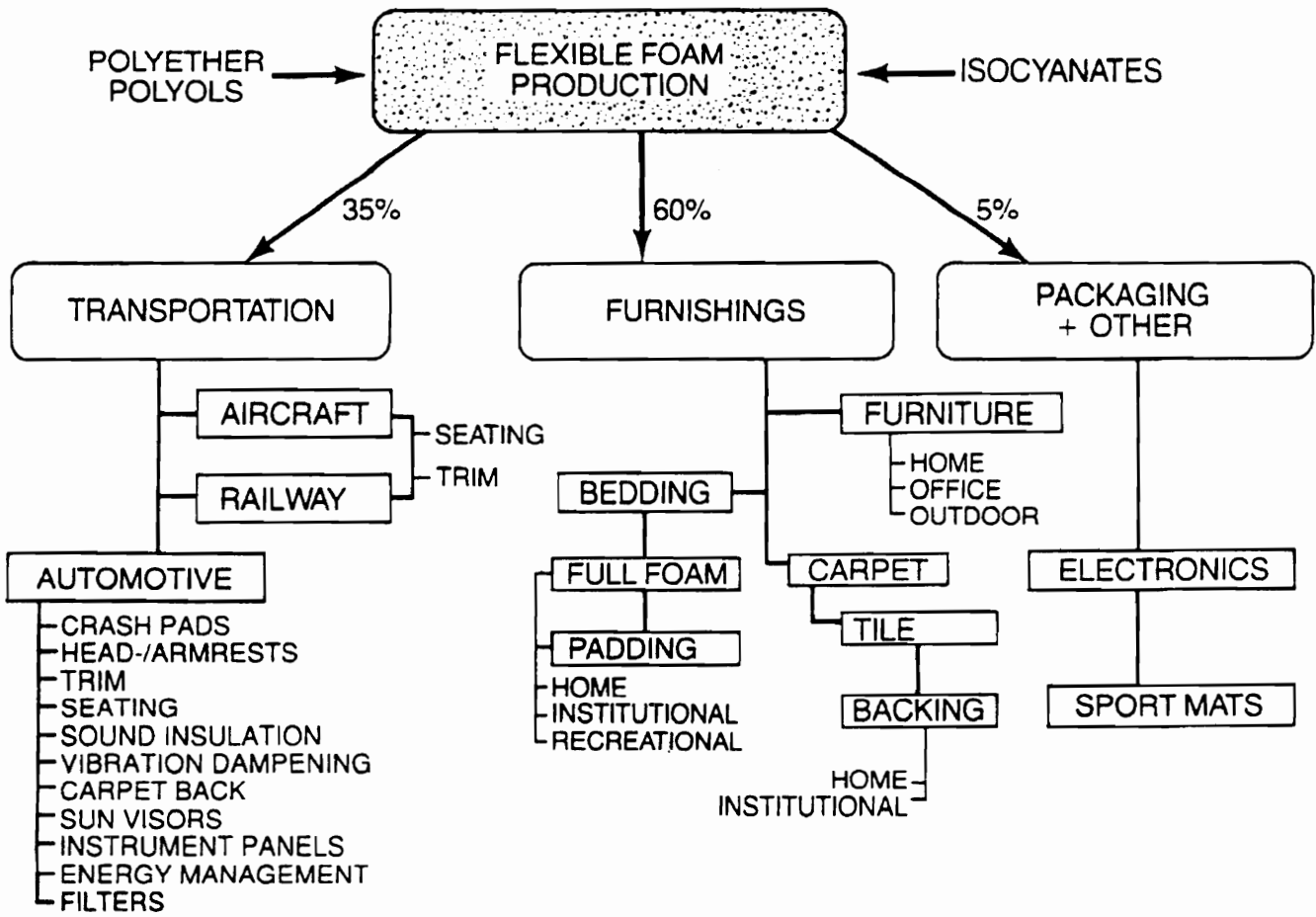


Figure 1.2. Applications of Polyurethane foams. [ref 5]

protective packing in packaging. By controlling the isocyanate and polyol, foams can be made ranging from soft low density foams to stiff high strength foams.

In view of the wide application base of these materials, a fundamental understanding of these materials is necessary, specifically how the formulation ingredients and processing techniques relate to the foam properties. While there exists within the scientific literature a wide range of data describing the various aspects of polyurethane foams, work which correlates the microscopic structure to the final foam properties is very limited. Roughly a decade ago, a joint venture between Dow Chemical Co. and the research group of Garth L. Wilkes began which focused on the structure-property behavior of slabstock polyurethane foams. The work presented in this dissertation is a continuation of this venture and reflects two major industrial trends: the increased manufacture of the higher productivity molded foams rather than slabstock, and the elimination of auxiliary blowing agents such as chloroflourocarbon (CFC). The majority of this work focuses on the structure-property relationships of molded foams to correlate the observed behavior to formulation ingredients and ensuing morphology using molecular arguments. The viscoelastic properties are given great consideration since they best simulate the end use treatment of these materials. These observations are then related back to the structural morphology of the foams. In addition, the results are compared to data obtained on conventional slabstock foams as obtained by similar methodology. In addition to characterization of the molded foams, the influence of altering the index, or amount on isocyanate included in the formulation relative to the amount required, was also investigated on a series of slabstock foams. This study reflects the trend of eliminating CFCs which has necessitated alternative methods of producing soft, low density foams. A potential method involves using a low index and a high water content.

The format of this dissertation begins with a literature review which presents relevant work carried out on mostly polyurethane foams. This review provides a good knowledge basis for the work that will be presented in this dissertation. While most of the

work that is presented is on foam, certain relevant features are portrayed by studies carried out on polyurethane elastomers and even cellular solids based on other polymers. Again, it is the intention of the author to emphasize specific conclusions that are based on molecular arguments especially with regard to mechanical properties. Many models have been presented, most empirical, which have shown good correlation with experimental data, but are limited in terms of physical meaning. A few have been presented here, but the focus has been on correlations to the molecular structure. Following the literature review, is a chapter describing the experimental materials and techniques utilized in this dissertation. Three chapters of results are then presented, beginning with a characterization of molded foams, followed by an investigation of a series of slabstock foams of varying index, and concluding with a small chapter presenting the influence of transient moisture conditions on the viscoelastic behavior.

Chapter 2

2.0 Literature Review

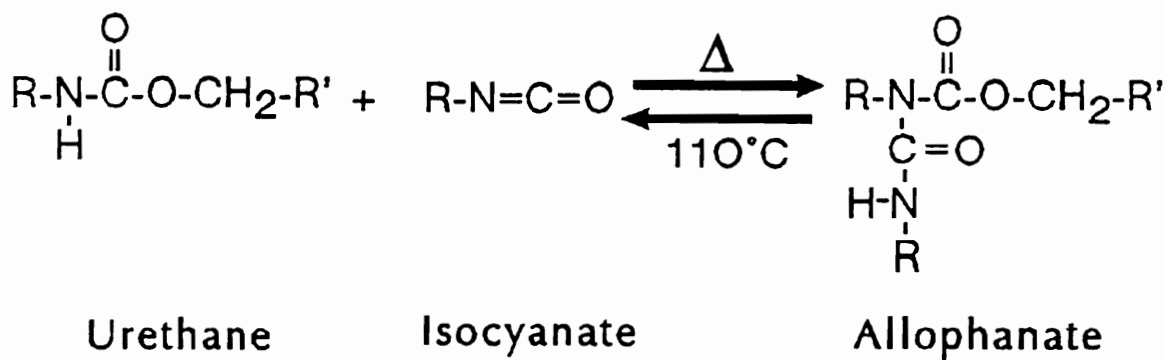
In this chapter, a summary of previous work on polyurethane foams is presented. Observations on other polymer foams and also some results on polyurethane elastomers are presented to convey certain relevant ideas. For example, in section 2.3.4, the mechano-sorptive behavior of many cellular materials is presented in view that it will be thoroughly investigated for the first time on polyurethane foams in this dissertation. Some of the other topics which are presented include the chemistry, morphology, mechanical properties, and viscoelastic properties of polyurethane foams and elastomers and even some other foams.

2.1 Chemistry

The chemistry of polyurethanes is based on reactions of isocyanates with active hydrogen-containing compounds, common examples being hydroxyl or amine functionalities. The hydroxyl or amine nucleophile adds to the isocyanate by a nucleophilic attack on the positive carbonyl carbon.

In the formation of polyurethane foams, there are at least two competing reactions. The first, illustrated in Fig. 2.1a., is the polymerization or gelling reaction. Here, an isocyanate group reacts with an alcohol or hydroxyl group to produce a urethane through

(A)



(B)

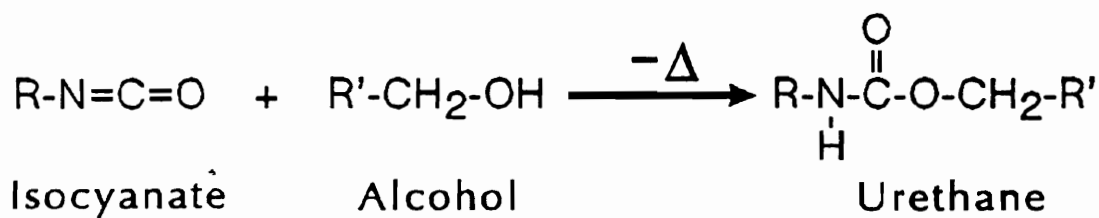


Figure 2.1. Reactions in urethane formation. (A) primary gellation reaction and (B) secondary reaction leading to allophanate.

an addition process with an exothermic heat of reaction of ca. 24 kcal/mole. When the alcohol is polyfunctional and the isocyanate is difunctional, a cross-linked polymer results. The urethane group can react further with an additional isocyanate to form an allophanate as illustrated in Fig. 2.1b. Allophanate formation can also cross-link the polymer. However, a significant amount is unlikely since high temperatures ($>110^{\circ}\text{C}$) are required for this reaction. Also, steric hindrance and the catalysts generally used for foam production tend not to promote allophanate formation.

The second and competing reaction is the blowing or gas-producing reaction. This reaction, shown in Fig. 2.2a., is known as the blowing reaction since the carbon dioxide formed serves to foam the polymer. This reaction is also exothermic releasing ca. 47 kcal/mole of heat. This reaction initially produces a thermally unstable carbamic acid which decomposes to an amine and carbon dioxide. Diffusion of the carbon dioxide through the reacting medium causes expansion of the bubbles primarily nucleated upon mixing and the production of a foam. The amine further reacts with an additional isocyanate to give a disubstituted urea shown in Fig. 2.2b. Additional cross-linking can be achieved from the reaction of the disubstituted urea and an isocyanate to give a biuret shown in Fig. 2.2c. However, as for the allophanate, reversibility and the high temperature ($>120^{\circ}\text{C}$) requirement for this reaction make any significant amount of biuret formation in the foam unlikely.

2.1.1 Formulation Components

The most common components used in the production of flexible polyurethane foam are listed in Table 2.1.

2.1.1.a Polyols

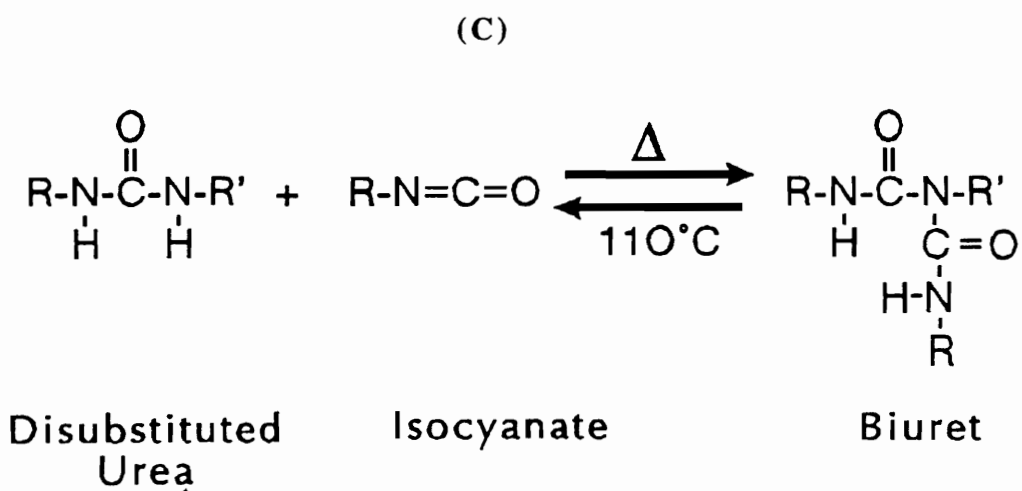
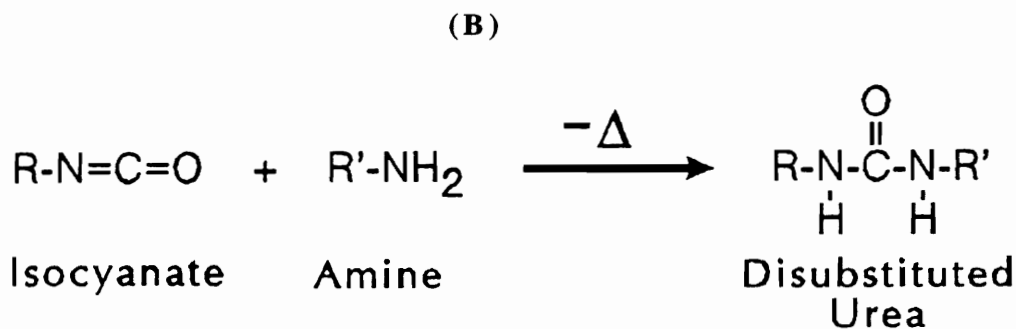
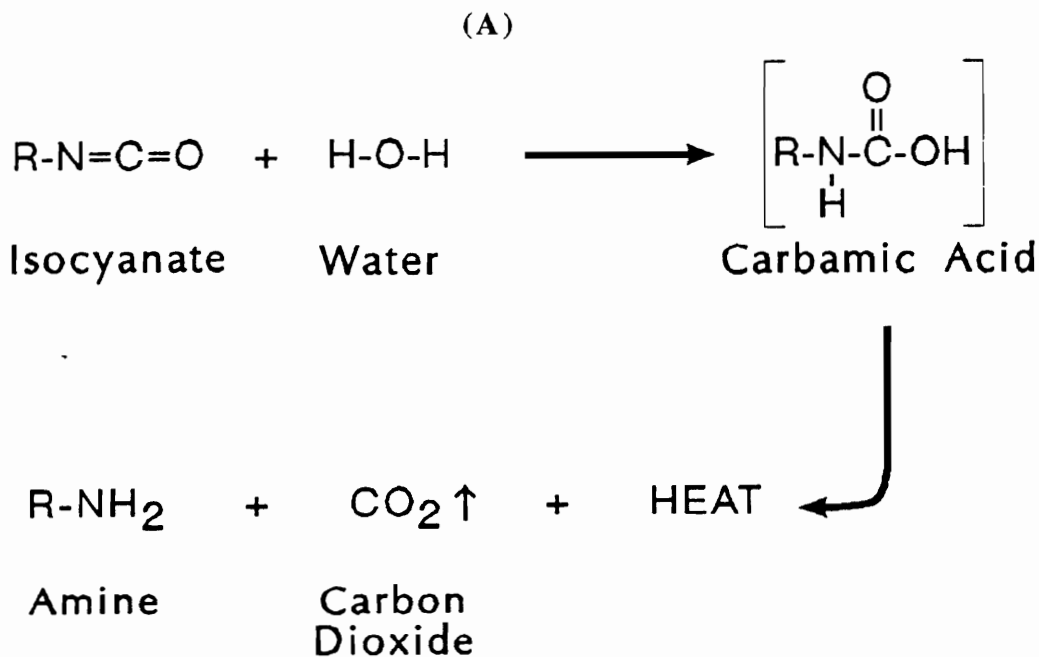


Figure 2.2. Reactions in urea formation. (A) primary blowing reaction, (B) chain extension reaction, and (C) secondary reaction leading to biuret.

Table 2.1. Basic Formulation Components for Flexible Polyurethane Foams

Component	Parts by Weight
Polyol	100
Inorganic Fillers	0 - 150
Water	1.5 - 5.5
Silicone Surfactant	0.5 - 2.5
Amine Catalyst	0.1 - 1.0
Tin Catalyst	0.0 - 0.5
Additive	Variable
Auxiliary Blowing Agent	0 - 35
Isocyanate	25 - 75

Nearly 90% of all flexible foams are produced using polyether polyols which are broadly grouped into the following categories:

- polyoxypropylene diols, triols, or tetrols
- ethylene-oxide endcapped diols, triols or tetrols
- random and block polymers of the above
- graft or copolymer polyols containing stable dispersions of solid such as styrene-acrylonitrile copolymers
- Cross-linkers typically short-chain polyfunctional molecules such as diethanolamine

Glycerol initiated polypropylene oxide polyols were initially used in the manufacture of flexible foams.³ Since then, polyols have also been based on polyethylene oxide, polypropylene oxide composition, polyethylene oxide endcapped polypropylene polyols, and finally a glycerol initiated copolymer from a mixture of polyethylene and polypropylene oxide.⁴ Polyether polyols are produced from reactions of organic oxides and initiators containing two or more active hydrogen groups. In the production of foams, glycerol is the most common initiator, however others are also used with functionalities as high as 8 such as that of sucrose. The alkoxide undergoes ring opening in the presence of a base catalyst. Figure 2.3 shows a triol which is produced from polypropylene oxide initiated by trifunctional glycerol. Side reactions are also known to take place. For example, small amounts of water may be present and may react with an epoxide to form a diol. Another side reaction which can occur is the base catalyzed isomerization of polypropylene oxide to form allyl alcohol. This alcohol can also react with an epoxide. Thus, in determining the net functionality of the polyol, these side reactions must be taken into consideration. For example, increased amounts of unsaturation or monol (mono alcohol) concentration lead to lower polyol functionality.

As mentioned previously, the two most widely used commercial alkylene oxides are polypropylene and polyethylene oxide. In the case of polypropylene oxide, the resultant

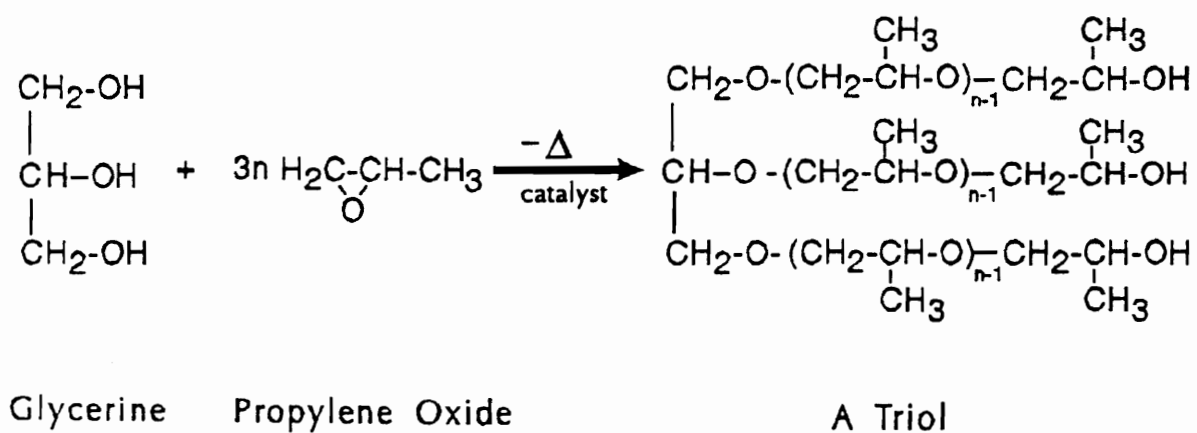


Figure 2.3. Formation of trifunctional polyol.

polyol has secondary terminal hydroxyl groups. When polyethylene oxide or polypropylene oxide endcapped with polyethylene oxide is used, the resultant polyol is a primary terminated hydroxyl which is illustrated in Fig. 2.4. Primary hydroxyl groups are generally ca. three times more reactive than secondary hydroxyl groups and are desirable in the production of molded foams where short production cycles are ideal. When a mixture of polypropylene oxide and polyethylene oxide is used, the result is a random copolymer polyol with improved water and isocyanate compatibility. The two epoxides can be added in sequential order to produce a block copolymer as shown in Fig 2.5.

Polyols can be modified with fillers to produce open-cell foams of higher hardness.^{6,7,8} The filler polymer is typically formed in situ through either a free radical or step addition polymerization of monomers. To prevent flocculation of the suspension, the particles are stabilized through a grafting process where either the base polyol or an added stabilizer molecule copolymerizes with the added monomer. The most common filler or dispersion in polyether polyols is produced through chain-growth polymerization where free-radicals are generated from an initiator molecule, typically an azo compound. These radicals can quickly react with the monomer to form undesirable high molecular weight polymer. To prevent this, low molecular weight chain transfer agents are often added which terminate the growing chain and initiate new polymer chain growth. The dispersions, originally based on acrylonitrile as the sole monomer, were used for the production of cold-molded high resiliency foam with increased hardness and strength. Due to deficiencies in certain properties such as flame resistance as well as a yellow appearance, styrene-acrylonitrile (SAN) mixtures are now used in place of acrylonitrile alone.⁵ In this case more efficient stabilizer molecules are required since copolymerization of the styrene and acrylonitrile is more favorable than either of those with the base polyol. One method of stabilization used is the grafting of a macromolecule functionalized with a vinyl moiety which copolymerizes with styrene-acrylonitrile and the base polyol (the method utilized in the molded foams studied in this dissertation).⁶ Here, polymerization begins with a graft

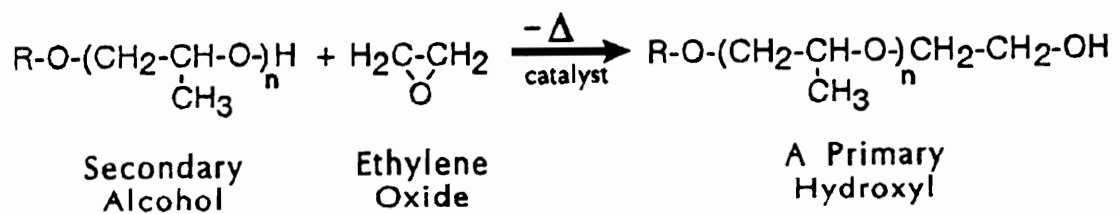


Figure 2.4. Formation of primary hydroxyl derived from ethylene oxide.

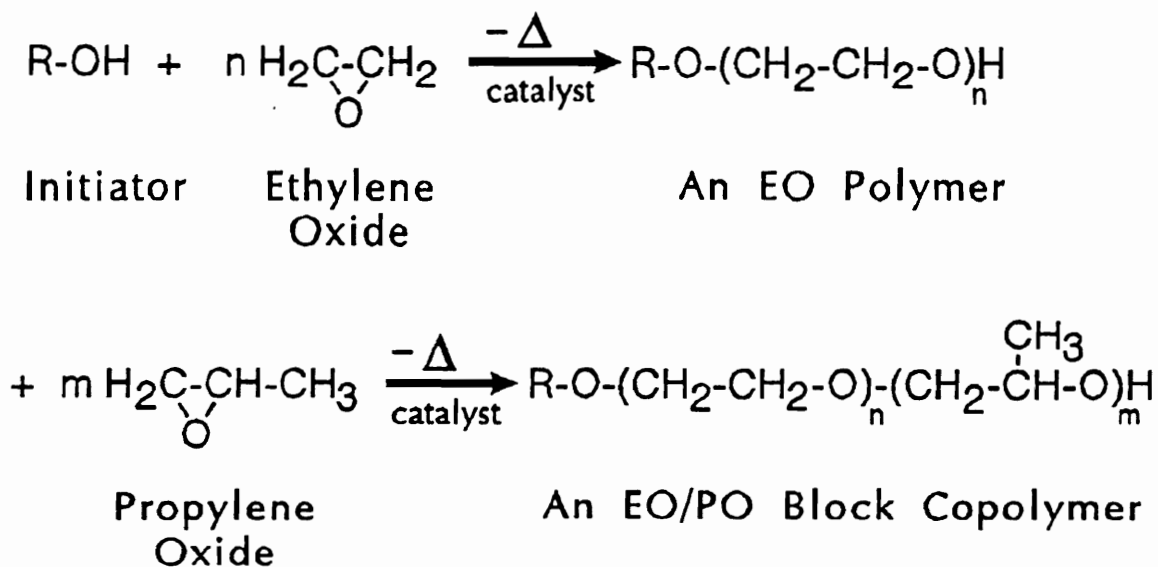


Figure 2.5. Formation of block copolymer polyol.

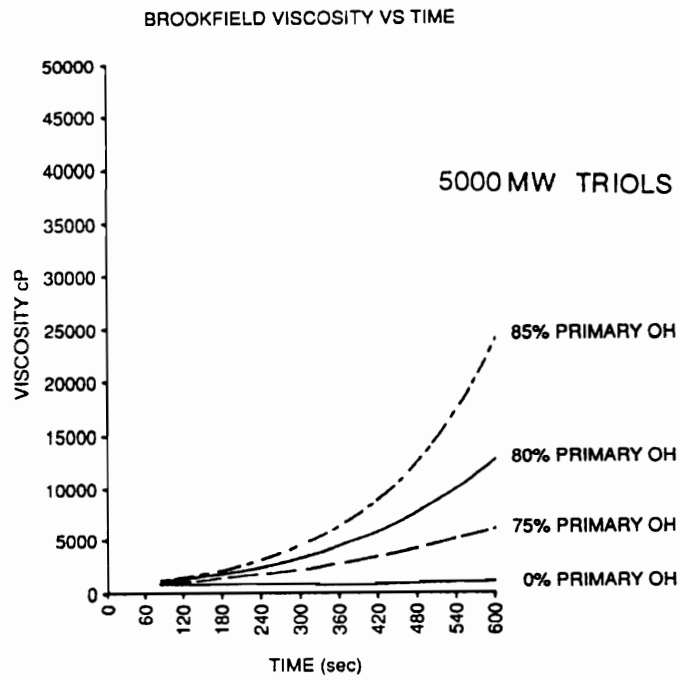
polyol where the backbone is the SAN copolymer chains and the teeth are the stabilizer molecules of the graft. As monomer and initiator are added, the comb polymers associate in a spherical structure where the insoluble copolymer portion, SAN, lies inside and the stabilizer chains extend outward. Once these particles have phase separated, polymerization occurs mainly inside these particles. During this stage, the particles grow from their initial size of 0.01-0.05 μm to a final size of 0.3-0.5 μm . High resiliency molded and sometimes slabstock foams are made with polyols having 10-40% solids and viscosities of 2500-4000 cp using this macromer process.

Although not as common, other fillers or dispersions are utilized in the production of polyurethane foams. For example, dispersions of polyurea particles known as the polyharnstoff dispersion (PHD) is one commercial protocol.^{9,10} These particles are prepared through step growth polymerization of a diamine with a diisocyanate which are dispersed in a polyether polyol. These polyurea oligomers quickly phase separate from the continuous phase as their molecular weight increases but are "naturally" grafted to the base polyurea through reaction of the diisocyanate to the polyol. Polyol grafting is thus lower than in the case of SAN polyols since the diamine - diisocyanate reaction is favored which also leads to a broader size distribution than achieved with the SAN dispersion. PHD polyols typically contain 20-30% solids and have viscosities of 3000-3500 cp. Along with polyurea particles, others such as polyurethane particles formed by the in situ reaction of an isocyanate with an alkanolamine and new epoxy fillers can also be utilized.

In general, there are many important characterizing factors of polyols which can influence the final foam properties. Factors such as functionality, hydroxyl number, primary hydroxyl content, and reactivity are now briefly discussed. The functionality arises from the choice of initiator and is defined as the average number of reactive sites per molecule. In determining the functionality, the level of monol and the level of diol must be considered since small amounts of either quickly decrease the overall functionality from the usual value of 3.0. The hydroxyl number is the amount of reactive hydroxyl groups

available for reaction per gram of polymer and thus is related to the equivalent weight of the polymer. It is typically determined by the number of milligrams of potassium hydroxide equivalent to the hydroxyl groups found in one gram of sample. The primary hydroxyl content is a measure of the distribution of primary and secondary hydroxyl groups as typically determined by NMR. As will be demonstrated throughout this dissertation, this factor is a very important one since it strongly influences the kinetics of the gelation reaction and therefore many other aspects such as cell-openness and microphase separation. In fact, all three factors (functionality, hydroxyl number, and primary hydroxyl content) greatly influence the reactivity and thus the morphology of the final polyurethane foam. For example, while polyethylene-oxide capping provides the primary hydroxyls, it also increases the compatibility between the hard and soft segments and may promote some phase mixing. This has been observed by noting the cloud point of a solution of the polyol in a water-isopropanol mixture which decreases as the molecular weight of the polyol increases and increases with increasing amount of polyethylene oxide. This suggests that increasing the molecular weight promotes phase separation while increasing the polyethylene oxide content promotes phase mixing. The reactivity is qualitatively the rate at which the polyol undergoes reaction which can be ascertained using viscosity measurements. Figure 2.6a is a Brookfield Viscosity Test of viscosity versus time illustrating the effect of increasing primary hydroxyl content on a polyethylene-oxide-capped 5000 MW triol. As can be seen, increasing the primary hydroxyl content significantly increases the rate of viscosity rise. Figure 2.6b illustrates the effect of primary hydroxyl as well as the effect of chain terminating monol (unsaturation) on the late stages viscosity in a typical molded foam. The unsaturation decreases the viscosity since it decreases the overall polyol functionality and slows down the rate of gelation. Both factors can dramatically influence the quality of the foam since certain events during the foam evolution must occur in a systematic order and precise timing. For example, the covalent

(A)



(B)

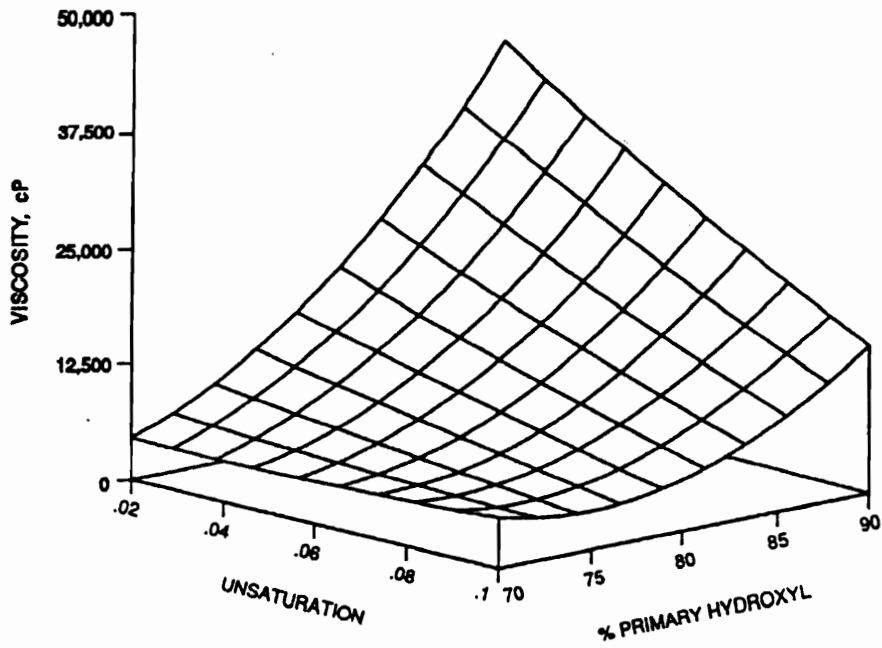


Figure 2.6. Reactivity of polyols. (A) effect of primary hydroxyl content (B) effect of monol and primary hydroxyl content. [ref 6]

gel point must occur just prior to cell opening in order for a good quality foam to be produced. The latter point will be presented with further detail throughout this dissertation.

2.1.1.b Isocyanates

All of the isocyanates used in the foam industry today contain at least two isocyanate groups per molecule. The most widely used method of producing isocyanates is the phosgenation of an amine as illustrated in Fig. 2.7.^{6,11} Several side reactions which can take place are illustrated in Fig. 2.8. The two most widely used isocyanates are toluene diisocyanate (TDI) and diphenylmethane diisocyanate (MDI) where TDI is used more in the manufacture of flexible foams and MDI is used more in the production of high resiliency, semiflexible, and rigid foams as well as elastomers. TDI is usually available as a mixture (80:20, or 65:35) of 2,4 and 2,6 isomers shown in Fig. 2.9. The 80:20 isomer mixture is obtained from the double nitration of toluene followed by reduction to the amine and then phosgenation to the diisocyanate as illustrated by the block diagram in Fig. 2.10. For a pure 2,4 isomer or a 65:35 blend, the reaction is stopped after the first nitration and the pure ortho- and pure para- nitrotoluene molecules needed to produce the desired isocyanates are obtained through crystallization procedures.^{12,13} The 2,4 isomer is more reactive than the 2,6 isomer primarily due to steric hindrance. The 65:35 isomer blend leads to higher load-bearing capabilities. Modified TDI or polymeric MDI reduces the hardness of the foam by interfering with the alignment or ordering of the polyurea hard segments and the foam's microphase separation.

Diphenylmethane diisocyanate (MDI) is prepared from aniline, formaldehyde, and a phosgenation according to the scheme in Fig. 2.11. The reaction mixture, resulting from the phosgenation of the polyamide mixture, contains a distribution of di, tri, and higher functionality isocyanates. Polymeric MDI is more widely used than pure MDI primarily due to the high reactivity of the sterically free pure 4,4' and 2,4' isomers. Also, pure two

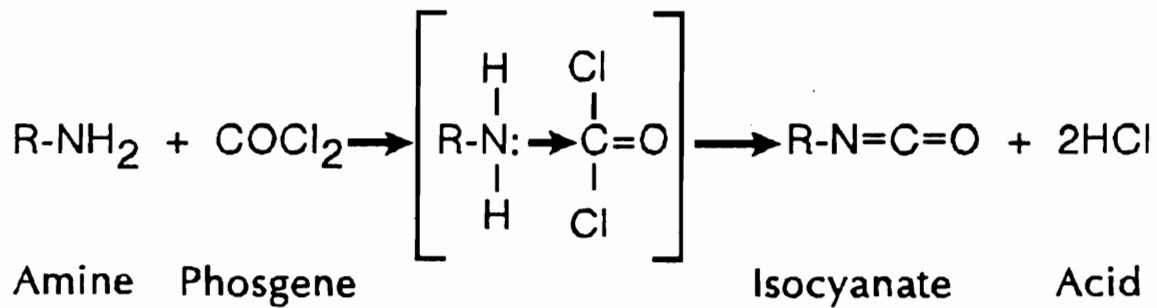


Figure 2.7: Formation of isocyanates.

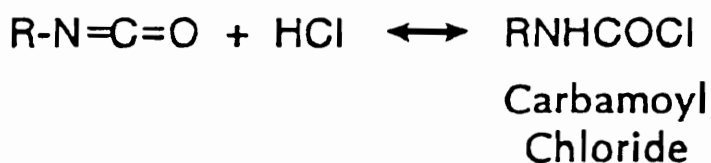
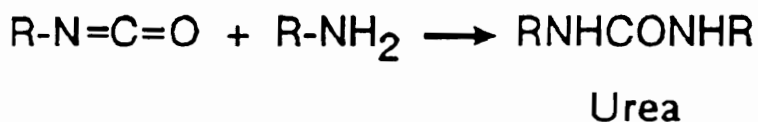
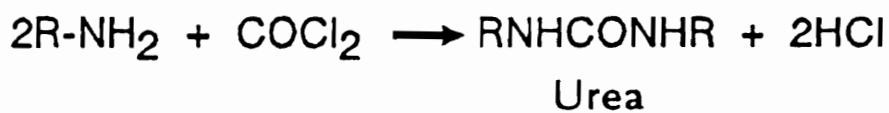
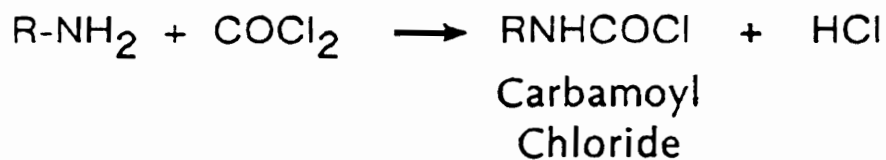
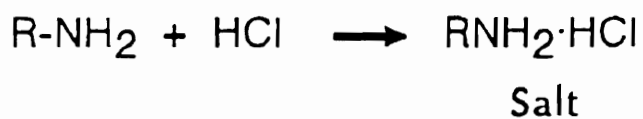
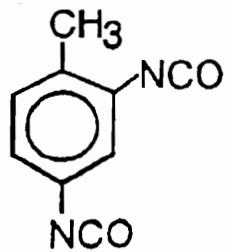
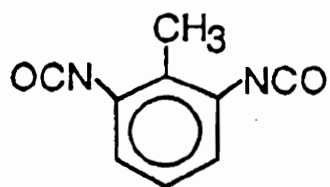


Figure 2.8. Secondary reactions in isocyanate formation.



2,4 Toluene Diisocyanate



2,6 Toluene Diisocyanate

Figure 2.9. Toluene diisocyanate isomers.

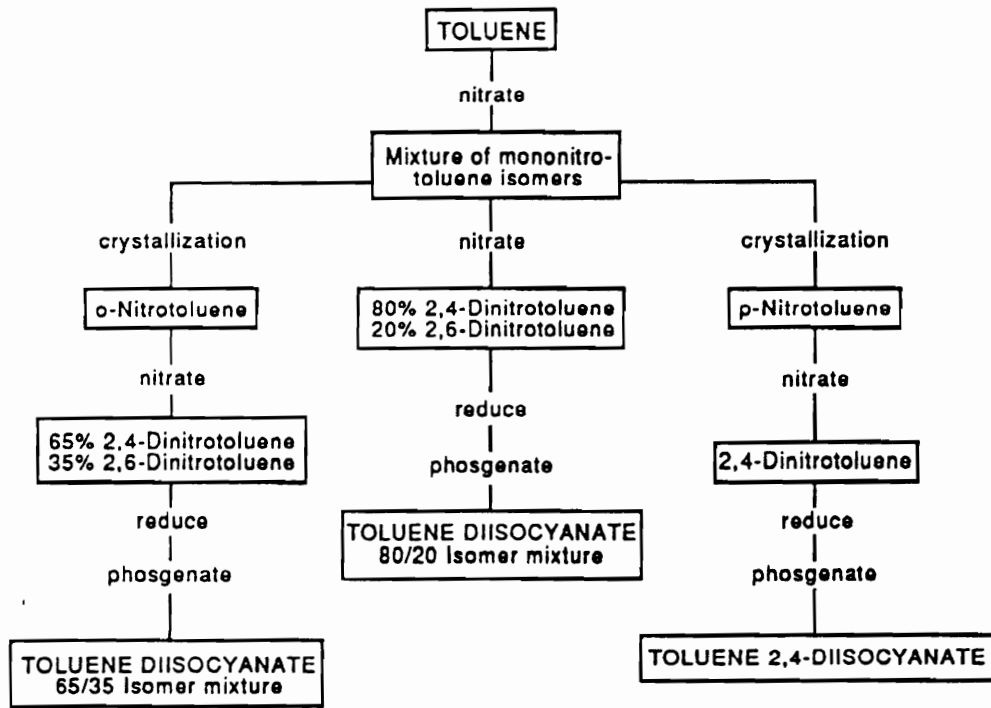


Figure 2.10. Production of 80:20 isomer mixture of toluene diisocyanate. [ref 6]

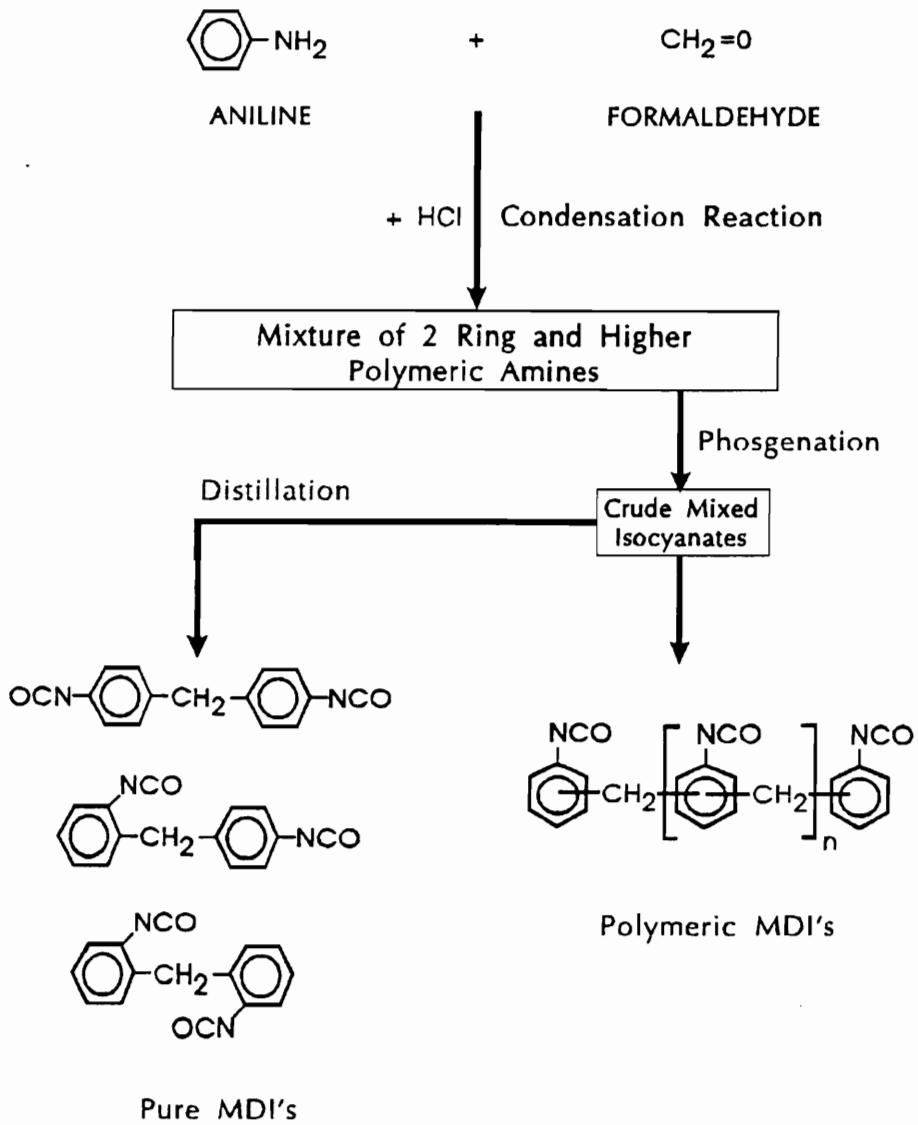


Figure 2.11. Production of diphenylmethane diisocyanate. [ref 6]

ring isomers require optimization of the reaction for maximum production and costly handling of the solids.

The stoichiometric amount of isocyanate required to react with the polyol may be adjusted to achieve the required final properties as will be later shown. The amount of isocyanate used relative to the theoretical equivalent amount is known as the isocyanate index. Thus, an isocyanate index of 100 refers to just enough isocyanate to react with all the active hydrogen sources. Excess isocyanate can lead to increased covalent cross-linking by further consuming any unreacted polyol and thus increased hardness in the final foam. This specific point will be investigated in series of foams varying in index in Chapter 6. Generally, the isocyanate index in the production of flexible slabstock foams ranges from 105 to 115 where the hardness can be readily controlled although there is a current trend to use a lower index. Common isocyanate indexes in molded foams range from 85 to 110. A distribution of indexes can be used to achieve multiples zones of hardness as is sometimes desired in automobile seats with lateral support.

2.1.1.c Water

Water is used to react with the isocyanate and produce carbon dioxide and polyurea. The carbon dioxide diffuses into the reaction mixture and aids in foam expansion by expanding the bubble size. The majority of the bubbles are nucleated in the early stages of the process specifically the mixing stages. In addition to the gas expansion, the bubbles can grow through consolidation of bubbles, the degree of which depends on the early stability of the growing bubbles.

2.1.1.d Surfactants

The main purpose of a surfactant is to stabilize the rising foam's cell walls. Without the cell wall stabilization, the cells would coalesce leading to a collapse of the foam. This delay in the thinning of the cell walls is due to an increasing surface viscosity by the surfactant. Also, elasticity of the membrane, known as the Gibbs-Marangoni effect, helps maintain the cell and prevent rupture.¹⁴ Along with this, however, a surfactant can also aid in the nucleation of bubbles during mixing and more importantly stabilize a growing bubble by basically lowering the bulk surface tension. Surfactants aid in nucleation by reducing the surface tension of the mixture and thus the energy required for bubble nucleation. This reduction in the surface tension also helps stabilize and promote growth of the bubbles. Finally, surfactants can also emulsify incompatible formulation ingredients. For example, the surfactant, as proposed by Rossmly et. al. disperses and incorporates the precipitated polyurea into the liquid reaction mixture.¹⁵

The amount of surfactant required for stable, quality foams displays a maximum or follows a bell-shaped curve. For example, insufficient amounts leads to coalescence, densification, splits, and "boiling" of the final foam. Increased amounts stabilize the mixture leading to well developed open-cell foams. Further increases in the surfactant amount overstabilizes the the cells leading to tighter, closed-cell foams with diminished physical properties.

The majority of flexible foams are made from polysiloxane-polyoxyalkylene copolymer surfactants. Here, the polyoxyalkylene end of the surfactant is responsible for the emulsification effect, while the siloxane lowers the bulk surface tension. The synthesis of silicone-glycol surfactants as described by Bryant and Stewart is illustrated in Fig. 2.12.¹⁶ First, sand is reacted with carbon and reduced to silicon. The silicon is then reacted with methyl chloride to produce a mixture of chlorosilanes. This mixture is then hydrolyzed to yield a substituted polysiloxane fluid which, in turn, is reacted with a hydroxyl-terminated polyglycol resulting in a silicon-oxygen-carbon type surfactant. A nonhydrolyzable type surfactant, derived from the reaction of the polysiloxane fluid with an

unsaturated polyglycol - i.e. an R group endcapped polyether repeat unit rather than a hydroxyl. The hydrolyzable surfactant would break apart when contacted with water into siloxane and polyol molecules and no longer act as a surfactant.

2.1.1.e Catalysts

The two most widely used catalysts are amines and organometallics. A combination of these are used to achieve a balance between the chain propagation or gelling reaction and the blowing reaction. These rates need to be controlled to assure that the gas is entrapped and allows the cell walls to develop sufficient strength and maintain their structure without collapse.

Tertiary amines, the most common blowing catalysts, enhance the blowing reaction since they have a lone pair of electrons and can form complexes with both isocyanates and water. Since they are strong nucleophiles, they can attack the carbon of the isocyanate group and can form stable hydrogen bonds with water. The formation of an isocyanate-amine complex through a nucleophilic attack on the carbon, as proposed by Baker and Holdsworth, is shown in Fig. 2.13.¹⁷ Once the complex has formed, the nitrogen atom on the isocyanate group is activated and readily reacts with hydrogen atoms from water or polyol. Figure 2.14 shows the formation of an active hydrogen-amine complex as proposed by Farkas and Strohm which supports the observation that increased basicity increases the catalytic activity.¹⁸

The most widely used metal in organometallic catalysts is tin. These organotins act as Lewis acids interacting with the basic sites. Although many mechanisms exist for the activated complex formation, the one presented in Fig. 2.15 incorporates the observed synergism between organometallic compounds and amine catalysts.⁶ Since tertiary amines are stronger Lewis bases than isocyanates and alcohols, their complexation to metal compounds such as organotins is likely. This complex reacts with a polyol to give a tin

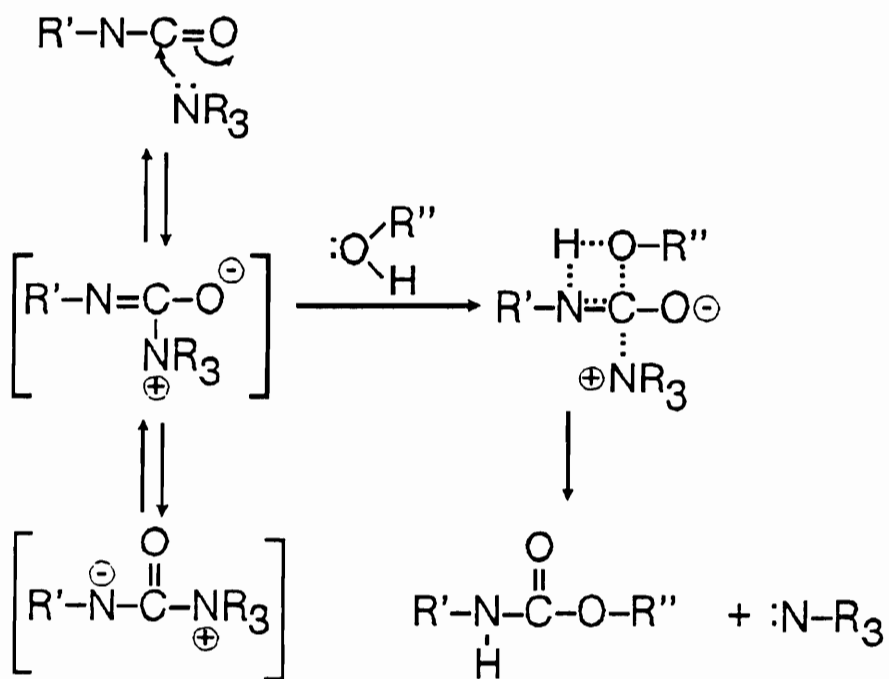


Figure 2.13. Formation of isocyanate-amine complex. [ref 5]

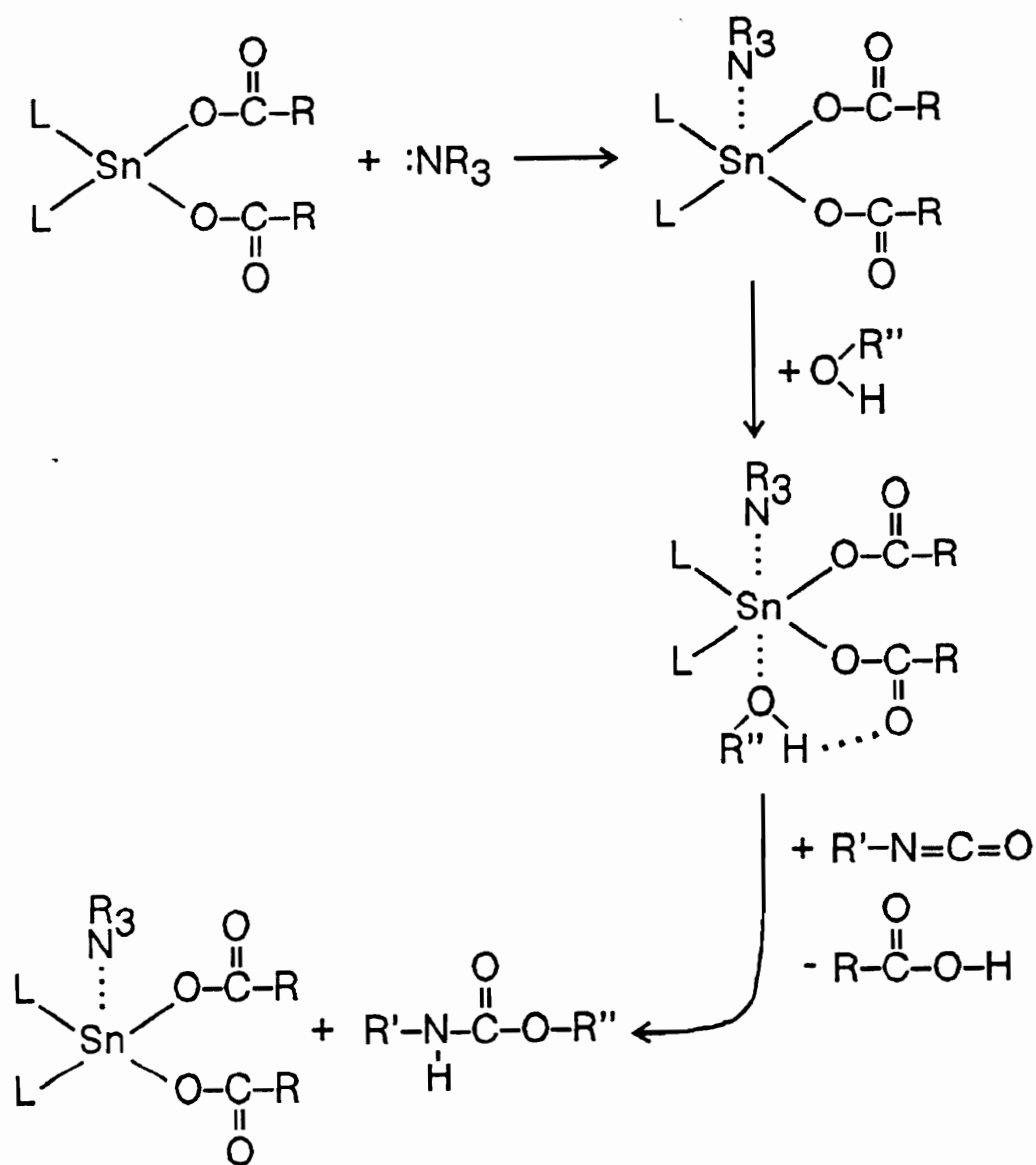


Figure 2.15. Mechanism for activated complex formation. [ref 5]

alkoxide. A carboxylate group accepts the proton from the polyol allowing for an isocyanate to enter and react with the polyol. The catalytic species is regenerated and can further react with an additional polyol to propagate the polymer.

As in the case of surfactants, the actual concentrations required must be determined experimentally and display an optimum for a desired set of properties. For example, when there is insufficient gellation, the expansion forces of the bubbles exceed the tensile strength of the cell walls and thus, foam splits may occur. This, however, can be compensated for by increasing the amount of organotin (usually stannous octoate for slabstock foams) catalyst. Further increases in catalyst can lead to shrinkage as the foam begins to gel faster, giving extremely strong cell-windows and tight foams.

High levels of catalysts, both amine and tin, are desired in molded foams to increase the rate of polymerization and cure in order to reduce mold occupation times.

2.1.1.f Blowing Agents

Auxiliary blowing agents may be used to aid in obtaining desired densities and softness. These are usually low boiling solvents and are inert in the chemical reactions. Since these are high volatile solvents, they vaporize providing additional gas as they absorb heat from the exothermic reactions. The blowing agent traditionally used in achieving extra-low densities is chloroflourocarbon 11 (CFC 11). However, due to environmental concerns that CFC 11 is a suspected ozone depleting agent, replacements such as halogenated chlorinated flourocarbons (HCFC-123 and HCFC-141) are also being utilized.^{19,20} These HCFC's are reported to have a much lower ozone depleting potential and also allow for foams to display similar physical properties to those blown with CFC 11. The drawback to HCFC's is that economical large scale production of these is difficult.

2.1.2 *Molded Foams*

In view of the fact that the majority of this dissertation deals with molded foams, a small section regarding some details and distinguishing features is appropriate. Specific details and aspects of molded foams are addressed and compared to conventional slabstock foams throughout this dissertation. Molded foams, a relatively newer technology, are foams in which a certain amount of formulation mix is either poured into a heated mold that is then closed or injected into a closed mold. Nearly half of all polyurethane foams produced commercially are molded foams as opposed to slabstock foams. The majority of molded foams are used in transportation seating and trim parts. However, they are also used in packaging, furniture, and novelty items. The biggest advantage is that the foam is molded into the intricate shape desired and, hence, the need for cutting is eliminated. Also, molded foams can be produced with reinforcements or multiple zones of hardness. Molded foams do not differ from slabstock foams in just that they are produced in molds rather than in a semicontinuous process but, in fact, are considerably more complicated. Generally, higher-molecular-weight, more reactive polyols are used in molded foams for reasons of increased productivity. Along with a higher reactivity formulation, factors such as size of individual shot, release agents, mold temperature gradients and curing times also contribute to the complication.

Molded foams are classified into two groups depending on how they were processed. The first, hot-cure, involves the application of heat to the mold to drive the reactions and decrease the cure time. The second classification, known as cold cure or high resiliency (HR) foams involves the use of a higher reactivity formulation so that no oven curing is necessary and less external energy is applied. The major differences between the two are illustrated in Table 2.2.

The largest application of hot-cured molded foams is as a contoured cushion for automotive seating. Formulation in these foams, is typically based on a 3000-molecular

Table 2.2. General Characteristics of Hot-Cure and HR Molded Foams

	Hot-Cure	HR
Isocyanate	80/20 TDI	80/20 TDI Blends w/MDI Polymeric MDI MDI prepolymers
Polyol Molecular Weight EO-Capped Copolymer Polyol	2800-3500 Yes Optional	4500-6500 Yes Optional
Cure Oven Temperature	180-300°C 356-572°F	75-200 °C 165-392 °F
Postcuring	No	Optional
Mold Temperature at Pour	25-45 °C 77-113 °F	50-70 °C 122-158 °F

weight polyethylene-oxide-capped triol. HR foams use a 5000-molecular weight polyethylene-oxide-capped triol. In processing the hot-cured foams, the molds moving on conveyors begin with preheating to approximately 43°C, from which they proceed to the pour station where the molds are charged with the reaction mixture. The mold lids are closed and then the molds proceed to the radiant heat oven where they are heated to approximately 121°C followed by a hot air oven at approximately 54°C. Finally, the molds are stripped, waxed and cooled to bring them back to the initial state. A typical molding cycle takes 30 minutes.

High resiliency foams have a dropping-ball-type resiliency (per ASTM D 3770-79) greater than 60%. Today, the term HR foams also refers to cold-cure foams. The greatest advantage of HR foams is that these foams have a superior support factor, ratio of 65% indentation force deflection (IFD) to 25% (IFD), relative to hot-molded foams or slabstock foams. Also, the amount of energy and time required for the HR process is considerably less. These foams are primarily based on 5000-molecular weight highly reactive polyethylene-oxide-capped polyether triols in combination with diamene cross-linkers. Grafted polymers and copolymers may also be included in the formulation. The formulation ingredients are mixed and dispensed into the waxed molds at a temperature of 49 to 71°C. In the case where some heat may be added, as in the case of low density seating foams, the molds are heated to 93°C for approximately 3 to 10 minutes. The foam is then removed and the molds are waxed and cleaned. The foam's cells are then immediately opened usually by means of mechanical crushing to minimize shrinkage upon cooling. HR foams usually require less gellation catalyst since the polyols are highly reactive and also require more blowing catalyst to accelerate the foam expansion. The latitude of the mold temperature at pour is normally 57°C to 77°C. Below this range, cold collapse can occur leading to a densified core while above this range, the skin becomes loose and flaky and large voids develop.

2.1.3 *Molded Foam Processing Technique*

Since the majority of this dissertation deals with molded foams, the process described here is a typical molded foam process. The processing technique for conventional slabstock foams has been described in detail in other references and is briefly presented in Chapter 3.⁷⁹ The majority of polyurethane foams are made by a "one-shot" process. The appropriate quantities of the chemical components are poured into a mixing head at controlled environmental conditions and agitation speed. At this point nucleation, controlled by bubbling air or nitrogen gas, begins. In less than one second, the nucleated liquid is dispensed into a preheated and waxed mold (for molded foams) where the bubbles begin to grow. The mold is preheated (usually to 38-49°C) to help prevent density variations due to temperature variations from the exothermic reaction. The mold lids are immediately closed and then conveyed to the radiant oven where they are heated to an internal surface temperature of ca. 120°C. During this induction or cream time (ca. 6-15 seconds), which is defined as the time between the discharge of the liquid and the beginning of the foam rise, the bubbles begin to grow and the liquid changes color. The surfactants and catalysts play a major role during this period. For example, as the surfactant reduces the surface tension, the bubble loss is lowered. Also, as the catalysts increase the rates of reaction, the cream time is shorter and thus the cells are smaller and fewer. Following the cream time, the foam mixture begins to rise due to the expansion of bubbles in the blow direction from the evolution of CO₂. These bubbles continue to grow until they come into contact with each other to form planar membranes. Due to the exothermic nature of the reacting mixture, the temperature rises, and at ca. 100°C, the cell walls rupture releasing the entrapped gas - the process of which is known as the blow-off. In 100-200 seconds after mixing, immediately following blow-off, the foam has reached its full rise. As the remaining isocyanate continues to react, the temperature continues to

increase. At the end of curing, the molds are opened automatically and the foam is removed. They are then stored to further cure for a period of about a week.^{3,21,22,35}

2.1.4 Reaction Sequences

With the use of FTIR, the reaction sequences in a foaming process can be followed to a high degree of accuracy. Many researchers such as Rossmly et. al. and Bailey and Critchfield have confirmed observations of absorption bands at 1710 cm^{-1} , 1660 cm^{-1} , and 1645 cm^{-1} during the early stages of the water-isocyanate reaction.^{15,23,24} The band at 1710 cm^{-1} was observed in the beginning of the reaction while the bands at 1660 cm^{-1} and 1645 cm^{-1} were observed at 50% and 75% of the rise time, respectively. It was proposed by both researchers that the band at 1645 cm^{-1} is due to a disubstituted urea. Rossmly et. al. suggested that the band at 1710 cm^{-1} is due to the soluble urea while the band at 1645 cm^{-1} is due to the insoluble urea. They also observed that as the reaction mixture went from clear to opaque, the IR shift went from 1710 cm^{-1} , corresponding to monodentate urea reflecting weak hydrogen bonding, to 1645 cm^{-1} , which reflects stronger hydrogen bonding. Hauptman et. al. and Hocker observed an IR shift from 1710 cm^{-1} to 1645 cm^{-1} when a diphenyl urea was dissolved in a good solvent (DMF) and then a poor solvent (THF).^{25,26} Bailey and Critchfield used gel/rise profiles to follow the foam process. A rise profile was initially observed showing a maximum in the rate of rise upon the first detection of the urea groups at 1645 cm^{-1} . The suggestion that the water-isocyanate reaction occurs first was further supported by Illeger et. al. by following the relative weight loss of isocyanate and water.²⁷

Both investigators also agree that the isocyanate-polyol reaction occurs later in the reaction near blow-off. Rossmly et. al. reported observing a urethane band at 1725 cm^{-1} at 75% of foam rise while Bailey and Critchfield reported observing a slow increase in the urethane band at 1730 cm^{-1} .^{23,24} This increase in the urethane absorption occurred for 30

min. after blow-off while no increase in the urea absorption was observed. Also, Bailey and Critchfield observed that the gel profile occurred during the period when urea formation was predominant and the rate of rise was decreasing.

Van Gheluwe and Leroux used temperature profiles to follow the foam formation.²⁸ They determined the rate of temperature rise as a function of varying water content and amine catalyst concentration. The temperature rate of the blowing reaction was generally greater than that of the gelling reaction primarily in the early stages of foam formation. Also, the rate of temperature rise increased with increasing water content. As this temperature rate began to level off for the blowing reaction, a steady increase in the temperature rate was observed for the gelling reaction.

Recently, McClusky et. al. used FTIR, SAXS and viscosity profiles to follow the foam evolution specifically the sequential development of the network.^{29,30} They have divided the matrix formation into four stages beginning with the initial reaction stage. Here, they observed initially the development of non-bonded urea and urethane. The rates of urea and urethane development were found to be a function of water content where the rate of urea intensity increase was higher than the rate of urethane intensity increase as the water content was increased. No hydrogen bonding was observed in this initial stage. The second stage, beginning at ca. 1 min. following mixing, was the onset of monodentate urea (at ca. 1700 cm^{-1} to 1640 cm^{-1}) as observed by FTIR which occurred at ca. 40% isocyanate conversion. During this time, there is no phase-separation or viscosity rise. The hard segments are still, for the most part, soluble in the soft phase. At ca. 100 sec., substantial amounts of isocyanate have reacted (65% conversion) and the onset of bidentate hydrogen bonding (at ca. 1640 cm^{-1}) was observed which reflects stronger, more stable multiple hydrogen bonds. Furthermore, SAXS data revealed phase separation and a sharp rise was observed in the viscosity in this third stage. McClusky et. al. referred to the final stage as an annealing stage where the foams slowly cool from their high temperatures and the ordering or perfection of the hard segment domains occurs.

A general conclusion from the presented research is that the isocyanate-water reaction occurs predominately in the early stages of the foam formation while the gelling reaction dominates when the foam has reached its maximum height. Also, it seems that the polyurea hard segments are initially soluble in the foam mixture and begin to precipitate out of solution at ca. 75% of the rise time suggesting polyurea aggregation via bidentate hydrogen bonding.

2.2 Morphology and Structure

The morphology of a flexible foam greatly influences the mechanical properties of the foam. In general, a typical polyurethane consists of a heterogeneous phase-separated morphology where discrete hard segment domains are dispersed within a continuous soft phase. The hard segment domains, resulting from the isocyanate-water reaction, are comprised of discrete polyurea segments which can form hydrogen bonds and phase separate from the continuous soft phase. In Fig. 2.16, which represents the phase-separated structure of a typical slabstock polyurethane foam, the hard segments are represented by the clustered thick lines which depicts them here as well ordered hard segment domains. These are covalently attached or entangled into the polyether or polyester soft phase. If a high water content is used in the formulation, the hard segment domains can aggregate and precipitate into polyurea "balls" or aggregates having a dimensions of about 3000 Å as observed using TEM.^{6,30} Due to the increased compatibility brought about by the additional components, these polyurea precipitates are not usually found in molded foams as will be shown later in this dissertation. Various techniques have been used in evaluating and determining the structure, both macroscopic and microscopic, of polyurethane foams. A general overview of the various aspects of polyurethane foams are given as well as the techniques used.

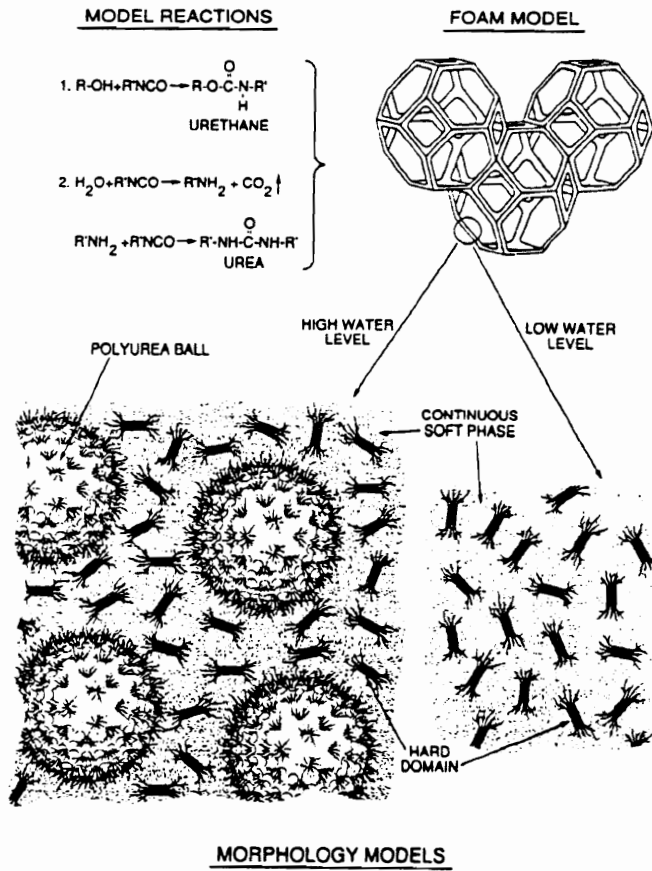


Figure 2.16. Representation of multiphase separated structure in conventional slabstock polyurethane foams. [ref 6]

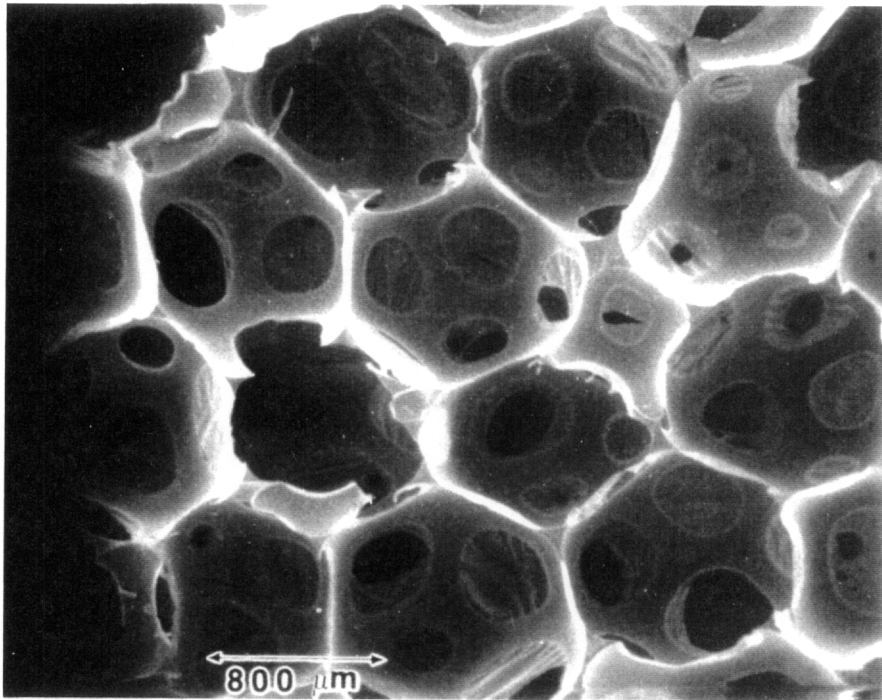
2.2.1 *Scanning Electron Microscopy*

Typical SEM micrographs of a slabstock foam are shown in Fig. 2.17 with the viewing direction parallel and perpendicular to the rise direction.³⁰ As can be seen, the foam contains large areas of voids or open cells with a continuous solid phase. The open cells are crucial not only from a comfort point of view but also to prevent the foam from shrinking or distorting in shape. Also, there exists a geometric anisotropy where, parallel to the blow direction, the cells appear spherical. Perpendicular to the blow direction, the cells appear ellipsoidal in shape with the major axis aligned with the blow direction. This anisotropy leads to differences in the foam properties with the foam having better bulk properties along the blow direction.

2.2.2 *Transmission Electron Microscopy*

Transmission electron microscopy has been used to observe features at magnifications in the range of 10,000X to 100,000X. Figure 2.18 shows TEM micrographs of four slabstock polyurethane foams increasing in water content from 2 to 5 with increasing foam number.³¹ Foam 1, micrograph (a), shows a grainy texture arising from most likely hard segment domains since it is not seen in the surrounding epoxy and since rough calculation of dimensions are within range of accepted dimensions. This micrograph does not show any distinct precipitate features as do the subsequent micrographs. Foam 2 (3 pph water content) shows the beginning of aggregations of polyurea precipitates. The white regions are the continuous soft phase and the dark regions are the precipitated urea rich aggregations. These regions are randomly dispersed and have a diameter of ca. 3000 Å. As the water content is increased, the regions become darker with greater contrast suggesting that the urea precipitates increase in number, size and "richness". This is clearly evident in micrographs (c) and (d).

(a)



(b)

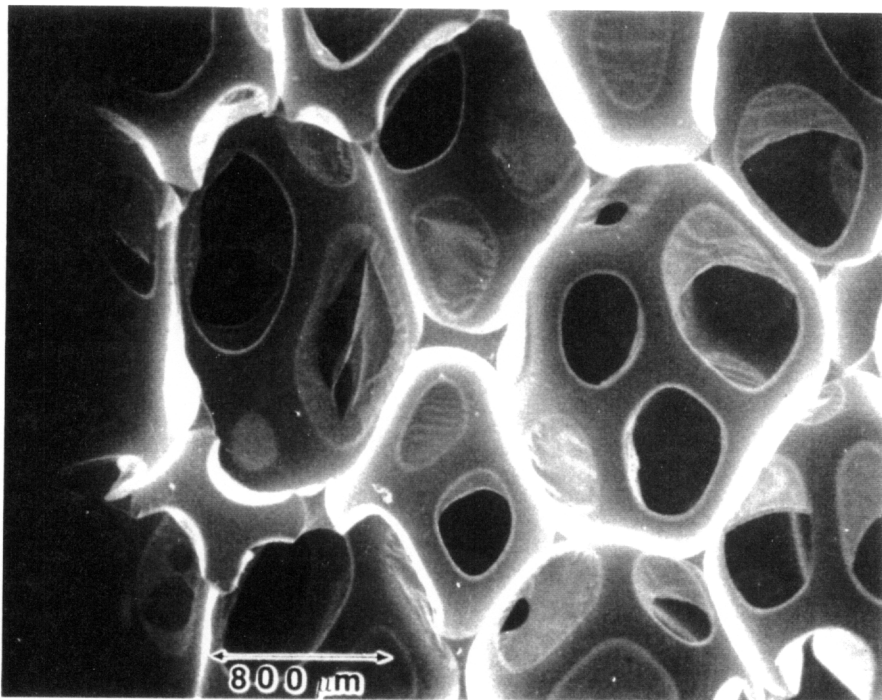
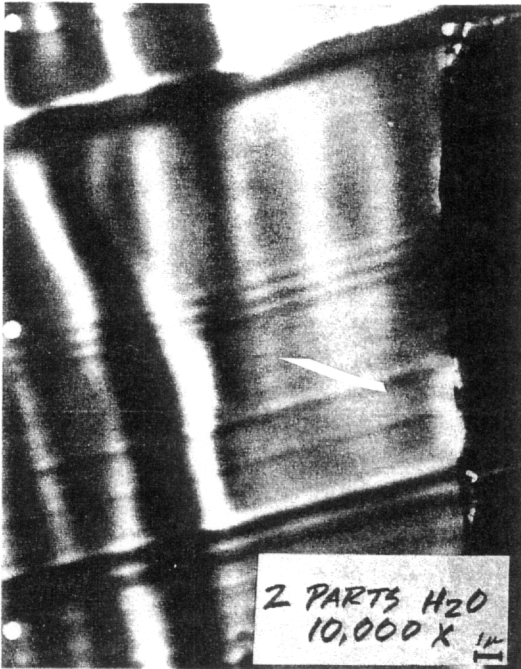


Figure 2.17. Typical SEM micrographs of a conventional slabstock polyurethane foam (a) parallel to the rise direction and (b) perpendicular to the rise direction. [ref 33]

(A)



(B)



(C)



(D)

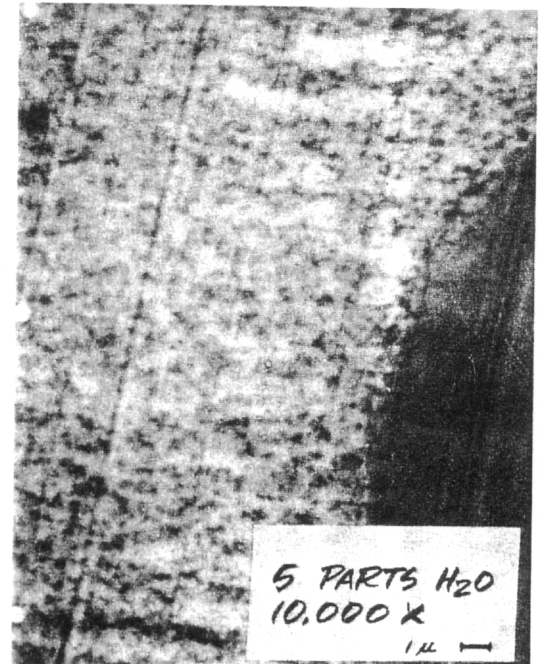


Figure 2.18: TEM micrographs of four slabstock polyurethane foams varying in water content (A) Foam 1 (B) Foam 2 (C) Foam 3 (D) Foam 4. [ref 33]

2.2.3 *Dynamic Mechanical Spectroscopy*

Dynamic mechanical spectroscopy (DMS) is a thermal analysis technique measuring the ability of a viscoelastic material to store and dissipate energy. The response of a multiphase polymer to an induced sinusoidal strain over a given temperature range can give information as to the stiffness and phase separation in the material.

Spell et. al. used DMS to arrive at the soft segment glass transition, obtain a temperature-dependent modulus, and to observe the possibility of any other thermal transitions in flexible polyurethane foams.²⁹ The DMS spectra are presented in Fig. 2.19 where the storage modulus, which was normalized for all samples to an arbitrary value typical of modulus values for the noncellular material below the glass transition, and tan delta are plotted for a temperature range of -160 to 300°C. At low temperatures, the modulus is high and the foams exhibit elastic behavior. The sharp transition observed at -40°C represent the soft segment glass transition. Here, the modulus drastically decreases and tan delta drastically increases. The soft segment glass transition is highly influenced by its molecular weight. At even higher temperatures where hydrogen bond disruption normally occurs, a rubbery plateau is observed. The fairly flat response in this region suggests the existence of a covalent cross-link network and/or well ordered hard segment domains also referred to as physical "cross-links". Finally, at even higher temperatures (ca> 230°C) a sharp decrease in the modulus is observed associated with thermal degradation.

In Fig. 2.19, higher water content in the formulation leads to a higher modulus due to increased amounts of the hard segment phase from the water-isocyanate reaction. These urea segment domains act as fillers producing a rise in the system modulus. The rather insensitivity of the glass transition as well as the sharpness of the transition to different amounts of water content suggests that there is significant phase separation.

2.2.4 *Differential Scanning Calorimetry*

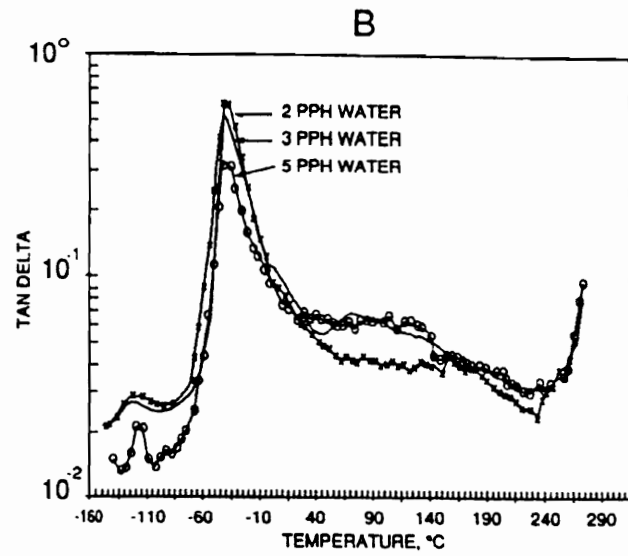
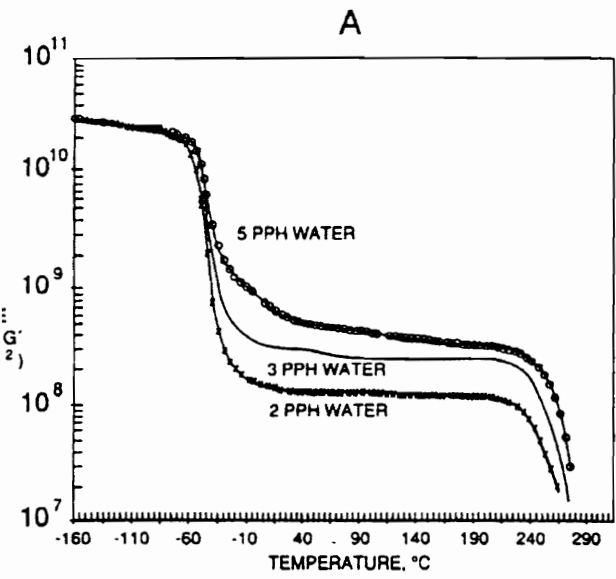


Figure 2.19. Normalized DMS spectra for slabstock polyurethane foams (a) storage modulus (b) $\tan \delta$. [ref 31]

Differential scanning calorimetry (DSC) has also been used to characterize slabstock polyurethane foams, primarily to determine the soft segment glass transition temperature or other thermal transitions.³⁰ Typical scans of conventional slabstock foams are illustrated in Fig. 2.20 with scans conducted at 10°C per minute over the range of 120 to 350°C. The results from DSC for the soft segment T_g show slight variations to those of DMS which are attributed to kinetic differences arising from the different scanning rates. The broad endotherms beginning at ca. 200°C reflect the onset of pronounced chemical degradation.

2.2.5 *Wide-Angle X-ray Scattering*

Wide-angle x-ray scattering (WAXS) has been carried out to examine for the presence of any crystallinity or packing order of the hard segment domains.. Figure 2.21 shows the x-ray diffraction patterns of four conventional slabstock polyurethane foams varying only in the water content as in the previous cases.^{30,31,32,40} All of the foams show a diffuse amorphous halo typical of liquid-like structures. However, for the 2 pph water content foams or greater, a scattering peak (actually ring) at 0.45 nm and a weaker peak (ring) at 0.59 nm are also displayed. The rings appear to sharpen with increasing hard segment content. The distinctness of the peaks indicates some degree of order, not just a maxima in the amorphous halos. Diffractometer scans have also verified this by showing two discrete peaks representing an ordered structure.³⁰ This increase in sharpness with hard segment content indicates that the local packing order of the hard segments is increasing. Tyagi and other authors have attributed the peaks to the short-range or paracrystalline ordering in the hard segment domains most likely arising from hydrogen bonding within the domains.³² In principle, the hard segment ordering can also arise from ordering within the urea aggregates observed in high water content slabstock foams using TEM.

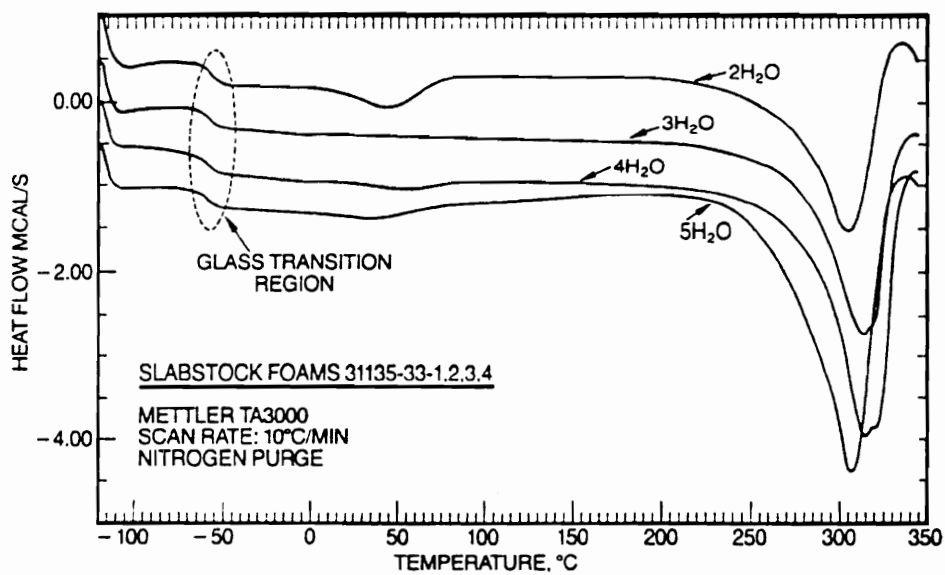


Figure 2.20. DSC thermogram of slabstock polyurethane foams varying in water content. [ref 6]

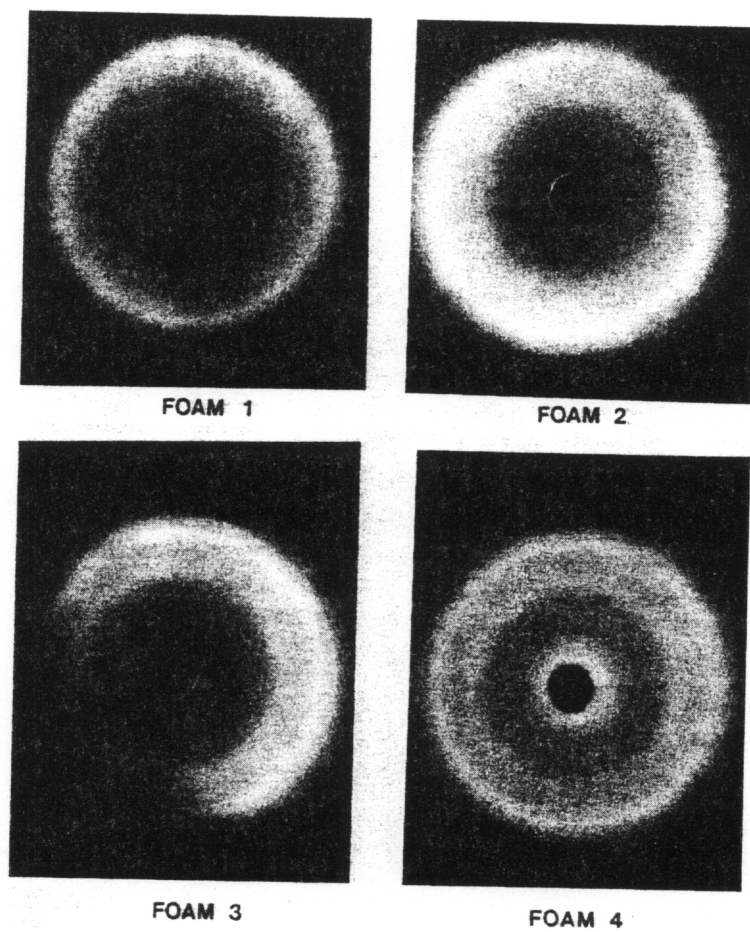


Figure 2.21. WAXS patterns for four slabstock polyurethane foams varying in water content. [ref 33]

2.2.6 *Small-Angle X-ray Scattering*

Along with wide-angle scattering, small-angle scattering has been used in understanding the morphology of polyurethane foams, primarily in obtaining the average size of the hard segment domains within the polymer matrix, the domain spacing, and the interfacial thickness.²⁹⁻³⁸ The first such work on foams was carried out by Wilkes et. al. on polyurethane foams that varied in water content TDI index, polyol molecular weight, and polyurea filler content.³⁸ They found that the foams with a high molecular weight polyol and polyurea filler content displayed the most distinct microphase separation. Upon altering the filler content, no appreciable change was observed in the SAXS profiles suggesting that the polyol molecular weight was the underlying factor. More recently, Armstead has evaluated the scattering characteristics of four slabstock polyurethane foams varying in water content (the same four foams shown in Figs. 2.17 - 2.21).^{32,33} Figure 2.22 shows the SAXS profiles of intensity versus scattering angle for the four foams varying in water content from 2 to 5 obtained by Armstead. These profiles did not exhibit sharp peaks but rather shoulders that appear at approximately the same scattering angle for each. Although the exact reasons for the lack of sharp peaks are unknown many factors can bring forth the observed results. These factors include the scattering features not being of uniform shape or size, and not being consistently separated by the same distances. By the application of Bragg's law to the shoulders, the interdomain distance between the scattering particles was calculated and found to systematically vary from ca 89 to 96 Å with increasing water content. Although, the numbers are only an estimate, they do show that the d-spacing increases with increasing hard segment content. These values as well as their increasing trend with water content are in agreement with what other researchers have reported.^{30,34,35,36} This suggests that the domains are increasing in size and thus the center-to-center distance is increasing.

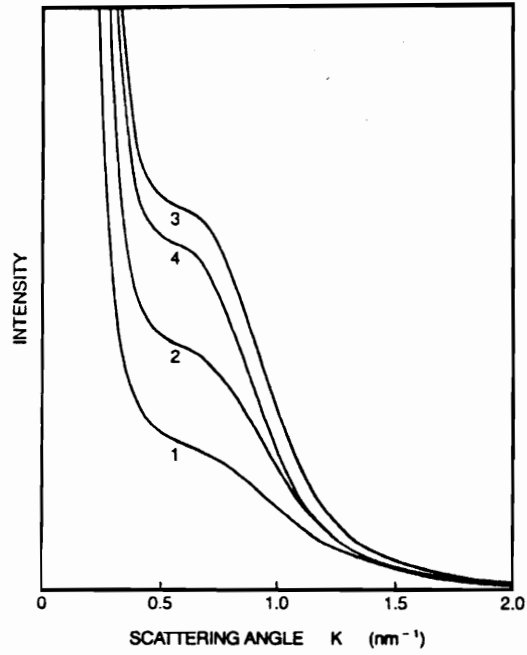


Figure 2.22. SAXS profiles for four slabstock polyurethane foams varying in water content. [ref 33]

Armstead et. al. also used the 1-dimensional and 3-dimensional correlation functions to compare the values obtained from the Bragg's spacing.^{32,33} The difference between the two correlation functions is in the assumed geometrical factors. For example, the 1-dimensional correlation function gives the interdomain distance between two scattering centers assuming a lamellar morphology where the 3-dimensional correlation function gives an estimate of the center-to-center spherical particle spacing. From these results, the authors concluded that no long range order existed and that the hard segment domains again have a center-to-center spacing of 65 to 95 Å depending on the hard segment content.³²

The thickness of the diffuse boundary between the hard and soft segments was calculated using Porod's law.^{30,33} This analysis gives an interfacial thickness parameter, σ , which represents the half-width of the assumed Gaussian distribution of the diffuse boundary. The Porod's law analysis obtained by Armstead gave a σ value of ca. 2 Å for the 2 pph water content foam which systematically increased to ca. 5 Å for the 5 pph water content foam.^{32,33} McClusky et. al. reported numbers in the range of 4 - 7 Å for roughly the same water content foams.³⁰ This is attributed to the increasing lengths of the chain-extended hard segments which are more polydisperse with increasing water content and thus, a more ordered interface is less possible with such dispersity in hard segment length.

SAXS has also been used to evaluate the degree of phase separation through an analysis of the invariant. The degree of phase separation is estimated by comparing the electron density variance for a completely phase separated system with the experimentally determined invariant. Armstead et. al. calculated the invariant as a function water content which showed to increase with increasing water content.³³ Thomas et. al. also determined the invariant in a similar manner but for a series of foams with different cross-link densities.³⁶ They found that the invariant and therefore the degree of phase separation decreased as the cross-link density was increased. This was attributed to the increased viscosity caused by cross-linking which restricted phase separation.

2.2.7 *Fourier Transform Infrared*

Fourier transform infra-red (FTIR) spectroscopy utilizes radiation to characterize the chromophoric groups of a molecule. It is a widely used technique which provides qualitative and quantitative information on the chemical nature, structural nature, type and degree of branching, static order, conformational order, physical arrangement of polymer chains, state of order, and the type and degree of preferential orientation of the polymer chain to name a few.

FTIR has also been used to obtain a better understanding of the morphological features in polyurethanes and polyurethane foams. More specifically, it has been used to study the degree of phase separation in polyurethanes. In the following cases, FTIR was used to characterize the phase separation and the hydrogen bonding as well as short range ordering among urea groups.

Senich and MacKnight used FTIR to study hydrogen bonding in segmented polyurethane elastomers.³⁶ The degree of interurethane hydrogen bonding and the enthalpy of hydrogen bond dissociation were used as indicators of phase separation both increasing with increased phase separation. Figure 2.23 shows the IR spectra at 29°C and 98°C in the N-H (ca. 3300 cm⁻¹) and the C=O (ca. 1700 cm⁻¹) stretching regions. In the N-H region, a decrease in the bonded N-H absorbance was observed, along with a shift in the maximum from 3283 to 3290 cm⁻¹ at the higher temperature. The C=O absorbance displayed similar behavior to the N-H with the exception of the maximum not showing a shift. Senich and MacKnight also determined the integrated absorbances in the range 3180 to 3470 cm⁻¹ (N-H stretch) and the range 1830 to 1630 cm⁻¹ (C=O stretch) at each temperature. The C=O band absorbance was independent of temperature up to a temperature of 100°C. The N-H band absorbance decreased linearly with temperature which was attributed a more sensitive extinction coefficient of the hydrogen bonded N-H

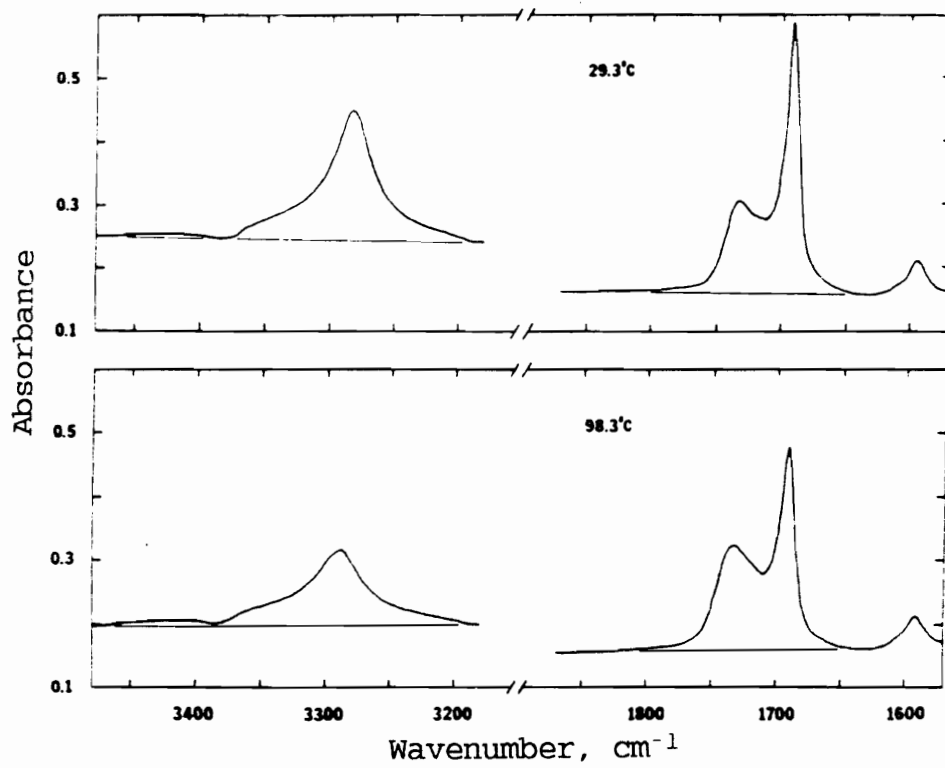


Figure 2.23. IR spectra in the N-H and C=O regions at 29°C and 98°C for a polyurethane elastomer. [ref 40]

absorbance. In the case of the carbonyl absorbance, both the free and bonded carbonyl bands have the same extinction coefficient. The upturn at 100°C was attributed to a new C=O band arising from thermal oxidation. They also reported that at the reference temperature, the fraction of bonded N-H was much higher than the fraction of bonded C=O indicating some degree of phase mixing.

Sung and Schneider examined the temperature dependence of hydrogen bonding in the N-H and carbonyl groups of a 2,4-TDI and a semicrystalline 2,6-TDI based polyurethanes and found that the nature of the soft and hard segments strongly influence the FTIR spectra and hydrogen bonding.⁴¹ Using curve resolving techniques, Sung and Schneider observed that the onset of hydrogen bond dissociation for the semicrystalline domains occurred around 60°C. Also, they found that 80% of the bonded N-H groups are bonded to urethane carbonyl groups which implies that almost all the urethane groups reside in the hard segment domains. With regards to the 2,4-TDI polyurethanes, Sung and Schneider found that at 0°C 95% of N-H groups are bonded and that 50% of those are bonded to carbonyl groups; the rest being hydrogen bonded to the soft segment indicating an extensive degree of mixing of the hard and soft segments. Within the carbonyl region, they observed that at 0°C the bonded carbonyl (at 1720 cm⁻¹) was about equal to the free carbonyl (at 1740 cm⁻¹). Furthermore, the onset of dissociation temperature was in the range of 40°C to 60°C depending, slightly lower than that of the 2,6-TDI based polyurethane. Koberstein, Gancarz and Clark used FTIR to investigate the effects of morphological transitions on the hydrogen bonding in polyurethanes.⁴² They, as with the previous authors found a strong dependence of hydrogen bonding on the morphology. They observed distinct changes in hydrogen bonding that coupled with the observation of morphological changes observed with DSC.

Coleman, Lee, Skrovanek, and Painter performed FTIR temperature studies on poly(1,4-butylene hexamethylene-carbamate), a semi-crystalline polyurethane.⁴³ As with previous researchers, Coleman et al. observed that the intensity of the bonded N-H

absorbance varied dramatically with temperature as shown in Fig. 2.24, where the sample was heated to 210°C and then cooled to 30°C. However, they did not attribute this to the transformation of bonded N-H groups to free N-H groups or vice versa, but instead to changes in the absorption coefficient which depends on the hydrogen bond strength. In the carbonyl region, three bands were observed. These are attributed to ordered hydrogen bonded carbonyl groups, disordered hydrogen bonded carbonyl groups, and free groups. As the temperature was raised, the ordered and disordered bonded bands decreased and gradually shifted to higher frequencies. At 150°C the ordered band vanished and the disordered band broadened. These two types of hydrogen bonding are similar as that observed in polyurethane foams with urea hard domains as will be soon demonstrated.

FTIR temperature studies have also been carried out on polyurethane foams which due to the presence of urea groups are significantly more complicated than polyurethane elastomers. Most of the FTIR work that has been carried out on polyurethane foams relates to foam kinetics and development of its morphology as was described earlier. For, example, McClusky et. al. used FTIR to follow the development of the ordered (bidentate) and disordered (monodentate) urea domains during foam evolution.³⁰ Recall that in the evolution of a foam, the first urea groups produced were observed to be soluble in the soft phase but shortly afterward began to phase separate into domains through initially monodentate hydrogen bonding and then later the more ordered bidentate hydrogen bonded domains. Table 2.3 and Fig. 2.25 show the carbonyl band assignments of the FTIR spectra of typical polyurethane foams.⁴⁴ It also simply illustrates the difference between monodentate and bidentate hydrogen bonding. Bidentate urea has been used to identify urea packing order, phase separation, and will be shown in this dissertation to correlate well with foam performance especially at elevated temperatures.^{45,46} Furthermore, McClusky et. al. evaluated and compared the ingredients of slabstock foams to those typically found in molded foams.³⁰ Interestingly, they observed strong bidentate absorbance bands in the slabstock foams but only weak monodentate absorbance bands in

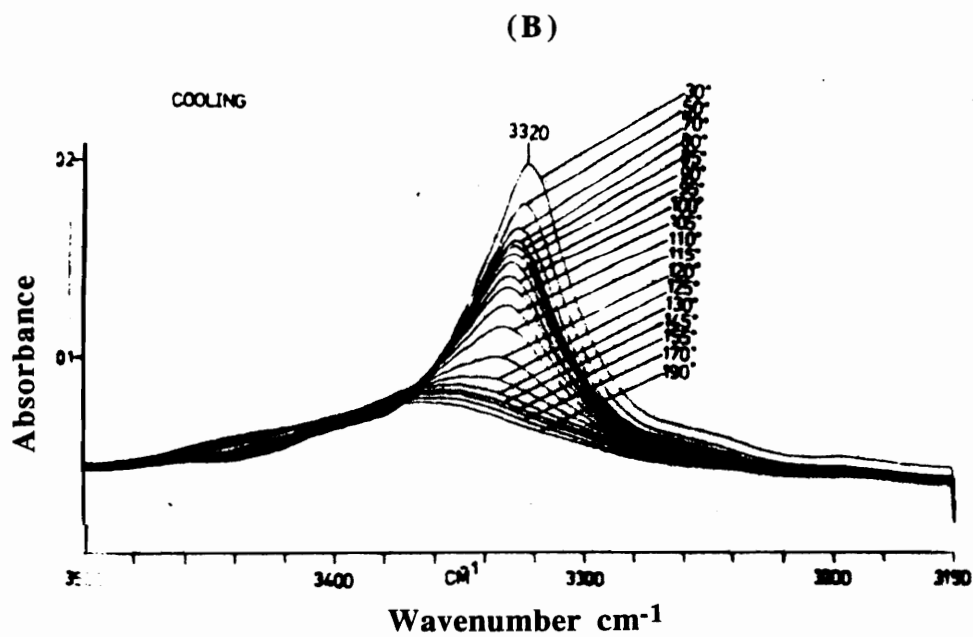
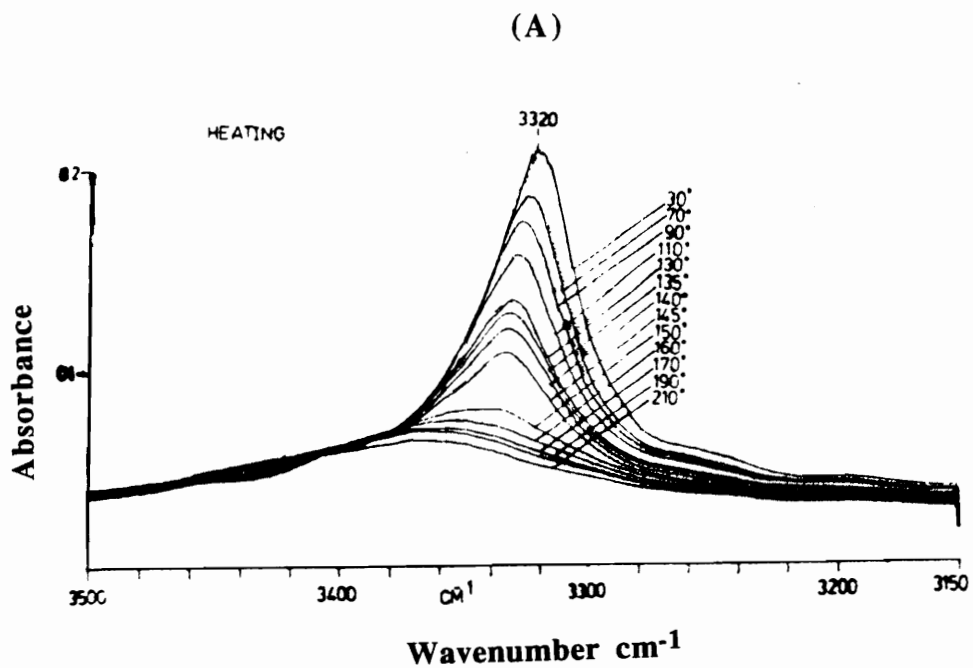


Figure 2.24. Temperature dependence of the bonded N-H region of semicrystalline polyurethane upon (A) heating and (B) cooling. [ref 43]

Table 2.3. Carbonyl Band Assignments

Free Urethane	1730 cm ⁻¹
Loosely Associated Urethane	1715 cm ⁻¹
Hydrogen Bonded Urethane	1700 cm ⁻¹
Free Urea	1715 cm ⁻¹
Loosely Associated "Monodentate" Urea	1700 cm ⁻¹ 1670 cm ⁻¹ 1650 cm ⁻¹
Hydrogen Bonded "Bidentate" Urea	1640 cm ⁻¹
Isocyanurate	1710 cm ⁻¹

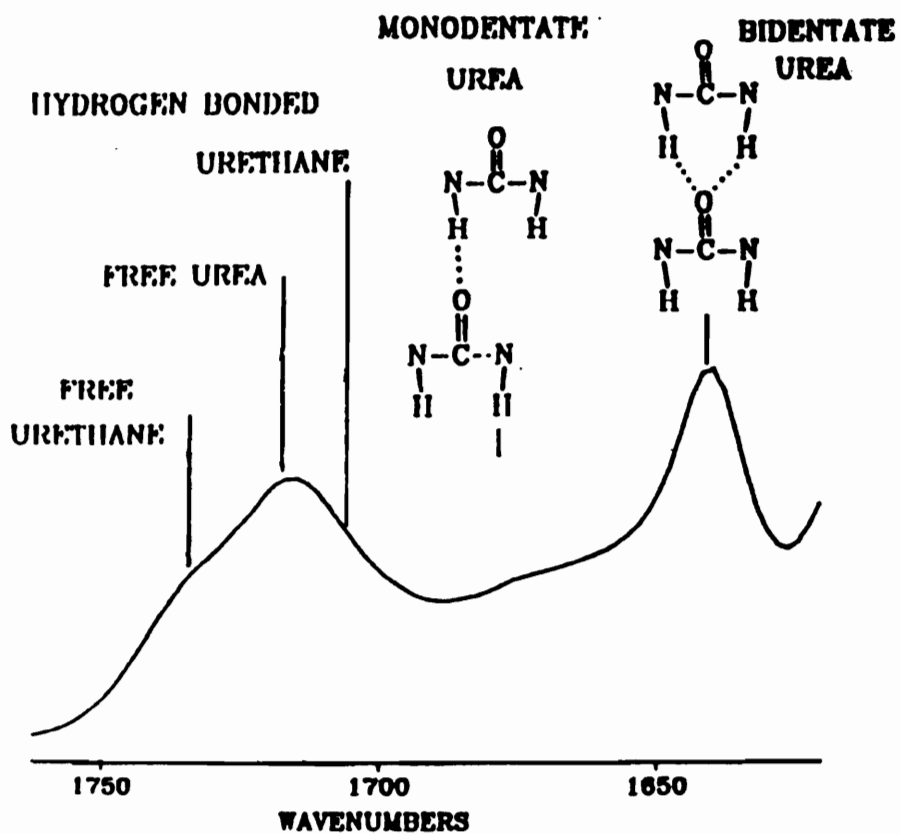


Figure 2.25. Carbonyl band frequency assignments. [ref 44]

the molded foams. This was attributed to the polyethylene oxide capped polyols and especially the additive, diethanol amine, a cross-linker, both of which are typically found in molded foams. These additives enhance the gelling reaction and are thus believed to interfere with the kinetics of the bidentate urea development. The work that will be present in Chapter 4 of this dissertation will evaluate this aspect further.

Thomas et. al. used FTIR to study the influence of cross-linking on the morphology of flexible molded polyurethane foams and films, based on a 4800 molecular weight polypropylene oxide/polyethylene oxide blend, 4 pph water and toluene diisocyanate (TDI).³⁶ Skorpenske et. al. also investigated the hard segment organization through FTIR analysis of the carbonyl region as a function of TDI index which as stated earlier influences the covalent cross-linking.⁴⁷ Both groups of researchers observed slight decreases in the bidentate absorbance bands with increases in cross-linking suggesting that the increased cross-linking results in a greater degree of phase mixing or higher disorder of the HS domains.

With respect to the thermal response of these groups in the carbonyl region, as expected hydrogen bonded bands decrease as the temperature is increased.⁴⁶ However, due to the complexities and convoluted nature of the bands in this region, it is difficult to determine if shifts are occurring from bonded to non-bonded or vice versa. For example, as the temperature is increased, the free urea band is expected to increase and the bonded urethane band is expected to decrease. However, due to the close proximity of the two bands (1715 cm^{-1} and 1705 cm^{-1}) coupled with the broadening of the bands that occurs with temperature, deconvolution of these peaks to determine the contribution of each band to the overall band is very difficult. The fact that both bonded and nonbonded urethane groups display absorbance bands in this region further complicate the analysis. In general, it has been determined that temperature has an adverse effect on hydrogen bonding specifically within the hard segment domains. In addition, certain formulation ingredients such as cross-linkers, higher reactivity polyols, or polyol functionality, can alter the foam

formulation kinetics and can also influence the hydrogen bonding structure. In addition to their effects on the structure and morphology, it is important to determine their effects of the physical properties of the bulk foam.

2.3 Mechanical Properties of Polyurethane Foams

As previously mentioned, the mechanical properties of polyurethane foams depend on the cell structure, morphology, and the chemical makeup of the foams. Basic physical properties include density measurements, indentation force deflection (IFD) tests which are a measure of the load-bearing properties of the foam, compression force deflection tests (CFD) which are similar to the IFD except that the sample size is different, compression set tests, stress-strain behavior, and tensile tests. Along with the mechanical properties, viscoelastic properties such as creep behavior, and stress-relaxation have also been investigated. These properties have been analyzed in terms of density, degree of openness, and the anisotropic shape as well as aspects of the of the solid portion of the foam such as cross-linking or morphology.

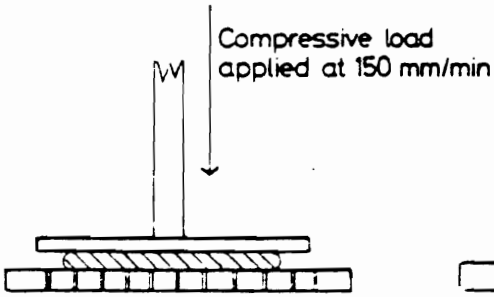
2.3.1 Basic Foam Properties

One of the most important properties of foams is density which is typically directly influenced by the water content. In addition to density, the water content strongly influences the physical properties as well since they are strongly dependent on the extent of microphase separation and perfection of the hard segment domains. Patten et. al. studied the effects of water content variations on the tensile strength, tear strength, and elongation of flexible polyurethane foams.^{39,48} They reported that an increase in the water content resulted in an increase in these properties up to a limiting point (4 pph) whereby no further increase in the properties was observed. This enhancement in the properties was attributed

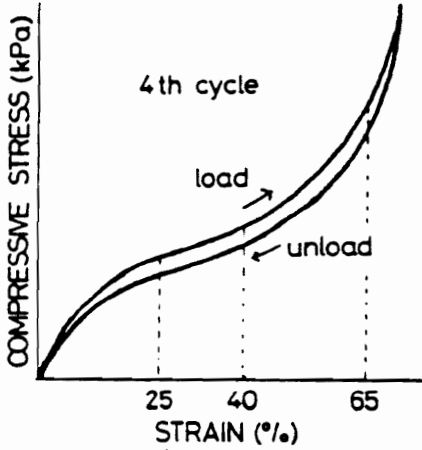
to an increasing hard segment content. Sung et. al. also observed the same trend on urea-urethane elastomers showing an increase in the modulus and tensile strength with increasing hard segment.⁴⁹

The indentation force deflection test (IFD) is another important property and, aside from density, is the most widely measured mechanical property. It is a measure of the force required to depress a small circular plate into the foam as illustrated in Fig. 2.30. Results are usually plotted as force versus indentation. The force is measured upon loading and unloading which gives an indication of hysteresis. Tabulated results are given as 25% IFD, 65% IFD, 25% return IFD, and % hysteresis return. The percentages represent the amount of deflection relative to the original height. The ratio of the 65% to 25% IFD value, known as the support factor or sag factor, gives an indication of the cushioning factor. A sag factor of 2.8 is considered sufficient cushioning. The hardness of a foam is shown to decrease with increasing water content due to decreasing density.^{3,22,50,51,52} Although increasing water content increases the hard segment content which leads to an increased modulus, the decreased density is the more dominant factor. However, if the density is normalized out, the higher hard segment foams do display higher hardness. Patten also showed that by holding the density constant through the use of a physical blowing agent, the hardness did increase with increasing water content. Along with water content, the isocyanate and the polyol structure can affect the hardness. An isocyanate index higher than 100 (an index of 100 is sufficient to react with all the active hydrogen atoms) can lead to harder foams due to additional cross-linking and the possible formation of biuret and allophanate structures provided that other conditions are favorable. In polyol structures, the molecular weight and functionality both influence the hardness. As both increase, so does the foam hardness. Finally, as expected, the cell geometry and its anisotropy affect the hardness. When loaded along the major axis of the ellipsoidal geometry, the foam displays a higher level of hardness.

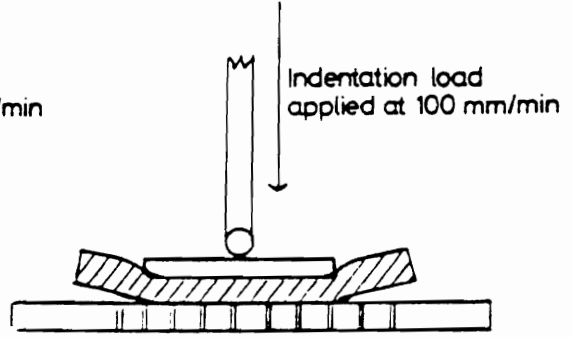
COMPRESSION HARDNESS



Compression hardness results expressed as compression stress in force/unit area



INDENTATION HARDNESS



Indentation hardness increases with increasing thickness of sample, increasing tensile strength and increasing sample size

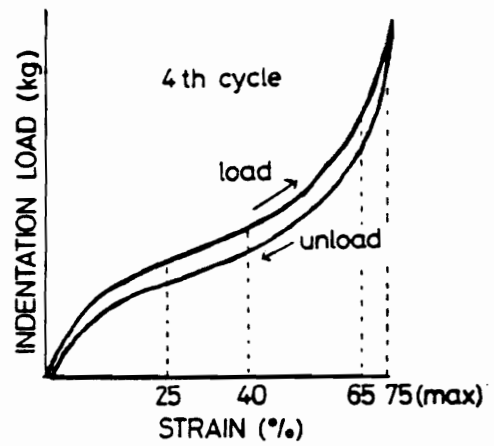


Figure 2.26. Compression hardness and indentation force deflection tests. [ref 3]

The compression force deflection (CFD) test is similar to the IFD except that in the CFD test, the entire foam sample, usually having dimensions of 4"x4"x1", is compressed.^{53,54,55} First the sample is conditioned by compressing it twice to 25%. Then, following a 10 min recovery period, the sample is compressed to 50% of its original height and the load is recorded after 60 sec.

2.3.2 *Stress-Strain Behavior*

Stress-strain loading is carried out to determine the foam modulus, transitions in the deformation mode, as well as mechanical hysteresis. Figure 2.27a is an illustration of the compressive stress-strain curves for an elastomeric open-celled foam which has been divided into three regimes by Gibson and Ashby as well as others.^{1,55,56,57} The first region is known as the linear elastic bending region. In this region, which occurs in the first 5-10 % strain, the cell walls begin to bend. The Young's modulus, E , is the initial slope of the stress strain curve and thus calculated in this region. The following region, known as the elastic buckling region, represents non-linear buckling of the cells, specifically the cell struts. Rigid foams would exhibit nonelastic deformation and plastic yielding in this second region. The last region is known as the densification region. Here, the cells completely collapse and opposing cell walls touch. Further strain compresses the solid portion itself thus giving dramatic increases in stress.

The response of an open-celled foam loaded in tension is shown in Fig. 2.27b. As with compression, the initial linear elastic response is caused by cell wall bending but here the linear region is longer. The non-linear region is smaller and finally, in the case of tension, the sample ruptures at higher strain levels.

In modeling the linear elastic behavior of a foam, many researchers have derived the expressions for the Young's modulus, the shear modulus, and Poisson's ratio, in terms of the solid modulus, and the relative density, defined as the foam density divided by the solid

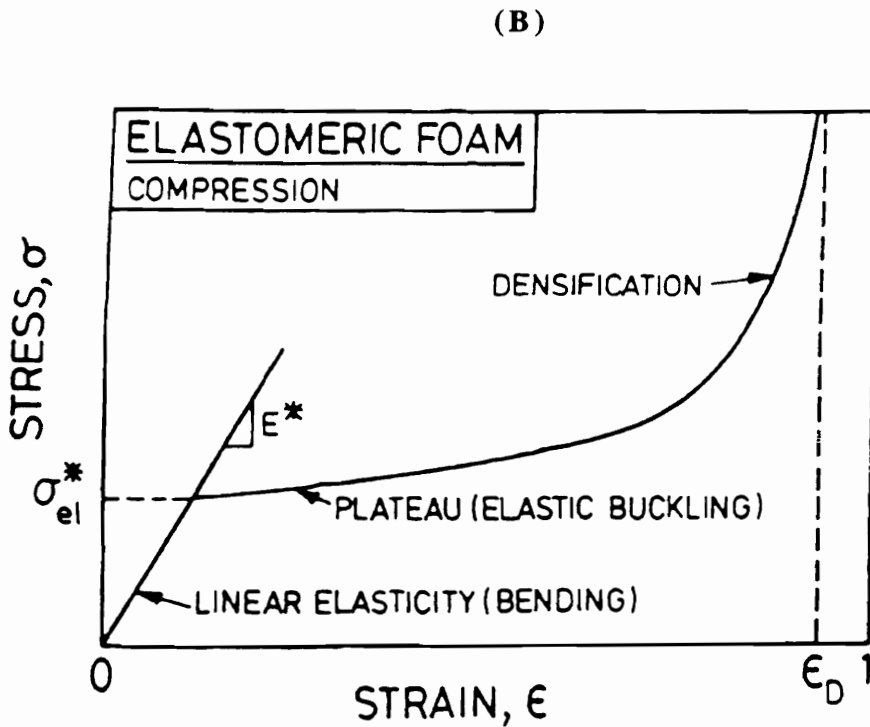
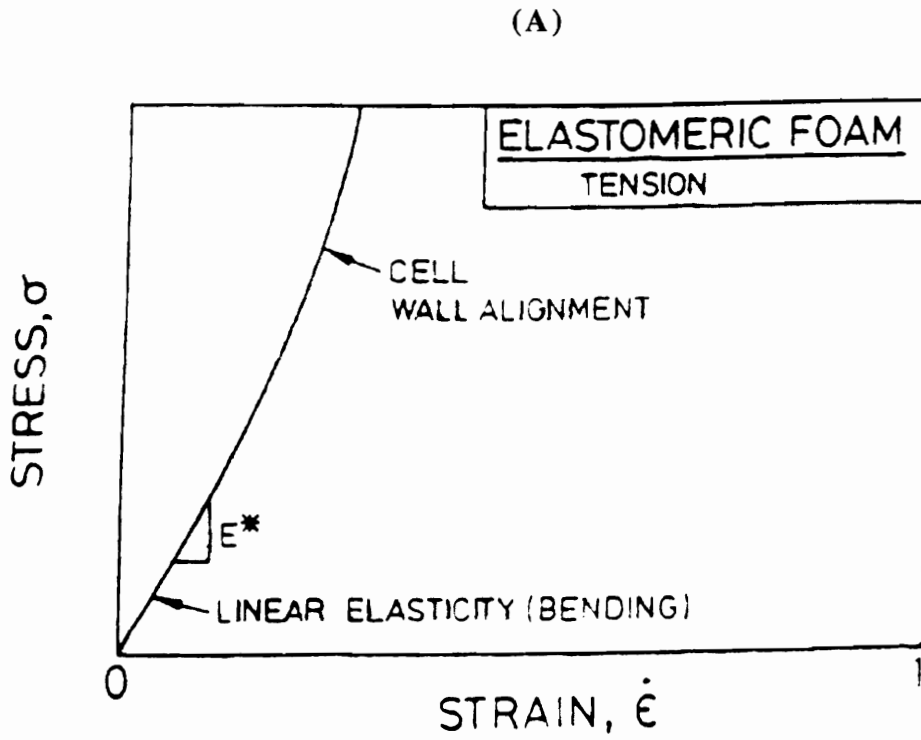


Figure 2.27. Stress-strain behavior for elastomeric foams in (A) compression and (B) tension. [ref 57]

density.⁵⁶⁻⁶⁰ The mechanism of linear elasticity depends on whether the cells are open or closed. If the cells are open, the mechanism is a bending of the cell walls where if the cells are closed the mechanism is stretching of the cell membranes along with compression of the cell fluid. Gibson and Ashby have provided an excellent treatise on the mechanical properties of foams, some of which is presented here.

2.3.2.a Open Cells

A foam has been modeled as a cubic array of membranes of length l and square cross-section of side t by Gent and Thomas and more recently Gibson and Ashby.^{56,58,59,60} This simple geometric shape is shown in Fig. 2.28a. The dimensions l and t are related to the relative density by

$$\frac{\rho^*}{\rho_s} \propto \left(\frac{t}{l}\right)^2 \quad 2.1$$

where ρ^* is the foam density and ρ_s is the solid density. Young's modulus for the foam is calculated from the linear-elastic deflection using standard beam theory with a given deflection δ and load F as shown in Fig. 2.28b. When this cubic array is subjected to a compressive force, F , a deflection δ occurs. This deflection was related to the force and the Young's Modulus of the solid by $\delta = Fl^3/E_s I$ (E_s = Young's Modulus and I = second moment of area) and defining the stress σ as F/l^2 and the strain ϵ as δ/l , the Young's modulus was determined. Young's modulus was then defined in terms of the solid foam modulus and the reduced density as

$$\frac{E^*}{E_s} = C_1 \left(\frac{\rho^*}{\rho_s}\right)^2 \quad 2.2$$

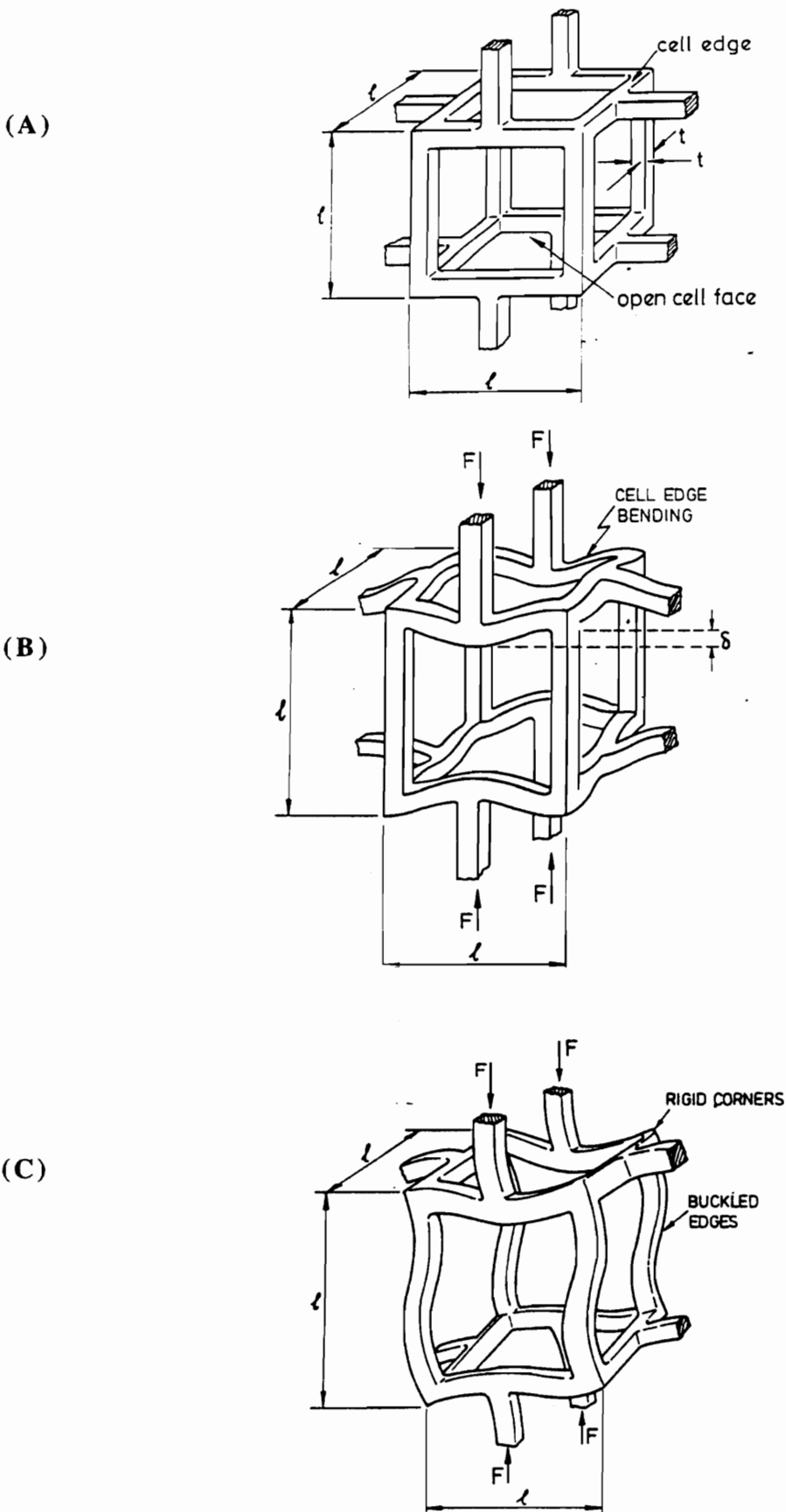


Figure 2.28. (A) Cubic model for an open-cell foam undergoing (B) cell edge bending and then (C) elastic buckling in cell walls. [ref 1]

where C_1 is a geometric constant which was experimentally determined to be unity. Again, this model is valid at small strains only since this model is only applicable in the linear elastic region. The shear modulus is calculated in a similar way to give

$$\frac{G^*}{G_s} = C_1 \left(\frac{\rho^*}{\rho_s} \right)^2 \quad 2.3$$

where C_2 has been experimentally shown to equal $3/8$. From the relationship between the shear modulus and Young's modulus, Poisson's ratio can be defined as

$$\nu^* = \frac{C_1}{2C_2} - 1 \quad 2.4$$

which is equal to ca. $1/3$ for the given values of C_1 and C_2 , consistent with many experimental observations. Since this ratio is the negative ratio of the lateral strain to the axial strain which are proportional to a single bending deflection, it is a constant affected only by the cell geometry.

Although this analysis contains many approximations such as double counting the density at the cell corners and the neglecting of the axial and shear displacements of the cell walls, Gibson and Ashby have shown that the simple models correlate well with the data. For example, Fig. 2.29 compares the model for Young's modulus to experimental data of various foams where the solid line represents the theory and the points represent actual data.

Foams can be and usually are compressed or stretched to strains much larger than the limited 5% for linear elasticity. Since the application of foams inherently places them under strains greater than 5%, this elastic but non-linear deformation is very important. Figure 2.28c illustrates a structural model undergoing elastic buckling. As in the case of linear elastic deformation, the behavior depends highly on the nature of cell openness. The

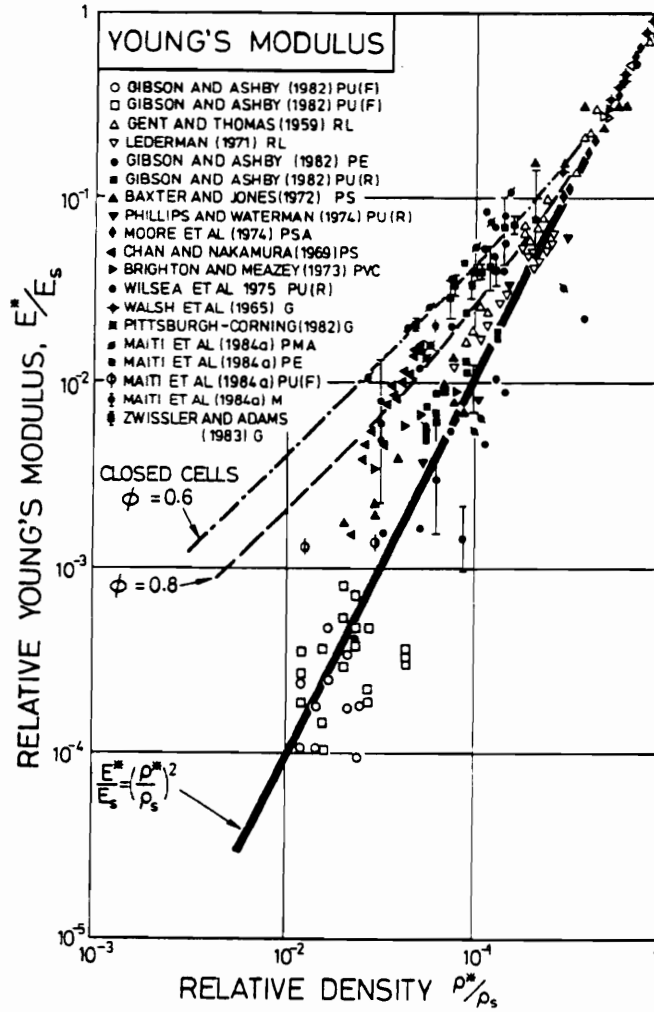


Figure 2.29. Comparison of theory to experimental data for Young's modulus. Solid line represents theory. [ref 57]

first step in this analysis was to calculate the force at which a cell edge begins to buckle and was done using Euler's formula

$$F_{crit} = \frac{n^2 \pi^2 E_s I}{l^2} \quad 2.5$$

where n^2 is the degree of constraint at the ends of the column and I is the second moment of area. The elastic collapse stress, σ_{el}^* , was written as the force divided by the cross-sectional area, F/l^2 . Relating the second moment of area to t^4 and introducing the relative density gives for the stress

$$\frac{\sigma_{el}^*}{E_s} = C_4 \left(\frac{\rho^*}{\rho_s} \right)^2 \quad 2.6$$

Gibson and Ashby introduced a density correction for reduced densities greater than 0.3 where the cell corners account for a significant part of the volume

$$\frac{\sigma_{el}^*}{E_s} = C_4' \left(\frac{\rho^*}{\rho_s} \right)^2 \left(1 + \left(\frac{\rho^*}{\rho_s} \right)^{1/2} \right)^2 \quad 2.7$$

Figure 2.30 is an illustration comparing these two models to experimental data for the elastic collapse stress which is plotted against the relative density. The solid line represents the theory while the points represent experimental data. The curves show very good agreement between the two.

At even larger strain levels beyond buckling, opposing walls of the cells crush together and the cell wall material is compressed. At this point, the stress rises steeply and the slope approaches E_s foam at a limiting strain of ϵ_D . The cell walls come together at a strain described by

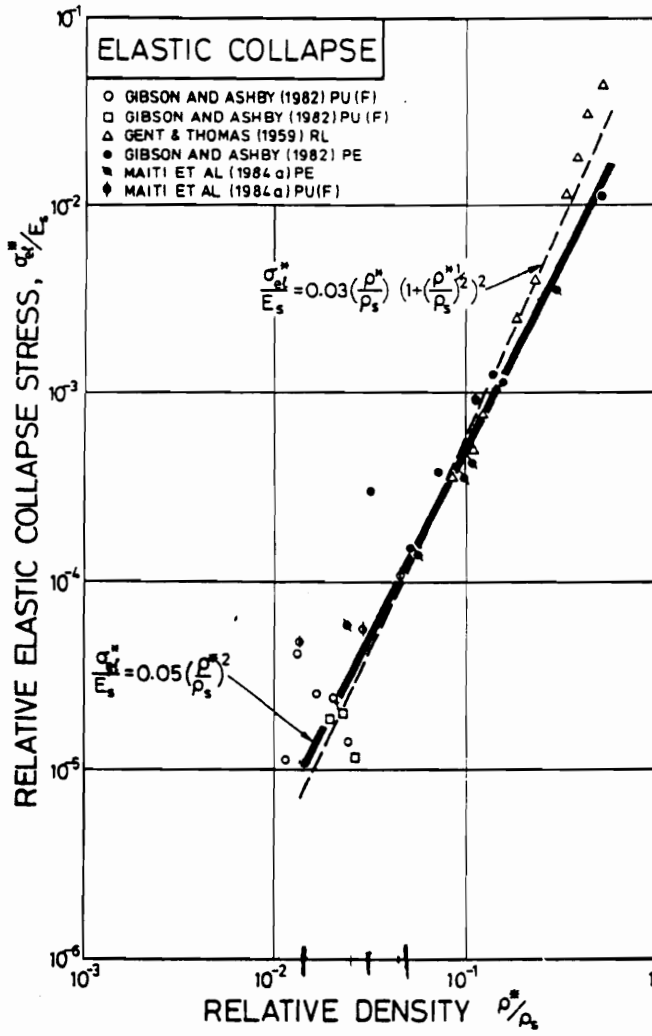


Figure 2.30. Comparison of theory to experimental data for the elastic collapse stress. Solid line represents theory. [ref 57]

$$\varepsilon_D = 1 - 1.4 \left(\frac{\rho^*}{\rho_s} \right) \quad 2.8$$

Again, Gibson and Ashby have demonstrated with their own as well as others that these simple models correlate well with experimental data.

2.3.2.b Closed-Cells

Although flexible molded foams are designed as open-cell foams, they inherently have many closed-cells even after mechanical crushing. Gibson and Ashby have extended their analysis to closed-cell foams as well, however, only a very brief sampling is provided to portray certain relevant ideas. While the foams evaluated in this dissertation are open-celled, the significant amount of closed cells that they contain are sufficient to contribute to the displayed physical behavior. Closed cells are much more difficult to model due to the added mechanisms involved when compressed. For example, the cell membrane can contribute to the stiffness of the foam, or due to the surface tension of the fluid, the membrane can be thinned leading to rupture during deformation. Gent and Thomas as well as Skochdopole and Rubens proposed that the Young's modulus for closed-cell foams is a sum of three contributions.^{59,60} The first contribution is the same as that in open-cell foams, cell-edge bending. The second contribution is provided by the compression of the cell fluid which was calculated using Boyle's law. The third contribution to the modulus is the stress exhibited by the cell membranes. As a closed-cell foam is compressed, the bending cell edges cause the cell faces to stretch.

The compression stress-strain behavior of flexible foams was investigated by Rusch.⁶⁴ He used four different foams to evaluate the effects of the structural features on this behavior. Two were low density reticulated polyurethane foams, Q and L, with Q

having a higher density. Another was a high density rubber latex foam with an irregular cell structure, R and the fourth was a nonreticulated polyurethane foam containing some closed cells and an irregular cell structure, E. The stress-strain behavior of each is shown in Fig. 2.31. From his analysis he concluded that the specific cell geometry has a great effect on the compressive stress-strain behavior. This is evident from the response of curves Q and L compared to curve R. Curve R from the rubber latex foam displayed only a slight transition into the buckling region but continued to increase with a large slope. The density and the cell size also showed considerable influence on the stress-strain behavior as evidenced by comparison of curves Q and L. As expected, the transitions from bending region to the buckling region and from the buckling region to the densification region occur at higher stress values for the higher density foam. Also, when a certain amount of closed-cells exist, the foam not only exhibits higher stresses at any given strain but continues to increase throughout the buckling range. One surprise is that the Young's Modulus appears independent of the nature of the cellular structure and density.

The stress-strain behavior in tension, illustrated in Fig. 2.27b, is similar to that in compression except that fracture can occur in tension. In tension, the modulus is determined by cell edge bending as with compression. At higher deformations however, buckling does not occur as in compression, but instead, the cell edges rotate towards the tensile axis and the bending moment acting on them decreases. At a strain of ca. 30%, the cell edges are substantially aligned in this direction and further deformation extends them axially.

Thomas et. al. evaluated the influence of cross-link density on the tensile stress-strain properties of a flexible polyurethane foam.³⁶ They noted that the nature of the solid portion of the foam also influenced this behavior in addition of the global cell geometry. Recall that both parameters are incorporated in the models provided by Gibson and Ashby. The higher level of cross-linking resulted in an increase in stress as a function of strain. The authors noted very little effect on the Young's modulus by altering the polyol

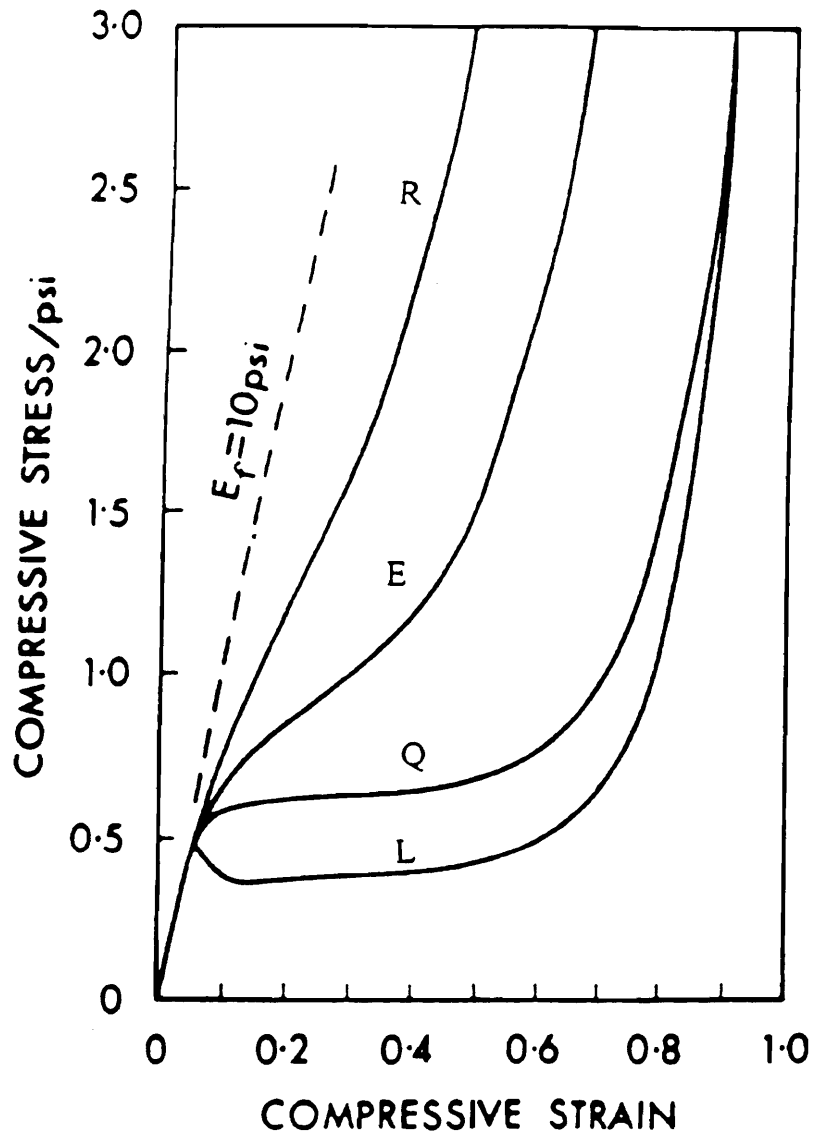


Figure 2.31. Compressive stress-strain. [ref 64]

functionality. The effect of cross-linking was more pronounced at higher elongations and at the point of failure. The higher cross-linked sample displayed a lower stress and elongation at break.

2.3.3 *Viscoelastic Properties*

The viscoelastic properties of foams are extremely important since they are a measure of a foams durability and recoverability. The load of these materials for a viscoelastic measurement is similar to the type of loading they undergo in an actual application such as seats. Furthermore, the viscoelastic properties are sensitive to the nature of the polymer. The structure and morphology dictate the type of response the foam will have and are influenced by both the covalent network and the hard segment domains or physical network. Measurement of these properties can thus provide an excellent evaluation of the network of the material.

The viscoelastic behavior of foams is characterized primarily through investigation of the stress relaxation and creep response as well as compression set. The first involves measurement of the time-dependent stress decay under a constant strain while the second involves the measurement of the strain under a constant load. Along with these, compression set and fatigue tests are conducted. Compression set is a measure of the deformation of a foam after it has been compressed at a given set of conditions. It is usually expressed as a percentage of the original compression. Along with indentation force deflection (IFD), it is one of the most widely measured properties and from a practical point of view may be the most important. Fatigue, another viscoelastic measurement, is usually reported as a percent indentation force deflection loss. This type of measurement is somewhat uncommon and is not undertaken in this dissertation. Again, the two main techniques focused on are stress relaxation and creep. Compression sets were also measured for comparison.

2.3.3.a Stress Relaxation

The viscoelastic properties of polymeric materials are often represented by relaxation curves. Stress relaxation curves have been used for the prediction of the cushioning factor of polyurethane foams. As mentioned above, the stress relaxation behavior is a measure of the stress decay under a constant deformation. Relaxation curves can be expressed by a generalized Maxwell model

$$Y(t) = \sum_{i=1}^n A_i \exp(-t/\tau_i) + Y_{\infty} \quad 2.9$$

where $Y(t)$ is the decaying parameter, Y_{∞} is the asymptotic residual value, A_i is a constant characteristic of the material, and τ_i is known as the relaxation time.⁶⁵ Many methods exist for evaluating relaxation data and arriving at the characteristic constants. Many polymer materials including polymer foams exhibit non-linear viscoelastic behavior in which the properties depend on the deformation history.

Tobolsky and Andrews have proposed that when materials are subjected to an external stress, "certain regions of elementary molecular movements" exist that allow readjustments to accommodate the stress. In the case of an elastomer such as natural rubber under an external stress, portions of the molecular chains between cross-links elastically uncoil and to some extent secondary bonds are broken and reformed in relaxed positions.⁶⁹ Secondary bonds, at low temperatures, initially contribute to the stiffness, but over time, will relax and reform in new positions producing a gradual decay in stress until equilibrium stress is reached. Ferry has added that at long-times, relaxation is related to the existence of branched structures in the presence of entanglements.⁷⁰ These dangling ends can eventually relax to an unperturbed conformation. Curro and Pincus investigated the long time relaxation behavior of natural rubber elastomers.⁷¹ In this investigation, they

used de Gennes' reptation theory for a single branched chain with topological constraints. For example, the mechanism by which the dangling chain ends equilibrate is viewed as a modified reptation process within a constraining tube. The theory presented by Curro predicts that certain parameters such as the asymptotic modulus E_{∞} and the relaxation time τ_0 are functions of the cross-link density. This was confirmed by Dickie and Ferry where their experimental results on natural rubber showed a similar relationship.⁷²

Hsiue, Chen, and Yeong-Kang investigated the relationship between the stress relaxation rate and domain structure of two thermoplastic elastomers, styrene-butadiene-styrene block copolymers (SBS) and 1,2-syndiotactic polybutadiene (1,2-PB).⁷⁵ Although these are not polyurethane systems, they have a common characteristic of domain morphology. They found that the structure of the domain whether it be amorphous as in SBS or crystalline as in 1,2-PB, has a significant effect on the stress relaxation.

Turner examined the stress relaxation behavior of reaction injection molded (RIM) polyurethanes.⁷⁶ He studied the influence of the hard segment domain structure and the influence of a glass fiber filler. The samples with the crystalline hard domains displayed higher stress levels and lower stress relaxation over the samples with amorphous hard domains. A similar phenomenon was observed with filled systems versus the non-filled systems. Glass fiber reinforcement increased the stress values and decreased the stress relaxation. Finally, Turner noted that in all systems, an increase in temperature caused increased stress relaxation and increased relaxation rates.

Dzierza and Seymour et. al. have shown that the relaxation process in polyurethane elastomers is dominated by the viscoelastic soft segment.^{73,74} Furthermore, they found that the relaxation process is also dependent on the functionality and molecular weight of the polyol. A higher molecular weight or functionality both lead to decreases in the level of relaxation. They also found that the hard segments exhibit little resistance to the relaxation and increases in the hard segment content lead to greater relaxation.

Morimoto et. al. examined the effect of different expansion ratios on the flexural stress relaxation of glass-fiber-reinforced and non-reinforced rigid polyurethane foams.⁷⁷ The results showed that a higher expansion ratio reduced the flexural modulus in both the reinforced and non-reinforced materials. This was expected based on the work of Gibson and Ashby. The stress relaxation increased with higher temperatures and a higher expansion ratio for the non-reinforced system. The expansion ratio was believed to influence the molecular weight between cross-links, M_c , where the higher expansion ratio increased M_c and thus decreased the number of elastically active chains.

Doherty and Ball reported that the viscoelastic decay of stress in slabstock foams increased with higher water content foams.⁷⁸ They related the decay to time by the following equation

$$\Delta L = At^x \quad 2.10$$

where t is the time, ΔL is the percent loss of a dimension such as stress and A and X are constants. The constant X is coupled with the relaxation rate and was shown to increase with increasing water content in the formulation and thus increasing hard segment content.

The stress relaxation behavior of flexible water-blown foams has been recently studied by Moreland.⁷⁹ Four foams, varying in hard segment content, were investigated including the effect of temperature and humidity on their behavior. Figure 2.32 shows the effect of temperature on the stress relaxation on a 2 pph water content foam. As the temperature was increased, the stress levels increased and the relaxation decreased up to a temperature of 100°C for where the stress sharply decreased. This increase initially was consistent with rubber elasticity theory which predicts an increase in stress with temperature for a network simply given as

$$\left(\frac{\partial f}{\partial T}\right)_{l,v} = -\left(\frac{\partial S}{\partial l}\right)_{T,v} \quad 2.11$$

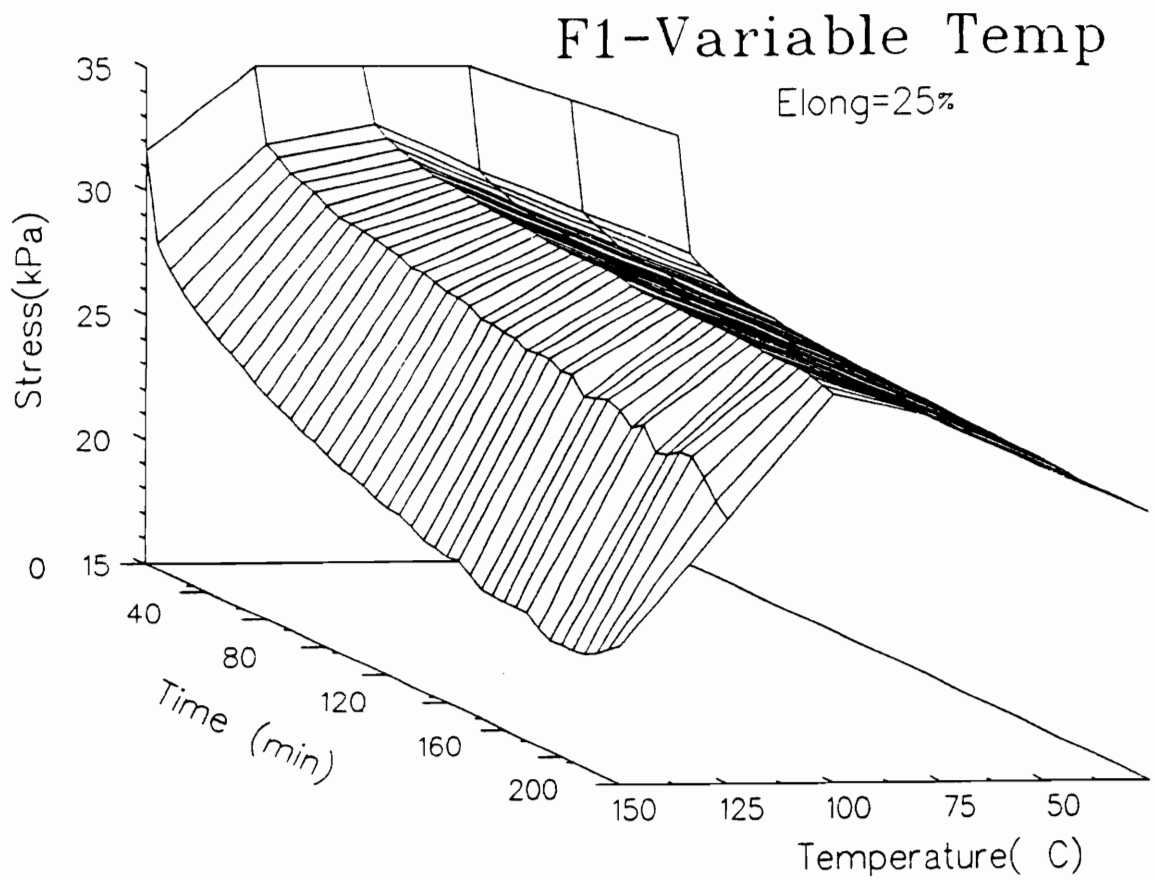


Figure 2.32. Effect of temperature on stress relaxation of 2 pph water content foam. [ref 79]

Also, the stress decay rate decreased up to a temperature of 100°C. Moreland stated that this decrease indicates that the stress relaxation approaches equilibrium faster with temperature. This is believed to be due to a faster relaxation of the soft segment chains and hydrogen bond disruption in the hard segments. Above 100°C, the stress relaxation increased significantly. Moreland attributed this increase to the dramatic disruption of hydrogen bonds, and in addition, to some chain scission which may be taking place primarily in the urethane linkage. In terms of the hard segment content, an increase in the stress levels as well as the amount of relaxation, was generally observed with an increase in hard segment content. Also, the amount of stress decay as a function of temperature was higher for the higher hard segment content foams. This is also evident in Fig. 2.33 which shows the effect of temperature on a 5 pph water content foam. At temperatures below 100°C, the influence of temperature on the high hard segment content foam was significantly different than that for the low hard segment content foam. Here, the stress levels decreased with increasing temperature for all temperatures above room temperature. This was attributed to the effect of temperature on the additional hydrogen bonding as a result of the higher hard segment content. Furthermore, since the hard segment content is higher, the lower soft segment content decreases the elasticity effect which induced the increases in stress with the 2 pph water content foams. In this 5 pph water content foam, the hard segments contribute more to the initial stiffness of the foam than in the 2 pph water content foam, and thus when the hydrogen bonding is weakened by temperature, greater stress relaxation occurs. Finally, Moreland also noted that increases in the relative humidity lowered the stress levels and increased the stress relaxation, similarly to temperature but to a lesser extent. This observation was attributed to the water acting as a plasticizer, primarily in the hard domains, promoting slippage. The influence of humidity was lower as the hard segment content increased.

Recently, Thomas et. al. evaluated the influence of cross-linking of molded polyurethane foams on a number of properties, one of which is stress relaxation.³⁶ The

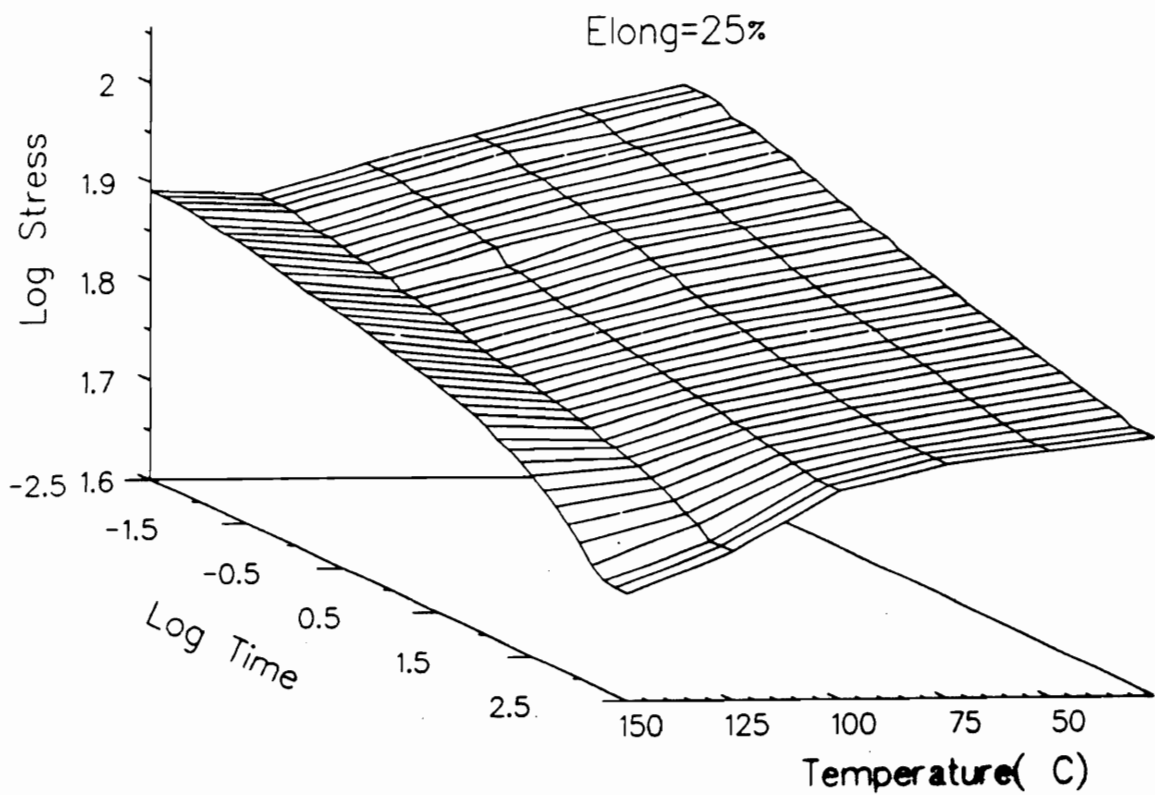


Figure 2.33. Effect of temperature on stress relaxation of 5 pph water content foam. [ref 79]

amount of cross-linking was varied by altering the polyol functionality through the introduction of mono-functional species. The data was fit to a power law relationship which was used to evaluate two foams varying in cross-linking. While the initial stress values were essentially the same, the relaxation rates were clearly different. These differences were also evident at longer times where the more cross-linked foam exhibited less decay. The power law exponent (related to the relaxation rate) was also lower confirming that the rate of relaxation and the amount of relaxation was lower for this higher cross-linked foam. They also pointed out that the hard segment domains have an overwhelming effect at room temperature since varying the polyol functionality produced a rather small effect.

2.3.3.b Creep

Along with stress relaxation, creep is also a common and very important property in evaluating the viscoelastic behavior. Creep is also important since it closely resembles the type of loading these materials undergo in actual applications. The creep behavior of a foam strongly depends on the solid portion of the foam. Many solid polymers are linear viscoelastic where the strain at any given time is proportional to the applied stress. At large strains or long times, the system may become nonlinear viscoelastic behavior where the strain is no longer just a linear function of the stress. As with stress relaxation many empirical equations for the linear and nonlinear viscoelasticity have been proposed.⁸²⁻⁸⁶ The examples from the literature presented here are chosen to relay certain ideas relevant to the present document.

Nolte and Findley compared the creep behavior of solid polyurethane to that of the foamed rigid polyurethane.⁸⁶ They found that for stress levels no greater than two-thirds of the plastic yield strength, the creep strain of the foam could be described as the creep strain of the solid portion multiplied by the ratio of the initial stiffness of the solid to that of

the foam. At higher levels of stress, where the foam began to display non-linear behavior, this simple method under-predicted the measured creep strains.

Huang and Gibson have recently analyzed and provided a model to describe the linear and non-linear creep of rigid polyurethane foams.⁸¹ Their derivation is based on the dimensional analysis used by Gibson and Ashby to model Young's modulus of an isotropic foam with linearly elastic cell-wall material and a geometric structure as shown in Fig. 2.28a. As presented earlier in Section 2.3.2.a, the Young's modulus was given as

$$E^*/E_s = C_1 \left(\rho^*/\rho_s \right)^2 \quad 2.2$$

Huang and Gibson then described the linear viscoelastic behavior in which the solid cell wall material creeps as

$$\varepsilon_s = \left(\varepsilon'_o + m't^n \right) \frac{\sigma_s}{E_s} \quad 2.12$$

where E_s is Young's modulus of the solid portion and σ_s is the stress of the solid portion. This was then used to derive the following equation describe the strain of the foam which is of the same form as the previous equation

$$\varepsilon(\sigma, t) = \left(\varepsilon'_o + m't^n \right) \frac{\sigma}{E^*} \quad 2.13$$

This was compared to experimental results obtained for four densities of rigid polyurethane foam by measuring their creep response when loading in shear and was found to display good agreement where the creep strains are predicted to within 10%.

D'Amore et.al. studied the flexural creep behavior of high density polyester foams.⁹⁰ They showed that the void content had no practical effect on the viscoelastic

response of the foam. Also, the exponent n used in Findley's and Huang's work was shown to increase with temperature. They found that while the foam modulus did depend on the void content, the viscoelastic behavior was independent of the void content. In another study by D'Amore et. al., the flexural creep behavior of glass reinforced polyester foams at different temperatures, fiber (filler) content, and foam density was investigated.⁹¹ Figure 2.34 shows the creep compliance as a function of time carried out at different temperatures. The compliance, calculated from the deflection and geometrical factors, increased with increasing temperature as shown. As can be seen, both the creep compliance and the creep rate systematically increased with increasing temperature. D'Amore et. al. also applied time-temperature superposition to the data of Fig. 2.34 thereby shifting the curves to obtain long time prediction of the data. The master curve, shown in Fig. 2.35, was constructed using horizontal shifts. These results were compared to transition state theory to check the validity of the shifting process which gives the temperature dependence of the shift factor. If the mechanisms are the same in each case, the data should follow a linear relationship providing a unique activation energy. D'Amore carried out such an analysis for the neat resin, unreinforced foam and reinforced foam; all fitting one line and having one activation energy. The authors interpreted this by suggesting that the void content and fiber content have no effect on the viscoelastic response. However, the master curve of the 45% reinforced foam appears to be lacking in continuity and thus the validity of such should be questioned.

Alperstein et. al. also investigated the creep behavior of reinforced rigid polyurethane foams; more specifically, the effects of density, glass fibers, temperature, and stress on the compressive creep of rigid polyurethane foams.⁹² As the temperature was increased, the creep rate was much higher along with the strain levels. The creep rate was assumed to follow an Arrhenius type relation with temperature. The activation energy was determined from the slope of the creep rate versus $1/T$ and was found to decrease with increasing stress. Finally, they did observe a slight decrease in the creep rate with

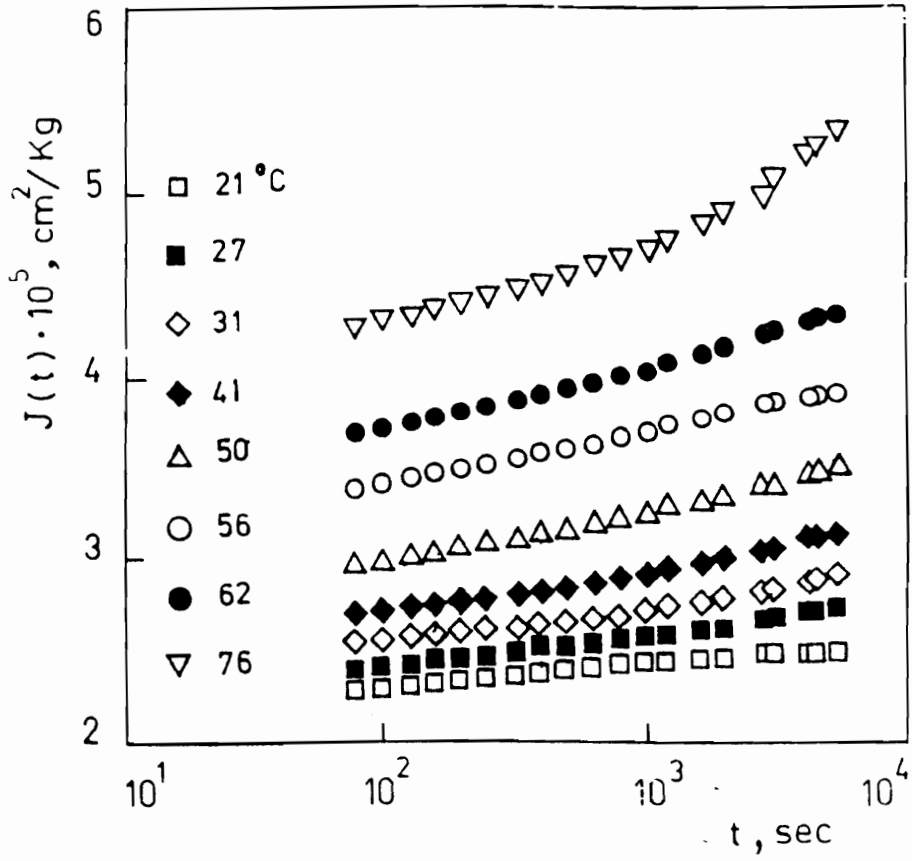


Figure 2.34. Flexural Creep for a 25% reinforced foam. [ref 91]

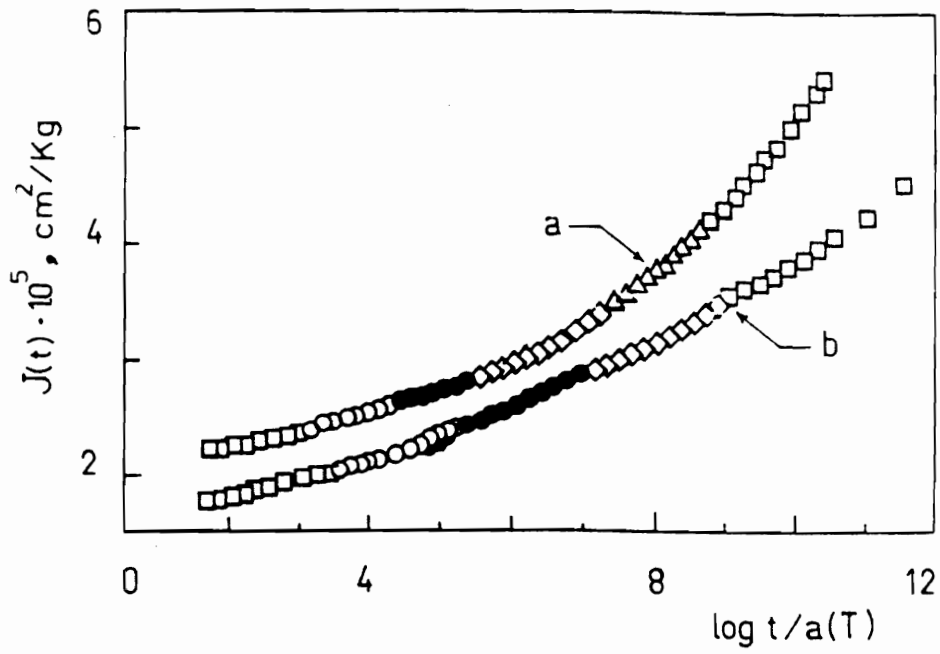


Figure 2.35. Master curves of flexural creep for (a) 25% and (b) 40% reinforced foams. [ref 91]

increasing filler content and with increasing density. The filler was more effective in the higher density foams.

Campbell investigated the compressive creep behavior of flexible polyurethane foams and the effect of polyol molecular weight and water content on the creep rate.⁸⁰ Comparing the creep rate of two foams; a high resiliency (cold-cure) foam and a hot-cure foam, the high resiliency foam displayed a much higher creep rate. For both foams, a higher stress (larger initial strain) led to a higher creep rate up to a deflection of 20% to 30% where it goes through a maximum. This deflection range where the creep rate is the highest is in the range where buckling occurs as described by Gibson and Ashby.⁵⁷ At further increases in the initial deflection, a decrease in the creep rate was observed. This deflection dependence of the creep rate is shown in Fig. 2.36, which is a plot of the creep rate versus initial deflection. Campbell qualitatively explains this phenomenon using the analogy of the buckling of a column. This buckling mode of failure is illustrated in Fig. 2.37. As the column is initially loaded, it will store much of the energy. Further loading causes the column to fail leading to large increases in strain. Campbell suggested that based on these results caution must be taken when evaluation of the processing or chemical aspects of the foams as how they influence the creep behavior.

In varying the density of the foam by packing the mold, changing the water content or changing the blowing agent content, Campbell found that only the altering of the water content had an influence on the creep behavior. More specifically, he concluded that increasing the water content caused an increase in the creep rate. Also, the creep rate was reduced following a 2 hr. postcure over that after a 20 min. postcure. Finally, Campbell tested the creep recovery of foams by first subjecting them to 400 hrs of dynamic compression loading and then testing them. The results showed a marked increase in the creep rate. Another sample was loaded for 2 hrs, unloaded for 4 hrs, loaded for 2 hrs and unloaded for 16 hrs. This process was repeated four times and tested, and also repeated seven times and tested. Here, the results showed an increase in the strain levels but a

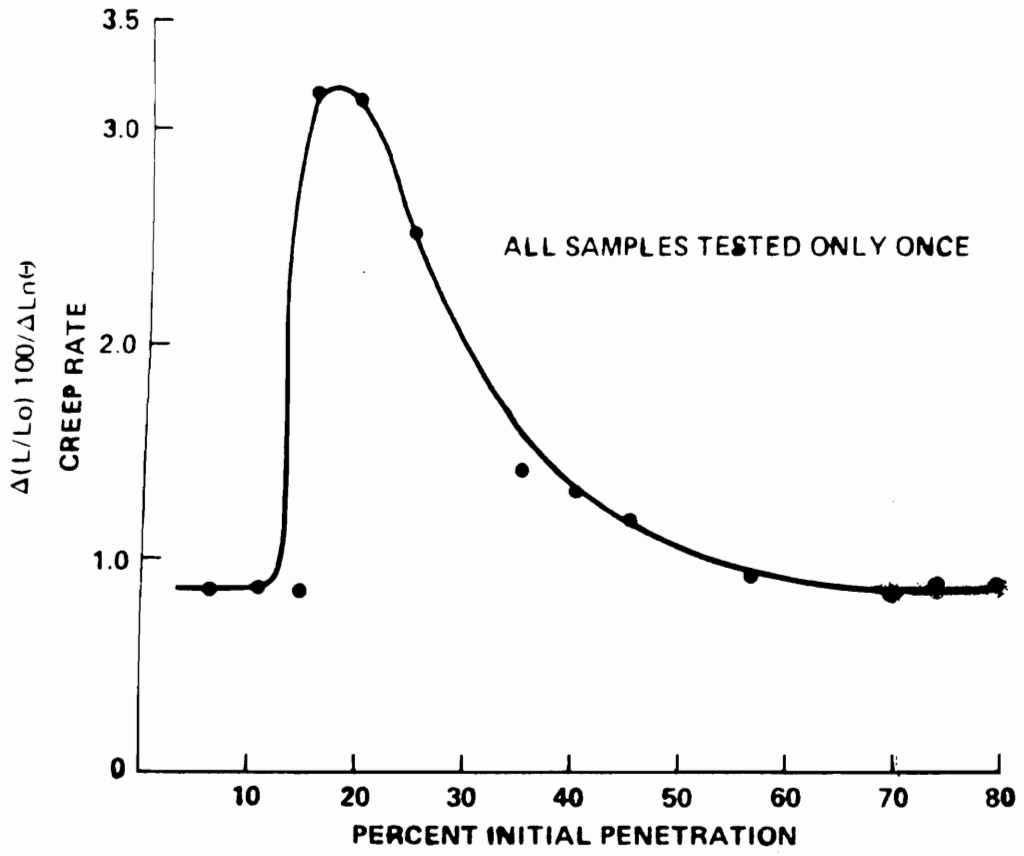


Figure 2.36. Creep rate as a function of initial penetration. [ref 80]

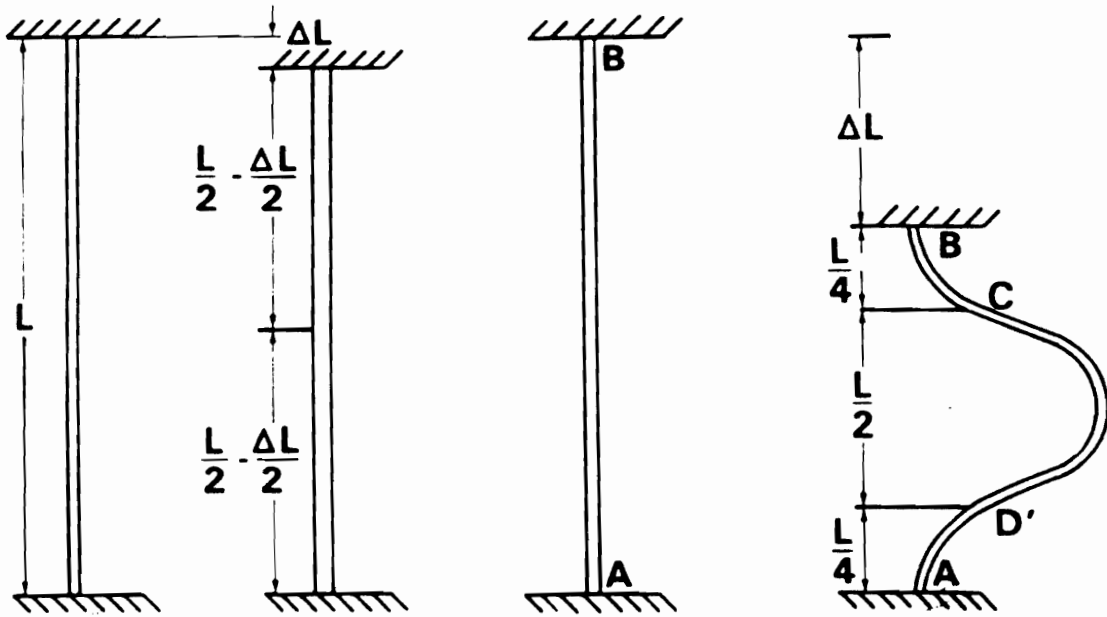


Figure 2.37. Long column buckling. [ref 80]

decrease in the creep rate for the sample that had undergone seven cycles over that which had undergone four cycles.

Moreland monitored the compressive creep behavior of flexible slabstock polyurethane foams for different loads, temperatures and relative humidity.⁷⁹ In Fig. 2.38, the compressive creep behavior is shown for two foams varying in hard segment content. Moreland reported that in all cases the behavior displayed a short induction period as shown by these curves. Following this initial induction period, the behavior was rather linear with log time for the three hour period. As evident in Fig. 2.38, as the hard segment content was increased, the creep rate also increased which was attributed to an increase in hydrogen bonding and their disruption. The creep rate displayed a strong dependence on the initial strain similar to the findings of Campbell. More specifically, the creep rate displayed a maximum with initial strain (at ca. 40%) which was attributed to cell buckling. As mentioned earlier, the buckling of the struts occurs in the range of 10% to 60% strain. Outside this range, the creep behavior is independent of cellular structure as suggested by both Campbell and Moreland. From the initial buckling of the strut, the creep rate simply increases as the localized strain increases.

The effect of temperature on the creep behavior was also investigated by Moreland. He first observed a non-linear creep response in logarithmic time at temperatures of 100°C or above. The creep rate initially decreased and then increased with temperature. Moreland claimed that the decrease in creep rate indicates that the approach to equilibrium is accelerated. The amount of viscoelastic decay increased with increasing temperature. The effect of temperature was greater as the hard segment content was increased that was attributed to more hydrogen bond disruption. At temperatures greater than 100°C, the amount of creep and the creep rate increased dramatically and with greater effect on the lower hard segment foams. This was attributed to additional mechanisms such as chain scission occurring in the urea and urethane groups.

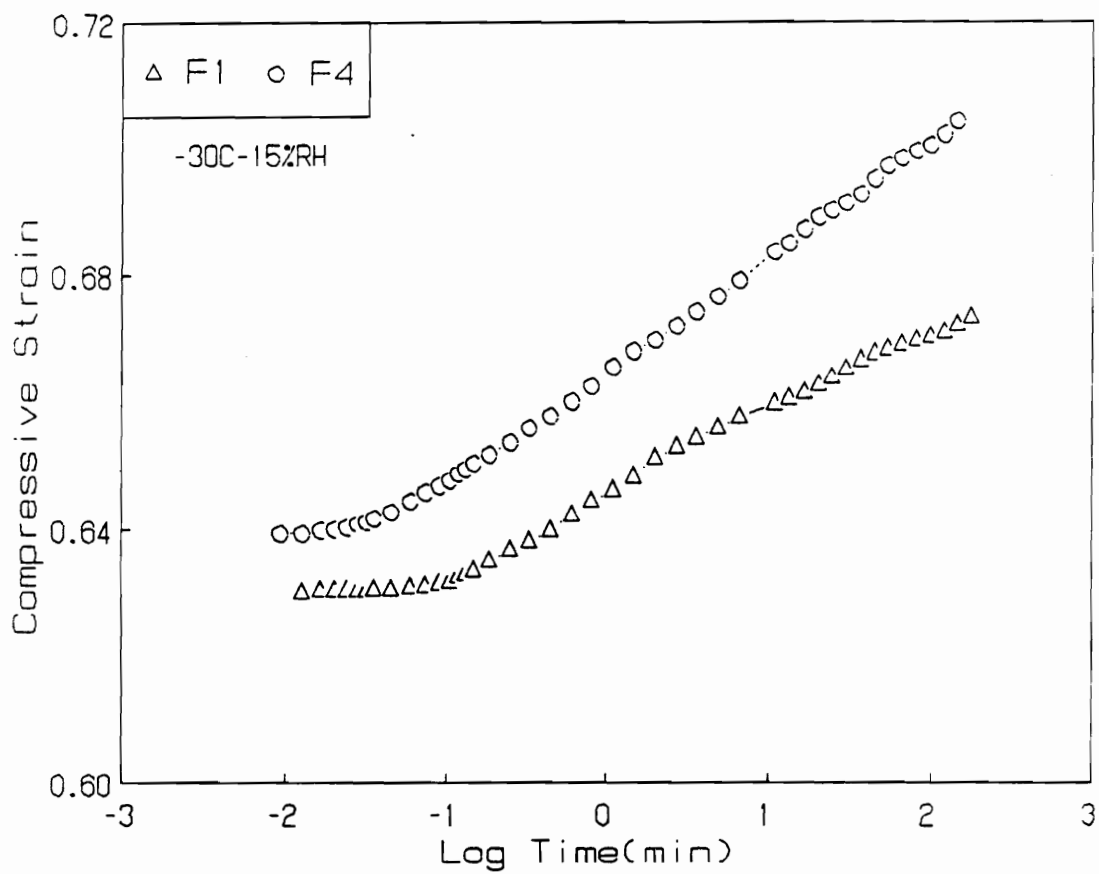


Figure 2.38. Compressive creep behavior for two foams varying in hard segment content. [ref 79]

As for the effect of relative humidity, Moreland reported that increasing relative humidity resulted in an increase in the creep rate. This behavior was more significant for a lower hard segment content foam. The increased humidity allows for water to act as a "plasticizer" allowing for further chain slippage to occur primarily at higher temperatures where the hydrogen bonds within the hard segments are weakened. This, in turn, allows for the penetration of water.

2.3.3.c Compression Set

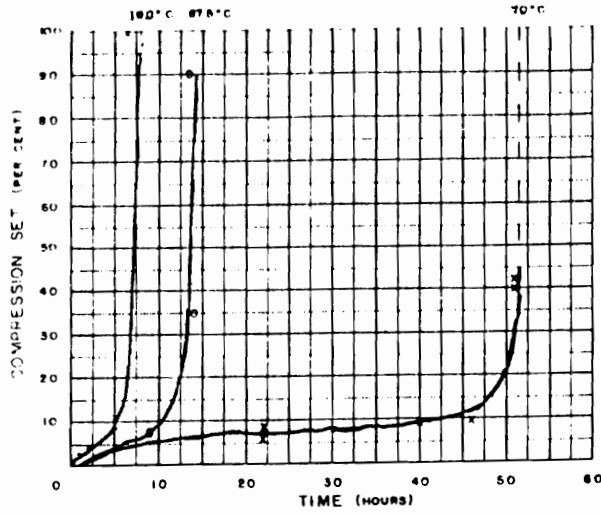
Compression set experiment is most widely measured property in evaluating the viscoelastic nature of foams since it best simulates end use. Typically, a compression set test involves compressing a foam sample to either 50, 75, and 90% of the sample's original height and held there at 70°C for 22 hr.⁶ The sample is then removed and allowed to recover for 30 min. The results for slabstock foams are reported as a percentage of the original thickness where for molded foams, the results are given as a percentage of the original deflection.

Compression set has been studied by several authors most of which have evaluated the formulation components such as water content or environmental conditions such as humidity.⁹³⁻⁹⁸ For example, Herrington and Klarfeld have studied the effects of temperature, humidity, and water content on the compression set properties of a series of molded foams.⁹³ They found that as the temperature was increased, the compression set level also increased. If the samples were treated to high humidity prior to the compression set experiment referred to as humid aged compression set (HASET), the compression set levels were dramatically increased and increased further as the temperature was increased during the humid aging. They also found that as the water content was increased, the compression set also increased in agreement with the trend reported by Patten and Seefried as well as Saotome.^{94,95} Herrington and Klarfeld attributed this behavior with the help of

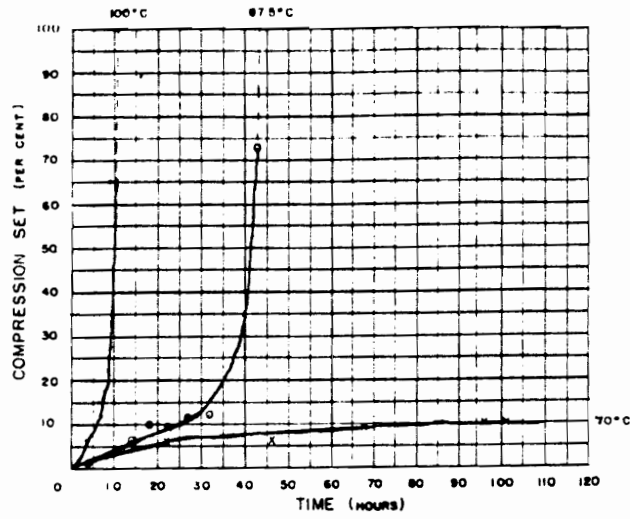
ATR spectroscopy to urea concentration; more specifically, hydrogen bond disruption. At high temperatures and humidity, intermolecular hydrogen bonds are disrupted by the water forming new hydrogen bonds. During the compression set process the foam is stressed at rather high temperatures (ca. 70°C) disrupting the new hydrogen bonds with water molecules driving the water away and leaving behind free volume which allows for chain slippage. The authors also noted that the isocyanate index had no influence on the compression set and that the foams exhibited recovery of the compression set which was enhanced at higher temperatures.

Terry also carried out compression set tests on flexible polyurethane foams.⁹⁶ Figure 2.39 represent the results where the compression set in plotted as a function of time under compression for three different temperatures and three different levels of deflection. Each curve showed a yield point where the slope dramatically changed from horizontal to vertical. As can be seen, the tests conducted at higher temperatures and higher deflections allowed for levels of compression set to be reached in shorter times consistent with previous authors. Also, any changes in temperature or deflection did not affect the location of the yield point in terms of the level of compression set but only the time to reach this point. The compression set was attributed to a decay in the restoring forces which come about from potential energy created where anchor points are strained. These anchor points are attractive forces between adjacent molecules such as covalent cross-links or secondary bonding forces such as hydrogen bonds. When the strain energy, for example, is greater than the activation energy for viscous flow, the potential energy decays. New secondary forces are now formed in the compressed state resisting the restoring forces and which after a period of time approach the magnitude of the restoring forces and a new equilibrium is formed. Thus, following removal of the load, no or little recovery occurs near the yield point. Terry was able to fit the data to a hyperbolic curve from which he calculated the compression set for a different set of conditions. He was also able to relate and predict the critical time (time to reach yield point) for one set of conditions to that of another. Terry

(A)



(B)



(C)

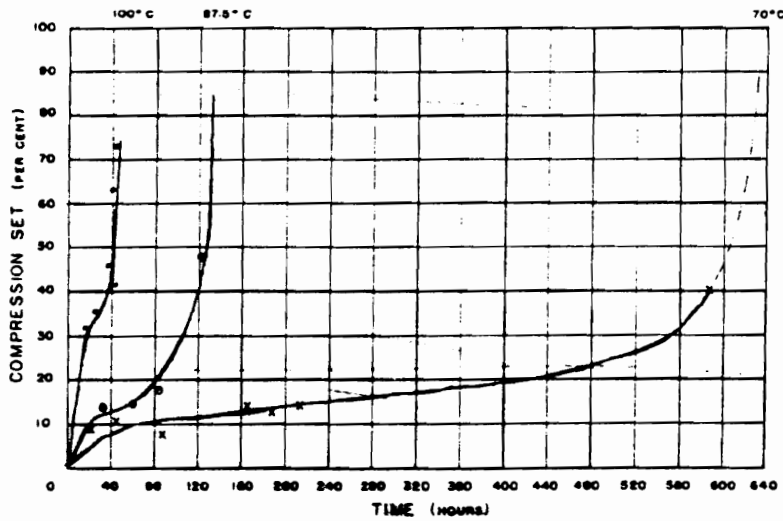


Figure 2.39. Compression set tests at (A) 90% deflection, (B) 75% deflection and (C) 50% deflection. [ref 96]

also conducted some stress relaxation studies on the same material. From the relaxation data, he was able to relate the stress relaxation to the compression set in terms of the initial and final loads and the initial and final heights of the foam. From this, Terry concluded that the same mechanism governs both stress relaxation and compression set.

Recently, Skorpenske et. al. presented a treatise on compression set and its mechanism. They found that both the physical "cross-links" and covalent cross-links can be used to describe this phenomenon. When evaluating the influence of TDI index on compression set, they observed an abrupt transition at ca. 100°C where the lowest index foam displayed the greatest compression set. Above or below this temperature, the differences between foams of different index foams were small. Again a higher hard segment content, higher temperatures and higher humidities increased the amount of compression set. A discontinuity was observed in the compression set data at ca. 100°C where the set dramatically increased. This was attributed to stress yielding of the hard segment domains. When the humidity was increased, the temperature at which this discontinuity occurred decreased due to the "plasticizing" effect. They found that by annealing the samples thereby improving the hard segment organization, the compression set improved. The covalent network of the foam impacted the recovery phase where the recovery is induced by the elastically active covalently cross-linked chains and which increased with increasing temperature. Finally, Skorpenske et. al. discovered that the cellular structure (density, cell-openness) had no bearing on the compression set.

2.3.4 Mechano-Sorptive Behavior

The effect of transient moisture sorption on the mechanical properties of hygroscopic materials is termed mechano-sorptive behavior.⁹⁸ Transient moisture conditions can affect the performance and mechanical properties of many materials and are of importance where materials are used for structural purposes. This phenomenon was

noted and systematically studied nearly thirty years ago primarily on wood and wood based products.^{99,100} More recently, studies have extended to paper, specific fabrics, natural fibers, and synthetic fibers, all of which have a common characteristic of molecular hydrogen bonding.¹⁰¹ Cyclic moisture conditions have been found to greatly increase the creep level over the creep level at the highest constant moisture content in the same time period as is shown in Fig. 2.40 where Hearmon and Patton showed the effect of cycling moisture on the deflection of Beech wood.¹⁰² Humphries and Schniewind observed this effect in Douglas-fir columns where the creep level was two orders of magnitude higher under transient moisture conditions than that observed when in a high constant humidity environment.¹⁰³ Hunt showed that in wood based panels, creep levels were three orders of magnitude larger under cyclic moisture content than under a high constant moisture.¹⁰⁴ Very recently, Wang and Dillard conducted similar tests on Kevlar® fibers and Kevlar® composites.¹⁰¹ They found that the level of creep was approximately 50% greater in cycling humidity and that the slope of a plot of creep versus log time, or the creep rate, increased dramatically when the moisture content was cycled either to lower or higher levels. Transient moisture conditions have also been noted to reduce the creep rupture life leading to failures in shorter times and lower loads. For example, Schniewind found that the creep rupture life of Douglas-fir beams was reduced by an order of magnitude when the moisture was cycled.^{105,106}

Many mechanisms have been proposed, yet one which fully explains such behavior has not been provided. However, the most widely accepted is that the entering and departing water molecules temporarily alter the localized hydrogen bonded structure - a common feature to all materials displaying the mechano-sorptive phenomenon. Based on this mechanism, originally proposed by Gibson, absorption of moisture disrupts the original bonds allowing for slippage.¹⁰⁷ Hoffmeyer and Davidson have proposed a "slip plane" mechanism.¹⁰⁸ After having observed failures at distinct planes through polarized microscopy, they proposed that the number of slip planes is affected and proportional to the

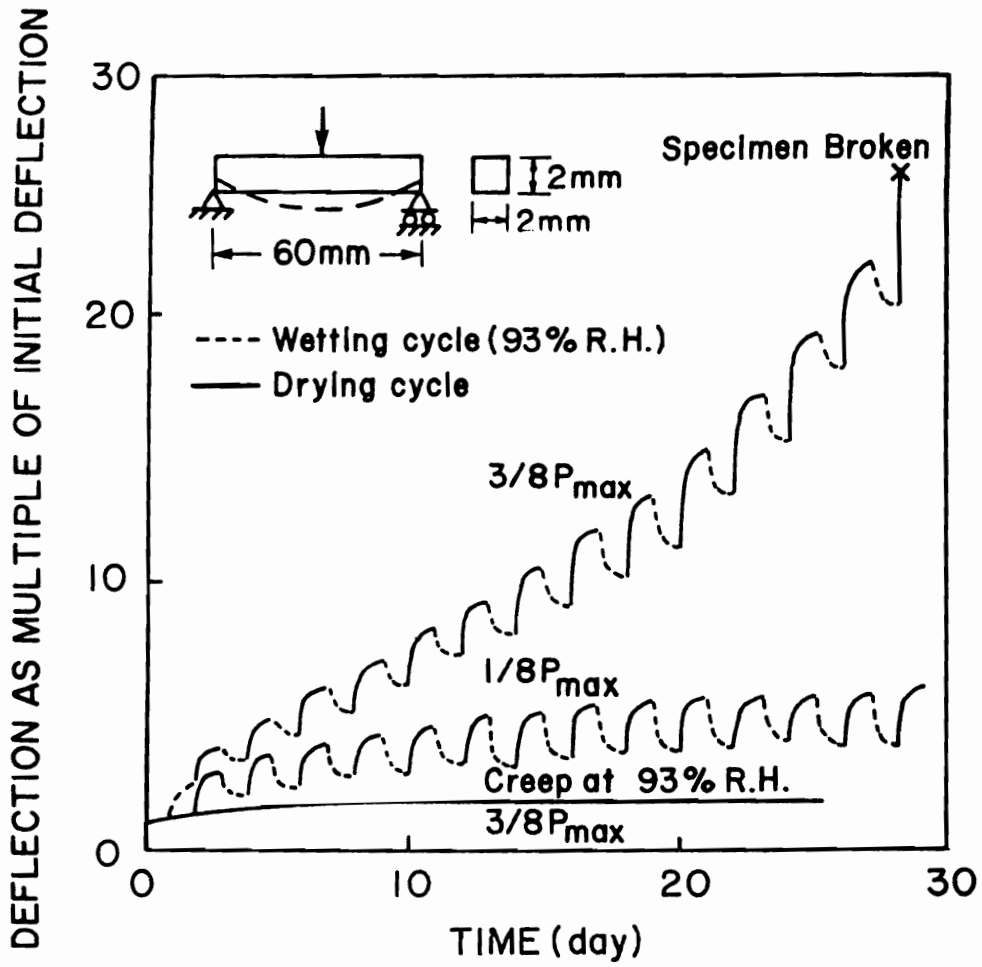


Figure 2.40. Creep and delayed failure of beech wood under cyclic moisture conditions. [ref 102]

amount of moisture change. In the case of Kevlar fibers, Wang and Dillard proposed a "crystallite rotation and slippage" mechanism.¹⁰¹ This mechanism proposes that during a absorption process, water molecules disrupt the hydrogen bonds which, in turn, allows for flow units (crystallites or molecular chains) to slip relative to each other and rotate towards the loading direction. Van de Put proposed that the mechano-sorptive behavior is due to the onset of "holes" or flow units which allow for an increase in molecular mobility.¹⁰⁹

2.4 Summary

Although polyurethane foams are found in many applications, the majority of them are used in furnishings. These foams are produced via the reactions between isocyanates, water, and polyols. From these reactions, CO₂ gas is given off which blows the foams resulting in a cellular structure. If both the solid phase and fluid phase are continuous, the foam is said to be open-celled. The morphology of the solid portion is typically a heterogeneous phase-separated morphology where discrete polyurea hard segment domains are dispersed within a continuous soft phase. These domains enhance the mechanical properties of the foam by acting as virtual "cross-links". These hard segments are strongly hydrogen bonded, usually between an N-H group and a carbonyl group. The hydrogen bonds also have a great influence on the mechanical properties.

There is an enormous amount of literature on polyurethanes and on their mechanical properties. There is also a large amount of literature concerning modeling, specifically on basic properties such as modulus and stress-strain properties on cellular solids in general. However, there is a relatively small amount of literature on the viscoelastic behavior of flexible polyurethane foams and an even smaller amount on molded polyurethane foams which is increasingly the process of choice in the production of polyurethane foams. The next few chapters describe the objectives of the present research as well as the results and conclusions which aim to characterize and relate the structure, morphology, and the

viscoelastic behavior of molded polyurethane foams to obtain a better understanding of these materials as presently exists for conventional slabstock foams.

Chapter 3

3.0 EXPERIMENTAL MATERIALS AND METHODS

3.1 Materials

In evaluating and pursuing the structure-property behavior of flexible polyurethane foams, the foams to be studied were formulated such that certain components were systematically varied to provide trends and allow for their influence on the bulk properties. To accomplish this, many series of foams were made, both molded and slabstock, where in each series a specific ingredient was varied. These samples reflect the activities of the evolving polyurethane foam industry which is rapidly moving to quicker, more efficient production cycles. In addition, certain formulation ingredients, such as auxiliary blowing agents, are in the process of being eliminated thereby requiring other methods of influencing cell-openness and density. Overall, 19 foam samples were made utilizing basically two techniques described below. The main area of interest within this research concerned the structure-property of molded foams. As mentioned earlier, the molding process as well as certain formulation additives in this class of foams provides many advantages over slabstock systems but at the same time also produces more challenges.

The molded samples of flexible water-blown polyurethane foams were made with a Hi-Tech RCM 30 foam machine at Dow Chemical in Freeport, Texas. This operation

consists of two hydraulic pistons to dispense the liquid components to the mixing head. The formulation components presented in Table 3.1A were prepared in two storage tanks, A and B. The A side consisted of the isocyanate. The B side consisted of the polyols, water, surfactants, and catalysts. Each stream consists of an adjustable orifice which allows for control of the impingement pressures into the mixing head. For example, the pressures were 1500 psig and 2100 psig for the B side and A side, respectively for the 2 pph water content foams. For the 4 pph water content foams, they were 2040 psig and 1785 psig for the B side and A side, respectively. After mixing, the mixture was poured (having a 6 sec. shot time) into a heated aluminum mold having dimensions of 15"x15"x4.5". This mold was heated to 140°F (60°C) before the foam mixture was dispensed into it. In 1.5 min. following the appearance of completed rise, the mold was then placed in an oven at 250°F (121°C) for 2.5 min. after which the foam was removed and immediately mechanically crushed. The mechanical crushing was accomplished by passing the pads through two steel rollers three times which is a common industrial practice for molded foams. The nomenclature of the samples presented in Table 3.1A is as follows: the letter "F" denotes a foam sample, the letter "m" denotes a molded foam sample, the third letter denotes the copolymer polyol used - "o" refers to no CPP utilized, "c" refers to a conventional CPP, "e" refers to an experimental CPP, and finally the number denotes the water content.

As mentioned in Chapter 2, a major objective when formulating molded foams is to decrease demold times thus increasing productivity. In view of this goal and other inherent challenges associated with molded foams such as cell opening, a higher number of components are utilized thereby making the overall formulation and reaction scheme more complex than that used for the simpler conventional formulations of slabstock systems such as those studied by Armstead and Moreland within this document.^{33,79} The molded foams studied in this dissertation used a blend of polyols where the base polyol in each foam was a 5000 g/mole molecular weight polyethylene oxide capped polypropylene oxide polyol that

Table 3.1A. Formulation Components of Molded Foams

Foam	Fmo4	Fmo2	Fmc4	Fmc2	Fme4	Fme2
V4703	100.00	100.00	50.00	50.00	64.70	64.70
CPP	0.00	0.00	50.00	50.00	35.30	35.30
WATER	4.00	2.00	4.00	2.00	4.00	2.00
DEOA	1.60	1.60	1.60	1.60	1.60	1.60
Y-10515	0.50	0.50	1.08	1.08	1.08	1.08
DC-5244	0.50	0.50	0.54	0.54	0.54	0.54
DC-5169	0.50	0.50	0.00	0.00	0.00	0.00
DABCO 33LV	0.34	0.34	0.43	0.43	0.31	0.31
NIAX A107	0.26	0.26	0.32	0.32	0.32	0.32
NIAX A4	0.26	0.26	0.32	0.32	0.32	0.32
XUS 16053	1.00	1.00	0.00	0.00	0.50	0.50
TDI-100 Index % Isocyanate	48.40	29.04	47.68	28.32	47.5	28.18
Density lb/ft ³	2.0	3.4	1.9	3.3	1.9	3.3

The values in the table designate the formulation amounts in terms of pph by weight of polyol.

The functions of each of the chemicals listed above are as follows: V4703 - 5,000 molecular weight glycerol initiated ethylene oxide capped propylene oxide; CPP - copolymer polyol particle based on styrene-acrylonitrile, these react into the network but are essentially reinforcing fillers (Table 3.1 (b). for greater details); Water - blowing agent; DEOA - diethanol amine, a cross-linking agent; Y-10515, DC-5244 - stabilizing and cell opening surfactants, respectively; DC-5169 - a surfactant used to control and eliminate basil cells (large irregular cells just beneath foam surface); DABCO 33LV, NIAX A107, NIAX A4 - tertiary amines primarily used for gelling, surface cure and blowing catalysts, respectively; XUS 16053 - cell opening polyol; and TDI - an 80/20 blend of the 2,4- and 2,6- isomers of toluene diisocyanate.

Table 3.1B. Copolymer Polyol Formulations

Copolymer Polyol	Control (Fmc4, Fmc4)	Experimental (Fme4, Fme2)
Base Polyol	62.5	62.25
Styrene	17.5	24.5
Acrylonitrile	7.5	10.5
Stabilizer*	12.5	2.75
VAZO		

Values designate weight percentages.

* Stabilizer used in control copolymer polyols is isocyanate capped triol and the stabilizer used in the experimental copolymer polyols is an isocyanate capped diol.

was initiated using glycerol. The polyethylene oxide capping was used in view of its more reactive primary hydroxyls which are 3x faster than the secondary hydroxyls provided by polypropylene oxide. This polyol contained ca. 20% EO capping which provided ca. 90% primary hydroxyls. Blended with the base polyol was a styrene/acrylonitrile copolymer dispersion phase commonly referred to as a copolymer polyol (CPP) which resulted in ca. 12.5% solids in the final foam. The make up of the CPP dispersion is shown in Table 3.1B which reveals that a stabilizer was included to improve wettability and dispersity of the particles and to some degree covalently grafts the particles to the base polyol. The two types of copolymer polyols used varied in the stabilizer molecule; functionality of and amount. As can be seen in Table 3.1B, the control copolymer polyol, V4925, utilized an isocyanate capped triol as the stabilizer while the experimental copolymer polyols utilized an isocyanate capped diol as the stabilizer. The inclusion of copolymer polyols is carried out to improve the firmness of the foams. Specifically, the indentation force deflection (IFD), one of the most widely measured properties of foams in industry is typically ca. 25% higher than that of foams lacking the particles. They also improve the processing latitude, demold times, and other mechanical properties such as tensile properties. The processing latitude is very important since a correct balance of the gelling and blowing reactions is required to produce a viable foam. Any disturbance to this balance can result in either complete collapse or severe shrinkage depending on the sequential occurrence of the gelling and blowing reactions. In view of the shorter production cycles, diethanolamine (DEOA) is added to increase the amount of cross-linking thereby providing a cross-linked polymer at the time of cell-opening which is crucial for stability of the foam. As can be seen in Table 3.1A, only a small amount by weight of DEOA is added relative to the amount of polyol. However, because of the much lower molecular weight of DEOA, the amount of functional groups supplied by the DEOA approaches the amount supplied by the polyol. For example, 2g of 105 molecular weight DEOA molecule gives nearly the same amount of functional groups as 100g of a 5000 molecular weight polyol molecule. The

inclusion of DEOA has some adverse effects such as reducing cell openness and the processing latitude requiring more extensive cell opening measures. These measures are reflected in the number of surfactants and catalysts used. For example, two stabilizing and cell opening surfactants are utilized. A common gel catalyst used in slabstock foams, stannous octoate, is omitted here which is not surprising since both the EO capping and DEOA enhance gelling. Instead, three catalysts, which are basically tertiary amines, are included which are generally regarded as blowing catalysts although they do have some minimum influence on the gelling reactions. The two other very important formulation components are water and the isocyanate. The isocyanate utilized was toluene diisocyanate (TDI) and was varied according to the water content. The higher water/TDI content foams had a lower density as the amount of CO₂ was increased. As will be shown in later chapters, the higher water/TDI content foams also contained a higher hard segment concentration. In addition, the TDI included relative to the weight amount required is referred to as the TDI index. In the molded foams, the index was 100 thereby signifying that just enough TDI was present to react, in principle, with all the active hydroxyls.

The molded foams lacking the copolymer polyols, whose formulation components are also given in Table 3.1A, were formulated to evaluate the influence of the CPP particulates. While the omitting of the CPP particles was the major difference, there were also some other minor variations which were necessary in order to produce a quality foam. The lack of the CPP dispersion required that an additional surfactant be utilized, DC-5169, which is regarded as a surfactant that eliminates basil cells, large irregular cells beneath the surface. In addition, the amount of XUS 16053, a proprietary additive which aids cell opening, is higher than in the experimental CPP containing foams. The other components are roughly the same in concentration as in the CPP containing foams.

Conventional slabstock water-blown foams which are used for research and development are produced using laboratory box-foaming machines. The conventional slabstock foam sample utilized in this study as a basis for comparison to the molded foams

was also made at Dow Chemical in a box-foaming operation. The ingredients utilized for this foam are shown Table 3.2. Here the components were prepared in three cycles; premix cycle, tin catalyst cycle, and isocyanate cycle. The specific process was as follows. First the polyol, surfactant, water, and amine catalysts were mixed for 30 sec. at 900 rpm. using a pin type 8 hp electric mixer. The tin catalyst was then added and the components were mixed for an additional 30 sec. Finally, the isocyanate was added and mixing took place for 5 sec at 1200 rpm at which point the components were poured into an open box having dimensions of 15"x15"x12" and allowed to cure. Following pour, the cream time, the amount of time it takes the mixture to begin to rise after pour, was noted which is typically ca. 10 - 15 sec. The so called rise is completed in ca. 150 - 200 sec. following the pouring of the components into the box. As the foam cools it continues to cure, the time of which strongly depends on the size of the foam pad. For example, commercial foams which can have dimensions of 50' x 10' x 5' exhibit higher temperatures for longer times than the experimental foams produced here. Furthermore, the temperatures of molded foams which are considerably smaller in size are even lower and cool rapidly. Typical maximum temperatures for a 4 pph water content slabstock foam are ca. 160°C (reached in ca. 50 min. following mixing) whereas typical maximum temperatures for a 4 pph water content molded foam are ca. 140°C (reached in less than 2 min.).

Compared to the molded foams, the slabstock foams utilized fewer and simpler components in its formulation. The polyol was a 3000 molecular weight, all polypropylene oxide initiated with glycerol. Although slower reacting, this polyol is more hydrolytically stable and less expensive and since time is not as much of an issue in fabrication, it is generally the polyol of choice for conventional slabstock systems. The isocyanate used was an 80/20 blend of the 2,4 and 2,6 isomers of toluene isocyanate, the same used in the molded foams. The water content was 4 pph which required ca. 50 pph of TDI at an index of 110 which is common for conventional slabstock foams. Two catalysts were utilized;

Table 3.2. Formulation Components of Slabstock Foams

Foam	F s2	F s4
V-3100	100	100
WATER	2	4
BF 2370	1	1
T-9	0.15	0.15
DABCO 33LV	0.3	0.3
TDI	30.79	52.06
Density lb/ft ³	1.9	1.4

The values in the table designate the formulation amounts in terms of pph by weight of polyol.

The functions of each of the chemicals listed above are as follows: V3100 - 3,000 molecular weight glycerol initiated propylene oxide polyol; Water - blowing agent; TDI - a blend of isomers of toluene diisocyanate; BF-2370- a silicone surfactant; T-9 - a tin catalyst commonly known as stannous octoate; and DABCO 33LV- tertiary amine primarily a blowing catalyst.

stannous octoate (T-9) which is regarded as a gelling catalyst and triethylenediamine in dipropyl glycol (DABCO 33LV) which is regarded as a blowing catalyst. Finally, a silicone surfactant (BF2370) was utilized. As can be seen less surfactants and catalysts are needed to balance the reactions and produce a quality foam. This is mostly due to the fact that no additives are incorporated other than the basic three components.

Other foams were formulated to evaluate the influence of specific formulation ingredients used in molded foams. Specifically, those formulation components were DEOA and the polyethylene oxide capped polyols. The foam systems developed from varying these components are regarded as model systems since they can be neither classified as molded nor slabstock foams. The two series of foams were formulated using the box-foaming operation described above but one series incorporated ingredients typically found in molded foams such as the EO capped 5000 molecular weight polyol. The other series utilized typical slabstock ingredients with minor modifications. The first series consisted of three foams labeled FeD-x where the variable "x" denotes the DEOA content in pph and the "e" suggests that EO capped polyols were used. The formulation components of each are listed in Table 3.3A. As can be seen, the DEOA content is varied from 0 pph to 2.0 pph. Similar to the molded foams discussed above, the polyol was a 5000 molecular weight glycerol initiated EO capped polypropylene oxide polyol. Here, a lower amount of polyethylene oxide capping was used than in the molded foams. Approximately 5 - 10% capping was used resulting in ca. 70% primary hydroxyls. Polyol V4701 is considered a rather low reactivity polyol for molded foams relative to V4703 which is considered a high reactivity polyol. Again, one surfactant, one gelling catalyst and one blowing catalysts were used since a lower reactivity polyol was utilized. As the DEOA level was increased, the tin level was adjusted (decreased) accordingly as was the TDI. For this series, samples FeD-0 - FeD-2, the TDI index was 103, between that of the highly reactive molded foam components and that of the conventional slabstock foams.

The second series of foams formulated with varying amounts of DEOA were made

Table 3.3A. Formulation Components of Foams Utilizing EO Capped Polyols Varying in DEOA Content

Foam	FeD-0	FeD-1	FeD-2
V4701	70	70	70
XAS10921	30	30	30
DEOA	0.0	1.0	2.0
WATER	5.0	5.0	5.0
DC-5169	1.1	1.1	1.1
DABCO	0.12	0.08	0.08
T-9	0.19	0.15	0.15
TDI	55.3	57.9	60.4

The values in the table designate the formulation amounts in terms of pph by weight of polyol.

The functions of each of the chemicals listed above are as follows: V4701 - 5,000 molecular weight glycerol initiated ethylene oxide capped propylene oxide; DEOA - diethanol amine, a crosslinking agent; Water - blowing agent; DC-5169 - a surfactant used to control and eliminate basil cells; T-9 - a tin catalyst commonly known as stannous octoate; DABCO 33LV - tertiary amine primarily a blowing catalyst; and TDI - a blend of isomers of toluene diisocyanate.

Table 3.3B. Formulation Component of Foams Varying in DEOA Content

Foam	FD-0	FD-0.5	FD-1
V-2100	100	100	100
DEOA	0	0.5	1.0
WATER	5.0	5.0	5.0
DC-5160	1.2	1.2	1.2
DABCO-8264	0.12	0.12	0.12
T-9	0.23	0.23	0.25
TDI	59.0	60.3	61.5

The values in the table designate the formulation amounts in terms of pph by weight of polyol.

The functions of each of the chemicals listed above are as follows: V2100 - 3,000 molecular weight glycerol initiated propylene oxide polyol; DEOA - diethanol amine, a crosslinking agent; Water - blowing agent; DC-5169 - a surfactant used to control and eliminate basil cells; T-9 - a tin catalyst commonly known as stannous octoate; DABCO 8264 - tertiary amine primarily a blowing catalyst; and TDI - a blend of isomers of toluene diisocyanate.

using a conventional polypropylene oxide polyol. These are labeled as FD-x where again the variable "x" denotes the DEOA content and whose value is given in Table 3.3B along with the other formulation components. Here the "e" is omitted to denote that no EO capping is present. The polyol utilized in this series of foams is the same as that used in the conventional slabstock foam, a 3000 molecular weight glycerol initiated polypropylene oxide system. The other components are the same as those used in the FeD-x series.

The final study undertaken in this dissertation reflects the trend to eliminate auxiliary blowing agents and produce soft low density foams utilizing a high water content and low TDI index. This study therefore involved varying the TDI index from 85 to 110 and determine the influence on the structure-property behavior of a series of slabstock foams formulated in a box-foaming operation. The foams were formulated using a relatively new polyol which is presented with the other components in Table 3.4. The polyol was initiated using a blend of glycerol and sucrose resulting in a nominal functionality of ca. 3.2. The oxide was a copolymer of polypropylene oxide and polyethylene oxide where the EO content was ca. 13% and the primary hydroxyl content ca. 35%. The water content was held constant at 6 pph as were the silicone surfactant and amine catalyst at 1.1 and 0.12 pph, respectively. The tin catalyst was varied according to the TDI index.

3.2 Experimental Techniques

The majority of this work involved molded foams and specifically characterizing these materials in terms of their structure-property behavior and the interaction between this behavior and specific formulation ingredients. Many techniques were used to characterize the cellular structure, morphology and viscoelastic behavior of these foams such as scanning electron microscopy (SEM), transmission electron microscopy (TEM),

Table 3.4. Formulation Components of Slabstock Foams Varying in TDI Index

Foam	Fs85	Fs90	Fs95	Fs100	Fs105	Fs110
Polyol	100	100	100	100	100	100
WATER	6.00	6.00	6.00	6.00	6.00	6.00
BF-2370	1.10	1.10	1.10	1.10	1.10	1.10
DABCO 8264	0.12	0.12	0.12	0.12	0.12	0.12
T-9			Varied			
TDI	57.9	61.3	64.7	68.1	71.5	74.9
TDI-Index	85	90	95	100	105	110
Density lb/ft ³	1.25	1.25	1.25	1.25	1.25	1.25

The values in the table designate the formulation amounts in terms of pph by weight of polyol.

The functions of each of the chemicals listed above are as follows: Polyol - 2700 molecular weight triol utilizing sucrose/glycerol initiator blend; Water - blowing agent; TDI - a blend of isomers of toluene diisocyanate; BF-2370- a silicone surfactant; T-9 - a tin catalyst commonly known as stannous octoate; and DABCO 8264- tertiary amine primarily a blowing catalyst; and TDI - a blend of isomers of toluene diisocyanate.

differential scanning calorimetry (DSC), dynamic mechanical analysis (DMA), small angle x-ray scattering (SAXS), wide angle x-ray scattering (WAXS), fourier transform infrared (FTIR), solvent extraction, tensile and compression stress-strain, load relaxation, creep, and compression set. A number of these techniques were used to determine the influence of DEOA as well as TDI index on the specific properties mentioned above.

3.2.1 Scanning Electron Microscopy

The cellular structure of these foams was evaluated and compared using scanning electron microscopy (SEM). Thin slices (3 - 4 mm) of foam were first obtained using a razor blade which were then adhered to aluminum stubs using silver paint. After ca 24 hr. for drying, a thin layer of gold was applied to the surface of the foam using a SPI model 13131 sputter coater. Micrographs were taken using a Cambridge Sterioscan model 100 operating at 20 kv and at a magnification of approximately 30x. In some cases, the micrographs were obtained on a Philips model 505.

3.2.2 Transmission Electron Microscopy

Transmission electron microscopy (TEM) was used for two reasons. One, to evaluate the size distribution and dispersity of the copolymer polyol particles. The other objective concerned with the effect of DEOA on the precipitated urea based structures which have been reported to exist in certain slabstock foams as discussed in Chapter 2.³³ The same procedure was used for both cases. Thinner samples were cut in a similar manner to those for SEM. From these samples, very thin sections were cryogenically microtomed by the investigator using a diamond knife on a Reincart Junt model FC40 ultramicrotome operating at -90°C. Ethanol was used to collect the sections onto 600 mesh copper grids. Some micrographs were taken using a Zeiss 10CA transmission electron

microscope equipped with a LaB₆ electron gun operating at an accelerating voltage of 80 kv. Others were taken using a scanning transmission electron microscope (STEM) operating at an accelerating voltage of 80 kv.

3.2.3 *Differential Scanning Calorimetry (DSC)*

Differential Scanning Calorimetry (DSC) was used to observe thermal transitions. The thermal scans were obtained using a Seiko model 5200. The samples were first cooled to -140°C and then heated to 140°C, held there for 5 min., cooled again to -140°C, and finally heated again to 140°C all at 10°C/min.

3.2.4 *Dynamic Mechanical Analysis (DMA)*

Dynamic mechanical analysis (DMA) was carried out using a Seiko model 210 in the tension mode. The samples were heated from -100°C to 140°C at a rate of 1°C/min. from which the storage modulus (E') and tan δ data were collected at a frequency of 1 Hz. The sample dimensions were approximately 6.8 x 6.8 x 25 mm with a grip-to-grip distance of 10 mm.

3.2.5 *Small Angle X-ray Scattering (SAXS)*

Some qualitative features of microphase separation were evaluated using small angle x-ray scattering (SAXS) the scans of which were obtained with a Philips model PW1729 generator operating at 40 kv and 20 ma. The smeared data were collected using a Kratky camera with nickel filtered CuK α radiation having a wavelength of 1.542Å passing through a slit collimator (0.03 x 5 mm). The detector used is a Braun OED 50 position-sensitive platinum wire detector. The raw data were corrected for parasitic scattering and

normalized using a Lupolen standard. The foam samples were cut approximately 10 mm thick and compressed to ca. 3 mm. This was done to increase the amount of material exposed to the x-ray beam. They were placed in the x-ray beam approximately 25 cm from the detector.

3.2.6 *Wide Angle X-ray Scattering (WAXS)*

Wide angle x-ray scattering (WAXS) patterns were obtained using a Philips x-ray generator model PW1720, a Statton camera and a fine focus tube with nickel filtered $\text{CuK}\alpha$ radiation having a wavelength of 1.542Å. Foam samples were cut approximately 10 mm thick and compressed to approximately 3 mm. The sample-to-film distance was 8 cm and exposure times were ca. 10 hr.

3.2.7 *Fourier Transform Infrared (FTIR)*

Fourier transform infrared (FTIR) was used to study the hydrogen bonding within the hard segments of the foams focused on within this dissertation. the relative degree of order of the hard segments of the molded foams and slabstock foams and how this local order is influenced by the specified formulation variables. The spectral profiles were obtained on a Digilab FTS-40 spectrophotometer equipped with an attenuated total reflectance (ATR) cell. For each sample, 64 scans were averaged taken in the range of 4000 cm^{-1} to 400 cm^{-1} with a resolution of 4 cm^{-1} . All scans were normalized to the absorbance of a CH stretch at 2945 cm^{-1} . The regions studied were: the amide I region ($1620 - 1800\text{ cm}^{-1}$), the N-H region ($3100 - 3500\text{ cm}^{-1}$), and the isocyanate region ($2200 - 2400\text{ cm}^{-1}$).

3.2.8 *Extraction Studies*

Extraction experiments were carried out on selected samples to qualitatively determine the level of cross-linking and how it is influenced by specific formulation ingredients. Samples of various shape and size (< 0.15 g) were cut from the center of the foam bun, dried under vacuum at 40°C and weighed. The samples were submerged in DMF (ca. 10x by volume) for a period of 48 hr. The samples were then removed from the DMF, dried under vacuum at 40°C for approximately 24 hr. and finally at 80°C for approximately an additional 48 hr. The weight of the samples was taken incrementally throughout the drying process.

3.2.9 Load Relaxation Measurements

Load relaxation experiments were performed using a similar procedure as that used and described by Moreland which was originally designed to mimic the ASTM procedure used for IFD testing.⁷⁹ Samples, having dimensions of 3.5"x 3.5"x 1", were cut from the foam bun using a band saw equipped with a "wavy edge" saw blade. Each sample was first dried under vacuum and at 40°C for 3.5 hr to give each sample an equal level of moisture. The samples were then placed in an environmental chamber preset at the testing conditions for ca. 60 min. The environmental chamber was purchased from Russells Technical Products and was equipped with a Watlow 922 microprocessor which controls temperature in the range of 0°C to 300°C and humidity in the range of 0 to 100%. The chamber was fit into the Instron frame (shown in Fig. 3.1) equipped with a model MDB-10 compression load cell manufactured by Transducer Techniques. The load cell was positioned within an aluminum cup having a small hole through which the arm attached to the load cell can pass into the chamber for which the foam sample can rest. The cup protects the arm and thus load cell from large lateral movement which can damage the load

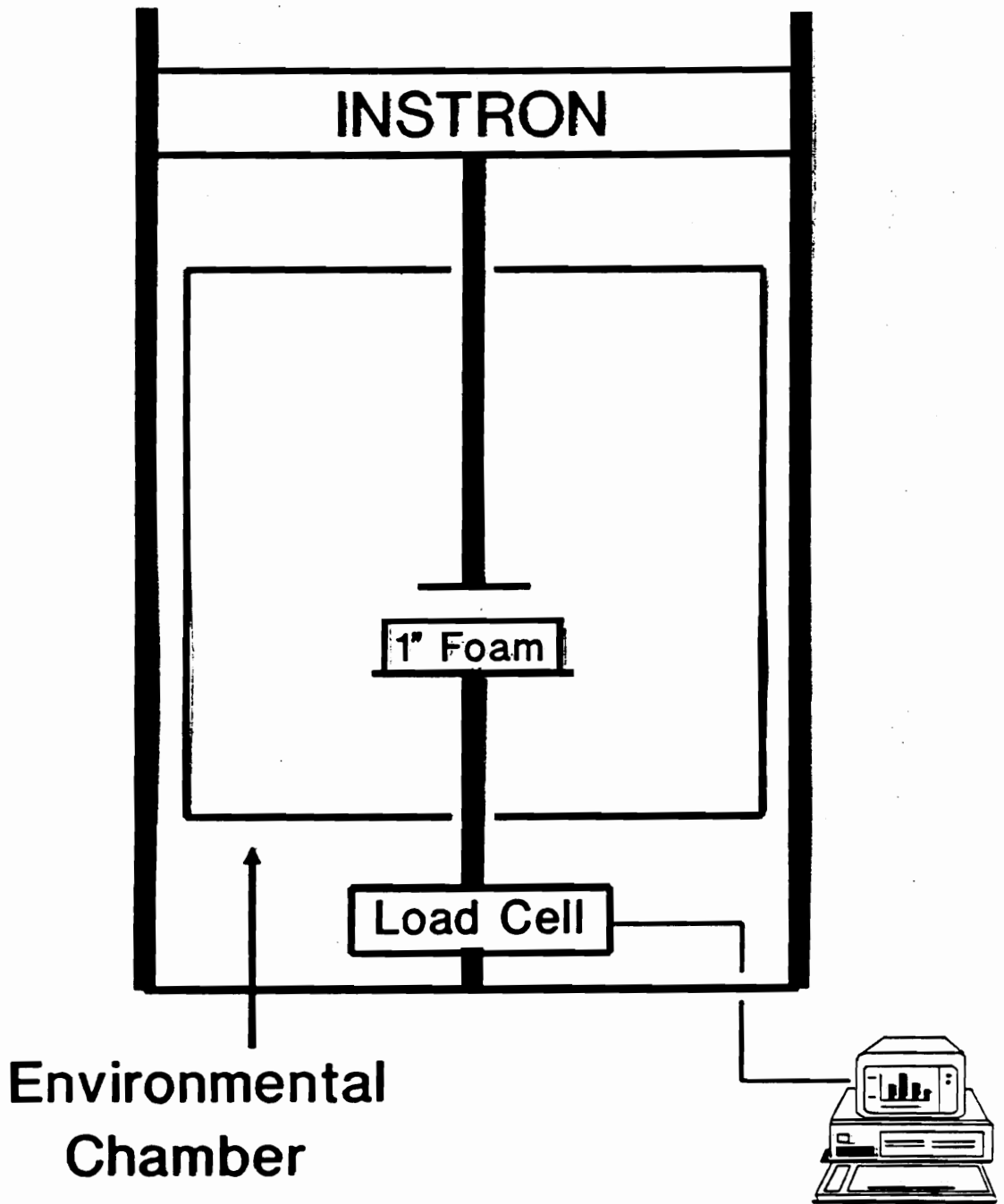


Figure 3.1. Illustration of load relaxation apparatus.

cell. Also illustrated in Fig. 3.1, this cup is also fitted with a line which provide a cool air purge to maintain temperature due to the load cell's sensitivity to temperature . The analog signal was converted to a digital signal using a QuaTech model ADM12-10 A/D converter from which the signal was sent to a computer.

Using a 2" indenter, initially at rest, the samples were twice compressed to 70% and released at a rate of 350 mm/min. After five minutes the samples were compressed to 65% strain at which point the load was immediately monitored via computer. The onset of densification for typical polyurethane foams occurs at approximately 65% compression above which relaxation occurs within the solid polymer independent of cellular structure.

3.2.10 *Compression Creep Experiments*

Compression creep experiments were carried out using a device consisting of a twin shaft assembly with a freely moving carriage manufactured by Thompson Inc. which is shown in Fig. 3.2 along with the environmental chamber. Attached to this carriage is an arm which extends into the environmental chamber and is capped with a 2" indenter. This indenter is initially set in contact with the top surface of the foam that is resting on a plate. Also attached to this carriage is the capillary of a linear voltage displacement transducer (LVDT) used to monitor any displacement in the thickness of the foams. The analog voltage signal is sent to a computer equipped with an A/D card converting it to a digital signal which is then converted to strain via a calibration procedure. As can be seen in Fig. 3.2, also attached to the carriage is a pulley system that enables the user to vary the applied load from approximately 100 g to 5 kg. Conditioning of the samples was carried out in a similar manner to the samples used in the load relaxation measurements. First, the samples were dried followed by a one hour conditioning in the environmental chamber. Following that, the arm with the indenter was allowed to freely drop compressing the foam while the strain was monitored.

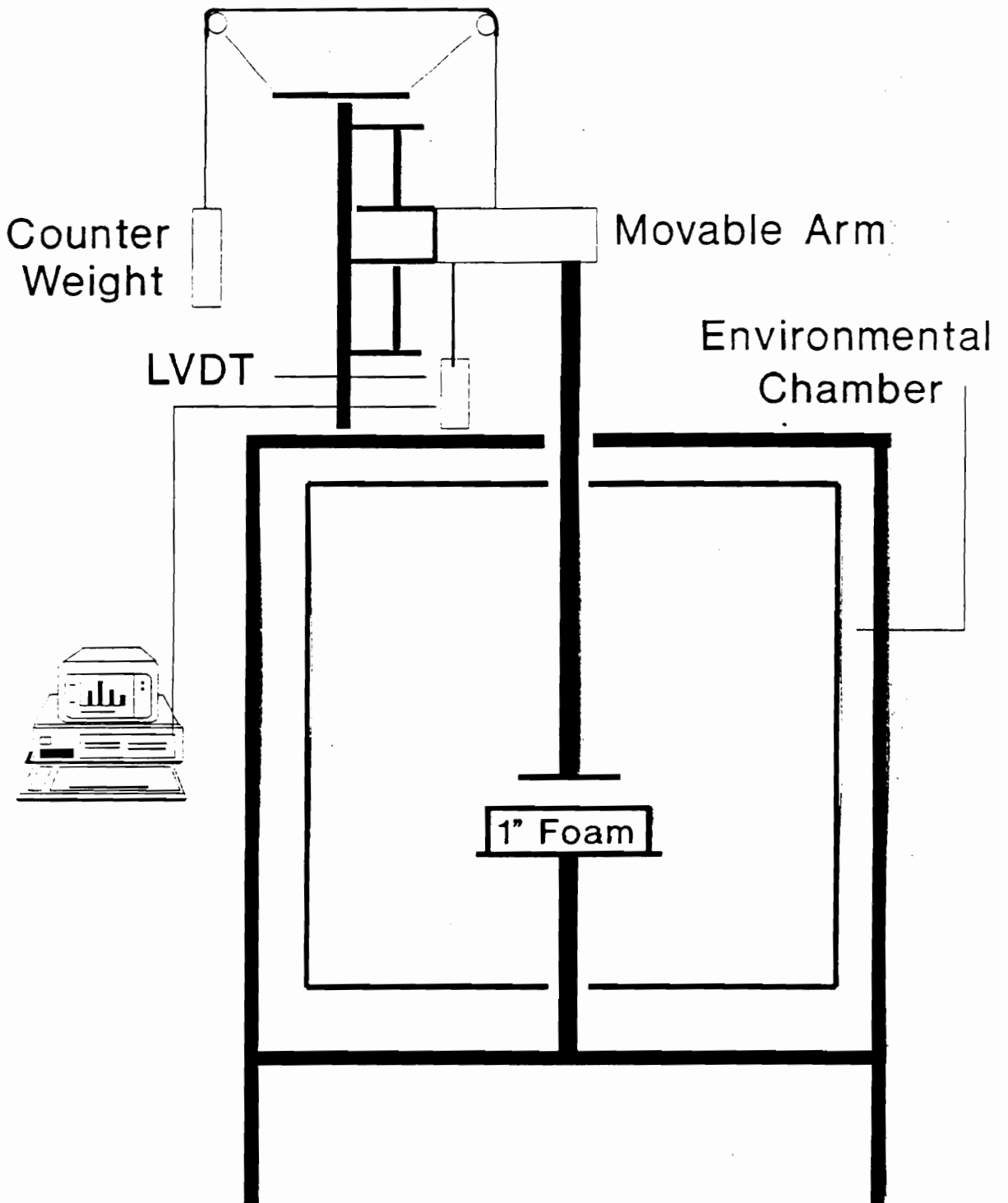


Figure 3.2. Illustration of creep apparatus.

3.2.11 *Compression Set and Recovery Experiments*

The procedure used for the compression set experiments was a non-ASTM procedure but was designed to reflect the load relaxation measurements. The samples were cut into dimensions of 2" x 2" x 1" in. and dried under vacuum for approximately 3.5 hr. They were then placed in the environmental chamber at the designated environmental conditions for one hour following which they were compressed to 65% for 3 hr. In completing the process, the samples were removed and placed in an oven set at 40°C after which thickness measurements were made.

Recovery experiments were carried out on the samples which displayed the greatest amount of compression set, specifically those carried out at 100°C-98%RH, in an attempt to recover some of the set. These samples which displayed considerable compression set were allowed to recover at room temperature for ca. a month. They were then placed in an oven at 100°C for one hr. This was done in an attempt to disrupt the hydrogen bonding and allow the elastically driven recovery to occur to relate it to the microstructure of the foams. Finally, the thickness of the foams were measured and the compression set calculated.

3.2.12 *Compression and Tensile "Stress"-Strain Determinations*

Compression load-strain measurements were conducted using the identical experimental setup used in the load relaxation measurements. An Instron frame equipped with a 10 lb compression load cell was utilized in conjunction with an environmental chamber. The 3.5"x 3.5"x 1" samples were first dried under vacuum and at 40°C for 3.5 hr and placed in an environmental chamber at 30°C-35%RH for c.a. 60 min. The samples

were then compressed at 15 mm/min. to ca. 80% strain and released. Data were collected using a computer as was done for creep and load relaxation.

Tensile stress-strain measurements were conducted using an Instron model 1122 equipped with pneumatic grips and again linked to a computer with an "in-house" program written in basic for data collection. The dogbone samples had dimensions of 2.8 x.6.7 x 24 mm with a grip to grip distance of 10 mm stretched at 3.6 mm/min.

3.2.13 *Mechano-sorptive Experiments*

The experimental equipment utilized for these experiments was the same as that used in the creep measurements. The mechano-sorptive procedure was different in that while the temperature and applied load were held constant, the relative humidity was cycled. A foam sample having dimensions of 4"x4"x1" was first placed in the chamber which was set at a constant temperature and approximately 10% RH. The foam was kept in the chamber for ca. one hour to reach the desired conditions in the chamber, the extension arm was released and allowed to drop onto the foam applying a constant load. A different load was used for each foam depending on the softness of the foam in order to achieve similar initial strains and to keep the creep response within the range of the LVDT. Following loading, the compressive strain was immediately monitored. After a period of ca. 60 min., the chamber humidity was rapidly increased to approximately 98%RH (occurring in a period of about 10 min.) while the computer continued to monitor the strain. After the specified amount of time, the humidity was then decreased again to 10%RH. This completed one absorption-desorption cycle. Each experiment consisted of 4 cycles excluding the initial loading cycle. The compressive strain was finally plotted versus time over the entire period of these four cycles.

Chapter 4

This chapter presents an extensive characterization of molded foams, specifically the structure-property behavior of these foams. As previously mentioned, molded foams are a newer, more complicated technology relative to slabstock foams and thus many of the observations are compared to those of conventional slabstock foams of equal water content. The important properties are the viscoelastic properties since these simulate the treatment of the foams in real applications. However, in order to best understand the displayed behavior, the microstructure and cellular structure are also investigated beginning with the cellular structure. Six foams varying in the content and structure of the copolymer polyols (CPPs) as well as the water/TDI content were used in this study designated Fmo4, Fmo2, Fmc4, Fmc2, Fme4, and Fme2. The important variables and some basic properties of each foam are shown in Table 4.4. Also given in Table 4.1 is that the foams with 4 pph water have a density of ca. 2 lb/ft³ while the 2 pph water foams have a density of ca. 3.3 lb/ft³.

4.1 Cellular Structure

The cellular structure of the molded foams was evaluated using scanning electron microscopy (SEM). These comparisons were made since the cellular structure of this class of materials significantly influences the physical properties of these foams as discussed in the literature review. The effects of altering certain formulation ingredients such as the

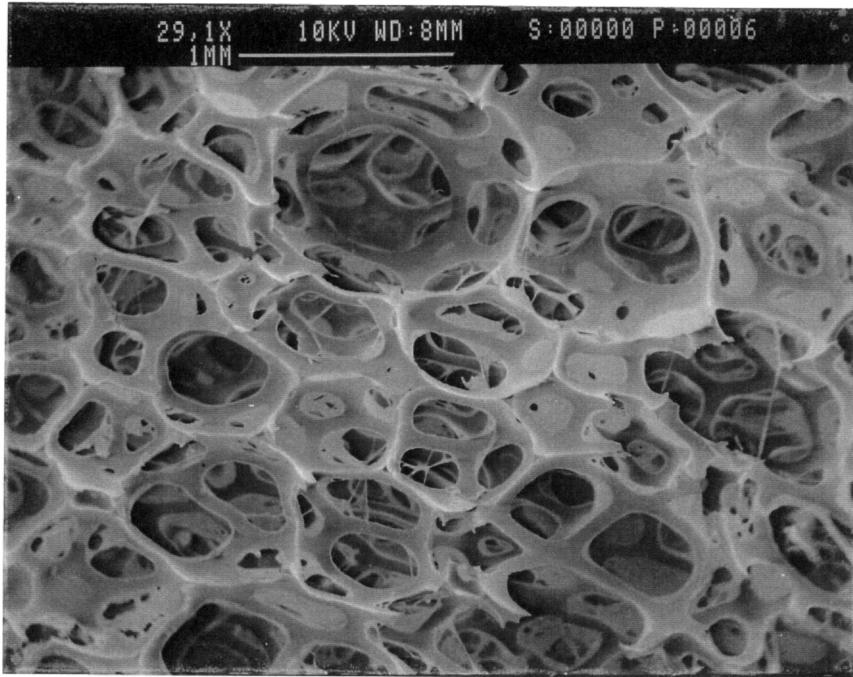
Table 4.1. Major Features of Molded Foams Studied

Foam	CPP	Water Content	Density, lb/ft ³
Fmo4	none	4 pph	1.9
Fmo2	none	2 pph	3.3
Fmc4	conventional ¹	4 pph	1.9
Fmc2	conventional ¹	2 pph	3.3
Fme4	experimental ²	4 pph	1.9
Fme2	experimental ²	2 pph	3.3

1. Based on graft copolymers of 3:1 ratio of styrene and acrylonitrile stabilized with 12% by wt. of isocyanate capped triol
2. Based on graft copolymers of 3:1 ratio of styrene and acrylonitrile stabilized with 3% by wt. of isocyanate capped diol

water/TDI content and copolymer polyols (CPP) were also targeted. This evaluation will help to delineate whether the observed behavior with respect to the mechanical properties is a result of differences in the cellular structure or in the solid portion of the foam. Figure 4.1 shows two micrographs of one of the molded polyurethane foams, Fmc4. Recall from Table 3.1 that Fmc4 is a 4 pph water content molded foam containing the CPP particles. The micrographs were taken in two orthogonal directions, a) parallel to the rise direction and b) perpendicular to the rise direction, in view of the geometric anisotropy that is known to occur in slabstock polyurethane foams.⁷⁹ With respect to the molded foams presented here, the rise direction was along the height dimension of the mold where the reacting mixture was poured into the mold and then allowed to rise, vertically. Comparing the two micrographs indicates that the pronounced geometric anisotropy which exists in slabstock foams does not exist for molded foams. As expected, the cells have essentially the same shape in both micrographs since the reaction mixture is being pressurized from all directions. However, to be consistent, the remaining micrographs were taken parallel to the rise direction. Although not overwhelmingly obvious here, these materials contain a relatively large amount of closed cells relative to conventional slabstock foams. The closed cells have also survived the mechanical crushing that they are subjected to in view of their more closed cell character common to molded foams. This was not only confirmed by comparison of micrographs of each molded and slabstock foam but also airflow measurements. The airflow measurement of a 4 pph water conventional slabstock foam was 5 ft³/min. In contrast, the airflow of Fm4 was only 1 ft³/min thereby providing further support that this molded foam has considerably more closed cells than the slabstock foam of equal water content. Finally, the cell struts are thicker in this molded foam (and all others investigated) relative to slabstock foams of comparable water content which, for equal cell size, inherently results in a higher density than for the slabstock foams. For example, foam Fmc4 had a density of 1.9 lb/ft³ while the 4 pph water content slabstock foam had a density of 1.4 lb/ft³. The thickness of the struts determined from these

(a)



(b)

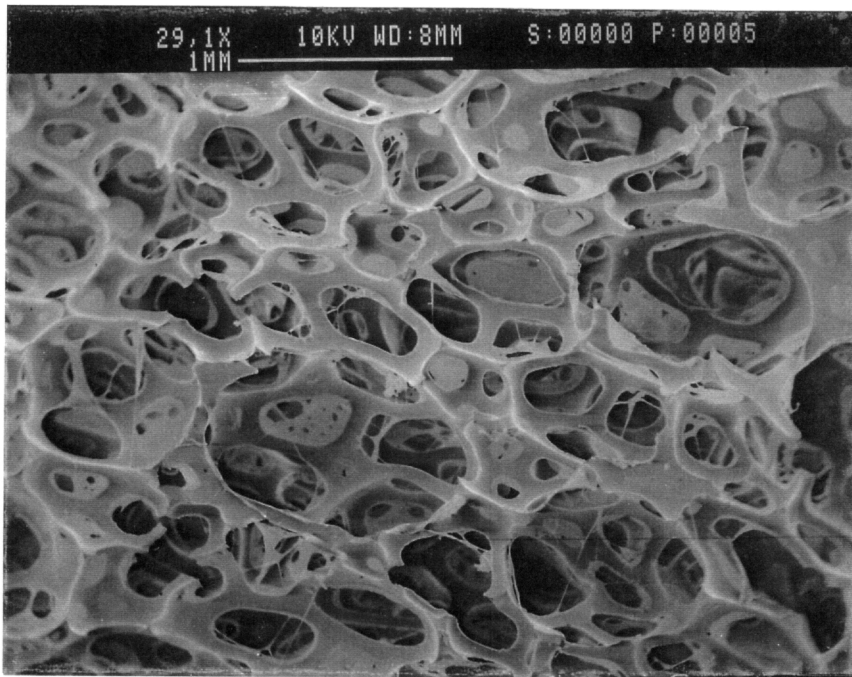


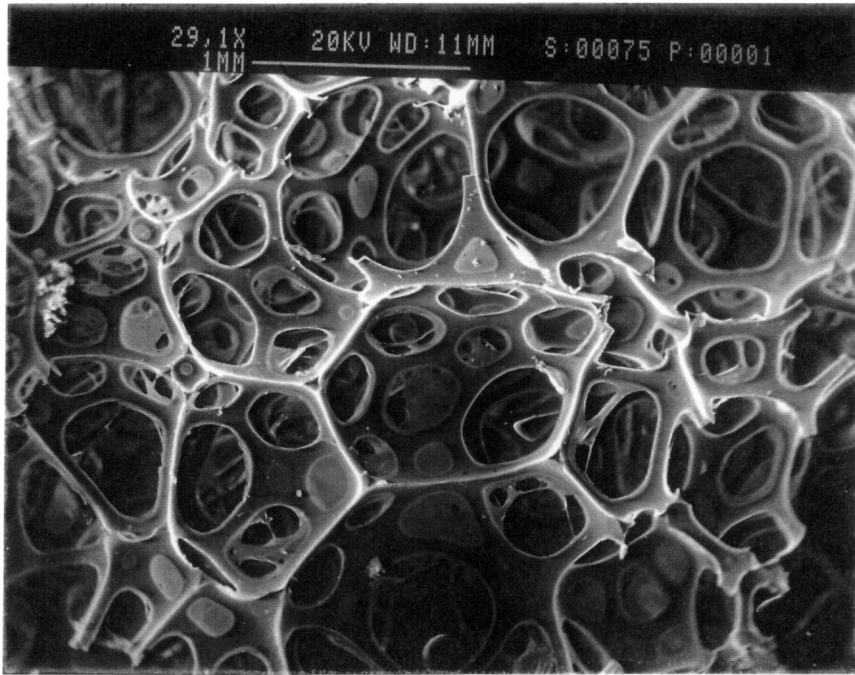
Figure 4.1. Scanning electron micrographs of foam Fmc4 shown both (a) parallel to the rise direction and (b) perpendicular to the rise direction.

micrographs was ca. 0.2 mm for the molded foams where the strut thickness of slabstock foams is usually ca. 0.1mm. Based on conventional wisdom, a thicker strut should have a strong influence on the bending or "flex" modulus of the foams.

4.1.1 Effect of Copolymer Polyols on Cellular Structure

Although copolymer polyols have been reported to aid in cell opening, very little difference between the micrographs of foams with and without CPPs was observed. The micrographs of Fmo4, Fmo2, Fmc4 and Fmc2 are shown in Fig. 4.2 so that the CPP effects as well as density effects could be investigated. Comparing the micrograph of Fmo4, shown in Fig. 4.2a, to that of Fmc4, shown in Fig. 4.2b, reveals that both foams have relatively the same amount of closed cells. Recall that all the micrographs were taken parallel to the rise direction and also note that the magnification is approximately the same at 30x. In fact, the only subtle difference observed is that the cells of foam Fmc4 appear smaller in size than those of Fmo4. The same is noted by comparing the cells of Fmo2, shown in Fig. 4.2c, to those of Fmc2, shown in Fig. 4.2d. Hence, the foams with CPPs have slightly smaller cells which naturally leads to the assumption that there is a higher density of cells early in the process when they are nucleated. Figures 4.3a through 4.3d show the same four foams as Fig. 4.2 however here they were taken at a magnification of 80x. From this set of micrographs it appears that along with the size of the cells being greater for the foams without CPPs, that the thickness of cell struts is also slightly larger. The thickness of the struts of Fmo4 as measured from Fig. 4.3a is ca. 94 μ m and only ca. 69 μ m for the struts of Fmc4 as measured from Fig. 4.3b. Comparing the structures of Fmc4 and Fmc2 to those of Fme4 and Fme2 whose CPP particles utilized the experimental stabilizer reveals no difference in cellular structure. The cellular structure of Fme4 is shown in Fig. 4.4.

(a)



(b)

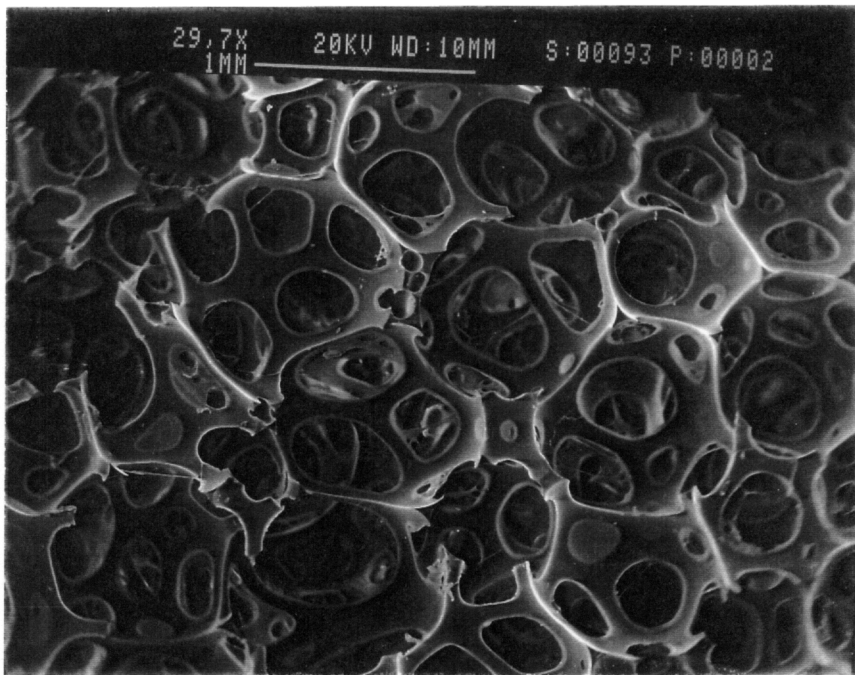
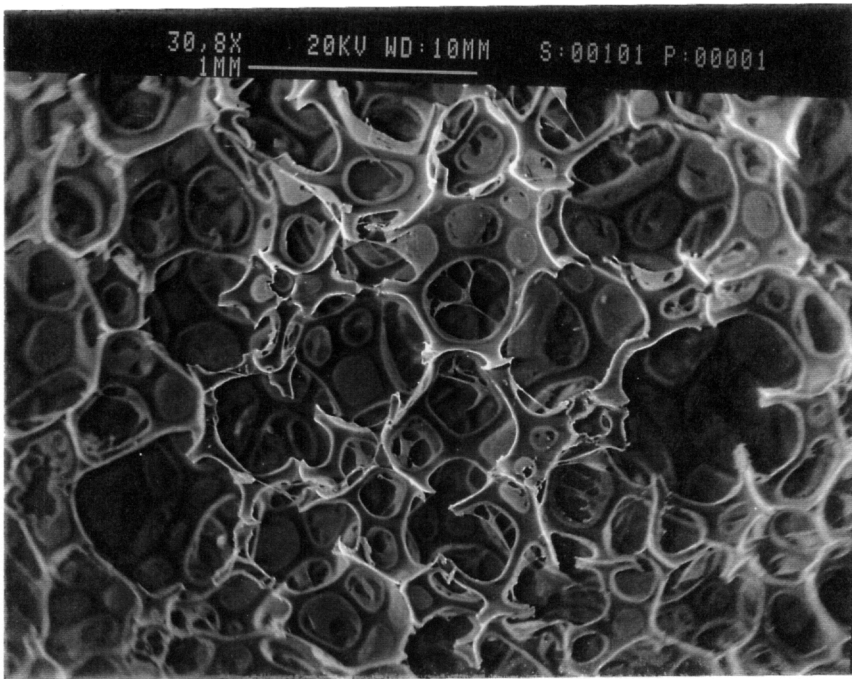


Figure 4.2. Scanning electron micrographs of foams (a) Fmo4, (b) Fmo2, (c) Fmc4, and (d) Fmc2. (mag = 30x)

(c)



(d)

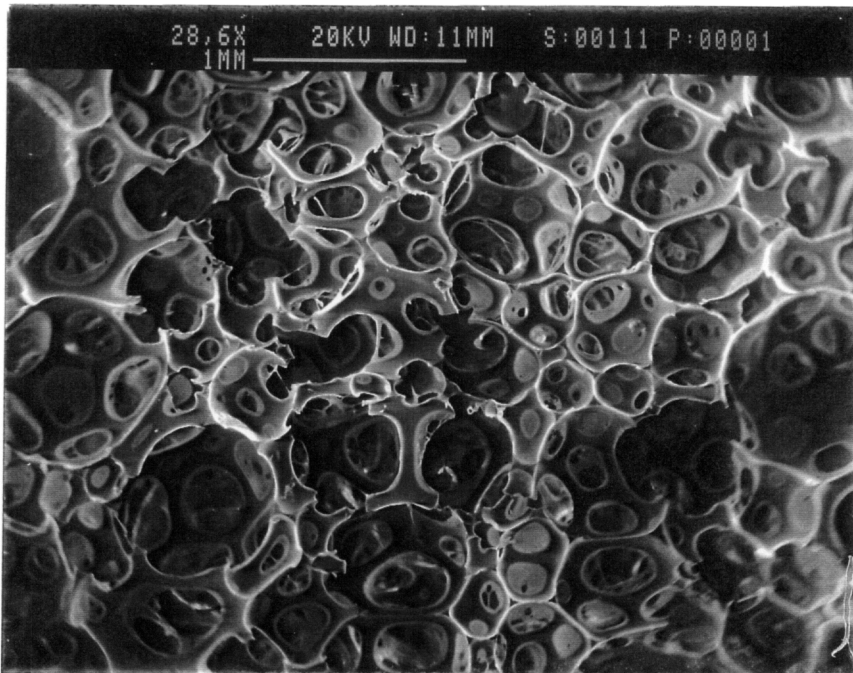
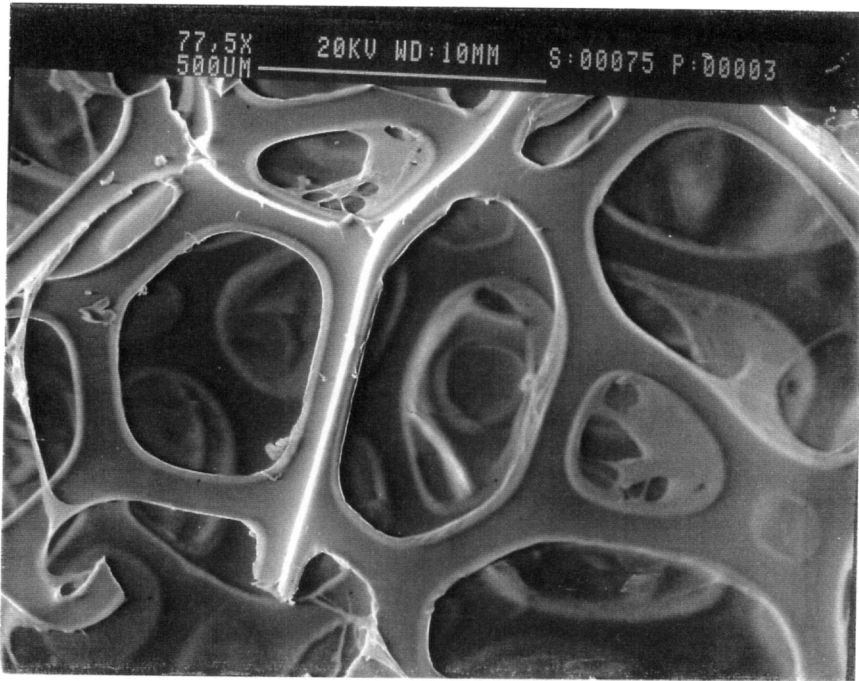


Figure 4.2 con't. Scanning electron micrographs of foams (a) Fmo4, (b) Fmo2, (c) Fmc4, and (d) Fmc2. (mag = 30x)

(a)



(b)

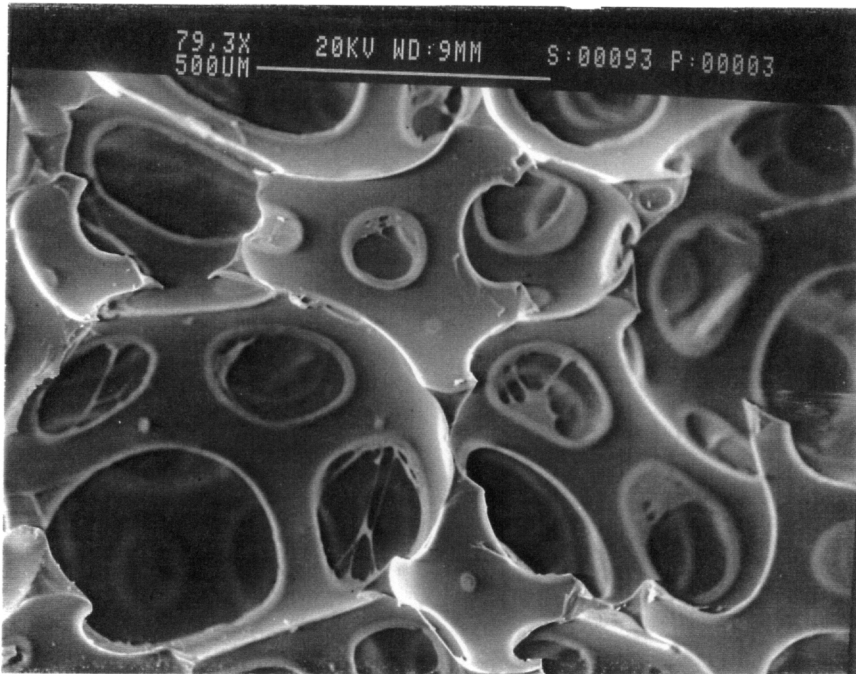
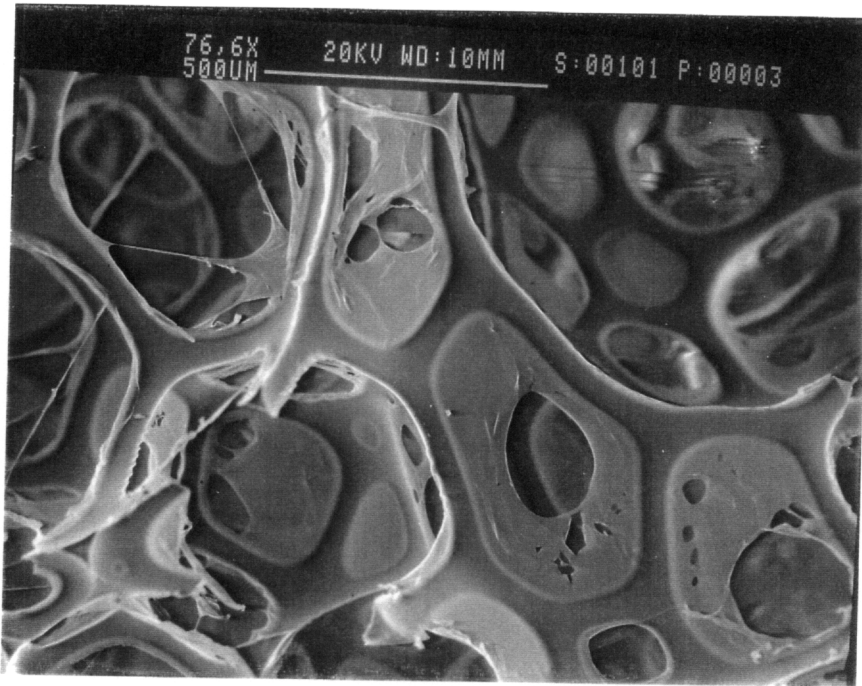


Figure 4.3. Scanning electron micrographs of foams (a) Fmo4, (b) Fmo2, (c) Fmc4, and (d) Fmc2. (mag = 80x)

(c)



(d)

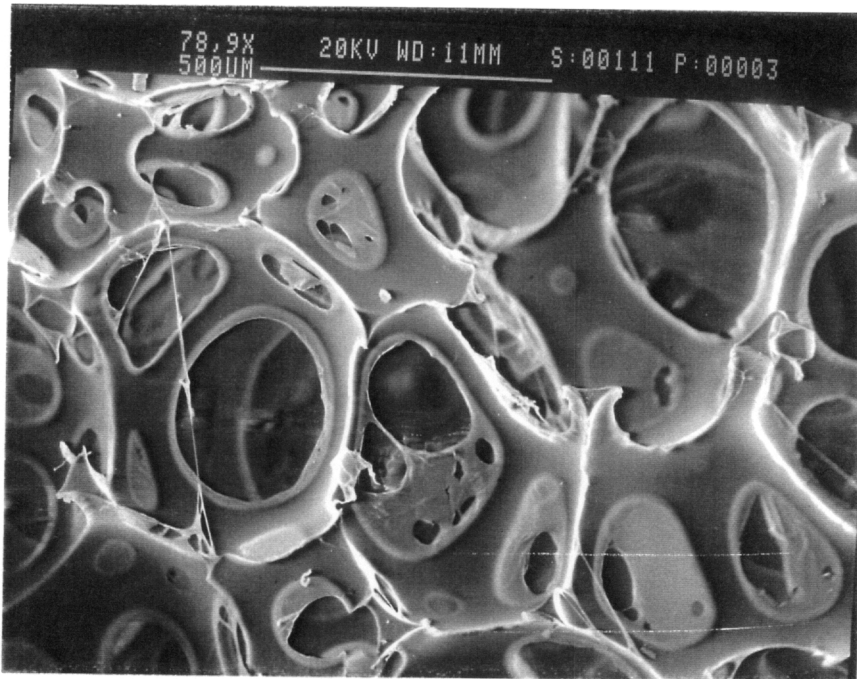
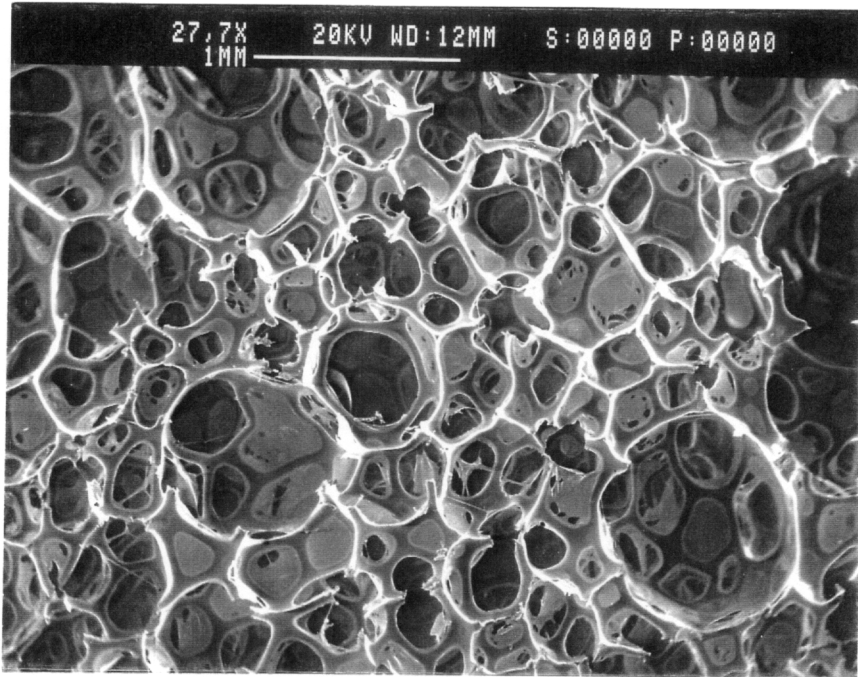


Figure 4.3 con't. Scanning electron micrographs of foams (a) Fmo4, (b) Fmo2, (c) Fmc4, and (d) Fmc2. (mag = 80x)

(a)



(b)

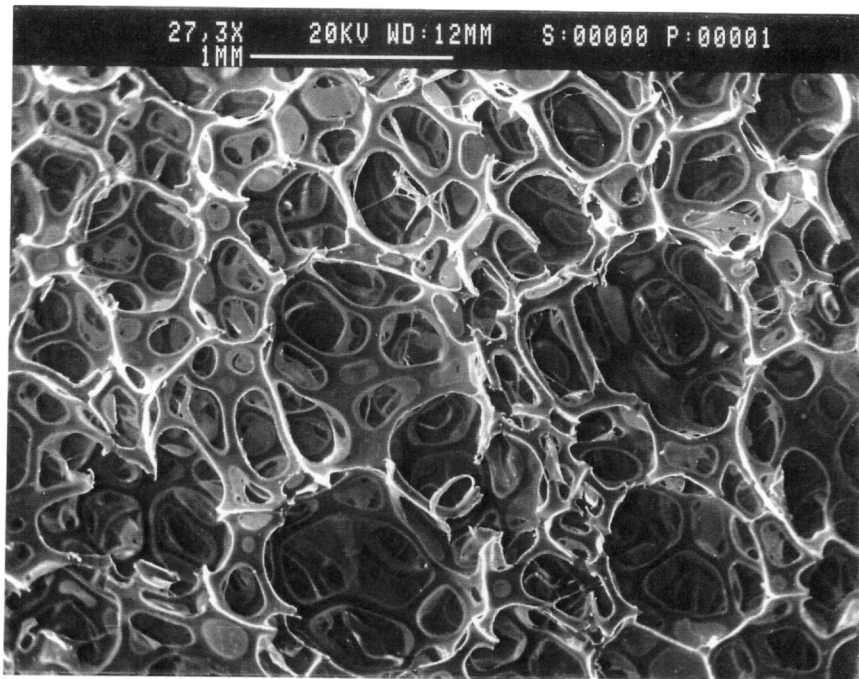


Figure 4.4. Scanning electron micrographs of foam Fme4 shown both (a) parallel to the rise direction and (b) perpendicular to the rise direction.

4.1.2 *Effect of Formulation Water/TDI content*

While somewhat surprising, the cellular structure appeared to be insensitive to the water/TDI levels incorporated in the formulation. For example, comparing foam Fmo4 to Fmo2 or comparing Fmc4 to Fmc2 in either Fig. 4.2 or Fig. 4.3 reveals very similar cellular structures. The cell openness, size of the cells, and the thickness of cell struts of the low and high water content foams are very similar. The cellular structures of foams Fme4 and Fme2 also appeared the same and were very similar to those of Fmc4 and Fmc2 and thus are not shown.

4.2 **Fine Structure**

As discussed in Chapter 2, one ingredient included in molded foam formulations to increase load bearing capabilities is the addition of copolymer polyols (CPP). In order for the effectiveness of the CPP phase to be maximized, they must be well dispersed. To prevent flocculation some type of steric stabilization is required which was accomplished by a "grafting" process thus allowing the dispersions to copolymerize with the base polyol. To evaluate the effectiveness of this stabilization and the final CPP dispersity, transmission electron microscopy (TEM) investigations were performed. Figure 4.5 is a TEM micrograph of foam Fmc4 and reveals a well dispersed particle structure which appears somewhat spherical. The particles range in size from ca. 0.25 to 0.6 μm . The CPP colloidal dispersions illustrate that the stabilization appears to have prevented flocculation. With respect to foam Fme4, in which the experimental stabilizer was utilized, while the particle size appears slightly larger, the structure and dispersity of the particles is very similar to that of Fmc4 as is demonstrated in Fig 4.6. The appearance of larger particles may not necessarily be due to flocculation or even larger dispersions but instead to the sample section being microtomed through different depths of the particles giving the

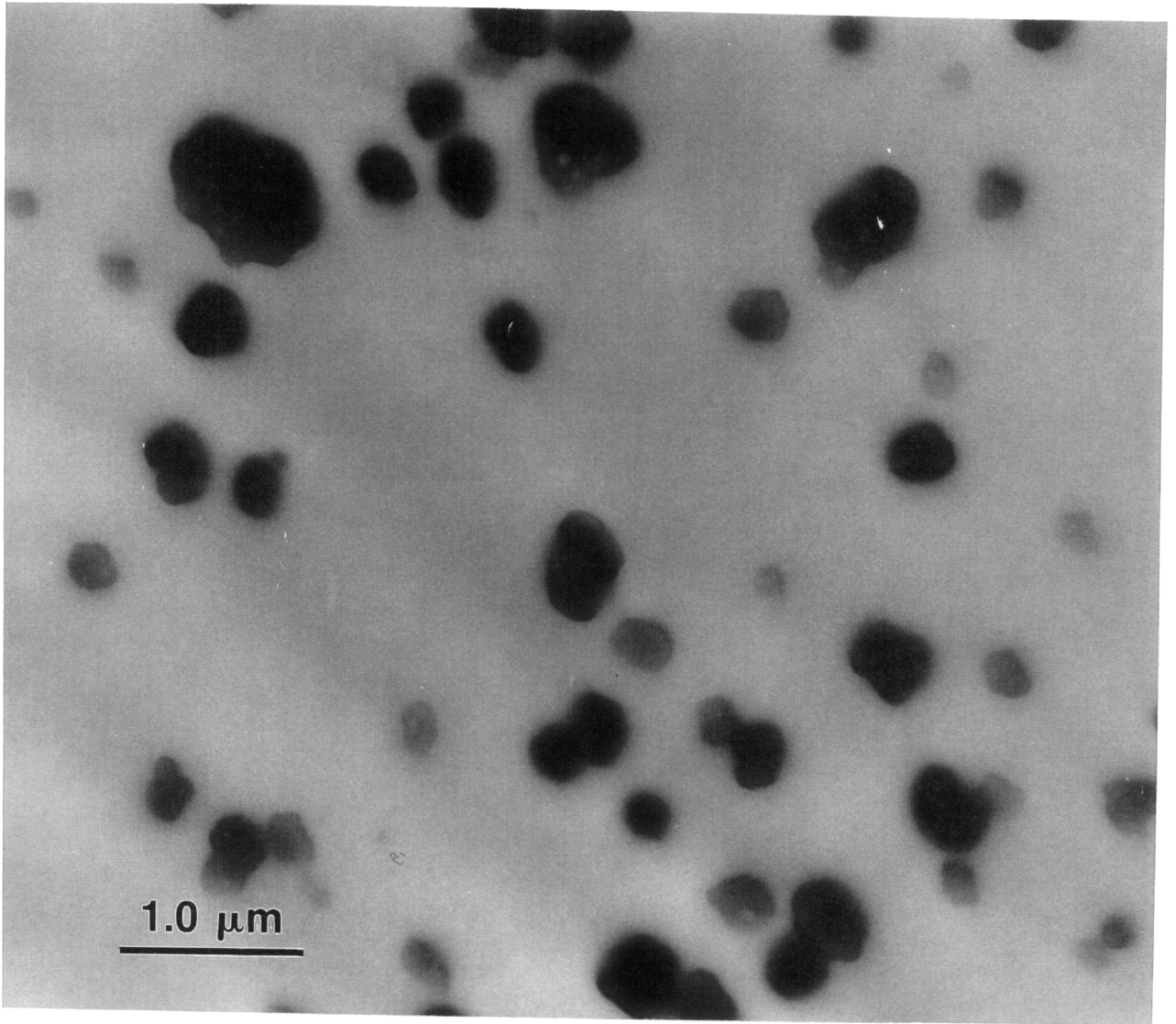


Figure 4.5. Transmission electron micrograph of foam Fmc4 (mag. = 27kx).

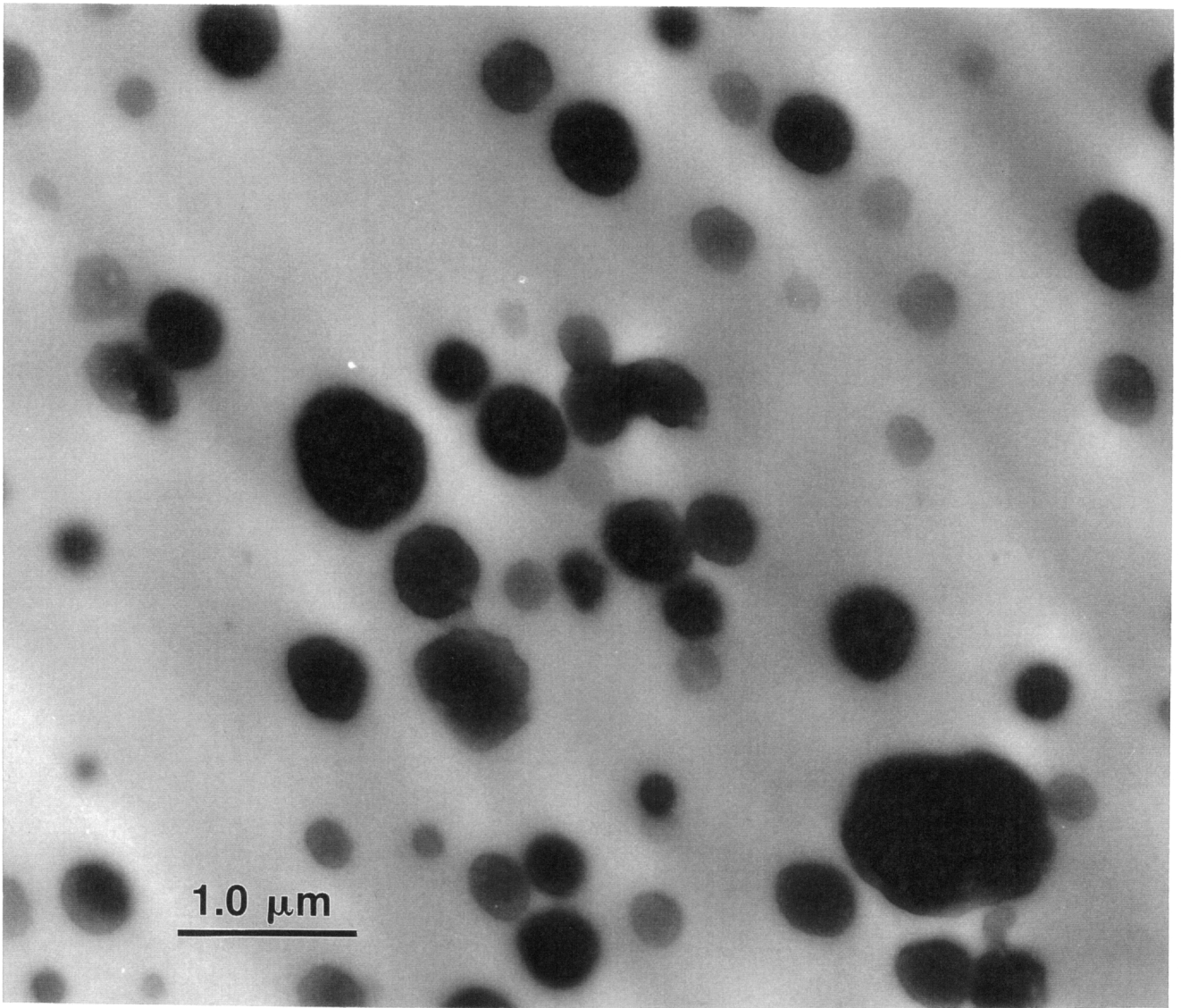


Figure 4.6. Transmission electron micrograph of foam Fme4 (mag. = 27kx).

appearance of different size. Thus it can be concluded that flocculation is also prevented by the experimental stabilizer, which is lower in amount and functionality than the conventional stabilizer. Again a colloidal dispersion is revealed for Fmc4.

Foam Fmc4 was subjected to 90% compression at 150°C (above the T_g of the CPP) to determine the stability of the CPP particles from a structural point of view. Such extreme treatment was chosen in light of earlier experiments at less harsh conditions leading to no displayed observable difference in size or geometry of the particles. The resultant particle structure is shown in Fig. 4.7 which reveals that this treatment promoted slight particle deformation where they now appear ellipsoidal instead of spherical. In view of the unlikelyhood of these materials being exposed to such conditions in "real" applications, it was concluded that the particles are structurally stable upon high loading under realistic temperature and humidity conditions that these materials would be subjected to.

4.3 Microphase Separation

Since the morphology of materials of this type is one of microphase separated domains (HS domains) embedded in a continuous soft phase, the foam properties are strongly dependent on the extent and perfection of this microphase separation. Hence, the phase separation including the perfection of the domains was investigated as well as the influence of the varying formulation ingredients. For example, the CPP and water/TDI content were the variables specifically targeted. Thereby, certain techniques, specifically thermal and x-ray analysis, were utilized to ascertain these aspects of phase separation.

4.3.1 Thermal Properties

Differential Scanning Calorimetry (DSC) was used to detect the presence of water, determine the soft segment glass transition, T_g , and the effects of the specific formulation

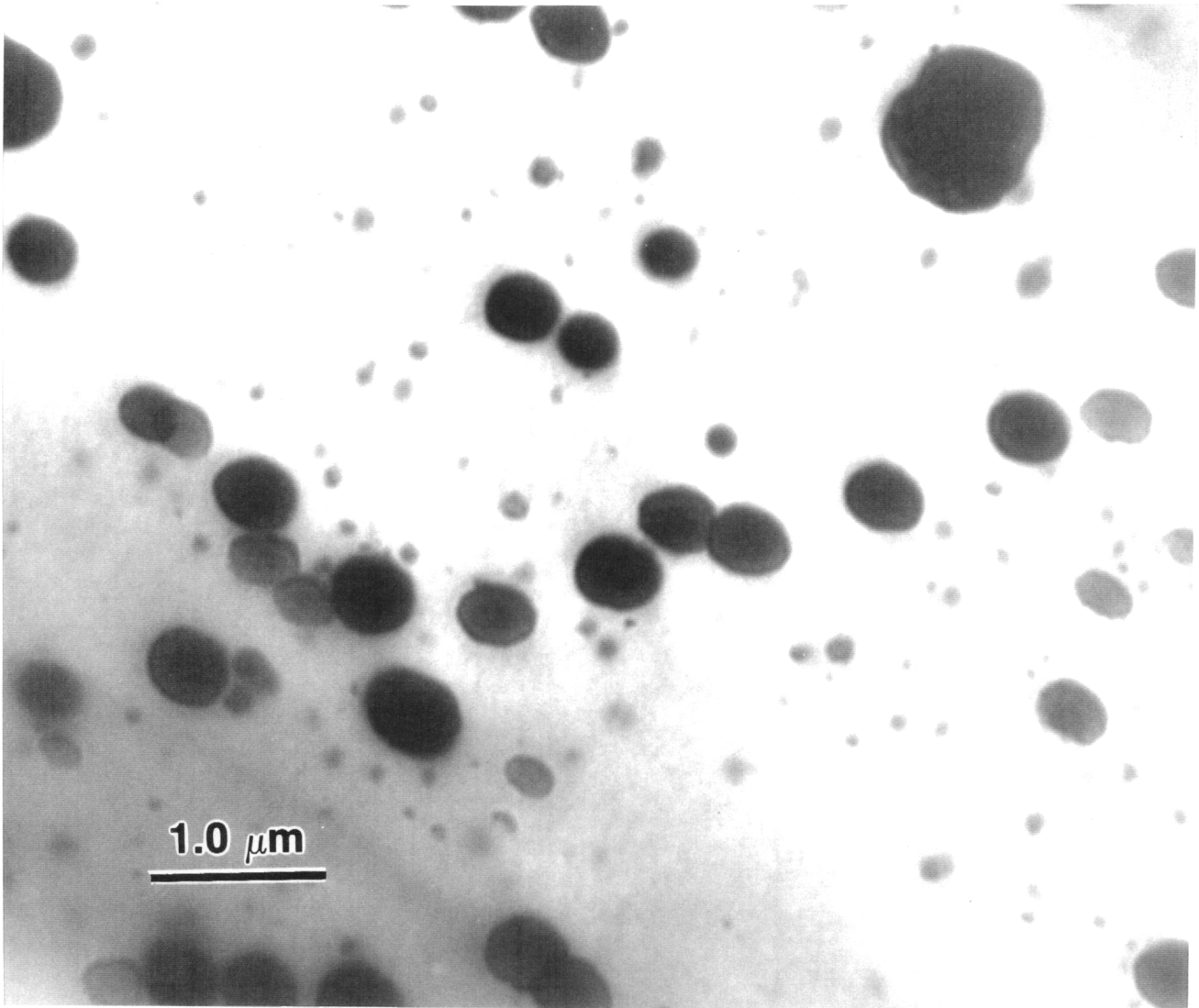


Figure 4.7. Transmission electron micrograph of foam Fmc4 after 90% compression at 150°C (mag. = 27kx).

components on this transition which can be qualitatively correlated to the extent of microphase separation. Figure 4.8 illustrates a typical DSC thermogram of a molded foam, foam Fmc4 in this case, showing both the first heat and second heat. Upon the first heating, a broad endotherm is observed in the range of 30°C to 100°C which can be attributed to the evaporation of absorbed water. As will be shown, all of the foams displayed a similar endotherm. Upon cooling the same sample to -140°C, and heating it to 140°C again, this endotherm is not observed. To further verify that this non-reversible endotherm was due to water evaporation, Thermo-Gravimetric Analysis (TGA) was carried out, the results being shown in Fig. 4.9. These results indicated that in this temperature range (30°C-100°C), 2% - 3% weight loss occurred which is likely due to water evaporation. Furthermore, oscillating DSC was carried out in which the thermogram was separated into a reversible and non-reversible contribution as shown in Fig. 4.10. This broad endotherm was shown to be an irreversible transition further supporting the claim of water evaporation. The soft segment glass transition T_g for the first as well as the second heat was ca. -59°C suggesting that the absorbed water had no significant influence on the T_g of the soft segment. Figure 4.11 shows the first and second heats of foam Fmo4. As with Fmc4, an endotherm was observed in the first heat while the soft segment T_g was unaffected by the absorbed water. The T_g was ca. -58°C for foam Fmo4. The fact that the soft segment T_g of both foams in both the first and second heating cycles were essentially the same suggests that this glass transition was insensitive to the absorbed moisture and whether CPPs were used. The DSC curves of the other molded foams were very similar to those of foams Fmc4 and Fmo4. Therefore, these figures are presented in Appendix 4.1. Again, the first heat displayed a broad endotherm associated with the release of absorbed moisture and the soft segment glass transition was ca. -59°C for both materials.

The use of copolymer polyols in molded polyurethane foams appeared to have no influence on the thermal behavior as indicated by DSC. In addition, based on the insensitivity of the soft segment T_g to the CPP system used (Table 4.2), it was suggested

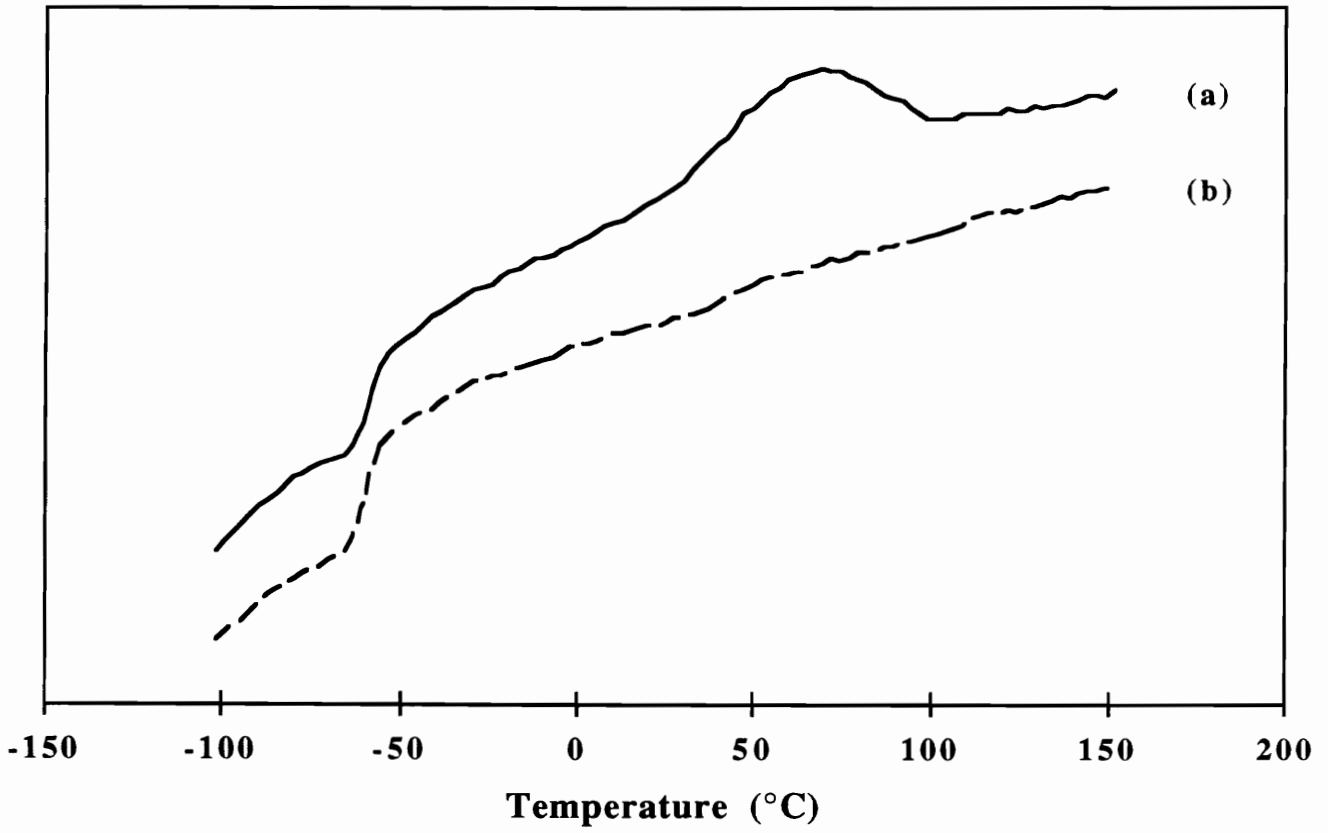


Figure 4.8. DSC thermograms of Fmc4 showing both the (a) first and (b) second heating cycles.

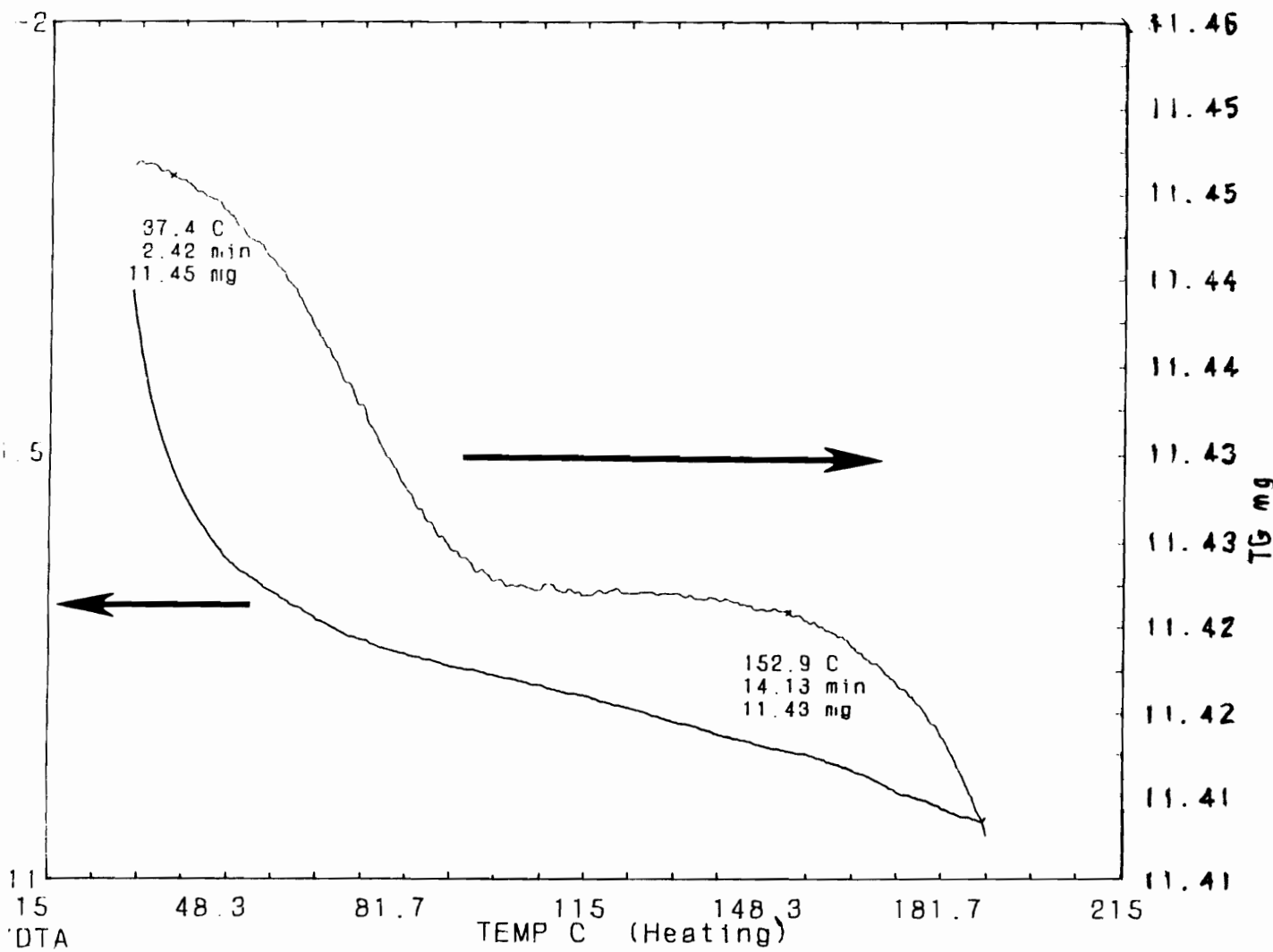


Figure 4.9. TGA thermogram of Fmc4 showing the weight loss associated with the observed endotherm.

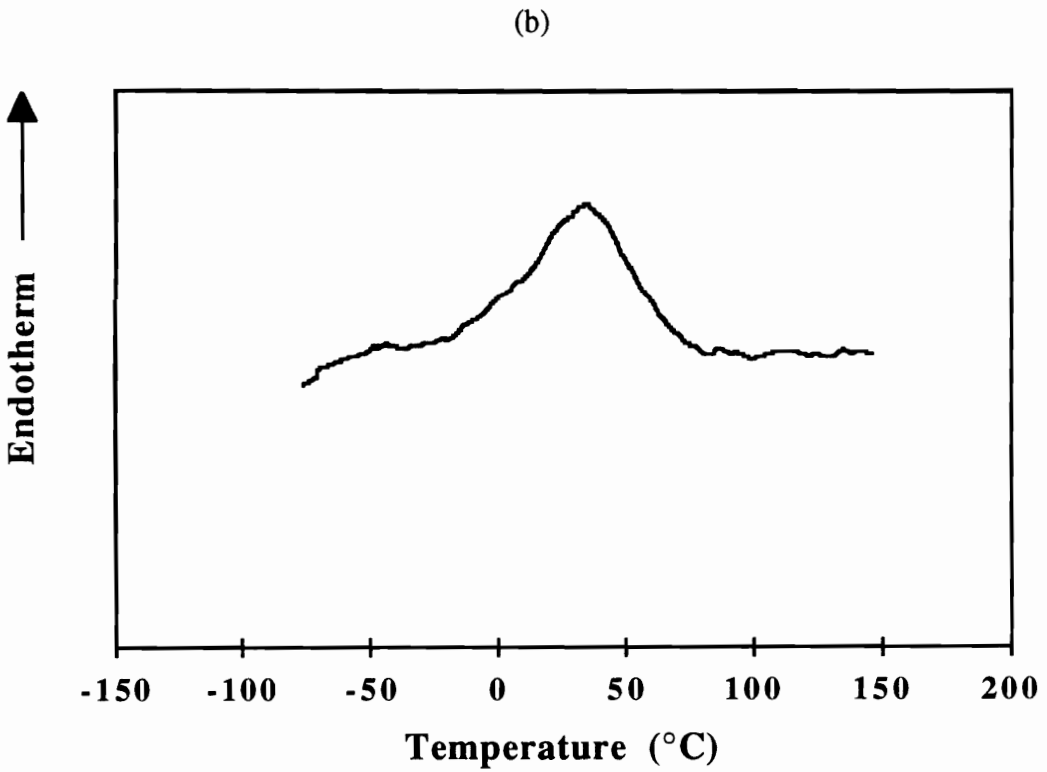
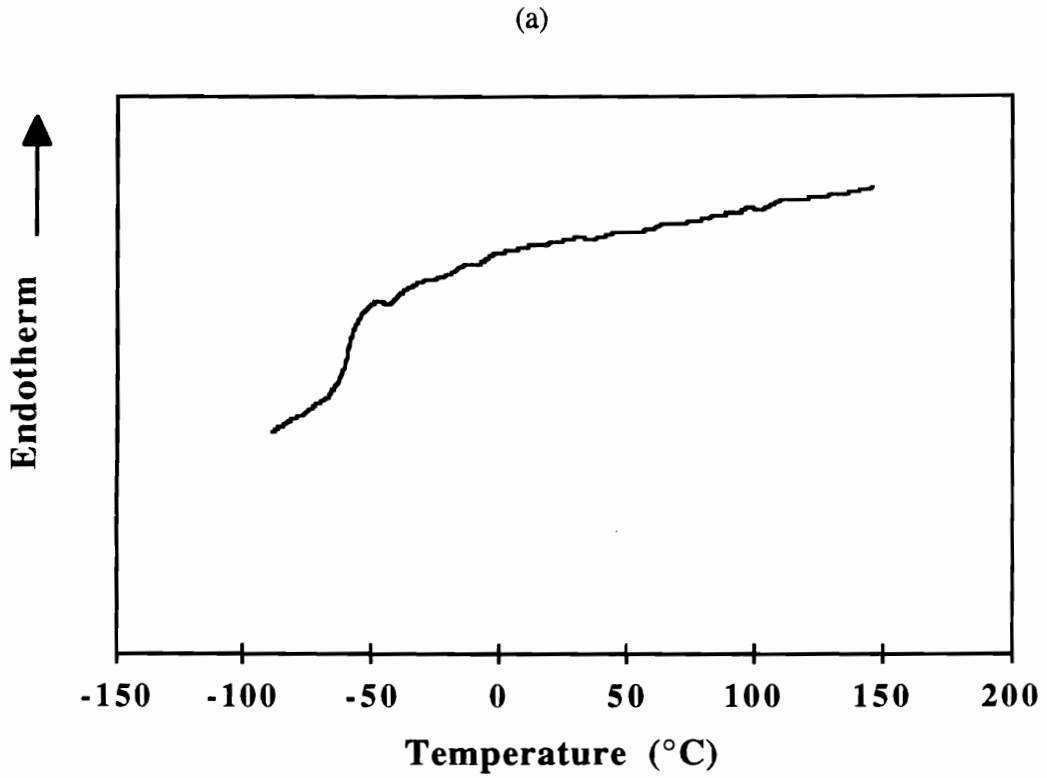


Figure 4.10. Oscillating DSC of Fmc4 illustrating both the (a) reversible and (b) irreversible transitions.

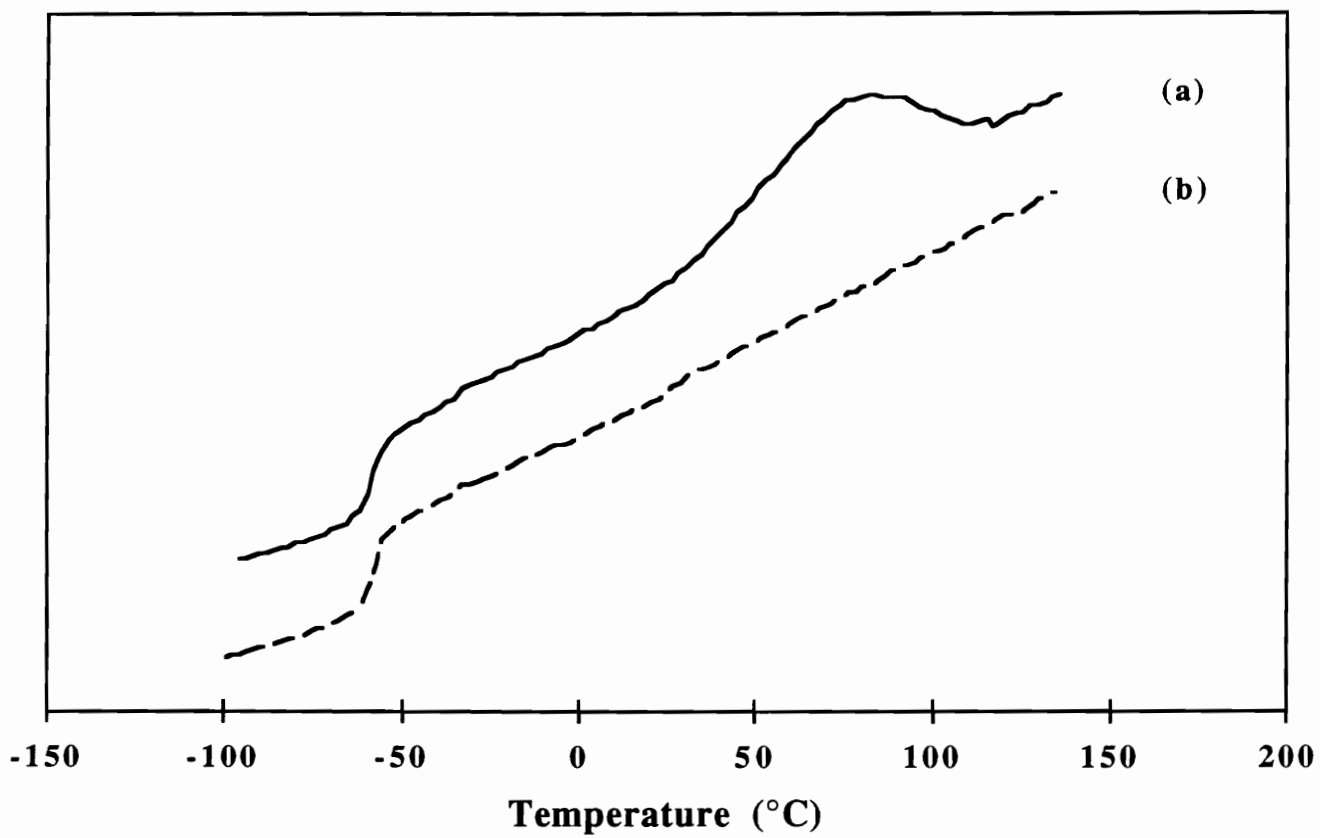


Figure 4.11. DSC thermograms of Fmo4 showing both the (a) first and (b) second heating cycles.

Table 4.2. Thermal Properties of Molded Foams

Foam	DSC	DMS	
	$T_g(^{\circ}\text{C})$	$T_g^1(^{\circ}\text{C})$	$T_g^2(^{\circ}\text{C})$
Fmo4	-57.9 ± 1.5	-57.6 ± 0.5	NA
Fmo2	-59.1 ± 1.0	-57.3 ± 1.0	NA
Fmc4	-58.8 ± 1.0	-58.1 ± 0.5	124.8 ± 2.0
Fmc2	-60.4 ± 2.0	-55.6 ± 2.0	125.7 ± 1.5
Fme4	-59.6 ± 1.0	-57.2 ± 1.0	124.3 ± 2.0
Fme2	-60.4 ± 1.5	-57.0 ± 1.5	125.4 ± 2.0

that altering the CPP provided no influence on the microphase separation. That is, regardless of whether CPPs were used or which CPP system was incorporated (conventional or experimental), the soft segment T_g was unaltered. In addition, no transition was observed at the reported T_g (125°C) of the CPP particulates. To either confirm or dispute whether the CPP component influenced the microphase separation of the HS domains, the other techniques mentioned earlier were used beginning with dynamic mechanical spectroscopy (DMS).

The soft segment T_g was also determined using DMS, specifically from the peak of the tan delta curve. The tan delta curves are shown in Fig. 4.12 which all exhibit a sharp peak at ca. -57°C . As with the DSC measurements, the soft segment T_g determined here (also given in Table 4.2) appears insensitive to water content and copolymer polyols. In addition, this T_g correlated well with the T_g measured using DSC for each sample. The magnitude of the tan delta peak was in general greater for the 2 pph water content foams. The higher magnitude displayed by the lower HS content foams is a result of the 2 pph water content foams having a greater soft segment content relative to the 4 pph water content foams. The hard segment phase makes up a higher volume fraction in the higher water content foams thus increasing the foam stiffness. Also observed was a small second tan δ peak at ca. 125°C displayed by the CPP containing foams - the origin being the T_g of the CPP particulates. This is more clearly exposed in Fig. 4.13. The tan delta curves of foams Fmo4 and Fmc4 reveal that both foams exhibited a peak centered at ca. -58°C , but Fmc4 also displayed the CPP peak centered at ca. 125°C . As suggested in Table 4.2, both the control and experimental CPP particles exhibited the same T_g . Based on the soft segment T_g determined by DMS and DSC it appeared that the microphase separation was not influenced by the variables in this study.

4.3.2 *Small Angle X-Ray Scattering*

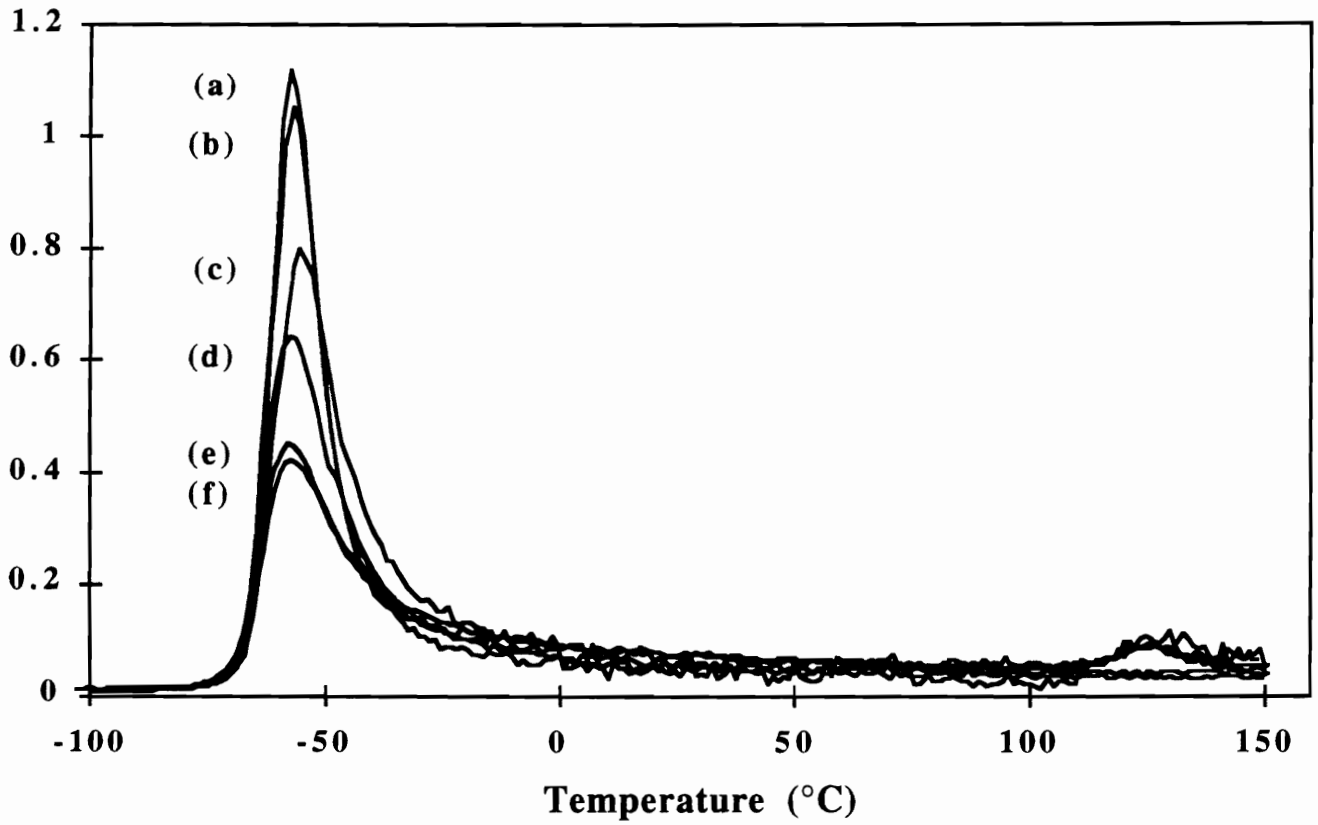


Figure 4.12. Influence of the formulation ingredients on the Tan Delta of the six molded foams. Foams are listed in terms of decreasing order of the magnitude of the tan delta peak: (a) Fmo2, (b) Fme2, (c) Fmc2, (d) Fmo2, (e) Fmc4, and (f) Fme4

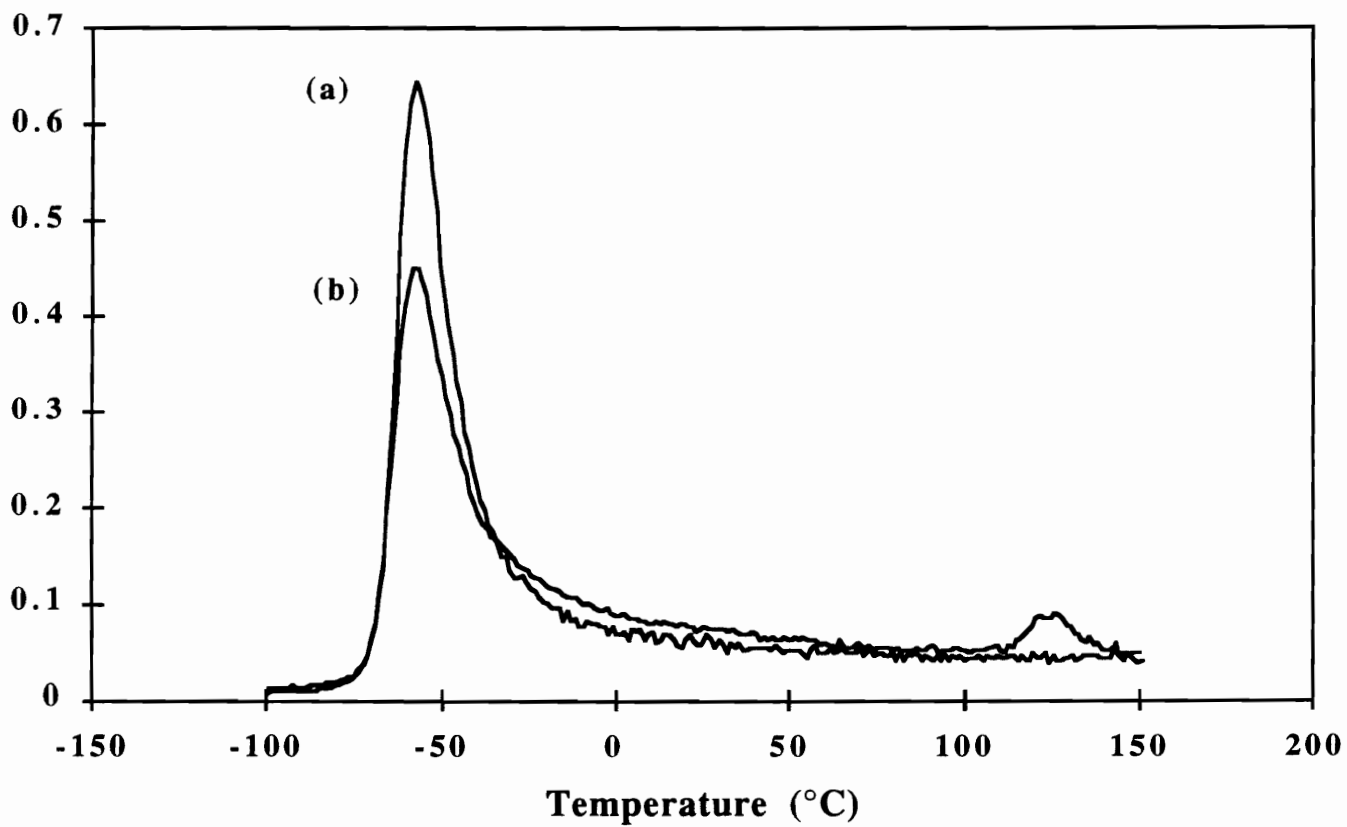


Figure 4.13. Influence of the CPP particles on the Tan Delta peak of the molded foams illustrated using (a) Fmc4 and (b) Fmo4.

Small angle x-ray scattering (SAXS) was undertaken to evaluate the microphase separation and the influence of the formulation variables on this behavior. The SAXS profiles for the four molded foams varying in water/TDI level and CPP particles content are presented in Fig. 4.14, which is a plot of the normalized smeared intensity as a function of the angular variable, $S = 2\sin\theta/\lambda$. A rough estimate of the average interdomain spacing or Bragg spacing can be calculated from the shoulder in the scattering profile through the application of Bragg's Law. The calculated d-spacings are 17-19 nm for Fmo4, Fmc4 and Fme4 and 13-15 nm for Fmo2, Fmc2 and Fme2. Also observed in Fig. 4.14 is that the measured intensity of the higher water/TDI content foams is higher than that of the lower content foams, i.e. the intensity of Fmc4 is higher than that of Fmc2. Although this difference can arise from differences in background scattering, it is more likely to arise from differences in the relative amounts of hard and soft segment. This will be further explored in the section below.

4.3.2.1 Effect of Water/TDI Content on SAXS

Based on Figs. 4.14 and 4.20 (which shows the influence of water content and experimental CPPs on the SAXS behavior), the water/TDI content and thus HS content had an influence on both the location of scattering angle associated with the shoulder and on the magnitude of the angular intensity. As expected, the higher water content or higher HS content lead to a greater interdomain distance, a result of larger hard segment domains. In addition to the d-spacing, the overall measured intensity was also greater for the 4 pph water content foams than those of 2 pph water as demonstrated in both figures. This is also a result of the 4 pph water content foams having a higher HS concentration. As will be later shown, theory predicts that for a sharp phase separated two component system, an increase in the integrated intensity (over all angles) occurs as the volume fraction of each phase approaches 0.5. Although the volume fractions are not 50/50, they are roughly

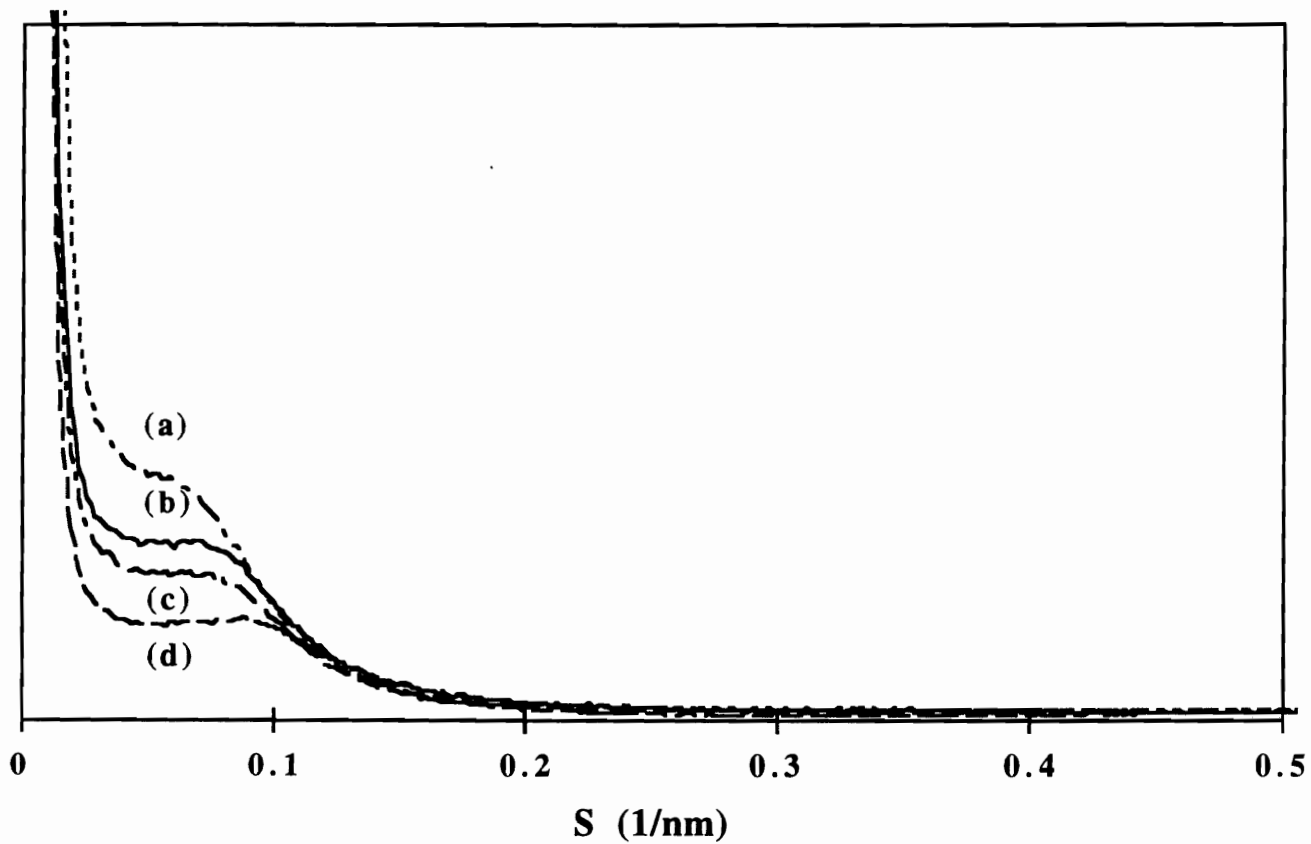


Figure 4.14. SAXS profiles of 4 molded foams illustrating the influence of the CPP particles and water/TDI content on the microphase separation: (a) Fmc4, (b) Fmo4, (c) Fmc2 and (d) Fmo2.

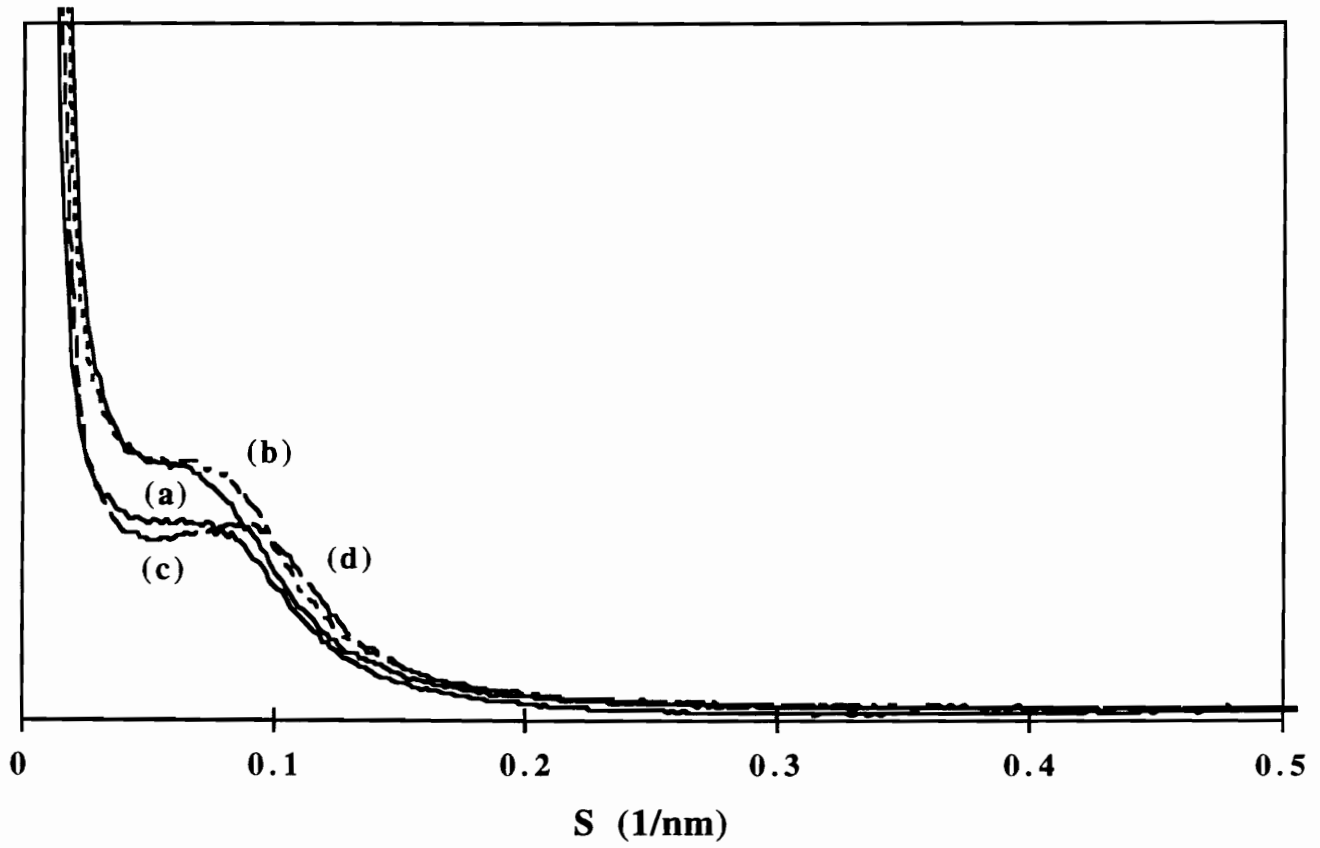


Figure 4.15. SAXS profiles of 4 molded foams illustrating the influence of the experimental CPP particles and water/TDI content on the microphase separation: (a) Fmc4, (b) Fme4, (c) Fmc2 and (d) Fme2.

33/67 for the 4 pph water content foams compared to ca. 23/77 for the 2 pph water content foams. The observed behavior with respect to the water/TDI content in Fig. 4.14 is therefore expected.

4.3.2.2 Influence of CPP Dispersions on SAXS

Figure 4.14 also reveals that the CPP containing foams displayed a higher scattering intensity over the foams lacking the CPP particles. Since the water/TDI content remains constant, the HS content is also constant and yet the intensity is influenced suggesting that the volume fraction of each phase may also vary. However, again, this is raw data not corrected for background scattering. However, it does appear that there is a small contribution to the microphase separation of the HS domains by the CPP particulates. These dispersions may also be influencing the volume fractions of each phase which can influence the scattered intensity. For example, the volume fraction of the soft phase is now lower relative to the hard segment volume fraction since some of the soft segment volume is now occupied by the CPP particulates. With respect to the experimental CPP foams, comparing the SAXS profiles of the control CPP containing foams to the experimental CPP containing foams shown in Fig. 4.15 reveals that the scattering angle associated with the d-spacing of the HS domains for the control CPP foams is slightly lower than those containing the experimental foams. The estimated d-spacing of Fmc4 is ca. 19 nm where for Fme4 the d-spacing is ca. 17 nm suggesting that the HS domains in the foams utilizing the control CPP particles are slightly larger or that there is a lower concentration of them. A possible speculation is that the different stabilization methods used between the two CPP systems, which alters the covalent cross-linking at the interface, could thus influence the phase separation behavior of the HS domains. Overall, as was expected, no peak was observed associated with the CPP particles for their size is too great to expect a scattering peak in this range with SAXS.

While SAXS was used to establish the presence of microphase separation, these same molded foams were shown to lack structural order or packing order within the HS domains. Both WAXS and FTIR were used to ascertain this lack of localized organization as will now be addressed.

4.3.3 *Wide Angle X-Ray Diffraction*

In addition to evaluating the microphase separation, the internal ordering of the hard domain was of interest and thus evaluated using two techniques. Recall, that the properties of a foam are strongly dependent on the perfection of the phase separated HS domains in addition to the level of covalent cross-linking. Wide angle x-ray scattering (WAXS) patterns were obtained to compare the amount of short range ordering or para-crystalline ordering of the HS domains and if it was influenced by any of the formulation components. For example, a less ordered domain might make that system more structurally labile under loading than one of higher order at a given environmental condition. As will be shown later in this chapter, the HS ordering correlates well with the foam's ability to resist temperature and humidity induced changes in the mechanical properties. The WAXS patterns of the six molded foams are shown in Fig. 4.16. As can be seen, while all the foams displayed a diffuse amorphous halo which is typical of liquid-like amorphous systems, none of the foams displayed sharp rings indicative of cohesive order as in the case of conventional slabstock foams such as those studied by Armstead shown earlier in Chapter 2 or that shown in Fig. 4.17a.³³ Figure 4.17 shows the scattering patterns of a 4 pph water content slabstock foam before (a) and after (b) extraction in DMF. As can be seen, the slabstock foam in addition to the diffuse amorphous halo, displayed two relatively sharp rings arising from the short range ordering of the HS domains. The patterns of the molded foams, however, resemble those of the slabstock foam after extraction (shown in Fig. 4.17b where the ordered urea segments are disrupted by the solvent treatment process.

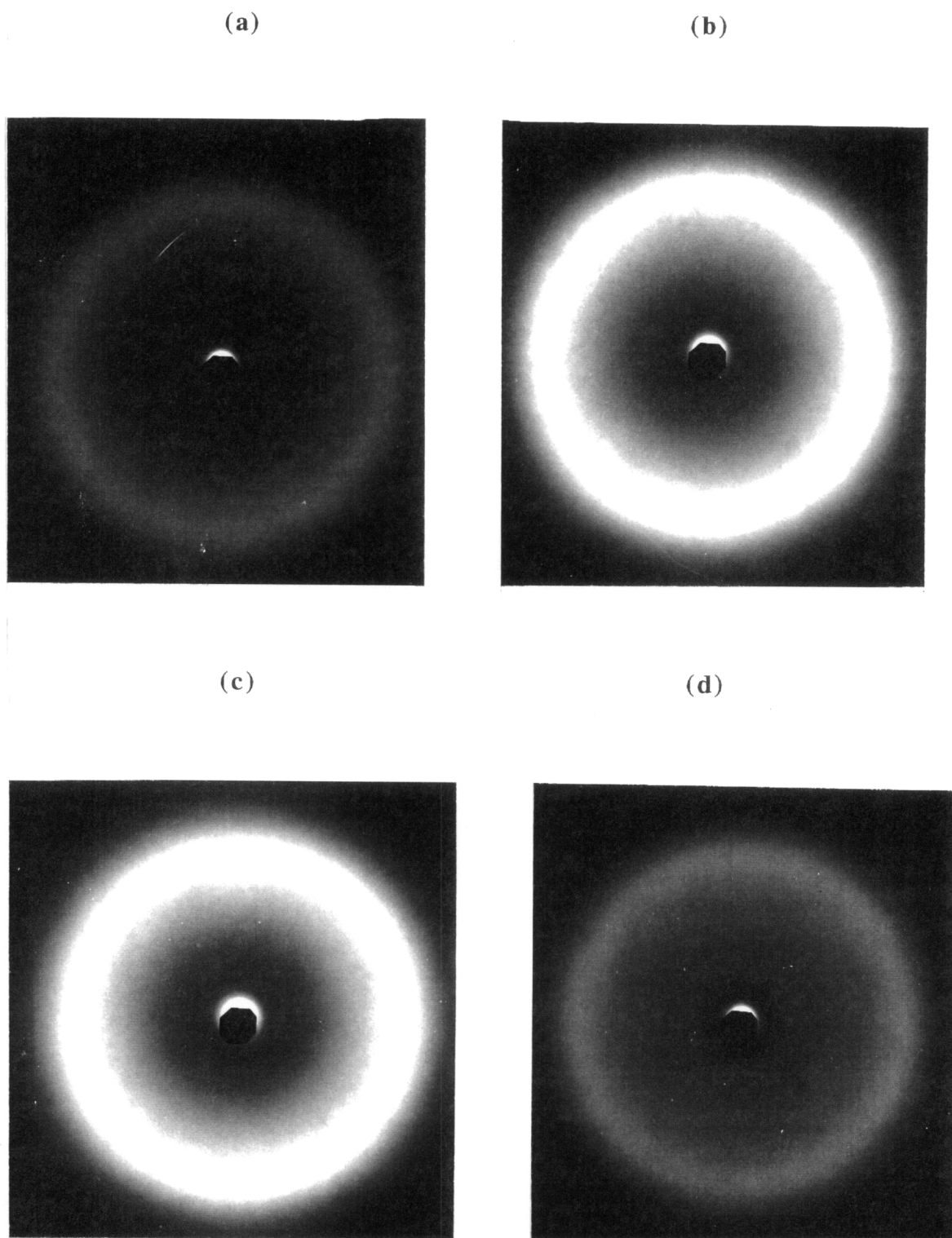
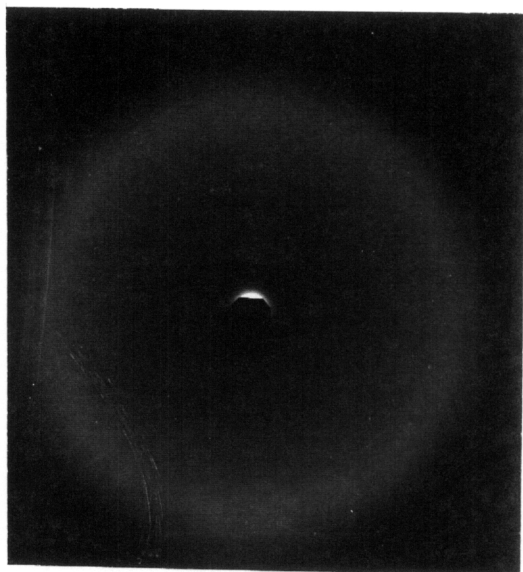


Figure 4.16. WAXS patterns illustrating the short range ordering of the HS domains of the molded foams: (a) Fmo4, (b) Fmo2, (c) Fmc4, (d) Fmc2, (e) Fme4, and (f) Fme2.

(e)



(f)

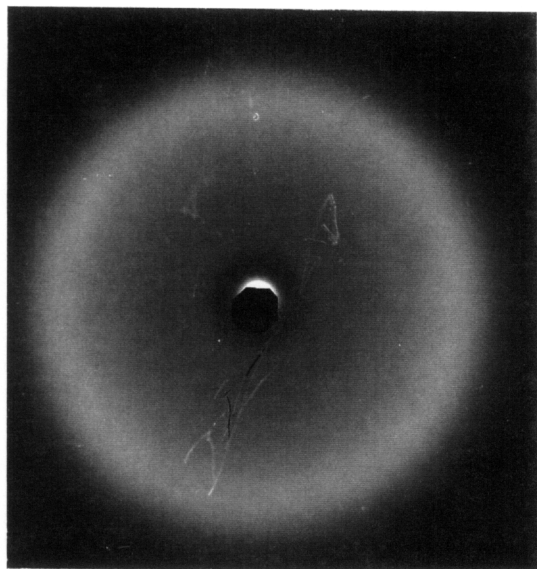


Figure 4.16. (con't)

WAXS patterns illustrating the short range ordering of the HS domains of molded foams: (a) Fmo4, (b) Fmo2, (c) Fmc4, (d) Fmc2, (e) Fme4, and (f) Fme2.

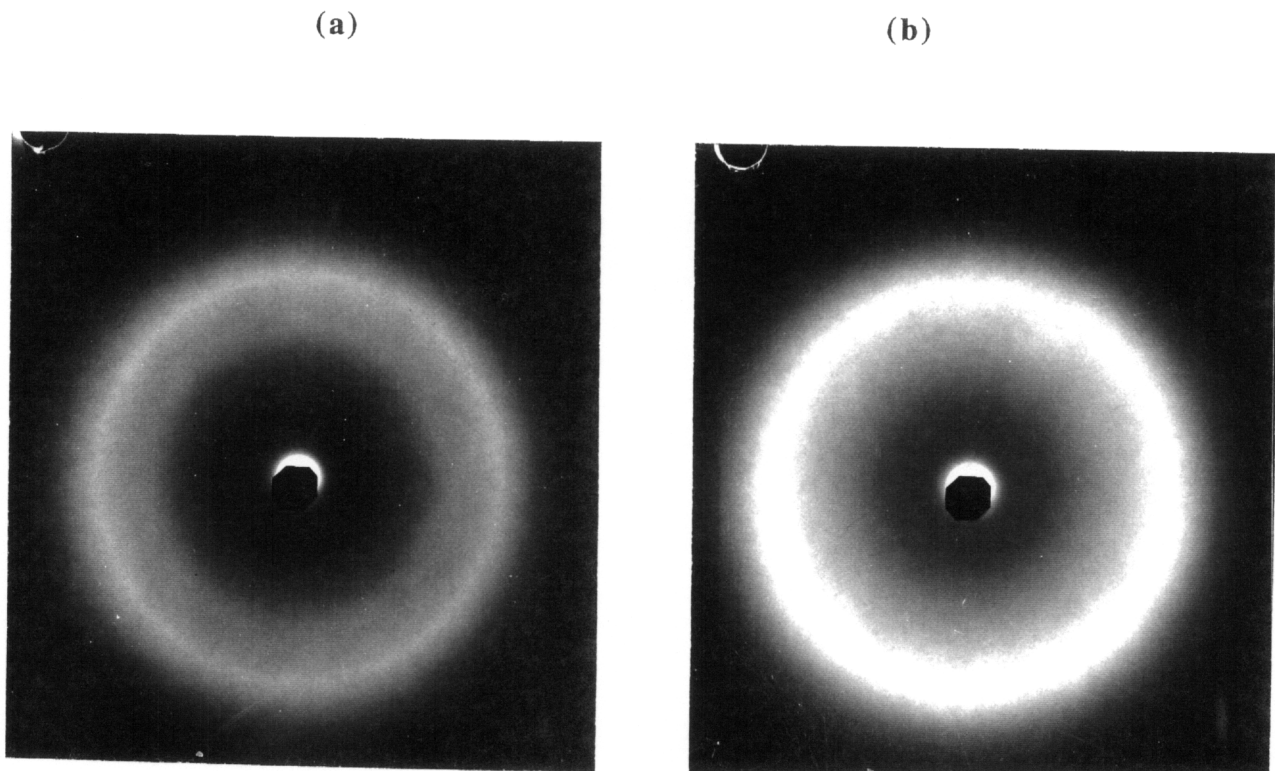


Figure 4.17. WAXS patterns illustrating the short range ordering of the HS domains of a conventional slabstock foam (a) before extraction and (b) after extraction.

The lack of sharp rings in the molded foams suggests that very little (if any) short range order exists amongst the hard segments and that the domains in the molded foams are more distinctly disordered with respect to the HS packing in slabstock foams. Therefore, based on this lack of order, the physical "cross-links" of molded foams allow for the easier "plasticization" by heat and humidity thereby making them more labile than those in slabstock foams. This lack of structural order observed within the hard segments is believed to be both kinetic and thermodynamic based. Hard domain formation is very sensitive to the solubility of the urea segments in the polyol soft phase which is greater in molded foams due to the stronger more favorable interactions between hard segments and the polyethylene oxide capped soft segments (used to endcap the polypropylene oxide to decrease demold times in view of its higher reactivity). In addition, bidentate hydrogen bonded urea must principally occur prior to the gel point of the covalent network. Recall that diethanolamine is also added in the formulation of molded foams to build hardness, speed up gelation and decrease demold times. The rapid cross-linking that occurs early on in the network development makes it very difficult for the urea segments to associate (through diffusion) and to pack and form multiple hydrogen bonds with other hard segments thereby limiting perfection of hard segment domain development.

Since the sharp rings in the x-ray patterns are of the same spacing, it can be concluded that the incorporation of copolymer polyols did not influence the ordering of the hard segments in any way. Any small differences that exist are differences in the brightness of the image which are a result of differences in the exposure of the material. This not to say that the CPP do not scatter x-rays and in fact are believed to contribute somewhat to the amorphous scattering.

4.3.4 Fourier Transform Infrared (FTIR)

In addition to the WAXS measurements, FTIR analysis was undertaken to evaluate the ordering or cohesiveness of the hard segments by evaluating the hydrogen bonding within the carbonyl region. Many researchers have utilized this technique to ascertain the level of phase separation which is not always applicable as will be shown. It is more accurately a reflection of the localized packing order of the hard segment domains which does not always depend on good phase separation between the hard and soft phases. In addition to the molded foams, a 4 pph water content conventional slabstock foam is included in the analysis to aid in the interpretation of the results. The amide I region (carbonyl region) was considered the most informative region and is thus shown for both molded foams and the slabstock foam in Fig. 4.18. The infrared results show significant differences between the slabstock foam and the molded foams. The slabstock foam displayed a strong bidentate absorption peak centered at 1640 cm^{-1} which is non-existent in the molded foams. This bidentate peak is indicative of hard segment ordering. All six molded foams displayed a strong monodentate urea absorbance centered at $1700\text{-}1650\text{ cm}^{-1}$ as well as free urea centered at 1715 cm^{-1} . For reasons mentioned above (specifically the addition of DEOA and EO capping in molded foams), it is concluded that the molded foams have much more disordered hard segment domains which, as will be demonstrated later allows for greater "plasticization" with temperature and humidity. The FTIR spectra of the molded foams free of the CPP particles are shown in Fig. 4.19. These also exhibit the monodentate and free urea absorbances, and again lack any indication of bidentate urea. No distinguishable differences were observed between these two molded foams and the other molded foams presented in Fig. 4.18.

In an attempt to verify that increased temperature disrupts hydrogen bonding, specifically in the viscoelastic studies (to be presented in later sections) FTIR - temperature studies were carried out and are shown in Fig. 4.20. The temperature was increased from room temperature to 140°C in increments of 10°C . As can be seen, the bidentate, monodentate as well as "loosely" bonded absorbances systematically decrease with

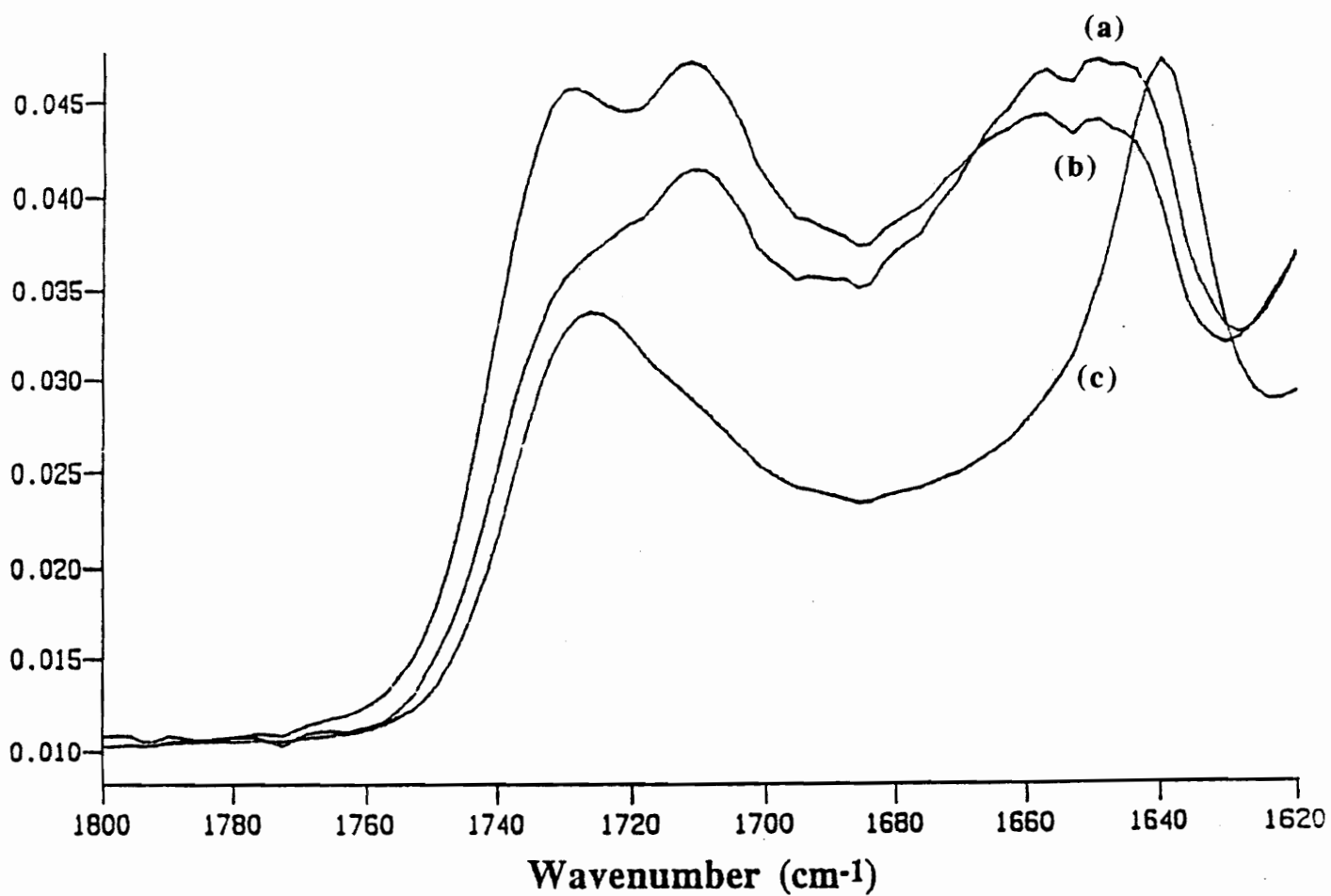


Figure 4.18. FTIR spectra in the carbonyl region of the molded foams (a) Fmc4 and (b) Fmc2 as well as slabstock foam (c) Fs5.

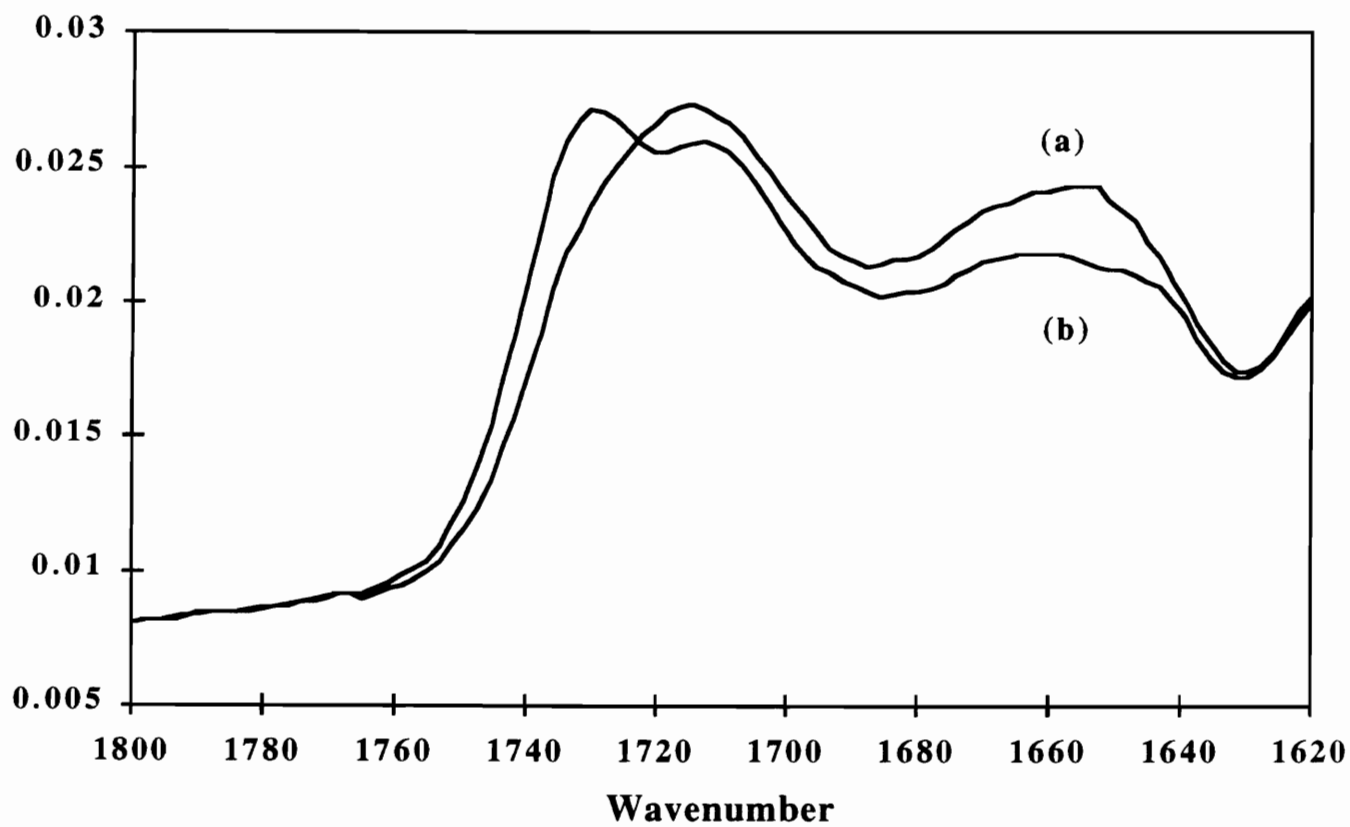


Figure 4.19. FTIR spectra in the carbonyl region of molded foams (a) Fmo4 and (b) Fmo2.

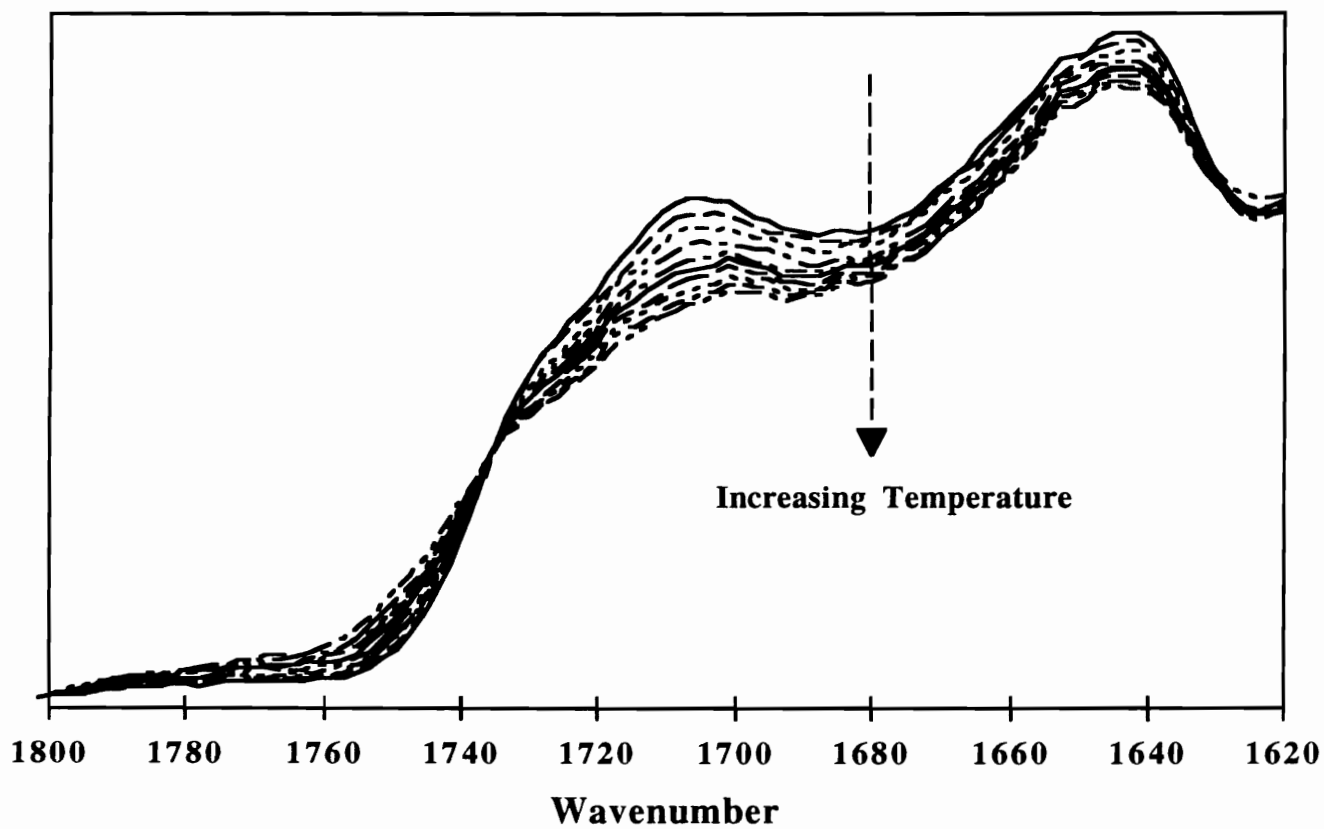


Figure 4.20. Influence of temperature on carbonyl absorbance in FTIR spectra of Fmc4.

increasing temperature. The decrease in absorbance is a result of decreasing hydrogen bond strength and even some dissociation. The decrease in the free or non-bonded carbonyl absorbance is a little surprising based on reports given in Chapter 2 which present an increase. However, Moreland also observed what appeared to be a decrease in the free carbonyl absorbance but attributed this to a broadening of this absorbance arising from spectral shifts to higher wavenumbers.⁷⁹ The evidence presented here complements the results which will be presented later in this chapter showing that the foams "soften" with temperature as based on direct mechanical property studies.

To aid the correlation between FTIR and WAXS that have been used to qualify the lack of local HS structural order, the 4 pph water content slabstock foam that was subjected to DMF and whose WAXS pattern showed a significant disruption of order, was also evaluated using FTIR. The carbonyl absorbance is shown in Fig. 4.21 along with the absorbance of the original sample. As can be seen, the original bidentate peak centered at 1640 cm^{-1} decreased in absorbance and shifted towards higher wavenumbers, now centered at 1645 cm^{-1} . The results here are in good agreement with the WAXS results suggesting that the extraction process disrupted some of the bidentate hydrogen bonding and ultimately some of the structural order of the HS domains. Clearly, FTIR is an excellent technique to evaluate the order of the HS domains but is somewhat lacking in correlating the FTIR observations to the extent of microphase separation. For example, as was shown, the molded foams displayed relatively strong SAXS "peaks" compared to slabstock foams yet showed poor bidentate hydrogen bonding and no Bragg-like rings in WAXS. In contrast, the slabstock foams which displayed very subtle SAXS shoulders, displayed strong bidentate absorbance and relatively sharp rings using WAXS.

Based on the similar infrared behavior exhibited by the CPP containing and CPP lacking foams, it is concluded that the copolymer polyols do not influence the bidentate absorbance and therefore do not influence the HS ordering. The small differences observed between the molded foams are due to differences in the water content where, as

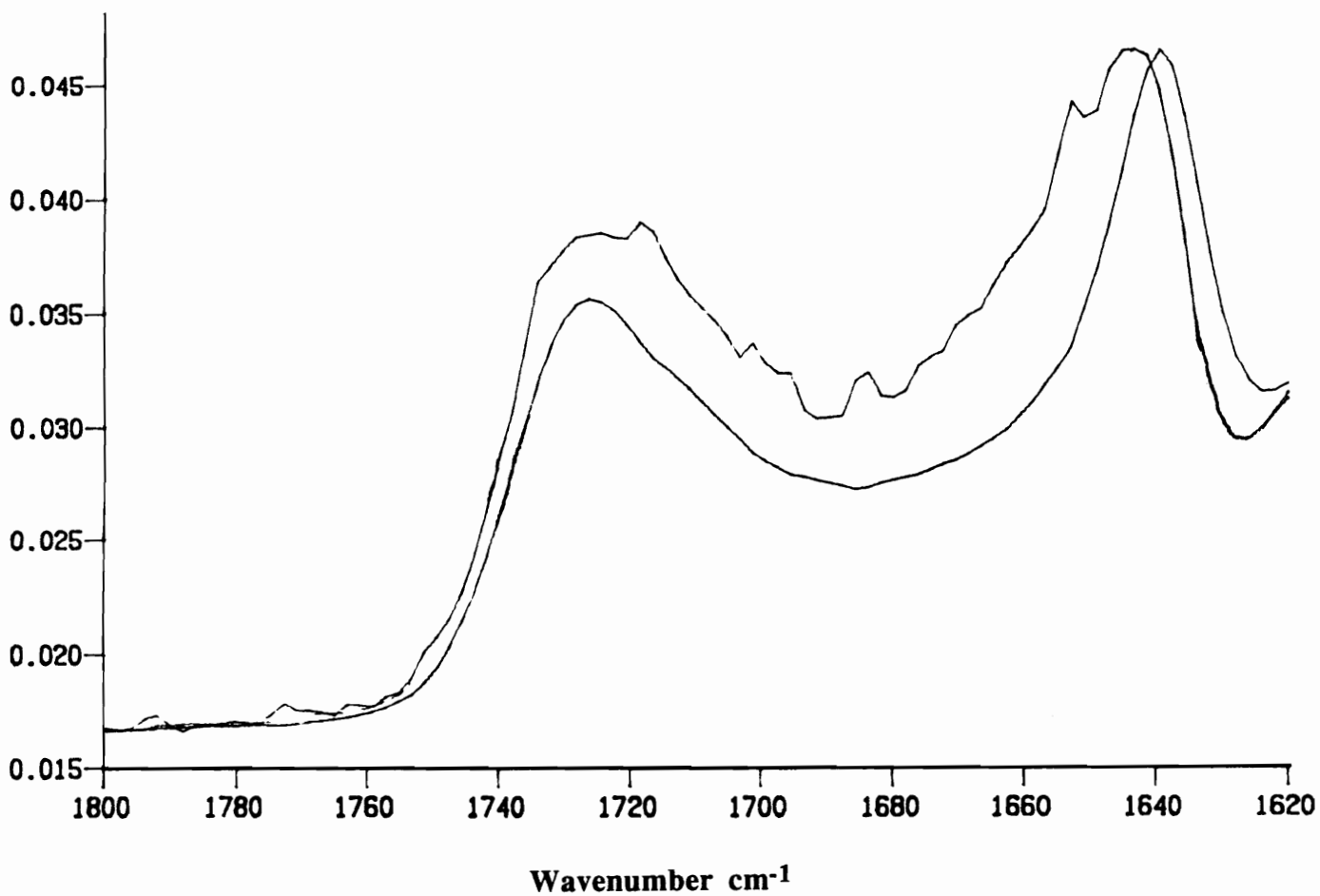


Figure 4.21. FTIR spectra in the carbonyl region of the slabstock foam (a) before extraction and (b) after extraction.

expected, the higher water/TDI content foams displayed slightly higher hydrogen bonded urea and naturally lower non-bonded urea. The indistinguishability exhibited between the CPP and non-CPP containing foams supports the results observed in the WAXS patterns.

4.4 Solvent Extraction Studies

The foam's covalent network was evaluated using extraction studies in dimethyl formamide (DMF) to compare the level of cross-linking as a function of the formulation ingredients. DMF was chosen in view of studies by Armstead in which a variety of solvents were used and DMF was found to be one of the better solvents - most likely a result of the solvent's polarity. The results, presented in Table 4.3, indicate that these foams are quite extensively cross-linked and that less than 8 wt.% can be extracted using DMF. A 4 pph water content slabstock foam similar to those studied by Moreland was also subjected to treatment in DMF, the results of which are also given in Table 4.2.⁷⁹ Following extraction, a wide angle x-ray scattering pattern (shown in Fig. 4.22) was obtained which revealed that much of the HS short range order exhibited by this foam had been disrupted by the extraction process. This suggests that the polar solvent DMF primarily disrupts and extracts any unattached urea based chains.. In addition, Armstead observed similar behavior with extraction studies on a slabstock foam and even analyzed the extract with infrared and found that the extract was primarily urea based.³³

4.4.1 Effect of Copolymer Polyols

From Table 4.3, it can be seen that the CPP containing foams displayed a greater amount of extractables than the foams lacking the CPP dispersion. In fact, the foams that incorporate CPPs lead to almost three times the amount of extractables over the foams free of CPPs. For example, the sol fraction of foam Fmc4 was ca. 9% where that of foam

Table 4.3. Solvent Extraction Results on Molded Foams

Foam	Sol fraction, %
Fmo4	3.0±0.2
Fmo2	3.8±0.1
Fmc4	8.8±0.1
Fmc2	8.3±0.2
Fme4	6.8±0.2
Fme2	7.0±0.2

Fmo4 was significantly lower, 3%. The values for the 2 pph water content foams also followed the same trend - the CPP containing foams exhibited a higher sol fraction. The results from this experiment strongly suggest that the CPPs are not as extensively reacted into the network as originally expected and that they may be interfaced to the surrounding soft segment principally only by secondary bonding. As was shown earlier, the stabilizer used prevented flocculation of the particles but may be less important in grafting the particles to the soft segment matrix. Restating this, these dispersions may only be linked to the soft phase by physical means such as hydrogen bonding. Further evidence supporting this will be presented in a later section (viscoelastic section) where the time-dependent properties of the CPP containing foams displayed much stronger sensitivity to temperature and humidity over those lacking CPP particles.

The experimental copolymer polyol foams also seemed to have a lower amount of extractables over the control copolymer polyol foams. Recall that the experimental CPPs were utilized in order to reduce the bulk viscosity of the reacting foam mixture early in the process. This was accomplished by two methods; first, the stabilizer of these CPPs was an isocyanate capped diol versus a triol and, second, less stabilizer was used in the case of the experimental CPPs. The amount of extractables for foam Fme4 was ca. 7%, slightly lower than that of Fmc4. The 2 pph water content foams displayed the same trend where the experimental CPP foam displayed a slightly lower sol fraction compared to the control CPP foam. The fact that this lower functionality stabilizer also prevented flocculation and displayed only a small effect on the extraction results also suggests that secondary bonding must be occurring.

4.4.2 Effect of Water/TDI Content

The water/TDI content in the formulation does not appear to have any significant effect on the amount of extractables. In some cases, it appeared that 2 pph water content

foams had a higher sol fraction while in others the trend was reversed. The sol fractions were only distinguished based on type of CPP utilized. Any variations in the observed mechanical properties as a function of water/TDI content appears to be attributable to differences in the HS domains, not covalent cross-linking.

4.5. Compression "Stress"-Strain

The compression loading-unloading response of the six molded foams was evaluated in terms of the formulation differences between them. The compression "stress"-strain behavior of foam Fmo4 is shown in Fig. 4.22. Figure 4.22a illustrates the loading and unloading curves while Fig. 4.22b illustrates the first loading and second loading after an intermediate 5 min. recovery. As can be seen, the curves can be divided into three deformation regions as has been well described by Gibson and Ashby: the linear bending region, the elastic buckling region, and the densification region.⁵⁷ The first region occurs in the first 10% strain and is representative of elastic bending of the cell struts. The second region represents buckling of the cell struts where the strain increases with small changes in load. The final densification region begins at ca. 65% strain which, in part, for that reason is also the level of compression chosen for the load relaxation measurements. Here the cells completely collapse and opposing cell walls come into contact. The fact that the loading and unloading curves are not superimposed confirms that these foams exhibit mechanical hysteresis.

Mechanical hysteresis is usually attributed to irreversible changes such as disentanglement of chains or plastic deformation, crazing, crack initiation, bond breaking, and even morphological changes such as crystallization and even other viscoelastic processes.⁸⁰ In polyurethane elastomers, hysteresis also originates from the disruption and displacement of domains primarily through hydrogen bond disruption.⁸⁰ Figure 4.22a shows that the foam was compressed to a maximum strain level of 76% which was chosen

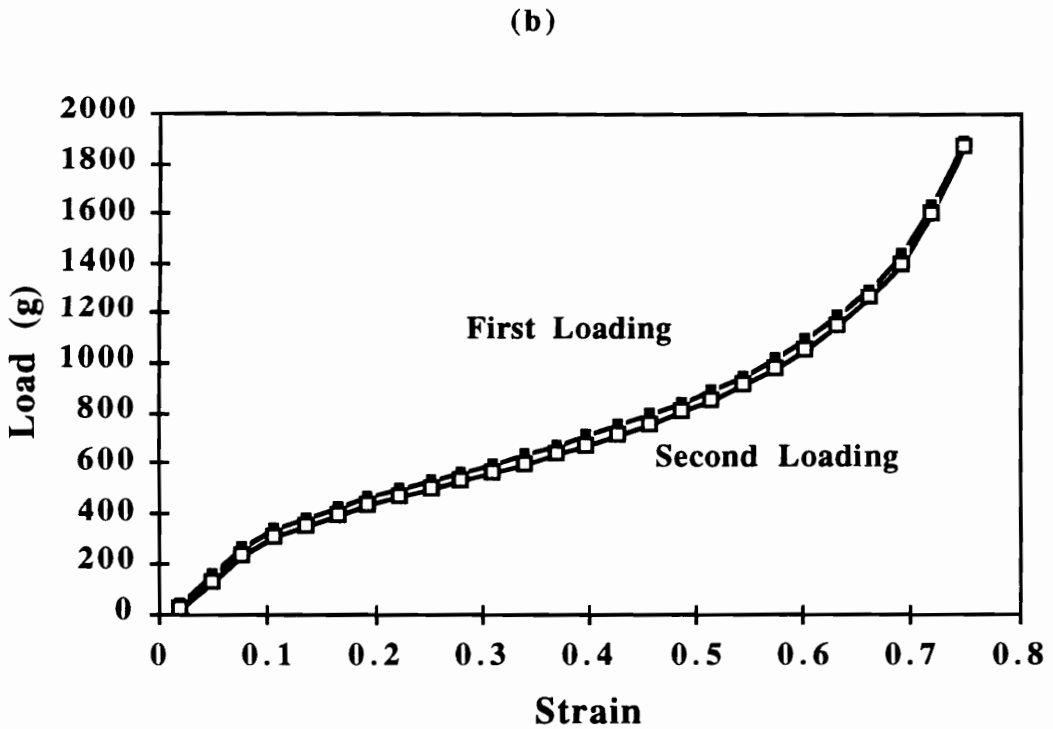
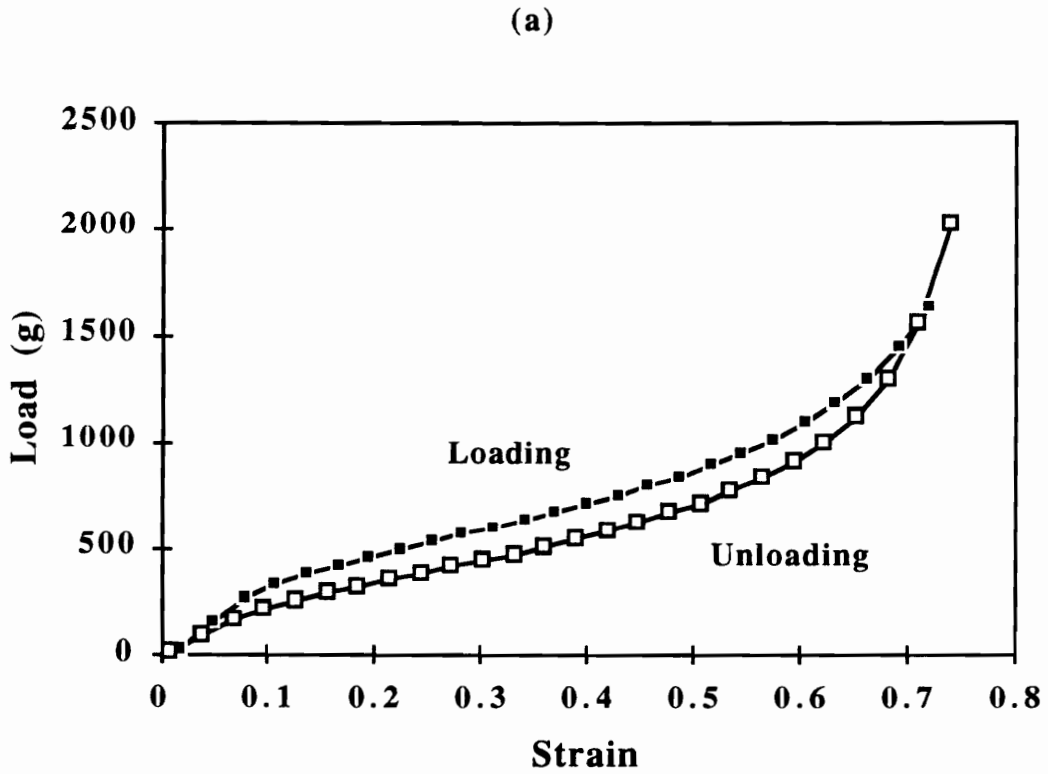


Figure 4.22. Load-strain behavior for Fmo4 illustrating hysteresis upon (a) loading-unloading and (b) first loading-second loading following a 5 min. recovery period.

in view of the physical limitation of the load cell. Figure 4.22b compares the first loading and second loading carried out 5 min. apart in light of the recovery period allowed in the load relaxation measurements. The two transitions from one region to the other occur at a strain of ca. 0.1 and 0.65, respectively. The loads at these strain values were 265g and 1300g respectively for the first loading. Naturally, on the second loading these values were slightly lower.

Figure 4.23 illustrates the loading-unloading as well as the first and second loading curves for Fmo2. The behavior is very similar to that of Fmo4 and the transitions occur at the same strain levels. The difference is that the loads are higher for Fmo2 than Fmo4. The higher density of Fmo2 is responsible for the higher loads at a given strain exhibited by this foam. In addition, Fig. 4.23b shows that very little difference exists between the first and second loading suggesting that considerable recovery has occurred in the 5 min. period and that the hysteresis is low. Figure 4.24a illustrates the loading-unloading behavior for Fmc4 and Fig. 4.24b illustrates the first loading and second loading of Fmc4. The compressive "stress"-strain behavior of Fmc2 is shown in Fig. 4.25. Likewise, Fig. 4.26 illustrates the load-strain behavior of foam Fme4. As can be seen, all foams exhibited similar behavior with the differences existing in the absolute loads and percent hysteresis. In order to demonstrate that the hysteresis was less during the second loading-unloading cycles relative to the first, the first loading-unloading cycle of Fmo4 is shown in Fig. 4.27a and the second loading-unloading cycle (after 5 min.) is shown in Fig. 4.27b. As can be seen, the amount of hysteresis is clearly less in the second cycle relative to the first.

In general, all foams demonstrated similar behavior exhibiting three deformation regimes resembling the description provided by Gibson and Ashby.⁵⁷ The differences between the foams lie in the load values and the amount of hysteresis. These points will be addressed in the following sections. In an attempt to compare the foams in terms of the percent load loss upon unloading the foam following compression, one strain value was picked from each deformation region. The load measured during unloading was related to

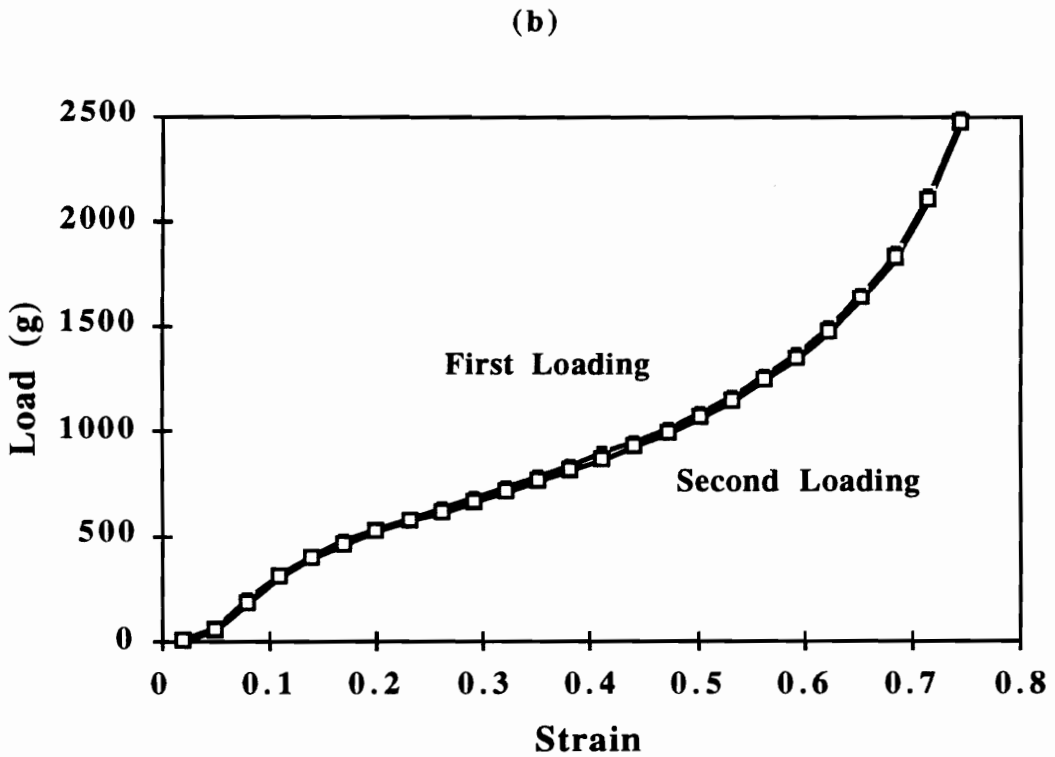
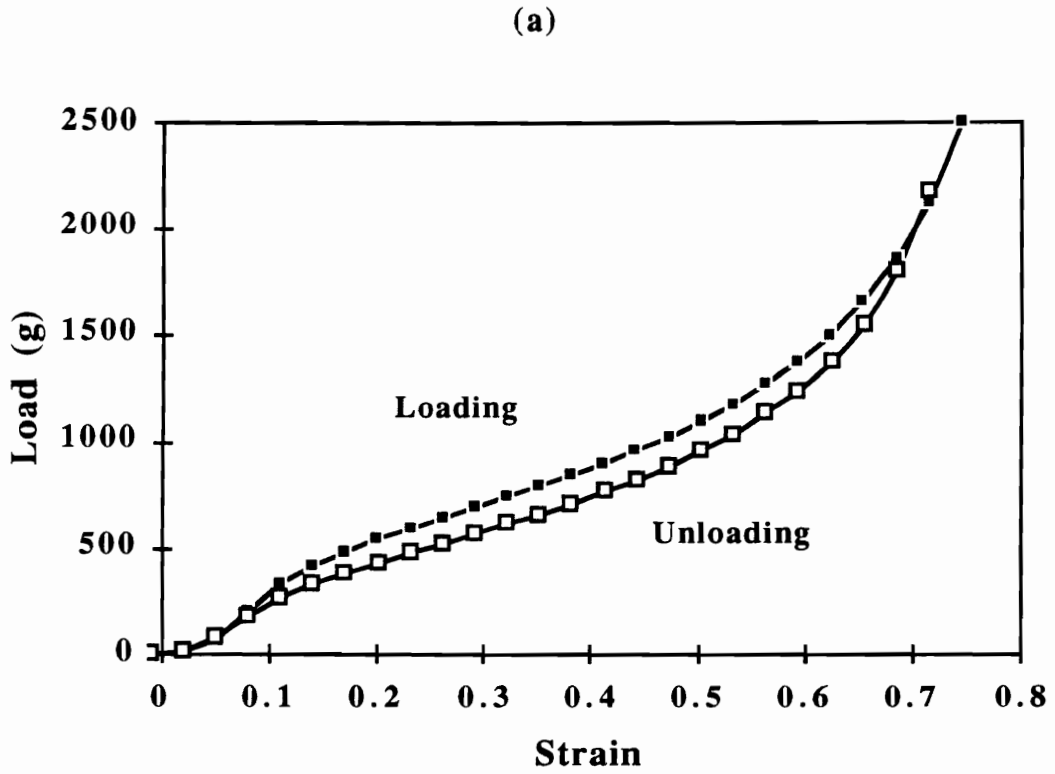


Figure 4.23. Load-strain behavior for Fmo2 illustrating hysteresis upon (a) loading-unloading and (b) first loading-second loading following a 5 min. recovery period.

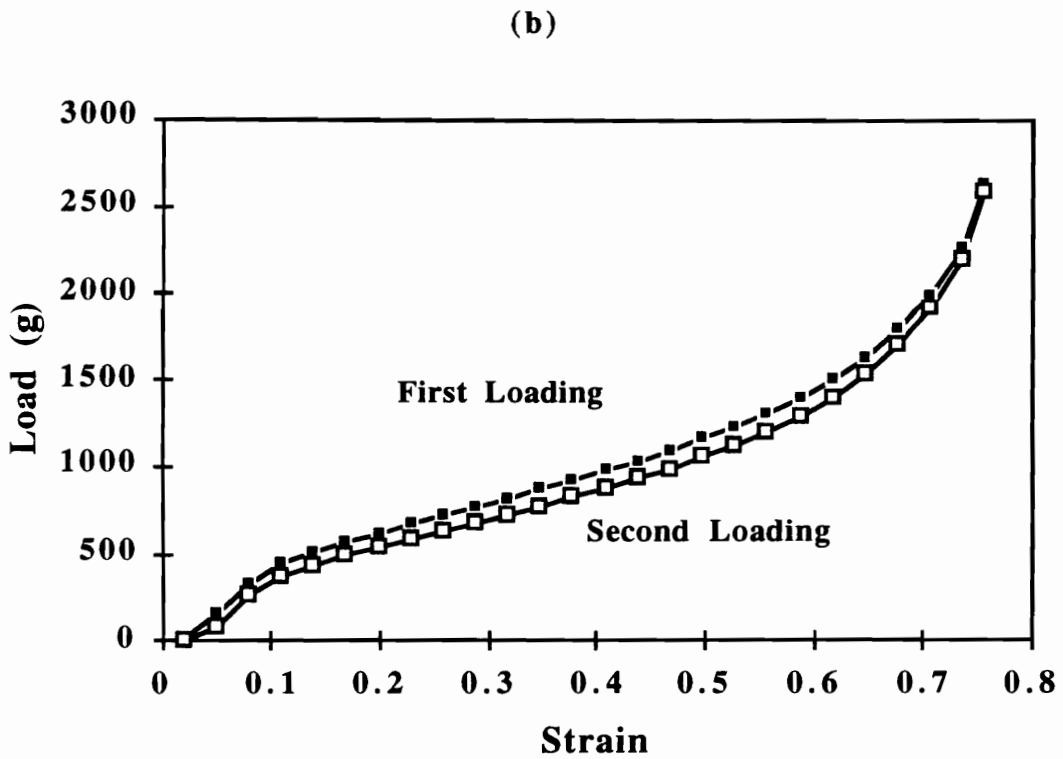
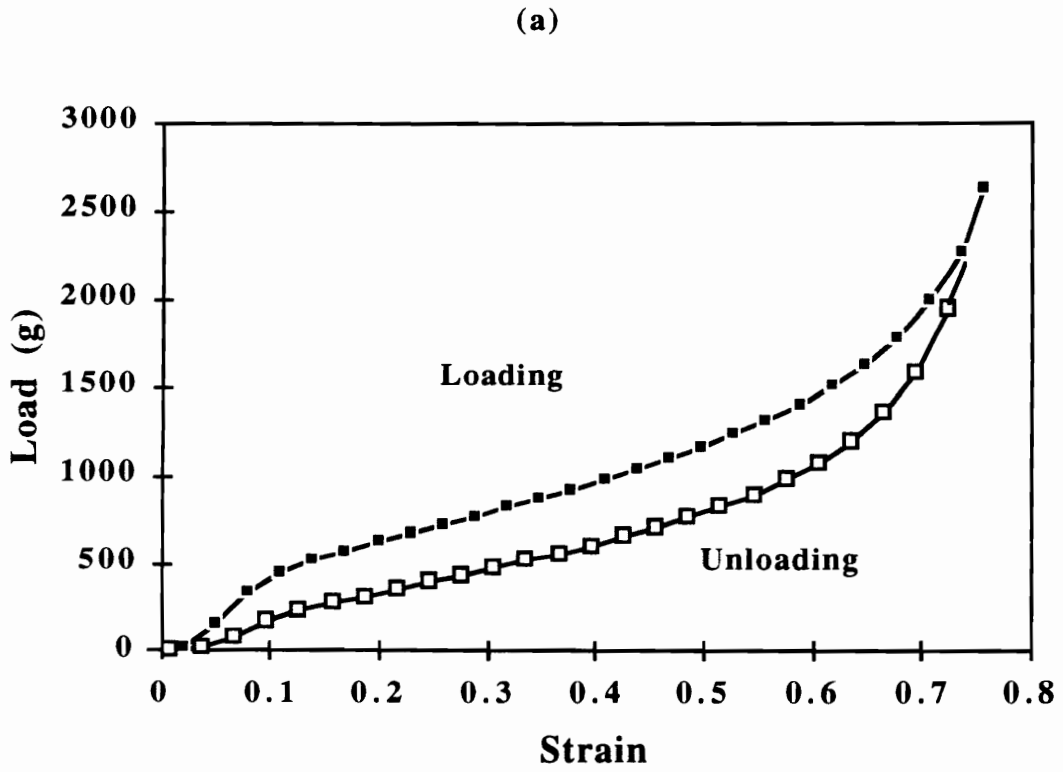


Figure 4.24. Load-strain behavior for Fmc4 illustrating hysteresis upon (a) loading-unloading and (b) first loading-second loading following a 5 min. recovery period.

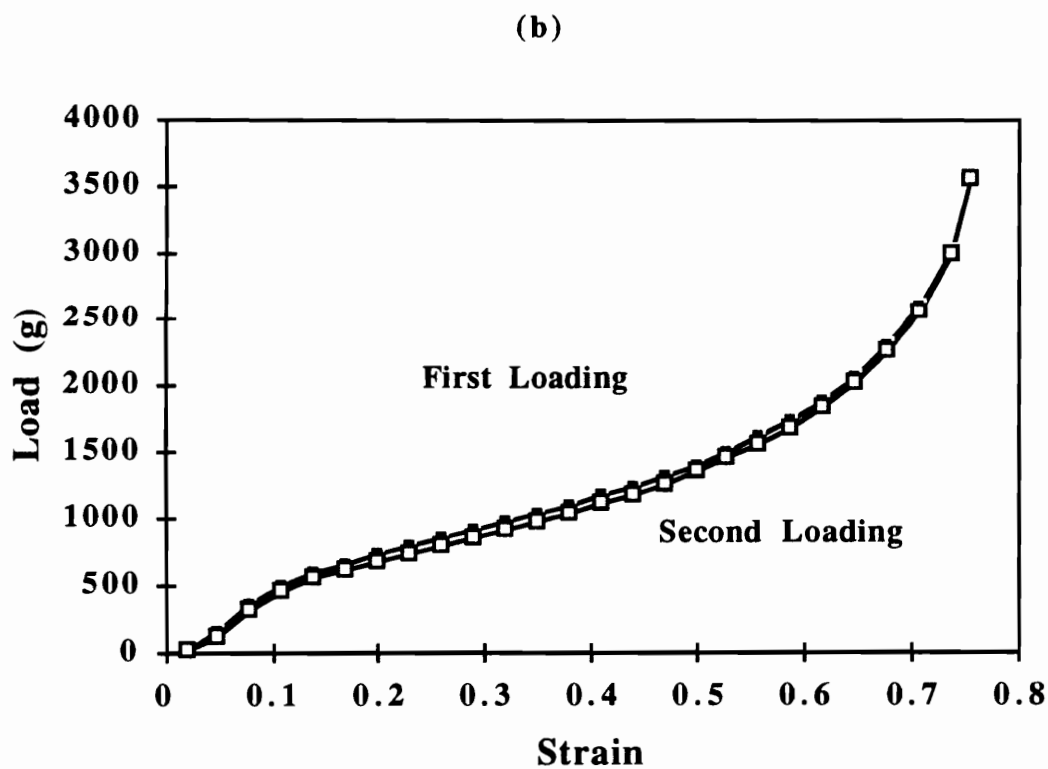
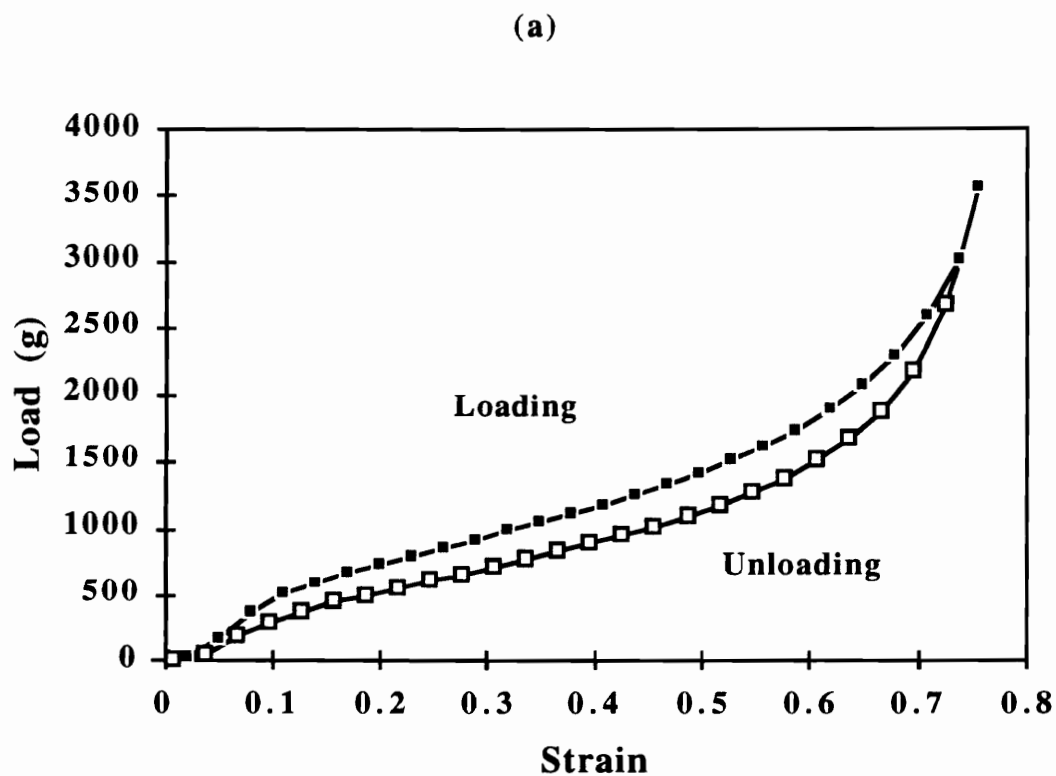


Figure 4.25. Load-strain behavior for Fmc2 illustrating hysteresis upon (a) loading-unloading and (b) first loading-second loading following a 5 min. recovery period.

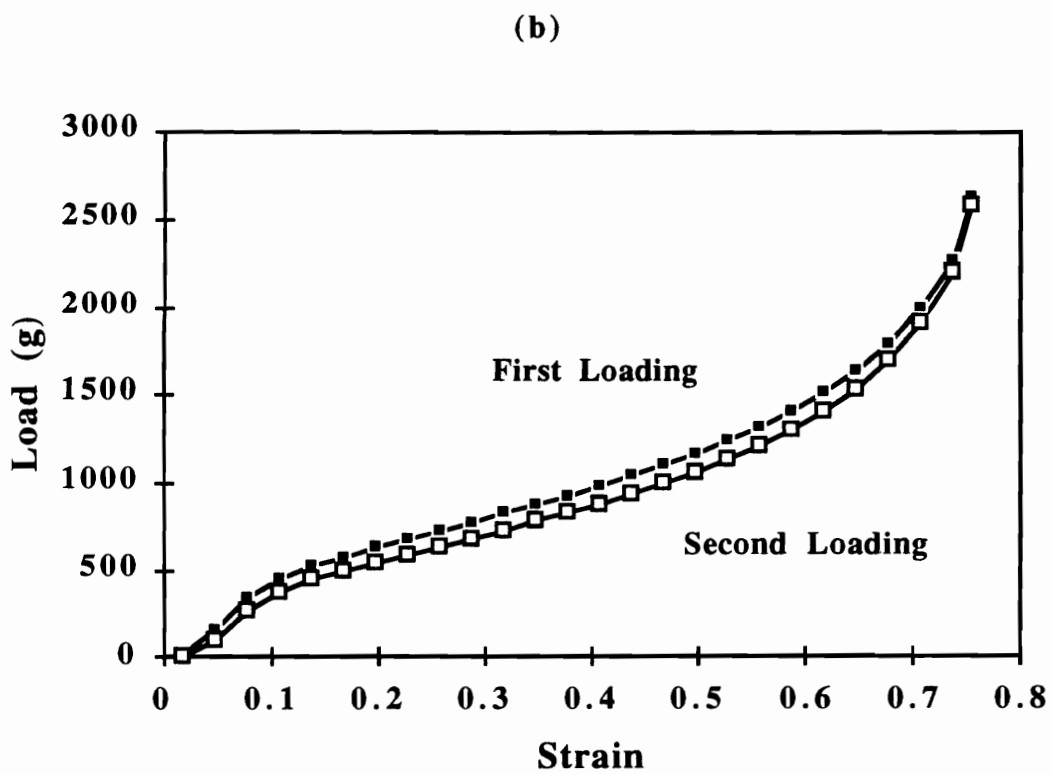
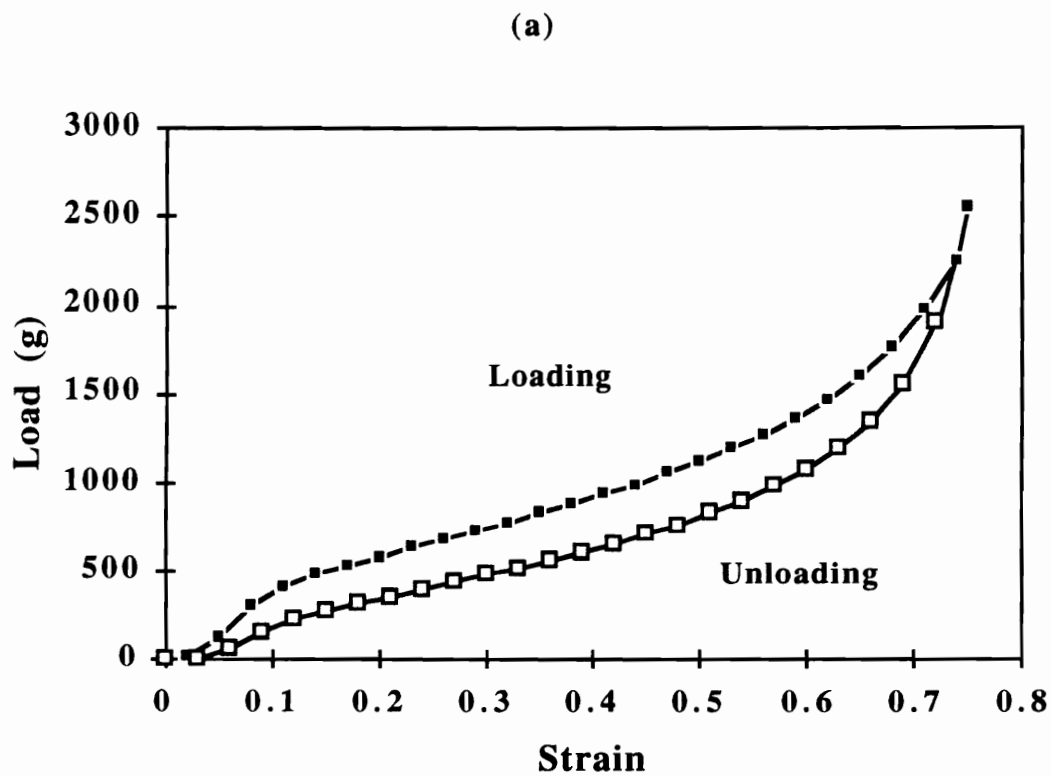


Figure 4.26. Load-strain behavior for Fme4 illustrating hysteresis upon (a) loading-unloading and (b) first loading-second loading following a 5 min. recovery period.

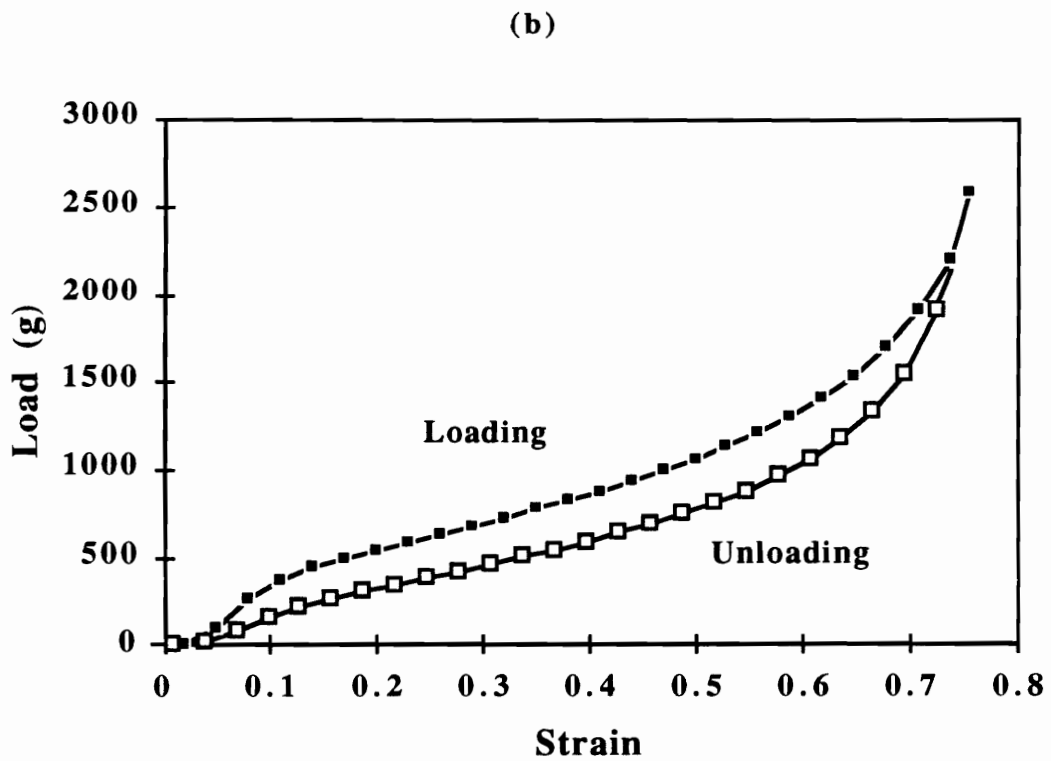
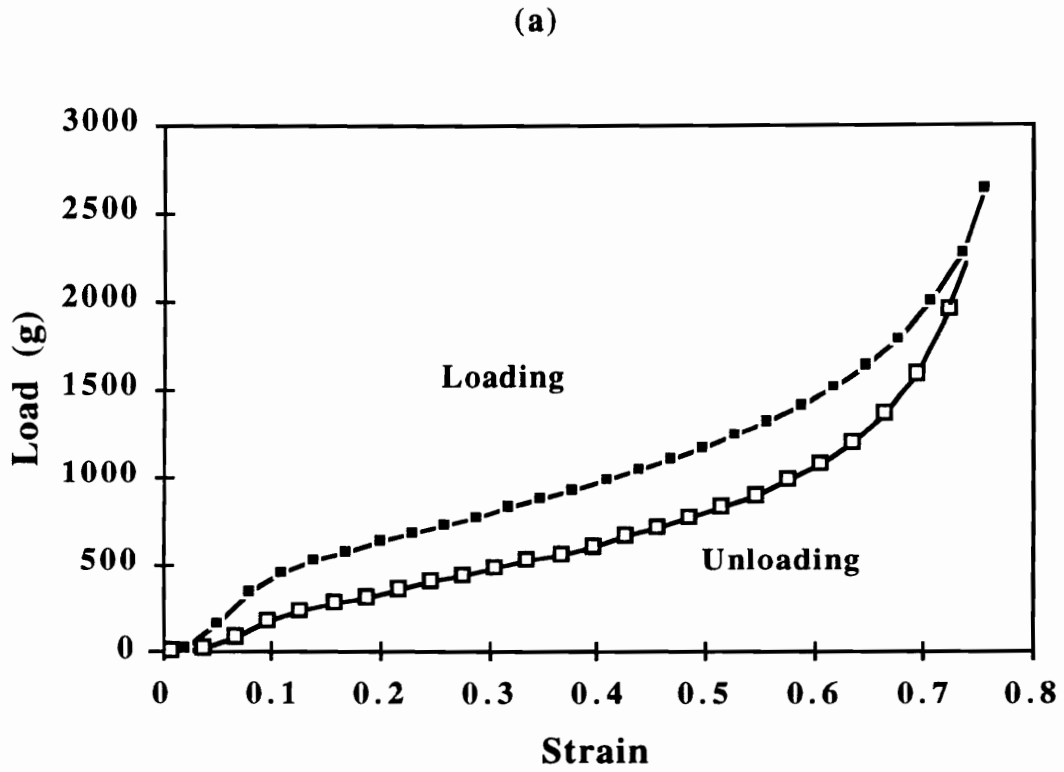


Figure 4.27. Load-strain behavior for Fmc4 illustrating hysteresis difference between (a) first loading-unloading and (b) second loading-unloading following a 5 min. recovery period.

the load during loading and is presented in Table 4.4 for each strain level. For example, in the bending region the chosen level of strain was 0.07 and the load loss was determined by $1 - L_u/L_l$ (where L_u is the load upon unloading while L_l is the load during loading) whose value is presented in Table 4.4. For foam Fmo4, the returning load was 30% lower than upon loading. In the buckling region ($\epsilon = 0.65$), the load loss was 20% and in the densification region, it was 7%. As displayed by all the foams, the load loss decreased as the level of deformation increased.

4.5.1 *Effect of Copolymer Polyols*

The influence of the copolymer polyols (CPP) on the load-strain behavior of these foams was the same for a given water/TDI content. In general, the inclusion of CPPs in the formulation increased the load at any given strain level. The measured loads were 25% to 35% higher for the CPP containing foams. For example, at a strain level of 0.4, comparing the loading curves of Fmo4 to Fmc4 reveals that Fmc4 displayed a load of 964g while Fmo4 displayed a load of 710g. The trend was similar at other strain levels as well, e.g. at a deformation level of 0.7, loads were 1945g for Fmc4 and 1504g for Fmo4. The 2 pph water content foams also portrayed a similar trend with in the inclusion of CPPs. Comparing Fig. 4.23 to Fig. 4.25 illustrates this point as do the values presented in Table 4.4. It can be concluded that the incorporation of this rigid filler into the formulation does indeed increase the foam "hardness" based on the increase in displayed loads at any level of deformation. In general, the loads of the CPP containing foams were ca. 25%-35% above those displayed by the foams free of CPPs. This point will also be confirmed by the observations in the following viscoelastic sections where the initial loads were ca. 25% greater for the CPP containing foams.

While the CPP containing foams displayed higher loads for a given strain during loading, the amount of hysteresis was also greater as presented in Table 4.4. For example,

Table 4.4. Loads Exhibited Upon Loading and Unloading as well as Loss of Load

Foam		Deformation Regions (strain)			Overall Hysteresis, %
		Bending(0.075)	Buckling(0.40)	Densification(0.70)	
Fmo4	Loading Load(g)	255	710	1504	16
	Unloading Load(g)	179	558	1404	
	Load Loss (%)	30	21	7	
Fmo2	Loading Load(g)	183	877	2006	11
	Unloading Load(g)	166	742	1983	
	Load Loss (%)	10	15	1	
Fmc4	Loading Load(g)	305	964	1944	31
	Unloading Load(g)	106	613	1645	
	Load Loss (%)	65	37	15	
Fmc2	Loading Load(g)	331	1161	2537	23
	Unloading Load(g)	210	892	2266	
	Load Loss (%)	37	23	11	
Fme4	Loading Load(g)	279	917	1902	28
	Unloading Load(g)	115	628	1675	
	Load Loss (%)	59	32	12	
Fme2	Loading Load(g)	311	1176	2682	20
	Unloading Load(g)	192	880	2436	
	Load Loss (%)	38	25	9	

comparing Fm04 (Fig. 4.22) to Fmc4 (Fig. 4.24) shows that the amount of hysteresis is greater for Fmc4, 30% compared to 16%. Furthermore, the values for the amount of load loss during unloading also presented in Table 4.4, indicate that the load is considerably less during unloading than loading for the CPP containing foams. For example, the load loss (strain of 0.075) was only 30% for Fm04 but was 65% for Fmc4. In the bending regime (strain of 0.4), the load loss was 21% for Fm04 but 36% for Fmc4. Finally, in the densification region (strain of 0.7), the load decreased by 7% during unloading over that of loading for foam Fm04 and by 15% for foam Fmc4. Again, the trend was the same for the 2 pph water content foams as clearly depicted in Table 4.4. The percent hysteresis for Fmc2 was 20% while for Fm02, it was 11%. The load loss was also lower in each deformation region for the foams lacking the CPP dispersions. From these results, it can be concluded the deformation mechanisms exhibit more hysteretic character for the CPP containing foams suggesting that these particles may increase the localized stress primarily at the interface because of their stiffness. The strain of the soft segment is greater since the soft segment area which accommodates the load is decreased as the CPP dispersions occupy a portion of the volume that would otherwise be occupied by the soft segment. This increased level of localized stress can further lead to disruption of hydrogen bonding at the interface resulting in more flow and greater hysteresis.

Comparing the amount of recovery that occurs in a 5 min. period between the CPP containing foams and those that do not contain any CPPs reveals that greater recovery is achieved for the foams not containing the CPP particles. Figure 4.22b shows that Fm04 recovers considerably in 5 min. where the first and second loading curves were within closer proximity. The recovery of Fmc4 after 5 min. from the initial loading shown in Fig. 4.24b is not as extensive as that of Fm04. The greater hysteresis exhibited by the CPP containing foams is believed to be a result of the rigid filler promoting increased localized stress and thus increased flow or chain slippage primarily disrupting hydrogen bonding at

the interface. The results suggest that the deformation these particles are subjected to results in permanent changes in structure.

With respect to the "experimental" copolymer polyols, they had little effect on the load-strain behavior relative to the "control" copolymer polyols. The loads were relatively unchanged but the amount of hysteresis decreased slightly. Table 4.4 shows that the load loss during reformation relative to deformation was slightly lower for the experimental CPPs than the control CPPs. In other words, the load loss upon reformation (removal of the load) was lower for the experimental CPPs compared to control CPPs such as Fme4 relative to Fmc4. A possible explanation is that the lower amount of grafting of these particles as a result of a lower surface functionality may allow them to respond more elastically thereby providing for more recovery and less hysteresis.

4.5.2 Effect of Water/TDI content

An increase in HS content produced a similar result in the hysteresis as did the incorporation of CPP particles discussed in the former section where the hysteresis increased. Strong evidence supporting that the mechanical disruption of hydrogen bonds is primarily responsible for the hysteresis observed is obtained by comparing the 2 pph water content foams to the 4 pph water content foams. Comparing Fig. 4.24 to Fig. 4.25, shows that Fmc4 displayed greater hysteresis than Fmc2. The amount of hysteresis of Fmc4 was 31% while that of Fmc2 was 23%. The more dense, lower HS content Fmc2 not only displayed higher loads at any given strain but also lower hysteresis. For example, at a strain level of 0.7, the deformation load displayed by Fmc2 was 2537g and that displayed by Fmc4 was 1945g. The higher loads displayed by Fmc2 was a result of this foam possessing a higher density than the 4 pph water content foam. Furthermore, the loss of deformation load upon reversing the strain was lower for Fmc2. This loss at a strain level of 0.7 was 15% for Fmc4 and 11% for Fmc2. Since Fmc4 does have a higher HS content

relative to Fmc2, it also has a higher hydrogen bonding content which may be mechanically disrupted. The HS domains increase the amount of localized stress leading to increased relaxation and hysteresis. Within the buckling region (strain of 0.4), the load loss was 37% for Fmc4 and 23% for Fmc2. This trend with water/TDI content was exhibited throughout this molded foam series regardless of the CPP utilized. While these hysteresis curves provide good information on the influences of HS content and CPP content, the viscoelastic properties are deemed more important since they more closely resemble the loading these foams undergo in end use.

4.6 Viscoelastic Behavior

The viscoelastic behavior of the flexible molded polyurethane foams and the influences of temperature and humidity on this behavior were evaluated using load relaxation, creep, and compression set. These measurements are excellent techniques that best simulate "real world" applications under different environmental conditions. In addition to being a good indication of the load bearing capabilities of the foams and the recoverability, the viscoelastic properties are sensitive to the network of the foam arising from both hard segment domains and covalent cross-links.

4.6.1 Load Relaxation Behavior

The compression load relaxation behavior is now presented which was performed at a constant 65% strain and under different temperature/humidity conditions. A strain of 65% was chosen based on earlier results which showed that the onset of densification occurred in this range and hence allows for evaluation of the polymer network. It is also the level of strain used by other researchers in relaxation measurements as well as in the well practiced industrial indentation load deflection (ILD) measurements and can thus allow

for qualitative comparisons. Figure 4.28 illustrates the load relaxation behavior for Fmc2 at 30°C-35%RH. The data have been plotted as a function of log time which allows for the observation of the results within this period and which can be used to qualitatively estimate a decay rate from the slope of the curves to be used for comparison purposes. As can be seen, the majority of the decay in load occurs within the first 20 min. As expected, the load does not decay to zero in this three hour period due to the covalent as well as physical (HS domains) network character of the foam. In all of the following figures, the load axis will not begin at zero but rather a higher load to allow for better visualization of differences that exist in these plots and between the different samples.

The variables evaluated and presented in the oncoming sections are as follows: a) the external variables of temperature and humidity and their influence on the relaxation behavior to ascertain the contribution to the viscoelastic properties by the covalent cross-links as well as the physical “cross-links”; (b) the influence of copolymer polyols, and (c) the influence of the water/TDI content in the formulation which inherently includes the density of the foams.

4.6.1.1. Effects of Temperature and Relative Humidity

The load relaxation behavior as a function of temperature and humidity for Fmo4 is shown in Fig. 4.29. An increase in temperature and/or humidity resulted in a shift of the relaxation curves to lower loads and an increase in the percent decay. The initial load decreased from 1597g at 30°C-35%RH to 1156g at 100°C-35%RH. Likewise, at the high humidity condition, the loads were 1135g at 30°C-98%RH, and 1049g at 100°C-98%RH. The percent decay dramatically increased as well from 27% at 30°C-35%RH to 51% at 100°C-98%RH. The results shown in Fig. 4.29 indicate that both temperature and humidity significantly "plasticize" the exhibited behavior. Table 4.5 gives the initial loads and the percent decays. The results clearly show that the load is decreased and the percent

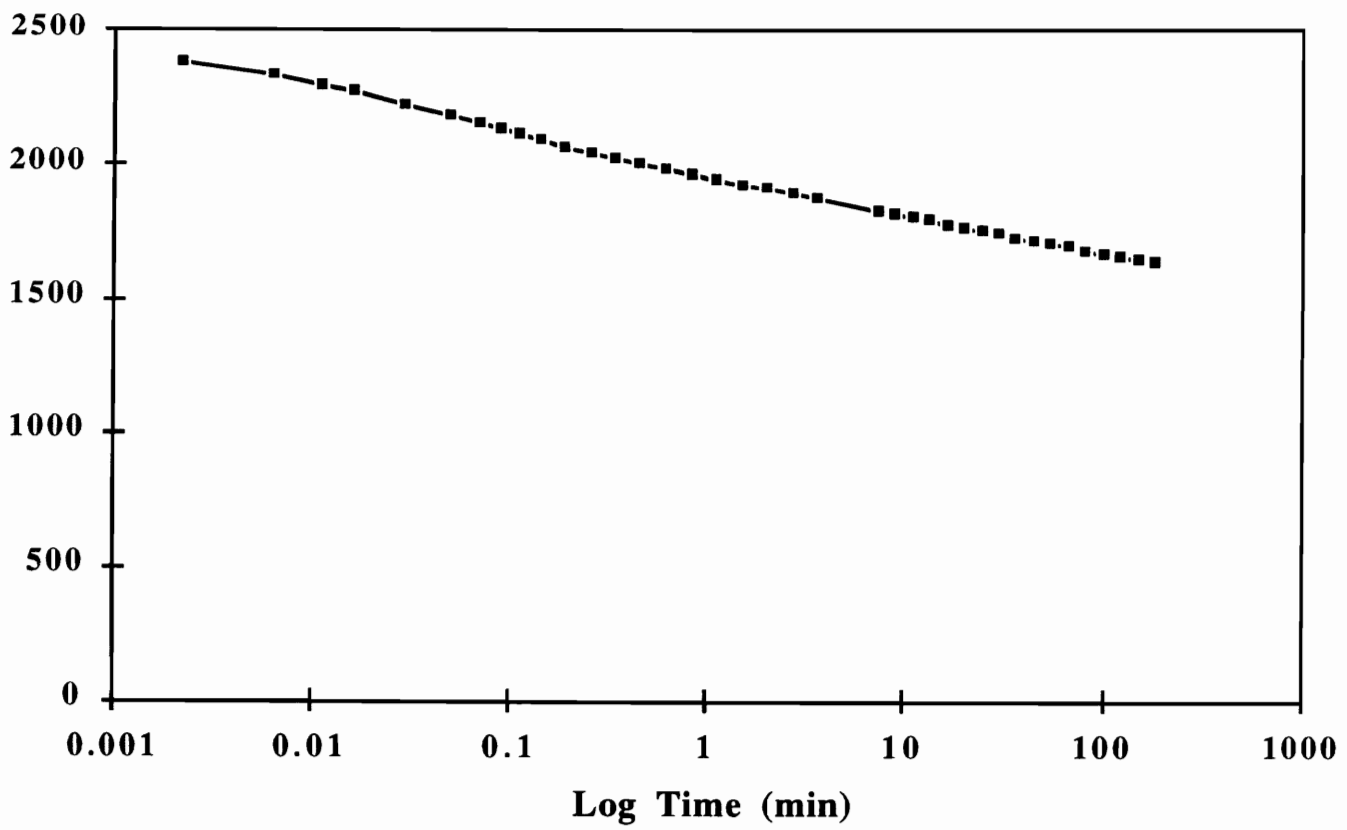


Figure 4.28. Load relaxation behavior of Fmc2 at 30°C-35%RH under a constant deformation of 65%.

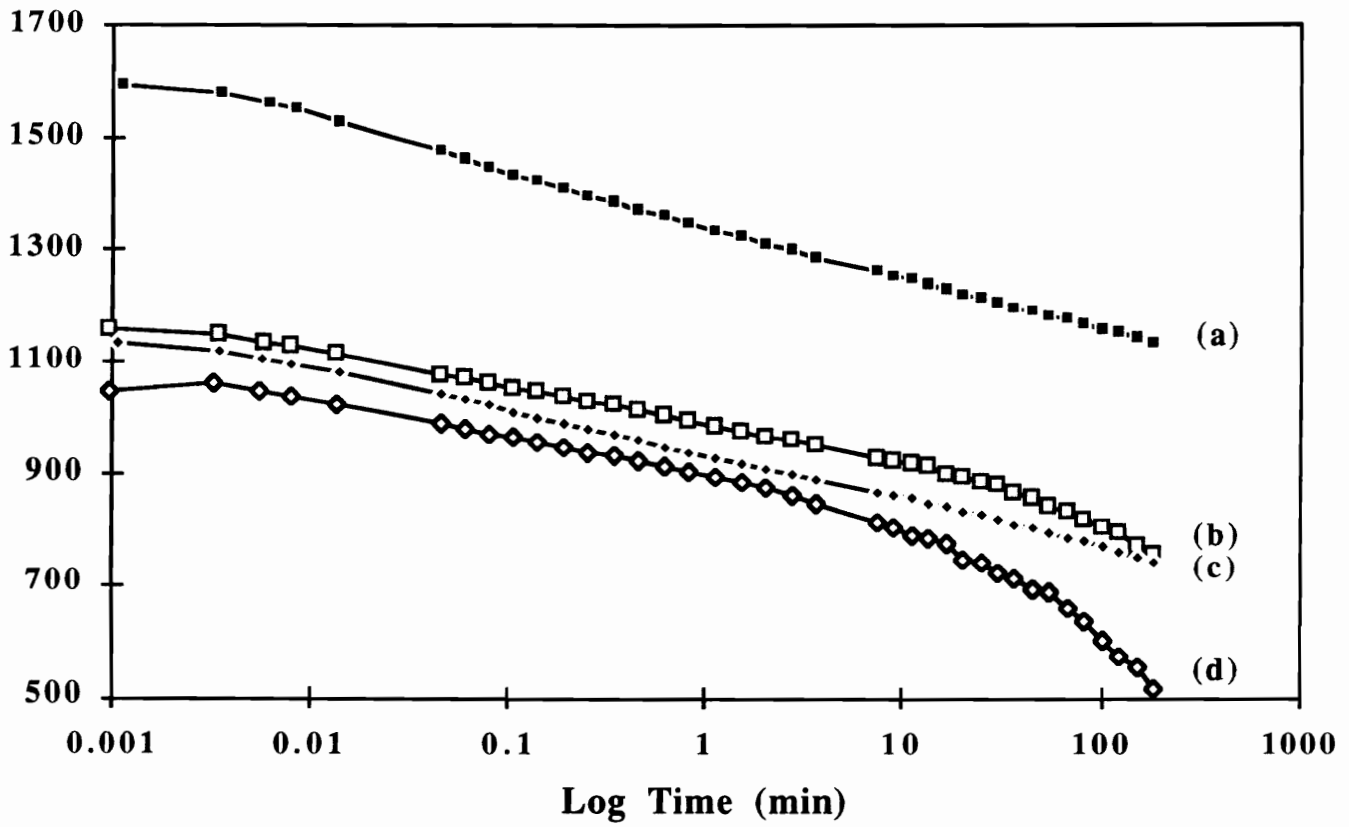


Figure 4.29. Load relaxation behavior of Fmo4 as a function of temperature/relative humidity, (a) 30°C-35%RH, (b) 100°C-35%RH, (c) 30°C-98%RH, and (d) 100°C-98%RH.

Table 4.5. Summary of Load Relaxation Measurements on Fm04

Temp-%RH (°C-%)	Std Dev. ¹ (±g)	Init. Load (g)	% Decay (%)
30-35	14	1597	27.0
100-35	38	1156	34.6
30-98	19	1135	34.4
100-98	153	1049	50.6

1. Based on two to three runs for each temperature and humidity.

decay is increased as the temperature and/or humidity is increased. This table also shows that only a small amount of scatter exists in this data. The decrease in load and increase in percent decay with temperature is primarily due to hydrogen bond disruption by the high temperature and/or high humidity therefore increasing the amount of chain slippage that occurs. This suggests that hydrogen bonding (predominately occurring within the hard segment domains) significantly enhances the foam properties, and when disrupted by temperature and/or humidity, these properties are severely altered. In addition, the increased soft segment mobility with temperature contributes to the increased percent decays and decreased initial loads. The nonlinearity observed at high temperatures, especially 100°C, suggests that the relaxation mechanism is enhanced or possibly an additional mechanism may be occurring. At the upper temperatures, the amount of hydrogen bond disruption is expected to dramatically increase. At the very highest temperature, the retroreaction or reversal of the urethane reaction may also occur as was shown by Moreland et al.⁷⁹ It is well known that temperature can disrupt hydrogen bonding, but it is clearly shown that humidity can also have a dramatic effect. As will be shown by several examples in this section, high humidity also plays a similar role to higher temperatures as might be somewhat expected. For example, increasing the humidity from 30% to 98% at 30°C resulted in a similar decrease in initial load as did increasing the temperature to 100°C at 35%RH. Table 4.6 lists the effects of increasing temperature and humidity on the initial load and percent decay illustrating the similar effects of both temperature and humidity. While in some situations, the temperatures of molded foams in vehicle seats may approach high temperatures (ca. 100°C), it is much more likely that they will be exposed to high humidities (ca. 100%RH) at lower temperatures instead. Therefore, the influence of relative humidity may be practically more important than temperature.

Figure 4.30 illustrates the load relaxation behavior and the temperature/humidity influences on this behavior for Fmo2. Increases in either temperature or humidity shifted

Table 4.6. Effect of Temperature and Relative Humidity on Load Relaxation of Fmo4

Effect of Temperature

Relative Humidity	Increasing Temp from 30°C to	Change in Init. Load* $\Delta(g_0) \%$	Change in Load Decay* $\Delta(\%) \%$
35%	100	-28	28
98%	100	-34	47

Effect of Relative Humidity

Temperature (°C)	Increasing %RH from 35% to	Change in Init. Load* $\Delta(g_0) \%$	Change in Load Decay $\Delta(\%) \%$
30	98	-29	27
100	98	-9	46

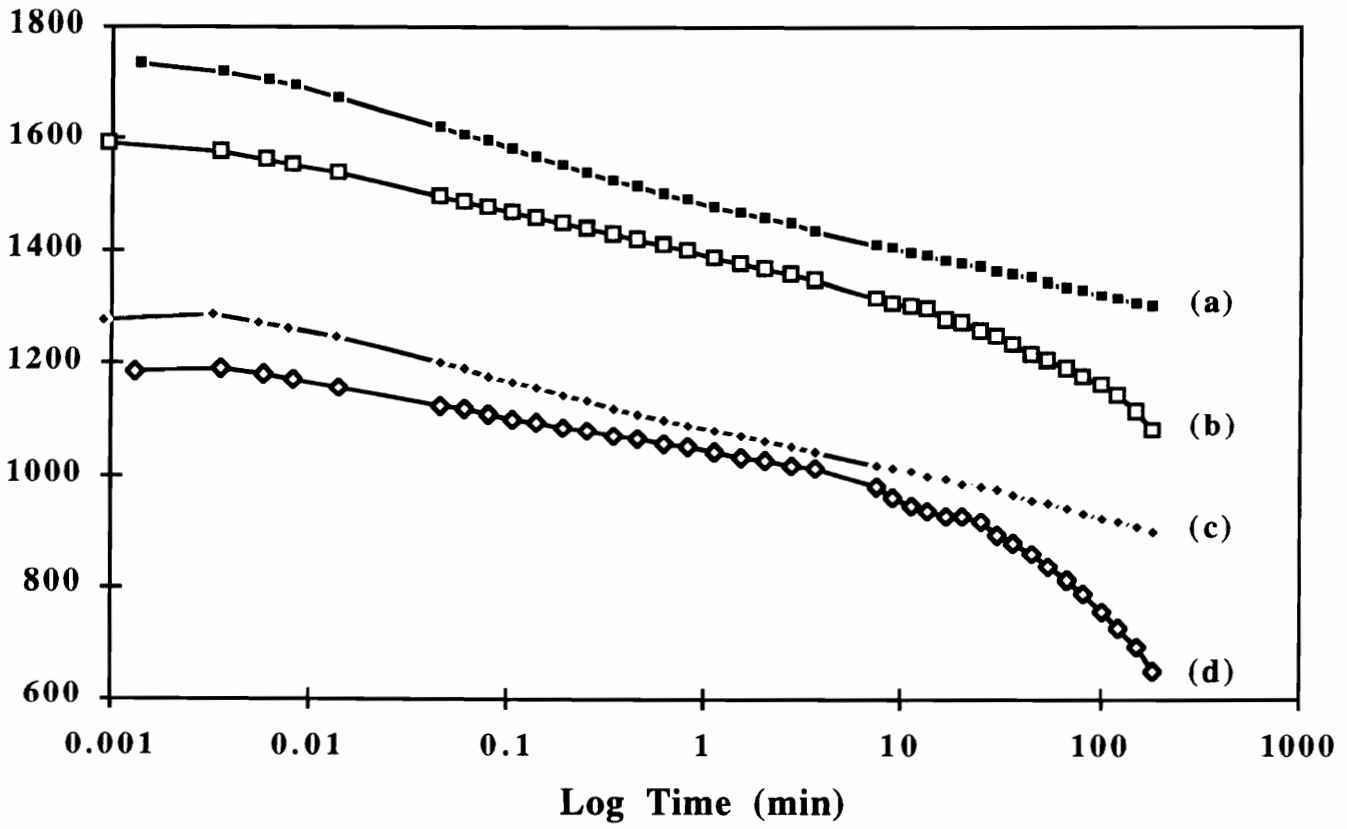


Figure 4.30. Load relaxation behavior of Fmo2 as a function of temperature/relative humidity, (a) 30°C-35%RH, (b) 100°C-35%RH, (c) 30°C-98%RH, and (d) 100°C-98%RH.

the load relaxation behavior to lower loads. The initial load at 30°C-35%RH was 1737g and at 100°C-98%RH it was 1186g. As with Fmo4 the percent decay also increased with an increase in temperature and/or humidity. These values were 25% at 30°C-35%RH and 45% at 100°C-98%RH. In addition, the data obtained at 100°C deviate from linearity indicating that this high temperature accelerated the relaxation mechanism. The overall results from this set of experiments are presented in Table 4.7. As with Fmo4, a minimum amount of scatter exists within these results. Table 4.8 gives the direct effects on the initial load and percent decay by temperature and humidity. Both tables as well as Fig. 4.30 suggest that the high humidity had a greater softening effect than temperature. The major difference between the behavior displayed by Fmo2 and that discussed previously displayed by Fmo4 is that the former displayed a higher load suggesting that this foam is stiffer - a result of it having a higher density.

The remaining foams that were investigated in the molded foam series contained CPP particles. With these foams, smaller increments in temperature were used to more closely follow the trend with temperature. The load relaxation behavior for Fmc4, as a function of temperature, is shown in Fig. 4.31 in a 3-dimensional surface plot where log-load is plotted versus log-time. As can be seen, an increase in temperature systematically shifted the relaxation curves to lower loads. This shows that the thermal “plasticization” occurs even at temperatures distinctly below 100°C. The initial load decreased from 2019g at 30°C-35%RH to 1271g at 100°C-35%RH while the percent decay in the three hour period increased from 36% to 54% as is exemplified in Table 4.9.

In general, any increase in temperature beyond 30°C resulted in a softening of the foam. Recall, that low water content slabstock foams displayed increases in load with initial increases in temperature as discussed in Chapter 2. In that case, the covalent cross-links dominate the load time behavior relative to the HS domains as noted by the pronounced rubber elasticity effect. In contrast, the molded foams studied here exhibited a softening effect with all temperature increases and at 98%RH as shown in Fig. 4.32. In

Table 4.7. Summary of Load Relaxation Measurements on Fmo2

Temp-%RH (°C-%)	Std Dev. ¹ (±g)	Init. Load (g _o)	% Decay (%)
30-35	183	1737	25.2
100-35	16	1590	31.9
30-98	4	1279	29.5
100-98	57	1186	45.1

1. Based on two to three runs for each temperature and humidity.

Table 4.8. Effect of Temperature and Relative Humidity on Load Relaxation of Fmo2

Effect of Temperature

Relative Humidity	Increasing Temp from 30°C to	Change in Init. Load* $\Delta(g_0) \%$	Change in Load Decay* $\Delta(\%) \%$
35%	100	-8	27
98%	100	-7	53

Effect of Relative Humidity

Temperature (°C)	Increasing %RH from 35% to	Change in Init. Load* $\Delta(g_0) \%$	Change in Load Decay $\Delta(\%) \%$
30	98	-26	17
100	98	-25	41

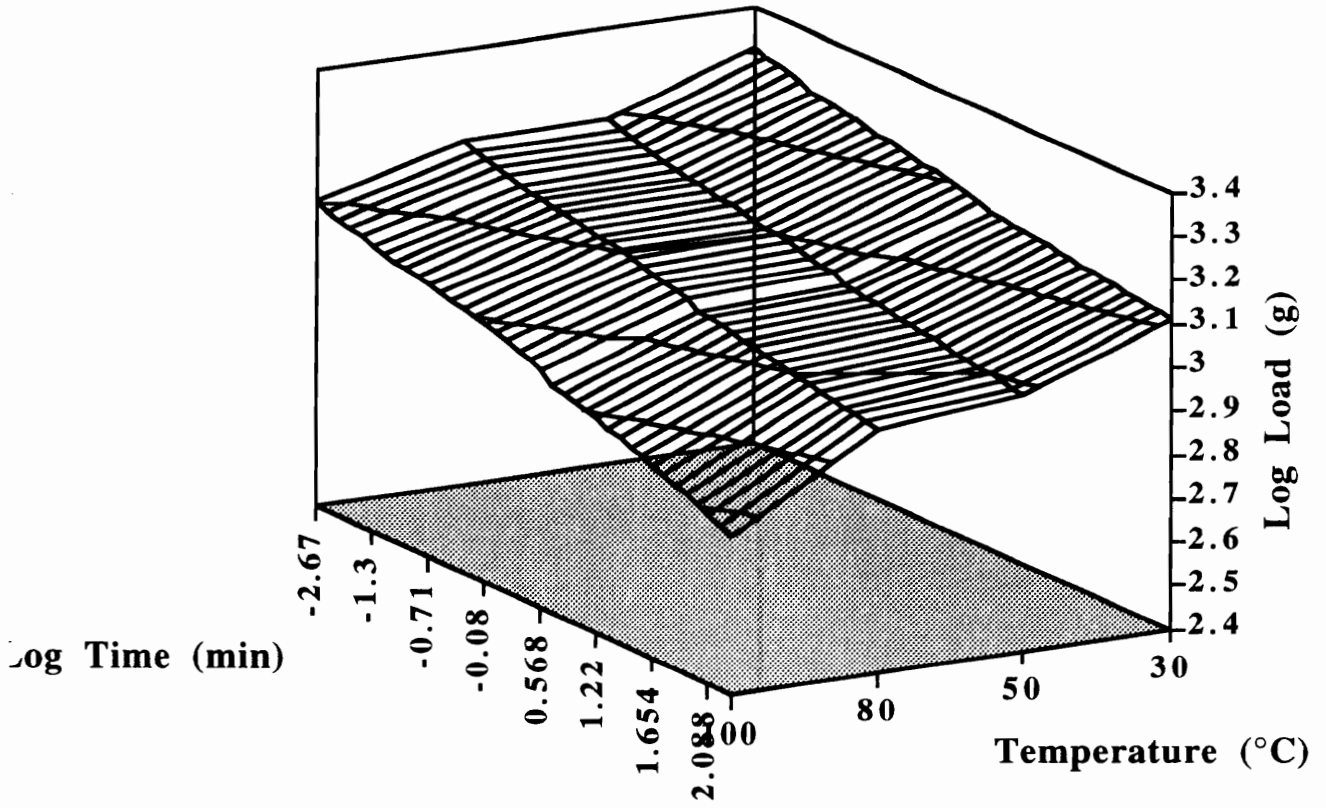


Figure 4.31. Variable temperature load relaxation behavior for Fmc4 at 35%RH.

Table 4.9. Summary of Load Relaxation Measurements on Fmc4

Temp-%RH (°C-%)	Std Dev. ¹ (±g)	Init. Load (g ₀)	% Decay (%)
30-35	286	2019	35.7
50-35	65	1557	37.7
80-35	35	1555	41.5
100-35	73	1271	54.3
30-98	13	1325	43.4
50-98	66	1218	47.9
80-98	49	1197	57.2
100-98	54	965	69.8

1. Based on two to three runs for each temperature and humidity.

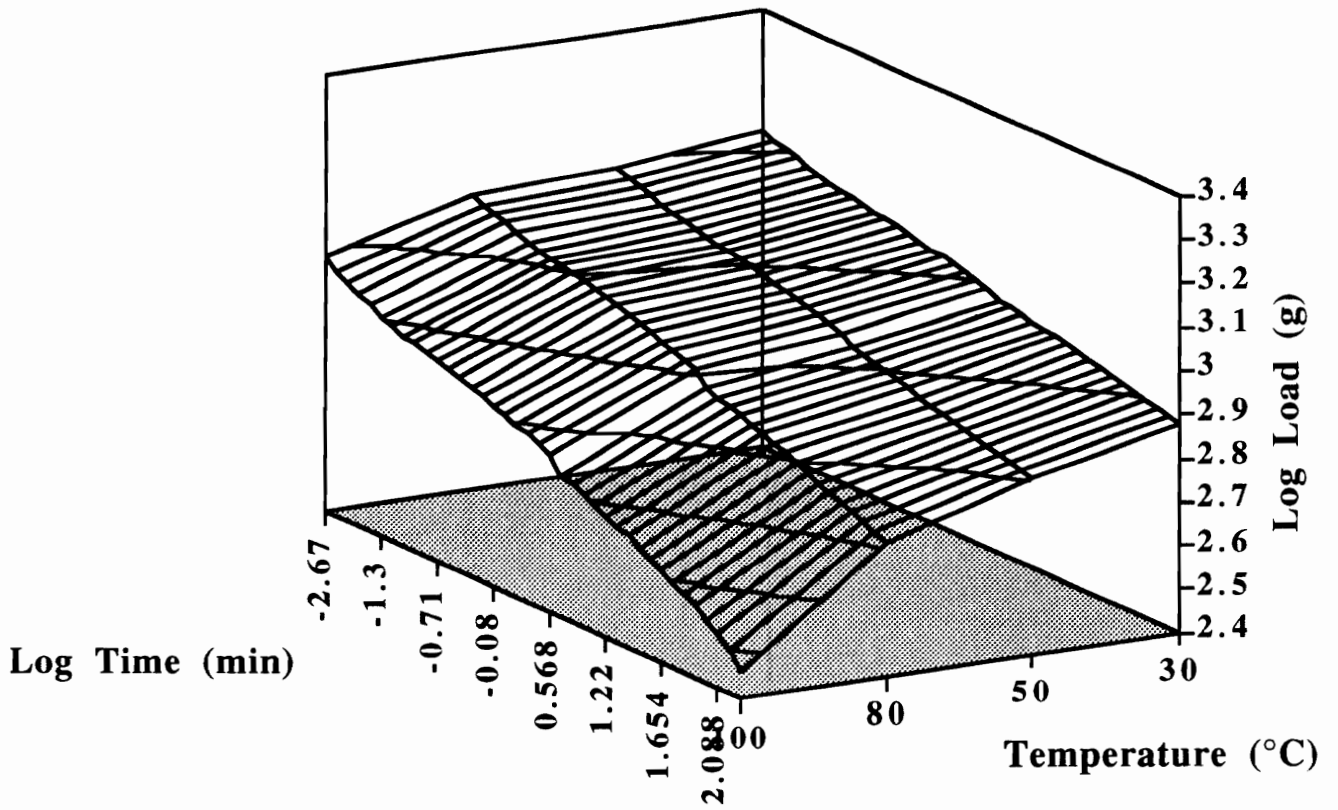


Figure 4.32. Variable temperature load relaxation behavior for Fmc4 at 98%RH.

this case, the initial load decreased from 1325g at 30°C-98%RH to 965g at 100°C-98%RH and the percent decay increased from 43% to 70%. Again, with each increase in temperature beyond 30°C, the loads decreased and the percent decays increased. A plot of the load versus $1/T$ revealed a positive slope which was inconsistent with rubber elasticity theory. Conversely, the conventional slabstock foams did follow rubber elasticity theory although they increasingly deviated from this theory with increases in the hard segment content to the worst case of a zero slope.⁷⁹ In order to consider the influence of increasing the humidity at each temperature, the data at all conditions were plotted together as shown in Fig. 4.33. This figure elucidates that high humidities have a similar effect to high temperatures at a low humidity. At a constant temperature, an increase in humidity from 35%RH to 98%RH had a similar effect as an increase in temperature from 30°C to 100°C at 35%RH. Table 4.9, which gives the overall relaxation results, as well as Table 4.10 that lists the direct influences of temperature and humidity on the initial loads and percent decays, clearly indicate the strong influence by humidity in addition to temperature. As can be seen, increasing the temperature from 30°C to 100°C decreased the loads roughly 20%-30% as did increasing the humidity from 35% to 98%. At temperatures above 80°C, the relaxation curves distinctly deviate from linearity regardless of the humidity level. This suggests that relaxation is occurring at a more significant rate relative to lower temperatures which may be due to an additional phenomenon. The thermal "plasticization" has traditionally been attributed to the disruption of hydrogen bonds by temperature or humidity which occur predominantly within the hard segment domains and to some extent between urea, urethane, and the ether groups of the soft segment. The degree of "plasticization" that occurs with temperature and humidity is evidence suggesting that the physical "cross-links" and associated hydrogen bonding play a significant role in the properties of the CPP containing foams as well at "room" conditions.

Figure 4.34 illustrates the influence of temperature on the load relaxation behavior of Fmc2 utilizing a 3D surface plot. The relaxation behavior for foam Fmc2 is very similar

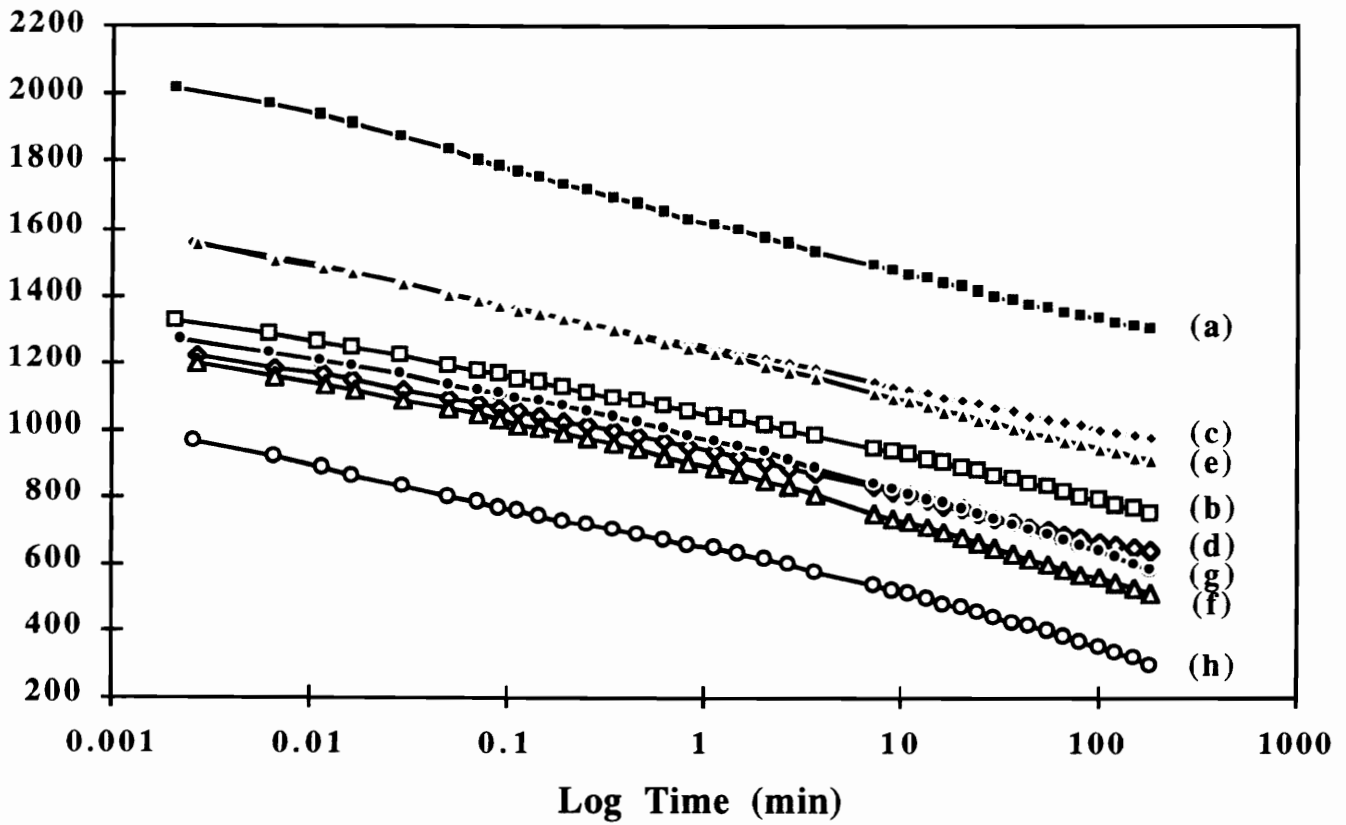


Figure 4.33. Load relaxation behavior of Fmc4 as a function of temperature/relative humidity, (a) 30°C-35%RH, (b) 30°C-98%RH, (c) 50°C-35%RH, (d) 50°C-98%RH, (e) 80°C-35%RH, (f) 80°C-98%RH, (g) 100°C-35%RH, and (h) 100°C-98%RH.

Table 4.10. Effect of Temperature and Relative Humidity on the Load Relaxation of Fmc4

Effect of Temperature

Relative Humidity	Increasing Temp from 30°C to	Change in Init. Load* $\Delta(\text{g}) \%$	Change in Load Decay* $\Delta(\%) \%$
35%	50	-23**	6
	80	-23	16
	100	-37	52
98%	50	-8	10
	80	-10	32
	100	-27	61

** Significant Data Scatter

Effect of Relative Humidity

Temperature (°C)	Increasing %RH from 35% to	Change in Init. Load* $\Delta(\text{g}) \%$	Change in Load Decay $\Delta(\%) \%$
30	98	-34	22
50	98	-22	27
80	98	-23	38
100	98	-24	29

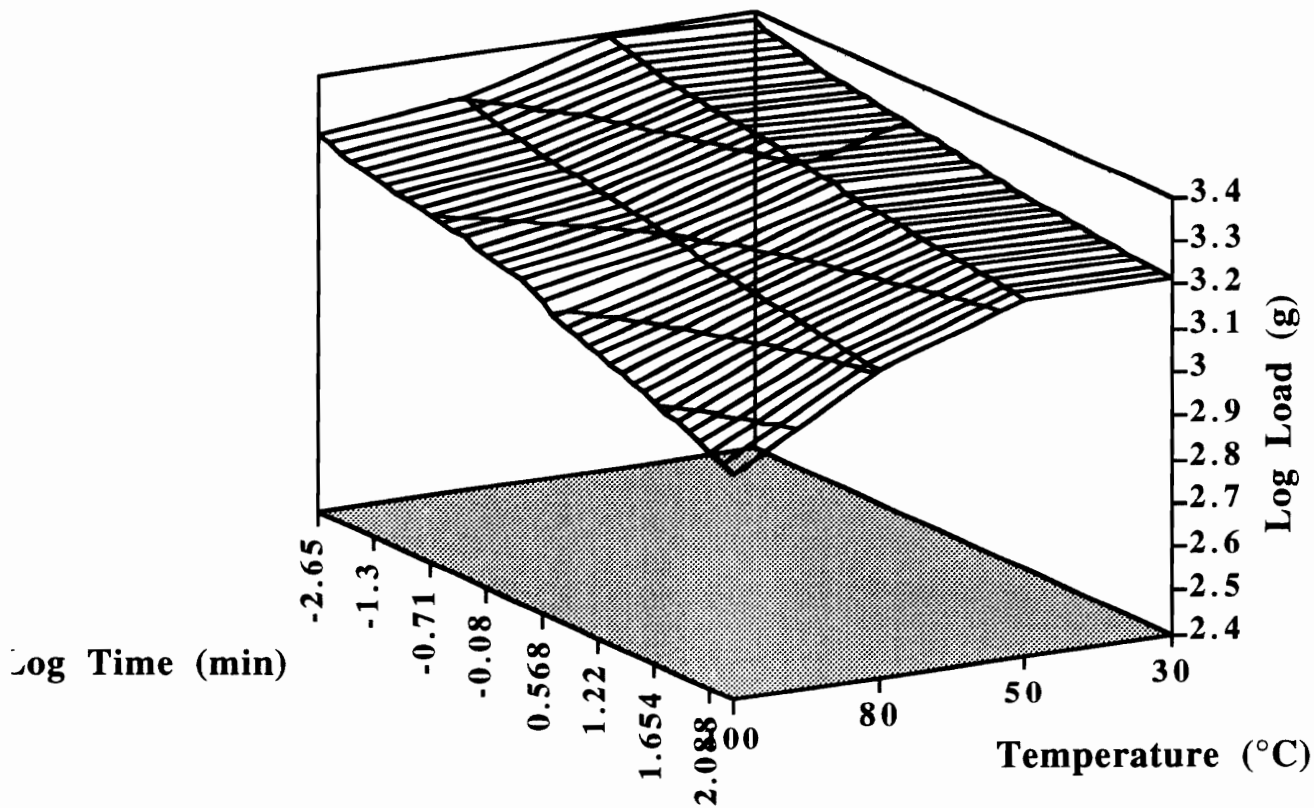


Figure 4.34. Variable temperature load relaxation behavior for Fmc2 at 35%RH.

to that of Fmc4 with a few exceptions. The influence of temperature is similar but the initial loads are greater and percent decays are lower for Fmc2 suggesting that foam Fmc2 is a stiffer foam than Fmc4 -yet it is principally a result of Fmc2 having a higher density. This trend is very similar to that displayed by the two foams without copolymer polyols, Fmo2 and Fmo4 where Fig. 4.34 and Table 4.11 reveal that increasing the temperature from 30°C to 50°C had little effect on the relaxation behavior. However, beyond 50°C, a softening occurred as expected. At 98%RH, shown in Fig. 4.35 the initial load was 2026g at 30°C and 1244g at 100°C while percent decay increased from 41% at 30°C to 67% at 100°C. Here, the foam was softened with all increases in temperature and the load systematically decreased while the percent decay increased. Figure 4.36, as well as Table 4.12, displays the data at all conditions depicting the strong influence of humidity. This shows that again an increase in humidity from 35% to 98% produce a similar response to increasing the temperature from 30°C to 100°C. In addition, the common non-linearity observed at temperatures above 80°C is also evident in foam Fmc2.

The next two foams that are discussed were synthesized using the experimental CPPs. Recall the experimental CPPs contained less "surface stabilizer" with a lower functionality. The load relaxation behavior, however, is almost identical to the foams made using the control CPPs. The influences of temperature and humidity on load relaxation are essentially the same as with the other molded foams and are shown in Fig. 4.37 for foam Fme4. Again, an increase in either temperature (beyond 50°C) or humidity had a softening effect on the exhibited behavior. The relaxation behavior for foam Fme4 was very similar to foam Fmc4. The initial load decreased from 1757g at 30°C-35% RH to 1540g at 100°C-35% RH while the percent decay increased from 35% to 52% as presented in Table 4.13. As in the earlier data, Table 4.14 exemplifies the direct effect of increasing temperature and humidity on the initial load and percent decay and clearly shows that increasing the temperature from 30°C to 50°C (at 35%RH) had very little influence. In addition, a strong humidity influence is also clearly presented.

Table 4.11. Summary of Load Relaxation Measurements on Fmc2

Temp-%RH (°C-%)	Std Dev. ¹ (±g)	Init. Load (g ₀)	% Decay (%)
30-35	66	2389	31.7
50-35	15	2471	33.0
80-35	102	2011	36.9
100-35	58	1860	55.5
30-98	169	2026	41.5
50-98	8	1822	43.4
80-98	45	1660	46.6
100-98	20	1244	66.8

1. Based on two to three runs for each temperature and humidity.

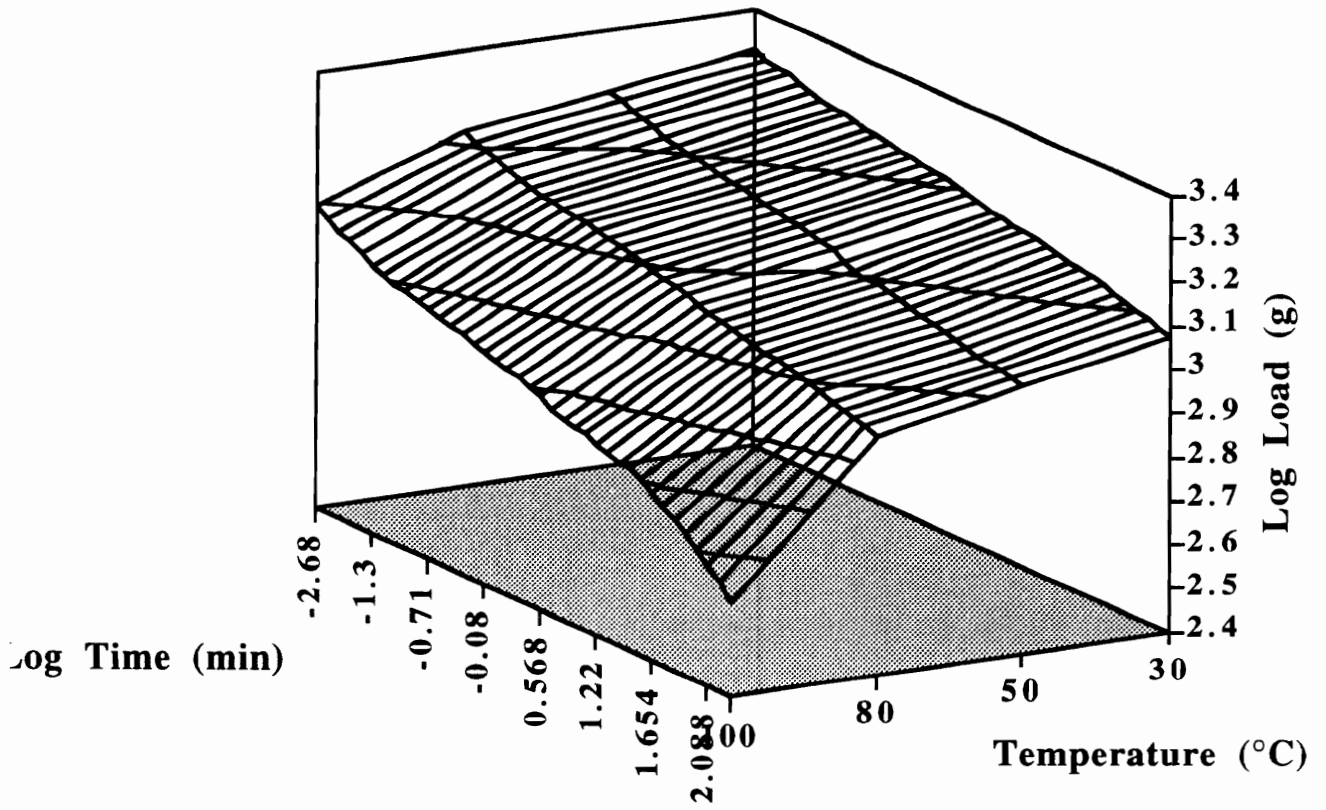


Figure 4.35. Variable temperature load relaxation behavior for Fmc2 at 98%RH.

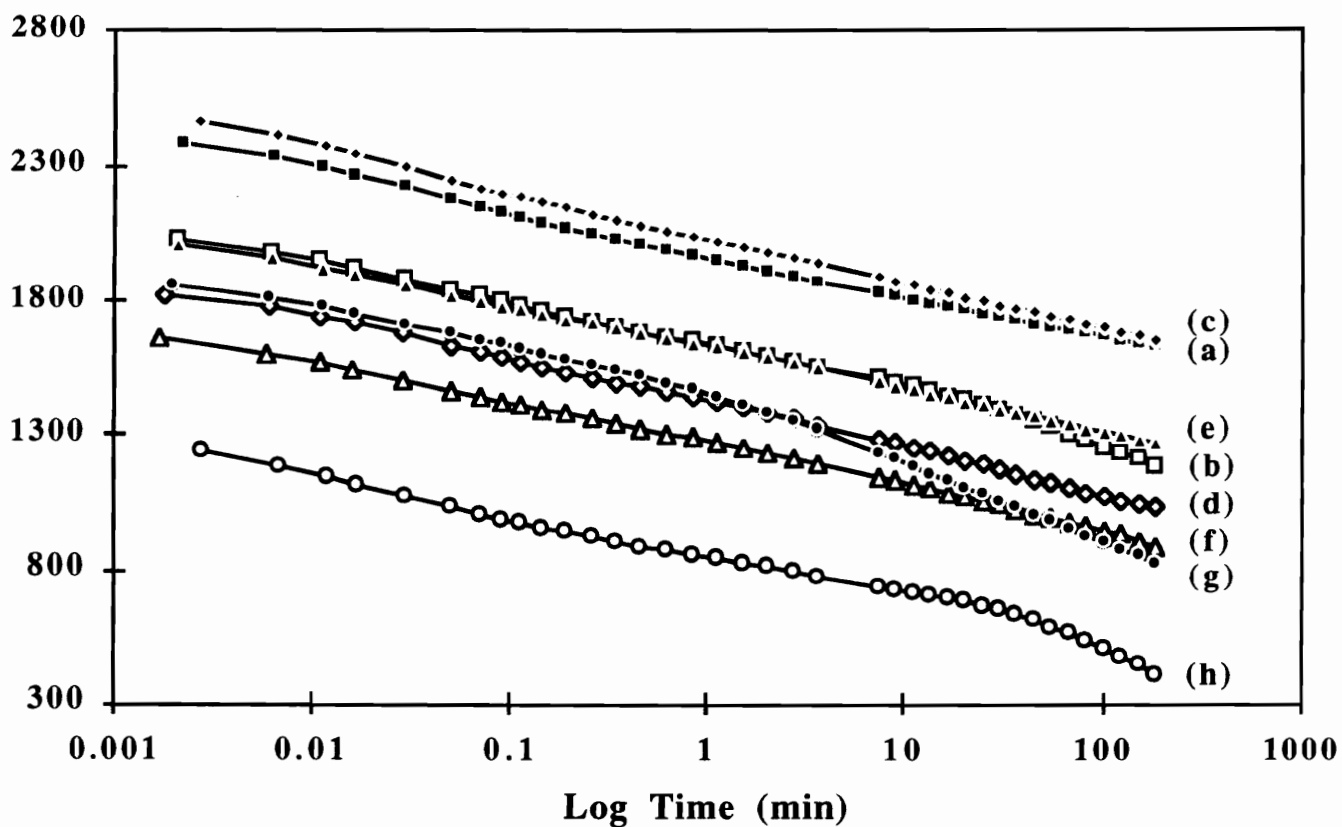


Figure 4.36. Load relaxation behavior of Fmc2 as a function of temperature/relative humidity, (a) 30°C-35%RH, (b) 30°C-98%RH, (c) 50°C-35%RH, (d) 50°C-98%RH, (e) 80°C-35%RH, (f) 80°C-98%RH, (g) 100°C-35%RH, and (h) 100°C-98%RH.

Table 4.12. Effect of Temperature and Relative Humidity on Load Relaxation of Fmc2

Effect of Temperature

Relative Humidity	Increasing Temp from 30°C to	Change in Init. Load* $\Delta(g_0) \%$	Change in Load Decay* $\Delta(\%) \%$
35%	50	3	4
	80	-16	16
	100	-22	75
98%	50	-10	5
	80	-18	12
	100	-39	61

Effect of Relative Humidity

Temperature (°C)	Increasing %RH from 35% to	Change in Init. Load* $\Delta(g_0) \%$	Change in Load Decay $\Delta(\%) \%$
30	98	-15	31
50	98	-26	32
80	98	-17	26
100	98	-33	20

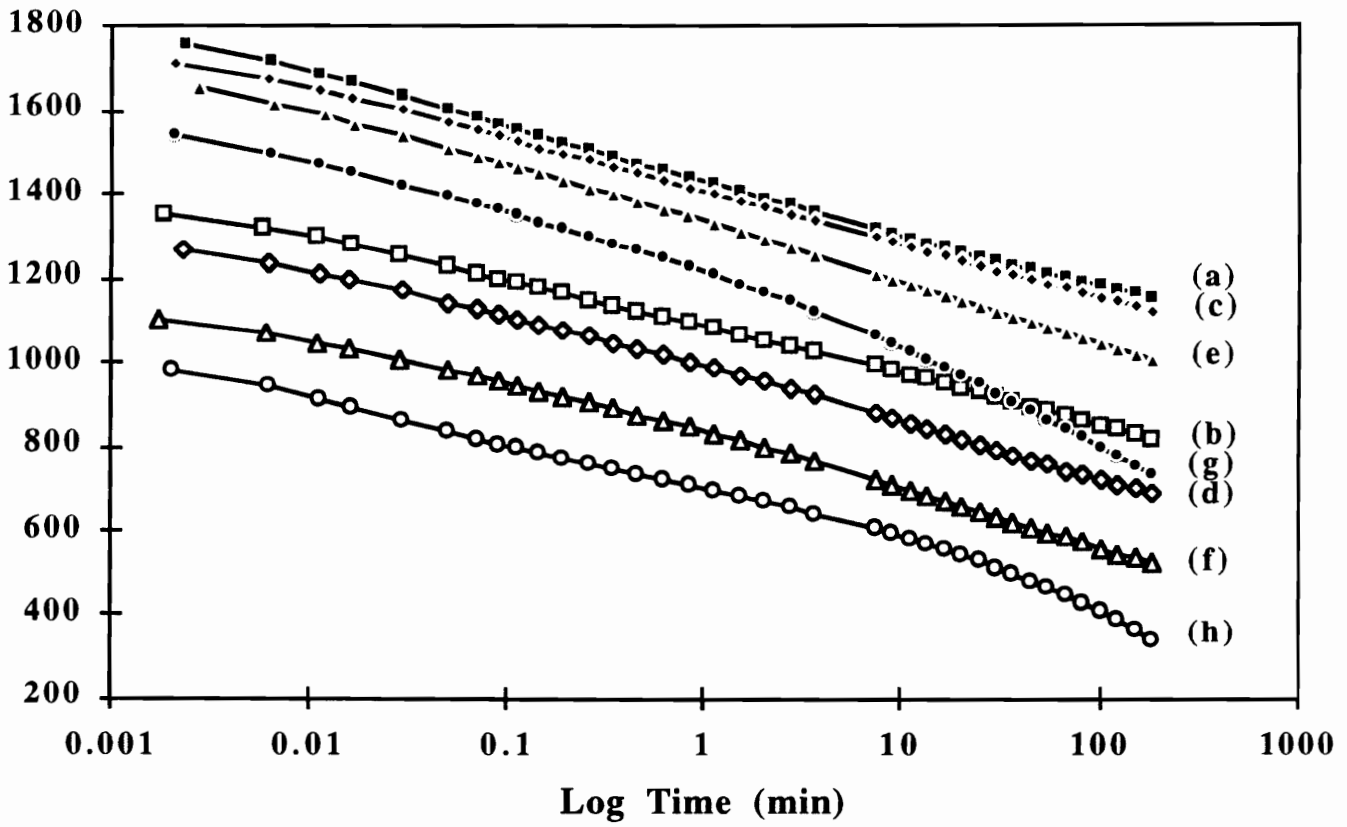


Figure 4.37. Load relaxation behavior of Fme4 as a function of temperature/relative humidity, (a) 30°C-35%RH, (b) 30°C-98%RH, (c) 50°C-35%RH, (d) 50°C-98%RH, (e) 80°C-35%RH, (f) 80°C-98%RH, (g) 100°C-35%RH, and (h) 100°C-98%RH.

Table 4.13. Summary of Load Relaxation Measurements on Fme4

Temp-%RH (°C-%)	Std Dev. ¹ (±g)	Init. Load (g _o)	% Decay (%)
30-35	52	1757	34.2
50-35	29	1716	34.4
80-35	33	1656	39.0
100-35	70	1540	52.3
30-98	4	1354	39.7
50-98	44	1268	45.5
80-98	55	1102	52.7
100-98	37	979	65.1

1. Based on two to three runs for each temperature and humidity.

Table 4.14. Effect of Temperature and Relative Humidity on the Load Relaxation of Fme4

Effect of Temperature

Relative Humidity	Increasing Temp from 30°C to	Change in Init. Load* $\Delta(g_0) \%$	Change in Load Decay* $\Delta(\%) \%$
35%	50	-2	1
	80	-6	14
	100	-12	53
98%	50	-6	15
	80	-19	33
	100	-28	64

Effect of Relative Humidity

Temperature (°C)	Increasing %RH from 35% to	Change in Init. Load* $\Delta(g_0) \%$	Change in Load Decay $\Delta(\%) \%$
30	98	-23	16
50	98	-26	32
80	98	-33	35
100	98	-36	24

Finally, the load relaxation behavior for Fme2 is shown Fig. 4.38. The displayed behavior of this foam resembled Fmc2 and was even slightly stiffer in the sense of displaying slightly lower percent decays. Tables 4.15 and 4.16 present the overall results from these load relaxation experiments. As with foam Fmc2, an increase in humidity from 35% RH to 98% RH had a similar effect as an increase in temperature from 30°C to 100°C at 35% RH.

In summary, increasing the temperature to 100°C (at 35%RH) lead to a decrease in the initial load in the range of 10% to 37%. Increasing the humidity to 98%RH (at 30°C) resulted in a decrease in the initial load in the range of 15% to 34% (essentially the same range as the previous case). However, when both the temperature and humidity are increased to 100°C-98%RH, the initial loads decreased even more significantly by 32% to 52% with the greater decreases surprizingly displayed by the foams *with* copolymer polyols. Similar trends were observed with the percent decays as the temperature and humidity were increased. In general, an increase in temperature from 30°C to 50°C at 35%RH resulted in a 5% increase in the percent decay. An increase to 100°C, again at 35%RH, resulted in an increase of 50% to 80% in the percent decay with the former increase occurring for the foams lacking CPPs. An increase to 98%RH increased the percent decays by 20% to 50% (depending on temperature) over those at 35%RH.

An attempt was made at time-temperature-superposition for the purpose of long term prediction. The relaxation curves for Fme4 carried out at four temperatures, 30°C, 50°C, 80°C, and 100°C, (all at 35%RH) were horizontally shifted to overlap and construct a master curve. The curve at 30°C was used as a reference and the other curves were shifted to overlap this set of data. The master curve, shown in Fig. 4.39a, indicates that time-temperature-superposition was not successful due to the curves not being completely superimposable. Both the nonlinear character at high temperature shown earlier and the non-superimposable nature in Fig. 4.39a are further evidence that the relaxation mechanism may be changing as a function of temperature. The curves corresponding to load relaxation

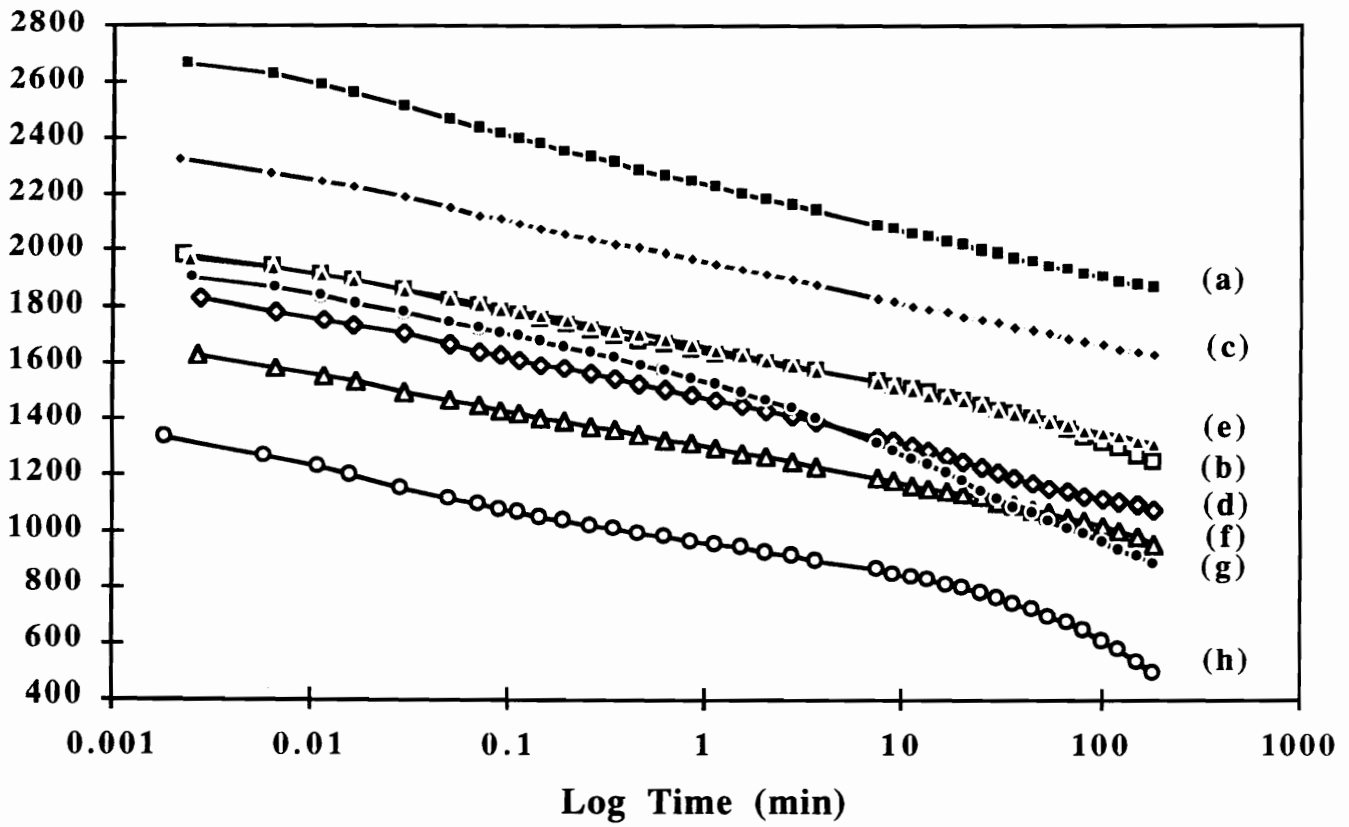


Figure 4.38. Load relaxation behavior of Fme2 as a function of temperature/relative humidity, (a) 30°C-35%RH, (b) 30°C-98%RH, (c) 50°C-35%RH, (d) 50°C-98%RH, (e) 80°C-35%RH, (f) 80°C-98%RH, (g) 100°C-35%RH, and (h) 100°C-98%RH.

Table 4.15. Summary of Load Relaxation Measurements on Fme2

Temp-%RH (°C-%)	Std Dev. ¹ (±g)	Init. Load (g ₀)	% Decay (%)
30-35	220	2670	30.1
50-35	198	2325	30.0
80-35	129	1977	33.6
100-35	117	1906	53.6
30-98	27	1987	37.2
50-98	6	1826	40.9
80-98	141	1627	41.2
100-98	41	1336	62.8

1. Based on two to three runs for each temperature and humidity.

Table 4.16. Effect of Temperature and Relative Humidity on Load Relaxation of Fme2

Effect of Temperature

Relative Humidity	Increasing Temp from 30°C to	Change in Init. Load* $\Delta(g_0) \%$	Change in Load Decay* $\Delta(\%) \%$
35%	50	-13**	0
	80	-26	12
	100	-29	78
98%	50	-8	10
	80	-18	11
	100	-33	69

**Significant Data Scatter

Effect of Relative Humidity

Temperature (°C)	Increasing %RH from 35% to	Change in Init. Load* $\Delta(g_0) \%$	Change in Load Decay $\Delta(\%) \%$
30	98	-26	24
50	98	-21	36
80	98	-17	23
100	98	-30	17

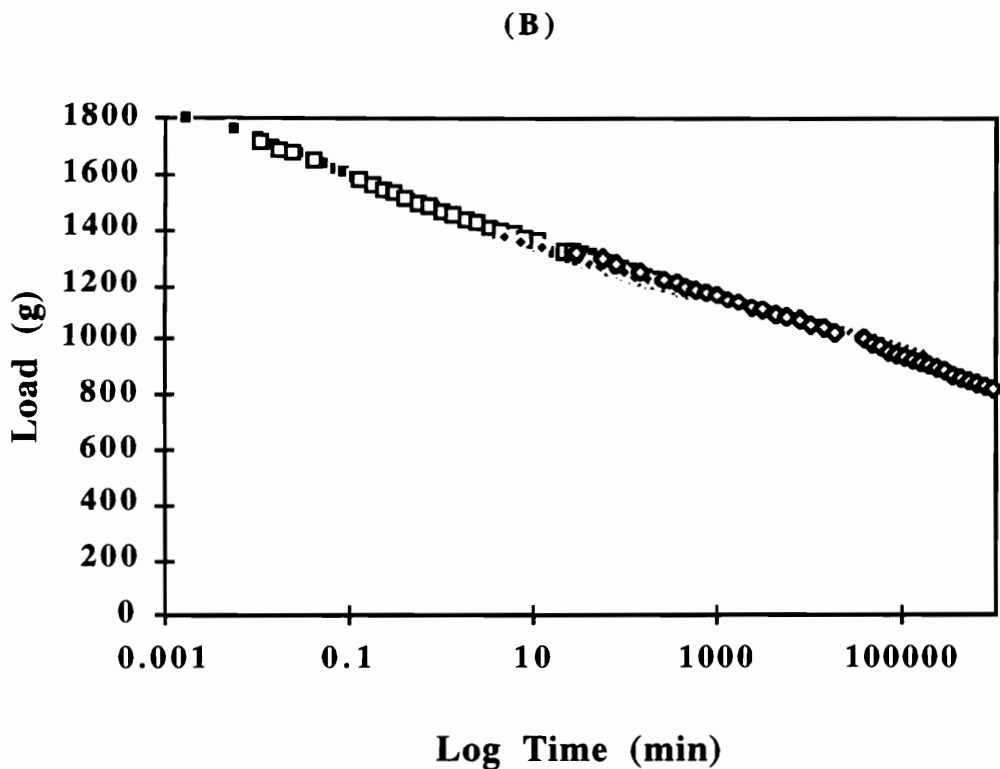
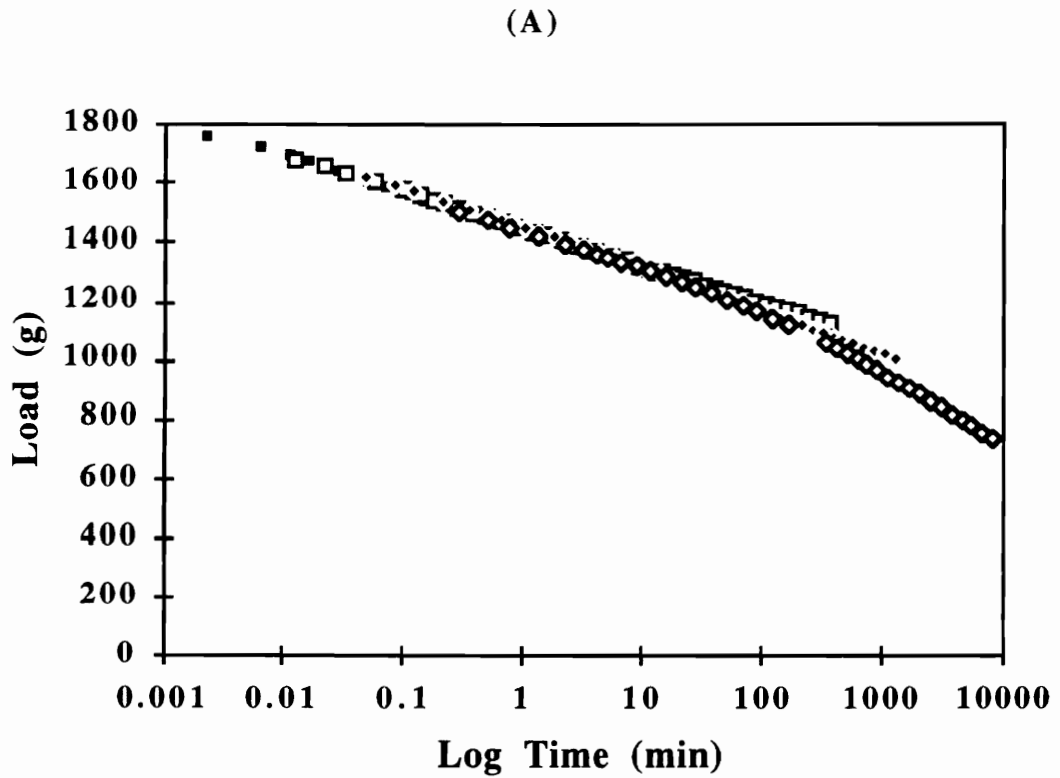


Figure 4.39. Master curves of the load relaxation behavior of foam Fme4 using horizontal shifts of curves at (A) different temperatures (ref. $T=30^{\circ}\text{C}$, $\text{RH}=35\%$) and (B) different humidity levels (ref. $\text{RH}=35\%$, $T=30^{\circ}\text{C}$).

carried out at different humidities were also shifted to create a master curve. The master curve shown in Fig. 4.39b suggests that time-"humidity"-superposition is feasible. The idea here is that the mechanism is constant over a range of humidities at a relatively low temperature. This was expected since the mechanism is not expected to vary with increasing humidity, only the degree of which is believed to change.

4.6.1.2 Effect of Copolymer Polyols

Copolymer polyols are commonly used in molded foams to improve foam hardness in view of the short cure cycles that are utilized. In addition, they have been shown to aid foam processing by improving cell-openness. Although limited work does exist in the literature regarding foam hardness, tensile properties, and processibility, little work exists regarding their influence on the viscoelastic properties. The effect on the viscoelastic properties is thus considered here. Figure 4.40 shows the behavior of the three, 4 pph water content foams, Fmo4, Fmc4, and Fme4, varying in the copolymer polyols carried out at 30°C-35%RH. As expected, foam Fmc4 with 12.5% solids displayed higher loads than Fmo4. The initial load was 1597g for Fmo4, 2019g for Fmc4 and 1757g for Fme4 suggesting that the foam hardness did indeed increase with the incorporation of CPP particles as expected. However, the slopes of the curves of the CPP containing foams are higher than that of Fmo4 as well as are the percent decays. The percent decays were 27%, 35%, and 34% for Fmo4, Fmc4, and Fme4, respectively. This suggests that while the copolymer polyols do increase the foam hardness, they cause the load to relax a greater amount leading to more time-dependent viscoelastic properties. The low water content foams, Fmo2, Fmc2, and Fme2 displayed the same trend with only the loads being higher as illustrated in Fig. 4.41. The initial loads were 1737g, 2389g, and 2670g for Fmo2, Fmc2, and Fme2, respectively. The percent decays were 25%, 32%, and 30% for the same three foams. Again, the incorporation of CPPs increased the foam hardness but also

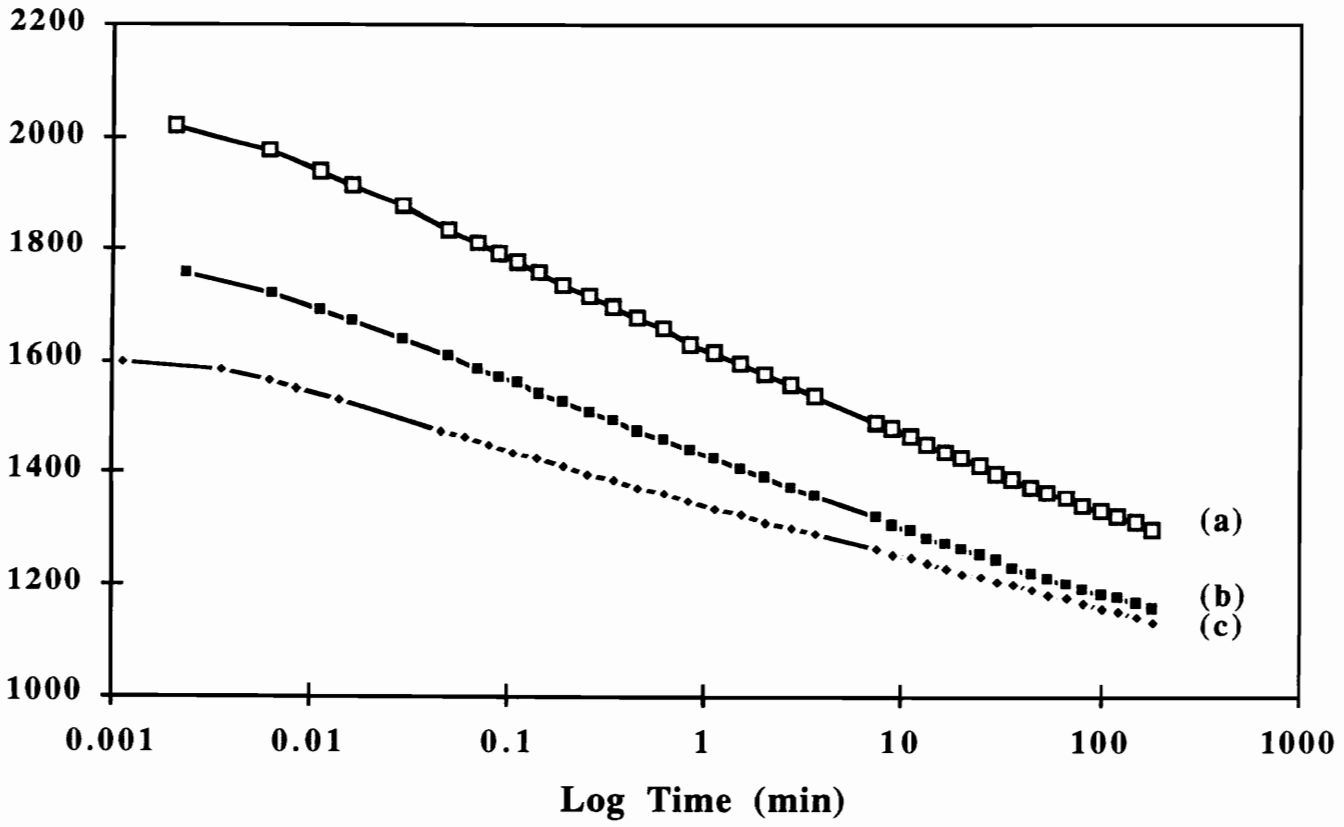


Figure 4.40. Load relaxation behavior at 30°C-35%RH for the 4 pph water content foams as a function of the CPP used, (a) Fme4, (b) Fmc4 and (c) Fmo4.

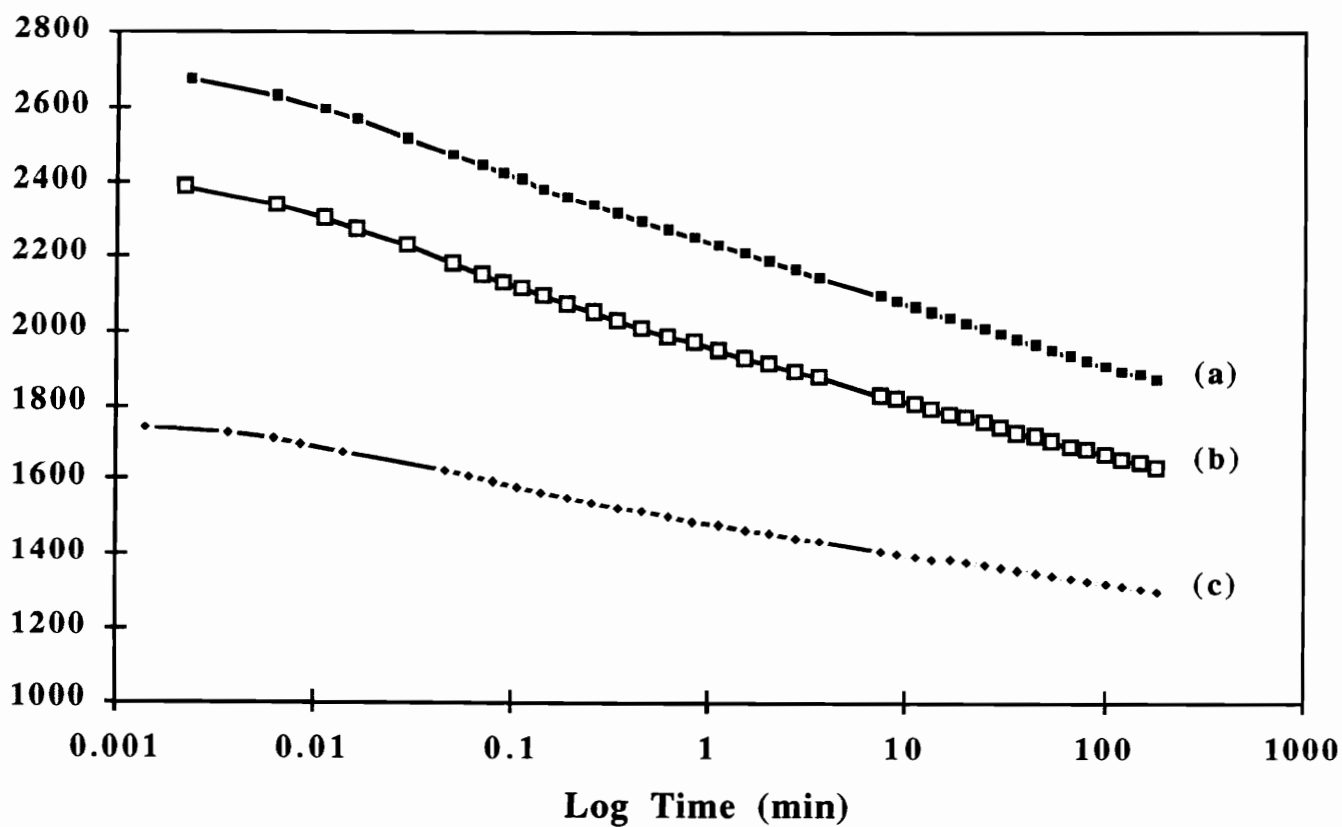


Figure 4.41. Load relaxation behavior at 30°C-35%RH for the 2 pph water content foams as a function of the CPP used, (a) Fme2, (b) Fmc2 and (c) Fmo2.

increased the viscoelastic decay. This decline in the viscoelastic properties is speculated to be in part due to a stress concentration effect by the rigid particles. The increased localized strain at the particle-matrix interface promotes further chain slippage. Restated, since stress relaxation is believed to predominately occur in the soft segment phase and there is less of it for the CPP containing foams, this soft segment is expected to relax or strain further thereby resulting in greater relaxation. Also, somewhat surprising is that the relaxation properties, specifically lower load decays, were slightly enhanced in the case of Fme2 where the experimental CPP was utilized.

The influence of the CPP particles in terms of viscoelastic decay was further enhanced at 100°C-35%RH as illustrated in Fig. 4.42 with the high water content foams and Fig. 4.43 with the low water content foam. At 100°C-35%RH (Fig. 4.42), the curves crossed where the CPP containing materials displayed higher initial loads but lower final loads at the end of the three hour experiment! For example, foam Fmo4 exhibited an initial load of 1156g, of which 35% decayed in three hours. In contrast, foam Fmc4 displayed an initial load of 1271g, of which 54% decayed in three hours - much more than that of Fmo4. Foam Fme4 displayed an initial load of 1540g and a percent decay of 52% - slightly less than that of Fmc4. Again, the relaxation properties of Fme4 appeared slightly improved over Fmc4. The 2 pph water content foams displayed similar behavior. For example, Fmo2 displayed an initial load of 1590g and a percent decay of 32%; Fmc2 displayed an initial load of 1860g and a percent decay of 56%; and Fme2 displayed an initial load of 1906 and a percent decay of 54%. *In both cases, low water and high water content, the slopes and percent decays are higher for the foams containing CPPs than those without.* This is strong evidence suggesting that hydrogen bonding is occurring with respect to the CPPs most likely at the interface which is disrupted at high temperatures resulting in a “cross-over” of the curves. Between the experimental and control CPPs, the properties of Fme4 and Fme2 are at best only slightly enhanced over those of Fmc4 and Fmc2. The

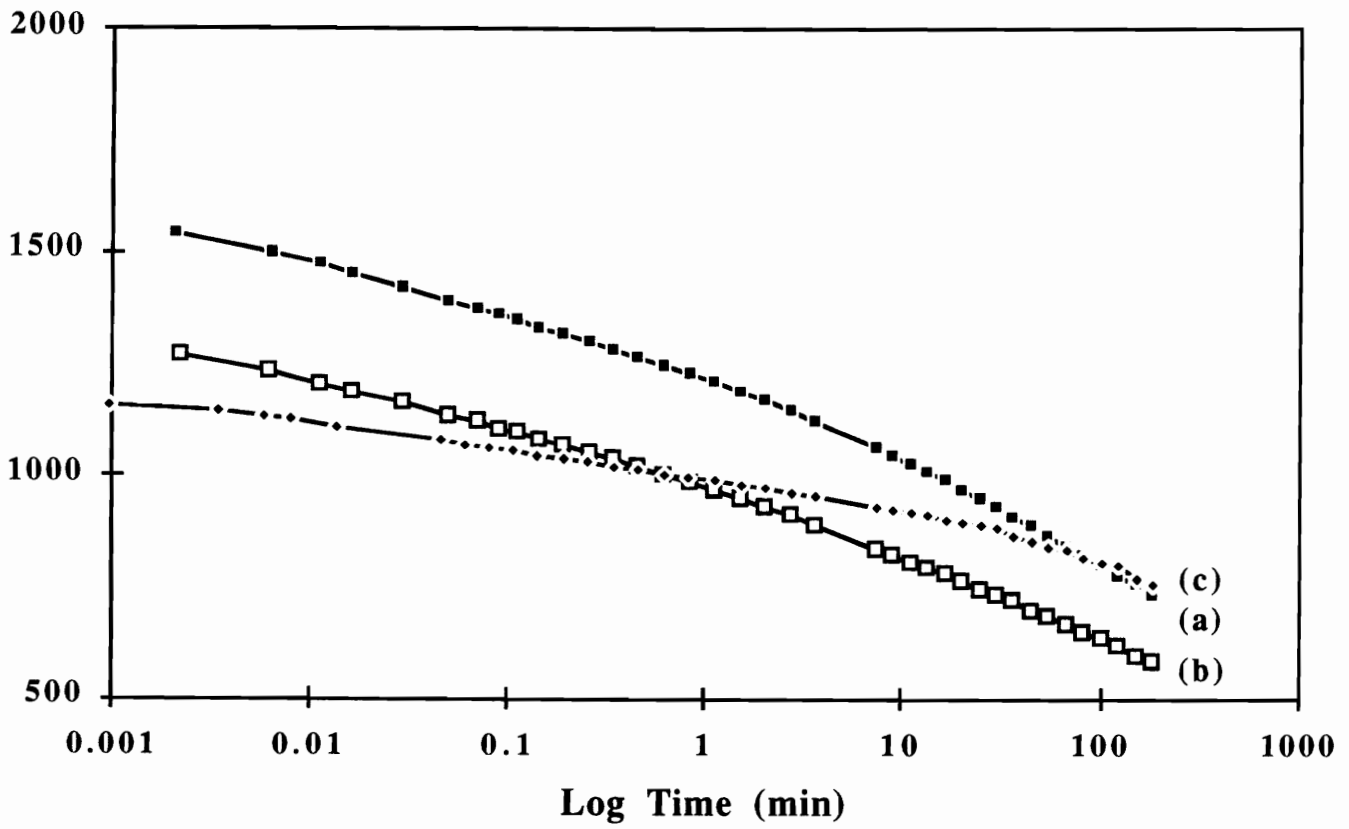


Figure 4.42. Load relaxation behavior at 100°C-35%RH for the 4 pph water content foams as a function of the CPP used, (a) Fme4, (b) Fmc4 and (c) Fmo4.

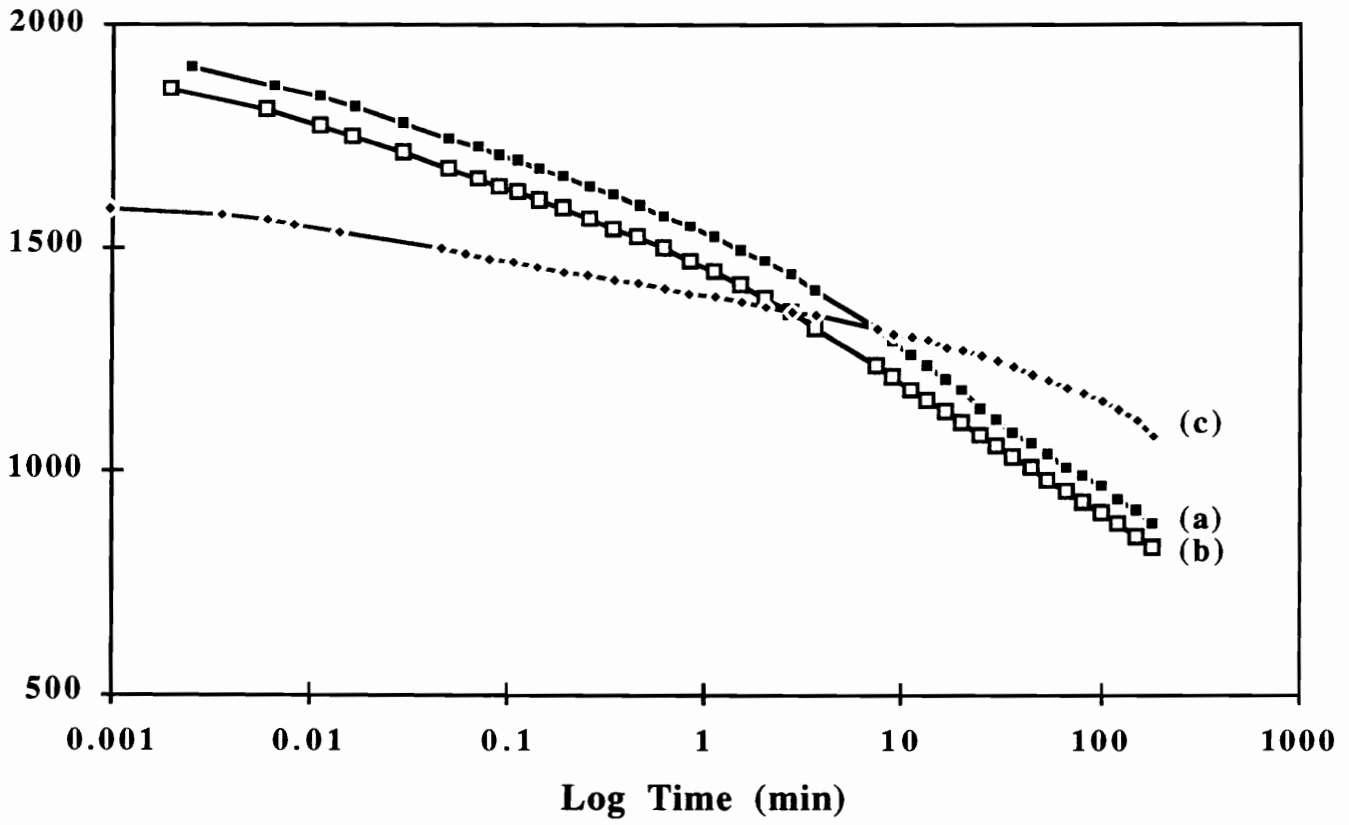


Figure 4.43. Load relaxation behavior at 100°C-35%RH for the 2 pph water content foams as a function of the CPP used, (a) Fme2, (b) Fmc2 and (c) Fmo2.

percent decays were only slightly lower for these materials where the experimental CPPs were incorporated.

A similar trend was observed at 30°C-98%RH as shown in Figs. 4.44 and 4.45 for the 4 pph water content foams and for the 2 pph water content foams respectively. In Fig. 4.44, the load relaxation curves for Fmo4, Fmc4 and Fme4 are presented. Once more, while the initial load was higher for Fmc4 over Fmo4, 1325g compared to 1135g, the percent decay was also higher, 43% compared to 34%, and the curves appear to “cross-over” right at the three hour point. The 40% decay for Fme4 was slightly lower than that of Fmc4 again suggesting that the properties were improved.

The relaxation curves of foams Fmo2, Fmc2, and Fme2 are shown in a similar manner in Fig. 4.45. Again, the materials with CPPs displayed both increased initial loads and increased percent decays. Also, of the two foams with CPPs, Fmc2 and Fme2, Fme2, which possesses the lower CPP surface functionality, displayed the lower percent decay. The values of initial loads were 1279g, 2026g, and 1987g for Fmo2, Fmc2, and Fme2, respectively while the percent decay values were 30%, 42%, and 37%, respectively. The greater percent decays observed at 30°C-98%RH dismisses the notion that the increased decay observed at 100°C is due to the proximity of this temperature to the T_g of the CPPs (ca. 120°C). In fact, this further supports the claim that principally hydrogen bonding may well be occurring primarily at the interface of the CPP dispersions since humidity as well as temperature can disrupt hydrogen bonding. In addition, this gives further support to the earlier solvent extraction results which showed that the percent extractables were higher for the CPP containing foams suggesting that these particles may not be covalently grafted to the soft phase to a great extent but may in part be only “interfaced” as a result of hydrogen bonding.

Figure 4.46 illustrates the load relaxation behavior of foams Fmo4, Fmc4, and Fme4 at 100°C-98%RH. Here the initial loads were essentially the same but the percent decays were dramatically different. The initial loads were 1049g, 965g, and 979g for

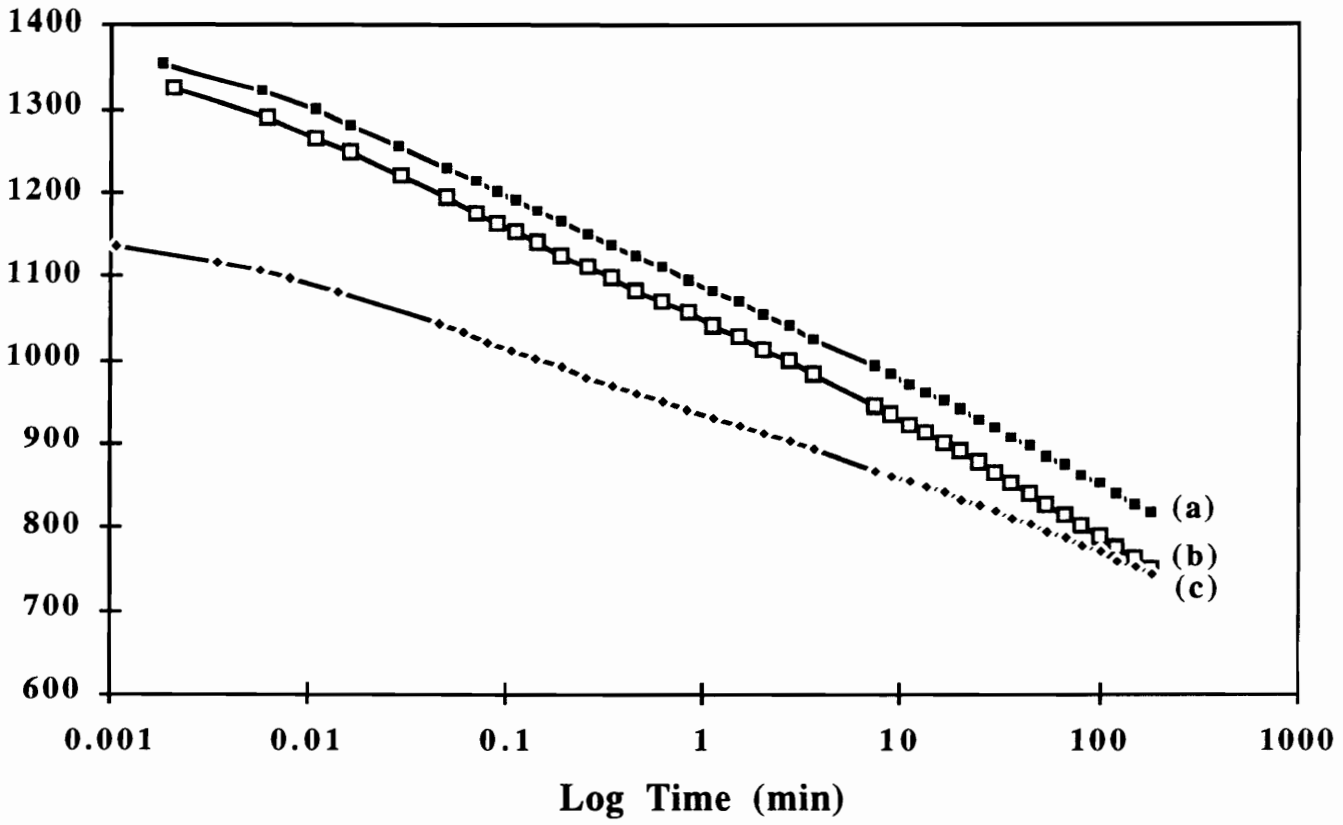


Figure 4.44. Load relaxation behavior at 30°C-98%RH for the 4 pph water content foam as a function of the CPP used, (a) Fme4, (b) Fmc4 and (c) Fmo4.

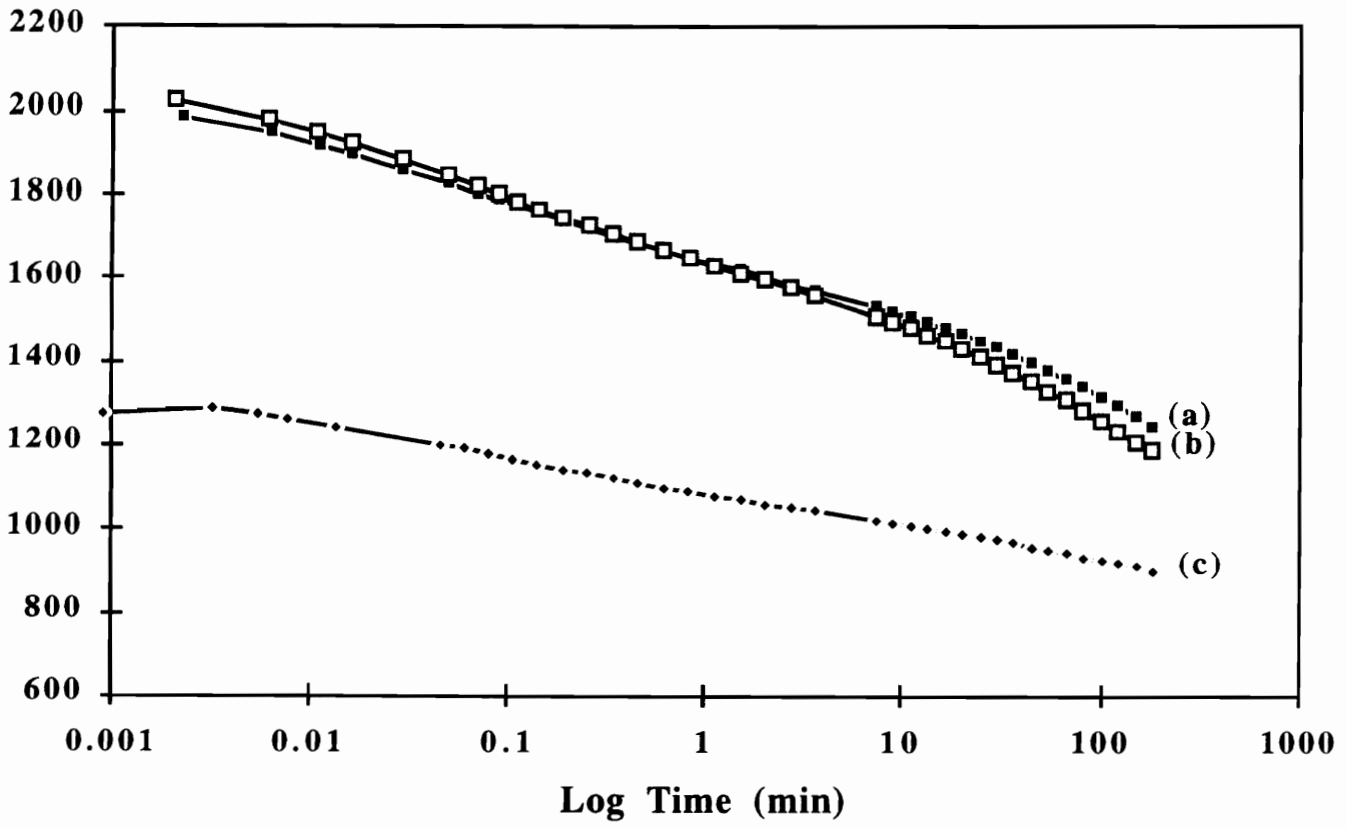


Figure 4.45. Load relaxation behavior at 30°C-98%RH for the 2 pph water content foams as a function of the CPP used, (a) Fme2, (b) Fmc2 and (c) Fmo2.

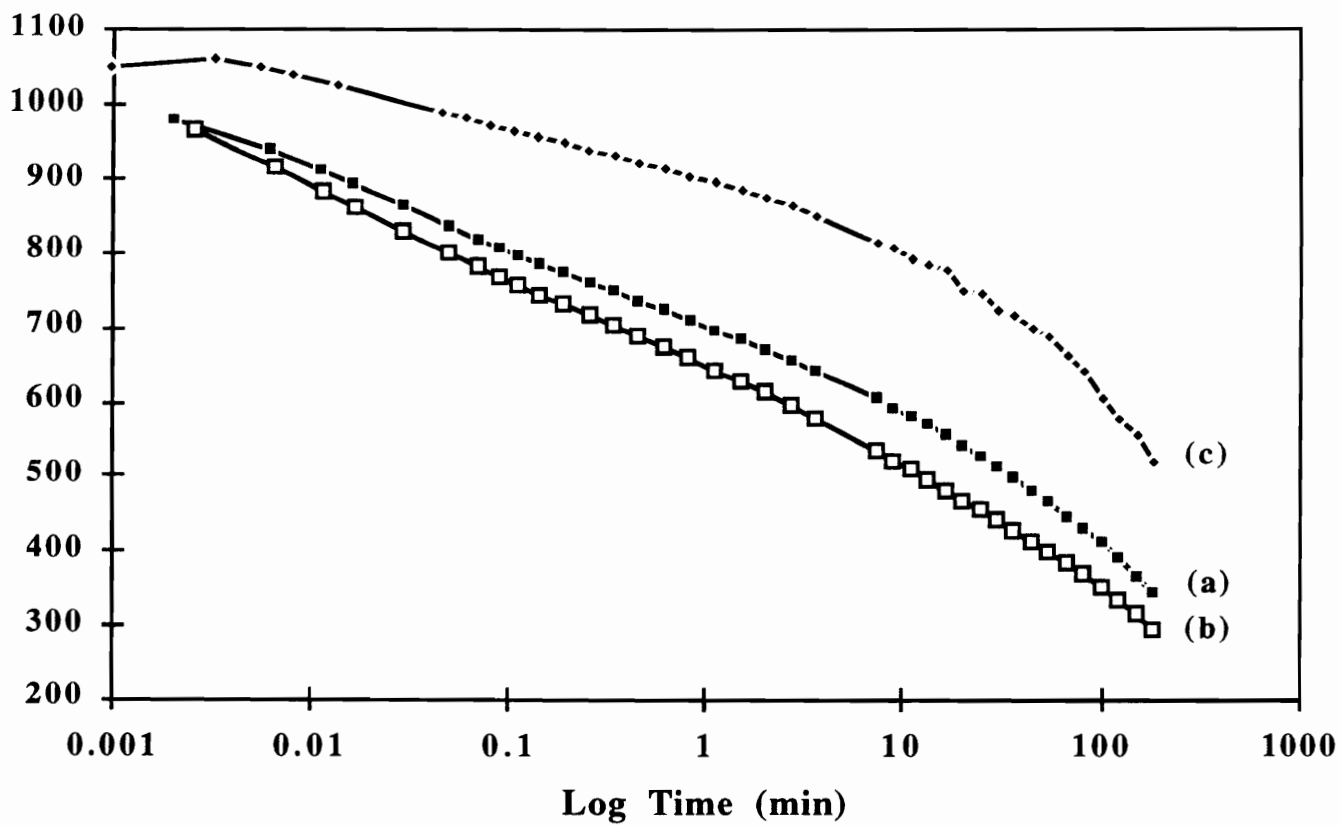


Figure 4.46. Load relaxation behavior at 100°C-98%RH for the 4 pph water content foam as a function of the CPP used, (a) Fme4, (b) Fmc4 and (c) Fmo4.

Fmo4, Fmc4, and Fme4 - within the experimental scatter based upon multiple runs. However, the percent decays were 51%, 70%, and 65% for the three foams respectively. Consistently, the percent decay increased for the CPP containing foams relative to the CPP-free foams and decreased for experimental foams relative to the control foams. The 2 pph water content foams, Fmo2, Fmc2, and Fme2 also displayed the same trend. Here, “cross-over” between Fmo2 and Fmc2 occurred early on as shown in Fig. 4.47. In fact, the initial loads are again within experimental error ranging from 1186g for Fmo2 to 1336g for Fme2. The percent decays in this case also followed the same trend; 45% for Fmo2, 67% for Fmc2, and 63% for Fme2.

In general, the initial loads increased ca. 10% to 30% with the incorporation of CPPs but the percent decays also increased ca. 30% to 50%. It appears that the mechanism of relaxation is different for the materials containing CPPs than for the materials that do not. Although the CPPs increased the initial loads they also increased percent decays. As mentioned earlier, one possible explanation for this is that these rigid particles can act as stress concentrators leading to increased levels of localized stress and thus promoting greater relaxation. In addition, relaxation within these particles can occur resulting in accelerated relaxation although this is not believed to occur to a great extent. The different behavior and thus different mechanisms exhibited by the CPP containing foams correlates well with the compression load strain measurements. In summary, the CPP containing foams demonstrated higher loads (initially), greater hysteresis, and greater relaxation in a three hour period than the CPP lacking foams.

Furthermore, the fact that either high temperatures or high humidities “plasticized” these CPP containing materials suggests that perhaps the accepted belief that the CPPs are tightly covalently grafted to the foam matrix may not be true. The slight improvement observed with the experimental CPPs may be due to a lower stress concentration effect and thus a lower localized stress effect. More importantly, the insensitivity of the observed trend to the stabilizer utilized further decreases the importance of its role in stabilization.

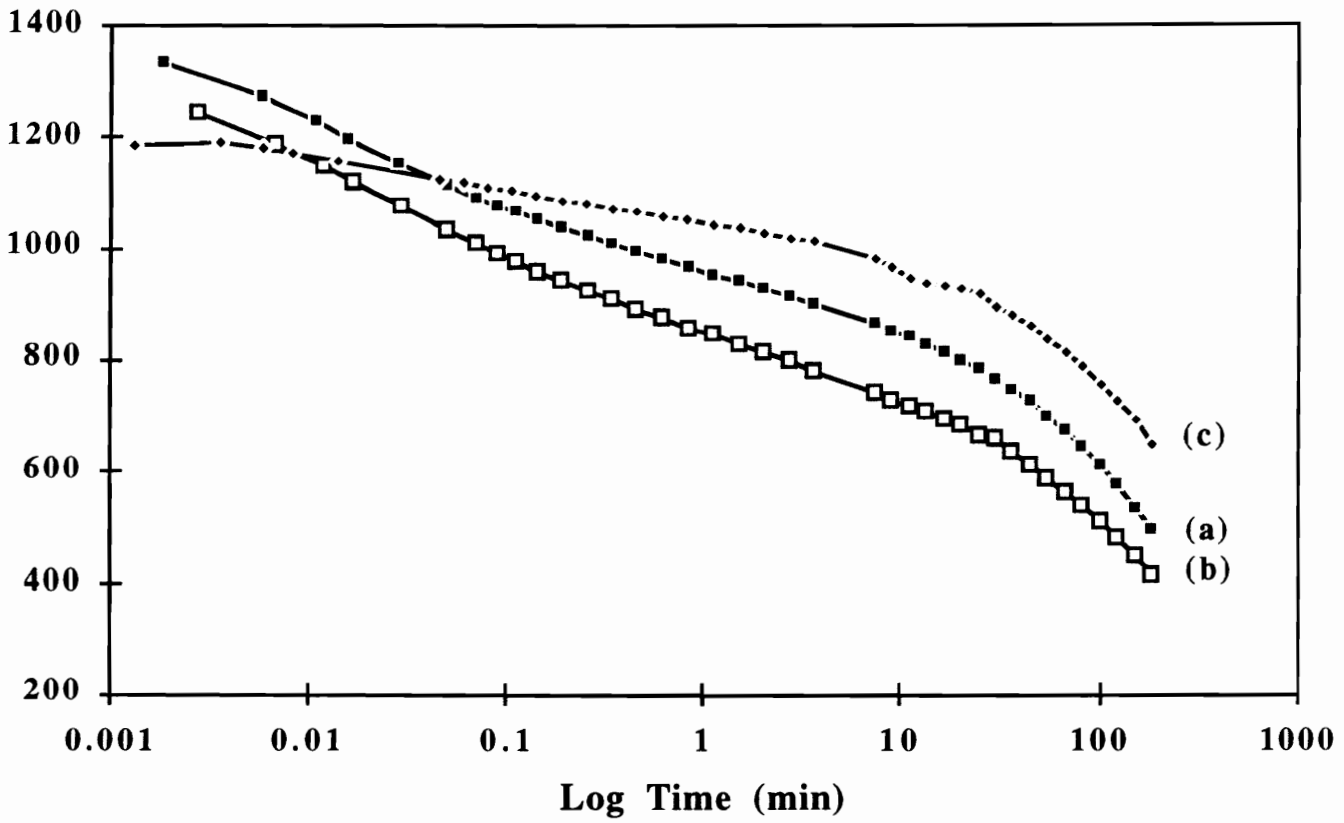


Figure 4.47. Load relaxation behavior at 100°C-98%RH for the 2 pph water content as a function of the CPP used, (a) Fme2, (b) Fmc2 and (c) Fmo2.

4.6.1.3 Effect of Formulation - Water/TDI Content

As the water/TDI content in the formulation is varied, the amount of evolved CO₂ also varied where more CO₂ is produced with increased amounts of water/TDI which in turn lowers the final foam density. In addition, the increased water/TDI content increases the amount of hard segment content. The effect of water/TDI content on the load relaxation behavior of the molded foams without CPPs is shown in Fig. 4.48 (plotted for the conditions of 30°C-35%RH). The data show that Fmo2 is a stiffer foam than Fmo4 (due to its higher density). The initial load is ca. 10% greater than that of Fmo4 and the percent decay is ca. 8% lower.

Figure 4.49 illustrates the effect of water/TDI content on the load relaxation behavior of the two molded foams containing CPPs - Fmc4 and Fmc2. Again the foam with the higher density displayed increased loads and a slightly decreased percent decay. The initial load was 2019g for Fmc4 and 2389g for Fmc2 and the percent decays were 36% and 32% for foams Fmc4 and Fmc2, respectively. When the loads are normalized with respect to density so that the specific load is plotted, Fmc4 displayed stiffer behavior as shown in Fig. 4.50. The foam with the higher hard segment content displayed higher specific loads as expected. Similar behavior was observed with the other foams varying in water/TDI content, Fme4 and Fme2 and at all environmental conditions and thus are not shown here.

4.6.2 *Compression Creep*

In addition to load relaxation, the change in thickness of the foam samples under a constant load in compression was also of interest since it directly measures the foam shape under load and closely simulates realistic application conditions. It was also used to

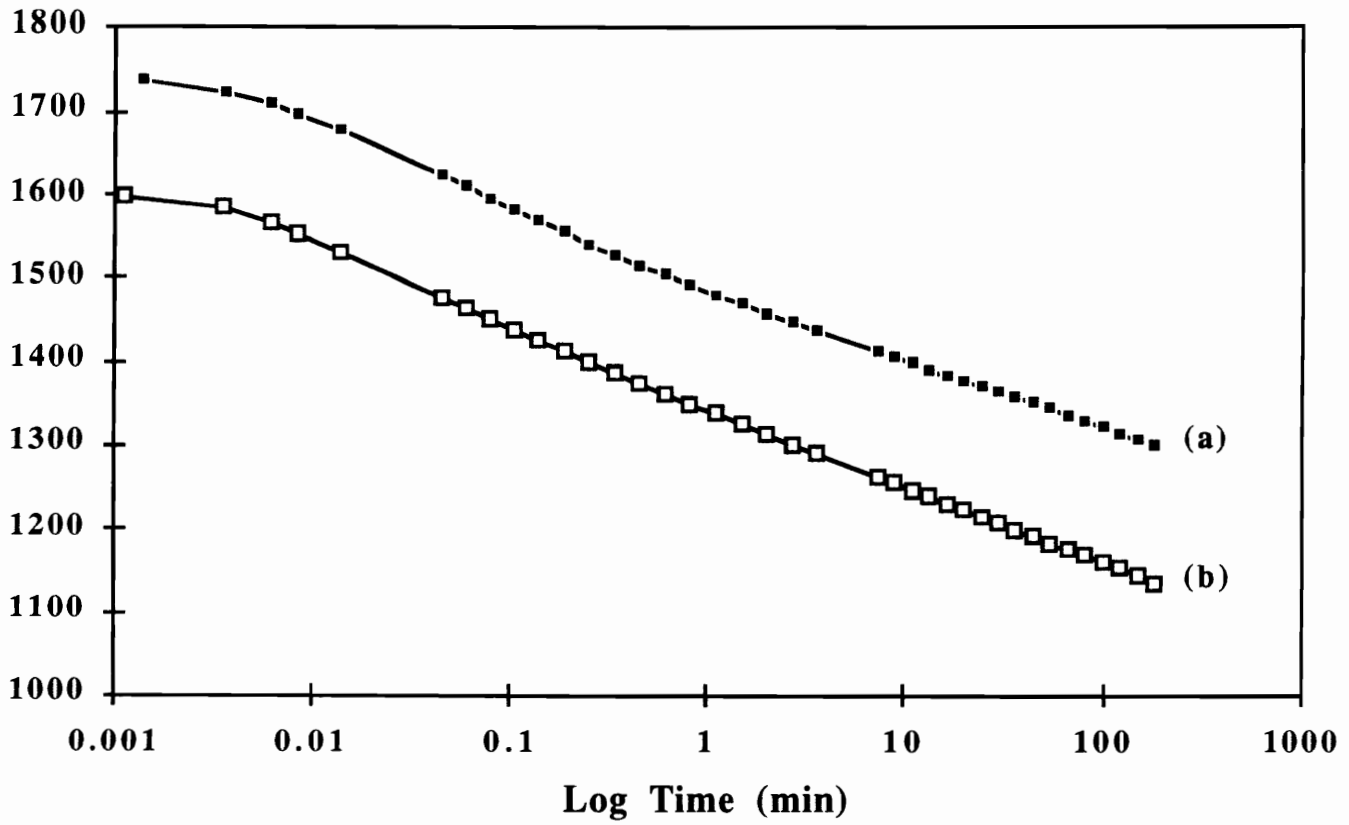


Figure 4.48. Load relaxation behavior at 30°C-35%RH of molded foams without the use of CPPs as a function of water/TDI content (or density), (a) Fmo2 and (b) Fmo4.

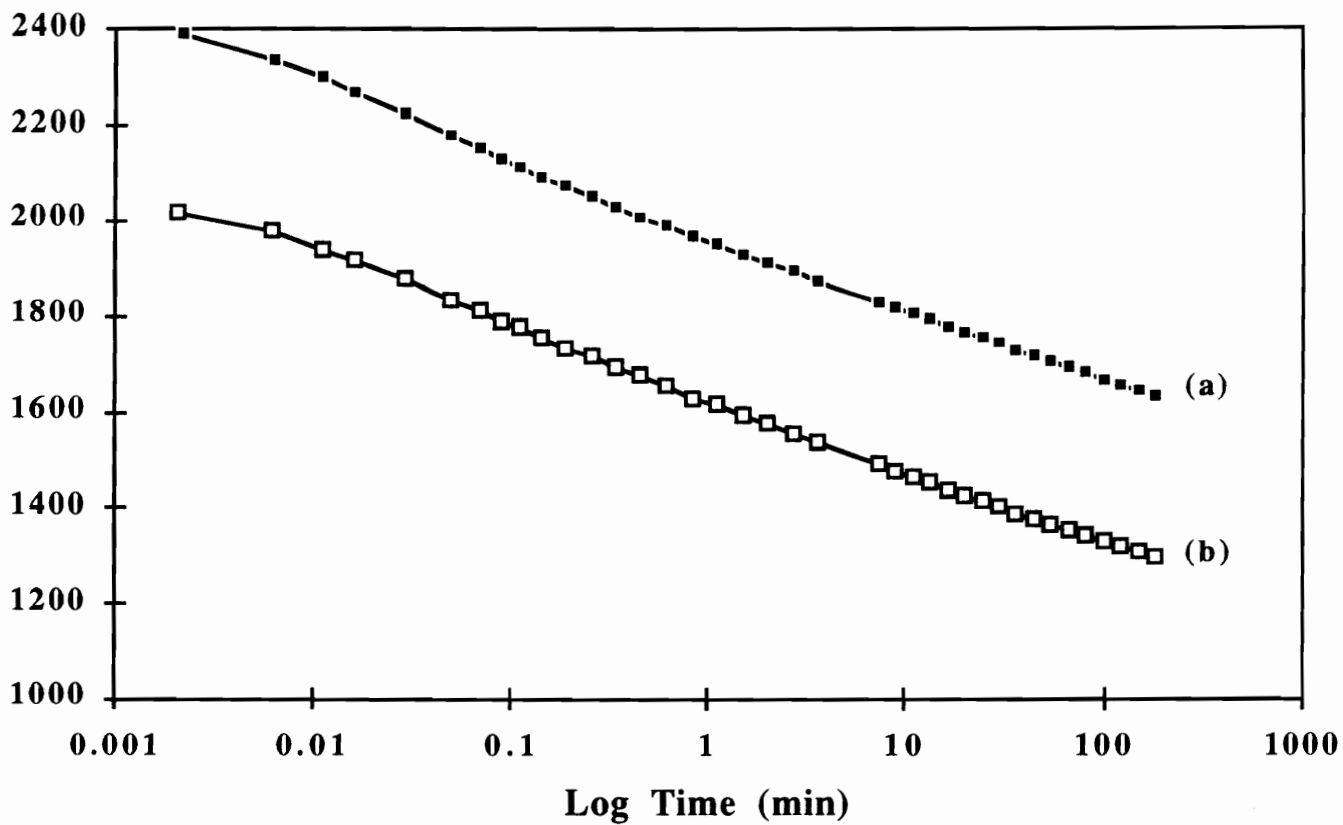


Figure 4.49. Load relaxation behavior at 30°C-35%RH for the CPP containing molded foams as a function of water/TDI content (or density), (a) Fmc2 and (b) Fmc4.

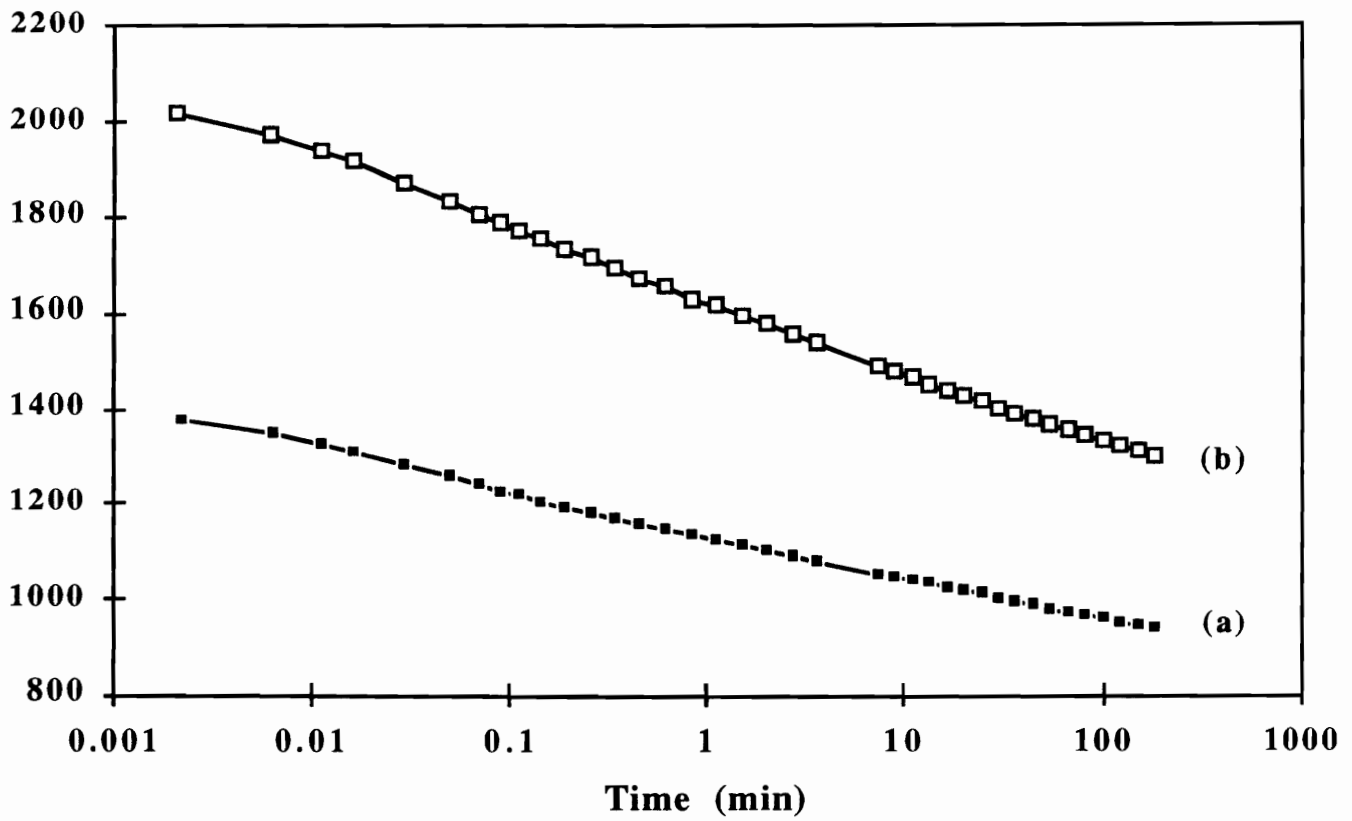


Figure 4.50. Normalized load relaxation behavior at 30°C-35%RH for the CPP containing molded foams as a function of water/TDI content, (a) Fmc2 and (b) Fmc4.

compliment the load relaxation findings since both tests reflect viscoelastic behavior. The six molded foam samples were compressed under a constant load and investigated using the same environmental conditions applied in the load relaxation measurements. The approach practiced was very similar to that used by Moreland as well as Cambell.^{79,80} In this case the applied load, 800g, was chosen to give an initial strain for low temperature, low humidity experiments of 0.2- 0.3. This value was chosen whereas it reflects the amount of strain that is normally observed in molded polyurethane foams used as automobile seats. The creep response was evaluated in terms of the formulation variables; copolymer polyols and water/TDI content in addition to specific environmental conditions.

4.6.2.1 Effect of Temperature and Relative Humidity

The creep response for Fmc4 under a constant load and varying temperature and/or humidity is shown in Fig. 4.51 and in tabular format in Table 4.17. As can be seen, a short induction period (ca. 6 sec.) is displayed at each environmental condition. Furthermore, this induction period slightly decreased with increasing temperature and/or humidity. Moreland observed similar behavior in evaluating conventional slabstock foams of water content greater than 2 pph and found this induction period to be insensitive to the water/TDI content and temperature. The exact origin of this induction is not known but is believed to be related to the CPP dispersion (in the molded foams) and the urea precipitates (in conventional slabstock foams). Recall from Chapter 2 that certain high water content slabstock foams exhibit another precipitate phase ca. 0.1-0.3 μm in size. Interestingly, as will be shortly illustrated, the molded foams lacking the CPP dispersions did not exhibit this induction period while the CPP foams as well as the slabstock foams did. Further evidence of the origin of this induction period can be obtained from another study carried out by Moreland et. al. where LiCl was added to the foam formulation which was shown to

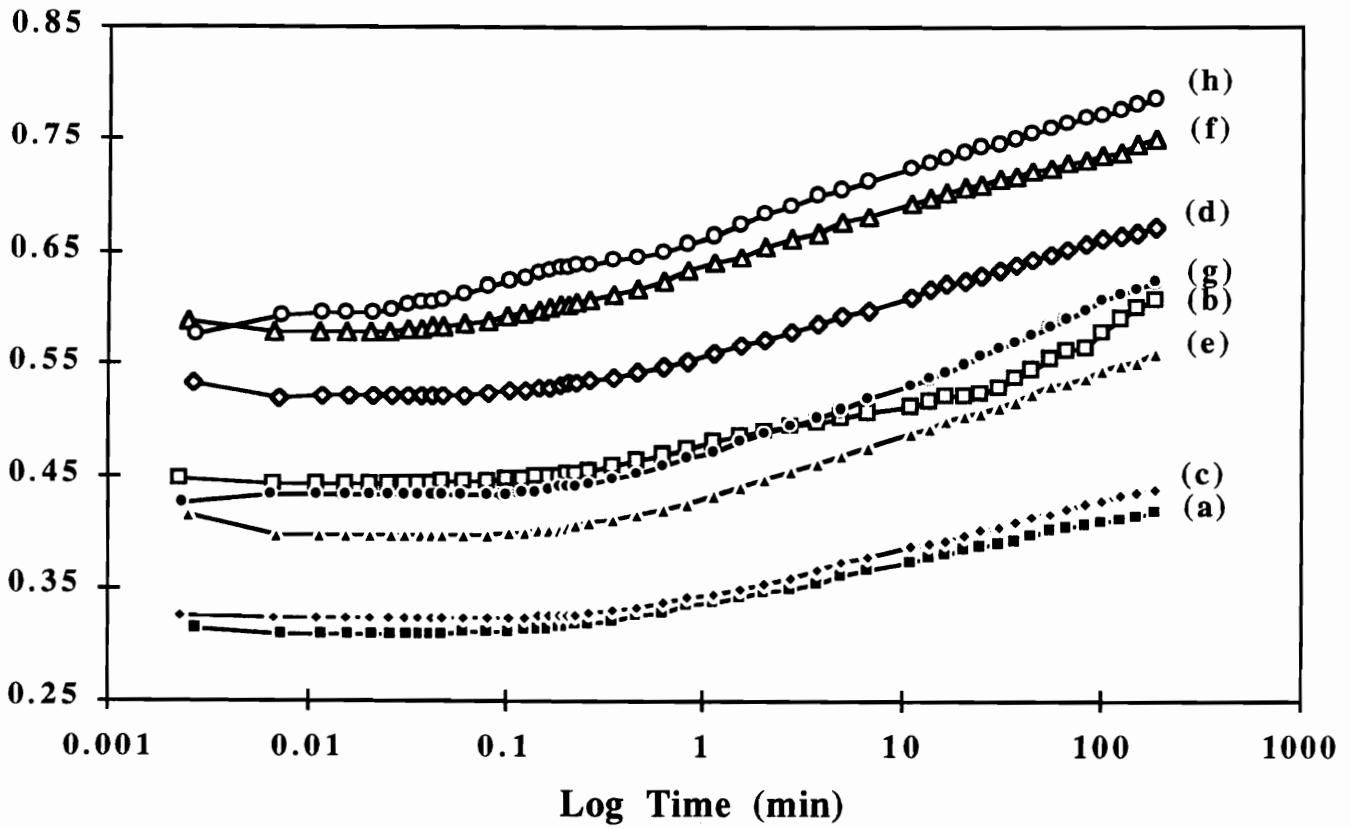


Figure 4.51. Creep response of Fmc4 as a function of temperature/relative humidity, (a) 30°C-35%RH, (b)30°C-98%RH, (c) 50°C-35%RH, (d) 50°C-98%RH, (e) 80°C-35%RH, (f)80°C-98%RH, (g) 100°C-35%RH (h) 100°C-98%RH.

Table 4.17. Summary of Creep Measurements on Fmc4

Temp-%RH (°C-%)	Std Dev. ¹ (±ε)	Init. Strain (ε ₀)	Δ Strain (Δε)
30-35	0.05	0.32	0.11
50-35	0.05	0.33	0.12
80-35	0.04	0.42	0.16
100-35	0.01	0.43	0.19
30-98	0.06	0.45	0.16
50-98	0.03	0.53	0.15
80-98	0.01	0.59	0.16
100-98	0.03	0.58	0.19

* Performed with a load of 800g.

1. Based on two to three runs for each temperature and humidity.

prevent formation of the precipitated urea based structures.⁷⁹ This plasticizer was also shown to eliminate the induction period which had been observed in foams without LiCl.

In addition to an induction period, Fig. 4.51 depicts that the effects of temperature and relative humidity on the creep behavior of these foams were similar to their effects on the load relaxation behavior, i.e. they had a "softening" effect. In this case, the initial strain as well as the additional three hour creep strain (amount of creep expressed in terms of strain) were recorded and are presented in Table 4.17. An increase in temperature and/or humidity resulted in increased initial strains and increased creep strains. This was especially true for temperatures greater than 50°C. At 30°C-35% RH, the initial strain was 0.32 and the additional creep strain after three hours was 0.11. At 100°C-98% RH, the initial strain was 0.58 and the amount of additional strain was 0.19. As in the load relaxation measurements, the behavior at 30°C-98%RH was similar to that at 100°C-35%RH, eg. curves (b) and (g) in Fig. 4.51. Table 4.17 also reveals that the initial strains and creep strains at these two conditions are similar. In general, increasing the temperature to 100°C or the humidity to 98%RH (from 30°C-35%RH) augmented both the initial strain and creep strain by ca. 50%. Increasing both the temperature and humidity resulted in an increase in both the initial strain and creep strain by ca. 100%. As with the load relaxation measurements, the high temperature results exhibited non-linear behavior. As discussed in the load relaxation section, the "plasticization" (increase in strain and creep strain) with temperature and humidity is primarily due to hydrogen bond disruption thereby increasing the amount of chain slippage. The non-linearity observed at high temperatures, especially 100°C, suggests that the relaxation mechanism is enhanced or an additional mechanism may be occurring. Here the amount of hydrogen bond disruption is dramatically increased. This further supports the conclusions from the load relaxation measurements that hydrogen bonding (predominately occurring within the hard segment domains) significantly enhances the foam properties. At elevated temperatures and/or humidities, these properties are severely impaired.

The creep behavior for Fmc2 is presented in Fig. 4.52. As with Fmc4, a "softening" effect is observed especially at temperatures greater than 50°C. Also, as in the load relaxation measurements, Fmc2 displayed stiffer behavior than Fmc4 - the loads were slightly lower as were the creep strains. Table 4.18 gives the initial strains and creep strains for the various environmental conditions as well as the scatter in the data. The initial strain at 30°C-35% RH was 0.21 with a creep strain of 0.08 resulting in a final strain of 0.28. At 100°C-98% RH, these two values were 0.53 and 0.23. Also, major changes in the behavior (initial strain and creep strain) were observed with increases in temperature beyond 50°C (@ 35%RH). As can be seen an increase in either temperature or humidity softened the response significantly. Again curves (b) and (g) are in very close proximity emphasizing the strong influence of humidity. The initial strain increased by ca. 40% upon increasing the temperature above 30°C to 100°C. Likewise, at any given temperature, an increase in humidity from 35% to 98% resulted in a 40% - 60% increase in the initial strain. Again the creep response exhibited an induction period similar to that of Fmc4 which decreased in length with increasing temperature.

The two foams, Fme4 and Fme2, exhibited very similar response when exposed to creep loading under various environmental conditions. The creep response of Fme4 is displayed in Fig. 4.53 and whose results are presented in Table 4.19. Both the initial strains and the creep strains were in close proximity to those of Fmc4. The initial strain values ranged from 0.28 at 30°C-35%RH, to 0.47 at 100°C-98%RH. The creep strains were 0.11 at 30°C-35%RH and 0.17 at 100°C-98%RH. Also similar to Fmc4 was the decreasing trend displayed with the induction period. Again, humidity as well as temperature displayed an intense influence on the creep response of this foam.

Foam Fme2 displayed a similar response to creep loading as foam Fmc2. Being of equal density, both displayed stiffer behavior than their corresponding 4 pph water counterparts. The creep response of Fme2 is illustrated in Fig. 4.54 and presented in Table 4.20. The two values, initial strain and creep strain, again increased with temperature

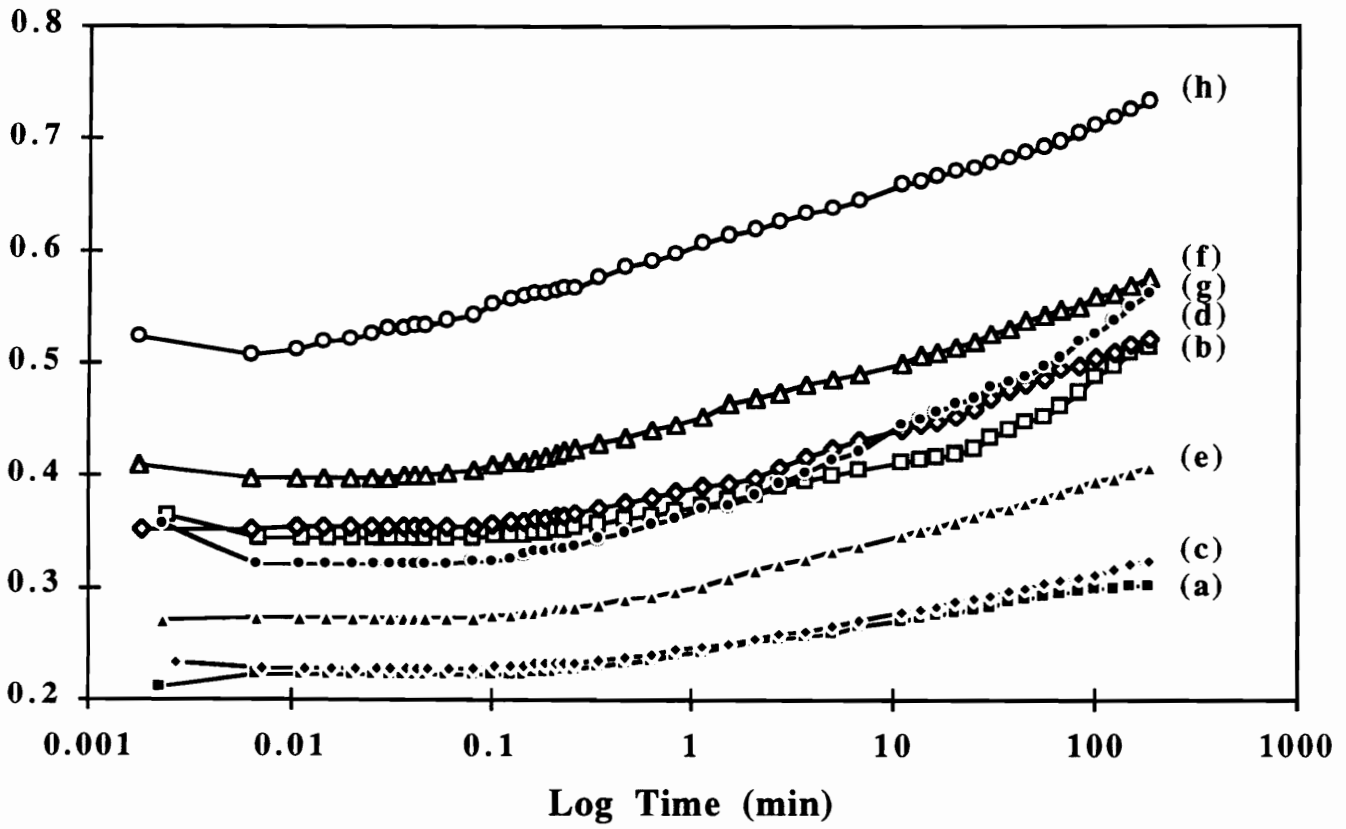


Figure 4.52. Creep response of Fmc2 as a function of temperature/relative humidity, (a) 30°C-35%RH, (b)30°C-98%RH, (c) 50°C-35%RH, (d) 50°C-98%RH, (e) 80°C-35%RH, (f)80°C-98%RH, (g) 100°C-35%RH (h) 100°C-98%RH.

Table 4.18. Summary of Creep Measurements on Fmc2

Temp-%RH (°C-%)	Std Dev. ¹ (±ε)	Init. Strain (ε ₀)	Δ Strain (Δε)
30-35	0.00	0.21	0.08
50-35	0.01	0.23	0.10
80-35	0.00	0.27	0.13
100-35	0.01	0.36	0.24
30-98	0.03	0.36	0.17
50-98	0.01	0.35	0.17
80-98	0.02	0.41	0.18
100-98	0.01	0.53	0.23

* Performed with a load of 800g.

1. Based on two to three runs for each temperature and humidity.

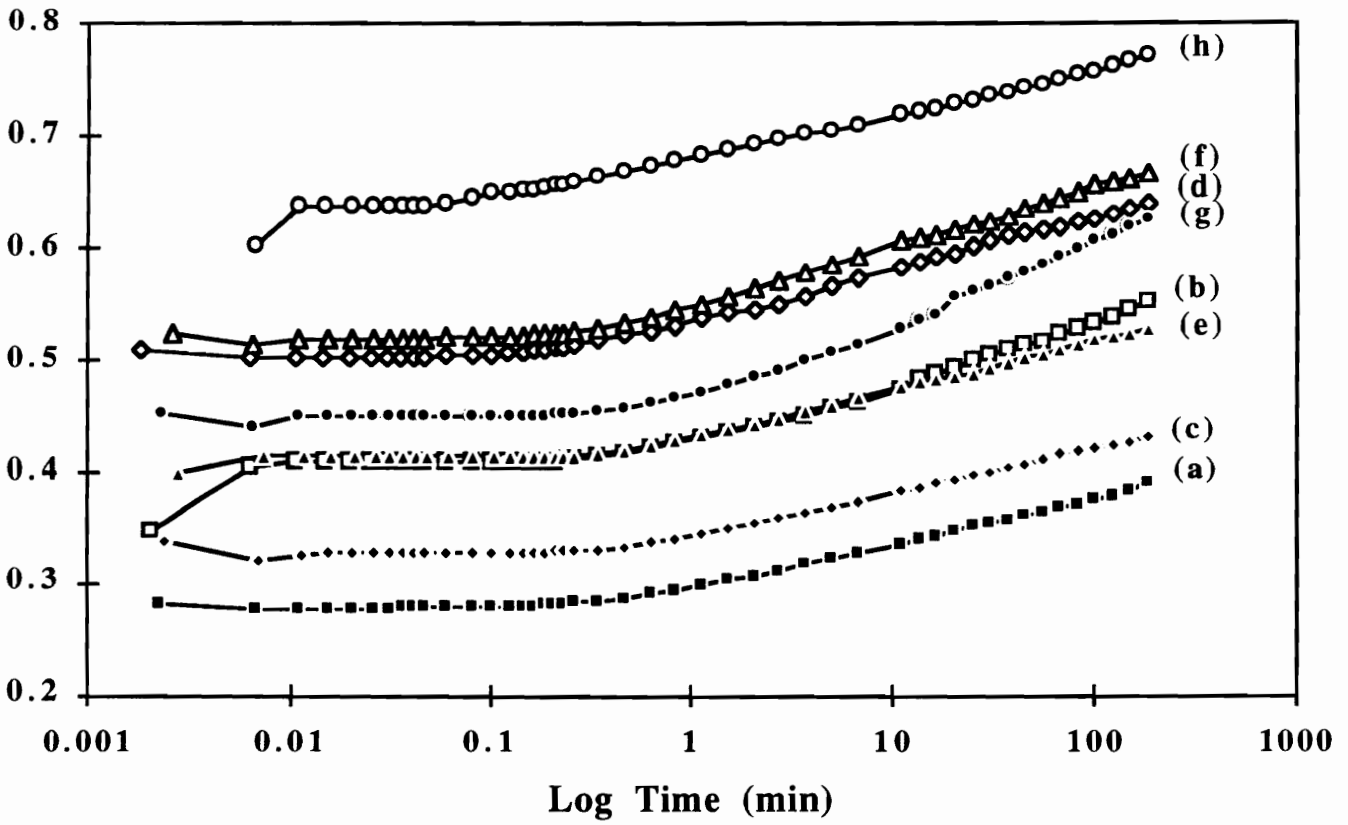


Figure 4.53. Creep response of Fme4 as a function of temperature/relative humidity, (a) 30°C-35%RH, (b)30°C-98%RH, (c) 50°C-35%RH, (d) 50°C-98%RH, (e) 80°C-35%RH, (f)80°C-98%RH, (g) 100°C-35%RH (h) 100°C-98%RH.

Table 4.19. Summary of Creep Measurements on Fme4

Temp-%RH (°C-%)	Std Dev. ¹ (±ε)	Init. Strain (ε ₀)	Δ Strain (Δε)
30-35	0.01	0.28	0.11
50-35	0.02	0.34	0.11
80-35	0.01	0.40	0.12
100-35	0.04	0.45	0.19
30-98	0.02	0.35	0.15
50-98	0.04	0.51	0.14
80-98	0.03	0.53	0.15
100-98	0.01	0.47	0.17

* Performed with a load of 800g.

1. Based on two to three runs for each temperature and humidity.

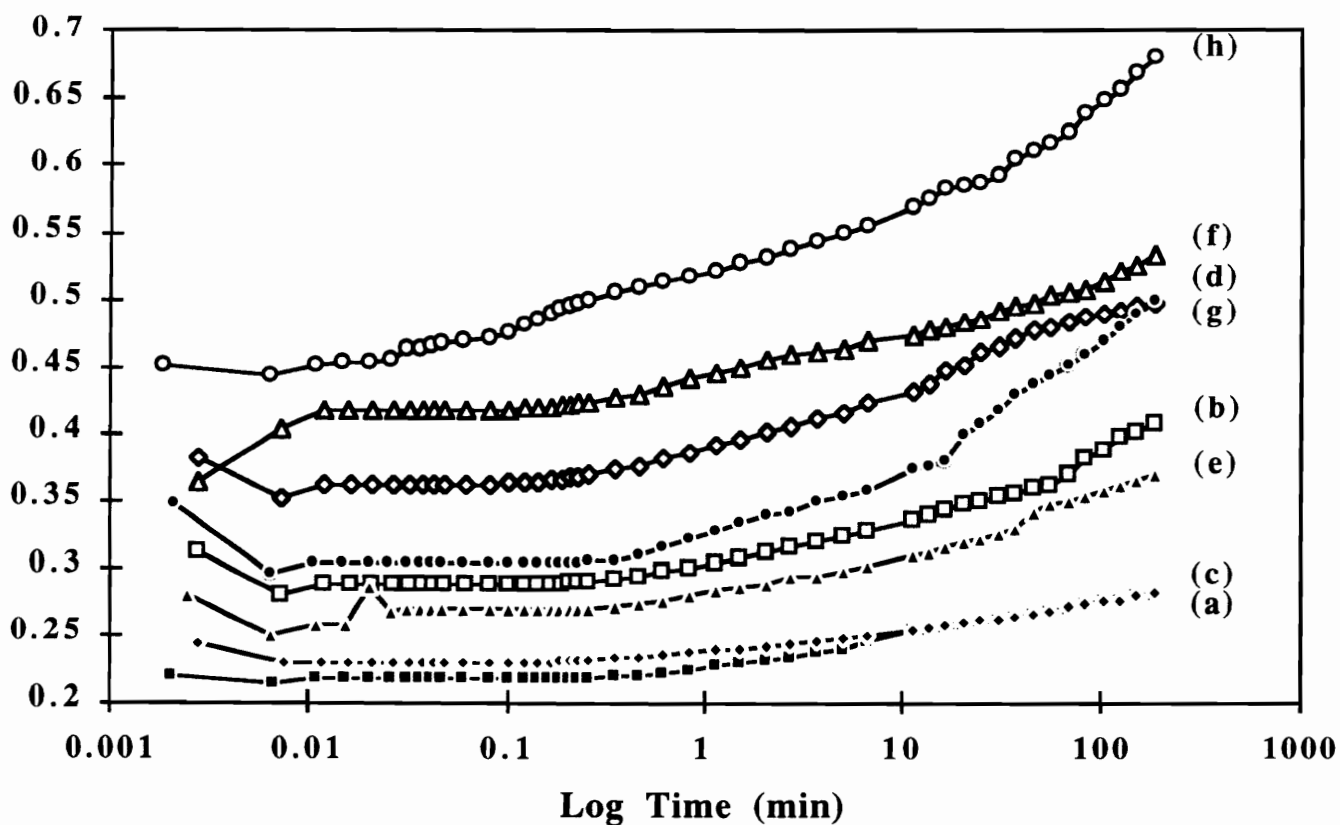


Figure 4.54. Creep response of Fme2 as a function of temperature/relative humidity, (a) 30°C-35%RH, (b)30°C-98%RH, (c) 50°C-35%RH, (d) 50°C-98%RH, (e) 80°C-35%RH, (f)80°C-98%RH, (g) 100°C-35%RH (h) 100°C-98%RH.

Table 4.20. Summary of Creep Measurements on Fme2

Temp-%RH (°C-%)	Std Dev. ¹ (±ε)	Init. Strain (ε ₀)	Δ Strain (Δε)
30-35	0.03	0.22	0.07
50-35	0.02	0.24	0.05
80-35	0.01	0.28	0.12
100-35	0.03	0.35	0.20
30-98	0.01	0.31	0.13
50-98	0.01	0.38	0.15
80-98	0.02	0.36	0.13
100-98	0.00	0.45	0.24

* Performed with a load of 800g.

1. Based on two to three runs for each temperature and humidity.

and/or humidity. The initial strain increased from 0.22 at 30°C-35%RH to 0.45 at 100°C-98%RH. The creep strain increased from 0.07 to 0.24, similar to Fmc2. Also similar to Fmc2 was that all curves displayed an induction period which decreased in time with increasing temperature. Again temperature and humidity "plasticized" the creep response indicating the susceptibility of hydrogen bonds to disruption by both.

The creep response of Fmo4, the 4 pph water content foam lacking the inclusion of CPPs, is shown in Fig. 4.55. The trend is again very similar to that displayed previously with the other molded foams - that is as the temperature and/or humidity was increased, the initial strain as well as the creep strain increased. As can be seen, the creep response carried out at 100°C-35% was similar to that carried out at 30°C-98%RH, ie. compare curves (b) and (c) of Fig. 4.55. However, one major difference was observed; the induction period observed in the creep response of the previous four foams was not exhibited here by foam Fmo4. As can be seen in Fig. 4.55, the strain increased immediately following loading and increased in a fairly linear fashion. Table 4.21 gives the creep results in terms of initial strain and creep strain for the four conditions as well as the standard deviations and shows that the initial strain increased by 50% upon increasing the environmental condition from ambient to the most extreme conditions. Aside from the lack of an induction period, all other aspects of this behavior are similar to that of the previously discussed foams.

Finally the response to creep loading of foam Fmo2 was investigated as well as its response to the various environmental conditions. The results are shown in Fig. 4.56 and presented in Table 4.22. As can be seen, both temperature and especially humidity "plasticized" the creep behavior. Table 4.22 reveals that the initial strain and creep strain increased by 25% - 50% going from ambient conditions to the extreme, highest temperature/humidity conditions. As with Fmo4, the creep curves lack an induction period as exhibited by all the foams containing the CPP particles. Here, the strain increased

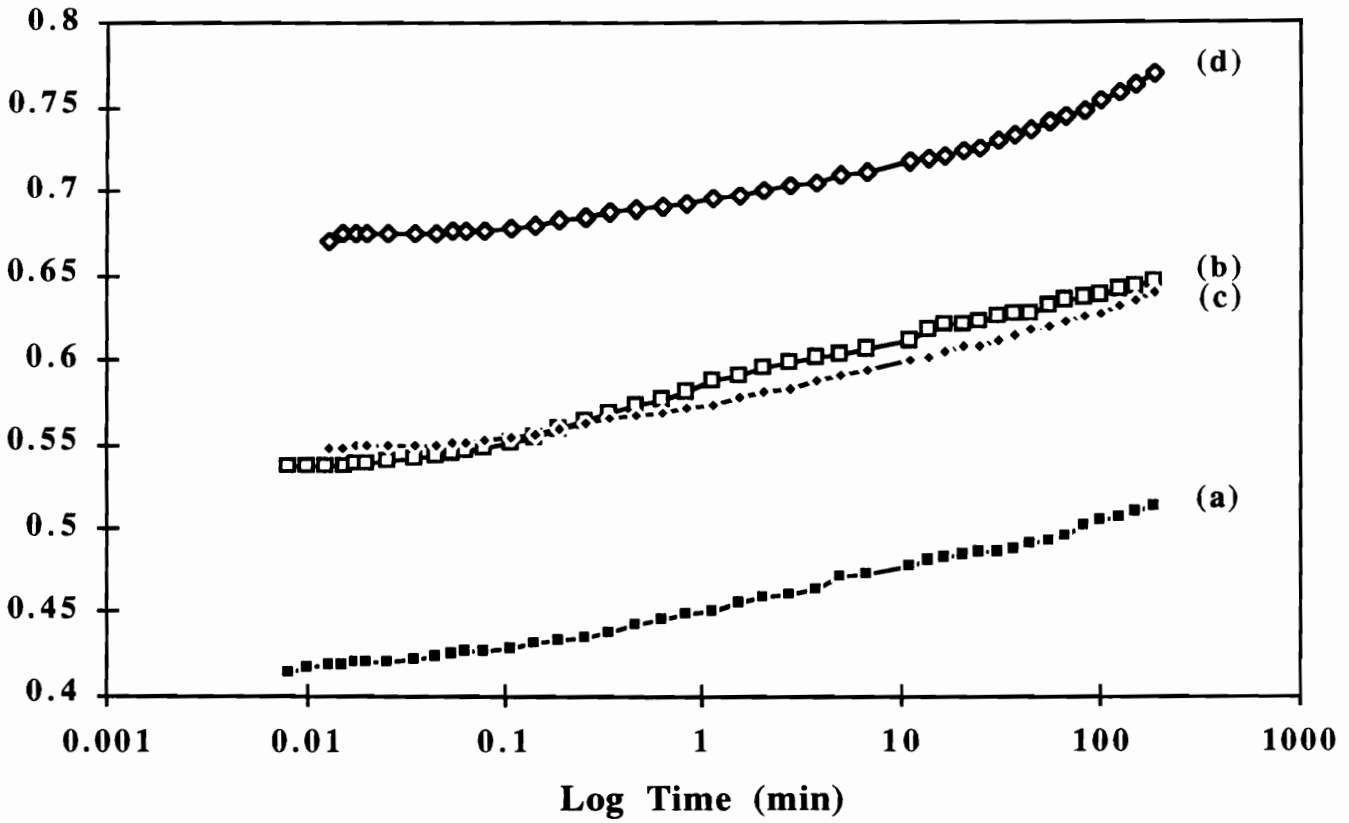


Figure 4.55. Creep response of Fmo4 as a function of temperature/relative humidity, (a) 30°C-35%RH, (b)30°C-98%RH, (c) 100°C-35%RH and (d) 100°C-98%RH.

Table 4.21. Summary of Creep Measurements on Fmo4

Temp-%RH (°C-%)	Std Dev. ¹ (±ε)	Init. Strain (ε ₀)	Δ Strain (Δε)
30-35	0.05	0.41	0.10
100-35	0.01	0.55	0.09
30-98	0.02	0.52	0.12
100-98	0.02	0.67	0.10

* Performed with a load of 800g.

1. Based on two to three runs for each temperature and humidity.

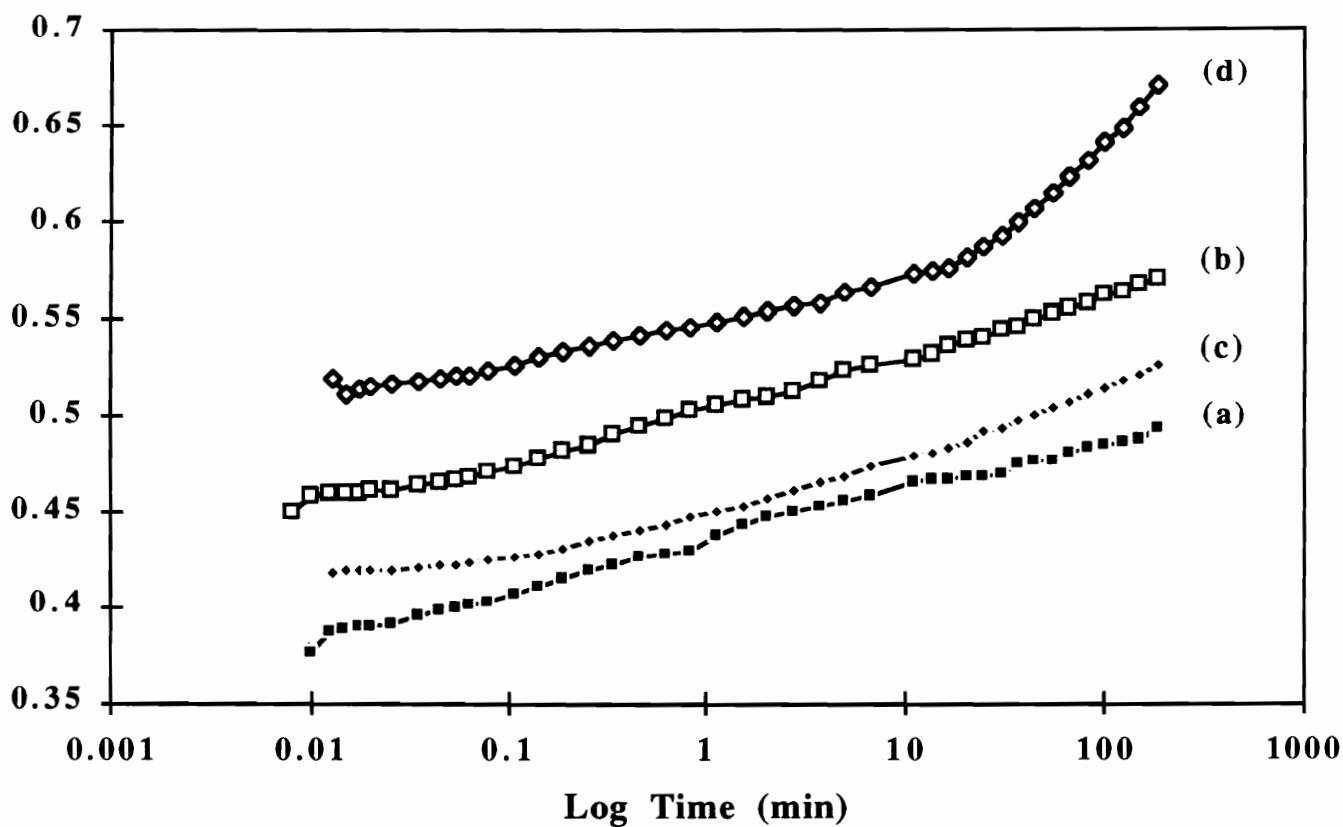


Figure 4.56. Creep response of Fmo2 as a function of temperature/relative humidity, (a) 30°C-35%RH, (b) 30°C-98%RH, (c) 100°C-35%RH and (d) 100°C-98%RH.

Table 4.22. Summary of Creep Measurements on Fmo2

Temp-%RH (°C-%)	Std Dev. ¹ (±ε)	Init. Strain (ε ₀)	Δ Strain (Δε)
30-35	0.05	0.39	0.09
100-35	0.02	0.42	0.11
30-98	0.02	0.45	0.12
100-98	0.01	0.51	0.15

* Performed with a load of 800g.

1. Based on two to three runs for each temperature and humidity.

immediately following loading. However, the high temperature non-linearity exhibited by the formerly discussed foams was also exhibited here by Fmo2.

Figure 4.57 more directly illustrates the effect of temperature at 35%RH on the initial strain for each foam. As clearly demonstrated, the initial strain systematically increased with each systematic increase in temperature for all foams. Likewise, the creep strain or total amount of change in strain also increased with temperature as shown in Fig. 4.58 where the creep strain is plotted versus temperature for each foam. This was especially true with the CPP containing foams. The fact that both the initial strain and creep strain were influenced by temperature and humidity strongly suggests that the foam behavior is dependent upon the solid polymer network of the foam and specifically that the physical network (HS domains) also plays an important role. Therefore long term behavior and dynamic fatigue of materials exposed to various environments depend on the characteristics of the HS domains. Hydrogen bonding which occurs predominately between carbonyl and NH groups within the HS domains has been shown to weaken with temperature and humidity thereby contributing less to any resistance to chain slippage. At elevated temperatures and humidities, the covalent network becomes more important.

4.6.2.2 Effect of Copolymer Polyols

The influence of the copolymer polyols (CPP) on the creep response was also investigated by varying only the CPP while maintaining all other formulation components constant. Such is the case in comparing foams Fmo4, Fmc4, and Fme4 whose creep response at 30°C-35%RH is displayed in Fig. 4.59. Both foams with CPPs, Fmc4 and Fme4 clearly displayed an induction period of ca. 6 sec. long while Fmo4 displayed no induction time. In addition, since the strains were lower, foams Fmc4 and Fme4 exhibited stiffer behavior than Fmo4. Recall that the initial strains for foams Fmo4, Fmc4 and Fme4 were 0.41, 0.32, and 0.28, respectively. However, while the use of CPPs did indeed

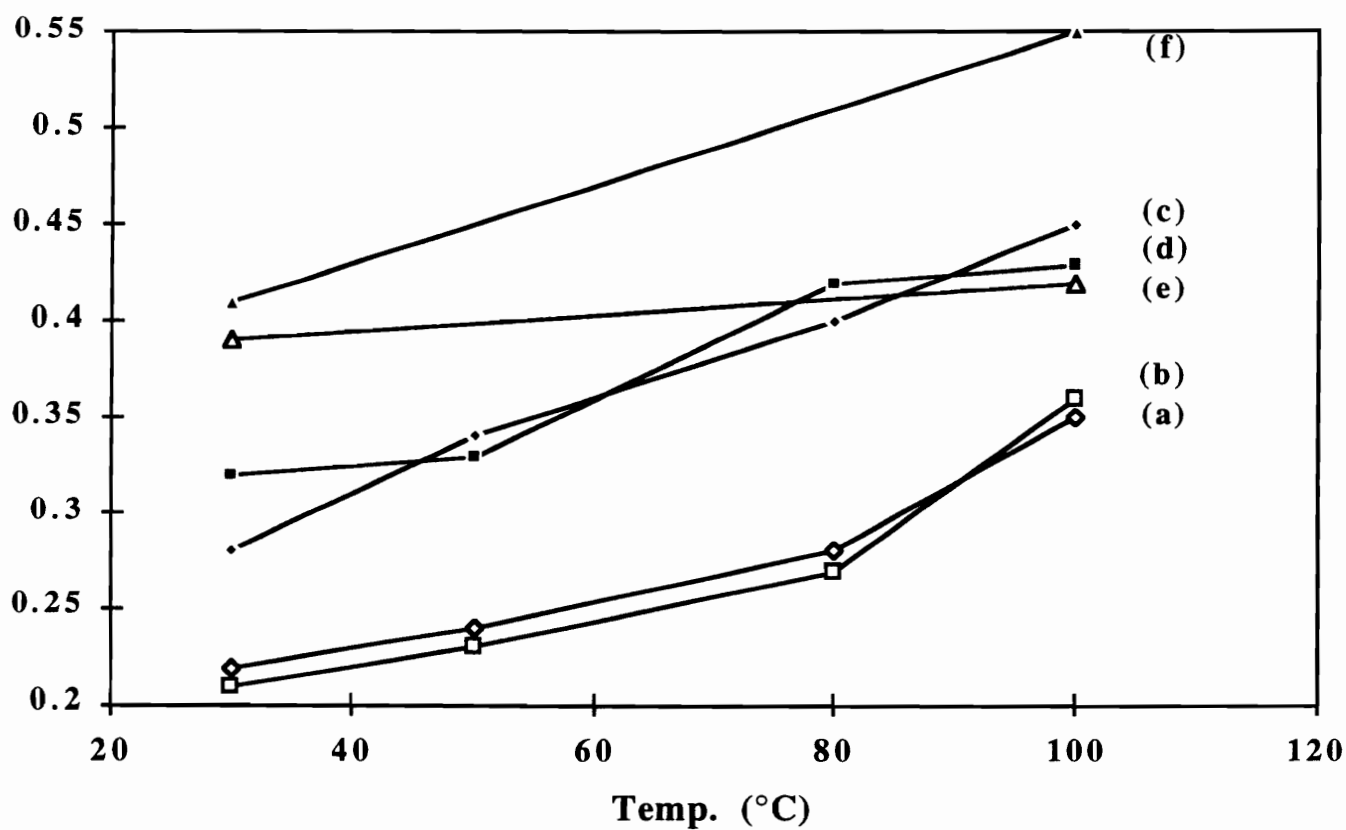


Figure 4.57. Effect of temperature on the initial strain at 35%RH, (a) Fme2, (b) Fmc2, (c) Fme4, (d) Fmc4, (e) Fmo2, and (f) Fmo4.

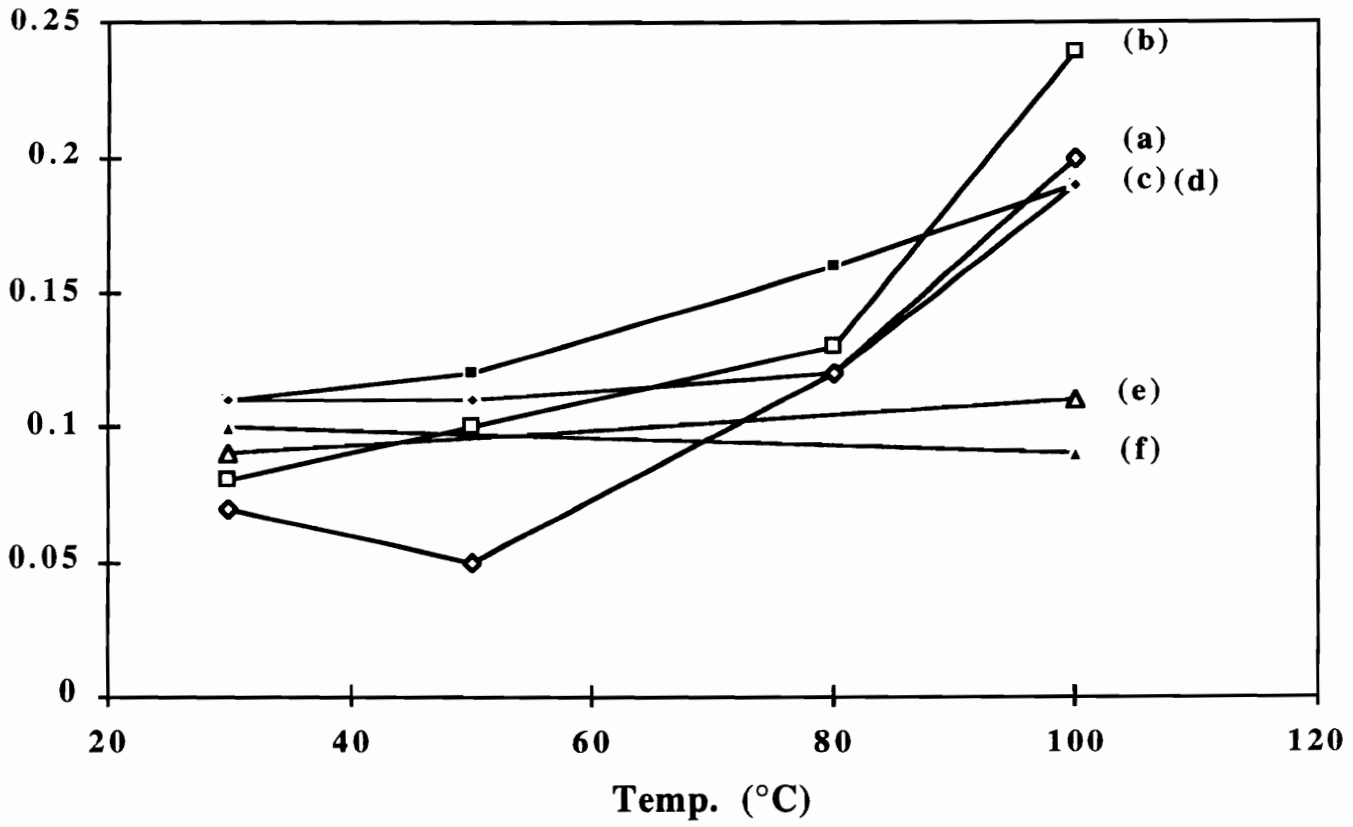


Figure 4.58. Effect of temperature on the creep decay at 35%RH, (a) Fme2, (b) Fmc2, (c) Fme4, (d) Fmc4, (e) Fmo2, and (f) Fmo4.

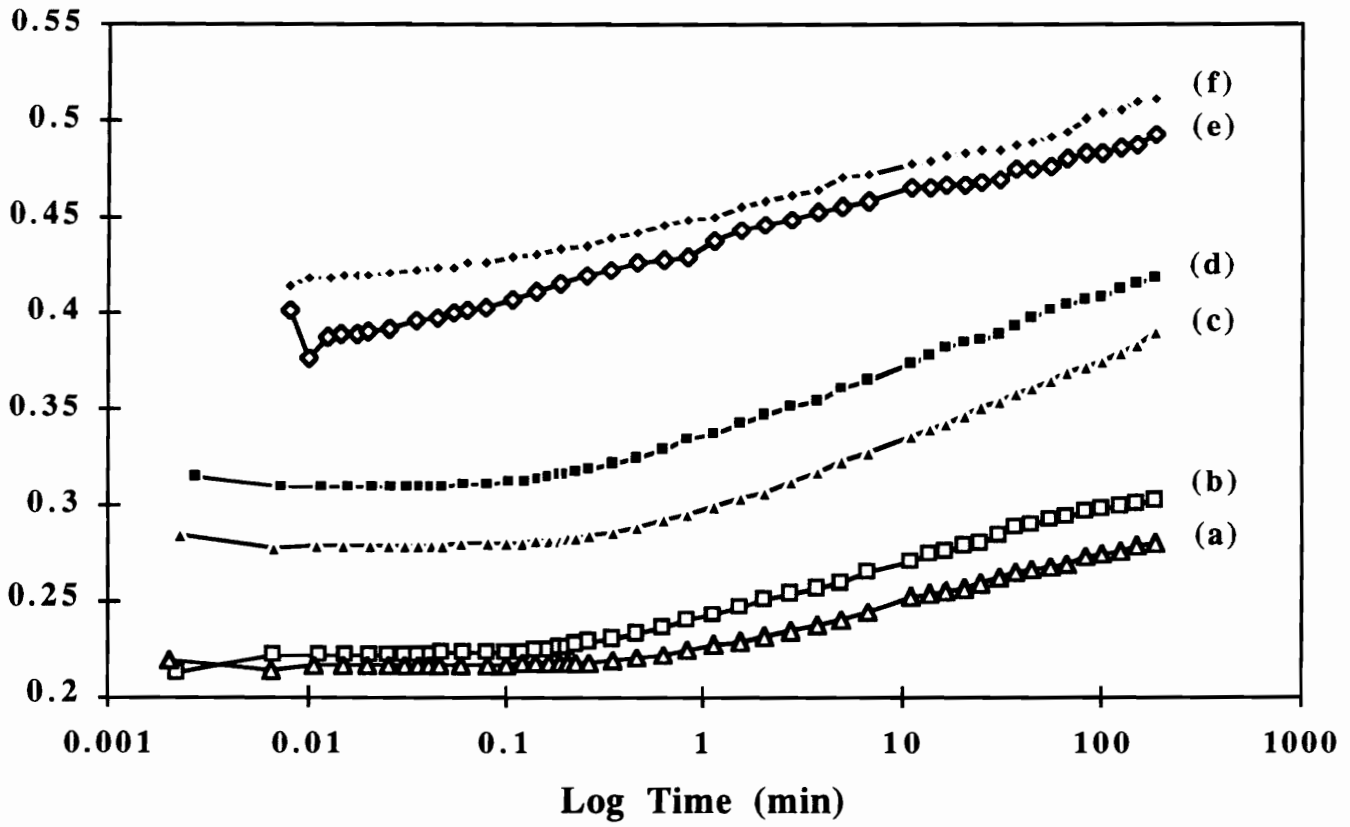


Figure 4.59. Creep response at 30°C-35%RH as a function of the CPP used and water/TDI content, (a) Fme2, (b) Fmc2, (c) Fme4, (d) Fmc4, (e) Fmo2, and (f) Fmo4.

improve initial foam "hardness" and even generated an induction period, they did not decrease the creep strains; in fact, these values were slightly greater than for the foams lacking CPPs. For example, the creep strains were 0.10, 0.11, and 0.11 for Fmo4, Fmc4 and Fme4, respectively. Likewise, within the 2 pph water content foams, that varied in the type of CPP particle utilized, similar results were demonstrated as also shown in Fig. 4.59. The incorporation of CPPs resulted in both lower initial strains and induction periods but had very little change on the creep rate and thus the creep strain. The strain levels were reduced by ca. 25% - 50% giving rise to an apparent stiffer foam. The use of the experimental CPP which possessed both less surface stabilizer and lower functionality, did not significantly alter the creep response as compared to the conventional CPP foams. The initial loads were essentially the same although the creep strains were slightly lower at 30°C as well as at the other conditions.

At 100°C-35%RH, the differences between the foams were accented even further specifically in creep strain behavior. Shown in Fig. 4.60 is the creep response of the six molded foams at this high temperature condition. Similar to the load relaxation results, the foams with CPPs displayed a much lower rate of creep and thus a much higher creep strain. The initial strains were again higher for the foams with CPPs, but the strain levels of these CPP containing materials surpassed those lacking CPPs. Here, the initial strains were 0.55, 0.43, and 0.45 for foams Fmo4, Fmc4 and Fme4, respectively. However, the creep strain values were 0.10, 0.19, and 0.19 for the same three foams respectively. As can be seen, the creep strain values for the CPP containing foams were almost twice as much as those without the CPP particles for the three hour period. This crossover of the strain levels between the CPP containing foams and those without CPPs occurred at ca. 80 min. for the high density foams. From extrapolation of the curves, the 4 pph water content foams appear to be heading toward crossover shortly after completion of the three hour experiment. Although the exact reason for the higher creep strains displayed by foams Fmc4 and Fmc2 is not known, it is believed that thermal "plasticization" in the matrix

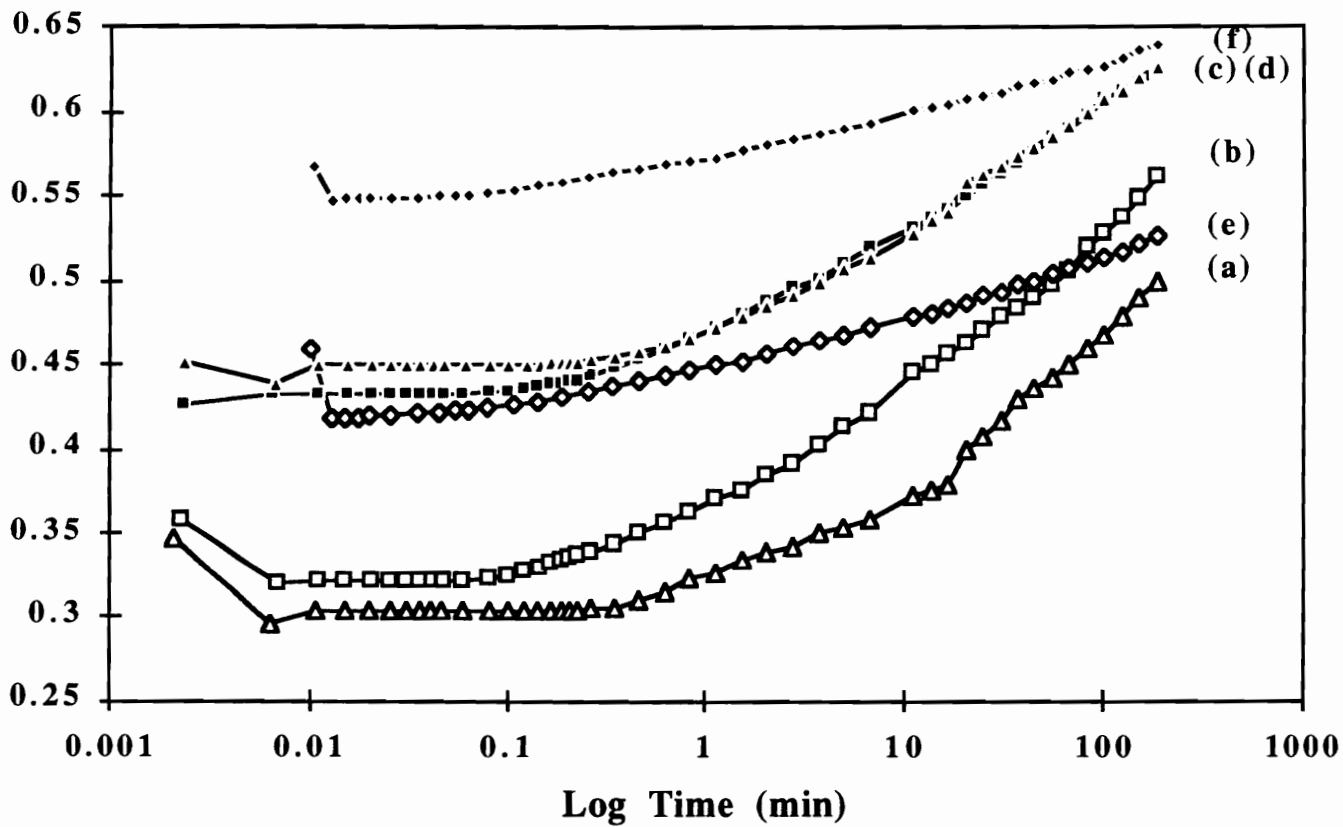


Figure 4.60. Creep response at 100°C-35%RH as a function of the CPP used and water/TDI content, (a) Fme2, (b) Fmc2, (c) Fme4, (d) Fmc4, (e) Fmo2, and (f) Fmo4.

polyol has led to greater creep and greater localized stress at the CPP-polyol interface. This stress concentration effect is thus promoting further chain slippage and increases in strain. In addition, creep may occur to a small extent within the CPP particles due to increased thermal mobility at this temperature which is close to the CPP T_g (ca. 125°C). As mentioned earlier, the strain on the soft phase is greater for the CPP containing foams due to the fact that a smaller fraction of soft segment is present to accommodate the applied load. Thus, the soft segment strains further for the CPP containing foams over the CPP lacking foams for a given total strain. Furthermore, secondary bonding such as hydrogen bonding is believed to exist at the interface which helps interface the particles to the soft phase. These secondary bonds may thereby be "plasticized" with temperature and/or humidity thus leading to further creep strain or increases in strain. This latter claim will be further considered in the next paragraph. Finally, the CPP containing foams consistently, exhibit a short induction period while the foams that do not contain this rigid filler do not exhibit an induction period suggesting that this induction period may be a consequence of the utilization of the CPP dispersed particles. However, this induction period decreased in length as the temperature was increased which may be a result of the hydrogen bond disruption associated with the CPP particles.

Comparing the above foams at the conditions of 30°C-98%RH reveals similar behavior to those given in Fig.4.60. Shown in Fig. 4.61, the CPP containing foams exhibited lower initial strains (ca. 20% lower) but higher creep strains (ca. 50% greater). For example, the initial strain was 0.52 for Fmo4, 0.45 for Fmc4, and 0.35 for Fme4. The creep strain was 0.12, 0.16, and 0.15 for the three foams respectively. Likewise, for the 2 pph water content foams, the initial strains decreased while the creep strains increased following the same trend. Although the curves do not cross-over, the slopes do imply that eventually the strains of the CPP containing foams would surpass those of the foams that do not contain CPPs. The evidence here suggests that creep is not occurring to a great extent within the CPP particles at 100°C-35%RH which approaches the CPP T_g . This was

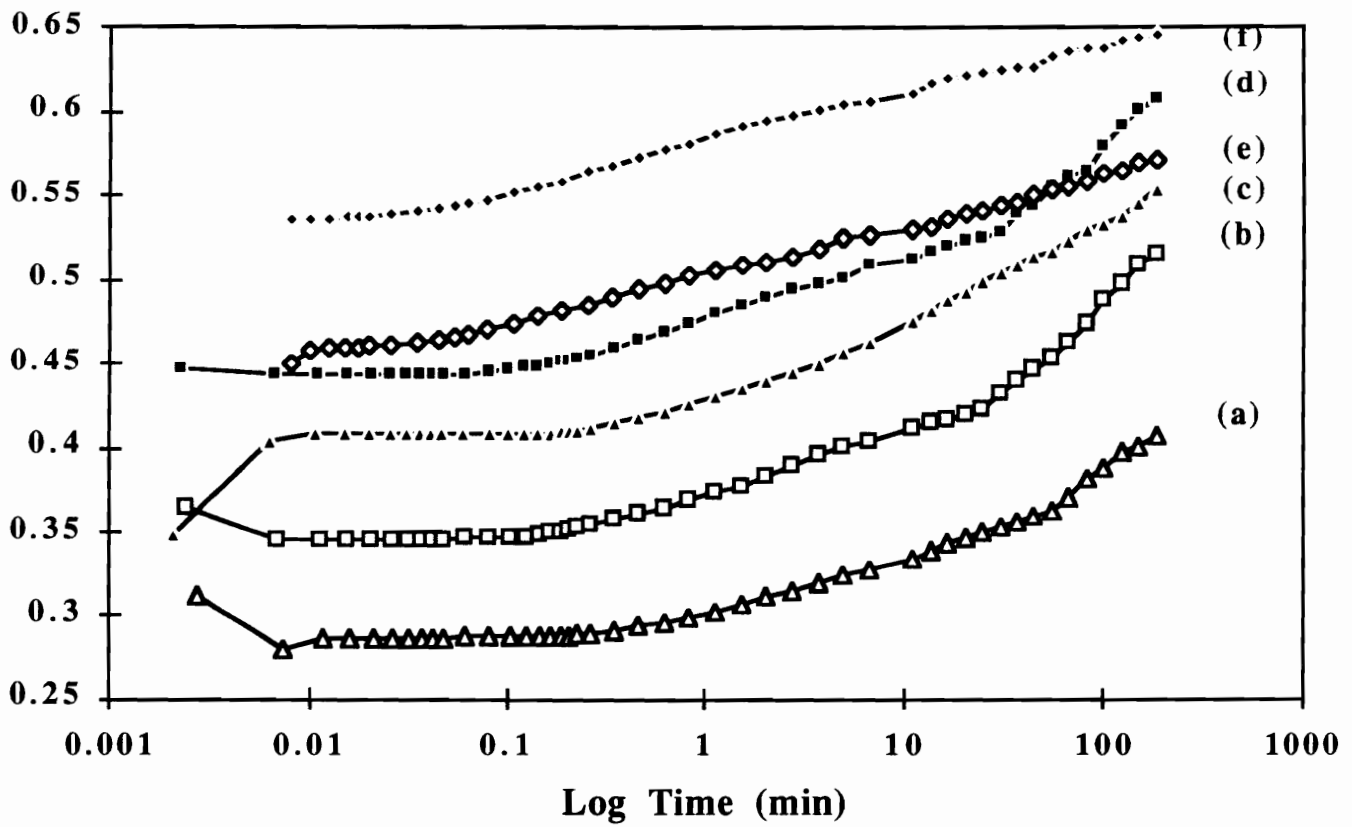


Figure 4.61. Creep response at 30°C-98%RH as a function of the CPP used and water/TDI content, (a) Fme2, (b) Fmc2, (c) Fme4, (d) Fmc4, (e) Fmo2, and (f) Fmo4.

concluded based on the similarity between the behavior at 30°C-98%RH and 100°C-35%RH. The creep strains were only slightly greater at 100°C-98%RH. Therefore, this "plasticization" or softening that was observed with both temperature and humidity is evidence supporting the claim that a significant degree of hydrogen bonding must exist at the interface of the particles and the base polyol. Again, the experimental CPP foams exhibited slightly improved behavior over the control CPP foams. This latter observation is further support that the covalent grafting may have less of an impact than hydrogen bonding since very little difference is observed with the major change in the stabilizer.

At 100°C-98%RH, the behavior exhibited by the six foams was very similar to that at the previous conditions as well as that observed in the load relaxation measurements. Recall that in the load relaxation measurements, the initial loads of the CPP containing foams and those without the particles (of equal water content) were essentially the same but decayed much more for the CPP containing foams. In the creep experiments shown in Fig. 4.62, while the initial strains of the CPP free foams are higher than the CPP containing foams, the creep strains surpass those of the CPP free foams within a 10 min to 100 min period. For example, the creep strain for Fmo4 was 0.10 while for Fmc4 the creep strain was 0.19. Again, the 2 pph water content foams portrayed the same trend. The trend of increasing creep strain in a three hour period with the incorporation of CPPs is consistent with previous results.

The results from the above experiments further confirms the findings of the load relaxation measurements where the incorporation of CPPs increased the foam stiffness by producing lower strains. While this was an initial goal (increase in ILD), the increase in the time dependent strain that accompanied this was definitely unexpected. Not only were the strain levels greater, but at elevated temperatures or humidities the strain levels of the CPP containing foams surpassed those of the foams lacking CPPs! This is clearly evident in Fig. 4.58 where the amount creep of each foam is plotted as a function of temperature which show dramatic increases at high temperatures and humidities. Again, the origin of

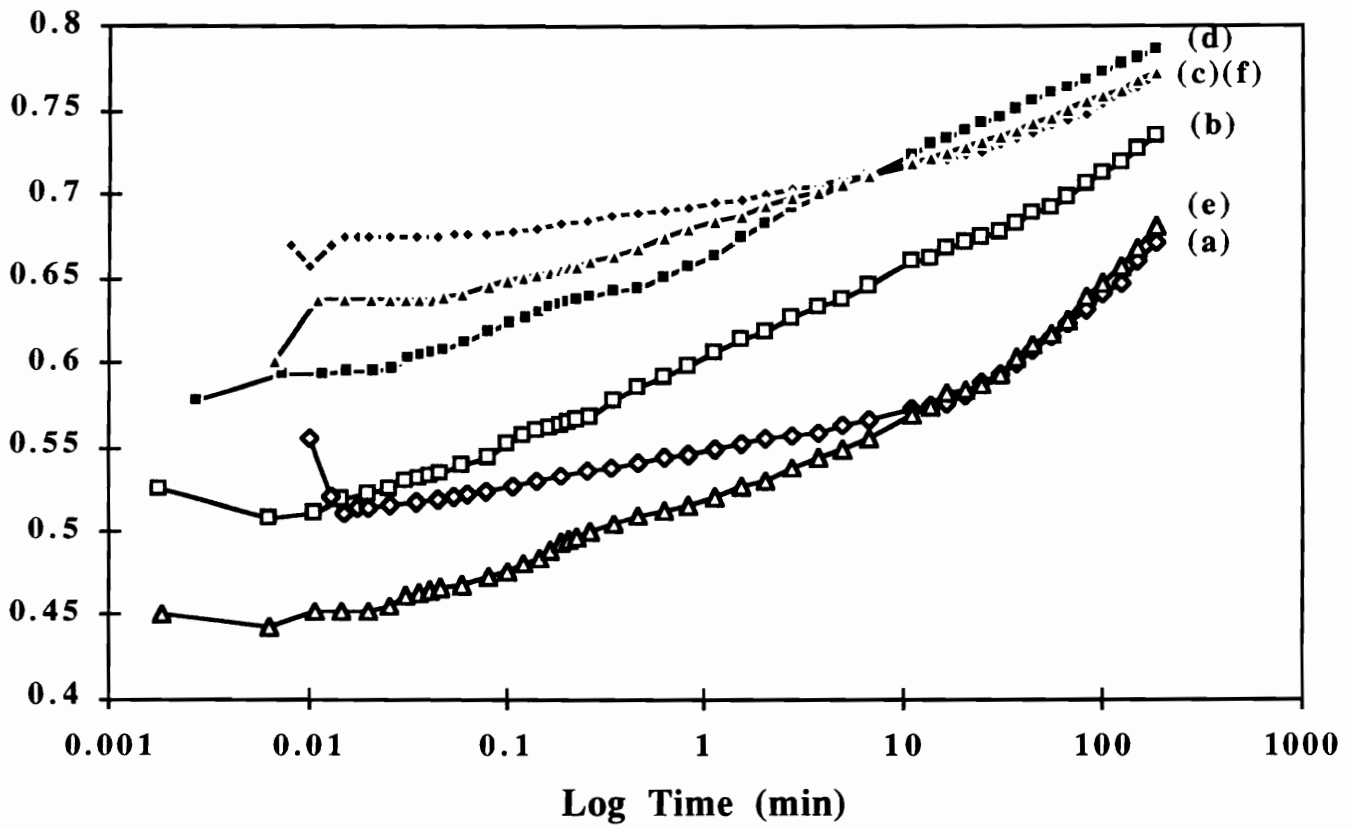


Figure 4.62. Creep response at 100°C-98%RH as a function of the CPP used and water/TDI content, (a) Fme2, (b) Fmc2, (c) Fme4, (d) Fmc4, (e) Fmo2, and (f) Fmo4.

this trend is believed to mainly lie in the particle-base polyol interface. The CPP particles, being rigid, are believed to act as stress concentrators thereby increasing the localized stress and eventually leading to increased strain. It is also believed that the particles exhibit hydrogen bonding at the interface. Thus, as discussed, these hydrogen bonds are disrupted by high temperatures and high humidity levels leading to further increases in the creep as well as load strains. Comparing the two foams incorporating CPPs revealed that the two foams with the experimental CPPs displayed slightly lower creep strains than those with the conventional CPPs. This is also well illustrated in Fig 4.58 which shows the change in strain for all six foams at the various temperatures.

4.6.2.3 Effect of Water/TDI Content

The influence of the water/TDI content on the creep behavior can also be investigated using Figs. 4.59 through 4.62. An increase in the water/TDI content resulted in more blowing and therefore a lower density. Similar to the load relaxation measurements, this also led to higher strains or softer foams. Recall that Gibson and Ashby determined that an open cell foam's modulus generally scales in proportion to density squared and thus it is no surprise that the lower density foams exhibited higher strains. Comparing the two foams without CPP's, Fmo4 and Fmo2, revealed that at 30°C-35%RH, the 4 pph water content foam had an initial strain of 0.42 while the 2 pph water foam displayed an initial strain of 0.39. At a humidity of 98% the trend was the same. In each case, the strain at any creep time was higher for the lower density foam.

The trend was the same for the CPP containing molded foams as illustrated in Figs. 4.59 through 4.62. In each case the higher water content foam exhibited strain values at any given strain ca. 15% to 60% higher (depending on temperature) than the low water content counterpart. For example, at low humidities the initial strain for the 4 pph water content foams (2 lb/ft³) displayed strains ca. 30% to 60% higher than the 2 pph water

content foams (3 lb/ft³) while at high humidities, the displayed strains of the 4 pph water content foams were ca. 10% to 50% higher than the 2 pph water content foams. In addition, the creep strains were different. Interestingly, the 4 pph water content foams displayed lower creep strains over the 2 pph water content foams (ca. 6% to 30% lower) at 98%RH whereas at 35% relative humidity these same 4 pph water content foams displayed increased creep strains (15% to 60%) relative to the higher density 2 pph water content foams. It appears that the increased hard segment content in the higher water/TDI content foams acts as to inhibit creep strain at high relative humidities compared to the lower hard segment content foams.

4.6.3 *Compression Set*

The compression set property of polyurethane foams used as load bearing materials may be the single most important property. Compression set is not only a direct measure of the thickness loss and recoverability of the foam, but is also sensitive to the foam's morphology and network structure. As with the previous viscoelastic measurements, this property was evaluated in terms the specific formulation variables as well as the environmental conditions.

4.6.3.1 *Effect of Temperature and Relative Humidity on Compression Set*

The compression set behavior as a function of temperature and humidity of the molded foams are presented in Table 4.23. As the temperature or humidity was increased, the compression set also increased - especially with temperature. For example, foam Fmc4 displayed only a small compression set of ca. 2% after a 65% compression at 30°C-35%RH for three hours. When the relative humidity was increased to 98%, the compression set increased to ca. 9%. This increase in the amount of set is mostly a result

Table 4.23. Compression Set and Recovery Results

Condition	30°C-35% RH	30°C-98% RH	100°C-35% RH	100°C-98% RH
Fmo4	1.7±0.2	4.0±0.5	10.7±0.5	63.0±0.1
Fmo2	0.5±0.1	2.7±0.3	9.5±0.5	62.0±0.2
Fmc4	2.5±0.1	9.5±1.5	59.0±0.3	64.3±0.1
Fmc2	1.2±0.2	5.3±0.3	59.6±0.6	63.2±0.1
Fme4	2.0±0.5	5.4±0.5	56.4±0.1	63.9±0.1
Fme2	1.1±0.1	4.0±0.1	59.6±0.5	63.0±0.1

Days after CS	Percent Compression Set			
	Fmo4	Fmo2	Fmc2	Conv. 4 pph Slab.
0	63.0±0.1	62.0±0.2	63.2±0.1	15.2±1.6
22 after 1 hr @ 100°C	61.3±0.1 60.2±0.1			9.5±1.0 5.9±0.3
70 after 1 hr @ 100°C		62.1±0.2 61.8±0.2		
89 after 1 hr @ 100°C			62.9±0.1 61.2±0.2	

of increased hydrogen bond disruption by the increased humidity. Thermal "plasticization" of the hydrogen bonding was enhanced when the temperature was increased to 100°C (at 35% RH) resulting in a dramatic increase in the compression set to 59%. Furthermore, at both high temperature and high humidity, 100°C-98%RH, the compression set was even greater, 64%. The trend was the same for the other CPP containing foams. The foams free of the CPP particles however exhibited severe compression sets only at 100°C-98%. At 100°C-35%RH, the compression sets were only ca. 10% for both Fmo4 and Fmo2. In general the primary mechanism driving compression set is the same as that for load relaxation and creep and as the temperature and/or humidity is increased, the amount of hydrogen bond disruption is also increased.

4.6.3.2 Effect of Copolymer Polyols

While the influence of copolymer polyols on the compression set behavior is minor in most conditions, they did display a major influence at 100°C-35%RH where the materials with CPPs displayed higher compression sets. Comparing foam Fmo4 to Fmc4 reveals that the compression set of Fmc4 was greater than that of Fmo4 at all conditions but especially at 100°C-35%RH. For example, at 30°C-35%RH, Fmo4 displayed a compression set of 1.7% while Fmc4 displayed a compression set of 2.5%. However, at 100°C-35%RH, Fmo4 displayed a compression set of ca. 11% while Fmc4 displayed a compression set of ca. 59% - a significantly higher value. Even at 30°C-98%RH, the compression set exhibited by Fmc4 was considerably higher than that of Fmo4 - 10% compared to 4% respectively. The particulates acting as stress concentrators promote greater relaxation and chain slippage as with load relaxation. Since it is principally the soft segment that strains further for a given overall strain, the amount of relaxation that occurs is more severe which can in turn result in the disruption of secondary bonds and lead to further chain slippage. Hydrogen bond disruption is believed to occur also with increases

in temperature or humidity with bonds specifically existing at the interface between the CPP particles and the surrounding soft segment which otherwise would not exist in the foams lacking the particulates. In addition, a small degree of chain slippage and flow may occur within the CPPs due to the proximity of this temperature to the T_g of these dispersions. A similar trend was displayed by the 2 pph water content foams, comparing foams both with and without CPPs. With respect to the experimental copolymer polyol foams, the compression set displayed by these foams was essentially the same as that displayed by the conventional CPP containing foams. Thus, while the experimental CPP containing foams displaced slightly lower compression sets, the differences in compression set were insignificant. As demonstrated earlier with load relaxation and creep and now with compression set, the time-dependent properties of the foams are diminished with the incorporation of the CPP particles.

4.6.3.3 Effect of Water/TDI content

The amount of water/TDI in the formulation and thus hard segment content and density, appeared to have little influence on compression set. Within each of the three sets of foams, the one with the lower water/TDI content displayed slighter lower compression sets. For example, comparing Fmc2 to Fmc4 reveals that at each environmental condition, Fmc2 exhibited a lower compression set. At 30°C-35%RH, the compression sets were ca. 1% and ca. 2% for foams Fmc2 and Fmc4, respectively. At 100°C-35%RH, these values were 5% and 9% for Fmc2 and Fmc4, respectively. The greater compression set exhibited by Fmc4 is a result of an increase in the amount of hydrogen bonds emerging from a greater water/TDI content and thus more hard segments. A similar trend was observed amongst the other foams varying in the water/TDI content.

4.6.3.4 Compression Set Recoverability

To further evaluate to foam network, physical and covalent, the foams retaining the greatest amount of compression set were subjected to thermal treatment at 100°C for one hour. The temperature of 100°C was chosen in view of earlier work and work by others which showed that severe hydrogen disruption occurs at this temperature.^{79,97} This was carried out to disrupt the newly formed hydrogen bonding (following the compression set treatment) which aided in maintaining the foam in a compressed state and thus allow for the covalent cross-links to induce recovery of the set. This treatment was also applied to a 4 pph water content conventional slabstock foam for later comparison. As can be seen in Table. 4.23, the compression set of this slabstock foam (ca. 15% after compression at 100°C-98%RH for three hours) decreased at ambient conditions and further decreased after the 100°C treatment (to a final value of ca. 6%). *The molded foams, however, did not exhibit any recovery.* Also shown in Table 4.23 is the compression set recovery of specific molded foams such as Fmc2 as a function of time (up to ca. three months) and after treatment at 100°C for one hour. *Again, all the molded foams displayed essentially no recovery.* These dramatic differences are clearly a result of differences in the solid morphology and/or covalent network content of the foams. Specifically the morphology as was shown earlier with WAXS and FTIR supplying evidence that the HS domains were much more ordered for the conventional slabstock foams than the molded foams. The more disordered HS domains allow for greater disruption and chain slippage thereby making reversal of the compression set difficult. The compression set results strongly compliment the other viscoelastic measurements as well as their response to high temperatures and humidities.

4.7 Characterization of Foams Made With Diethanolamine

As mentioned early in the molded foam section, one important formulation ingredient utilized in the production of molded foams is diethanolamine (DEOA). Recall, this is primarily used to increase the level of covalent cross-linking in a relatively short amount of time so that the foam can achieve sufficient strength early and decrease demold times without foam collapse. In an attempt to understand the influence of DEOA on the morphology and properties, two sets of foams were prepared in a box-foaming process which is the method used in slabstock formulations. One series incorporated traditional molded foam polyols (5000 molecular weight EO capped polyols providing ca. 20% primary hydroxyl groups) and another series utilized typical polyols (3000 molecular weight all PO providing all secondary hydroxyl groups) found in conventional slabstock. The latter series of foams was formulated to delineate the effects of the EO capping (and thus the primary hydroxyl content) which has been reported to promote reagent compatibility. While the higher molecular weight would favor greater phase separation, the EO capping promotes some phase mixing. In addition to compatibilizing hard and soft segments, EO capping is also known to be more hydrophilic than PO. It was of interest, based on the correlation between HS ordering and viscoelastic response, to evaluate the correlation (if any exists) between DEOA and HS ordering.

4.7.1 Influence of Diethanol Amine on Structure and Properties

In view of the growing trend to use cross-linking additives such as DEOA, foams were produced where the DEOA content was systematically varied. These foams were then analyzed in terms of structure. The formulations used for this series of model polyurethane foams are shown in Table 3.3A. As can be seen, the DEOA content was varied from 0 pph to 2 pph. The 0 pph DEOA and 2 pph DEOA content foams were evaluated which encompassed the processing latitude utilized in production. Note that while these seem to be only a small amount by weight, because of the low molecular weight of DEOA, 2 pph

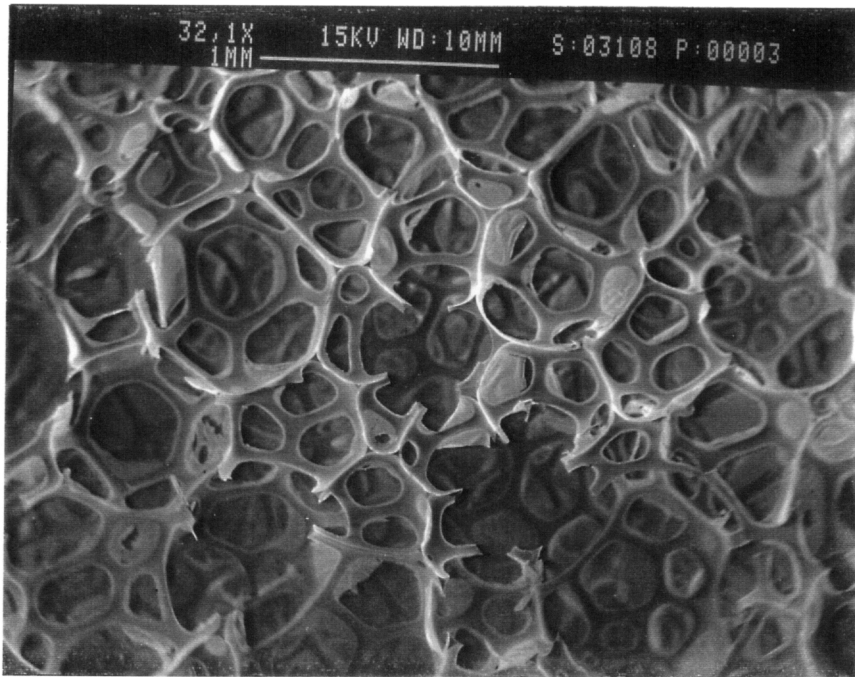
provides roughly the same amount of functional groups as about 100 pph of the triol! This can quickly increase the amount of covalent cross-linking as will be shown. Furthermore, it should also be pointed out that 2 pph DEOA is slightly beyond the amount used (ca. 1 - 1.5) by foam formulators but was intentionally chosen here to emphasize the influences. The fact that 2 pph is slightly beyond the optimum amount will be made evident in this section. The areas of interest that will now be addressed with respect to the influence DEOA are the cellular structure, fine microstructure including phase segregation as well as HS structural order and finally, the mechanical behavior.

4.7.1.1 Influence on Cellular Structure

The cellular structure of these foams was studied using scanning electron microscopy and indirectly using airflow measurements. The cellular structure of foam FeD-0 is shown in Fig. 4.63 which shows a structure typical of a polyurethane foam. Recall that the "e" denotes polyethylene oxide which endcapped the polypropylene oxide polyol. With the exception of a few closed windows, the foam appears to be an open-celled foam. Comparing this foam to foam FeD-2, shown in Fig. 4.64 reveals that the 2 pph DEOA content added resulted in an extremely high number of closed windows. Airflow measurements that were carried out also reflected this. The airflow measurement of foam FeD-0 was ca. 5.0 ft³/min. The airflow of foam FeD-2 was ca. 0.4 ft³/min., much lower suggesting that indeed many more cell windows are still in tact in this foam. The closed and larger cells are a consequence of cross-linking occurring prematurely before maximum bubble growth which prevents the rupture of the cells. The additional cross-linking provided by the DEOA over-stabilizes the cell walls thus preventing rupture when growing bubbles impede.

4.7.1.2 Influence on Fine Structure

(a)



(b)

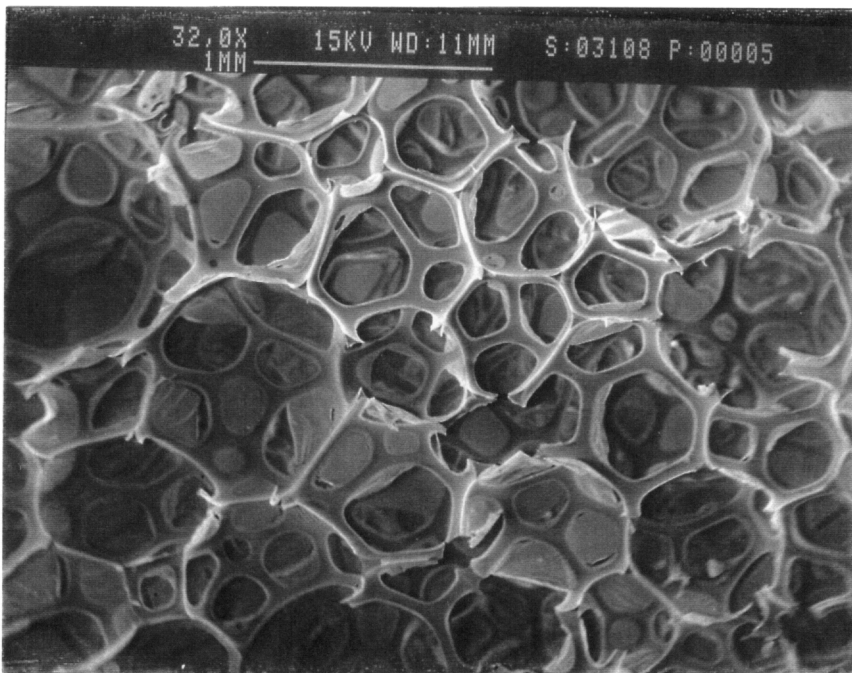
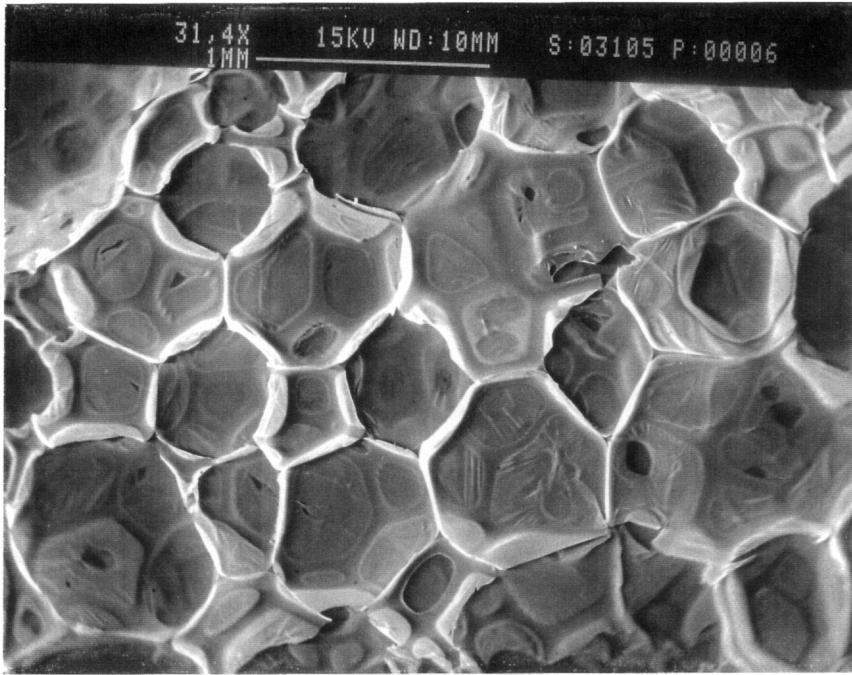


Figure 4.63. Scanning electron micrographs of foam FeD-0 shown both (a) parallel to the rise direction and (b) perpendicular to the rise direction.

(a)



(b)

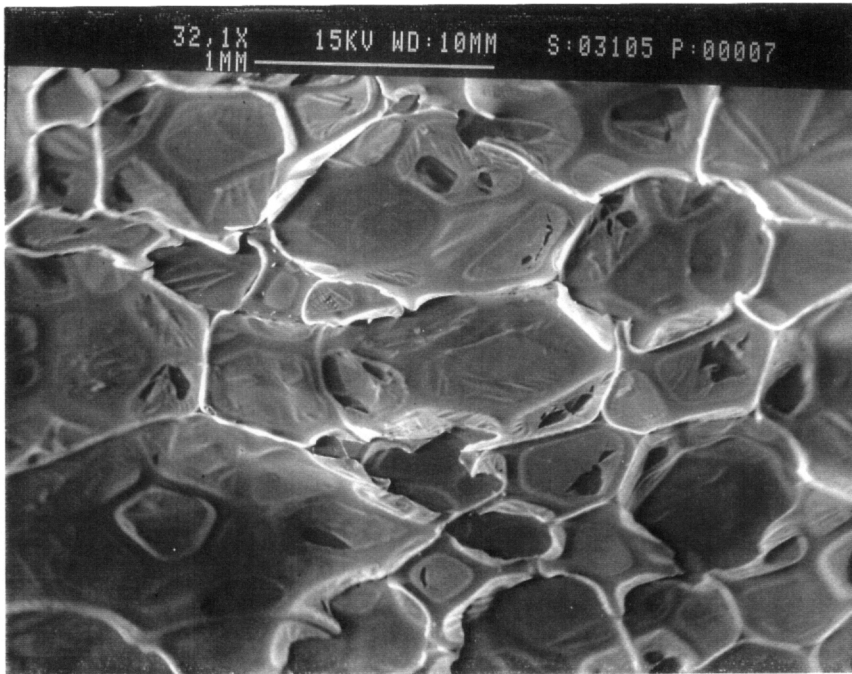


Figure 4.64. Scanning electron micrographs of foam FeD-2 shown both (a) parallel to the rise direction and (b) perpendicular to the rise direction.

In an attempt to determine whether DEOA had any influence on the fine structure of these foams, transmission electron micrographs were taken of the foams in this series and are presented in Fig. 4.65 where micrograph (a) shows the structure of FeD-0 at a magnification of 69.6Kx and micrograph (b) shows the structure of FeD-2 at the same magnification. As can be seen, both micrographs show a similar texture with essentially no differences between them.

4.7.1.3 Influence of DEOA on Solvent Extraction Behavior

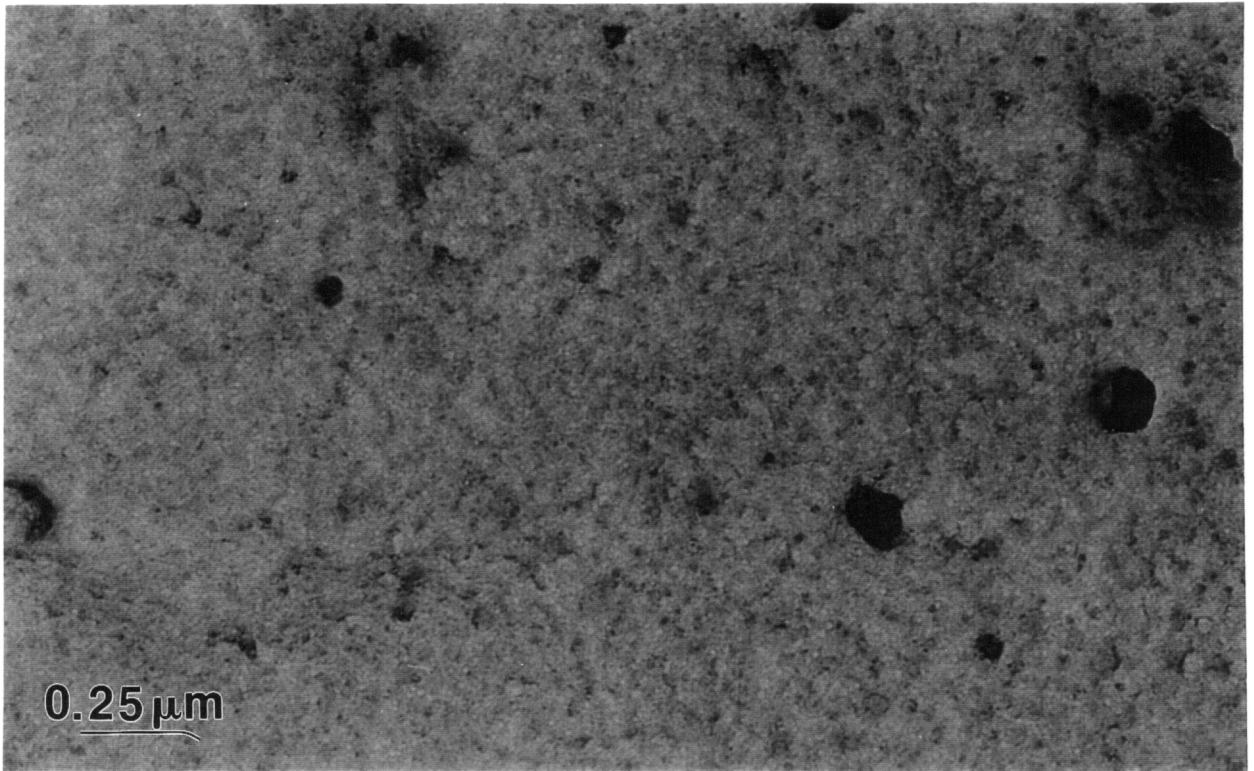
Solvent extractions using DMF were carried out to evaluate the amount of covalent cross-linking as a function of DEOA content. Table 4.24 presents the results of this treatment which clearly show that the amount of covalent cross-linking is increasing with increasing DEOA content. The amount of extractables decreased from 18.5% for FeD-0 to 6.5% for FeD-2. This further verifies that the resultant cellular structure is principally a result of altering the covalent network.

4.7.1.4 Influence of DEOA on Microphase Separation

The microphase separation as a function of DEOA content was evaluated in view of the well documented influence of cross-linking affecting the phase behavior of segmented materials, in general, promoting phase mixing.³⁶ Both thermal analysis and x-ray scattering were used to ascertain the amount of phase-separation and structural order of the HS domains.

4.7.1.4a Thermal Analysis

(a)



(b)

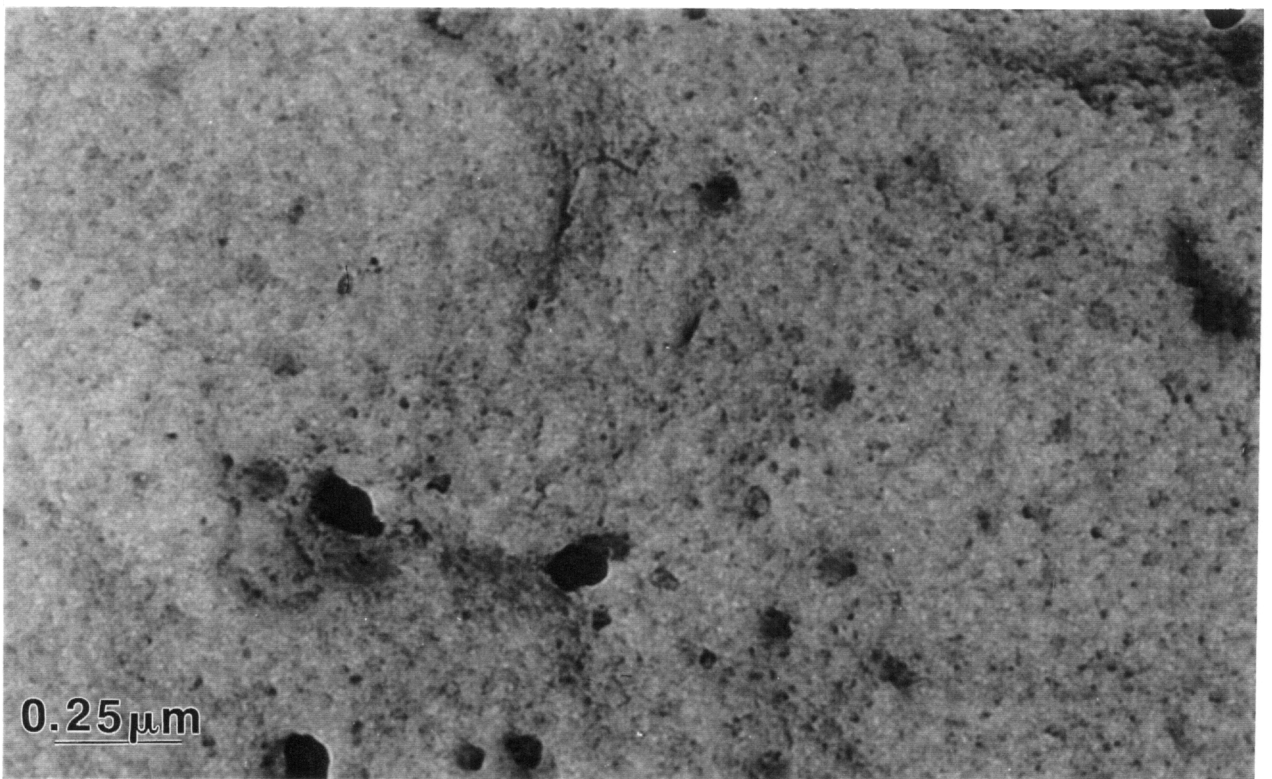


Figure 4.65. Transmission electron micrographs of foam (a) FeD-0 and (b) FeD-2 at a magnification of 69.6kx.

Table. 4.24. Solvent Extraction Results for EO Capped Foams Varying in DEOA Content

Foam	Sol Fraction (%)
FeD-0	18.5
FeD-2	6.5

Differential Scanning Calorimetry (DSC) was utilized to follow the soft segment T_g as a function of DEOA content. The first heating scans of each foam are shown in Fig 4.66 and second heating scans are shown in Fig. 4.67. As with the molded foams discussed earlier, the first heating scans displayed a broad endotherm which was previously suggested to be associated with the evaporation of absorbed water. The T_g of the soft segment for each foam was ca. -57°C and was unaltered by DEOA content. The dynamic mechanical behavior (DMA) revealed the same information. The soft segment T_g determined from DMA was also ca. -57°C and insensitive to DEOA content as is shown in Fig. 4.68. Overall, DMA analysis suggested that the influence of DEOA content on the soft segment T_g and storage modulus was minimal.

4.7.1.4b Small Angle X-ray Scattering

Small angle x-ray scattering (SAXS) was undertaken to more directly evaluate the microphase separation and the influence of the DEOA content on this behavior. The SAXS data for the two foams are presented in Fig. 4.69 which is a plot of the normalized smeared intensity as a function of an angular variable s defined as $s = 2\sin\theta/\lambda$. The average interdomain spacing was not determined due to the fact that a sharp peak is not displayed but rather only a weak shoulder. As can be seen, the overall measured intensity of the FeD-2 was lower than that of FeD-0. In this case, the HS content is constant and therefore the difference in intensity over all angles suggests that phase-mixing was promoted by the increased cross-linking brought about by the higher DEOA content. More accurately, the increased cross-linking prevented phase separation from occurring to the extent it occurs in foam FeD-0. This was concluded based on the simplified interpretation of the invariant which for an ideal two phase system with sharp boundaries is given as

$$\overline{\Delta\rho}^2 \approx \varphi_1\varphi_2[\rho_1 - \rho_2]^2 \quad 4.1$$

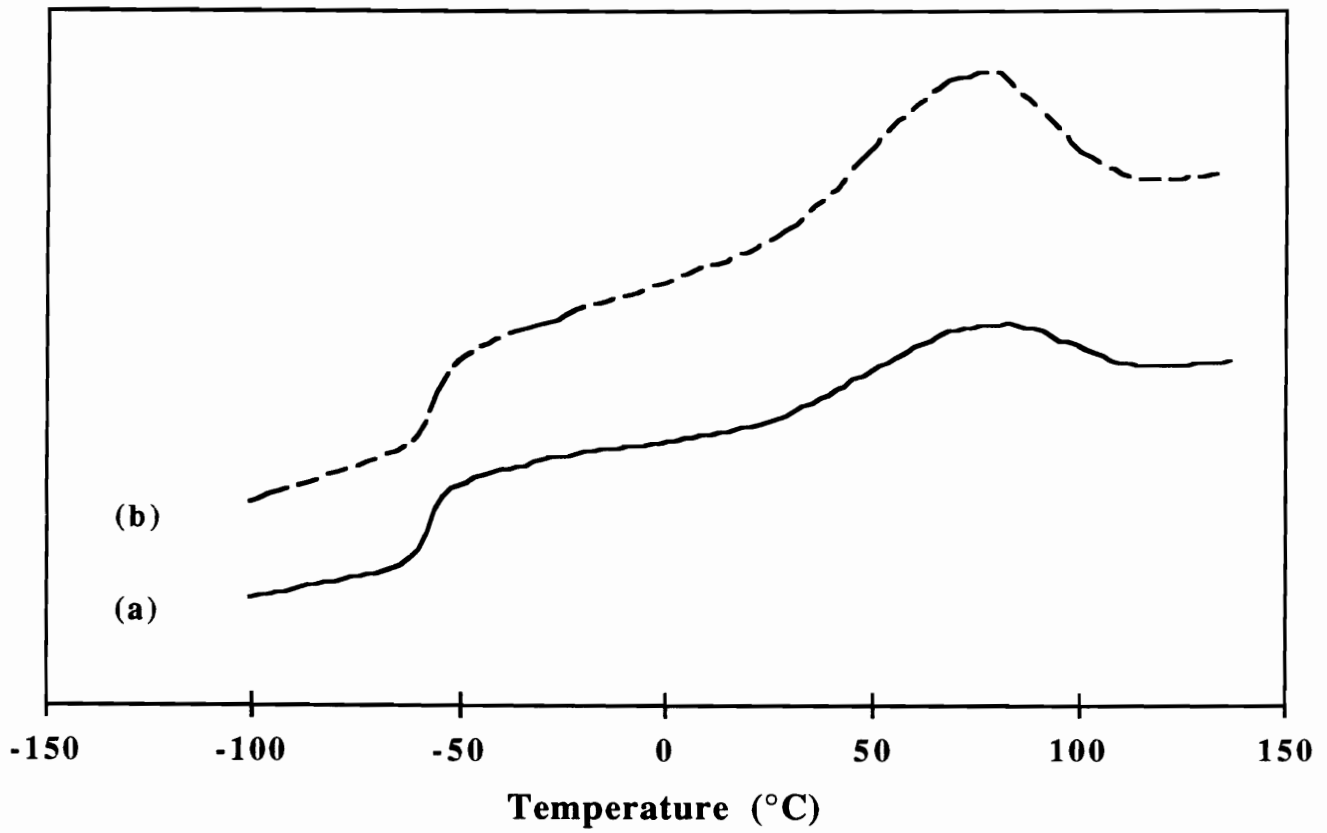


Figure 4.66. DSC thermograms of the first heating cycles of (a) FeD-0 and (b) FeD-2.

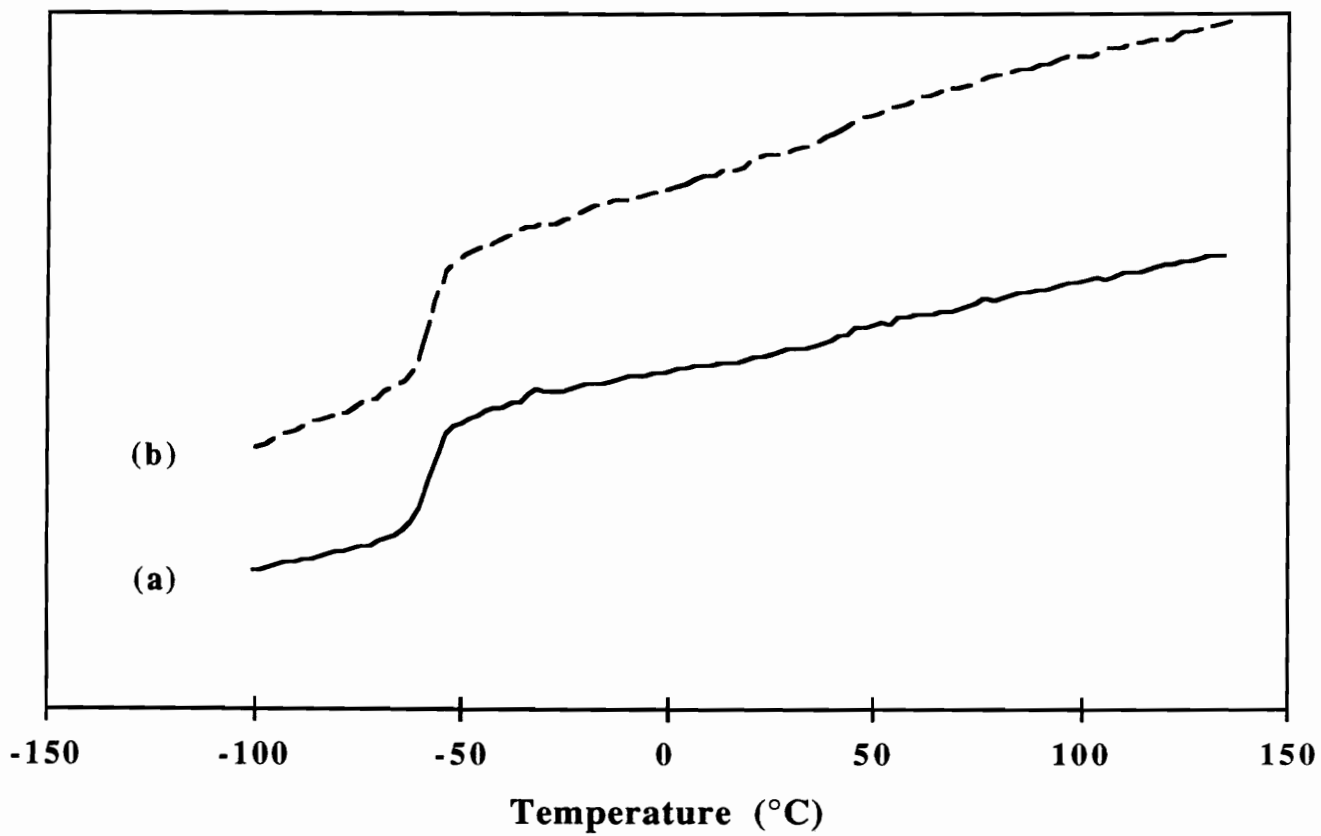


Figure 4.67. DSC thermograms of the second heating cycles of (a) FeD-0 and (b) FeD-2.

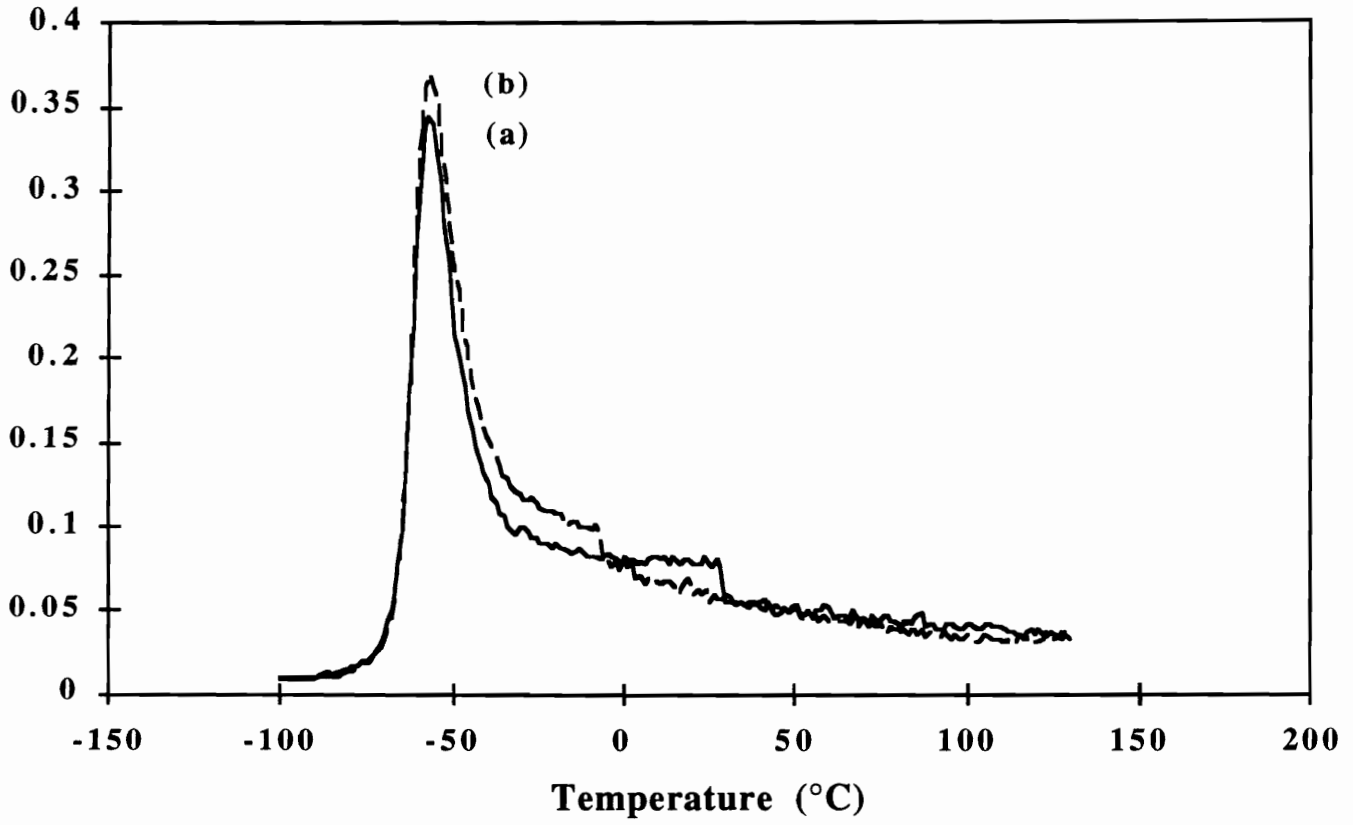


Figure 4.68. Influence of the DEOA content on the Tan Delta peak of the molded foams: (a) FeD-0 and (b) FeD-2.

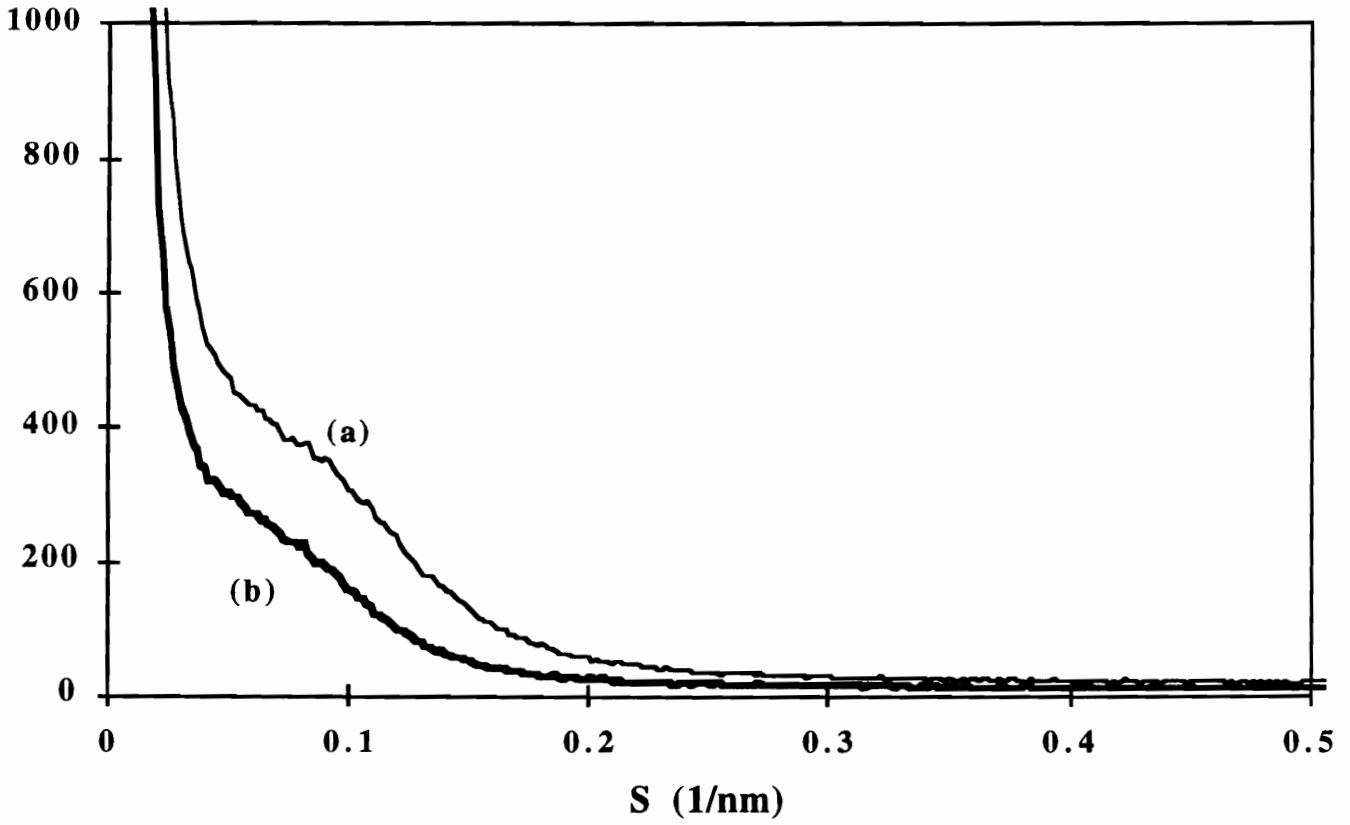


Figure 4.69. SAXS profiles of (a) FeD-0, (b) FeD-2 illustrating the influence of the DEOA content on the microphase separation.

where ϕ_1 and ϕ_2 are the volume fractions of each phase and $[\rho_1 - \rho_2]$ is the electron density difference between the two phases. Thus, the invariant achieves a maximum for a 50/50 mixture (assuming the electron density difference does not change) of each phase and decreases as the volume fraction deviates from 50/50. Experimentally, the invariant is determined by an integration of the intensity times the scattering vector squared

$$\overline{\Delta\rho}^2 \approx \frac{2}{V} \int_0^\infty I(s) s^2 ds$$

where again s is the scattering vector and $I(s)$ is the scattered intensity. Therefore, by taking a ratio of the experimentally determined and theoretically calculated invariants, a qualitative estimate of phase separation could in principle be obtained. Before determination of the invariant, various corrections are necessary including zero angle extrapolation, and background removal must be also carried out. Although the analysis was not undertaken, the different intensities of each foam shown in Fig. 4.69 suggest that the invariant is higher for foam FeD-0 and that even though the HS content is the same for both foams (equal water/TDI contents), more hard segments are solubilized within the soft phase rather than in the HS domains. Although not evident in the thermal analysis, the SAXS results suggest that the microphase separation is influenced by the DEOA content and the extent of which decreases with increasing DEOA content. The reasons why no influence on the soft segment T_g were observed are not known but there are other factors involved in these systems which influence the phase behavior such as polyol molecular weight, polyol functionality and the polyethylene oxide endcapping that was used.

4.7.1.4c Wide Angle X-ray Scattering

In addition to SAXS and more importantly, wide angle x-ray scattering (WAXS) was carried out to ascertain the HS short range ordering. Figure 4.70 illustrates the

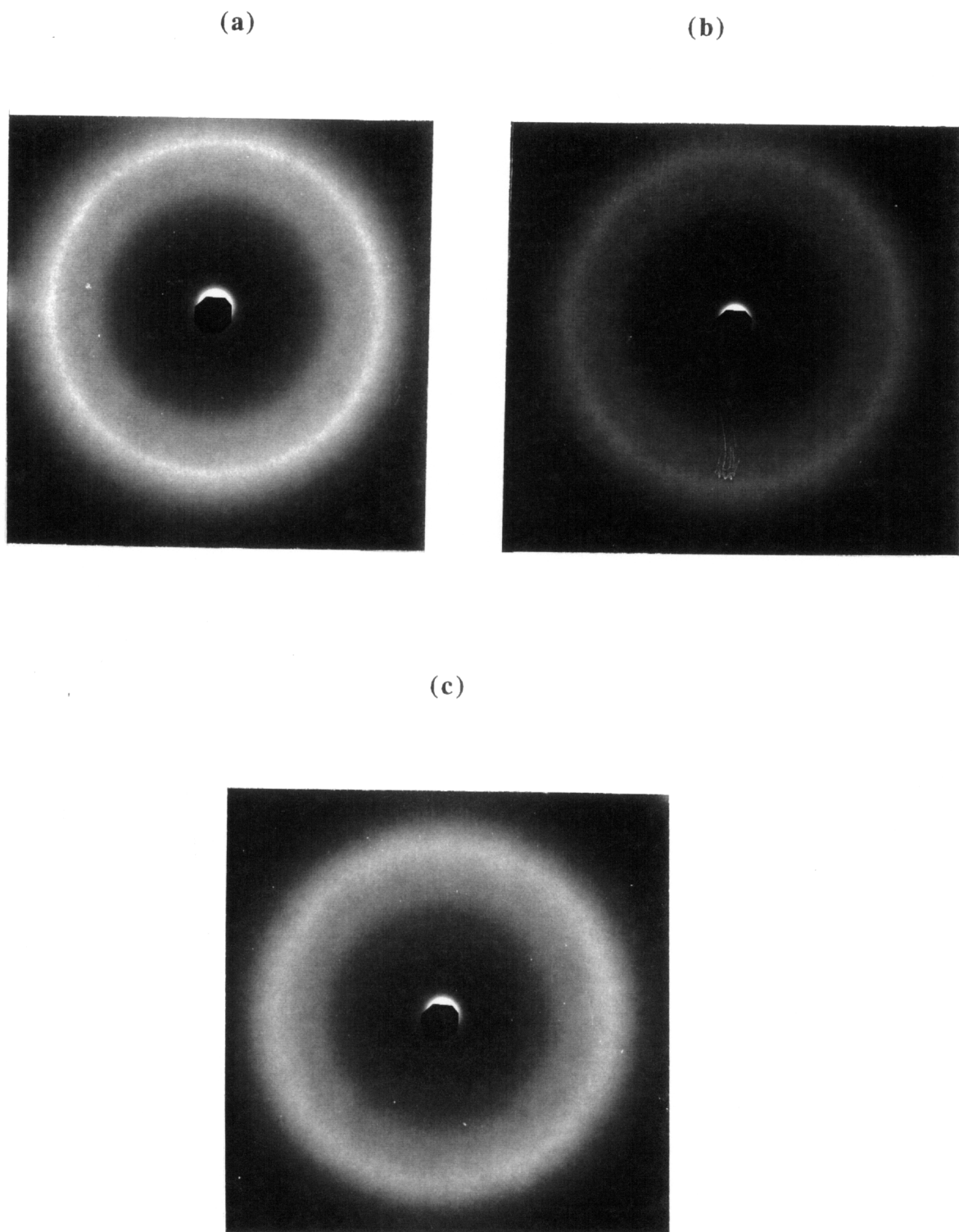


Figure 4.70. WAXS patterns illustrating the influence of DEOA content on the short range ordering of the HS domains: (a) FeD-0, (b) FeD-1 and (c) FeD-2.

scattering patterns of foams FeD-0, FeD-1 and FeD-2. As can be seen, along with a broad amorphous halo each pattern shows the presence of two relatively sharp rings which is indicative of short range or paracrystalline ordering. The origin and meaning of these rings has already been discussed but in short relates to the local packing order of the hard segments. Also evident in Fig. 4.70 is that the sharpness of these rings distinctly decreases as the DEOA content is increased suggesting that this ordering is also decreased. The differences are clearly evident where the DEOA included in FeD-2 has drastically disrupted the ordering of the HS domains. The sharp rings of Foam FeD-0 shown in Fig. 4.70a become much more diffuse for FeD-2 as shown in Fig. 4.70c. The results are systematic where, with each increase in DEOA content, a subsequent decrease in HS ordering results as evidenced by the decreasing sharpness of the two rings. This evidence suggests that while DEOA increases the level of cross-linking, it also disrupts the hard segment ordering as suggested earlier. As discussed earlier in the molded foam section, this can allow for the easier "plasticization" by heat and humidity thereby making these domains more labile at these elevated conditions. The rapid cross-linking that results with the addition of DEOA makes it more difficult for the urea segments to associate (through diffusion) and to pack and form multiple bidentate hydrogen bonds with other hard segments thereby limiting perfection of the hard segment domain development.

4.7.1.4d Fourier Transform Infrared

To further verify the WAXS results, fourier transform infrared (FTIR) was carried out which also showed that the influence of DEOA on the structural order of the HS domains was one of a disrupting nature. The FTIR spectral profiles of foams FeD-0 and FeD-2 are shown in Fig. 4.71 which displays absorbances in the carbonyl region. Evident here is that the well ordered bidentate absorbance centered at 1640 cm^{-1} decreased significantly by the inclusion of 2 pph DEOA. Again, this strongly supports the evidence

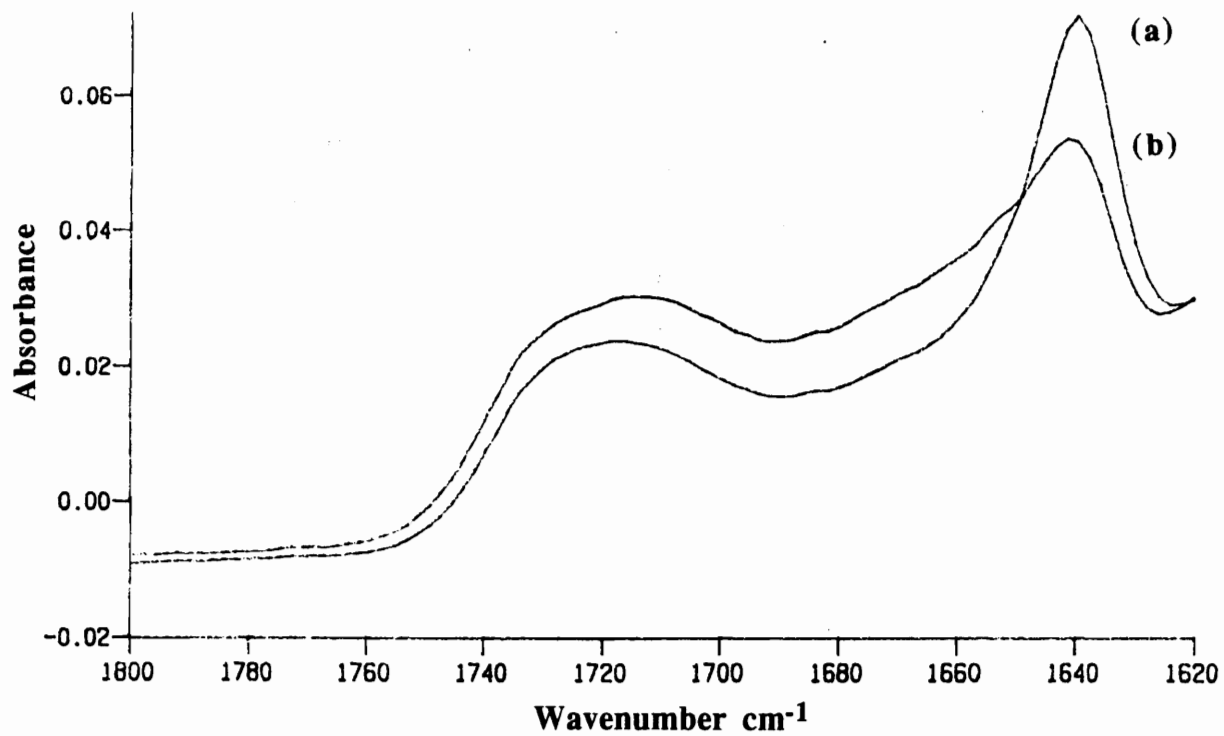


Figure 4.71. Influence of DEOA content on bidentate absorbance in the FTIR spectra of foams (a) FeD-0 and (b) FeD-2.

acquired in the WAXS analysis that DEOA does prevent the perfection of the HS domains or physical "cross-links". Furthermore, the results are in good agreement with those presented by McClusky in which the urea band was followed with time for two foams, one with DEOA and one without. The foam containing DEOA did not show evidence of a bidentate peak while the foam lacking DEOA displayed a sharp bidentate peak developed ca. 105 sec. following pour.³⁰

4.7.1.5 Load Relaxation Behavior

Finally, the influence of DEOA on the physical properties, specifically the load relaxation behavior, was also of interest. The load relaxation behavior of FeD-0 as a function of temperature and humidity is presented in Fig.4.72a and that of FeD-2 in Fig. 4.72b. Similar to the behavior of the molded foams presented earlier, both temperature and humidity "plasticized" this behavior shifting the curves to lower loads with increases in either. The initial loads for FeD-0 are in the range of ca. 3000g to 2300g depending on the conditions. The percent decays for this foam are ca. 21%. The load relaxation behavior of FeD-2 drastically differs from that of FeD-0. FeD-2 displayed much higher initial loads, ca. 4700g, but also greater percent decays which are a direct consequence of the numerous closed cells possessed by this foam. The higher compression loads are due to pressure from the trapped gas contained within the bubbles. In addition, the cell membranes may also contribute somewhat to the foam stiffness. The gas encapsulated then diffuses out as a load is applied which leads to significant decay of this load. Rupturing of the cell membranes is also occurring especially during the high rate of loading, all of which results in greater decay in load. The percent decays in three hours were ca. 75% where the loads decreased to as low as 500g. Both foams were compared on one plot shown in Fig. 4.73. Regardless of the environmental condition, within 6 sec. the load exhibited by FeD-2 which was initially significantly higher than that of FeD-0, decayed to a value below that of

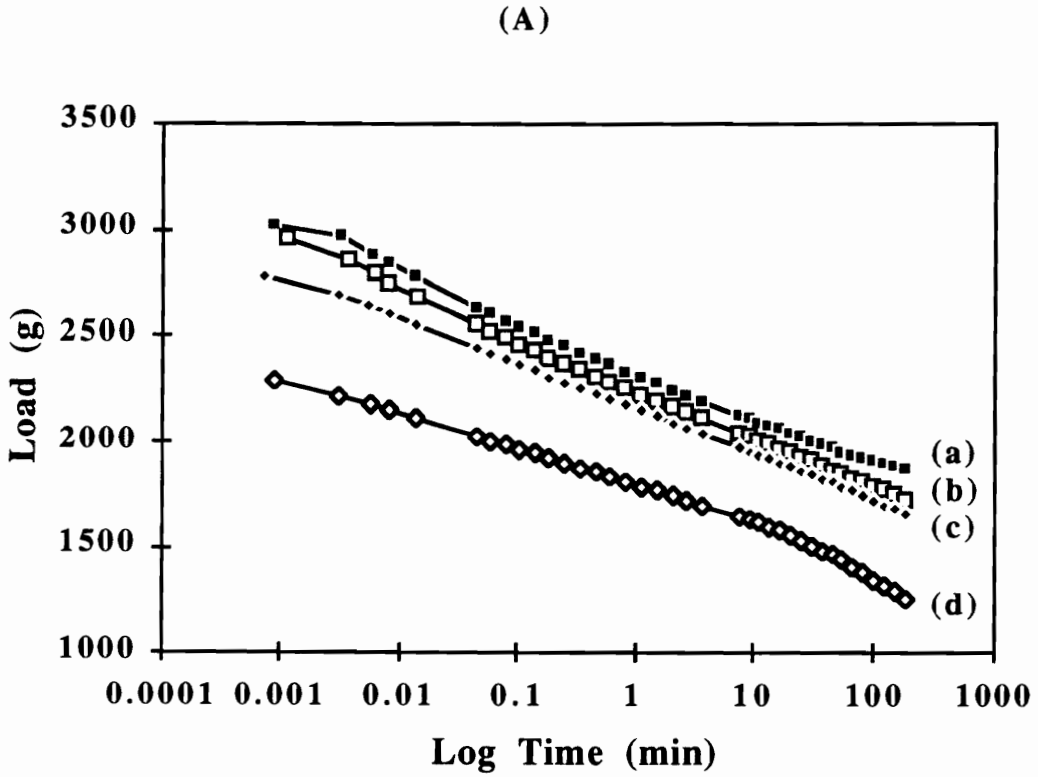


Figure 4.72. Influence of temperature and relative humidity on the load relaxation behavior of (A) FeD-0 and (B) FeD-2. In each figure the letters designate the following conditions: (a) 30°C-35%RH, (b) 30°C-98%RH, (c) 100°C-35%RH, and (d) 100°C-98%RH.

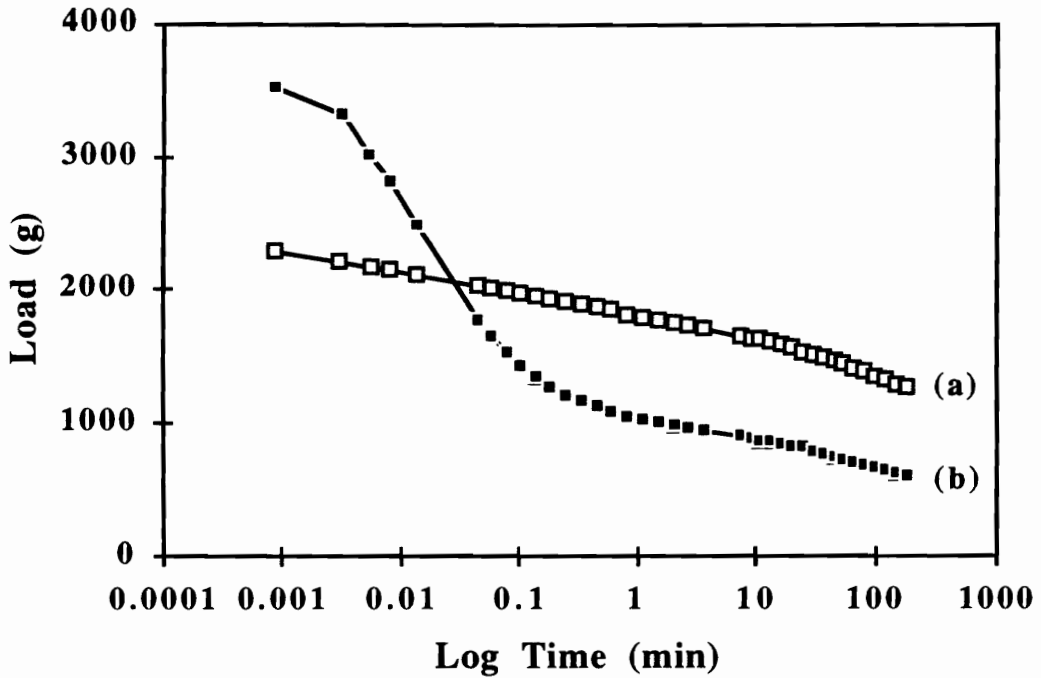
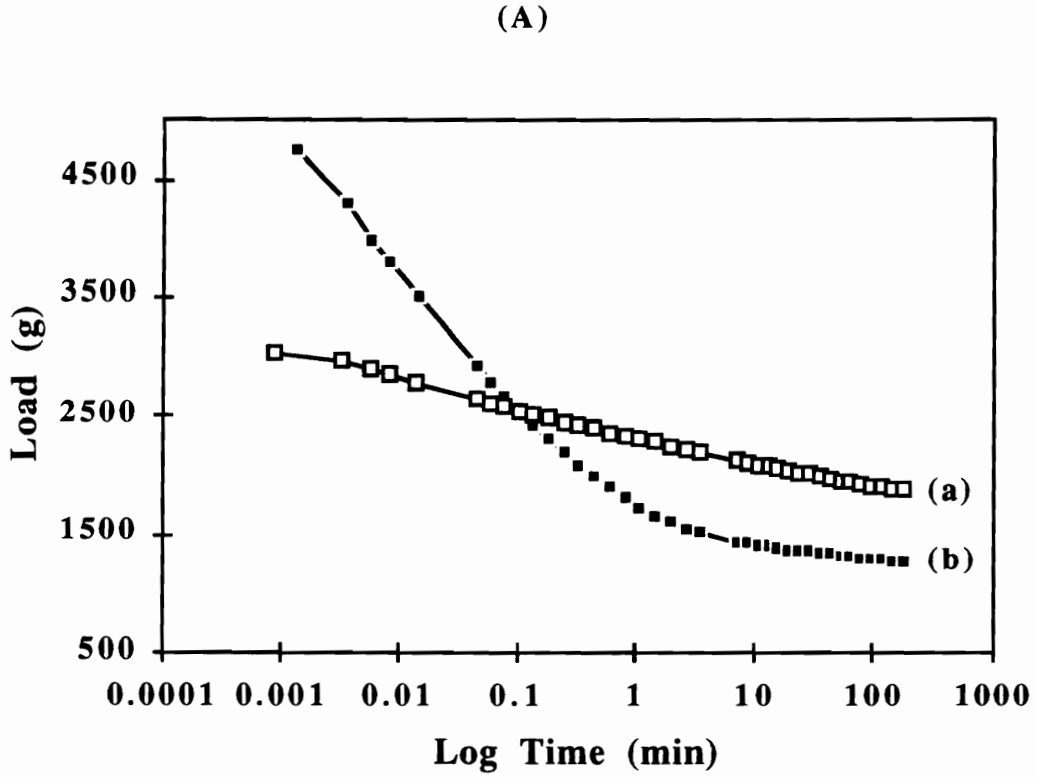


Figure 4.73. Influence of the DEOA content on the load relaxation behavior at (A) 30°C-35%RH, and (B) 100°C-98%RH. In each figure the letters designate: (a) FeD-0 and (b) FeD-2.

FeD-0. As mentioned above, the mechanisms are clearly different and thus the influence of DEOA could not be accurately deciphered.

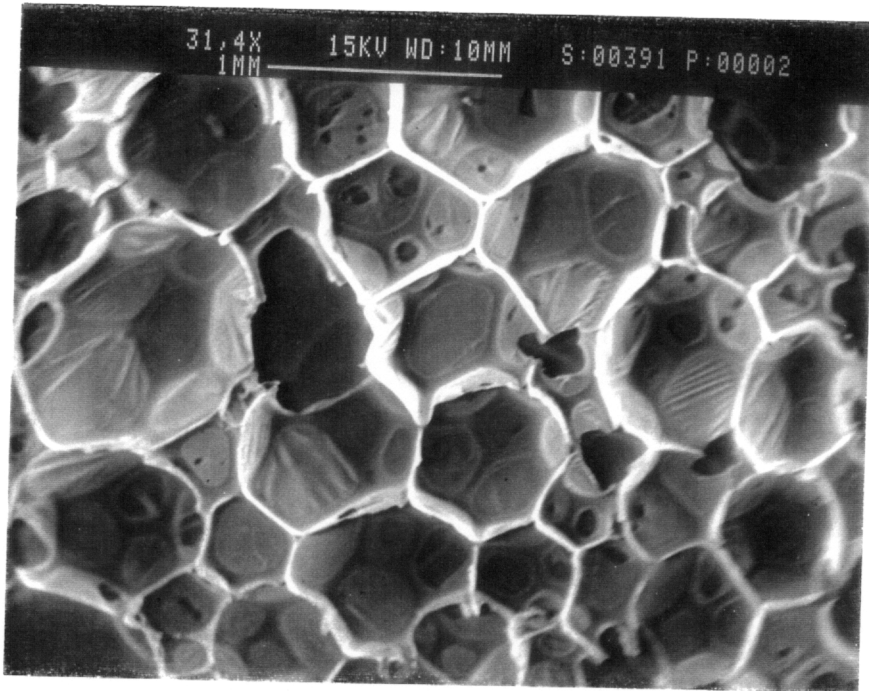
4.7.2 Influence of Diethanol Amine on Structure and Properties of Foams Made with a 3000 MW All PO Polyol

As mentioned at the beginning of this section, two series of foams were produced where the only significant difference between them was the polyol used. Again, the first series which was just discussed consisted of a 5000 molecular weight EO capped polyol. The other series which will now be discussed utilized a 3000 molecular weight PO triol which provided all secondary hydroxyls as presented in Table 3.3B. The second model series allows for the evaluation of DEOA irrespective of the effects of the EO capping. Furthermore, qualitative evaluation of the effects of the EO capping can be obtained by comparing general features of each series of foams. The appropriate measurements were then undertaken as in the previous section to evaluate these materials in terms of their structure, morphology, and properties. As with the previous series, the investigation began with SEM to evaluate the influence of DEOA content on the cellular structure.

4.7.2.1 Influence on Cellular Structure

The cellular structure of these foams was studied using SEM and airflow measurements. The cellular structure of foam FD-0 is shown in Fig. 4.74 both parallel and perpendicular to the rise direction depicting the geometric anisotropy. As can be seen, this foam has an unusually large number of closed windows. This is most likely a result of the relatively high amount of gelling catalyst used which results in an improper balance between blowing and gelling and ultimately a greater number of closed cells. Comparing these micrographs to those of foam FD-0.5, shown in Fig. 4.75 also reveals a relatively

(a)



(b)

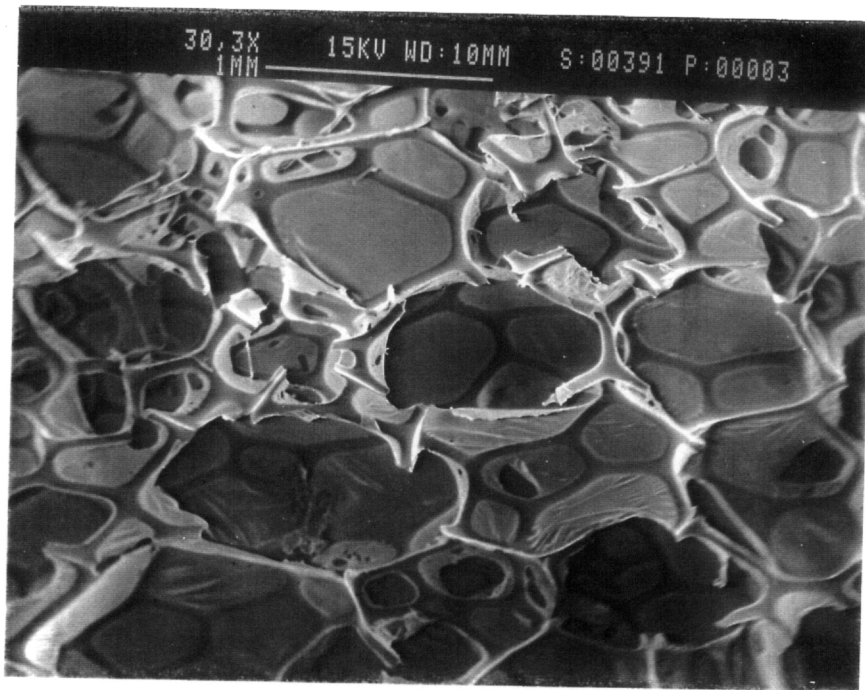
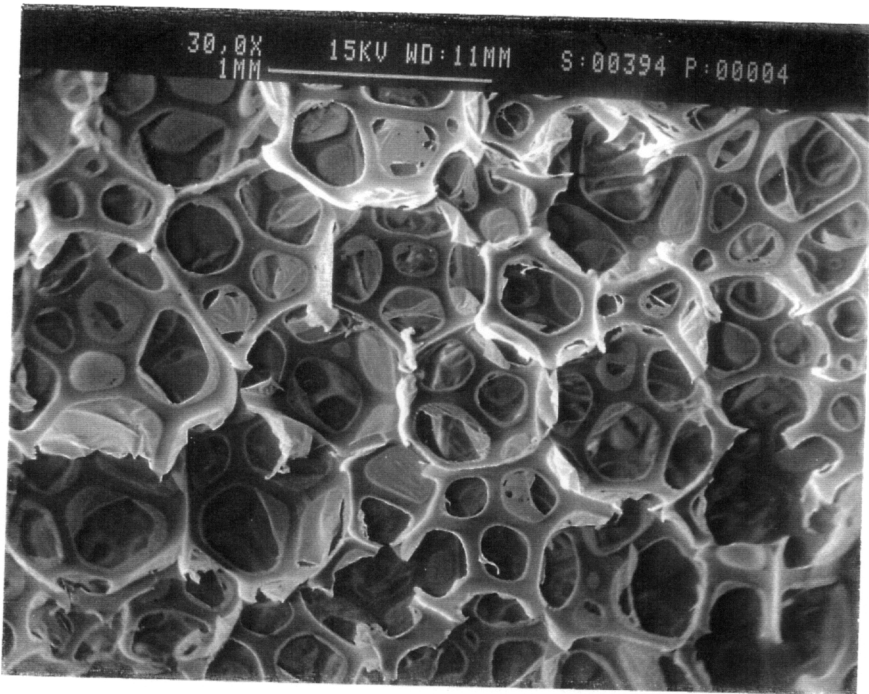


Figure 4.74. Scanning electron micrographs of foam FD-0 shown both (a) parallel to the rise direction and (b) perpendicular to the rise direction.

(a)



(b)

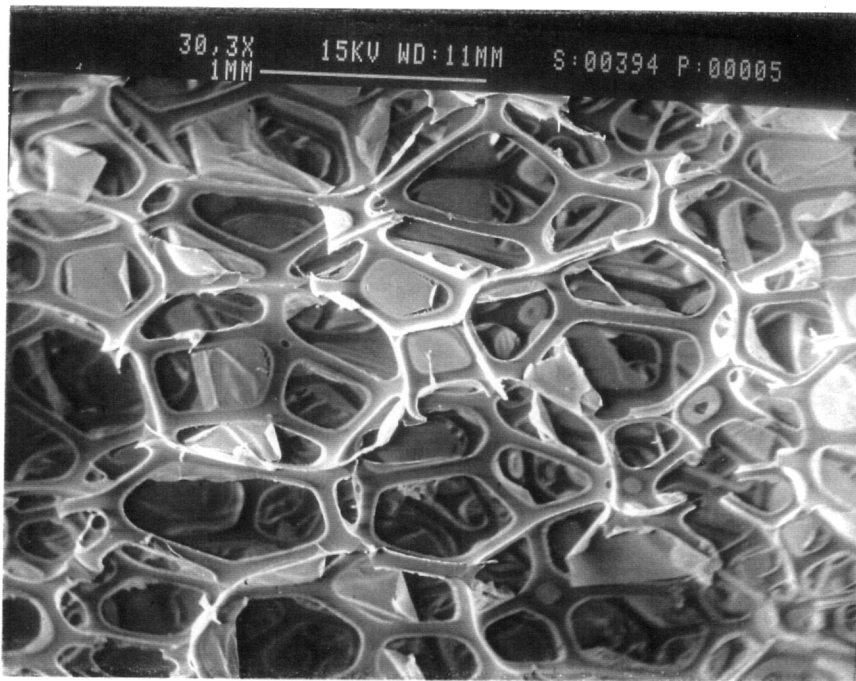


Figure 4.75. Scanning electron micrographs of foam FD-0.5 shown both (a) parallel to the rise direction and (b) perpendicular to the rise direction.

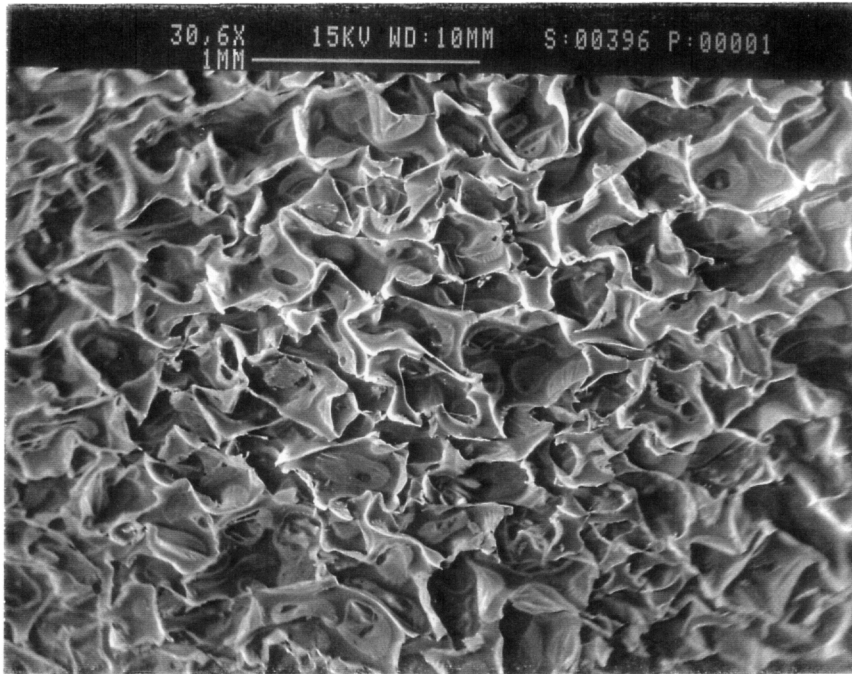
high amount of closed windows. Again, the geometric anisotropy is clearly evident where parallel to the rise direction, Fig. 4.75a, the cells appear circular and perpendicular to rise direction, Fig. 4.75b, they appear ellipsoidal. Based on the micrographs both foams appear similar in cell-openness and size. The airflow data, however, suggest otherwise. The measured airflow of FD-0 was ca. 5.0 ft³/min. and that of FD-0.5 was 0.2 ft³/min. suggesting that FD-0.5 has considerably many more closed windows and that the continuous flow of air through the foam is hindered. In the case where the DEOA content was increased to 1.0 pph, the result was severe foam shrinkage due to the cooling and thus contraction of the entrapped gas within the closed cells whose cell window membranes have significantly increased in strength by the additional DEOA. The resultant cellular structure is shown in Fig. 4.76 which clearly shows a severely altered structure. Although the foams still display a geometric anisotropy, the cells nowhere near display the polyhedron cellular structure typical of polyurethane foams.

4.7.2.2 Influence on Fine Structure

Transmission electron microscopy (TEM) was carried out to observe the presence of any influences on the fine structure of these foams as a function of DEOA content. In addition, based on reports of the presence of what are referred to as urea precipitate or aggregate structures in all PO high water content foams, it was desired to determine whether these structures would be observed in this series of foams, and furthermore whether DEOA had any influence on them. As stated in Chapter 2, these precipitates were observed by Armstead for foams of at least 4 pph water content. Moreland also observed a similar morphology and added that the geometry or structure of these aggregates is possibly more lamellar-like than spherical as based on infrared dichroism - orientation studies.⁷⁹

The TEM of foam FD-0 is presented in Fig. 4.77 and that of FD-0.5 is shown in Fig. 4.78. Both figures display the appearance of large electron dense regions unlike those

(a)



(b)

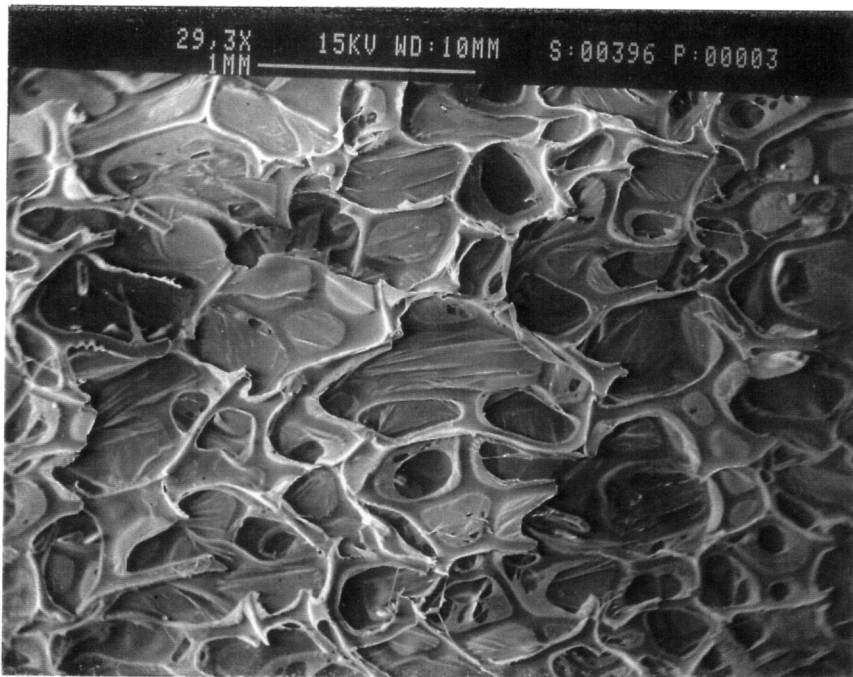


Figure 4.76. Scanning electron micrographs of foam FD-1 shown both (a) parallel to the rise direction and (b) perpendicular to the rise direction.

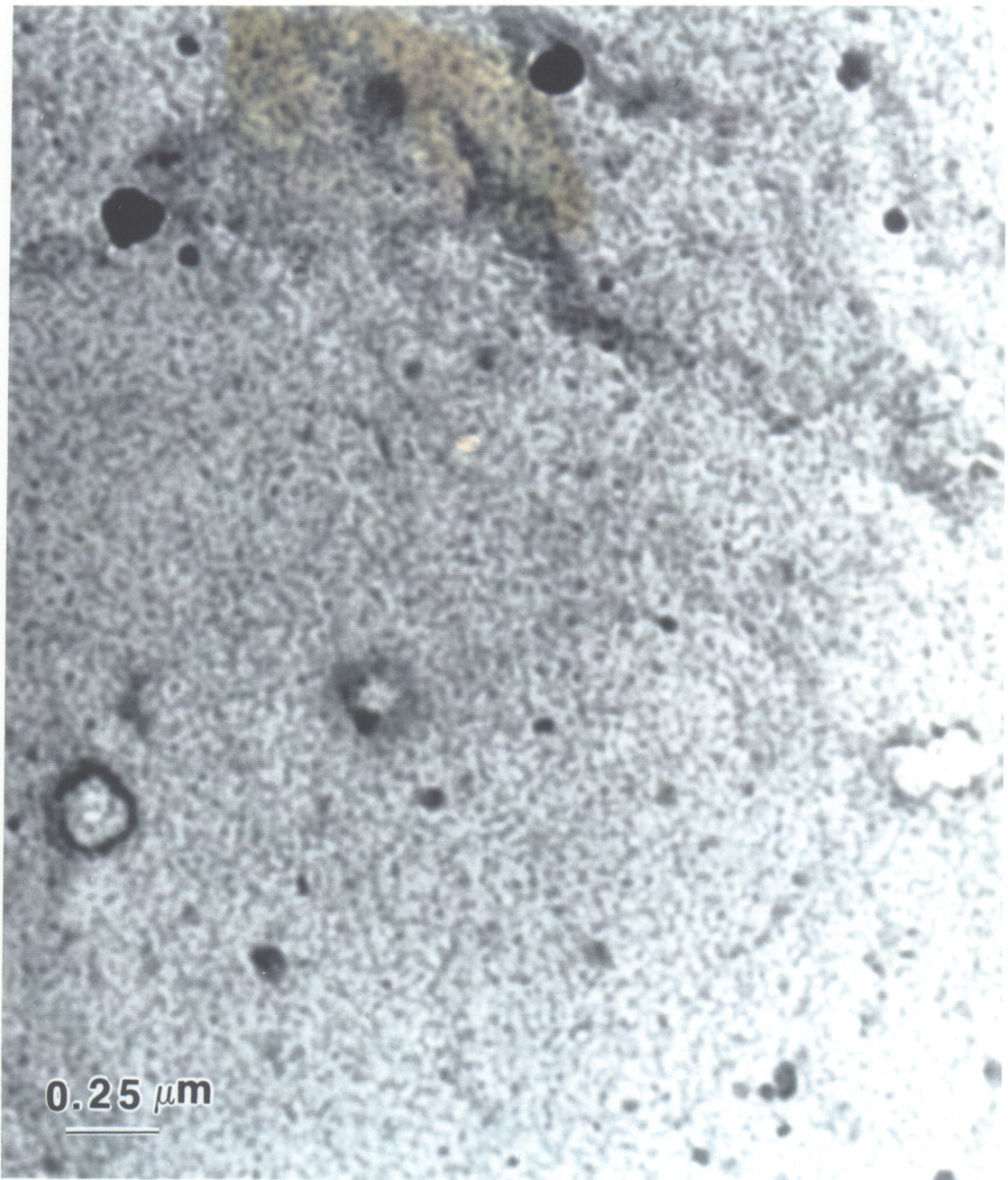


Figure 4.77. Transmission electron micrographs of foam FD-0 at a magnification of 54kx.

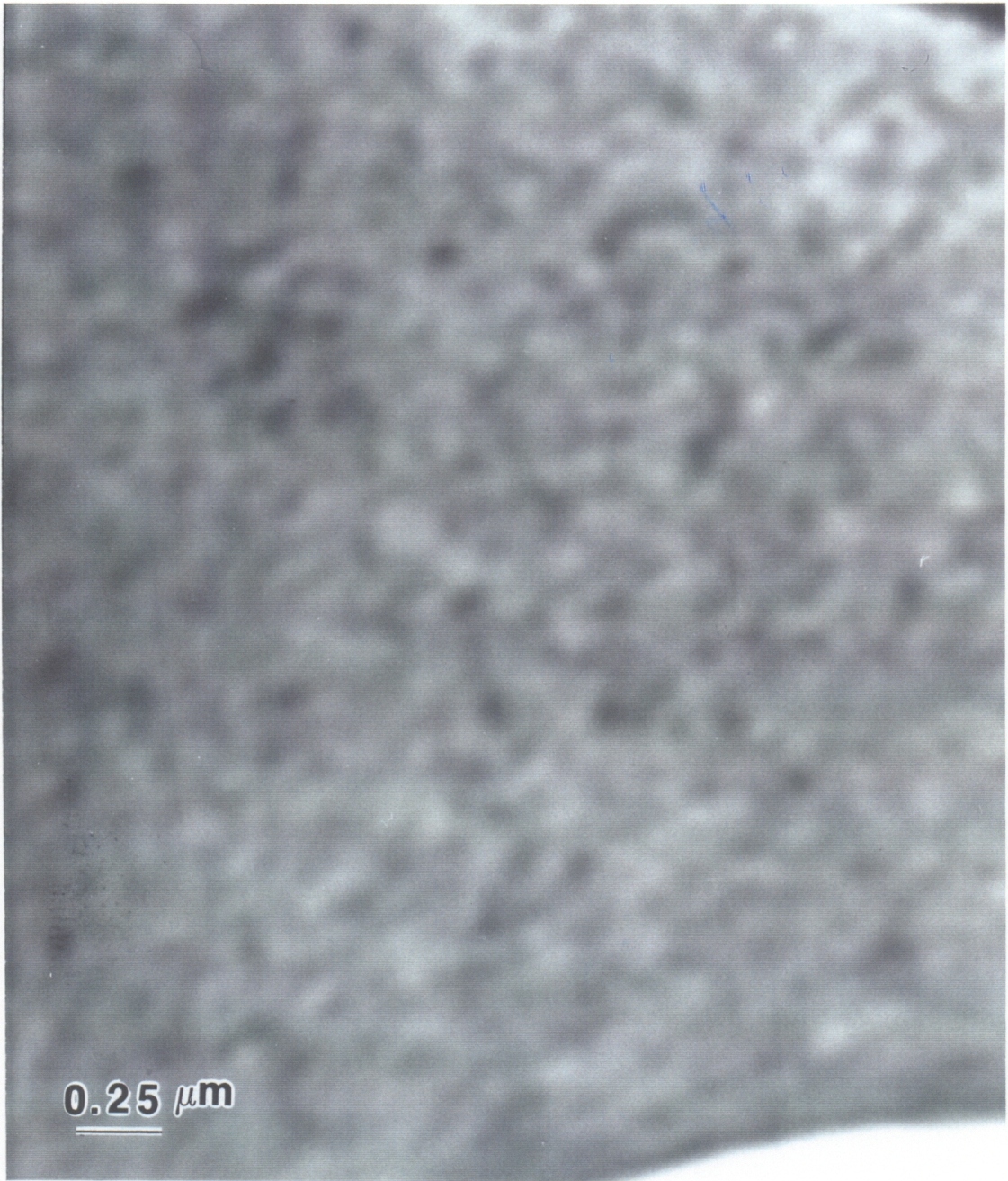


Figure 4.78. Transmission electron micrographs of foam FD-0.5 at a magnification of 54kx.

exhibited by either of the EO capped foams, FeD-0 or FeD-2, which are shown in Fig. 4.65. The dark regions in Figs. 4.77 and 4.78 range in size from 100 - 150 nm and are believed to urea-rich precipitates or urea aggregates in a continuous soft phase. These are believed to be the same structures which have been observed by others in high water content conventional slabstock foams.^{33,79} Upon comparing the micrograph of FD-0 to that of FD-0.5, it appears that the urea aggregates are more discrete with higher contrast in foam FD-0 where in FD-0.5 they appear somewhat gray and slightly larger. This may be a result of this area consisting of a mixed morphology which is still urea rich but now having more soft segment mixed in.

4.7.2.3 Influence of DEOA on Solvent Extraction Behavior

As with the EO capped foams varying in DEOA content, the direct influence of DEOA content on the covalent network of all PO foams was also of interest. Therefore, solvent extractions in DMF were carried out to evaluate the amount of covalent cross-linking as a function of DEOA content. Table 4.25 presents the results of this treatment which confirm that the amount of covalent cross-linking is distinctly increased with increasing DEOA content. The amount of extractables decreased from 7.8% for FD-0 to 5.7% for FD-0.5, to 3.2% For FD-1.5. Clearly, the amount of material secured within the network is increasing with increasing DEOA. Not surprising, these results as well as those presented in the previous section depict how a small amount of DEOA (by weight) results in dramatic differences in the covalent network. Recall that because of the low molecular weight of this additive, relative to the polyol, even a small amount on a weight basis cross-linking sites provides for many functional groups.

4.7.2.4 Influence of DEOA on Microphase Separation

Table 4.25. Solvent Extraction Results for All PO Foams Varying in DEOA Content

Foam	Sol Fraction (%)
FD-0	7.8
FD-0.5	5.7
FD-1	3.2

As it was shown that DEOA influenced the phase behavior in the previous section with the FeD-x series, its effect on the phase behavior of this series of foams followed a similar trend. The usual techniques discussed throughout this chapter were administered to ascertain the influence of DEOA on phase-separation and structural order of the HS domains.

4.7.2.4a Thermal Analysis

Dynamic Mechanical Analysis (DMA) was applied to follow the soft segment T_g as a function of DEOA content with the intention to qualitatively relate it to the level of phase separation. The tan delta curves of the three foams FD-0, FD-0.5 and FD-1 are shown in Fig. 4.79. Here, the T_g of the soft segment slightly increased with increasing DEOA content increasing from -48°C for FD-0 to -45°C for FD-1. Although subtle, the results indicate that the soft segment T_g is increasing due to more hard segments being "locked" within the soft segment phase thereby preventing their association within the hard segment domains. It is not clear why in this foam series, altering the DEOA content does have an impact on the soft segment T_g while in the previous series it did not. Speculation only leads to the different polyols where in addition to a lower molecular weight, this series possessed an all PO system. The storage modulus which is shown in Fig. 4.80 was also influenced by the DEOA content. While no difference was displayed between foams FD-0 and FD-0.5, foam FD-1 exhibited a modulus ca. a half order of magnitude greater than the other two. Although the increased covalent network undoubtedly had an impact, the higher modulus of foam FD-1 also reflects the dramatic difference in cellular structure (and inherently density) demonstrated by this foam earlier using SEM.

4.7.2.4b Wide Angle X-ray Scattering

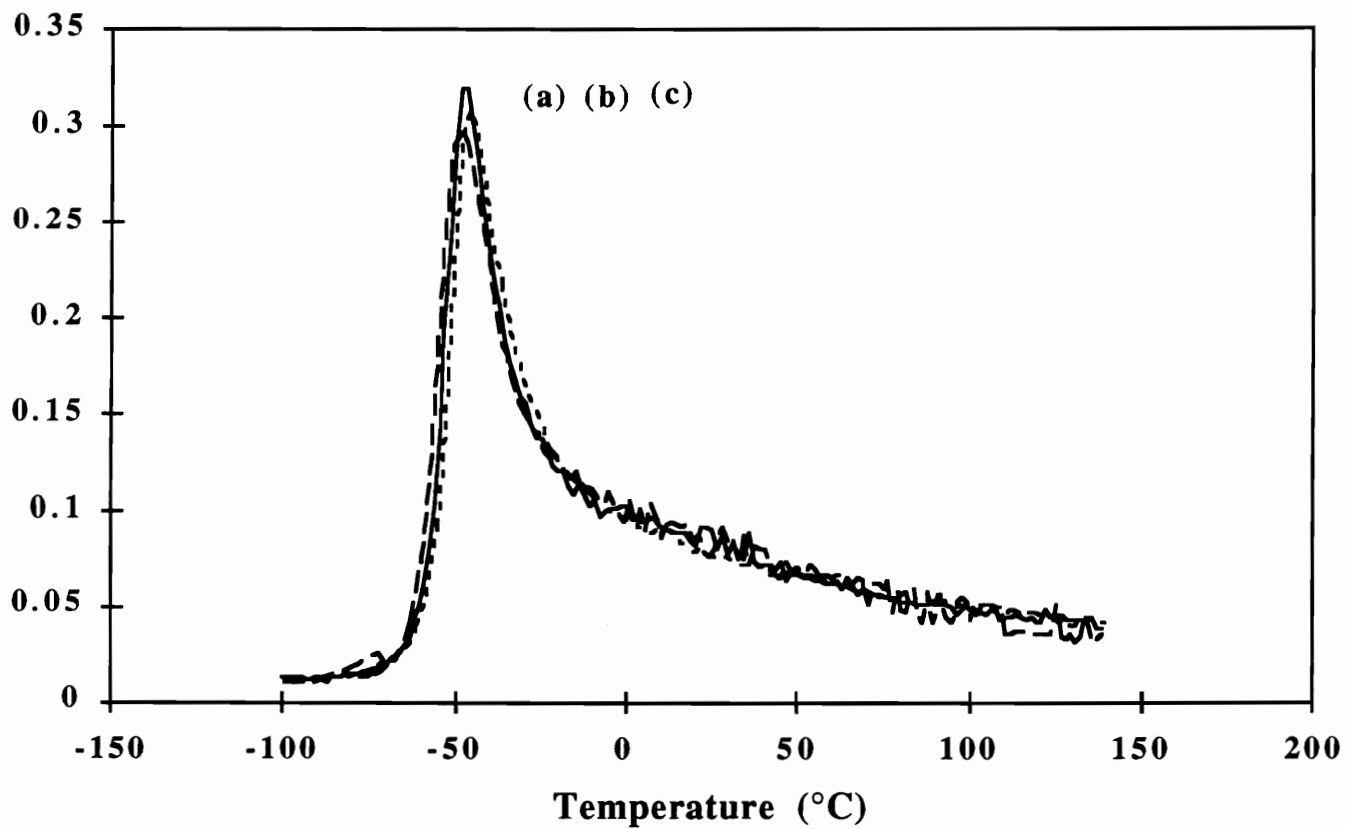


Figure 4.79. Influence of DEOA content on the Tan Delta peak of foams (a) FD-0, (b) FD-0.5 and (c) FD-1.

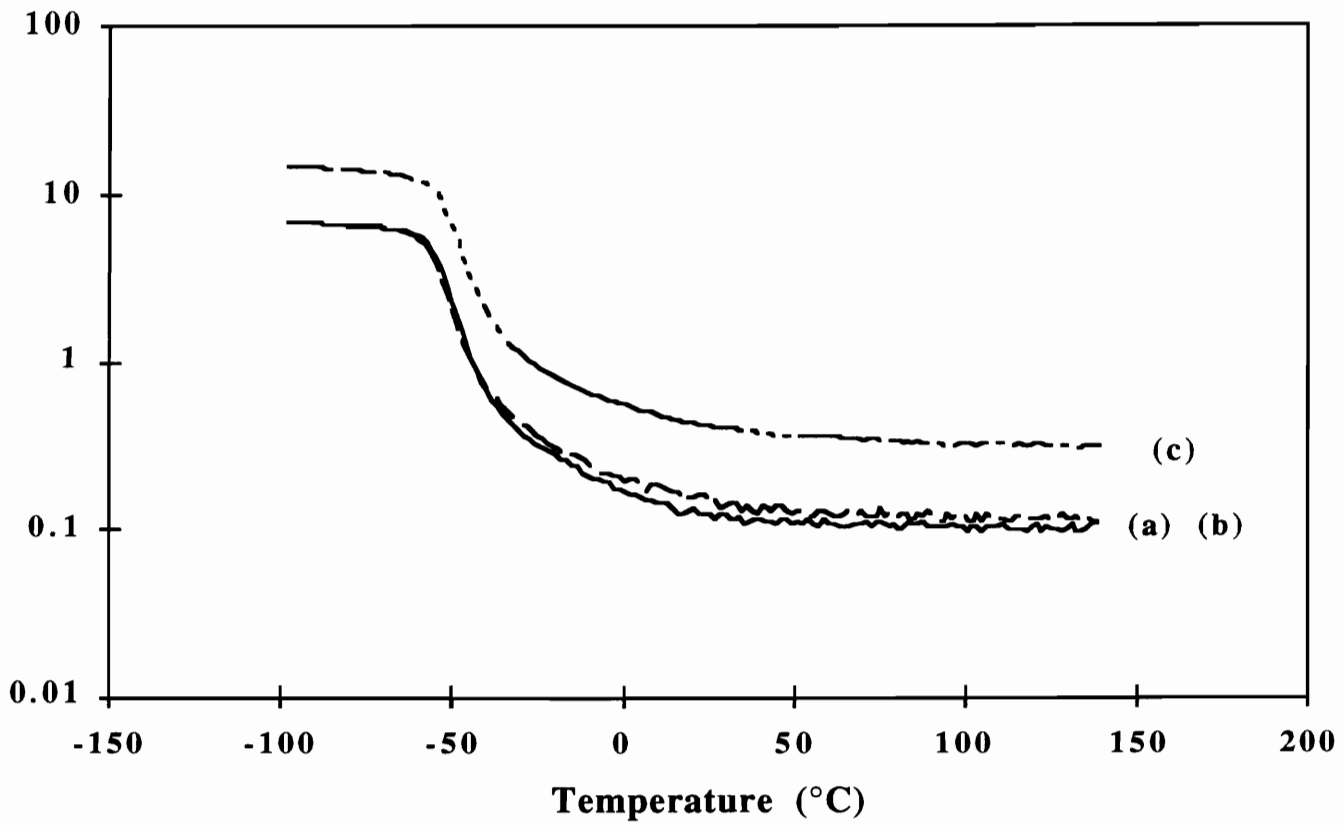


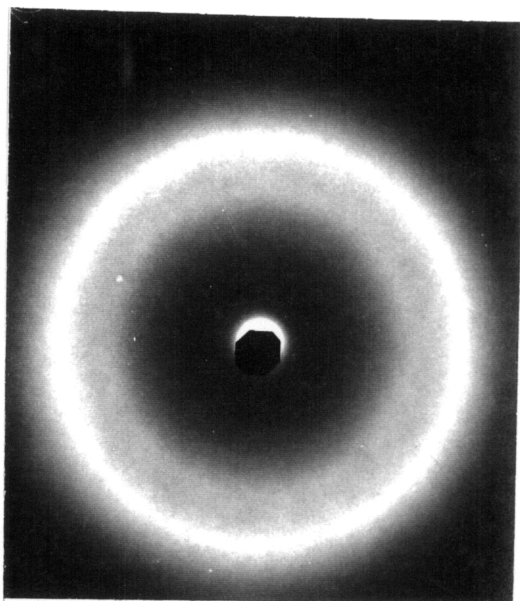
Figure 4.80. Influence of DEOA content on the storage modulus of foams (a) FD-0, (b) FD-0.5 and (c) FD-1.

Wide angle x-ray scattering (WAXS) was carried out to ascertain the short range ordering and the influence of DEOA content on this local packing order of the hard segments within this series of foams. Figure 4.81 illustrates the WAXS patterns of the foams FD-0 and FD-0.5, and FD-1. Again, in addition to the amorphous halo, two relatively sharp rings (indicating localized packing order) are displayed. As with the previous series of foams, increasing the DEOA content disrupted the ordering of the HS domains as denoted by the subtle decrease in ring sharpness especially with FD-1. The sharp rings displayed by FD-0 shown in Fig. 4.81a have become slightly more diffuse for FD-0.5 as shown in Fig. 4.81b and even more diffuse for FD-1, shown in Fig. 4.81c. Clearly, this evidence confirms the earlier results that while DEOA increases the level of cross-linking, it also disrupts the hard segment ordering although the disruption is slightly more severe in the case where the polyol is EO capped. As mentioned earlier, EO has been shown to compatibilize soft and hard segments promoting some phase mixing which can also lead to HS domain disruption.

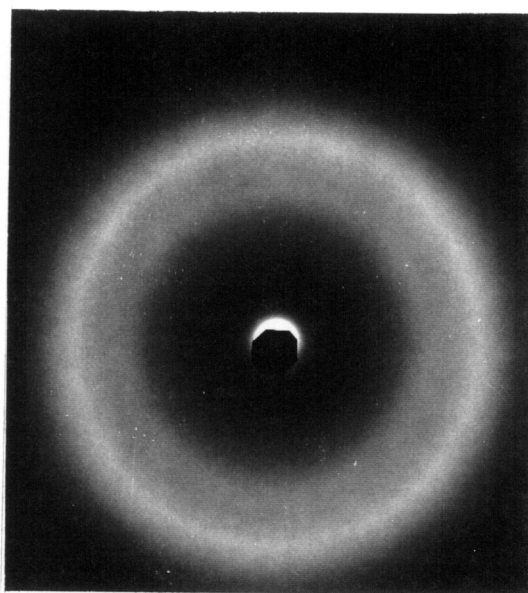
4.7.2.5 Load Relaxation Behavior

The load relaxation behavior of this series of foams as influenced by the DEOA content was investigated. Since FD-1 had severely shrunk and a severely disrupted cellular structure, only foams FD-0 and FD-0.5 were evaluated. The load relaxation behavior of FD-0 as a function of temperature and humidity is presented in Fig. 4.82a and that of FD-0.5 in Fig. 4.82b. As expected, temperature and especially humidity dramatically "plasticized" the load relaxation behavior shifting the curves to lower loads; approximately 15% lower than at ambient conditions. More directly comparing the two foams to each other as shown in Fig. 4.83 reveals that DEOA enhances the loads particularly at ambient conditions. The loads were increased by ca. 20% at 30°C-35%RH with the inclusion of 0.5 pph DEOA in the formulation. At 100°C-98%RH however, the small amount of DEOA

(a)



(b)



(c)

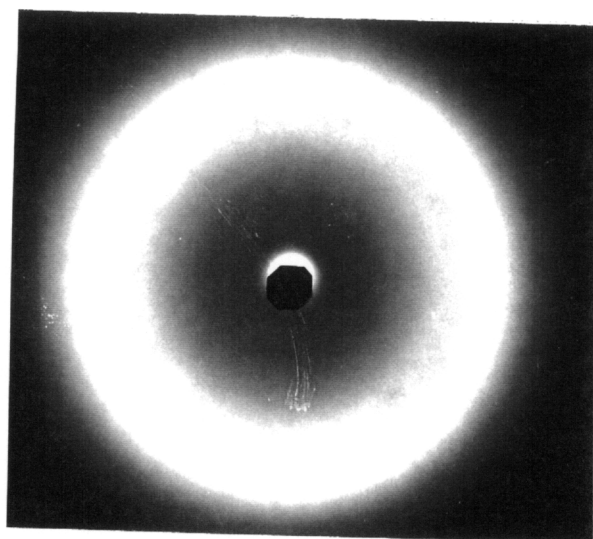


Figure 4.81. WAXS patterns illustrating the influence of DEOA content on the short range ordering of the HS domains: (a) FD-0, (b) FD-0.5 and (c) FD-1.

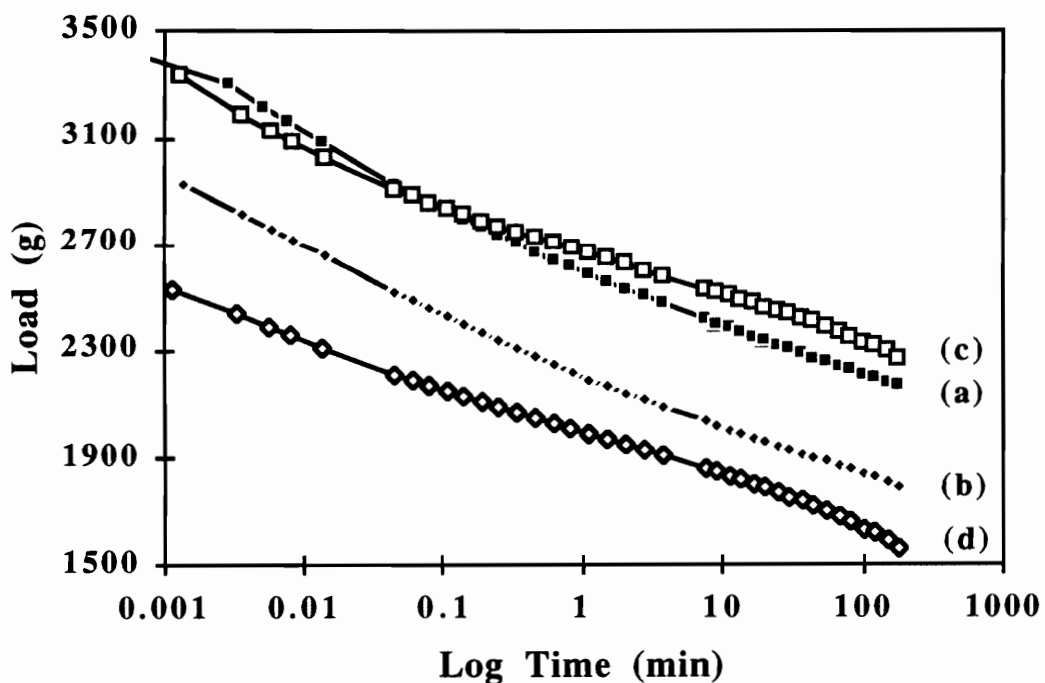
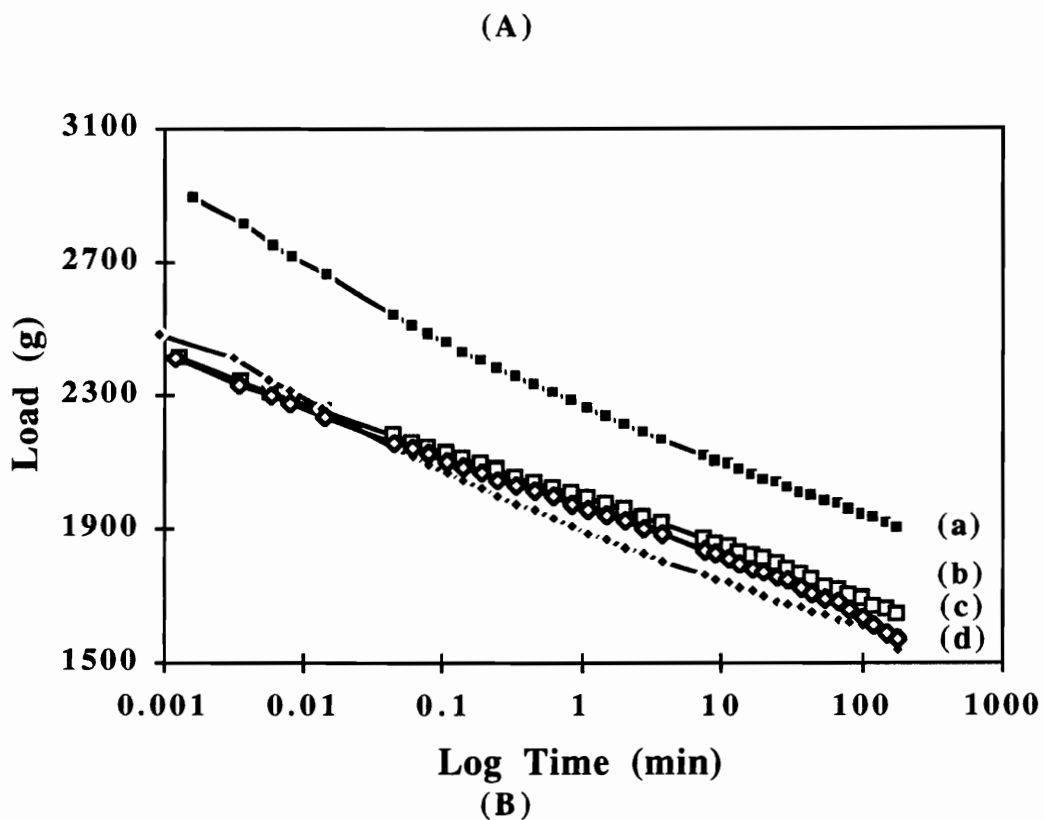


Figure 4.82. Influence of temperature and relative humidity on the load relaxation behavior of (A) FD-0 and (B) FD-0.5. In each figure the letters designate the following conditions: (a) 30°C-35%RH, (b) 30°C-98%RH, (c) 100°C-35%RH, and (d) 100°C-98%RH.

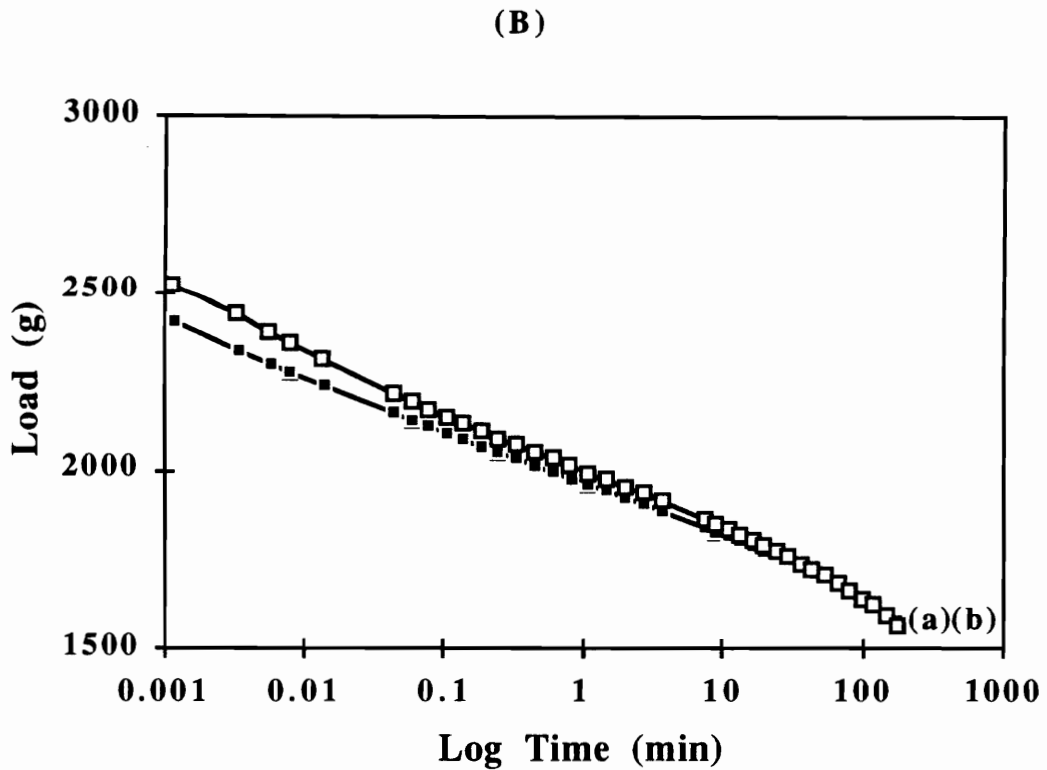
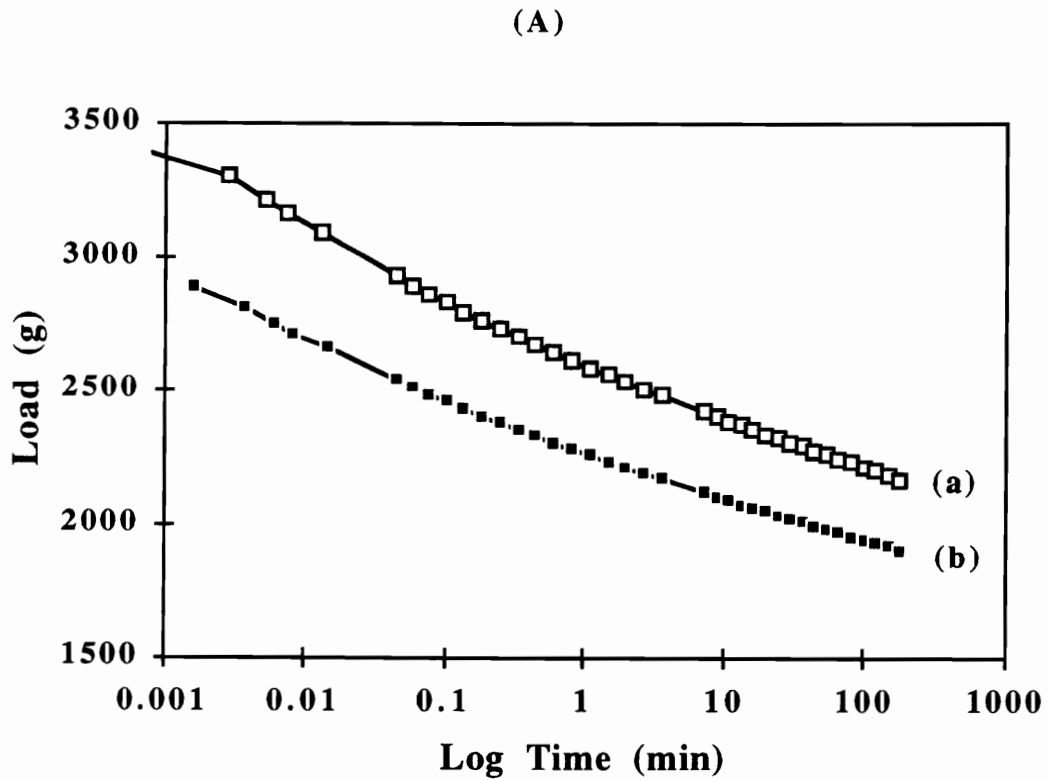


Figure 4.83. Influence of the DEOA content on the load relaxation behavior at (A) 30°C-35%RH, and (B) 100°C-98%RH. In each figure the letters designate: (a) FD-0 and (b) FD-0.5.

in the formulation had little influence on the relaxation behavior implying that while the DEOA increases the covalent cross-linking it also "loosens" by disordering the HS domains for which water and temperature can disrupt their hydrogen bonding even further than in FD-0. It must also be pointed out that the different cellular structures exhibited by these two foams as witnessed by the airflow measurements may also influence the load relaxation behavior. For example, the increased cross-linking, in addition to strengthening the struts, produced more closed windows which greatly reduced the airflow further increasing the load levels.

4.7.3 Influence of EO Capped Polyols

The influence EO capping was qualitatively ascertained by comparing foams from each of the two series in which the other components were comparable. For example, both series of foams contained a foam having 1 pph DEOA content as well as 5 pph water content although some of the other components slightly varied. Therefore, these comparisons are intended to be qualitative and only reflect trends.

Comparing the solvent extraction results of each series indicates that the FeD-x series displayed a higher amount of extractables suggesting that less material is covalently connected within these foams than foams FD-x. This result can be attributed to the major difference in the molecular weight of the polyols, where the 5000 molecular weight polyol, having a greater molecular weight, corresponds to a greater molecular weight between cross-links.

The cellular structures were also different for each series of foams as implied by the SEMs in Figs. 4.63, 4.64, 4.74, 4.75, and 4.76. The foams formulated with the all PO polyols exhibited greater closed cell character at lower DEOA levels. For example, foam FeD-2 displayed a greater airflow rate than FD-0.5, 0.4 ft³/min. compared to 0.2 ft³/min. Furthermore, foam FD-1 had such a high fraction of closed cells that it underwent

significant shrinkage as a result. Foam FeD-2, however, also displayed a high fraction of closed cells but did not show any signs of shrinkage. These observations are most likely a result of over-stabilization of the foam brought about by the higher level of surfactants utilized in the FD-x series and the greater amount of T-9 (a gelling catalyst) also utilized in this series. Both the higher amount of surfactants, as well as gelling catalysts can stabilize the evolving foam much prior to the cell opening point which will result in a significant amount of closed cells.

Of all the differences observed in this comparison, the greatest was in the TEM analysis where the foams incorporating primary hydroxyl groups lacked the evidence of any precipitated structures as those observed for the foams containing all secondary hydroxyl groups. In fact, only a grainy texture on the order of 150 Å was observed in the micrographs of the FeD-x series where the precipitated structures of the FD-x series were on the order of 100 - 150 nm. The EO capping used in the "molded" polyol increases the compatibility between the two phases, hard phase and soft phase, that precipitation of the urea-based features does not occur.

Within the range studied, the EO capping appeared to have little influence on the short range HS ordering. The sharpness of the rings in the WAXS patterns of each of the foams, FeD-1 and FD-1, were very similar suggesting that while EO may influence the phase separation, the ordering is not influenced.

With respect to the load relaxation behavior, the results were comparable and within range of each other although many other factors different in each series can also have a bearing on this behavior. However, comparing both foams lacking DEOA displayed similar initial loads and load decays at all studied environmental conditions.

4.8 Summary

The clear and significant advantages achieved with molded foams such as allowing intricate shapes to be produced, are also accompanied by many complexities. For example, in order to achieve these advantages, the formulation components are more complex usually requiring faster, more reactive ingredients as well as additional ingredients that serve this purpose. Since these differences can dramatically alter the foam process and important balance between the gas-producing and gelling reactions, more complex surfactant/catalyst packages are required. The key factor is that, while the complexities can be overcome by the use of various surfactants and catalysts, the structure within the solid portion of the foam is also dramatically influenced and influenced in an unfavorable manner. This point was substantiated throughout this chapter beginning with the cellular structure of the foams.

The cellular structure as evaluated by SEM demonstrated that cell opening is a major concern in molded foams, even after mechanical crushing has been undertaken. The micrographs showed that many windows still remain unopened. Furthermore, it was evident that these materials have densities higher than slabstock foams of comparable water content. The struts of each cell in molded foams average ca. twice the thickness of slabstock foams. Another important observation was that the molded foams lacked the geometric anisotropy with respect to rising direction that slabstock foams possess. The CPP dispersions included in the formulation displayed only a small influence on the cellular structure. The cells of the foams containing these particles were slightly smaller than those lacking them which was attributed to a difference in the amount of nucleated bubbles at the beginning of the process. While the water/TDI content strongly influenced the density, it appeared to have no bearing on the size and structure of the cells.

Thermal analysis and x-ray analysis showed evidence of microphase separation. The effects of water/TDI content and CPP dispersions were rather small. A greater water content shifted the SAXS shoulder to lower angles suggesting that the spacing between scattering centers is greater. The CPP particles slightly influenced the SAXS profiles

where the foams containing these particles exhibited higher overall scattering implying that they influence the microphase separation between the HS domains and continuous soft segment.

One of the most important discoveries in this chapter was the fact very little order was observed within the HS domains of the molded foam. WAXS patterns revealed only a broad amorphous halo without the presence of sharp rings which have been observed in slabstock foams and attributed to local packing of the HS domains. This was also confirmed with FTIR by following the hydrogen bonded urea absorbance. The molded foams also lacked the presence of any bidentate absorbance and only displayed monodentate and free urea absorbances. Slabstock foams do typically show a strong more stable bidentate absorbance associated with the structural order of the HS domains. This order or lack of was shown to correlate well with the viscoelastic behavior of the foams at elevated temperatures and humidities. FTIR also showed that the hydrogen bonded absorbance decreased with increasing temperature confirming the disruption of these secondary bonds by temperature.

In evaluating the influence of the CPP dispersions, solvent extraction revealed that the foams containing the particles displayed higher sol fractions. The higher extractables suggested that the particles or a portion of them can be extracted thereby also suggesting that these particles are not as extensively covalently grafted to the soft segment matrix. These foams also exhibited greater hysteresis than the foams lacking the CPPs - this behavior attributed to the rigid particles increasing the local stress and furthering the irreversible flow or chain slippage and disruption of hydrogen bonds at the interface. As the HS content was increased, the amount of hysteresis was also increased - this also due to a greater number of hydrogen bonds being disrupted.

The viscoelastic properties of the molded foams revealed a strong dependence on the environmental condition. For example, in load relaxation, increases in temperature and/or humidity "plasticized" the behavior dramatically. Unlike slabstock foams which

displayed very little change with increases in temperature and even increases in load (attributed to a rubber elasticity effect) except at very high temperatures, the molded foams studied here displayed decreases in load and increases in load decay with even small increases in temperature. Furthermore, increases in humidity ensued similar effects where the relaxation curves were shifted to lower loads. Creep experiments revealed similar behavior. Increases in either temperature or humidity caused the both the initial strains and the amount of creep to increase systematically and significantly. The primary mechanism driving the dramatic decrease in the properties over a three hour period with increases in temperature and humidity is hydrogen bond disruption. While hydrogen bond disruption occurs in slabstock foams, it occurs to a greater extent and with greater ease and less energy in molded foams. The reason for this is the lower HS ordering exhibited by the molded foams.

The viscoelastic properties of the CPP containing foams were more time-dependent than of the foams lacking these particles. As expected, the incorporation of these particles increased the initial load and decreased the initial strain over the foams lacking the particles suggesting that the initial stiffness of these materials (such as that measured by ILD) was increased. However, over a period of time, the amount of this initial load that decayed was greater for the CPP containing foams and furthermore, at elevated conditions, the load decreased to levels below those of the CPP lacking foams. That is, the load of the CPP containing foams was lower than that of the CPP free foams at the end of the three hour period. The increased relaxation is a result of greater localized stress occurring for the "filled" materials since there is less soft segment leading to greater localized strain. Furthermore, disruption of the hydrogen bonding existing at the interface enhances this phenomenon.

Compression set results followed a similar trend. First as the temperature and/or humidity was increased the amount of compression set increased, especially at high temperature and humidity. As with the load relaxation and creep, the molded foams

exhibited greater set at a given temperature than typical slabstock foams. Within the molded foams, those containing the CPP particles revealed higher compression sets at either high temperature or high humidity than those lacking the particles.

Finally, one major reason for the decreased order among the HS domains of the molded foams as well as poorer viscoelastic properties was the incorporation of the additive, DEOA. It was shown that as small amounts of DEOA significantly increased the covalent cross-linking, they also distinctly disrupted the ordering of the HS domains as illustrated by WAXS and FTIR. Depending on the polyol utilized, it also showed some evidence of phase mixing suggested by slight shift in the soft segment T_g as well as SAXS. Another observation which came out of this small study of DEOA was the development of the larger urea precipitate structures were not evident in the foams which incorporated polyols that were EO capped. This suggests that the EO capping to some extent compatibilizes the urea groups and ether containing soft segments.

Chapter 5

5.0 Influence of TDI Index on Structure-Property Behavior of Flexible Slabstock Polyurethane Foams

The broad application base of polyurethane foams inherently requires them to be made with varying levels of "stiffness". Traditionally, this was accomplished by the use of low boiling liquids or auxiliary blowing agents which influenced the density and softness of the foam. However, due to the concerns about the effects of CFCs and other blowing agents on the ozone layer of the earth's atmosphere, these materials have been nearly phased out from the formulation of polyurethane foams. This has therefore led urethane foam manufactures to alter foam formulations and derive novel components to meet the changing and evolving application base. Modifications to the existing formulation components include altering polyol molecular weight, polyol functionality, isocyanate functionality, isocyanate molecular weight, isocyanate amount (isocyanate index), as well as the amounts of water, catalysts, surfactants, etc.

In this study, a new proprietary polyol (nominal functionality 3.15) was used in conjunction with 6 pph water content as presented in Table 3.4. The isocyanate index was thus systematically varied from 85 to 110 (samples F85 - F110) thereby altering the foam stiffness - via varying the level of covalent cross-linking and level of hard segment content. The objective was to characterize the foams as a function of index in view of the trend just

mentioned. Along with the physical properties, other properties such as cellular structure and micro-structure were also investigated as a function of TDI index. It is to be noted from Table 3.4 in Chapter 3 that the density of all the foams was maintained at 1.25 lb/ft³.

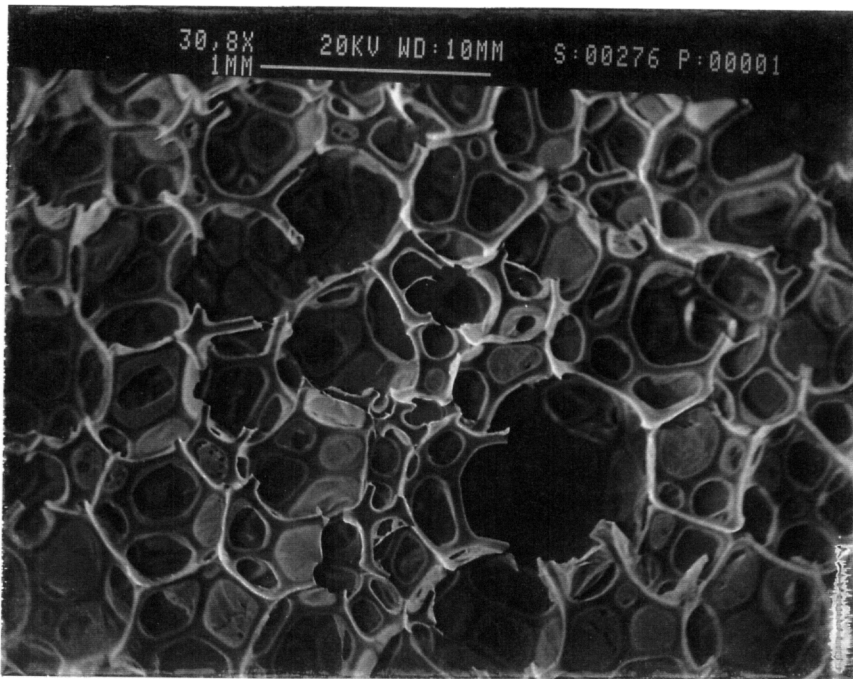
5.1 Influence of Index on Cellular Structure

Scanning electron micrographs were taken of the foam samples to observe any distinct differences in the cellular structure as a function of index which can inherently influence their mechanical properties. Figure 5.1 is a micrograph depicting the cellular structure of F85 shown parallel and perpendicular to the rise direction. The shape of the cells is a polyhedral or multi-sided shape which is a result of the impedance of the growing bubbles. The closest approximation to the cell shape is a tetrakaidecahedron which denotes a fourteen-faced cell. The majority of the faces are hexagons with the presence of some pentagons and four sided faces. As can be seen, the cells are elongated along the rise direction. The micrograph taken perpendicular to the rise direction illustrates this with the cells displaying an ellipsoidal shape. Parallel to the rise direction, the cells appear "circular" in shape as described earlier. In addition, the majority of the cells are open although a few closed windows do exist.

The structure of F100, which is shown in Fig. 5.2, was very similar to that of F85. Again, the cellular structure is typical of a slabstock foam where the majority of the cells are open and exhibit the typical polyhedral shape. Figure 5.2b shows the remains of cell membranes that have ruptured. This rupturing can arise during foaming or perhaps later during preparation for evaluation by SEM which requires high vacuum treatment.

Based on analysis of the SEM micrographs, the TDI index had very little influence on the cellular structure. Even the cellular structure of F110, shown in Fig. 5.3, appeared very similar to that of the two previously discussed foams. Evaluation of these micrographs lead to the conclusion that the cellular structures were relatively unaffected by

(A)



(B)

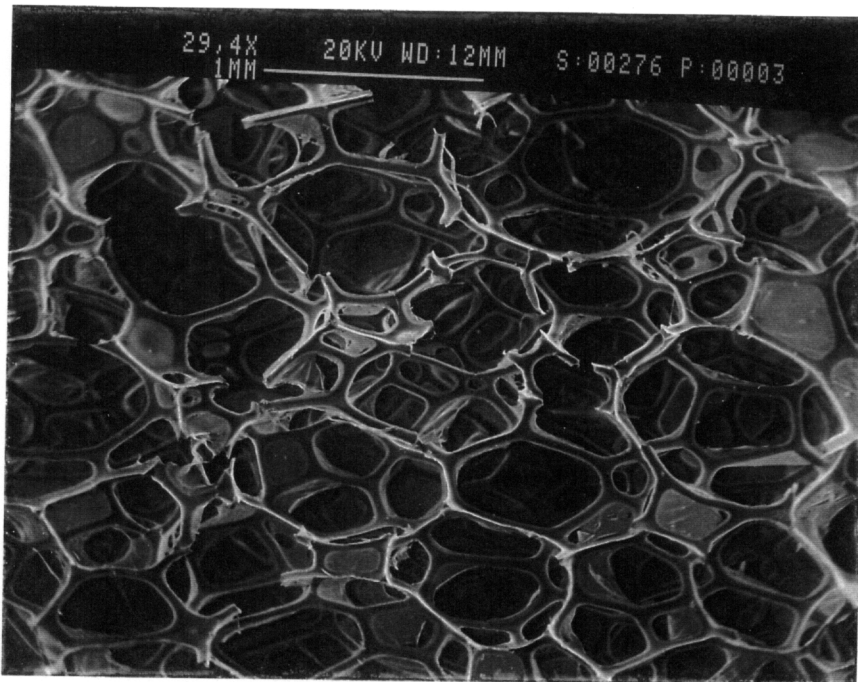
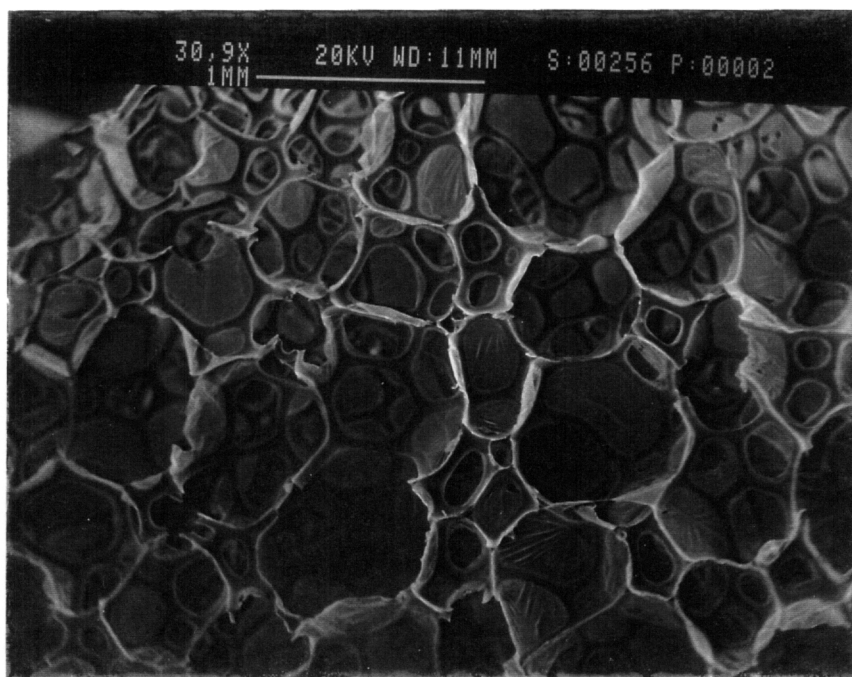


Figure 5.1. Scanning electron micrographs of foam F85 shown both (A) parallel to the rise direction and (B) perpendicular to the rise direction.

(A)



(B)

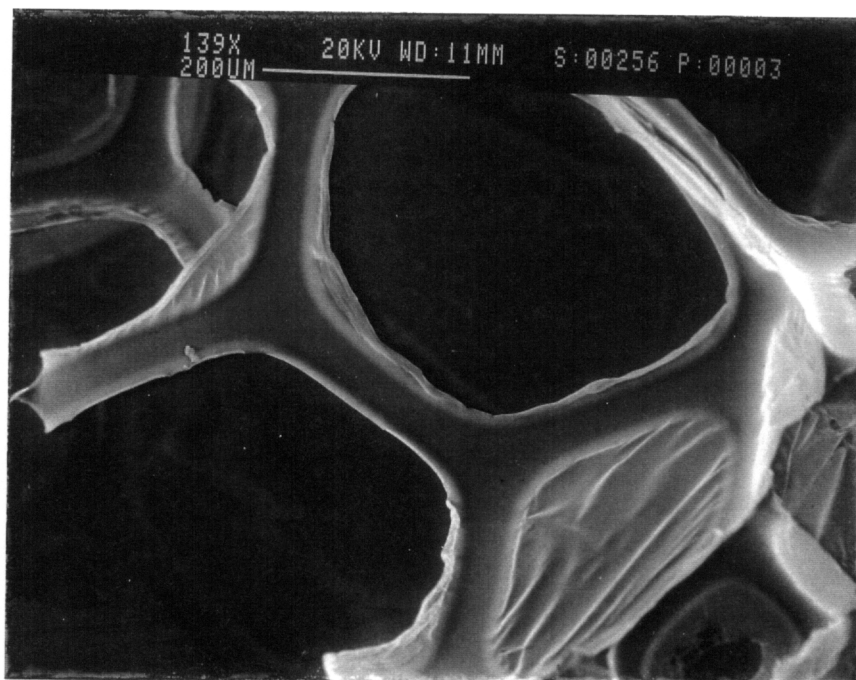


Figure 5.2. Scanning electron micrographs of foam F100 shown at a magnification of (A) 30x and (B) 140x.

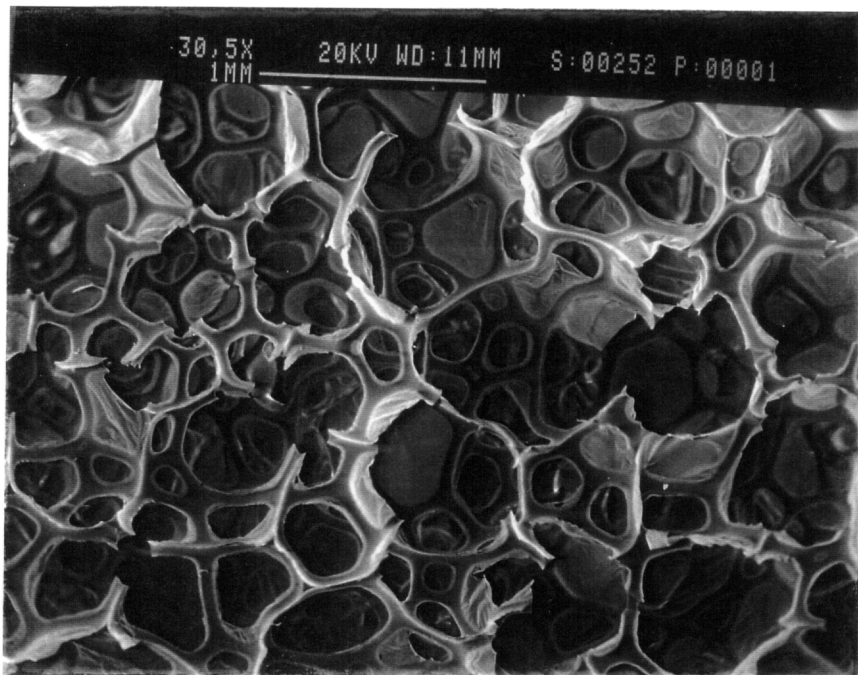


Figure 5.3. Scanning electron micrographs of foam F110 at a magnification of 30x.

altering the TDI index. Again, while all foams are open-celled, all have some closed cells. Further support of the cellular structure's insensitivity to TDI index was obtained by comparing the airflow measurements of each of these foams. All foams displayed airflow rates of ca. 5 ft³/min. confirming that the cellular structure is relatively unaltered by the different TDI indexes. Therefore, physical property differences between the foams of varying index are most likely not a result of different bulk cellular structures but instead a result of differences within the solid morphology of the foams.

5.2 Influence of Index on Solvent Extraction Results (Covalent Cross-linking)

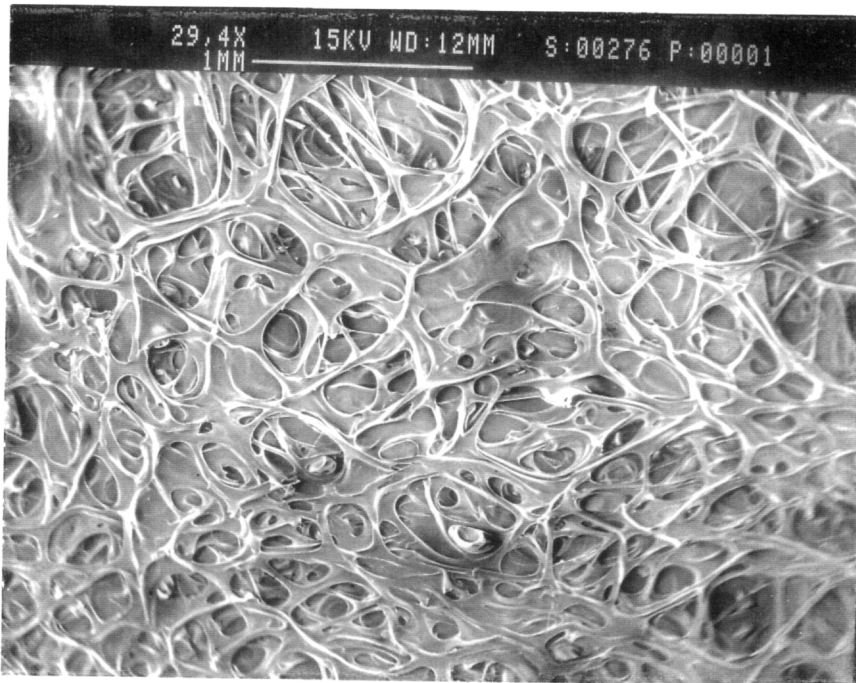
The influence of index on the covalent cross-linking was qualitatively ascertained by solvent extractions in DMF. Results from the 48 hr extraction studies are given in Table 5.1. As can be seen in Table 5.1, the lowest index foam, F85, displayed a sol fraction of ca. 31%. As the TDI index was increased, the amount of extractables decreased suggesting that the amount of covalent cross-linking increased as expected. The sol fractions decreased to ca. 6% for the highest index foam, F110. However, it also appears from these results that at an index of 100 or above that the sol fraction (and thus the gel fraction) remains essentially constant. This may in part be due to residual DMF because of the strong interactions between the hydrogen bonding moieties and the polar solvent. Nevertheless, it can be easily concluded from these results that increasing the TDI index does increase the overall covalent cross-linking. Further evaluation of the cross-linking as a function of index was also addressed in the viscoelastic measurements.

Following the DMF treatment, SEM micrographs were obtained of the foams to relate the induced changes in the cellular structure to the TDI index. The strong dependence of the structural integrity on the TDI index is clearly evident. Figure 5.4 shows the cellular structures of foams (a) F85, (b) F100 (c) F110 following treatment in DMF. Micrograph

Table 5.1. Percent Sol from Solvent Extraction Studies Using DMF

Foam	Sol fraction, %
F85	31.3±0.5
F90	15.0±0.6
F100	5.6±0.5
F110	6.0±0.4

(A)



(B)

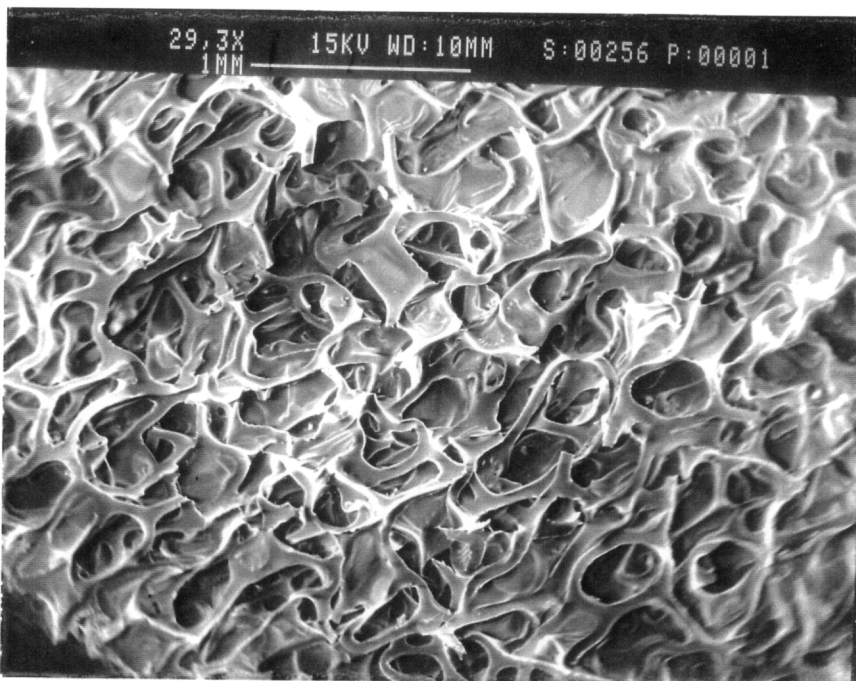


Figure 5.4. Scanning electron micrographs of foams following extraction process: (A) F85, (B) F100, and (C) F110.

(C)

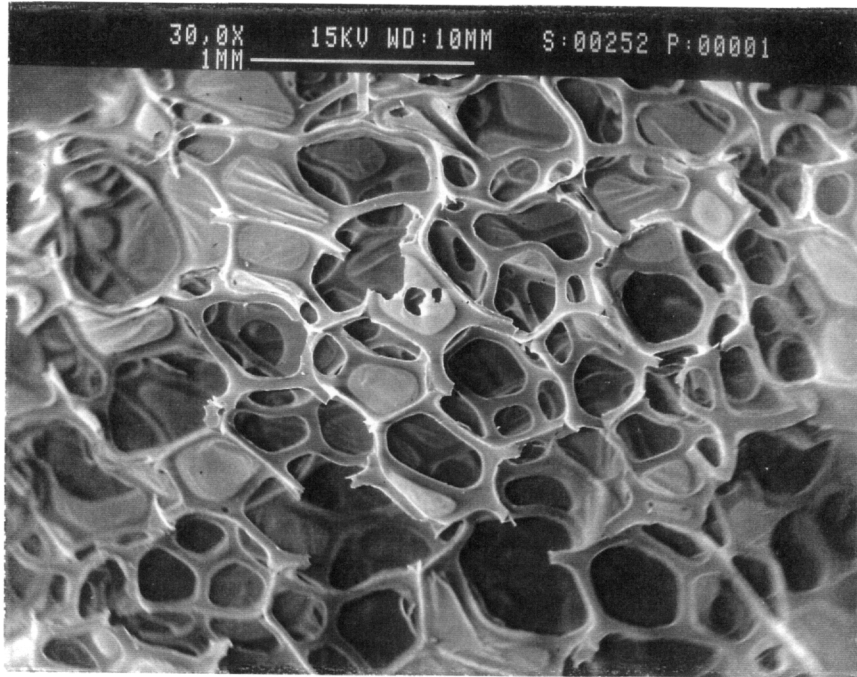


Figure 5.4 con't. Scanning electron micrographs of foams following extraction process: (A) F85, (B) F100, and (C) F110.

(a) illustrates the dramatic structural changes promoted by the extraction process that has caused the foam to essentially collapse into a much more dense, nearly film-like material. As the index increased, the foam's resistance to the extraction process increased. The resultant structure of F100, shown in Fig 5.4b, although still altered from its original state, resembles a foam much more than did F85 following extraction. While the cellular structure has been severely altered, it is much improved over that of F85 illustrating the significant contribution by the enhanced covalent network. Further increases in index increased the foam's resistance to structural changes by DMF as illustrated in Fig. 5.4c. In this case, after extraction, the foam is only partially altered but the cellular structure is quite similar to its unextracted form. As will be substantiated throughout this chapter, the systematic improvement in the structural integrity with index substantiates the conclusion that the varying TDI index has a direct correlation to the level of covalent cross-linking.

5.3 Influence of TDI Index on the Microphase Separation

The results of the solvent extraction studies indicated that the index had a direct effect on the covalent cross-linking and since cross-linking has been shown to influence the phase separation characteristics, they were also investigated using a number of techniques. Recall, as discussed in Chapter 2, that increasing the covalent cross-linking decreases the extent of phase separation.^{30,36} In view of this observation, as well as the observations with DEOA on the microphase separation in Chapter 4, it logically follows that the TDI index may also influence the hard segment ordering. For example, if a high index (or level of cross-linking) promote phase mixing, it may also influence the diffusion of the hard segments and perfection of the domains. Thus, the microphase separation and domain structure of the polyurethane foams were evaluated through a number of techniques beginning with thermal analysis.

Differential Scanning Calorimetry (DSC) was utilized to follow the soft segment T_g and relate shifts in this parameter as a function of index to changes in the amount of microphase separation. Figure 5.4 illustrates the first heating cycles of four foams varying in index from 85 to 110. As expected, in addition to the T_g , a broad endotherm is displayed which again is attributed to the evaporation of absorbed water. Figure 5.5 shows the second heating cycle for the same four foams. As with the other foams investigated within this dissertation, no observable difference was exhibited between the first and second heats of each foam with the exception of the broad endotherm. More importantly was the observation of the T_g with index. Although subtle, the T_g slightly shifted towards higher temperatures with increasing index suggesting that the HS content soluble in the soft segment phase is increasing. The specific values of T_g (determined from the inflection point) are presented in Table 5.2, from which it can be seen that the T_g does increase with increasing index. Along with the DSC determined T_g , the T_g as determined by DMA is also given in this same table as will be now discussed.

Dynamic mechanical analysis (DMA) was also carried out to follow the change in T_g with altering TDI index. The $\tan \delta$ results for the four foams are shown in Fig. 5.6. Similar to the DSC results, the T_g shifted towards higher temperatures as can be gathered from Fig. 5.6. Again the gradual and systematic shift in T_g indicates a phase mixing phenomenon which arises from the increased cross-linking preventing phase separation from occurring to the extent that it does for the lower index foams. The decreasing magnitude of the $\tan \delta$ peak indicates that the material "stiffens" with increasing index. However, the stiffening is not only a result of the increased cross-linking but also that the soft segment content is lower.

Small angle x-ray scattering (SAXS) was finally carried out to ascertain the presence of phase separation and how it was affected by the index. The SAXS data for the two foams, F85 and F110, are presented in Fig. 5.7 which is a plot of the normalized smeared intensity as a function of an angular variable s , defined as $s = 2\sin\theta/\lambda$. Although

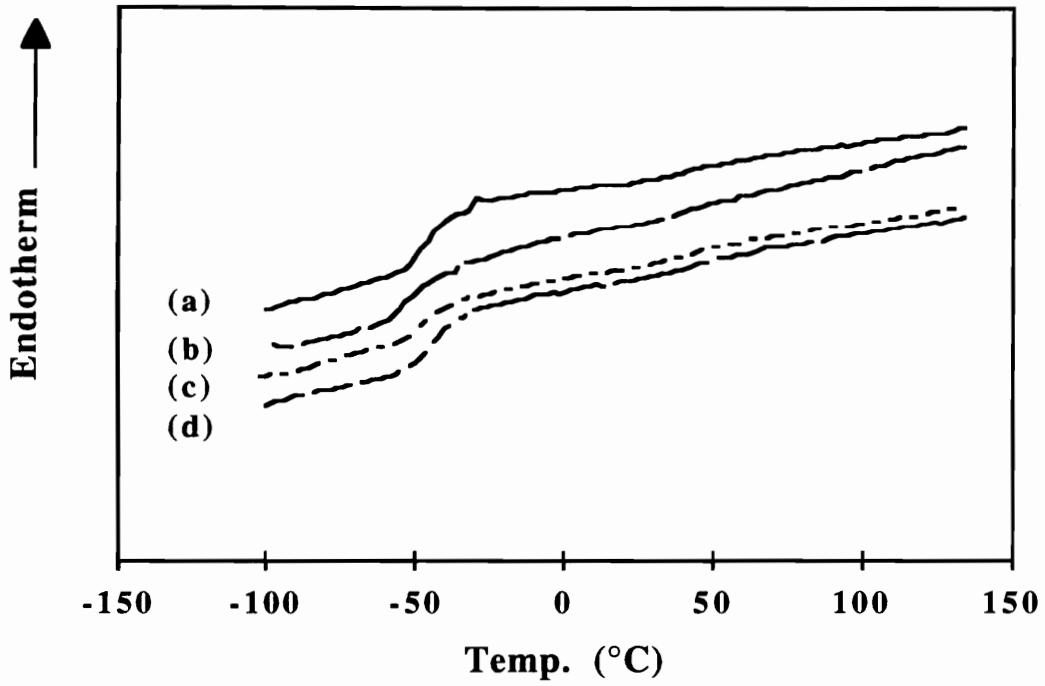
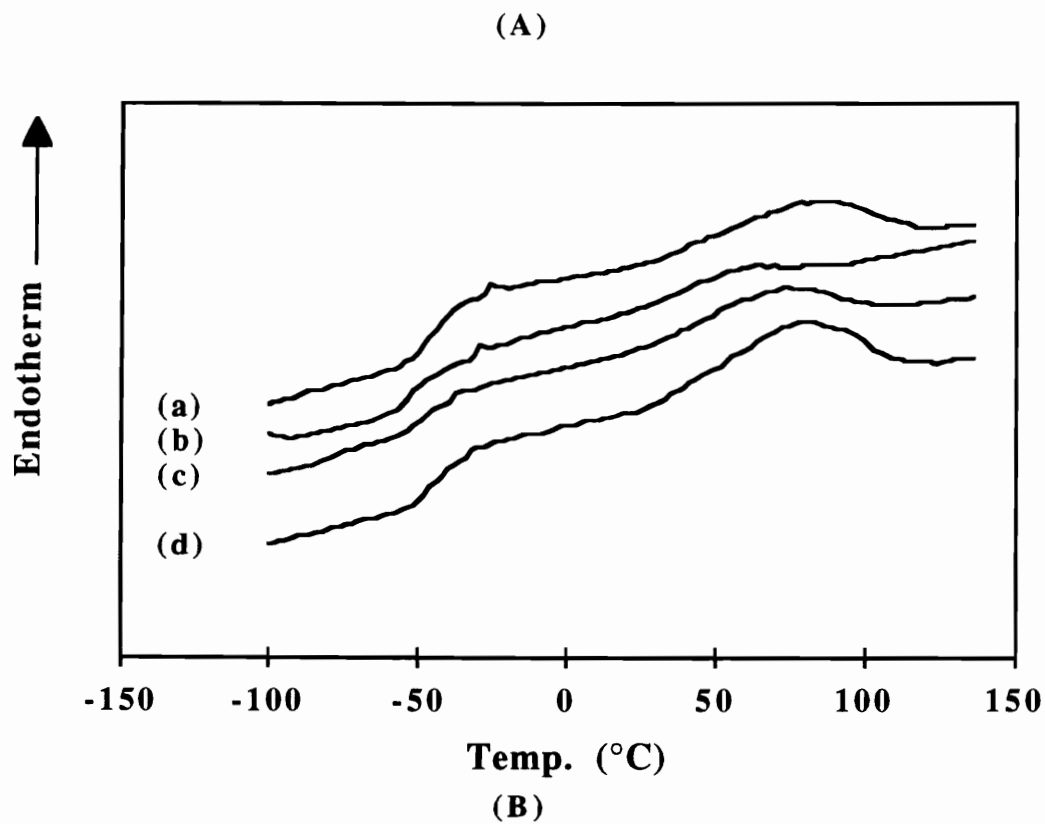


Figure 5.5. DSC thermograms of the (A) first heating scans and (B) second heating scans. In each figure letters designate the following foams: (a) F85 and (b) F95, (c) F100, and (d) F110.

Table 5.2. Thermal Properties*

Foam	T_g (°C) by DMA	T_g (°C) by DSC
F85	-53±1	-51±3
F95	-51±1	-52±1
F100	-48±1	-48±1
F110	-45±1	-45±1

Reported soft segment T_g is based on the inflection point in DSC and on the tan δ peak for DMA

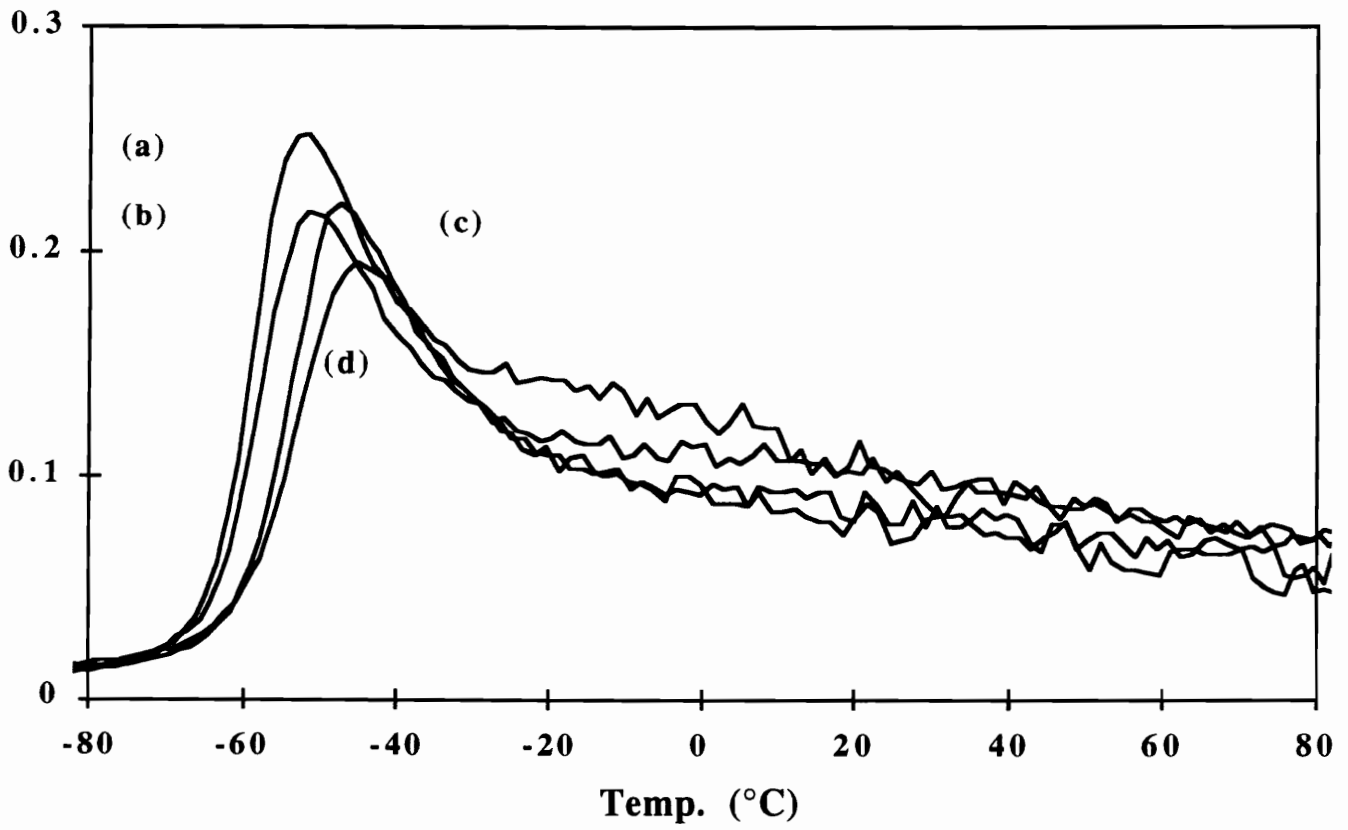


Figure 5.6. Influence of the TDI index on the tan delta peak: (a) F85 and (b) F95, (c) F100, and (d) F110.

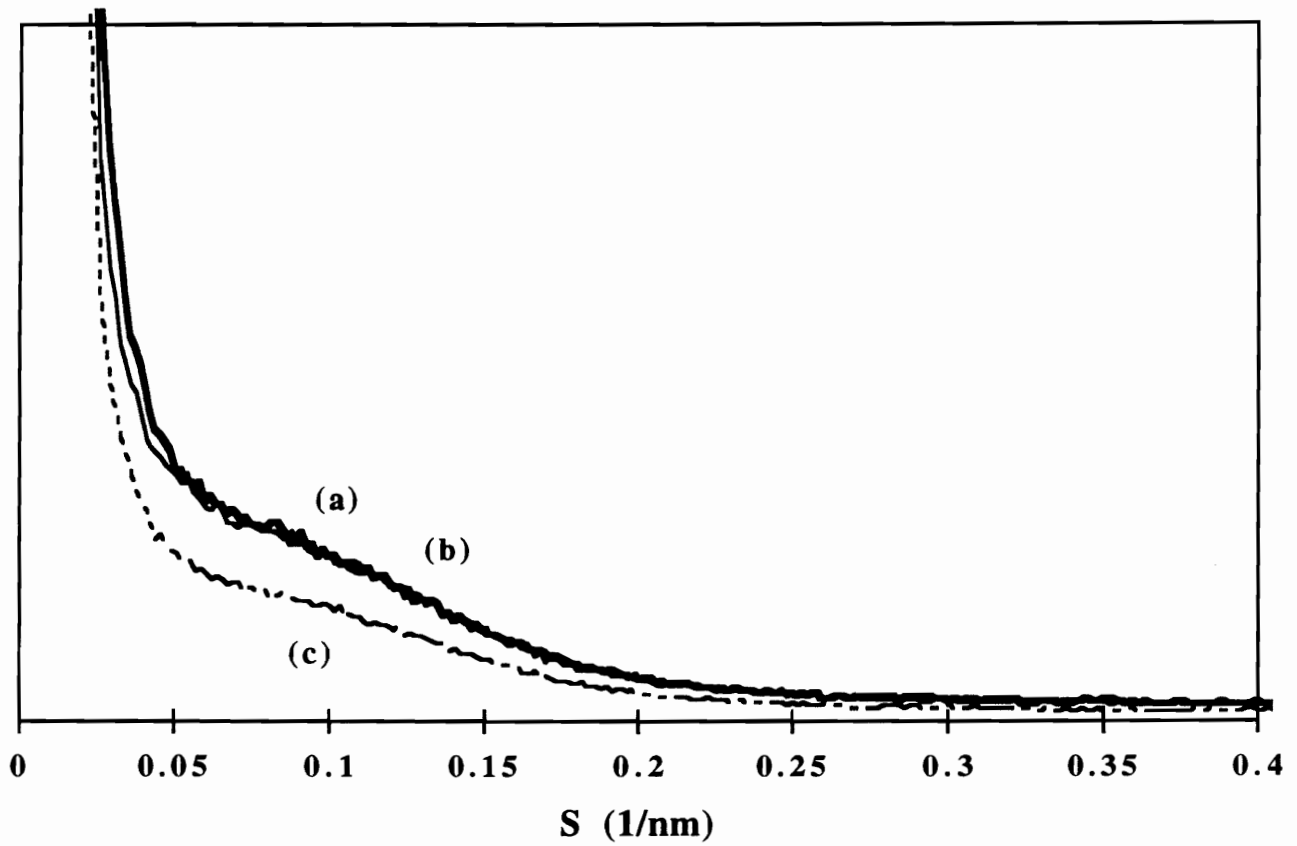


Figure 5.7. SAXS profiles of slabstock polyurethane foams (a) F85, (b) F100, and (c) F110 varying in the TDI index.

not very distinct, a weak shoulder occurs ($s \approx 0.1 \text{ nm}^{-1}$) indicative of microphase separation. The average interdomain spacing was not determined due to the fact that a sharp peak is not displayed but rather only a weak shoulder. Distinctly evident was that the overall measured normalized intensity of F110 was lower than that of F85. This result supports the thermal analysis data since it also indicates that the highest index foam has a higher amount of phase mixing occurring. The increased cross-linking prevented phase separation from occurring to the extent it occurs in foam F85. This was concluded using the same argument as that used in Chapter 4 which is based on the simplified interpretation of the scattering invariant which for an ideal two phase system with sharp boundaries is given as

$$\overline{\Delta\rho}^2 \approx \phi_1\phi_2[\rho_1 - \rho_2]^2 \quad 4.1$$

where ϕ_1 and ϕ_2 are the volume fractions of each phase and $[\rho_1 - \rho_2]$ is the electron density difference between the two phases. Again, for a given value of $[\rho_1 - \rho_2]$, the invariant achieves a maximum where each volume fraction is 0.5. As the volume fractions deviate from 0.5, the invariant decreases. Thus, an estimation of the amount of phase separation can be obtained by comparing this theoretical invariant to the experimentally determined invariant by

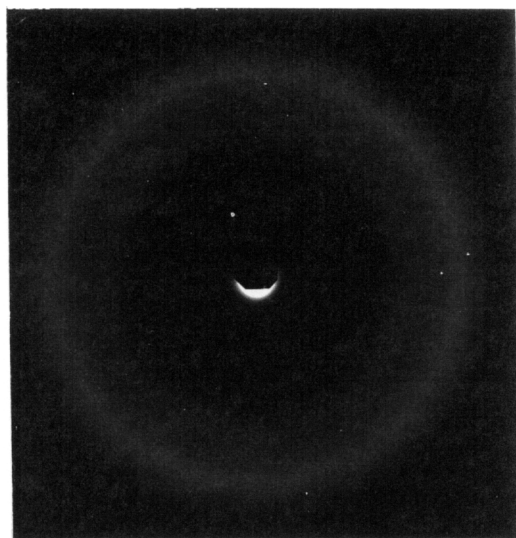
$$\overline{\Delta\rho}^2 \approx \frac{2}{V} \int_0^\infty I(s)s^2 ds \quad 4.2$$

where again s is the scattering vector and $I(s)$ is the smeared scattered intensity. Therefore, by taking a ratio of the experimentally determined and theoretically calculated invariant, a qualitative estimate of phase separation can be obtained. This analysis was not carried out but the results presented in Fig. 5.7 of the normalized intensity also indicate that the invariant for foam F85 is higher than for F110 suggesting that even though the HS content

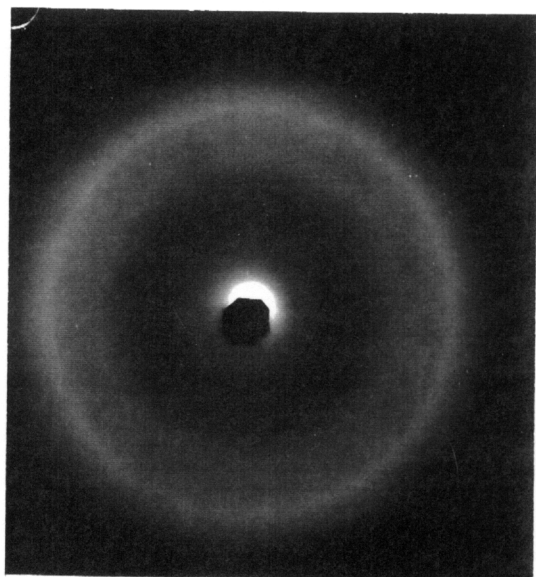
is higher for foam F110, more hard segments are solublized within the soft phase rather than in the HS domains. Again, the data were only normalized and treatments such as de-smearing, and background removal have not been undertaken. However, it is assumed that this type of treatment would not influence the trend demonstrated by the data as presented. Therefore, the SAXS results, if nothing else, do not contradict the thermal analysis results and even compliment them, all of which impart that the extent of microphase separation decreases as the covalent cross-linking increases.

The short range ordering or local packing order of the segment domains was studied using wide angle x-ray scattering (WAXS) which was shown in the previous chapter to correlate well with the response of the bulk foam's physical properties to varying environmental conditions. The WAXS patterns for foams F85, F100, and F110 are shown in Fig. 5.8 all of which exhibit two characteristics. The first is a broad amorphous halo as has been seen in the WAXS patterns of other foams and which is typical of amorphous systems. Second, all foams show two relatively sharp rings having a corresponding Bragg spacing of approximately 4.5 (outer ring) and 6.0 Å (inner ring) similar to the slabstock foams presented in Chapter 4. These peaks originate from the non-crystalline or paracrystalline HS ordering. The sharpness and intensity of the rings can be used to qualitatively ascertain the level of ordering of the hard segments. The rings (esp. 6.0 Å) are sharper for F85 than for F110 which was again attributed to the disruption of this packing ordering by the additional covalent cross-linking in F110. Diffractometer scans were taken to confirm the subtle differences in the patterns since the inferences can be somewhat subjective. The results are presented in Fig. 5.9 which is a plot of intensity versus the angle, 2θ . The scans depict two peaks which correspond well with the spacings of the rings in the scattering patterns. In addition the scans in Fig. 5.9 also compliment the trend observed with the patterns which shows that the intensity of F110 is both lower and broader than that of F85 confirming the interpretations of a disruption of the HS ordering as induced by the increased cross-linking.

(A)



(B)



(C)

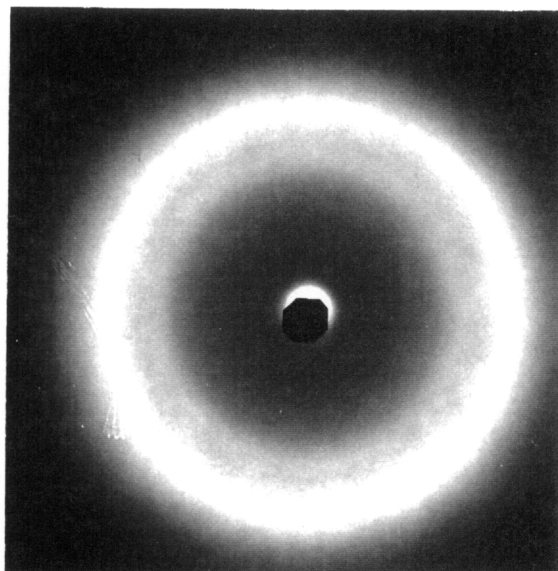


Figure 5.8. WAXS patterns illustrating the influence of TDI index on the short range ordering of the HS domains: (A) F85, (B) F100 and (C) F110.

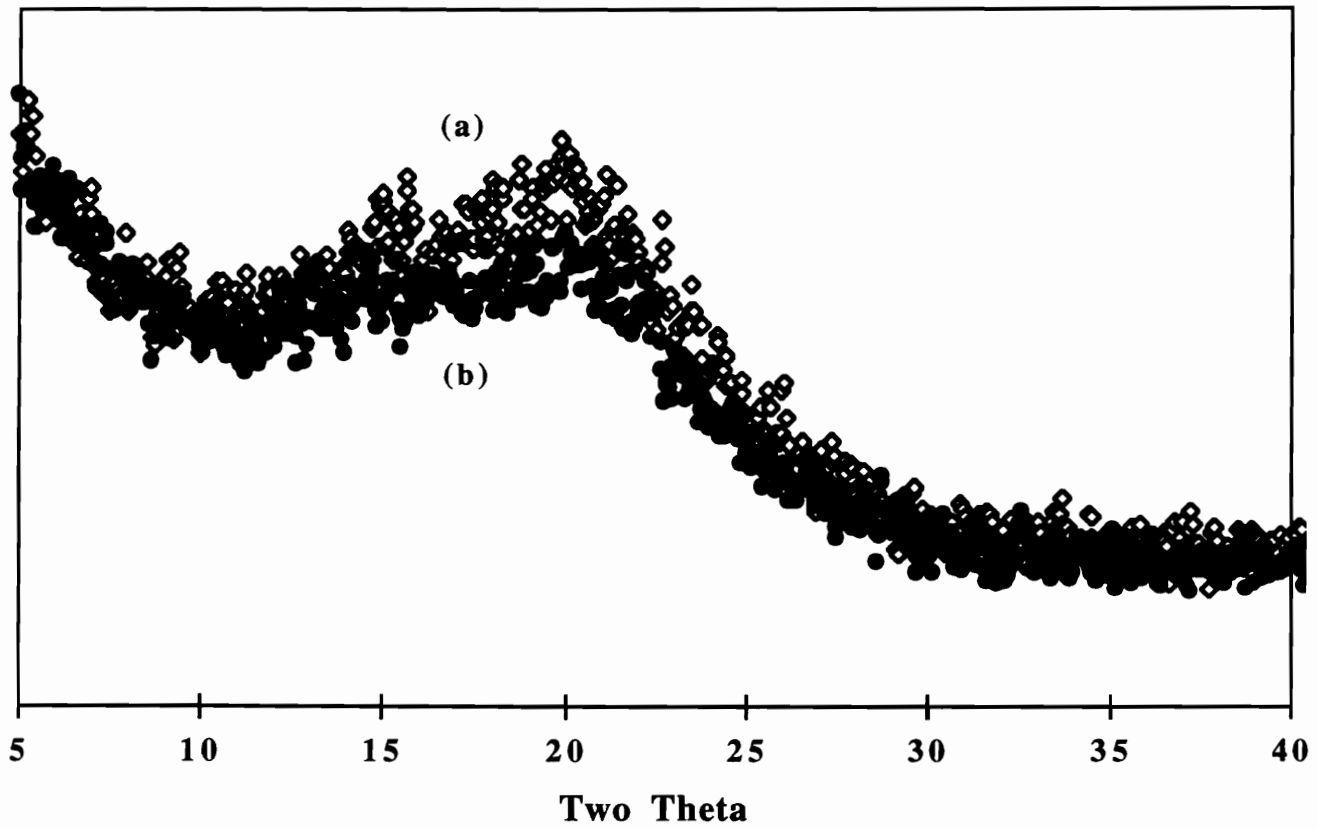


Figure 5.9. WAXS diffractometer scan illustrating the influence of TDI index on the short range ordering of the HS domains: (a) F85 and (b) F110.

Fourier transform infrared (FTIR) spectroscopy was also utilized to study the ordering of the hard segments by focusing on the hydrogen bonding in the carbonyl and N-H regions. Recall that well ordered HS domains exhibit bidentate hydrogen bonding shown in Fig. 2.25 and thus has been utilized as an indication of the level of HS ordering.³⁰ The FTIR carbonyl spectral profiles for the three foams, F85, F100, and F110 are shown in Fig. 5.10. The bidentate peak centered at ca. 1640 cm^{-1} shows that the bidentate absorbance and thus HS ordering displays a maximum as a function of index. Foam F100 exhibited a stronger bidentate absorbance than F85 which is due to a higher concentration of well ordered HS domains arising from a higher HS content. This trend strongly suggests that the development of HS domains further progresses with initial increases in index (up to ca. 100 index). The bidentate absorbance for F110, however, is significantly lower than either F85 and especially F100. The trend in the N-H absorbance region, shown in Fig. 5.11, is similar to that in the carbonyl region. The hydrogen-bonded N-H absorbance, centered at about 3280 cm^{-1} , is highest for F100 and lowest for F110 with the absorbance for F85 lying between. The lower absorbance of F110 was expected and is a result of the disruption of the HS ordering by the increased covalent cross-linking. The increased covalent cross-linking that occurs in this high index foam makes it more difficult for the urea segments to associate (through diffusion) and to pack with other hard segments thereby limiting perfection of the HS domains which must principally occur prior to the gel point. Although the non-bonded urea and urethane, centered at ca. 1695 cm^{-1} and 1730 cm^{-1} , respectively, appear to increase with increasing index, it is difficult to conclusively confirm this due to the convoluted nature in this region (1695 cm^{-1} to 1750 cm^{-1}). This is due to the fact that contributions from free urea groups, bonded urethane groups, free urethane groups, allophanate groups, and biuret groups all display absorbance peaks here. Figure 5.12 shows the FTIR spectral profiles of the three foams in the isocyanate region. Not surprising, this figure shows an increase in the amount of free isocyanate suggesting that as the TDI index is increased, the amount of unreacted

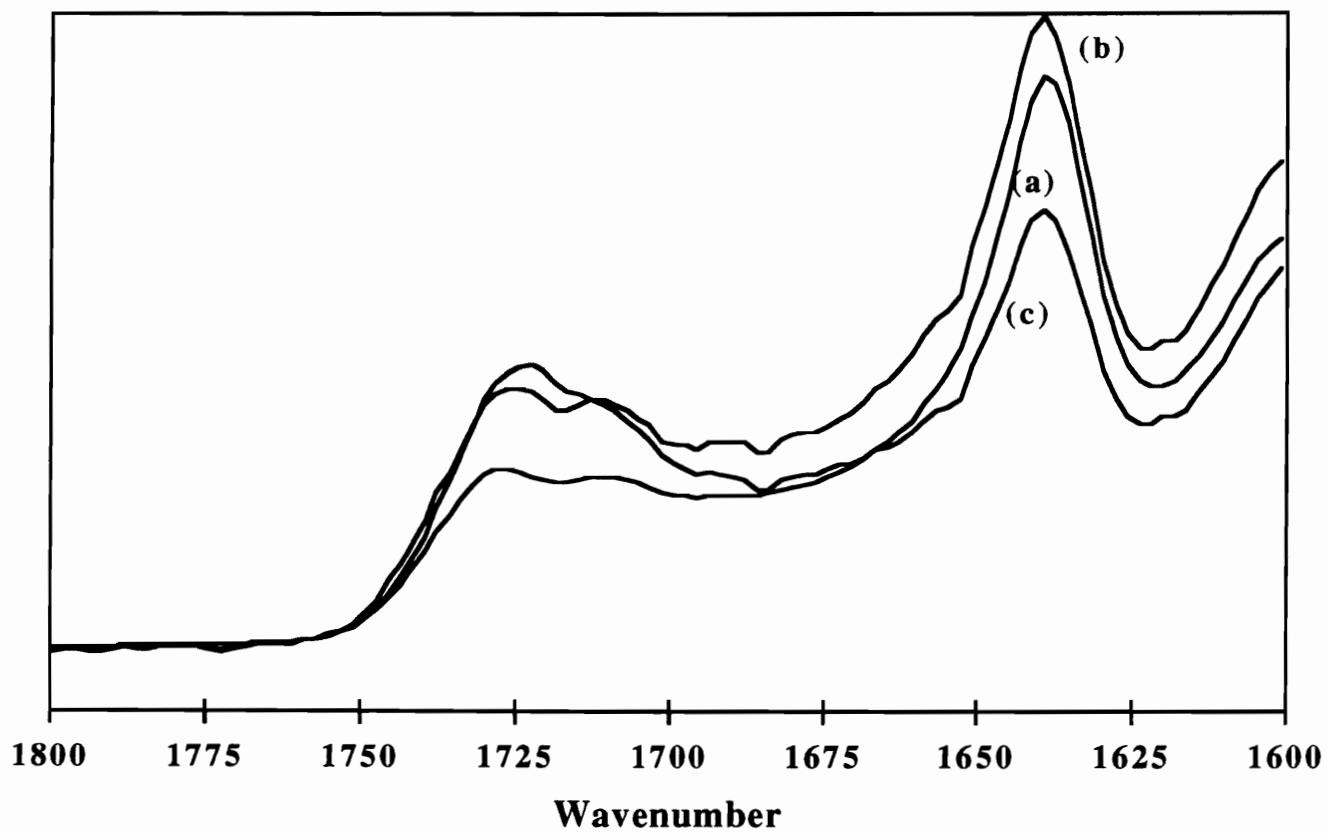


Figure 5.10. Influence of TDI index on bidentate absorbance (1640 cm^{-1}) in the FTIR spectra of foams (a) F85 and (b) F100, and (c) F110.

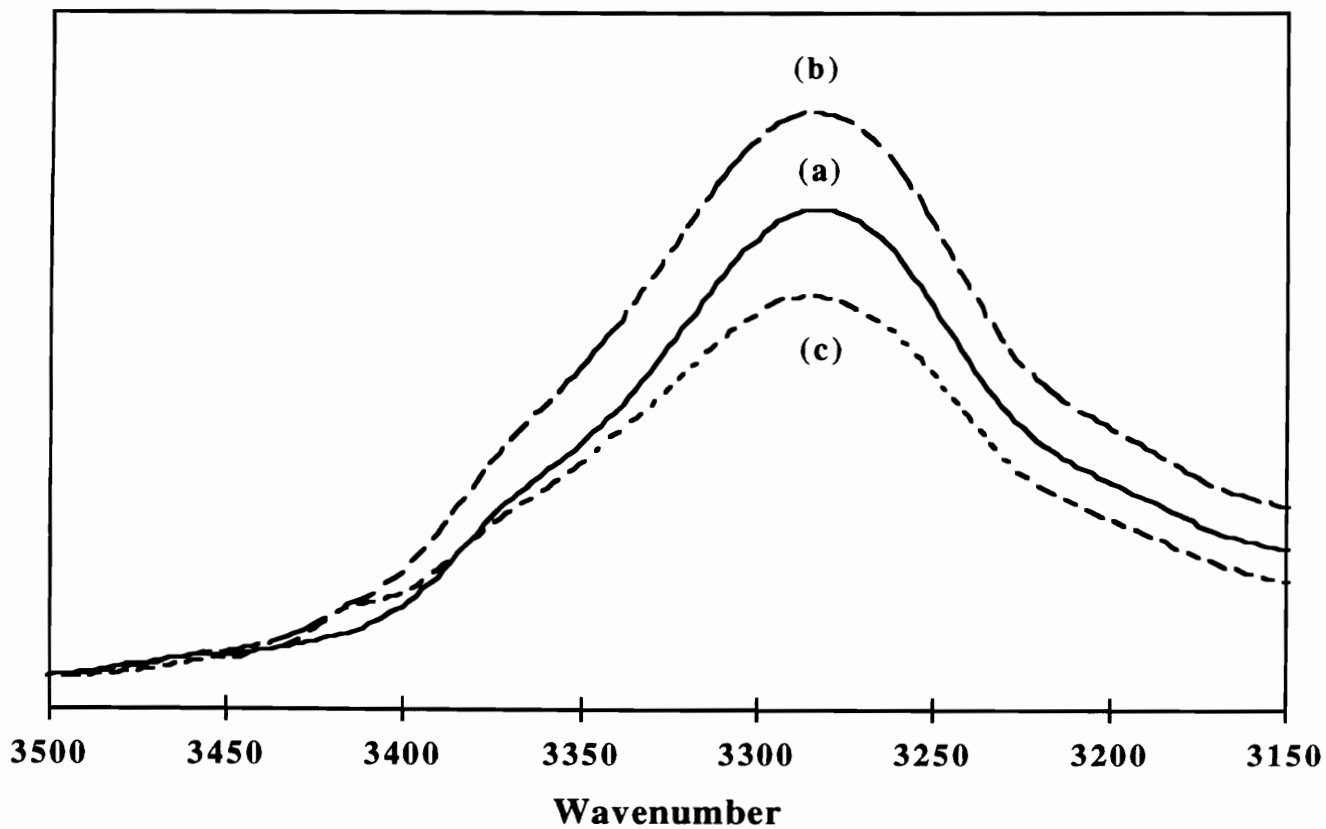


Figure 5.11. Influence of TDI index on the NH absorbance in the FTIR spectra of foams (a) F85 and (b) F100, and (c) F110.

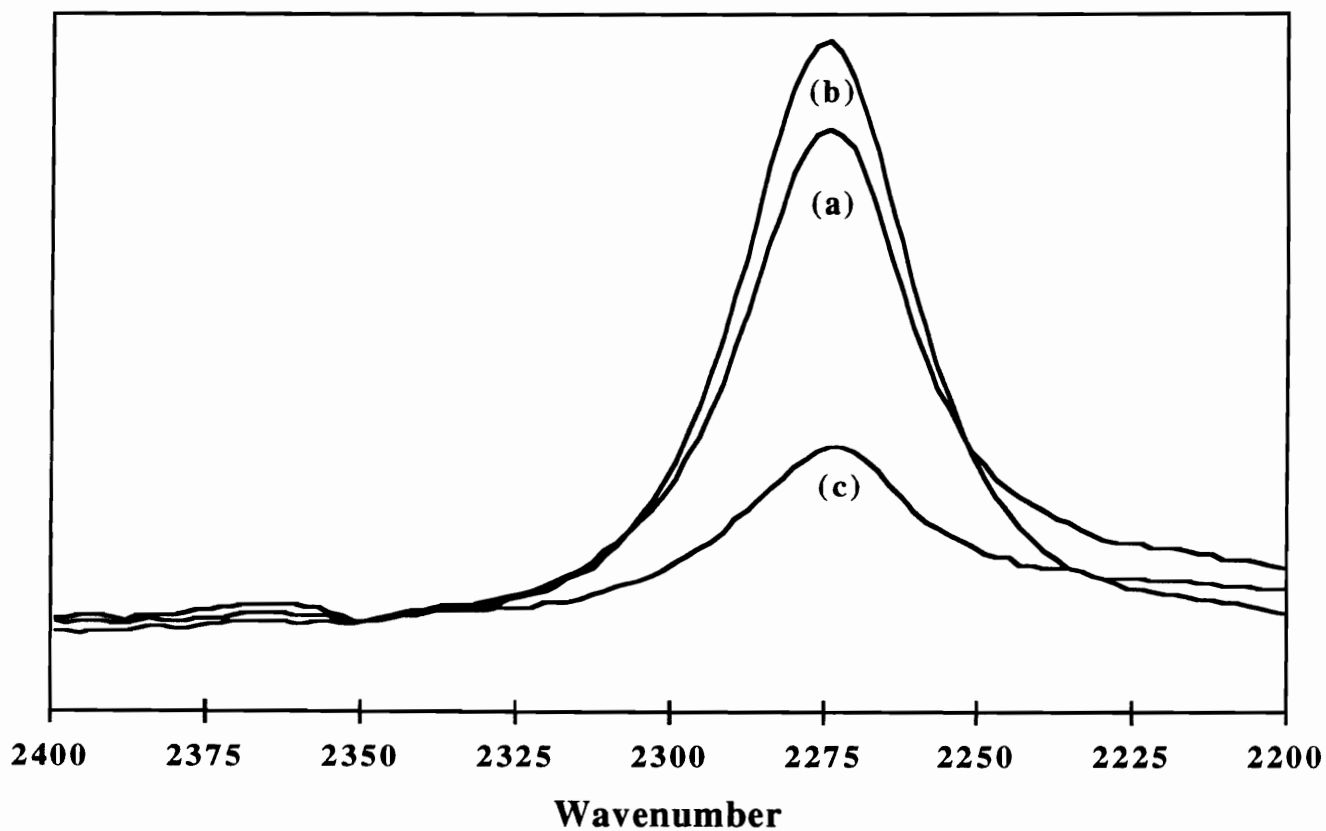


Figure 5.12. Influence of TDI index on the free isocyanate absorbance in the FTIR spectra of foams (a) F85 and (b) F100, and (c) F110.

isocyanate is also increased. Overall, the FTIR analysis further supports the conclusions of the WAXS behavior.

5.4 Effect of Index on the Mechanical Properties

The tensile properties were investigated to determine the influence of index on the modulus as well as the stress and strain at failure. The tensile stress-strain results carried out on dogbone foam samples are shown in Fig. 5.13. Surprisingly, Young's modulus of all foams (ca. 0.1 MPa) appears to be insensitive to the TDI index up to approximately 15% strain beyond which an increase in index leads to an increase in stress as a function of strain. Repetitive runs revealed the same behavior where the modulus did not change. As is well known, the hard segment domains as well as the covalent cross-linking strongly influence the mechanical properties. It is surprising and not well understood that the modulus is independent of both since both are influenced by the TDI index. Recall that Gibson and Ashby have related the modulus of a foam to the modulus of the solid portion as well as the reduced density. A speculation is that the small change in the solid portion modulus within the index range studied may not be reflected in the foam modulus. An insensitivity to cross-linking of the foam modulus was also observed by Thomas et. al.³⁶ The effect of index is more pronounced at strain levels beyond 15%. Both the stress at failure and strain at failure increased with index up to an index of 100 where they displayed a maximum. Foam F110 followed the same curve as F100 up to 75% strain (and a stress level of ca. 0.11 MPa) where it failed. F100 failed at a strain of ca. 140% with a stress of 0.1 MPa. Finally, F105 failed at a slightly higher stress (ca. 0.13 MPa) although the strain level was roughly the same. The maximum displayed by an index of 100 - 105 may be in part due to an increase in the concentration of urea groups and thus hard segment domains over that of lower index foam samples in addition to increased cross-linking. Further increases in index and thus cross-linking prevents elongation to the same extent as in F100

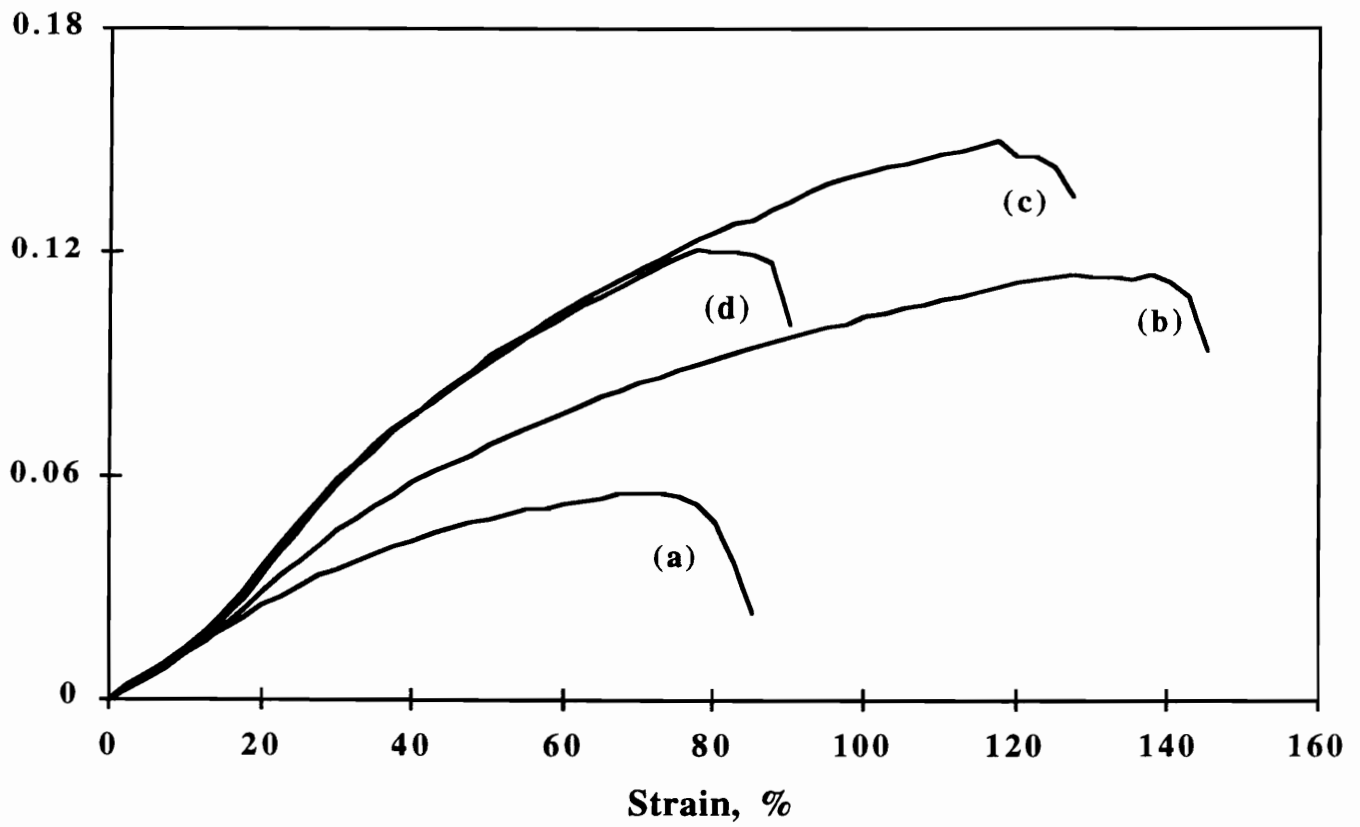


Figure 5.13. Tensile stress-strain behavior for the foam (a) F85, (b) F100, (c) F105, (d) F110.

or F105. In summary, the stress and strain at failure increased with index with the exception of the highest index foam which failed at a lower value of stress and strain than F100.

5.5. Influence of TDI Index on the Viscoelastic Behavior

The viscoelastic behavior was used to address the time-dependent behavior of these materials as well as the influences of the TDI index on this property. It was also measured to evaluate the influence of the physical "cross-links" in addition to the covalent cross-links. Figure 5.14 illustrates the load relaxation behavior for foam F85 as a function of temperature/humidity. As with the molded foams, both temperature and/or humidity "plasticized" the behavior. At 30°C-35%RH, the initial load was 1973g and decayed 43% to 1125g in the three hour loading period. At 100°C-35%RH, however, the initial load was 1373g, 30% lower than that at 30°C while the percent decay was roughly the same. As can be seen in Fig. 5.14, increasing the relative humidity also shifted the relaxation curves to lower loads. The initial load decreased from 1973g at 30°C-35%RH to 1435g at 30°C-98%RH. The percent decay increased slightly from 43% at ambient conditions to 46% at the highest condition which is also given in Table 5.3. As with the molded foams, this "plasticization" is attributed to the disruption of hydrogen bonds by temperature and/or humidity. Recall that the hydrogen bonding occurs predominantly within the hard segment domains but to some extent between urea, urethane, and ether soft segment groups. The degree of "plasticization" that occurs with temperature and humidity is evidence suggesting that the virtual "cross-links" play a very significant role in the properties of the foam at ambient conditions. This is especially true in this case where a relatively high water/TDI content was used resulting in a high urea content and hence a high hydrogen bonding content. For example, as was shown in Fig. 5.14, both high humidity and temperature resulted in a "pasticization" effect where increasing the humidity to 98%RH from 35%RH

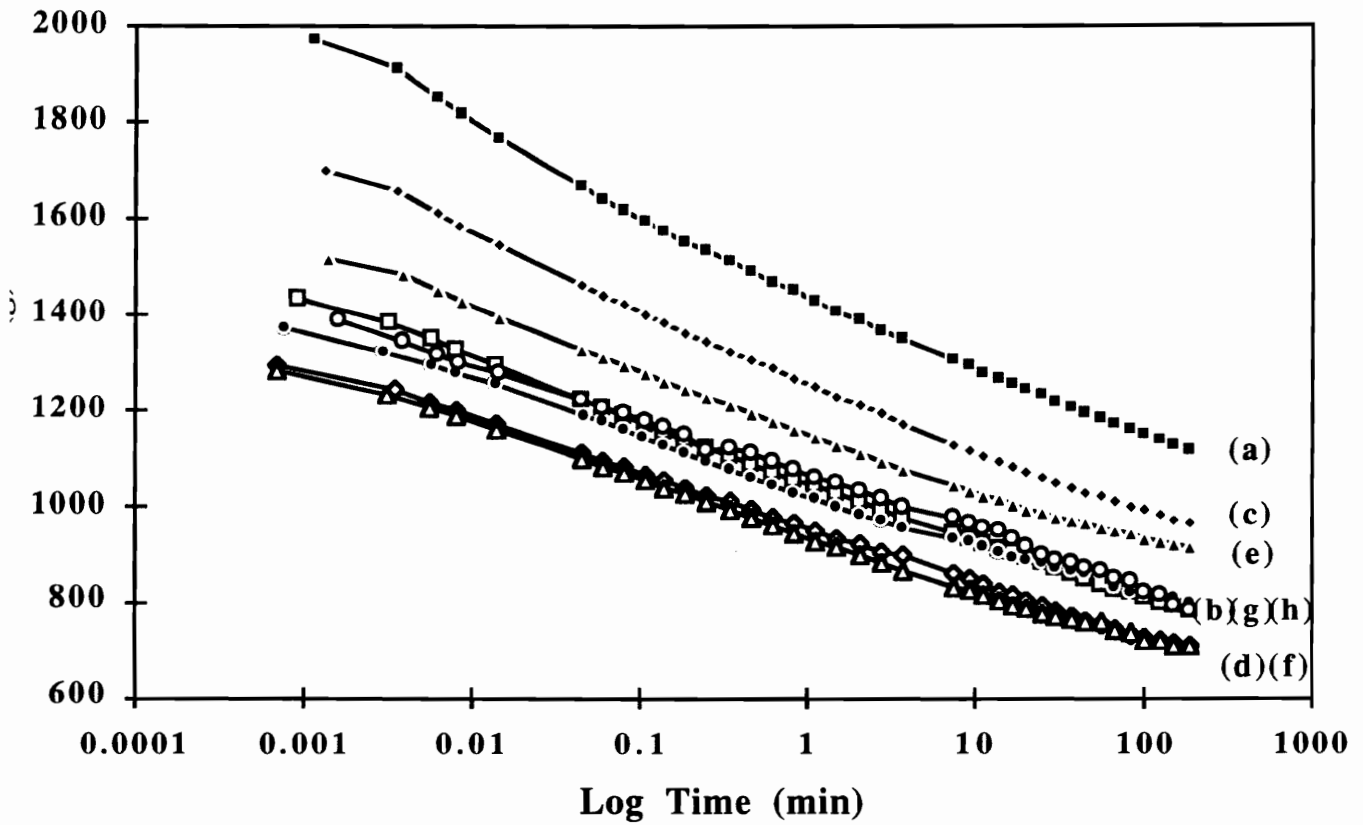


Figure 5.14. Load relaxation behavior of F85 as a function of temperature/relative humidity, (a) 30°C-35%RH, (b) 30°C-98%RH, (c) 50-35%RH, (d) 50-98%RH, (e) 80°C-35%RH, (f) 80°C-98%RH, (g) 100°C-35%RH, and (h) 100°C-98%RH.

Table 5.3. Summary of Load Relaxation Results for Three Foam Samples

F110

Temp-%RH (°C-%)	Init. Load (g)	% Decay (%)	Std. Dev. (±g)
30-35	4218	37.1	102
100-35	2899	31.6	82
30-98	3319	40.0	74
100-98	2799	38.5	21

F100

Temp-%RH (°C-%)	Init. Load (g)	% Decay (%)	Std. Dev. (±g)
30-35	3490	39.9	26
100-35	2847	29.2	50
30-98	3053	39.6	156
100-98	2420	39.0	71

F85

Temp-%RH (°C-%)	Init. Load (g)	% Decay (%)	Std. Dev. (±g)
30-35	1973	43.3	40
100-35	1373	41.7	39
30-98	1435	45.5	30
100-98	1387	43.4	20

shifted the curve to lower loads as did increasing the temperature from 30°C to 100°C at 35%RH. Both treatments reduced the initial load (at 30°C-35%RH) by ca. 30%. This behavior was very similar to that displayed by the molded foams (lacking CPPs) but was very different from that of the slabstock foams investigated by Moreland, both of which have been previously discussed. This implies that the hard segments domains (and their local packing) are critical in the foam properties and furthermore, the higher the HS content, the more "plasticization" occurs as the temperature or humidity is increased.

All of the six foams varying in index exhibited a similar response to increasing temperature and humidity and the differences between them are subtle. Therefore, the load relaxation results as a function of temperature and/or humidity of foams F90, F95, F100, and F105 are not shown. However, to portray the differences between the foams, the load relaxation behavior of the highest index foam is shown in Fig. 5.15. These results are illustrated in a similar manner to those of F85; as a function of temperature/humidity. With a few exceptions, the displayed behavior was similar to that of F85. The temperature and humidity "plasticized" the behavior to a great effect, but the initial loads were greater and percent decays were lower for F110 suggesting that this foam is stiffer than F85. Table 5.4 provides the initial loads and percent decays at each condition. As with the low index foam, humidity, in addition to temperature, "plasticized" the load relaxation behavior for F110, although to a somewhat lesser extent. For example, the initial load was 4218g at 30°C-35%RH and 2789 at 100°C-35%RH. At 30°C-98%RH this load was 3319g, ca. 20% lower than at 30°C-35%RH. Interestingly, the foams which exhibited the greatest resistance to either temperature or humidity were F100 and F105. An increase in temperature to 100°C reduced the initial load by ca. 20% and an increase in humidity to 98% reduced the initial load by ca. 15%. This is strong evidence of the importance of both a covalent network and well-ordered HS domains! Recall, that both of these foams were shown to exhibit a maximum in the covalent and physical network within the index range studied. Overall, all foams displayed a "plasticization" with temperature and/or humidity

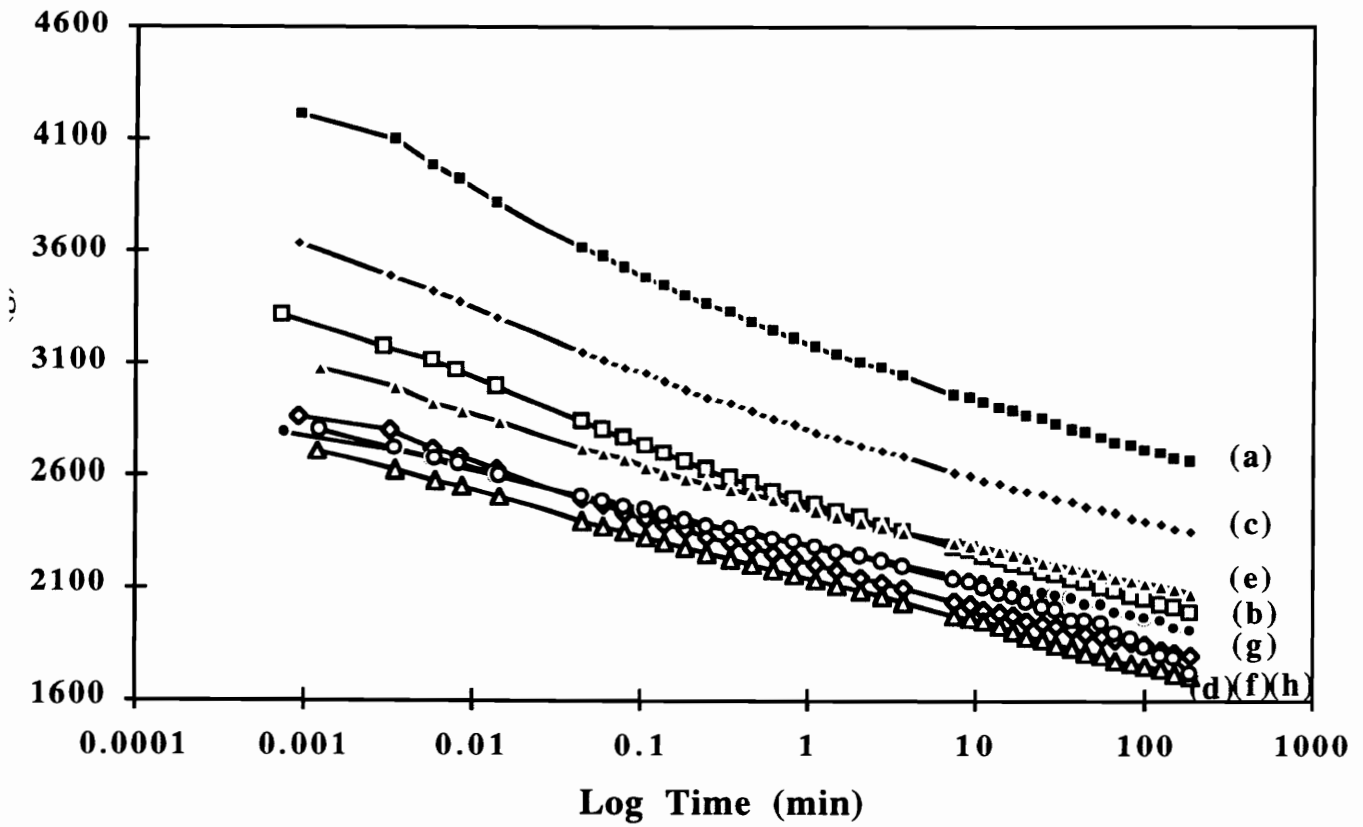


Figure 5.15. Load relaxation behavior of F110 as a function of temperature/relative humidity, (a) 30°C-35%RH, (b) 30°C-98%RH, (c) 50-35%RH, (d) 50-98%RH, (e) 80°C-35%RH, (f) 80°C-98%RH, (g) 100°C-35%RH, and (h) 100°C-98%RH.

suggesting that hydrogen bonding and thus the physical "cross-links" *still* play a significant role in the properties regardless of the amount of covalent cross-linking. In addition, the trend of increased cross-linking arising from the increasing index is clearly evident as is best shown by the following figures.

To directly observe the differences in load relaxation behavior as influenced by the index, the results were plotted as a function of index at a single environmental condition. For example, Fig. 5.16 displays the load relaxation results at 30°C-35%RH for all six foams. In general, an increase in index shifts the curves to higher loads. The initial loads increased and the percent decays decreased as is suggested in Table 5.3. Although there is some scatter in the data, a trend is clearly evident in Fig. 5.16. The initial load of the highest index foam was more than twice that of the lowest index foam. It appears that at this low temperature and humidity where hydrogen bonding contributed significantly, the curves group in pairs. The contribution of the two types of cross-links is high and therefore, small changes in index are not reflected in this relaxation property. However, when these hydrogen bonds were disrupted by either high temperature or humidity, the curves spread apart while maintaining the same trend as illustrated in Fig. 5.17. Here, at 100°C-35%RH, while the curves have all been shifted to lower loads relative to 30°C-35%RH, they still lie in a systematic order of increasing index with the exception of F105 and F110 being essentially indistinguishable. These two foams displayed very similar relaxation behavior throughout this study indicating that there is little difference between the two. At 30°C-98%RH, the initial loads were 1435g and 3319g for foams F85 and F110, respectively as shown in Fig. 5.18 and given in Table 5.3. These loads, although slightly higher than those at 100°C-35%RH, are again considerably lower than those at 30°C-35%RH depicting a strong softening effect by humidity. The trend with index was again the same where the curves systematically increased in load with increasing index with the exception of F110 and F105 being superimposed. Finally, Fig. 5.19 shows the load relaxation behavior at 100°C-98%RH and the trend with index is consistent with the trend

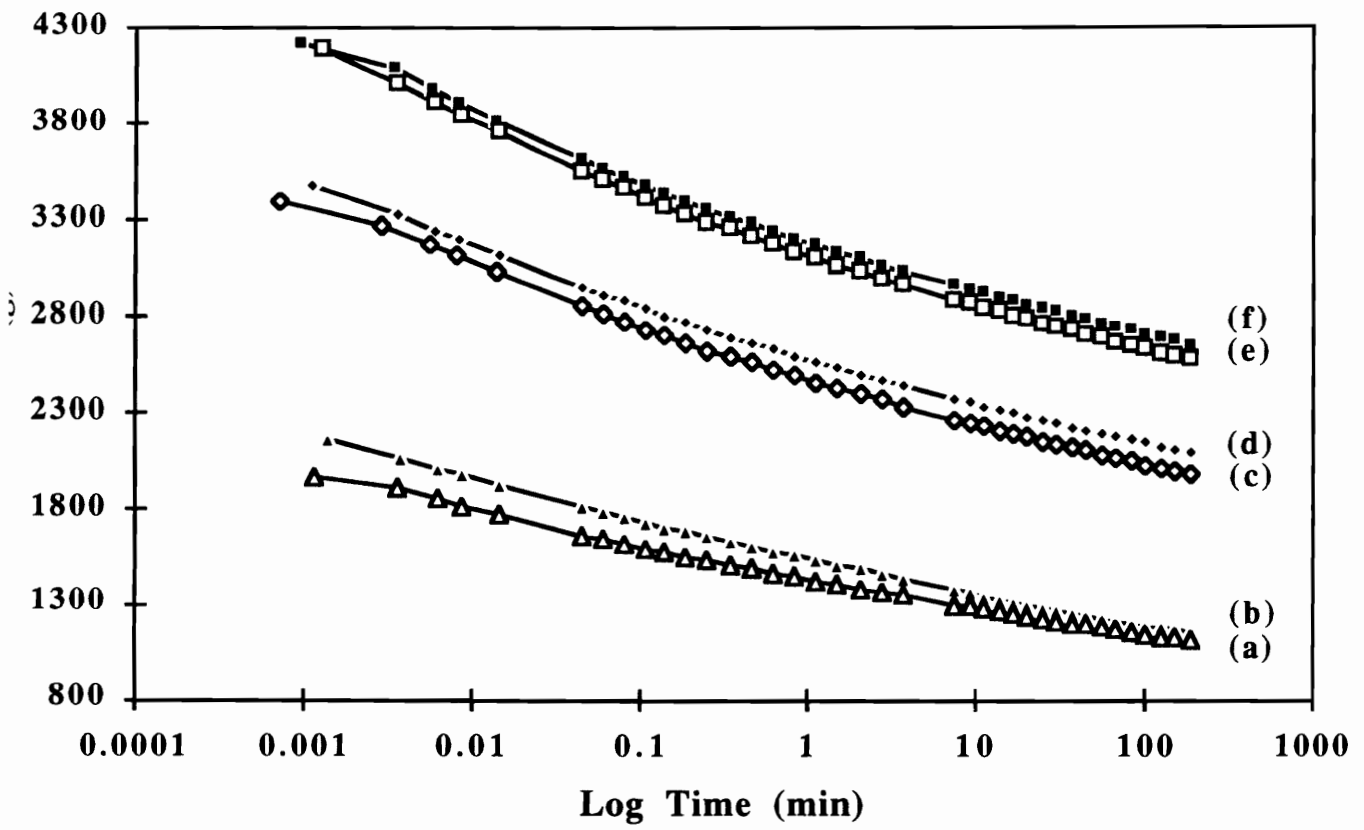


Figure 5.16. Load relaxation behavior at 30°C-35%RH of the foams varying in index (a) F85, (b) F90, (c) F95, (d) F100, (e) F105, and (f) F110.

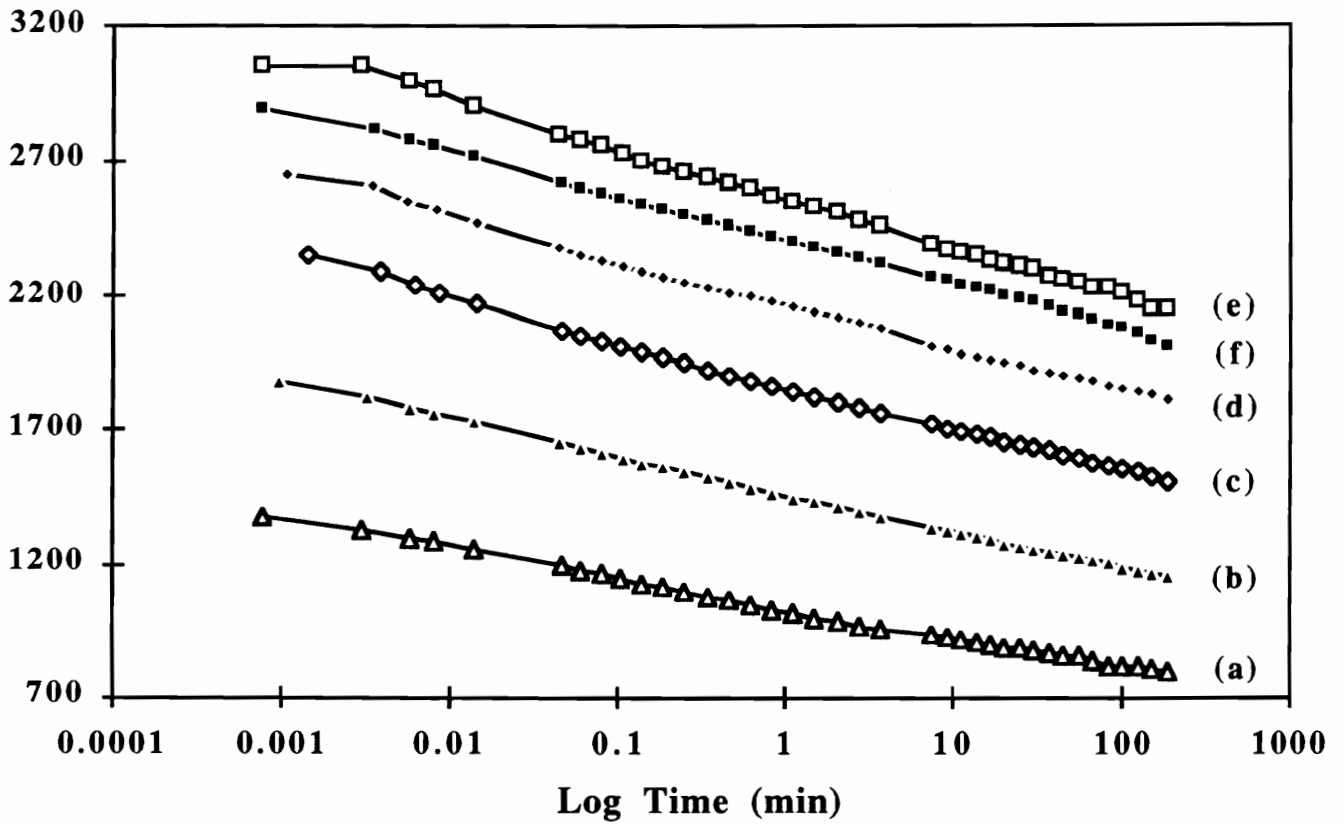


Figure 5.17. Load relaxation behavior at 100°C-35%RH of the foams varying in index (a) F85, (b) F90, (c) F95, (d) F100, (e) F105, and (f) F110.

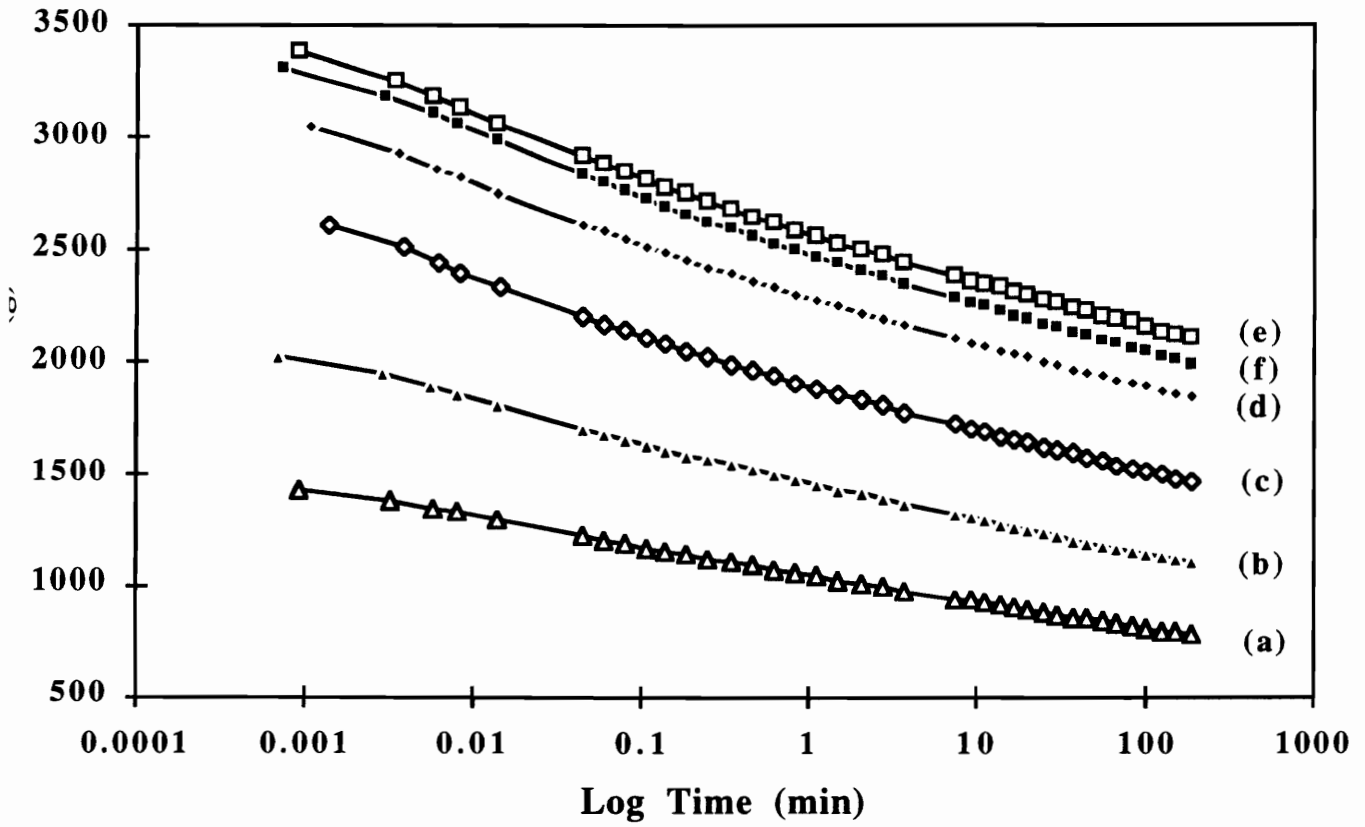


Figure 5.18 Load relaxation behavior at 30°C-98%RH of the foams varying in index (a) F85, (b) F90, (c) F95, (d) F100, (e) F105, and (f) F110.

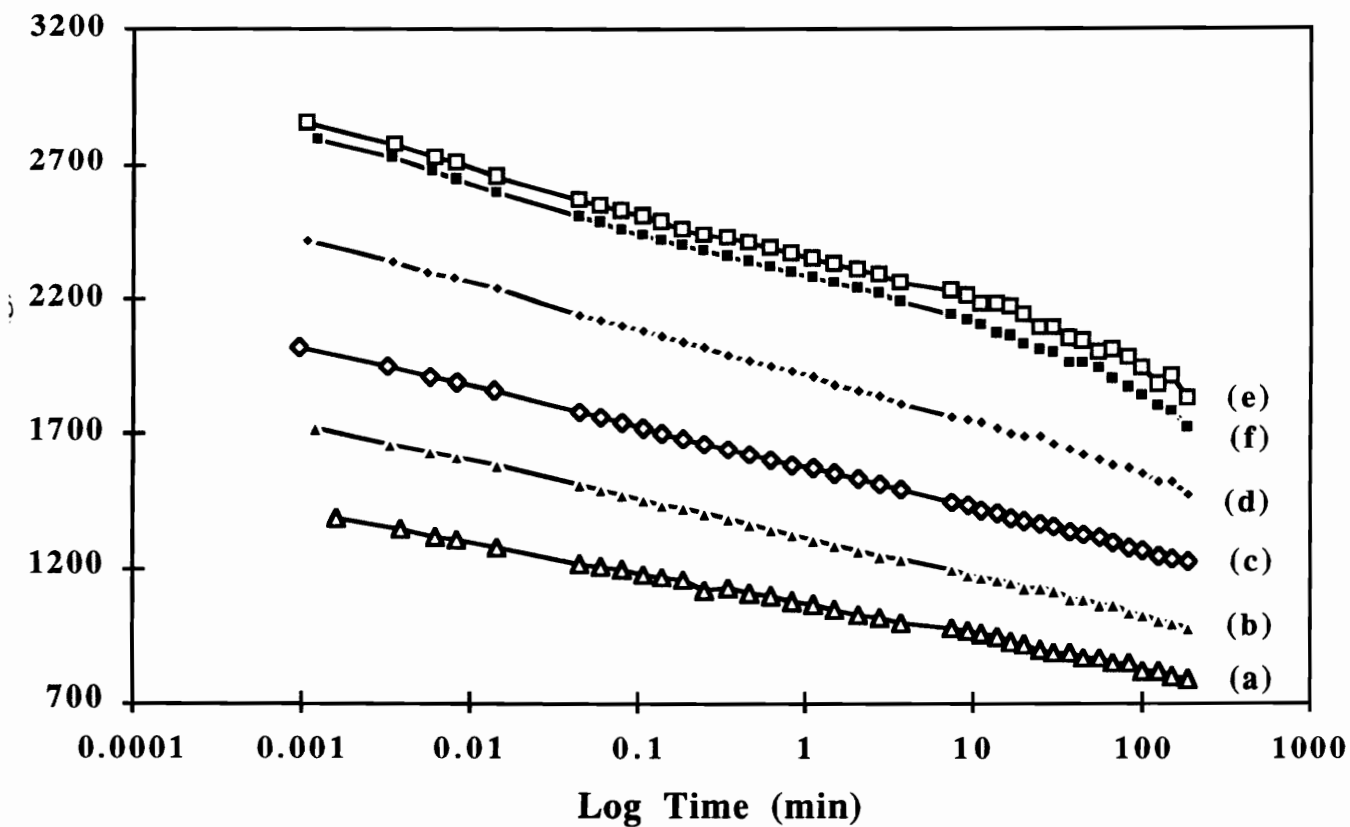


Figure 5.19. Load relaxation behavior at 100°C-98%RH of the foams varying in index (a) F85, (b) F90, (c) F95, (d) F100, (e) F105, and (f) F110.

at other conditions including the indistinguishability between the two high index foams, F110 and F105. It is noted that at this condition, the initial loads have been dramatically decreased with respect to ambient conditions, here being 1387g and 2799g for F85 and F110, respectively. All foams displayed similar softening effects at this condition where the initial loads decreased by ca. 30% relative to ambient conditions. In addition, the curves display some non-linear behavior (relative to the curves at ambient conditions) suggesting that the rate and amount of hydrogen bond disruption has been greatly accelerated. Nevertheless, the TDI index displayed a strong bearing on the load relaxation behavior especially at increased temperature and/or humidity.

The creep behavior as influenced by TDI index was also investigated at different environmental conditions. However, due to a strong influence of index on the stiffness of the foam, it was impossible to maintain a constant load through this series. To do so would have resulted in drastically different initial strains and thus different time-dependent behavior. Recall that Campell and Moreland et. al. have shown that the creep rates are very much dependent on the initial strain or region of deformation.^{80,79} Therefore, support that the index increased the foam stiffness as illustrated in the load relaxation behavior, was obtained by the fact that similar strains were displayed by the foams increasing in index yet the applied load was also increased. An attempt was made to maintain similar strains by adjusting the applied load. The creep response for the lowest index foam F85 and highest index foam F110 are shown in Fig. 5.20. In both figures, the strains lie in the range of 0.30 to 0.85 the latter being well into the densification range. However, the applied loads are very different where in the case of F85 a constant load of 1629g was applied and in the case of F110 a load of 3064g was applied, roughly twice that of F85. The load was required to increase with index in order to maintain strains in this range. Also evident in Fig. 5.20 is the large softening effects by temperature and humidity causing the data (and therefore the creep mechanism) to cross over from the buckling region into the densification region as noted by the dramatic change in the slopes of the curves.

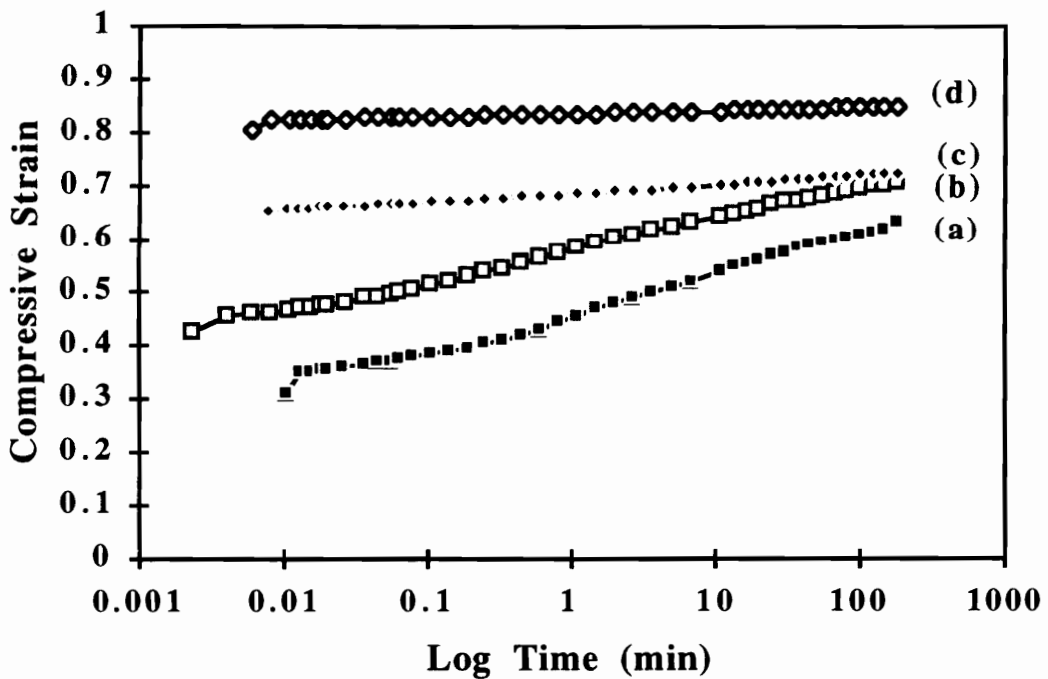
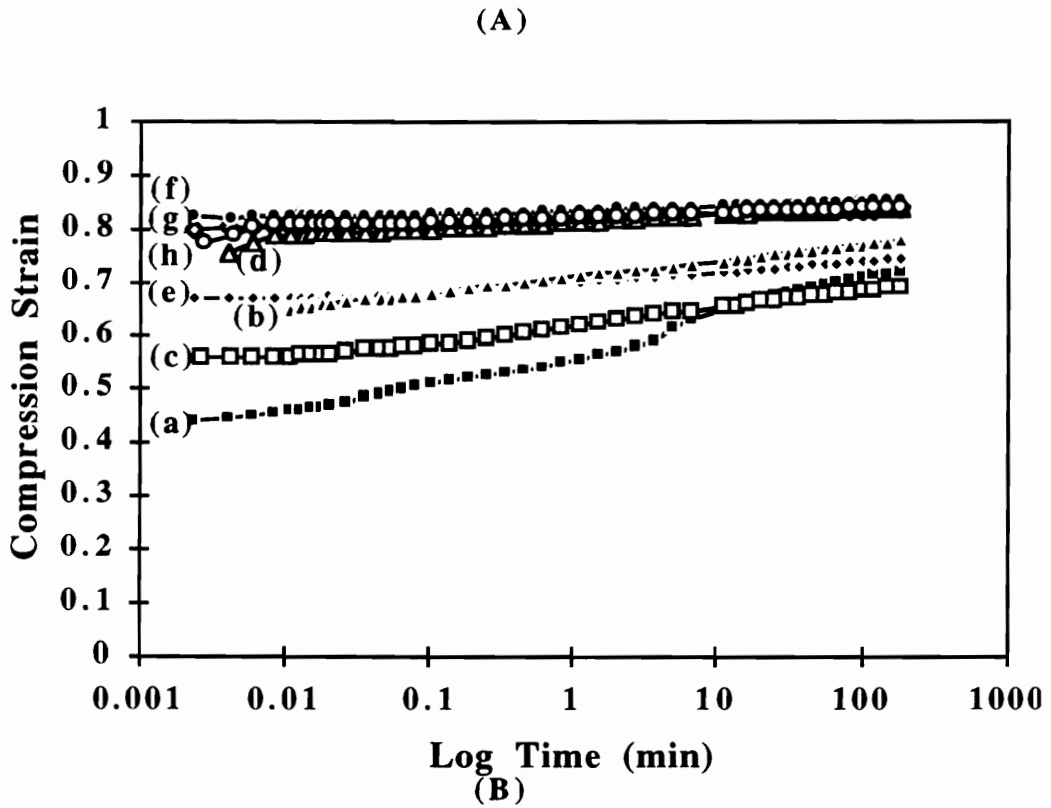


Figure 5.20 Creep response of (A) F85 and (B) F110 as a function of temperature/relative humidity, (a) 30°C-35%RH, (b) 30°C-98%RH, (c) 50-35%RH, (d) 50-98%RH, (e) 80°C-35%RH, (f) 80°C-98%RH, (g) 100°C-35%RH, and (h) 100°C-98%RH.

To further evaluate both the physical and covalent network of the foams as influenced by the index, they were subjected to 65% compression for three hours under the specified environmental conditions. The thickness of the foam was then measured and recorded relative to the original thickness. The compression set results are presented in Table 5.4. As expected, the amount of compression set systematically increased as the temperature or humidity was increased and especially when both variables were raised. The compression set increased from ca. 2% at ambient conditions to ca. 55% at 100°C-98%RH. The mechanism responsible for this compression set is the same as that behind load relaxation and creep. The "plasticization" by temperature and humidity occurs primarily in the hard segment domains due to disruption of the hydrogen bonding. Surprisingly, there appears to be very little influence on the compression set by the TDI index. All foams exhibited similar compression sets at each condition. The independent behavior of the compression set relative to index may be explained in terms of compression set (as other mechanical properties) being influenced by both the physical "cross-links" and the covalent cross-links which are both being altered by the varying TDI index. For example, at low index, not only is the covalent cross-linking low, but also the low hard segment content prevents the development of well ordered domains thereby making them easily plasticized. At high index, the additional covalent cross-linking was shown to prevent perfection of the domains by preventing diffusion of the hard segments into domains. The end result is again lower hydrogen bonding and easier plasticization. The influence of index is strongly projected in the compression set recovery which is driven by the soft segment elasticity. When comparing the thermally induced recovery results (@ 100°C), the effect of TDI index is very significant as shown in Fig. 5.21. As is well known, a covalent network significantly enhances the rubber elasticity effect. Therefore, the higher fraction of covalent, elastically active chains in the higher index foams allows the foam to recover toward its original state once the hydrogen bonds are "softened" by this high temperature. Furthermore, the high temperatures, in addition to "softening" the

Table 5.4. Compression Set Results of Foams Varying in TDI Index

Condition	F85	F100	F110
30°C-35% RH	1.7±0.0	2.5±0.2	2.2±0.1
30°C-98% RH	3.8±0.3	5.3±0.3	5.1±0.5
100°C-35% RH	15.2±1.6	12.2±2.0	12.0±0.5
100°C-98% RH	54.8±1.4	55.4±1.8	56.4±1.2

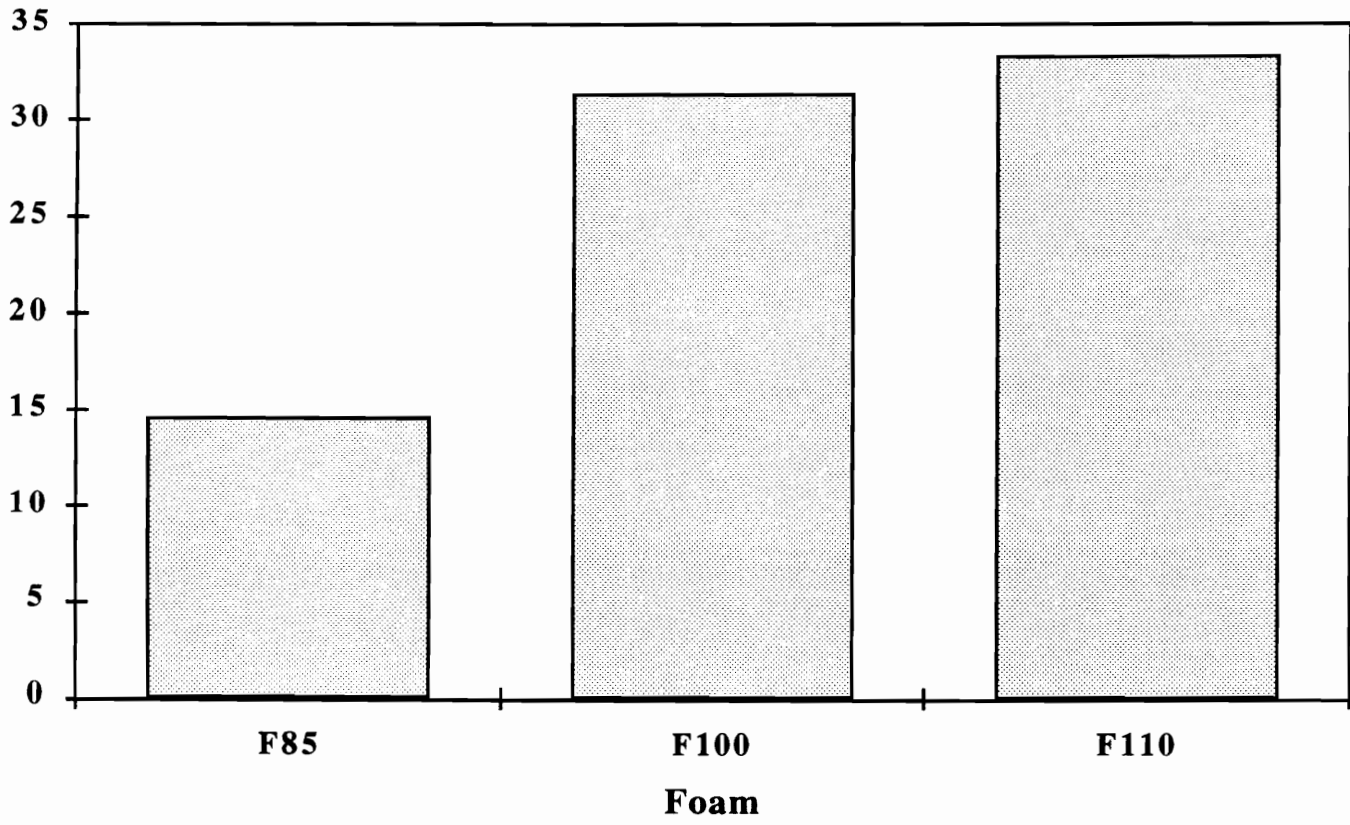


Figure 5.21 Compression set recovery as a function of index.

hydrogen bonds, increase the rubber elasticity effect further increasing the recovery of the compression set. The fact that as the index is increased, the amount of recovery is also increased, is strong evidence supporting the previously shown results of increased covalent cross-linking with higher index.

5.6 Summary

Flexible slabstock polyurethane foams were produced using a high water content formulation without the use of auxiliary blowing agents and varying levels of TDI to influence the softness of the foams. As the TDI index was increased, the "stiffness" of the material also increased suggesting that the higher index in the formulation resulted in a higher hard segment content and/or a higher covalent network. Solvent extraction experiments indicated that covalent cross-linking was a direct consequence of altering the TDI index. The amount of extract decreased systematically with increasing index. However, there was essentially no difference between the 100 index foam and the 110 index foam suggesting that the amount of cross-linking reached a maximum at about 100 index.

The mechanical and viscoelastic properties also complimented the above findings. The stress and elongation at break increased as a function of index with the exception of the highest index where the sample broke much earlier. The initial loads systematically increased with increasing index with the exception of the two highest index foams. Likewise, the percent decays systematically decreased with increasing TDI index. All foams were significantly "softened" by either temperature or humidity and especially both. Although the compression set properties appeared to be independent of TDI index, the different TDI index was clearly evident in the recovery experiments. Higher recovery from compression set was achieved for the higher index foams in a systematic fashion. The

increasing recovery with increasing index is attributed to and viewed as strong evidence for the direct correlation between the TDI index and covalent cross-linking.

Along with investigating the influence of index on the physical properties of polyurethane foams, it was desired to investigate its effect on morphology of these materials as well. SAXS results indicated that the lowest index foam had better phase separation than the highest index foam which displayed a lower intensity. This was supported by DSC and DMA measurements where the observed glass transition region in both techniques increased in temperature with increasing TDI index.

The level of short range ordering of the hard segments was studied by FTIR and WAXS which showed that the amount of well ordered bidentate urea dropped off either increasing or decreasing the index from 100. The 100 index foam displayed the highest amount of bidentate suggesting this material has the highest concentration of well organized hard segments. This evidence strongly supports the claim that the increased covalent cross-linking prevents hard segment domain perfection. WAXS results confirmed this claim which showed that increasing the index caused the rings, associated with short range order, to become more diffuse attributed to a disordering phenomenon.

Chapter 6

6.0 Mechano-Sorptive Behavior

Since water-blown flexible polyurethane foams are most widely used in load bearing applications that undergo transient moisture conditions such as seating material etc., the mechano-sorptive phenomenon is very important particularly in view of the high specific surface of these open cell structures. Recall that the effect of transient moisture had been reported to induce creep strains beyond those at constant humidity conditions, either high or low, in materials with the common characteristic of hydrogen bonding. In this study, compressive creep and load relaxation was monitored under cycling moisture conditions and constant temperature. While an increase in humidity is expected to promote increased creep, a decrease in humidity is expected to "plasticize" the hydrogen bonds to a lesser degree thereby slowing down the rate of creep. As will be shown, the contrary was observed which demonstrates that in attempting to predict the behavior in actual applications, static conditions may fall short since in most places, the environment is in a dynamic mode.

6.1 Effect of Transient Moisture Conditions on the Creep Response

Three foams were studied which showed many similar features as those observed for wood and wood based products under transient moisture conditions.^{99,100} Figure 6.1 shows the mechano-sorptive behavior for foam Fs4 under a constant load of 1558g. Curve (a) in Fig. 6.1 corresponds to the creep response of Fs4 under constant 10% RH. The initial strain is approximately 0.17 and extends to approximately 0.22 after 550 min typical of creep curves presented in Chapter 4. Curve (b) corresponds to the creep response under constant 98% RH. The behavior here is again typical of what is expected where the initial strain was 0.25 and increased to about 0.33 after 550 min. The final curve shown in this figure, curve (c), corresponds to cyclic moisture conditions beginning at 10% RH. The strain, initially 0.18, extends to 0.22 after 60 min. at which point the humidity was increased to 98% RH. During this time the largest increase in strain was observed, i.e. the strain increased to 0.32 followed by a decrease in the creep rate as noted by a near flat response. As the humidity was then decreased to 10%, the strain rapidly increased to 0.34. The second cycle began with absorption where no increase in strain was displayed until the onset of desorption when the strain increased to 0.36. Interestingly, subsequent absorption steps did not display increases in strain although subsequent desorption steps did and the strain level reached 0.38 after 550 min.; higher than it did at a constant 98%RH. These results are very similar to those obtained by other researchers on cellulose based materials as well as other exhibiting hydrogen bonding. This point will be addressed later.

The results of transient moisture conditions on the higher hard segment foam, Fs5, are illustrated in Fig. 6.2. As can be observed, the compressive strain under a constant load of 1900g, follows the same trend as foam Fs4. Curve (a) in Fig. 6.2 is the creep response under constant 10% RH. The strain increased from an initial value of 0.20 to 0.36 after 600 min. Curve (b) represents the creep response under constant 98% RH. Here the strain level increased from 0.34, initially, to 0.50 in the same time period. Curve (c) represents the effect of transient moisture conditions on the creep response of Fs5. The response observed here was similar to that of foam Fs4. That is, the first absorption cycle

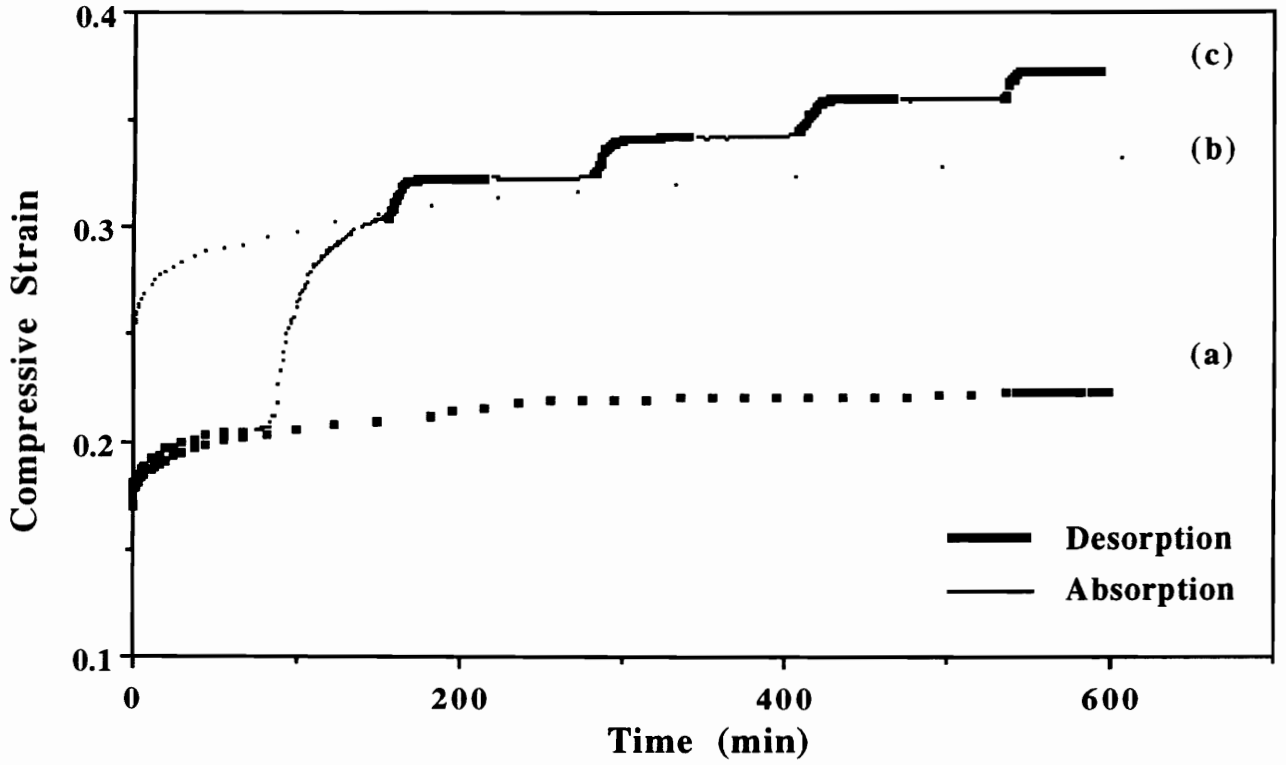


Figure 6.1. Mechano-sorptive behavior for slabstock foam Fs4 under a constant load and temperature (40°C). Curves correspond to (a) constant 20%RH (b) constant 98%RH, and (c) cyclic moisture conditions.

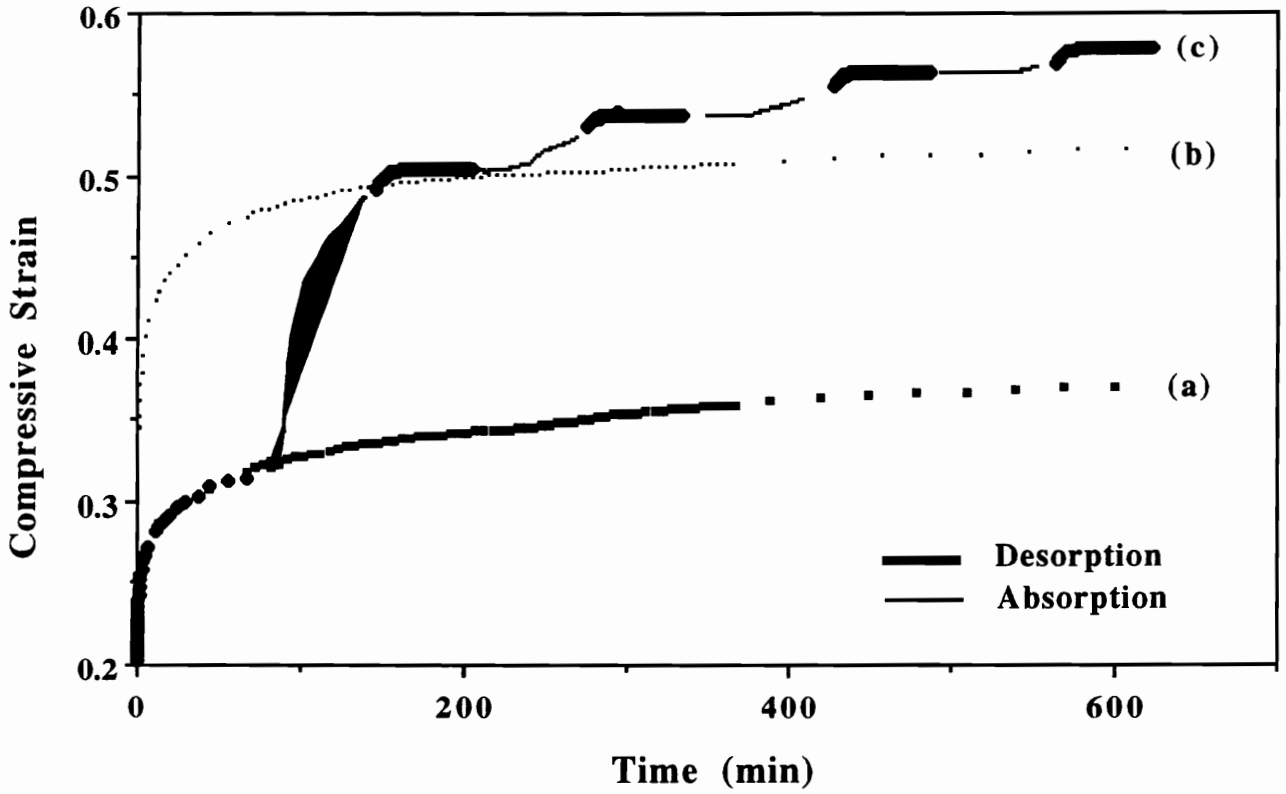


Figure 6.2. Mechano-sorptive behavior for slabstock foam Fs5 under a constant load and temperature (40°C). Curves correspond to (a) constant 20%RH (b) constant 98%RH, and (c) cyclic moisture conditions.

displayed the biggest increase in strain as did each desorption step thereafter. The only exception here was that small increases in strain were observed during subsequent absorption steps which may be a result of the higher applied load. The final strain for this material reached a final level of 0.58 after 600 min.; again much higher than that at a constant 98%RH .

A similar creep experiment was carried out on a molded foam in view of their different structure and properties determined earlier. Figure 6.3 illustrates the mechano-sorptive behavior displayed by the molded foam, Fme2, under a constant load of 684g. As in the previous cases, curve (c) representing the strain response under transient moisture conditions exceeds the strain in each case (low or high RH) where the humidity was held constant. For example, the final strain under transient moisture conditions was 0.38 where under a constant 98%RH it was 0.34. With respect to curve (c) obtained under transient moisture conditions, the increases in strain were displayed only during desorption cycles and the first absorption cycle. The increasing strain level continued as the moisture cycling occurred until a point was reached where the covalent network of the foam accommodated the stress. Further increases in strain led to densification of the foam which is due to the compression of the struts and remaining cell texture into a less porous solid.

The mechano-sorptive phenomenon observed in Figs. 6.1 to 6.3 is due to the polar water molecules interacting with hydrogen bonds within the solid portion of the foams - particularly the hard segment regions. As illustrated in the simplified morphological model given in Fig. 6.4, this causes hydrogen bonds to be formed between the molecular structure of the foam and the water molecules thereby disrupting or loosening portions of the intermolecular forces within the foam and hence, causing slippage and creep. In desorption, these hydrogen bonded regions with water are again disrupted or temporarily broken as the water diffuses from the system leaving increased regions of free volume thereby causing the foam to once again be less resistant to creep. The flux of water molecules into or out of the cellular structure, whether in absorption or desorption, disrupts

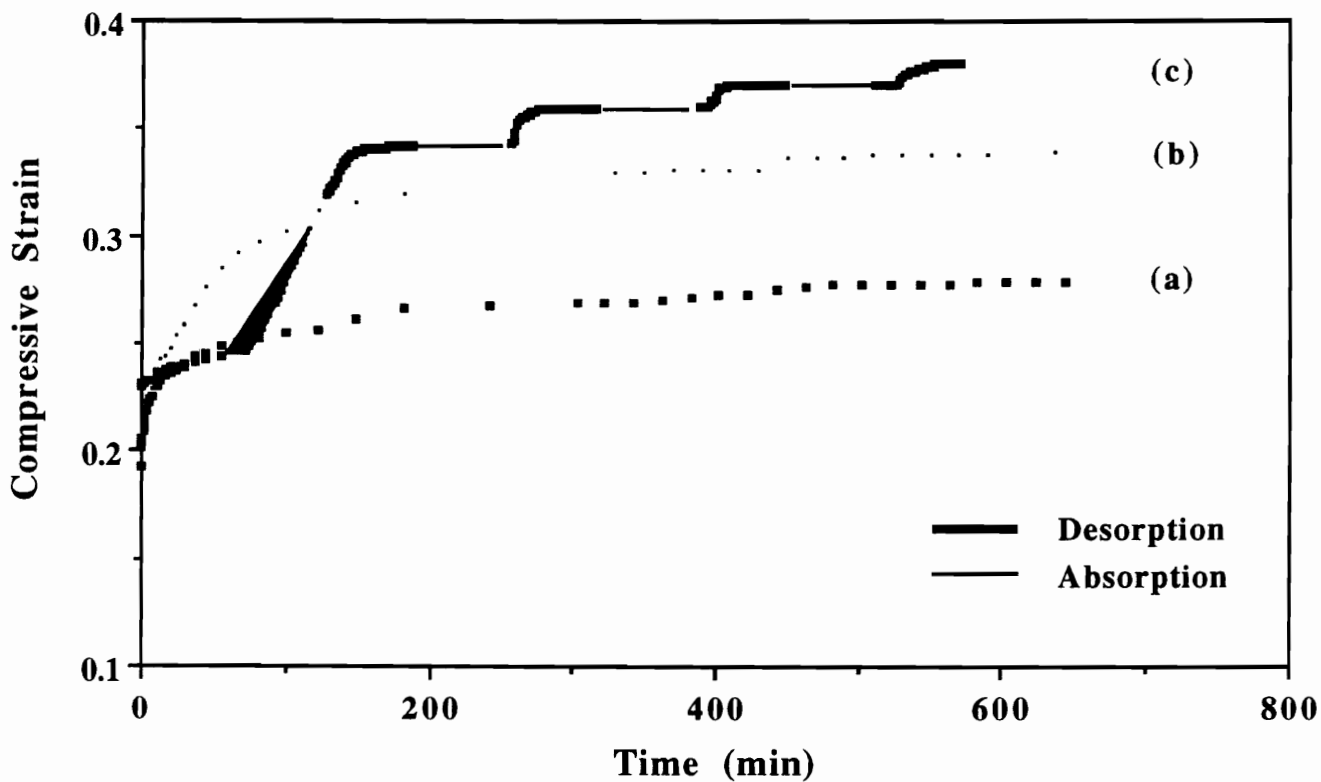


Figure 6.3. Mechano-sorptive behavior for slabstock foam Fme2 under a constant load and temperature (40°C). Curves correspond to (a) constant 20%RH (b) constant 98%RH, and (c) cyclic moisture conditions.

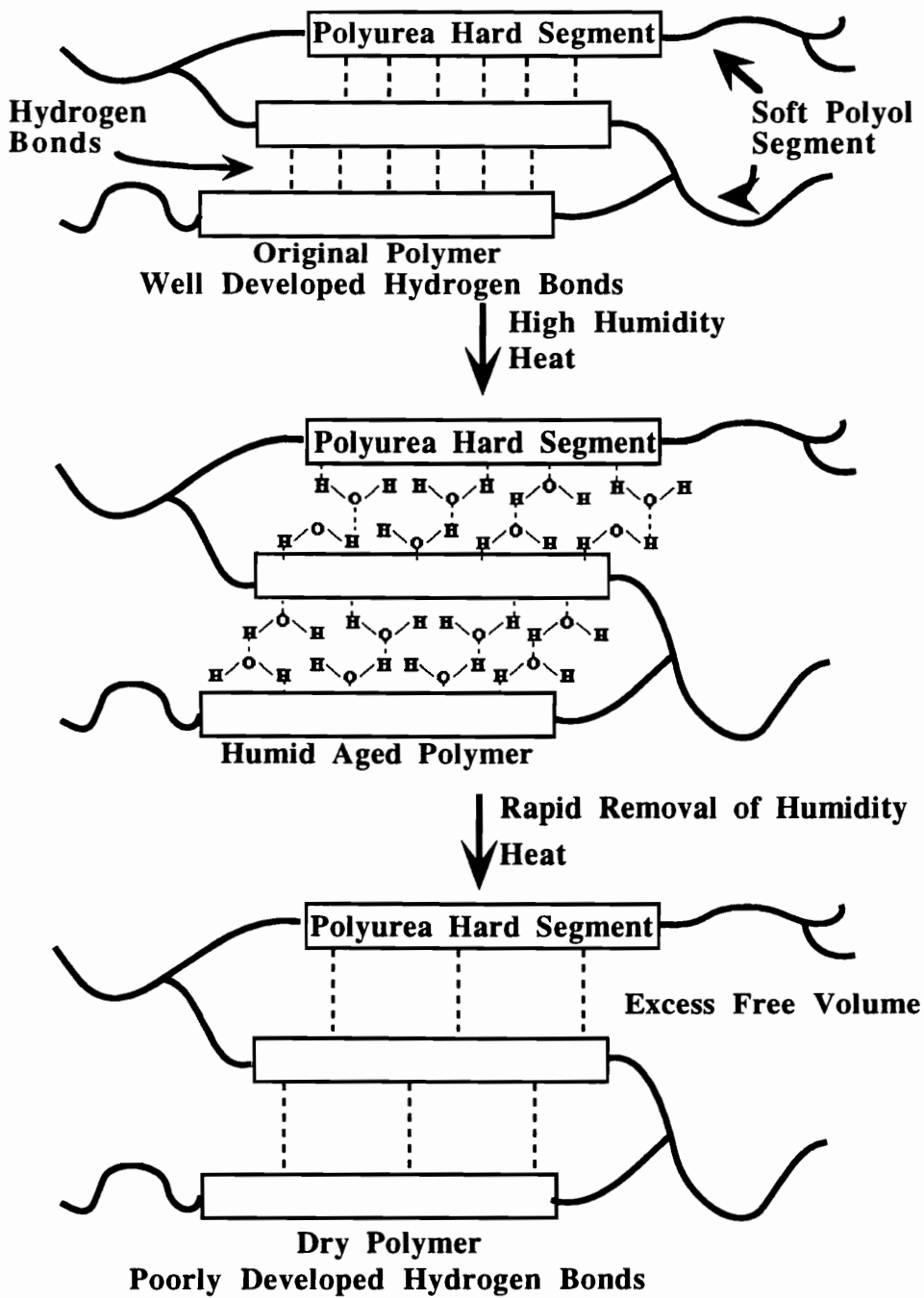


Figure 6.4. Simplified morphological model illustrating the mechanism behind the observed mechano-sorptive behavior.

the dynamic equilibrium of the hydrogen bonds causing bonds to be temporarily broken and reformed and, in turn, promotes greater molecular mobility or creep within the mechanically loaded foam. Also, shrinking and swelling may have a small effect on the creep behavior as well - particularly swelling at high humidity in the case of soft foam structures. In absorption, the foam may actually swell a small amount causing the strain to remain nearly unchanged - recall that during the latter absorption cycles, no significant creep occurred. In addition, the degree of this behavior is dependent upon the load as well as the nature of the foam. Restated, the molecular interactions between the water and the foam which tend to promote creep may be somewhat balanced by the swelling of the foam during absorption. In desorption, swelling is not expected to occur and thus the creep strain increases. For example, a similar mechano-sorptive experiment was performed on Fs5, however it was carried out at a high temperature (90°C) and under a lower applied load (1560g) than for the results shown earlier in Fig. 6.2. The creep response of this foam is shown in Fig. 6.5 which reveals a similar behavior to that in Fig. 6.2 with the exception that in this case, a small recovery was displayed during absorption cycles after the first. Here, since the temperature is higher (requiring considerably more water vapor) and the load is lower, the swelling pressure of the absorbed water may exceed the creep force thereby inducing a slight recovery and thus decreasing the creep strain. This exhibited behavior offers support that the lack of creep observed earlier during absorption is most likely a result of swelling and also dependent on the applied load. The mechanism proposed here is basically in agreement with that proposed by previous authors describing observed behavior on wood and wood based materials with the exception that the present approach emphasizes that changes in the time dependent free volume are also important - particularly as a result of desorption.

In view of the proposed model, a similar experiment was carried out on a molded foam Fme2 (shown to be easily "plasticized" by temperature and humidity relative to slabstock foams) at a higher temperature where the hydrogen bonding is more mobile. The

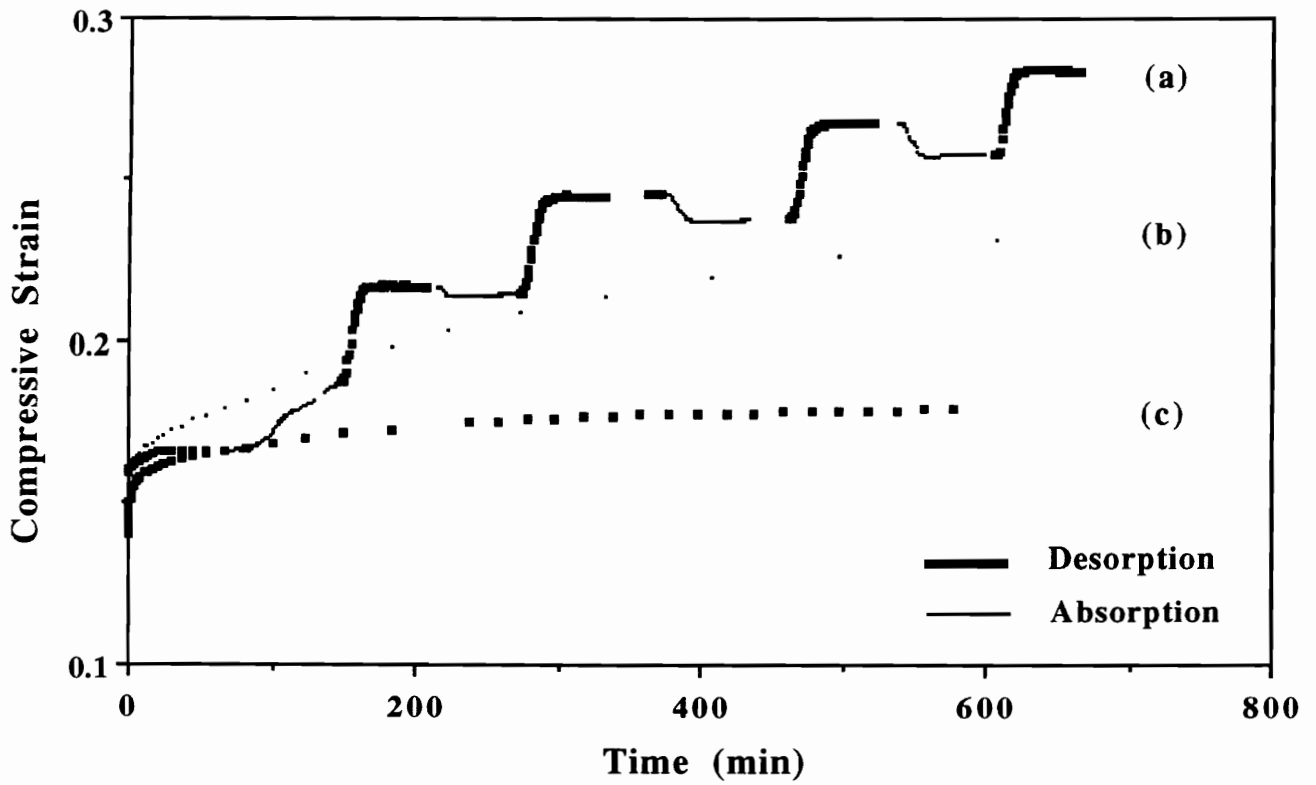


Figure 6.5. Mechano-sorptive behavior for slabstock foam Fs5 under a lower constant load and a high temperature (90°C). Curves correspond to (a) constant 20%RH (b) constant 98%RH, and (c) cyclic moisture conditions.

mechano-sorptive behavior was less evident in the sense that the creep level under cyclic humidity does not exceed that at the highest constant humidity. As can be observed in Fig. 6.6, the creep response displayed at constant 98% RH was indeed very similar to that obtained under cyclic humidity conditions in the sense that the strain levels were nearly the same. At this temperature, the hydrogen bonds within the foam are much more labile than at the earlier lower temperature of 40°C. The weaker hydrogen bonded structure in this system at the high temperature, coupled with the high humidity further "plasticize" the foam causing strain levels to exceed those in Fig. 6.3. In Fig. 6.3, the strain levels for curves (b) and (c) reached 33% and 38% ,respectively. However, in Fig. 6.6, the strain levels for curves (b) and (c) reached 55% and 57%, respectively. The increased strain levels along with the similar response on curves (b) and (c) of Fig. 6.6 further support the proposed mechanism.

Further support for the importance of the free volume as well as surface area such as that exhibited by foams as well as from the cellular structure of wood is given in Fig. 6.7 which illustrates the creep response of a noncellular polyurethane elastomeric film in tension under transient moisture conditions. The displayed response is similar in the sense that increases in strain occurred in a step-wise manner but these increases occurred only during absorption, not desorption. Following the first cycle at 10%RH, only absorption steps produced further strain. Both the "plasticization" of hydrogen bonds and slight swelling that occurs with the absorption of water, contributed to the increase in creep strain. During desorption, the *slow* diffusion of water out of the material allows for the re-establishment of hydrogen bonds with no observed changes in strain. Since these films lack the cellular structure and large surface area of foams which makes the diffusion of water in and out slower.

6.2 Effect of Transient Moisture Conditions on the Load Relaxation Behavior

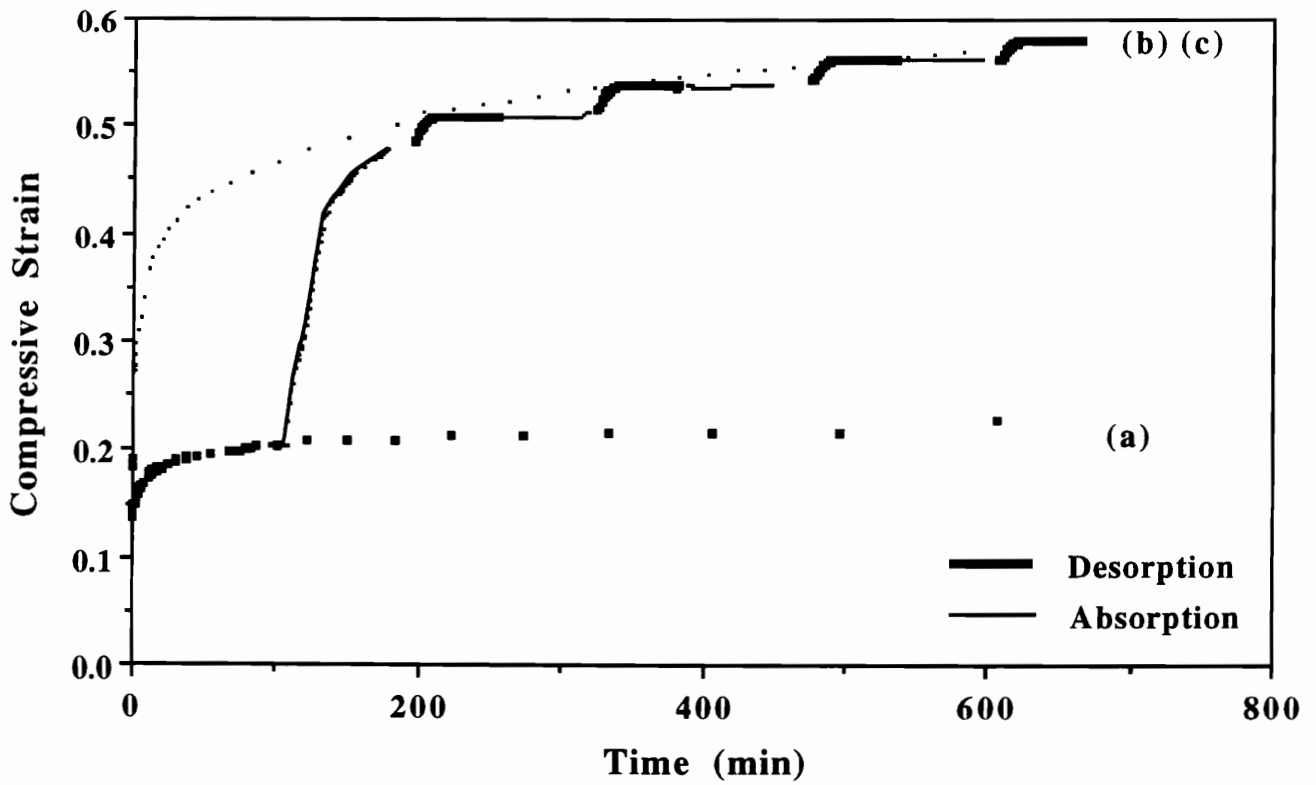


Figure 6.6. Mechano-sorptive behavior for slabstock foam Fme2 under a constant load and a high temperature (90°C). Curves correspond to (a) constant 20%RH (b) constant 98%RH, and (c) cyclic moisture conditions.

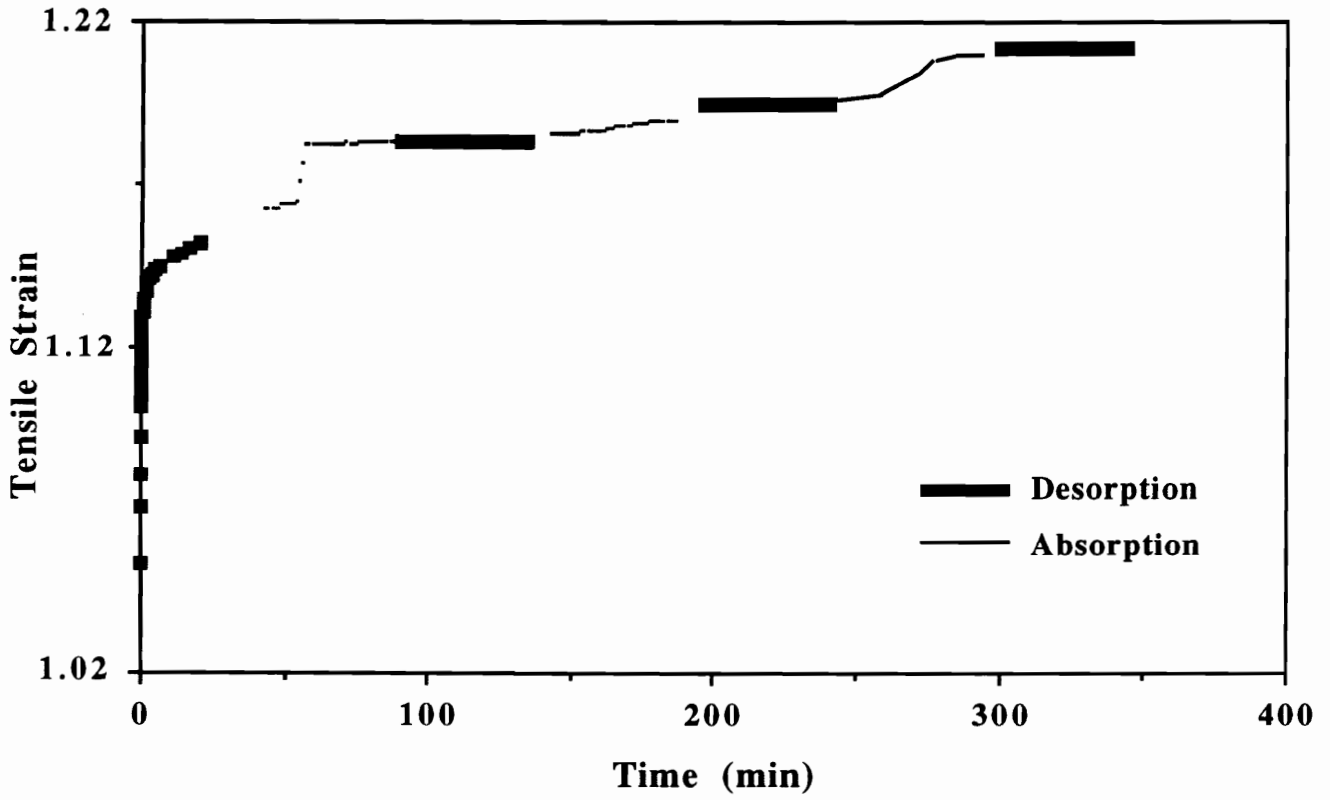


Figure 6.7. Mechano-sorptive behavior for a polyurethane elastomer under constant load and temperature (40°C), but cyclic moisture conditions.

A comparison of the creep response under transient moisture conditions to the load relaxation behavior under transient moisture conditions was carried out to obtain further support of the proposed mechanism. This involved compressing the foam to 65% in the same manner as for the load relaxation results described in Chapter 4. While the temperature was held constant, the humidity was cycled from 10%RH to 98%RH while the load was monitored.

The results of the 65% compression load relaxation experiment under transient moisture conditions are displayed in Fig. 6.8 which are very similar to the observed behavior under creep loading. Following the initial dry loading (showing typical decay in load), the first absorption cycle produced a step-like decrease in load and thereafter, only the desorption steps displayed decreases in load for during absorption the load always increased. At 40°C, the load decreased from ca. 2000g to 1600g during the initial low humidity cycle. During the following absorption cycle, the load decreased to ca. 1400g and then during the following desorption cycle, the load further decreased to ca. 1150g. Each subsequent absorption step results in a ca. 200g increase in load while each subsequent desorption step resulted in a ca. 250g decay in load thereby leading to an overall decay of the load with time. The recovery or increase in load during absorption is due to a swelling pressure which has a greater impact in load relaxation than creep due to the greater sensitivity in small changes in the displayed load. Thus this pressure overrides the softening effect resulting from the disruption of the hydrogen bonds. As the water is removed, the excess free volume as well as the disruption of the newly formed hydrogen bonds between the molecular structure and water molecules induce significant decreases in load. The behavior was the same at 90°C with only the curve being shifted to lower loads as illustrated in Fig. 6.9. At 40°C, the initial load was ca. 2000g and the final load was ca. 980g while at 90°C, the initial load was ca. 1580g and the final load was ca. 700g. The trend was the same, where except for the first absorption, each absorption step produced an

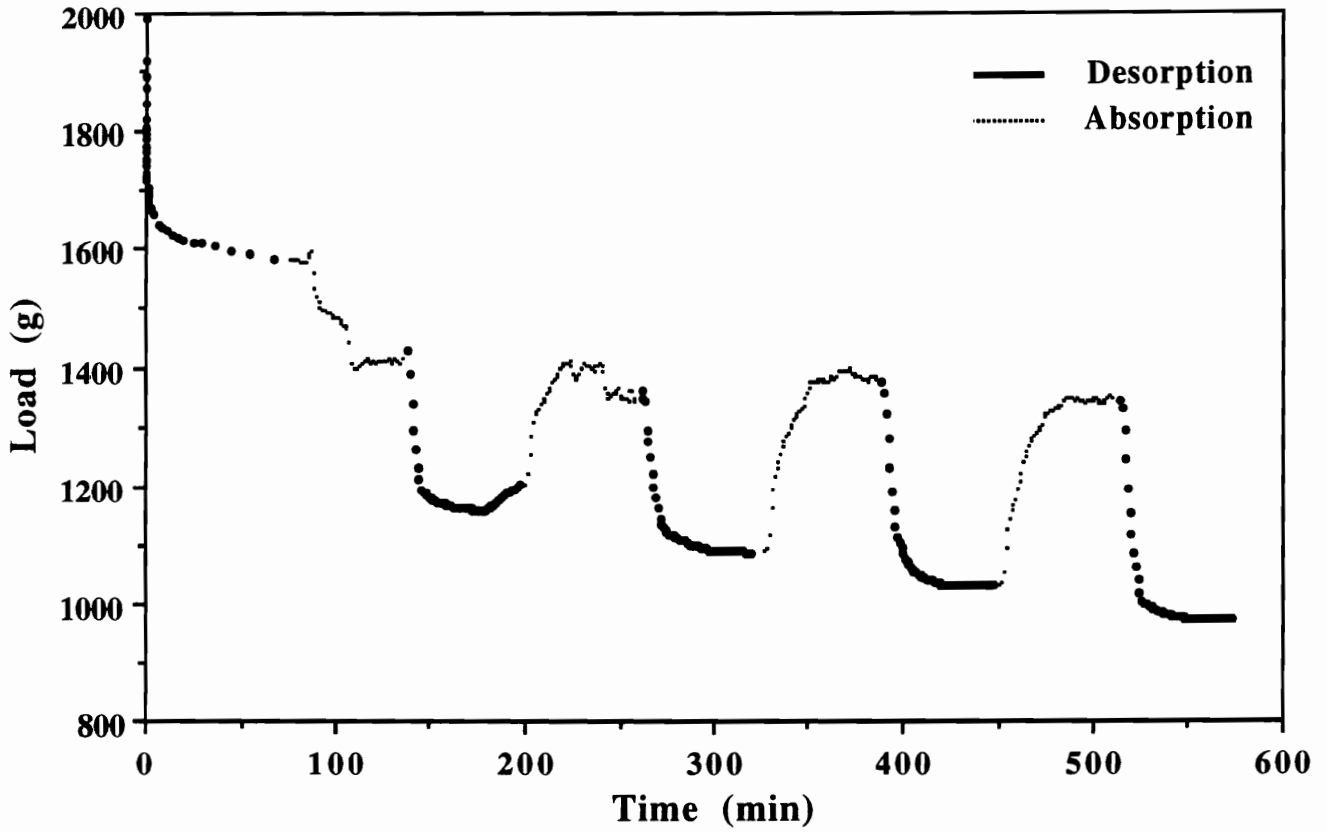


Figure 6.8. Influence of cyclic moisture conditions on the load relaxation behavior of Fs5 at a constant 65% strain and constant 40°C.

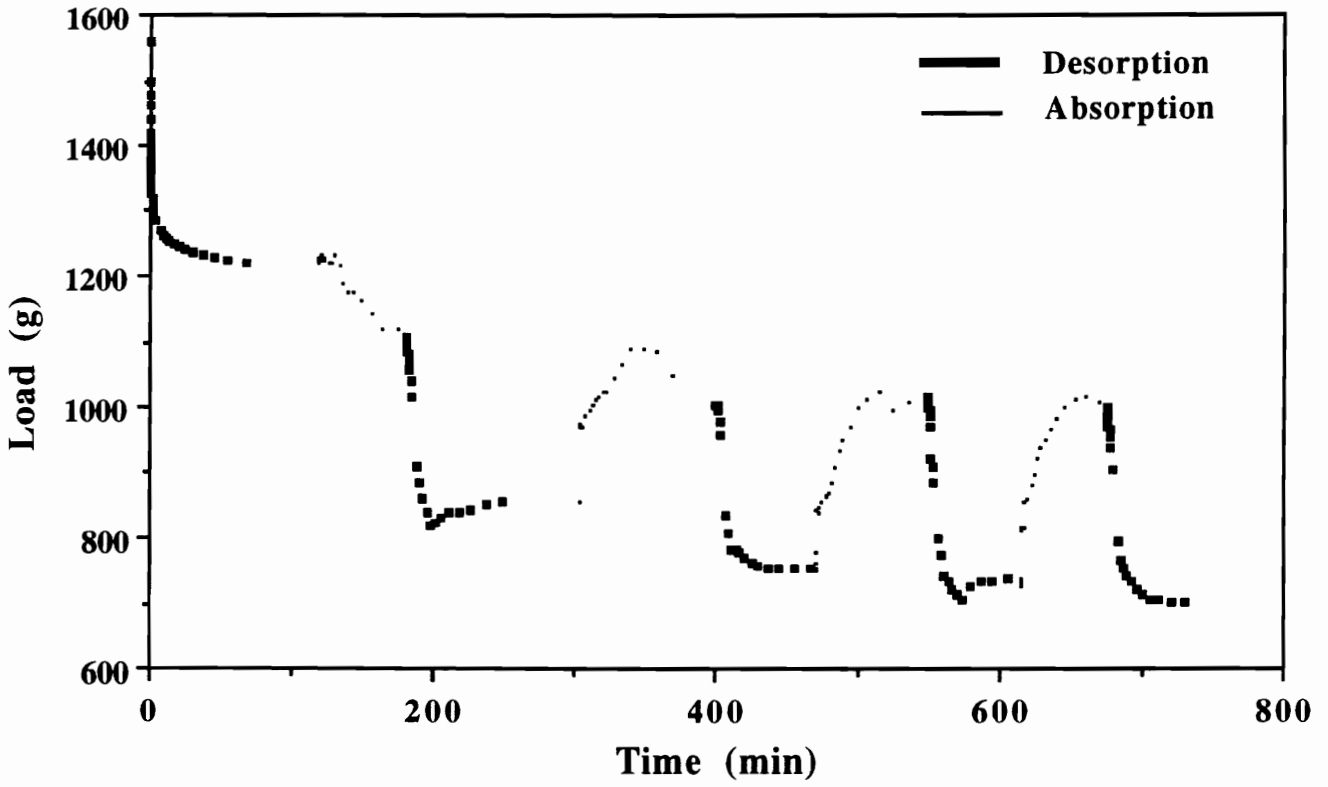


Figure 6.9. Influence of cyclic moisture conditions on the load relaxation behavior of Fs5 at a constant 65% strain and constant 90°C.

increase in load while every desorption step produced a decrease in load or a load decay. Again, even at 90°C, the overall trend is one of a decaying load over all absorption-desorption cycles.

6.3 Summary

Cyclic moisture conditions were found to have a pronounced effect on the viscoelastic behavior of flexible water-blown polyurethane foams. Both slabstock and molded foams were compressed under a constant load (or constant strain) and constant temperature in a changing moisture environment, while the strain (or load) was monitored. The mechano-sorptive phenomenon was evident with all three foams following a similar trend where at 40°C the strain level surpassed those under constant relative humidity, either high or low. In creep loading, the creep level increased with the first absorption cycle. Then, in each subsequent absorption cycle, minute changes in strain, if any, were observed, while in each desorption cycle, increases in strain were evident. The effect of cyclic moisture content on creep is believed to be due to the interaction of the water with the hydrogen bonded structure within the foams causing them to be temporarily broken and reformed and hence, causing the foam to undergo enhanced creep in correspondence to each change in moisture conditions. Of major significance is that during desorption, the increased free volume, along with the less ordered hydrogen bonds, allows for further increases in the creep strain in a step-like manner. Further support to this mechanism was given when the mobility of the hydrogen bonds was enhanced by increasing the temperature instead of cycling humidity. In this case, the final creep strain level reached was in close proximity to that where the humidity was cycled. Since polyurethane foam materials are inherently placed in changing environmental conditions - i.e. changing weather conditions, it is clear that the mechano-sorptive phenomenon is very important due to the application of foams in load bearing and structural purposes.

Chapter 7

7.0 CONCLUSIONS AND RECOMMENDATIONS

7.1 Conclusions

Many conclusions can be drawn from the work presented thus far regarding flexible molded as well as slabstock polyurethane foams. The conclusions presented here are specifically made from Chapters 4 through 6 and are presented in that general order beginning with statements concerning molded foams. The important aspects addressed are the structure, morphology and viscoelastic properties.

The molded foams had dramatically different cellular structures compared to slabstock. They possessed many more closed cells whose geometric shape was isotropic relative to slabstock foams which displayed a geometric anisotropy oriented along the rise direction. In addition, the cell struts of the molded foams were much thicker all of which results in a higher density than a slabstock foam of comparable water content. Varying the water content or CPP particulate content did not appear to significantly influence the cellular structure. TEM micrographs displayed evidence of the CPP particles distributed in a rather smooth continuous phase. They lacked the "grainy" texture observed with slabstock foams which has been attributed to the urea precipitates.

The molded foams displayed microphase separation as was observed using SAXS where the scattering peaks corresponded to a Bragg spacing of ca. 130 - 170 Å which varied slightly depending on the water content or CPP content. One of the most important discoveries of the work presented in this document was arrived at using WAXS. The WAXS patterns of the molded foams lacked any signs of structural order associated with the packing order of the HS domains but only displayed a broad amorphous halo. The conventional slabstock foam exhibited two relatively sharp peaks associated with local packing order of the hard segments. This was confirmed with FTIR which revealed that the molded foams lacked bidentate urea associated with well ordered hydrogen bonding and only displayed monodentate urea. In contrast, the slabstock foams again exhibited evidence of short range packing with the observation of a strong bidentate urea absorbance. Another important observation was the good agreement between FTIR and WAXS which suggested that FTIR is a good technique for assessing HS order but may be lacking in relating the results to the degree of microphase separation in polyurethane foams. Furthermore, the WAXS and FTIR results correlated well when carried out on an extracted slabstock foam where both techniques revealed that the order had been disrupted. As expected, the CPP particles did not appear to influence the HS ordering.

The viscoelastic properties varied significantly especially when the test temperature and/or humidity was increased. Comparing the load relaxation behavior, the molded foams exhibited a strong temperature and/or humidity dependence where at elevated conditions the relaxation curves resulted in lower loads and greater load decays. Initial increases in temperature resulted in increases in load (for the low water content foams) with no changes in the load decays of conventional slabstock foams. Humidity also had a dramatic softening effect on the relaxation behavior of molded foams inducing a similar "plasticization" effect. In general, the temperature beyond which significant softening was observed was ca. 50°C for the molded foams where this temperature was ca. 100°C for the slabstock foams. The softening effect was shown to be primarily a result of hydrogen

bond disruption (most of which exists within the hard segments) which occurs with greater ease in the molded foams than in the slabstock foams. This ease of "plasticization" displayed by the molded foams is a result of these foams having HS domains which are much less ordered and possess weaker monodentate hydrogen bonds. The other viscoelastic measurements, creep and compression set, also confirmed that the viscoelastic properties of the slabstock foams were superior to those of the molded foams. Not only was the compression set lower for the slabstock foam, but this system also displayed significant recovery whereas the molded foams did not.

Within the molded foams, varying the CPP content produced significant changes in the mechanical and viscoelastic properties. As expected, the foams containing this "filler" displayed greater initial stiffness such as initial loads in load relaxation or higher loads at any given strain in load-strain measurements. With respect to the load-strain measurements, the CPP containing foams exhibited greater hysteresis than those lacking the particles. Surprisingly, the viscoelastic properties of the foams containing the CPP dispersion were more time dependent than the foams free of these particles. The percent decays, in load relaxation, were higher for the CPP containing foams compared to the CPP free foams, especially at elevated temperatures or humidity. The lower amount of soft segment within the CPP containing foams relative to the CPP free foams resulted in greater strain within the soft segment for a given applied load since the rigid particles are not expected to strain. The particles are believed to act as stress concentrators thereby increasing the relaxation decay. At elevated temperatures and/or humidities, hydrogen bond disruption existing at the interface is disrupted which leads to further chain slippage. In creep, the CPP containing foams displayed lower initial strains, but during the creep experiment, the strain levels surpassed those of the CPP free foams. Higher compression set values were displayed by the "filled" foams confirming the load relaxation and creep results. Solvent extraction results surprisingly revealed that the foams incorporating the

CPP dispersion displayed a higher amount of extractable suggesting that these particles are completely grafted to the base polyol.

Another important ingredient incorporated in molded foams, DEOA, was evaluated by systematically varying its concentration. Solvent extraction results confirmed that as the DEOA was increased, the amount of covalent cross-linking also increased. However, the increased cross-linking also promoted many closed cells which dramatically altered the mechanical properties and even caused shrinkage of the foam pad as it cooled. High levels of DEOA also appeared to disrupt the rather large urea aggregates observed with TEM for the all propylene oxide polyol based foams. These aggregates appeared to have more of a mixed morphology for the high DEOA content foams which was attributed to the prevention of the full development of these structures by the added DEOA.

Increasing the DEOA content also influenced the microphase separation between the HS domains and the soft segment phase. As the DEOA was increased, the extent of phase separation decreased which was especially true for the lower molecular weight all propylene oxide polyol based systems. This was concluded using SAXS which exhibited a decreased overall intensity with the higher DEOA content foams as well as with DSC which revealed that the soft segment T_g increased in temperature as the DEOA content was increased.

The higher cross-linking provided by increasing the DEOA content also severely disrupted the hard segment ordering confirmed by both WAXS and FTIR. The sharpness of the rings in the WAXS patterns significantly decreased as the DEOA content was increased. In addition, FTIR illustrated that the bidentate urea absorbance also decreased as the DEOA content was increased. This observation is extremely important and believed to be in part responsible for the observed lack of packing order exhibited by the hard segments within the molded foams. It was also concluded that the inclusion of DEOA allowed these hard segment domains to be more labile at elevated temperatures thereby diminishing the foam's performance.

The high amount of closed cells was clearly evident in the load relaxation behavior. The high DEOA content foam displayed significantly higher initial loads but also displayed significant decay of the load in a three hour period. Comparing foams with relatively comparable cellular structures demonstrated that increasing the DEOA content increased the displayed load in load relaxation measurements at room temperatures. At elevated temperatures, however, no significant difference was observed as a function of DEOA content. This was attributed to a balance between the "tightening" of the covalent network and a "loosening" of the physical network (HS domains) as the DEOA content was increased.

The influence of the ethylene oxide capping was also evaluated by comparing the two series of foams where one contained a higher molecular weight polyol that was ethylene oxide end capped. The greatest effect was observed with TEM where the ethylene oxide containing polyol based foam contained small regions or domains on the order of ca. 150Å. The all propylene oxide polyol based foam also displayed larger regions on the order of ca. 150 nm which were attributed to urea aggregates.

Slabstock flexible polyurethane foams were produced using high water content formulations without the use of auxiliary blowing agents and varying levels of TDI index which influenced the softness of the foams. As the TDI index was increased, the "stiffness" of the material also increased which was a result of higher cross-linking and higher hard segment content arising from the higher index. Solvent extraction experiments also indicated that cross-linking was a direct result of altering the TDI index. The amount of extract with DMF decreased systematically with increasing index. Further evidence of covalent cross-linking was brought about by comparing the SEM micrographs of the foams after extraction as a function of TDI index which showed that the cellular structure of the highest index foam was much less affected than the cellular structure of the lowest index foam which appeared to have lost its integrity.

The mechanical and viscoelastic properties also compliment the above findings. The stress and elongation at break increased as a function of index with the exception of the highest index foam which failed at a lower stress and strain value than the 100 to 105 index foams. The viscoelastic properties also systematically improved with TDI index. In load relaxation, the initial loads systematically increased with increasing index with the exception of the highest index foam which throughout this study showed no significant difference to its predecessor. The percent decays systematically decreased with increasing TDI index. All foams were significantly "softened" by either temperature or humidity and especially both variables. As with the molded foams, the "plasticization" was attributed to the disruption of the hydrogen bonding (which is considerable in these high water content foams) by temperature and/or humidity . Although the compression set properties appeared to be independent of TDI index, the different TDI index strongly influenced the recovery experiments. Higher recovery from compression set was achieved for the higher index foams in a systematic fashion. The increasing recovery with increasing index is attributed to and viewed as strong evidence for the direct correlation between the TDI index and covalent cross-linking.

Along with investigating the influence of index on the physical properties of polyurethane foams, its effect on the morphology of these materials was investigated as well. SAXS results indicated that the lowest index foam had better phase separation than the highest index foam which displayed the lower intensity. This was supported by DSC and DMA measurements where the observed glass transition region increased in temperature with increasing index.

More importantly, the level of short range ordering of the hard segments was studied first by FTIR which showed that the highest amount of well ordered bidentate urea was displayed by the 100 index foam. This foam displayed the highest amount of bidentate urea suggesting this material has the highest concentration of well organized hard segments. The other foams having an index either above or below 100 displayed a

bidentate absorbance lower than that of the 100 index foam. This evidence strongly supports the claim that the increased covalent cross-linking prevents hard segment domain perfection. WAXS results confirmed this claim which showed that increasing the index caused the Bragg rings, associated with short range order, to become more diffuse due to a disordering of the hard segments.

Finally it was found that cyclic moisture conditions have a pronounced effect on the viscoelastic behavior of flexible water-blown polyurethane foams. The mechano-sorptive phenomenon was evident with both slabstock and molded foams. All foams followed a similar trend where at 40°C the strain level under transient moisture conditions surpassed those under constant high relative humidity. The creep level increased dramatically with the first absorption cycle. Then, in each subsequent absorption cycle, minute changes in strain, if any, were observed, while in each desorption cycle, increases in strain were clearly evident. The effect of cyclic moisture content on creep was attributed to the interaction of the water with the hydrogen bonded structure within the foams causing the hydrogen bonds to be temporarily broken and reformed and hence, causing the foam to undergo further strain in correspondence to each change in moisture conditions. Of major significance is that during desorption, the increased free volume, along with the less ordered hydrogen bonds, allowed for further increases in the strain in a step-like manner. Further support to this mechanism was given when the mobility of the hydrogen bonded structure was enhanced by increasing the temperature instead of cycling the humidity. Here, the final strain level was almost identical to that where the humidity was cycled. Since polyurethane foam materials are inherently placed in changing environmental conditions - i.e. changing weather conditions, it is clear that the mechano-sorptive phenomenon is very important due to the application of foams in load bearing and structural purposes.

7.2 Recommendations

In view of molded foams continually growing in their application, further evaluation of these materials should be pursued. While the work presented within this dissertation has significantly contributed to the general understanding of these materials, continuation of this study can further verify some of these observations. For example, the copolymer polyols, an important component added to molded foams to improve load bearing capabilities, were shown to promote diminished viscoelastic properties. Furthermore, the foams containing these particles were also shown to display a greater amount of extractables relative to the foams free of these particles. This aspect should be expanded upon by further evaluating extent that these particles are covalently linking to the base polyol. The particles should be separated from the polyol serum phase and then subjected to an extraction treatment. They should then be evaluated as to whether they contain polyol that was not extracted. In addition, FTIR can be carried out on the extract of a foam containing the particles to demonstrate any bands attributed to the components comprising the particles.

Another important aspect of molded foams is the ethylene oxide capped polyols that are utilized for greater productivity taking advantage of their greater reactivity. A series of foams should be formulated where the primary hydroxyl content is systematically varied by varying the amount of ethylene oxide capping thus allowing a more direct evaluation of its influence on the structure-property behavior. Special attention should be paid to the hard segment ordering since it was shown here to be an extremely important parameter in predicting a foam's mechanical behavior.

Finally, further work should be dedicated to evaluating the existence and influence of the urea aggregate structures. For example, these structures were observed in the slabstock foams utilizing all propylene oxide polyols. When ethylene oxide was included such as in the molded foams, these structures are not evident. Furthermore, the existence of these structures can in part explain the fact that the molded foams exhibit sharper SAXS

peaks than did the slabstock foams. If a large part of the hard segments are located within these aggregates, a SAXS peak is not expected in view of their larger size while sharp WAXS peaks and bidentate order are still possible. The lack of the aggregates in the molded foams can then promote the occurrence of the hard segments in domains (or mixed in the soft phase) thereby increasing the sharpness and intensity of the SAXS peaks.

References

1. N.C. Hilyard, "Mechanics of Cellular Plastics," Macmillan Publishing Co., Inc., New York(1982).
2. O. Bayer, *Modern Plastics*, **24**, 149-152, 250-262(1947)
3. G. Woods, "Flexible Polyurethane Foams:Chemistry and Technology," Applied Sci. Publishers, LTD, New Jersey(1982).
4. R.D. Duffy and R.D. Whittman, *J. Cell. Plastics*, **14**(3), 161(1978).
5. F.E. Critchfield, J.V. Koleske and D.C. Priest, *Rubber Chem. Tech.*, **45**, 1467-1487(1972).
6. R. Herrington and K. Hock, "Flexible Polyurethane Foams," Dow Chemical Co., Midland, Michigan,(1991).
7. K.E.T. Barrett, "Dispersion Polymerization in Organic Media," John Wiley and Sons, London(1975).
8. D.H. Napper, "Polymer Stabilization of Colloidal Particles," Academic Press, London(1983).
9. K.G. Spitler and J.J. Lindsey, *J. Cell. Plastics*, **17**(1) 43(1981).
10. P. Vehlewald, *Kustoff*, **73**(8), 439(1983).
11. A.A.R. Sayigh, H. Ulrich and W.J. Farrissey, "Diisocyanates In Condensation Monomers," Wiley-Interscience, New York(1962).
12. D.H. Chadwich and T.H. Cleveland, *Kirk-Othmer Encyclopedia of Chemical Technology, Third Edition*, John Wiley & Sons, New York, **13**, 789-818(1982).
13. K.E. Lunde and L.C. Bratt, *Process Economics Program Reprot No. 1*, Stanford Research Institute, Menlo Park, California,(1963).
14. B. Kanner and T.G. Decker, *J. Cell. Plastics*, **4**, 32(1969).

15. G. Rossmly, H.J. Kollmeier, W. Lidy, H. Schator and M. Wiemann, *J. Cell. Plastics*, **17**(6), 319(1981).
16. R.M. Bryant and H.F. Stewart, *J. Cell. Plastics*, **9**(2), 99-102(1973).
17. J.W. Baker and J.B. Holdsworth, *J. Chem. Soc.*, 713-726(1947).
18. A. Farkas and P.F. Strohm, *Ind. Eng. Chem. Fund.*, **4**(1), 32-8(1965).
19. *Rubber and Plastics News*, Oct. 15,(1990).
20. *Proceedings(Abstracts) of SPI Polyurethane Division Conference*,(1990).
21. G. Woods, "The ICI Polyurethanes Book," ICI and John Wiley & Sons, Netherlands,(1987).
22. Dow Chemical Co., "The Flexible Foam Handbook," Dow Chem. USA, Urethane Dept., Midland, Michigan.
23. G. Rossmly, W. Lidy, H. Schator, M. Wiemann and H.J. Kollmeier, *J. Cell. Plastics*, **13**(1), 26(1977).
24. F.E. Bailey and F.E. Critchfield, *J. Cell. Plastics*, **17**, 333(1981).
25. G. Hauptman, K.H. Dorner, J. Hocker and G. Pfister, *Proceedings of the 5th International SPI-Conference*,(1980).
26. J. Hocker, *J. Appl. Polym. Sci.*, **25**,2879(1980).
27. H.W. Illeger, K.H. Dorner and H. Hettel, *Polyurethane World Congress*, 305(1987).
28. P. Van Gheluwe and J. Leroux, *J. Appl. Polym. Sci.*, **28**, 2053(1983).
29. J. V. McClusky, R. E. O'Neil, R. D. Priester, Jr. and R. B. Turner, *J. Cell Plastics*, **26**, 346(1990)
30. J. V. McClusky, R. D. Priester, Jr. and W. R. Willkomm, M. A. Capel, M. D. Heaney, *Polyurethanes World Congress*, 507(1993)
31. R.B. Turner, H.L. Spell and G.L. Wilkes, *SPI 28th Annual Technical/Marketing Conference*, 244(1984).
32. J.P. Armistead, G.L. Wilkes and R.B. Turner, *J. Appl. Polym. Sci.*, **35**, 601(1988).
33. J.P. Armistead, MS Thesis, Virginia Polytechnic Institute and State University, Chem. Eng. Dept., Blacksburg, Virginia(1989).
34. D. Tyagi, Ph.D. Thesis, Virginia Polytechnic Institute and State University, Chem. Eng. Dept., Blacksburg, Virginia(1985).
35. J. T. Koberstein, R. S. Stein, *J. Poly. Sci., Polym. Phys. Ed.*, **21**, 1439, (1983)

36. O. Thomas, R. D. Priester, Jr., K. J. Hinze, and D. D. Latham, *J. Polym. Sci., Part B: Polym. Phys.*, **32**, 2155(1994).
37. Y.P. Chang and G.L. Wilkes, *J. Polym. Sci.*, **13**, 455-476(1975).
38. G.L. Wilkes and S. Abouzahr, *J. Cell. Plastics*, 248(1983).
39. W. Patten and D.C. Priest, *J. Cell. Plastics*, **8**, 134(1972).
40. G.A. Senich and W.J. MacKnight, *Macromol.*, **13**, 106(1980).
41. C.S. Paik Sung and N.S. Schneider, *Macromol.*, **10**, 452(1977).
42. J.T. Koberstein, I. Gancarz and T.C. Clarke, *J. Poly. Sci: Part B: Polymer Physics.*, **24**, 2487-2498(1988).
43. M.M. Coleman, K.H. Lee, D.J. Skrovanek and P.C. Painter, *Macromol.*, **18**, 2149(1986).
44. R. D. Priester, Jr., J. V. McClusky, D. I. Cortelek, P. S. Carleton, J. R. Porter, J. A. DeHaseth, *34th Annual Polyurethane Technical/Marketing Conference*, 206(1992)
45. J. V. McClusky, R. E. O'Neil, R. D. Priester, Jr. and W. A. Ramsey, *34th Annual Polyurethane Technical/Marketing Conference*, 535(1992)
46. Personal communication with John McClusky
47. R. G. Skorpenske, R. Solis, R. A. Kuklies, A. K. Schrock, and R. B. Turner, *34th Annual Polyurethane Technical/Marketing Conference*, (October 1992).
48. W. Patten, C.G. Seefried, R.D. Whitman and D.E. Pollart, *J. Cell. Plastics*, July, 172(1974).
49. C.S. Paik Sung, C.B. Hu and C.S. Wu, *Macromol.*, **13**, 111(1980).
50. K.C. Frisch and J.H. Saunders, "Plastics Foams: Part 1," Marcel Decker Inc., New York(1972).
51. Hilyard, "Mechanics of Cellular Solids," Applied Sci. Publishers, LTD, New Jersey,(1980).
52. W. Patten and C.G. Seefried, *J. Cell. Plast.*, Sept./Oct., 306(1985).
53. Anon, *Plast. Tech.*, **8**(4), 26-32(1962).
54. A. Lambert, *J. Cell. Plastics.*, **10**(1), 35-42(1974).
55. W.A. Ashe and O.M. Grace, *J. Cell. Plastics*, **25**(4), 371-390(1989).
56. M.F. Ashby, *Mettalurgical Trans.*, 14A, 1755(1983).
57. L.J. Gibson and M.F. Ashby, "Cellular Solids," Pergamon Press, New York(1988).

58. A.N. Gent and A.G. Thomas, *J. Appl. Polym. Sci.*, **1**, 107(1959).
59. A.N. Gent and A.G. Thomas, *Rubber Chem. Tech.*, **36**, 597(1963).
60. Skochdopole and Rubens
61. L.J. Gibson and M.F. Ashby, *Proc. R. Soc. Lond.*, **382**, 43(1982).
62. Zang and Ashby
63. S.K. Maiti, L.J. Gibson and M.F. Ashby, *Acta Metal.*, **32**, 1963(1984a)
64. K.C. Rusch, *J. Appl. Polym. Sci.*, **13**, 2297(1969).
65. J.D. Ferry, "Viscoelastic Properties of Polymers," John Wiley & Sons, New York(1961).
66. J. Miltz and O. Raman, *Polym. Eng. and Sci.*, **26**, 1305(1986).
67. M. Peleg, *J. Rheology*, **24**, 451(1980).
68. H.S. Michley, T.K. Sherwood and C.E. Reed, "Applied Mathematics in Chemical Engineering," McGraw-Hill, New York(1957).
69. A.V. Tobolsky and R.D. Andrews, *J. Chem. Phys.*, **13**(1), 1945).
70. J.D. Ferry, "Viscoelastic Properties of Polymers," John Wiley & Sons, New York(1970).
71. J.G. Curro, P. Pincus, *Macromol.*, **16**(4), 559-562(1983).
72. R.A. Dickie and J.D. Ferry, *J. Phys. Chem.*, **70**, 2594(1966).
73. W.J. Dzierza, *J. Appl. Polym. Sci.*, **27**, 1487(1982).
74. R.W. Seymour, G.M. Estes, D.S. Huh and S.L. Cooper, *J. Polym. Sci.*, **10**(A-2), 1521(1972).
75. G. Hsiue, D. Chen and Yeong-Kang, *J. Appl. Polym. Sci.*, **35**, 995-1002(1988).
76. R.B. Turner, *Polym. Composites*, **5**(2), 151-4, Apr.(1984).
77. K. Morimoto, T. Suzuki and R. Yosomiya, *Polym. Eng. and Sci.*, **24**(12), Aug.(1984).
78. D.J. Doherty and G. M. Ball, *J. Cell. Plastics*, **3**(5) (1967)
79. J.C. Moreland, Ph.D. Thesis, Virginia Polytechnic Institute and State University, Chem. Eng. Dept., Blacksburg, Virginia(1991).
80. G.A. Campbell, *J. Appl. Polym. Sci.*, **24**,709-23(1979).
81. J.S. Huang and L.T. Gibson, *J. Materials Sci.*, **26**, 637-47(1991).

82. Y.H. Pao and J. Marin, *J. Appl. Mech.*, **19**, 478(1952).
83. Y.H. Pao and J. Marin, *J. Appl. Mech.*, **20**, 245(1953).
84. W.N. Findley and G. Khosla, *J. Appl. Mech.*, **26**, 821(1955).
85. W.N. Findley and C.A. Stanley, *J. Mater.*, **3**, 916(1968).
86. K.G. Nolte and W.N. Findley, *Trans. ASME J. Basic Eng.*, **92**, 105(1970).
87. J.M. Davies, *Struct. Eng.*, 435(1987).
88. M. Just, *Ifl-Mitt.*, **22**, 3(1983).
89. M. Zaslowsky, *SPE J.*, **240**, 62(1968).
90. A. D'Amore, L. Nicholais and M. Narkis, *J. Cellular Plastics*, **22**, p³(1986).
91. A. D'Amore, J.M. Kenny and L. Nicholais, *J. Cellular Plastics*, **24**, 473(1988).
92. D. Alperstein, M. Narkis and S. Kenig, *Polymer Composites*, **5**(2), 155(1984).
93. R. M. Herrington, and D. L. Klarfeld, *Proceedings of the SPI Annual Technical/Marketing Conference*, 177(1980)
94. Patten
95. Soatome
96. S.M. Terry, *J. Cell. Plastics*, **12**, 156(1976)
97. R. G. Skorpenske, A. K. Schrock, and G. E. Beal, *J. Cellular Plastics*, **27**, 560(1991).
98. P.A.U. Grossman, *Wood Science and Technology*, **10**, 163(1976)
99. L.D. Armstrong and R.S.T. Kingston, *Nature*, **185**, 863(1960)
100. B.H. Mackay and J.G. Downes, *J. of Applied Polymer Science*, **II**(4), 32(1959)
101. John Z. Wang, David A. Dillard, and Frederick A. Kamke, *J. Mat. Sci.*, **26**, 5113(1991)
102. R.F.S. Hearmon and J.M. Paton, *Forest Products Journal*, Aug. 357-9(1964)
103. Michael Humphries and Arno P. Schniewind, *Wood Science*, **15**(1), 44(1982)
104. D.G. Hunt, *Wood Science*, **2**, 212(1970)
105. Arno P. Schniewind, *Wood Science and Technology*, **1**, 278(1976)
106. E.L. Bryan and A.P. Schniewind, *Forest Products Journal*, **15**, 143(1965)

107. E. J. Gibson, *Nature*, **206**, 213(1965)
108. P. Hoffmeyer and R.W. Davidson, *Wood Sci. and Tech.*, **23**, 215(1989)
109. T.A.C.M. van de Put, *Wood and Fiber Sci.*, **21**(3), 219(1989)

Vita

Dimitrios (Jim) Dounis was born of Bill and Pat Dounis in the riverfront town of Wyandotte, Michigan. He grew up in a wonderful small suburb named Riverview, Michigan and in 1986 graduated from Riverview High School. He immediately began studies at Michigan State University and graduated with a B.S. in Chemical Engineering in 1990. That fall, he moved to Blacksburg, Virginia and joined the Chemical Engineering Department at Virginia Polytechnic Institute and State University. He began pursuing a Ph.D. under the guidance of Professor Garth L. Wilkes .